UNIVERSIDADE DE SÃO PAULO
FACULDADE DE CIÊNCIAS FARMACÊUTICAS
PROGRAMA DE PÓS-GRADUAÇÃO EM FARMÁCIA
(FISIOPATOLOGIA E TOXICOLOGIA)
ÁREA DE FISIOPATOLOGIA

Milena Fronza Broering

Novas formulações de Anexina A1 como estratégia terapêutica para a colite experimental

São Paulo
2024

UNIVERSIDADE DE SÃO PAULO
FACULDADE DE CIÊNCIAS FARMACÊUTICAS
PROGRAMA DE PÓS-GRADUAÇÃO EM FARMÁCIA
(FISIOPATOLOGIA E TOXICOLOGIA)
ÁREA DE FISIOPATOLOGIA

Milena Fronza Broering

Novas formulações de Anexina A1 como estratégia terapêutica para a colite experimental

Versão Original

Tese para obtenção do Título de Doutora em Ciências

Orientadora:
Profa. Dra. Sandra Helena Poliselli Farsky

São Paulo
2024

Ficha Catalográfica elaborada eletronicamente pelo autor, utilizando o programa desenvolvido pela Seção Técnica de Informática do ICMC/USP e adaptado para a Divisão de Biblioteca e Documentação do Conjunto das Químicas da USP

Bibliotecária responsável pela orientação de catalogação da publicação:
Marlene Aparecida Vieira - CRB - 8/5562

B863n

Broering, Milena Fronza
Novas formulações de Anexina A1 como estratégia terapêutica para a colite experimental / Milena Fronza Broering. - São Paulo, 2024.
320 p.

Tese (doutorado) - Faculdade de Ciências Farmacêuticas da Universidade de São Paulo. Departamento de Análises Clínicas e Toxicológicas.
Orientador: Farsky, Sandra Helena Poliselli

1. Anexina A1. 2. Ac2-26. 3. Doença inflamatória intestinal. 4. Nanocápsula multiparede de núcleo lipídico. 5. SBA-15. I. T. II. Farsky, Sandra Helena Poliselli , orientador.

Milena Fronza Broering

Novas formulações de Anexina A1 como estratégia terapêutica para a colite experimental

Comissão Julgadora

Tese para obtenção do Título de Doutora em Ciências

_____

Prof. Dr. Orientador/presidente

_____

1º examinador

_____

2º examinador

_____

3º examinador

São Paulo, _____ de 2024.

DEDICATÓRIA

À minha mãe, Flavia, e aos meu avós Arno e Aneide que foram fundamentais para eu trilhar meu caminho até o dia de hoje e muitas vezes tiraram de si para que eu pudesse realizar meus sonhos. Vocês sempre foram minha força e o maior exemplo para me tornar alguém melhor. Nada disso seria possível sem vocês.

Ao meu noivo, Fernando, que me conheceu no início do doutorado e acompanhou minha caminhada até esse momento. Você me inspira a ser alguém forte e confiante. Obrigada por ser meu porto seguro e acreditar em mim mais do que eu mesma.

DEDICATÓRIA

À minha orientadora, profa. Dra Sandra Farsky, que sempre quis a melhor formação para seus alunos e faz de tudo ao seu alcance para isso. Que me acolheu em momentos difíceis e me mostrou que sempre somos capazes de superar nossos limites. Obrigada por acreditar em mim e me ajudar alcançar meus sonhos!

AGRADECIMENTOS

À Fundação de Amparo a Pesquisa do Estado de São Paulo - FAPESP pela concessão do apoio financeiro durante o doutorado (Projeto nº 2018/26383-7), pela bolsa BEPE (Projeto nº 2022/05777-2) que me possibilitou alcançar a oportunidade de expandir meus conhecimentos na pesquisa.

À Faculdade de Ciências Farmacêuticas (FCF-USP) por proporcionar a oportunidade de fazer parte desse programa que me acolheu como aluna, pela infraestrutura e professores necessários para a minha formação.

À CAPES, pelo apoio ao desenvolvimento e consolidação do Programa de Pós-Graduação em Farmácia.

À meu querido orientador de iniciação científica e mestrado José Roberto Santin que me inspirou a ser uma cientista, que sempre acreditou em mim e me ajudou a trilhar o caminho do conhecimento desde a graduação.

À meus colegas e amigos de bloco 13B: Pablo, Silvana, Pamela, Luana, Vítor e André. E aos que já saíram de lá: Gustavo e Marina. Cada dia vivido no laboratório foi melhor por que vocês estavam lá para compartilhar as felicidades, angústias, almoços e cafés comigo.

À meu amigo Matheus Leão, que me ajudou a entender o mundo das nanocápsulas e transferiu todo seu conhecimento para mim, no início uma estranha, da melhor forma possível.

À meu amigo Pablo Scharf, que desde o primeiro dia que iniciei na USP foi um ombro amigo dentro e fora do laboratório. Que nunca mediu esforços para me ajudar e estar presente para me dar seus conselhos sinceros.

À minha amiga Silvana Sandri, uma pesquisadora com o conhecimento e o coração maiores do mundo. Seus ensinamentos foram são para a vida.

À minha amiga Pamela Pacassa, que me acolheu e fez do seu, o meu lar tem um momento que precisei de um ombro amigo. Que me ajudou a concluir diver experimentos enquanto eu estava no BEPE.

À professora Soumita Das (Universidade Massachusetts Lowell) que abriu as portas de seu laboratório para me receber durante o BEPE.

À meu mentor do BEPE, Ibrahim M. Sayed (Universidade Massachusetts Lowell). Você mudou o destino do meu BEPE e me acolheu como uma de suas alunas. Obrigada por todo o conhecimento repassado e amizade.

À meus amigos Stefania Tocci e Noah Sout (Universidade Massachusetts Lowell) que dentro e fora do laboratório foram o motivo de eu aguentar os momentos difíceis e de solidão.

À meus colaboradores que foram essenciais para o desenvolvimento da minha tese e artigos publicados nesse perído: Professora Márcia Fantini, Professor Marco Antonio Stephano, Dr Luís Cides e Dr. Pedro Oseliero, obrigada por me receberem em seus laboratórios e abraçarem esse projeto da SBA-15 junto conosco. Às professora Silva Guterres e Adriana Pohlmann que forneceram todo suporte científico para o desenvolvimento da MLNC. Ao Professor Lionel Gamarra e seu aluno Fernando que colaboraram para os experimentos de PET/SCAN e enriqueceram nosso trabalho.

EPÍGRAFE

Cada dia
traz sua alegria
e sua pena,

e também
sua lição
proveitosa

José saramago

RESUMO

BROERING, M. F. **Novas formulações de Anexina A1 como estratégia terapêutica para a colite experimental.** 2024. 316 f. Tese (Doutorado em Ciências) – Faculdade de Ciencias Farmacêuticas, Universidade de São Paulo - SP, 2024.

A Anexina A1 (AnxA1) é uma proteína de 37 kDa que controla o desenvolvimento da reação inflamatória inata, e favorece a eferocitose e o reparo tecidual. Em doenças inflamatórias intestinais (DIIs), tanto a AnxA1 endógena, como a sintética e o peptídeo sintético mimético ao N-terminal da proteína (Ac2-26) inibem o desenvolvimento de doença e induzem a cicatrização. O presente projeto teve o objetivo de obter novas formulações para carrear a AnxA1 recombinante (rAnxA1) ou o Ac2-26 e testar suas eficácias no modelo de colite experimental induzida pelo dextram sulfato de sódio (DSS, 0-6 dias) em camundongos C57Bl/6 machos. A rAnxA1 foi funcionalizada em nanocápsulas de núcleo lipídico de parede múltipla (MLNC) pela ligação Zn^{2+}, com alta eficência de incorporação (92%) e adminsitrada pelas vias oral, intravenosa ou intraperitoneal durante a fase latente da doença (6°-9° dia). Somente o tratamento intraperitoneal com MLNC-AnxA1 (12,5 µg/mL) reduziu significativamente os sinais clínicos da doença, restaurou a integridade da estrutura colônica e a proliferação celular, bem como aumentou expressão de junções celulares da barreira intestinal. Ainda, MLNC-AnxA1 induziu a polarização de macrófagos para o fenótipo M2 *in vivo* no tecido inflamado e *in vitro* após estímulo com lipopolissacarídeos (LPS) bacteriano. Na tentativa de obter uma formulação terapêutica com atividade por vial oral, o peptídeo Ac2-26 foi incorporado em sílica mesoporosa ordenada SBA-15 e revestidos com Eudragit® L30-D55. A incorporação do peptídeo foi efetiva (88%) e a administração oral de Eudragit-SBA15-Ac2-26 (6°-9° dia; 200 µg/camundongo; 8 mg/kg) reduziu significativamente os sintomas clínicos e inflamação. De fato, ensaios de PET-SCAN mostraram que o SBA-15 permaneceu no intestino por até 16 horas após a administração e promoveu a liberação do peptídeo no intestino inflamado. Em cultura celular de epitélio (Caco-2), Eudragit-SBA15-Ac2-26 favoreceu a internalização de Ac2-26. Em conjunto, as duas estratégias expermentais de entrega do rAnxA1 ou Ac2-26 foram eficientes e os resultados obtidos sugerem que mais estudos devem ser realizados para a confirmação das estratégias de tratamento. Com o intuito de buscar ferramentas para ampliar estes estudos, durante estágio BEPE foram realizados estudos em cultura de células epiteliais baseado em células-tronco adultas diferenciadas *in vitro*. Os resultados mostraram que rAnxA1 ou Ac2-26 protegeram a integridade epitelial após desafio com LPS, pela regulação positiva da expressão das junções oclusivas e aderentes e redução da expressão de claudina-2, responsável pelo aumento da permeabilidade intercelular; pela modulação negativa decitocinas pró-inflamatórias CXCL-1 e MCP-1, e positiva de citocina anti-inflamatória IL-10. Desta forma, padronizamos um novo modelo de cultura celular ainda não testada para a AnxA1 ou Ac2-26, que poderá ser empregada para desvendar os mecanismos da MLNC-AnxA1 e do Eudragit-SBA15-Ac2-26.

ABSTRACT

BROERING, M. F. **New formulations of Annexin A1 as a therapeutic strategy to experimental colitis.** 2024. 316 f. PhD thesis – School of Pharmaceutical Sciences, University of São Paulo- SP, 2024.

Annexin A1 (AnxA1) is a 37 kDa protein that controls the development of the innate inflammatory reaction, and favors efferocytosis and tissue repair. In inflammatory bowel diseases (IBDs), both endogenous and synthetic AnxA1 and the synthetic peptide mimetic to the N-terminal of the protein (Ac2-26) inhibit the development of disease and induce healing. The present project aimed to obtain new formulations to carry recombinant AnxA1 (rAnxA1) or Ac2-26 and test their efficacy in the experimental colitis model induced by dextram sodium sulfate (DSS, 0-6 days) in C57Bl/6 mice. rAnxA1 was functionalized into multiwall lipid core nanocapsules (MLNC) by Zn^{2+} binding, with high incorporation efficiency (92%) and administered orally, intravenously or intraperitoneally during the latent phase of the disease (6º-9º day). Only intraperitoneal treatment with MLNC-AnxA1 (12.5 µg/mL) significantly reduced the clinical signs of the disease, restored the integrity of the colonic structure and cell proliferation, as well as increased the expression of intestinal barrier cell junctions. Furthermore, MLNC-AnxA1 induced macrophage polarization to the M2 phenotype *in vivo* in inflamed tissue and in vitro after stimulation with bacterial lipopolysaccharides (LPS). In an attempt to obtain a therapeutic formulation with oral activity, the Ac2-26 peptide was incorporated into ordered mesoporous silica SBA-15 and coated with Eudragit® L30-D55. Peptide incorporation was effective (88%) and oral administration of Eudragit-SBA15-Ac2-26 (6º-9º day; 200 µg/mice; 8 mg/kg) significantly reduced clinical symptoms and inflammation. PET-SCAN assays showed SBA-15 remained in the intestine for up to 16 hours after administration and promoted the release of the peptide in the inflamed intestine. In epithelial cell culture (Caco-2), SBA15-Ac2-26 favored the internalization of Ac2-26. Taken together, the two experimental delivery strategies for rAnxA1 or Ac2-26 were efficient and the results obtained suggest that more studies should be carried out to confirm the treatment strategies. In order to seek tools to expand these studies, during the BEPE internship, studies were carried out in epithelial cell cultures based on adult stem cells differentiated *in vitro*. The results showed rAnxA1 or Ac2-26 protected epithelial integrity after challenge with LPS, by upregulating the expression of tight and adherens junctions and reducing the expression of claudin-2, responsible for increasing intercellular permeability; by negative modulation of pro-inflammatory cytokines CXCL-1 and MCP-1, and positive modulation of anti-inflammatory cytokine IL-10. In this way, we standardized a new cell culture model that has not yet been tested for AnxA1 or Ac2-26, which could be used to unravel the mechanisms of MLNC-AnxA1 and Eudragit-SBA15-Ac2-26.

LISTA DE FIGURAS

LISTA DE TABELAS

SUMÁRIO

Introdução

Doenças inflamatórias intestinais

A inflamação é um complexo processo fisiopatológico desencadeado em resposta a agentes agressores ao organismo, sejam eles infecciosos ou não, que culmina na ativação de fatores plasmáticos e de células imunes e epiteliais, com a subsequente ativação de vias de sinalização inflamatória (MEDZHITOV, 2010). Dentre as diversas doenças de base inflamatória, encontram-se as doenças inflamatórias intestinais (DIIs), como a doença de Crohn (DC) e a retocolite ulcerativa (RCU), caracterizadas pela presença crônica e recorrente de inflamação no trato gastrointestinal, com ênfase no intestino grosso. Esses distúrbios, considerados idiopáticos, podem ter sua origem associada a fatores como alterações na microbiota intestinal, ambientais, autoimunidade e predisposição genética. Além disso, trata-se de condições incuráveis que alternam entre períodos de latência e remissão. Os principais sintomas dessas enfermidades incluem diarreia persistente, dores abdominais, presença de sangue nas fezes e fadiga. Ainda, cerca de 25% das pessoas acometidas podem apresentar alguma manifestação não intestinal, como lesões cutâneas, orais e oculares. Pacientes com DIIs têm risco significativo de desenvolvimento de câncer colorretal e as implicações sociais consideráveis decorrentes da situação debilitante enfrentada pelo doente (COLOMBEL; NARULA; PEYRIN-BIROULET, 2017; FEUERSTEIN et al., 2019; LEE; KWON; CHO, 2018; WILHELM; LOVE, 2017).

Entre 1990 a 2017 registrou-se um aumento considerável na incidência de DIIs em diferentes regiões do mundo. Um dos fatores associados a esse aumento inclui mudanças no estilo de vida e comportamento, exposição à poluição ambiental e alteração na dieta. Estes fatores estão associados às diferenças culturais, juntamente com a industrialização. Atualmente as maiores prevalências de DIIs encontram-se nos Estados Unidos, China e Europa Ocidental, com cerca de 150 casos para 100.000 habitantes. Houve aumento de aproximadamente 50% de prevalência e 68,75% de aumento da morbidade relacionada a DIIs quando comparados os períodos entre 1990 e 2019 (WANG et al., 2023). Contudo, no período entre 2016 e 2019, a morbidade das DIIs alcançou estabilidade em países ocidentais. Essa estabilização foi principalmente atribuída aos avanços nas terapias específicas desenvolvidas para o tratamento dessas condições (KAPLAN; NG, 2017; PARK et al., 2020; WANG et al., 2023).

O diagnóstico de DIIs ocorre comumente em pessoas com idade entre 15 e 35 anos e é baseado em uma combinação de sintomas, análises colonoscópicas e histológicas, além cultivo de fezes para descartar a possibilidade de outras infecções (MAGRO et al., 2017; SHIVASHANKAR et al., 2017). O diagnóstico diferencial de RCU e DC ocorre, principalmente, pela colonoscopia que avalia a aparência intestinal e coleta de tecido para biópsias seriadas de cada segmento intestinal. Na RCU, os pacientes apresentam lesões contínuas, marcadas por ulcerações, que se limitam ao cólon e se iniciam no reto e atingem até a região proximal, podendo atingir todo o cólon de forma ascendente (NIKOLAUS; SCHREIBER, 2007). A biópsia apresenta infiltrado celular majoritariamente de neutrófilos e se caracteriza por inflamação na região mucosa, podendo apresentar edema de cripta e alteração da histoarquitetura Pacientes portadores de DC apresentam envolvimento em todo o trato gastrointestinal, com lesões em regiões alternadas, mas que acometem principalmente a região ileal na maioria dos casos. A biópsia pode apresentar características similares a RCU; no entando, a inflamação ocorre de forma transmural e grande parte dos casos apresenta granulomas e o infiltrado celular é majoritariamente de células mononucleres (GEBOES et al., 2000; SILVERBERG FRCPC et al., 2005; WOLFSON et al., 1982).

Diferentes mecanismos podem estar associados a etiologia de DIIs, por se tratarem de doenças crônicas, remitentes-recorrentes e imuno mediadas, o que também acarreta complexidade da gênese dessas doenças (LINDEN et al., 2008) (Figura 1). A heterogeneidade no padrão de distribuição das DIIs ao redor do mundo indica a importância crucial dos fatores ambientais em seu desenvolvimento. Entretanto, é relevante observar que variações genéticas desempenham um papel significativo, influenciando as modificações principalmente no sistema imunológico (GRAHAM; XAVIER, 2020; SHI et al., 2019). Uma característica de pacientes com RCU é a redução da camada de mucina, a qual é responsável por manter as bactérias afastadas da barreira intestinal (JOHANSSON et al., 2014). Além disso, a redução do gene fucosiltransferase 2 (*FUT2*), que está associado a função da barreira mucosa, é relacionado ao aumento da suscetibilidade para o desenvolvimento de DC (MCGOVERN et al., 2010). A camada de mucina secretada sobre o epitélio intestinal é considerada uma barreira física e a primeira linha de defesa para impedir a invasão das bactérias luminais (LINDEN et al., 2008).

Figura 1. Representação gráfica dos fatores envolvidos no desenvolvimento das DIIs

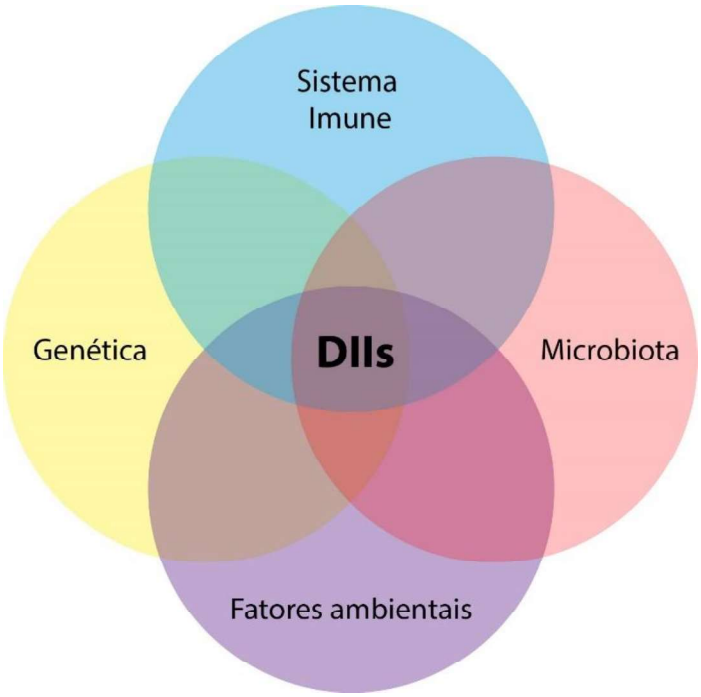

As DIIs são doenças multifatoriais e podem ter sua patogênese associada a uma ou mais condições simultaneamente. Fonte: o autor

Na RCU, o aumento da permeabilidade da barreira epitelial está associado a redução da síntese e secreção de mucina 2 (MUC2). Diferentes fatores podem estar relacionados a diminuição da espessura e composição do muco intestinal, como a presença de células calciformes (*goblet cells*) imaturas e a redução do número dessas células, responsáveis pela produçãoe manutenção do muco intestinal (GROOTJANS et al., 2013; SHAOUL et al., 2004). Pacientes com DC ou RCU também podem apresentar aumento de muco intestinal, no entanto tal característica não impede a permeação de bactérias pela barreira epitelial. Nesses casos é observado alterações estruturais secundárias no muco, como perda da função viscoelástica. A qualidade do muco intestinal está intimamente relacionada à composição da microbiota intestinal e a produção de seus metabólitos, uma vez que pacientes com DIIs apresentam comumente defeitos em glicosilação e sulfatação na estrutura do muco, tornando-o ineficaz como barreira (GROOTJANS et al., 2013; PARIKH et al., 2019).

Além disso, muitas alterações genéticas associadas ao desenvolvimento de DIIs ocorrem especificamente entre a interação do sistema imune e a microbiota. Uma das modificações genéticas mais notáveis e correlacionadas às DIIs refere-se a alterações no gene responsável pela codificação do receptor intracelular de domínio

de oligomerização de ligação a nucleotídeos 2 (NOD2), cuja função é o reconhecimento de componentes da parede bacteriana e a promoção da função antimicrobiana celular por meio da ativação de vias pró-inflamatórias. A alteração no gene NOD2 está associada à modificação do microbioma e aumenta a suscetibilidade e recorrência à DC (KOBAYASHI et al., 2005; MUKHERJEE et al., 2019; SHARMA et al., 2023).

A disbiose, reconhecida como um fator significativo para a manifestação e evolução das DIIs, destaca-se pela influência crucial da composição da microbiota intestinal no desenvolvimento dessas condições. Bactérias simbióticas presentes no intestino reforçam a barreira anti-inflamatória e a regulação das células imunes intestinais (PICKARD et al., 2017). A ruptura desse equilíbrio mutualístico que existe no microambiente intestinal leva a redução de metabolitos anti-inflamatórios produzidos por essas bactérias, como ácidos graxos de cadeia curta (*short-chain fatty acids* – SCFA), butirato e ácido indoleacrílico (FRANK et al., 2007; GAUDIER et al., 2004; WLODARSKA et al., 2017). Adicionalmente, a exposição a poluentes ambientais, como elevados níveis de dióxido de enxofre (SO2) e dióxido de nitrogênio (NO2), está correlacionada à maior propensão ao desenvolvimento das DIIs (MOLODECKY; KAPLAN, 2010).

Os intestinos desempenham papel vital no funcionamento do corpo humano, destacando-se pelo tecido epitelial que se auto-renova de forma rápida, superando outros mamíferos. As vilosidades e microvilosidades das criptas intestinais, presentes em ambos os intestinos delgado e grosso, são essencias para a absorção de nutrientes e na preservação da homeostase, oferecendo respostas imunes contra bactérias do microbioma e patógenos (BARKER, 2014; BARKER et al., 2007; DE SOUSA E MELO; DE SAUVAGE, 2019). A estrutura e integridade das criptas são mantidas pela renovação eficiente do epitélio intestinal, que se completa a cada 7 dias. Nas DIIs ocorre a perda da integridade de junções celulares que compõem o epitélio intestinal. Estas junções, compostas por proteínas transmembranares e citosólicas, se subdividem em *tight-junctions*, *adhesion-junctions* e desmossomos, desempenhando um papel crucial na coesão entre as células intestinais. Essa coesão forma a barreira intestinal, essencial para a homeostase do trato gastrointestinal. (AHMAD et al., 2014; GÜNZEL; YU, 2013; RESCIGNO, 2011; ZEISSIG et al., 2007).

A principal função das junções é atuar como um “portão” que sela o espaço paracelular, regulando a entrada de moléculas por esse espaço e formando canais que possibilitam a entrada de nutrientes (CHELAKKOT; GHIM; RYU, 2018; DIAMOND, 1978). As *tight junctions* estão localizadas na região apical das células e são compostas por diferentes proteínas transmebranas e citosolicas, dentre elas estão as zonulas de oclusão (ZOs), claudinas e ocludinas. Enquanto as junções de adesão estão localizadas em uma região subapical e são compostas por filamentos de actina e citoqueratina. Abaixo das junções de adesão estão localizados os desmossomos que interagem com as proteínas de junção de adesão e juntas fazem a forte adesão celular (FARQUHAR; PALADE, 1963).

Alterações na expressão e funcionamento das proteínas presentes nas junções epitelaiis estão associados ao desenvolvimento de doenças, uma vez que essas agem em conjunto e interagem entre si. A expressão de ocludina no tecido é igualmente correlacionada com a integridade da barreira, sendo a mais abundante junção expressa por essas células. As claudinas, em especial a claudina 2 é responsável pela formação dos canais de água na região paracelular e o aumento da expressão dessa porteína é associado a ampliação da permeabilidade de barreira nas DIIs (CHELAKKOT; GHIM; RYU, 2018; HARHAJ; ANTONETTI, 2004; ZEISSIG et al., 2007). Por outro lado, o aumento da expressão das claudinas 1, 5 e 8 é correlacionado ao aumento da integridade da barreira epitelial (GÜNZEL; YU, 2013). ZO-1 é responsável por interagir com ocludina, claudinas e junções de adesão formando ligações através da interação com proteínas do citoesqueleto celular F-actina e miosina (CUNNINGHAM; TURNER, 2012).

O controle da expressão das junções ocorre de maneira altamente regulada. Embora muitos dos mecanismos que envolvem a regulação dessas proteínas sejam ainda desconhecidos, sabe-se que a resposta imune exerce grande papel na sua regulação. Enquanto o fator de crescimento transformador β (TGFβ) atua aumentando a integridade pela regulação positiva de claudina 1 (HOWE et al., 2005), o fator de necrose tumoral α (*tumoral necrosis factor* α – TNFα) e o interferon γ (IFNγ) são capazes de atuar sobre a regulação negativa da integridade dessas junções. O TNF é capaz de alterar a expressão de ocludina, induzindo a internalização dessa proteína, enquanto o IFNγ reduz a expressão de ZO-1 e ocludina (UTECH et al., 2005; WANG et al., 2005). Dado o fato de que DIIs são doenças imuno mediadas, o estudo das junções de adesão é crucial para a compreensão das DIIs (DIIs), sendo essencial

tanto para desvendar os mecanismos subjacentes à patogênese quanto para o desenvolvimento de abordagens terapêuticas eficazes.

O sistema imune na patogênese das DIIs

O sistema imune que controla a homeostase intestinal é composto de um equilíbrio complexo entre a imunidade funcional (inata e adaptativa) e anatômica (mucosa e sistêmica). As células imunes na mucosa intestinal podem ser encontradas em linfonodos secundários e são, majoritariamente, compostas de linfócitos, macrófagos e células dendríticas que promovem o controle imune frente a antígenos inócuos (MALOY; POWRIE, 2011).

As células dendríticas, componentes essenciais do sistema imunológico, mantêm um contato contínuo com antígenos luminais através de seus dendritos que permeiam as células epiteliais. Esta função de "vigilância" desempenhada pelas células dendríticas é crucial para a detecção de organismos estranhos, que podem manifestar-se como PAMPs (Padrões Moleculares Associados a Patógenos) ou DAMPs (Padrões Moleculares Associados a Dano). Este processo de vigilância está intrinsecamente associado ao controle rigoroso entre o que é considerado "self" e "non-self" pelo sistema imunológico. ao manterem uma vigilância constante, desempenham um papel crucial na detecção e resposta a ameaças potenciais, contribuindo para a homeostase imunológica e a defesa eficaz do organismo contra patógenos e lesões (FARACHE et al., 2013; GROSS; SALAME; JUNG, 2015).

Linfócitos B agem promovendo o equilíbrio na resposta a antígenos via imunoglobulinas (Ig) e podem adquirir seu fenótipo de plasmócitos e secretar a imunoglobulina A (IgA), para neutralizar os patógenos e toxinas sem a ativação da cascata inflamatória. Além disso, alguns pacientes com DC e RCU apresentam um subtipo de IgG contra a microbiota comensal, associado ao aumento da resposta inflamatórias nesses pacientes (BOURGONJE et al., 2022). Adicionalmente, outro estudo demonstrou que pacientes com RCU produziram autoanticorpos contra a integrina αvβ6, que mantém a barreira epitelial através da adesão celular (KUWADA et al., 2021).

Os linfócitos T que residem no intestino passam por um processo de maturação nos órgãos linfoides associados ao intestino, conhecidos como *Gut-Associated Lymphoid Tissues* (GALTs). Destacam-se entre essas regiões os linfonodos

mesentéricos e as placas de Peyer, fundamentais componentes do GALT. Nesses órgãos, os linfócitos T adquirem características específicas de linfócitos intestinais antes de migrarem para regiões designadas do intestino delgado ou grosso em resposta a estímulos específicos. Os linfócitos T que se encontram no tecido epitelial intestinal podem ser subdivididos em duas categorias principais: as células intraepiteliais (LIE) e os linfócitos T localizados na lâmina própria. As LIE desempenham um papel crucial na regulação da autoimunidade e na promoção da tolerância intestinal. Por outro lado, os linfócitos T presentes na lâmina própria estão diretamente envolvidos na resposta imunológica do intestino contra agentes infecciosos. As células não intraepiteliais (LIE) atuam na promoção da tolerância imunológica no intestino, desempenhando um papel fundamental na supressão de respostas autoimunes prejudiciais. Elas contribuem para a manutenção do equilíbrio entre a defesa imunológica e a prevenção de reações excessivas contra antígenos próprios do organismo. Por outro lado, os linfócitos T localizados na lâmina própria desempenham uma função predominante na defesa contra infecções no intestino. Estas células respondem a estímulos provenientes de patógenos, promovendo respostas imunes adaptativas eficazes para combater invasores microbianos e garantir a integridade do sistema gastrointestinal (AGACE, 2008; CAMPBELL; BUTCHER, 2002; MA; TAO; ZHU, 2019). Um breve resumo do microambiente intestinal em homeostase está ilustrado na Figura 2.

Figura 2. Tecido intestinal em homeostasia

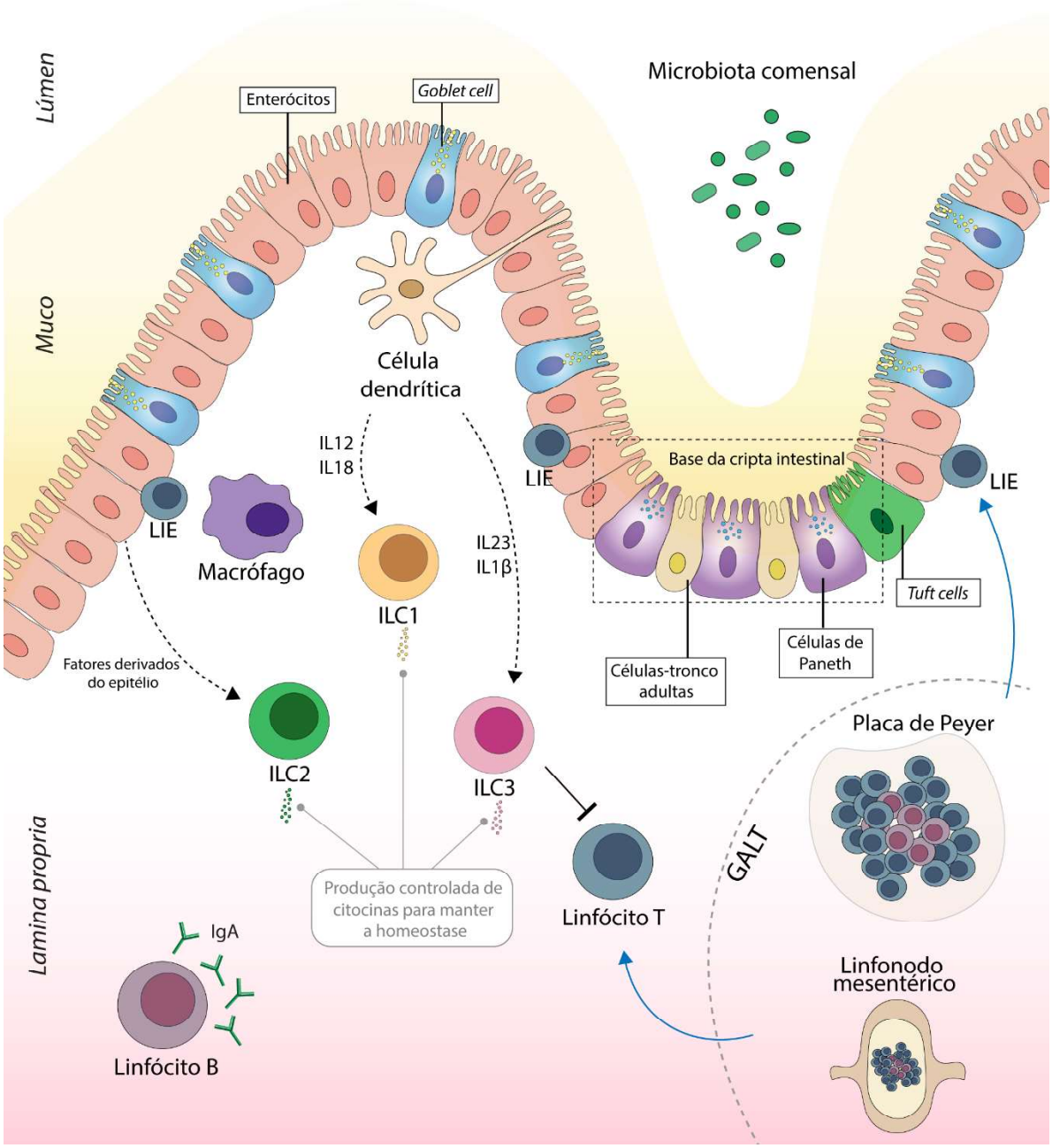

Diferentes tipos celulares compõem a barreira epitelial e são fundamentais para manter a integridade do tecido. Na base da cripta intestinal se localizam as células que darão origem a todo o conjunto celular formador da barreira. Células tronco adultas e células de Paneth controlam a proliferação e formação da cripta. Células calciformes *(Goblet cells),* produzem o muco que reveste a barreira celular em contato com o lúmen intestinal com objetivo de reduzir o contato bacteriano e barreira. Essas células se alternam entre os enterócitos. Ainda, linfócitos intraepiteliais (LIE) localizados entre os enterócitos fazem o pepl de controle da autoimunidade frente a antígenos. Na região da lâmina própria o equilibro imune ocorre pela presença de células dendríticas, macrófagos residentes e linfócitos T e B. Células linfóides inatas (ILC) são encontradas no intestino e regulam tanto o sistema imunológico quanto a integridade da barreira epitelial pela produção controlada de citocinas, em especial as interleucinas (IL) 12, 18, 23 e 1β. Linfonodos mesentéricos e a placa de Peyer são tecido linfóides associados ao intestino ou *Gut-Associated Lymphoid Tissues* (GALT) e são responsáveis pela maturação de linfócitos T intestinais. Linfócitos B representam o sistema imune adaptativo liberanto IgA (não ativa sistema complemento e cascata inflamatória). Fonte: o autor.

As células T desempenham papel crucial na patogênese das DIIs. Células T ativadas deslocam-se dos gânglios linfáticos mesentéricos para a corrente sanguínea, onde circulam de forma contínua e dirigem-se para a lâmina própria. Esse direcionamento ocorre por meio da interação entre a integrina α4β7 e a molécula-1 de adesão celular de endereçamento vascular (MAdCAM-1) (LAMB et al., 2018; MEENAN et al., 1997). Os linfócitos que migram para o compartimento epitelial exercem regulação positiva sobre a integrina αEβ7, que interage com a E-caderina nas células epiteliais, promovendo a retenção dos linfócitos e amplificação da inflamação (CHANG; WHERRY; GOLDRATH, 2014; LAMB et al., 2016).

A resposta mediada por células T pode assumir diferentes fenótipos de acordo com o perfil de citocinas produzidas pelas células apresentadoras de antígenos. A resposta de células T efetoras CD4+ do tipo T helper T_H1 e T_H17 estão associadas a ativação dos fatores de transcrição T-bet e RORγt, respectivamente. A resposta do tipo T_H1 promove o recrutamento de macrófagos, células *natural killer* e células T CD8+ via produção de interferon-γ, enquanto a resposta via T_H17 promove o recrutamento de neutrófilos e produção de IL-17A, IL-17F e IL-22. Ambos perfis celulares podem ser observados em pacientes com DC e RCU, no entanto os níveis de IL-17 são consideravelmente mais altos em pacientes com DC (BRITTON et al., 2019; FUJINO, 2003). No quadro de RCU a resposta das células T ocorre por meio da ativação de células T_H2 via fator de transcrição GATA-3 e tem como característica a produção das citocinas IL-5 e IL-13, associadas à ruptura das células epiteliais, além de IL-4, IL-6 e TNFα (FUSS et al., 2004) ; ou T_H9 produzindo IL-9 (KURMAEVA et al., 2014).

Outro subtipo celular proveniente do progenitor linfóide que está presente na mucosa intestinal tanto em perídos de homeostase quanto de infecção são as células linfóides inatas (ILCs). Constituindo uma subcategoria especializada do sistema imunológico, as ILCs manifestam tanto similaridades fenotípicas quanto funcionais com linfócitos T, sendo estrategicamente localizada em locais caracterizados por uma exposição intensificada a influências externas, como a mucosa intestinal, onde as infecções iniciais são propensas a ocorrer. Diferentemente de outras células que respondem a estímulos diretos, as ILCs respondem primordialmente a sinalização por citocinas provenientes tanto de células imunes quanto epiteliais (BERNINK et al., 2013; SIMONI et al., 2017; YOO; OH, 2023; ZENG et al., 2019).

As ILCs desempenham um papel significativo na patogênese das DIIs. A interação sinérgica de diversas citocinas pode induzir alterações substanciais no microambiente. O ciclo de ativação e plasticidade entre ILC1 e ILC3 é modulado pela produção significativa de citocinas, incluindo IL-12, IL-18, IL-23 e IL-1β por macrófagos e células dendríticas. A ativação de ILC1 resulta na produção de TNFα e IFNγ, causando danos diretos à barreira epitelial. Por outro lado, a ativação de ILC3 é desencadeada por estímulos de IL-1β e IL-23, culminando na liberação de IL-12, IL-22, IL-17 e GM-CSF. O GM-CSF, por sua vez, induz células dendríticas (DCs) e macrófagos a gerar ácido retinoico, o qual também ativa ILC1, amplificando o ciclo inflamatório associado a esse subtipo celular (BERNINK et al., 2013; SIMONI et al., 2017; YOO; OH, 2023; ZENG et al., 2019).

Após permear a barreira epitelial, as bactérias são reconhecidas por macrófagos e células dendríticas, por meio de receptores do tipo toll (*Toll-like receptor* - TLR), capazes de distinguir os antígenos bacterianos, como o LPS (HART et al., 2005). Desta forma, ocorre a ativação de vias inflamatórias e fatores de transcrição responsáveis pela propagação do sinal inflamatório e perpetuação da resposta. O fator nuclear *kappa* B (NF-κB) é um dos mais reconhecidos pelo seu papel inflamatório, resultando no aumento de citocinas, como o TNF-α, IL-1β, IL-6, IL-12 e IL-23, entre outras (A JERSMANN et al., 2001; KAPLAN; JESS, 2016; ZHANG et al., 1999). Citocinas e quimiocinas atuam na sinalização celular para promover a quimiotaxia de células imunes para o sítio inflamatório. Os neutrófilos migrados para esse tecido assumem um papel microbicida fundamental para conter a infecção desencadeada pela translocação bacteriana, operando por meio da liberação das armadilhas extracelulares de neutrófilos (*neutrophil extracellular traps* - NETs), compostas por cromatina e proteínas dos grânulos intracelulares (BRINKMANN, 2004); grânulos contendo mieloperoxidase e elastase, bem como a geração de espécies reativas de oxigênio (ROS) e de nitrogênio (RNS) exercem funções líticas sobre as bactérias (BJERG BENNIKE et al., 2015), além de secretarem inúmeras citocinas pró-inflamatórias que contribuem para a exacerbação do processo inflamatório (HELLER et al., 2008; STEEL et al., 2011).

Dentre os mediadores que exercem papel fundamental na patogênese das DIIs, vale ressaltar o TNFα. Esse mediador solúvel produzido por macrófagos, neutrófilos, linfócitos e células epiteliais promove aumento da expressão de moléculas de adesão

pelas células endoteliais, induzindo o aumento da migração de células imunes (SANDBORN; HANAUER, 1999). O remodelamento tecidual, via fibroblastos com aumento de metaloproteinases e síntese de colágeno, contribue para ulceração e degradação da mucosa, além de contribuir para o aumento da permeabilidade das células epiteliais intestinais, o que leva a prejuízos na função de barreira (PALLONE et al., 2003; LOUIS, 2001).

Macrófagos são células da resposta inflamatória inata, a partir do reconhecimento antigênico associado tanto PAMPs quanto DAMPs. No entanto, essas células também são as principais responsáveis pelo processo ativo de resolução do processo inflamatório. O processo inflamatório intestinal pode progredir de duas formas: (1) cronificação e (2) resolução (MANTOVANI; BONECCHI; LOCATI, 2006; SCHETT; NEURATH, 2018). As DIIs são doenças inflamatórias com um curso crônico associado também a perda de tolerância dos macrófagos intestinais frente aos antígenos. Durante o processo inflamatório intestinal, ocorre o acúmulo de macrófagos imaturos que contribuem para a ativação de células T_H1 e T_H17 via citocinas IL-12, IL-23 e IL-1β e cronificação da inflamação (BAIN et al., 2013, 2014). A perda dae função tecidual consequente da resposta inflamatória crônica e exacerbada, bem como a resposta inflamatória inefetiva estão associadas a necessidade de cirurgia em casos de DIIs (HWANG; VARMA, 2008).

O curso natural de uma inflamação é a resolução do processo e diversos mediadores proteicos e lipídicos estão associados a esse evento celular. Os principais eventos celulares associados à resolução da inflamação são: (1) redução da quimiotaxia de neutrófilos; (2) apoptose dos neutrófilos presentes no tecido; (3) mudança fenotípica dos macrófagos; (4) remoção desses neutrófilos apoptóticos por meio da eferocitose realizada pelos macrófagos (SERHAN; SAVILL, 2005; SCHETT; NEURATH, 2018; SUGIMOTO et al., 2019). Dentre os mediadores lipídicos que contribuem para a resolução, destacam-se a lipoxina A4, resolvina D1, resolvida E1 e a maresina 1 (UDERHARDT et al., 2012). As principais citocinas associadas são a IL-10 e o TGFβ, responsáveis pela diferenciação de macrófagos inflamatórios M1 em macrófagos anti-inflamatórios M2, reparo tecidual e apoptose de neutrófilos (LOPES et al., 2016; POE et al., 2013; SCHETT; NEURATH, 2018). Além disso, outros mediadores contribuem para completar o ciclo de resolução como o ligante indutor de apoptose relacionado ao fator de necrose tumoral (TRAIL) produzido por linfócitos T (MCGRATH et al., 2011), o ligante de Fas (FASL) (BROWN; SAVILL, 1999) e a

proteína AnxA1, que está relacionada a todos os eventos que envolvem a resolução da inflamação (PERRETTI, 2012; PERRETTI; D'ACQUISTO, 2009a).

Alguns dos principais eventos que promovem a resposta inflamatória e a resolução do processo inflamatório nas DIIs bem como a sua complexidade celular e molecular estão exemplificados na Figura 3.

Figura 3. A resposta inflamatória e resolutiva que ocorre nas DIIs.

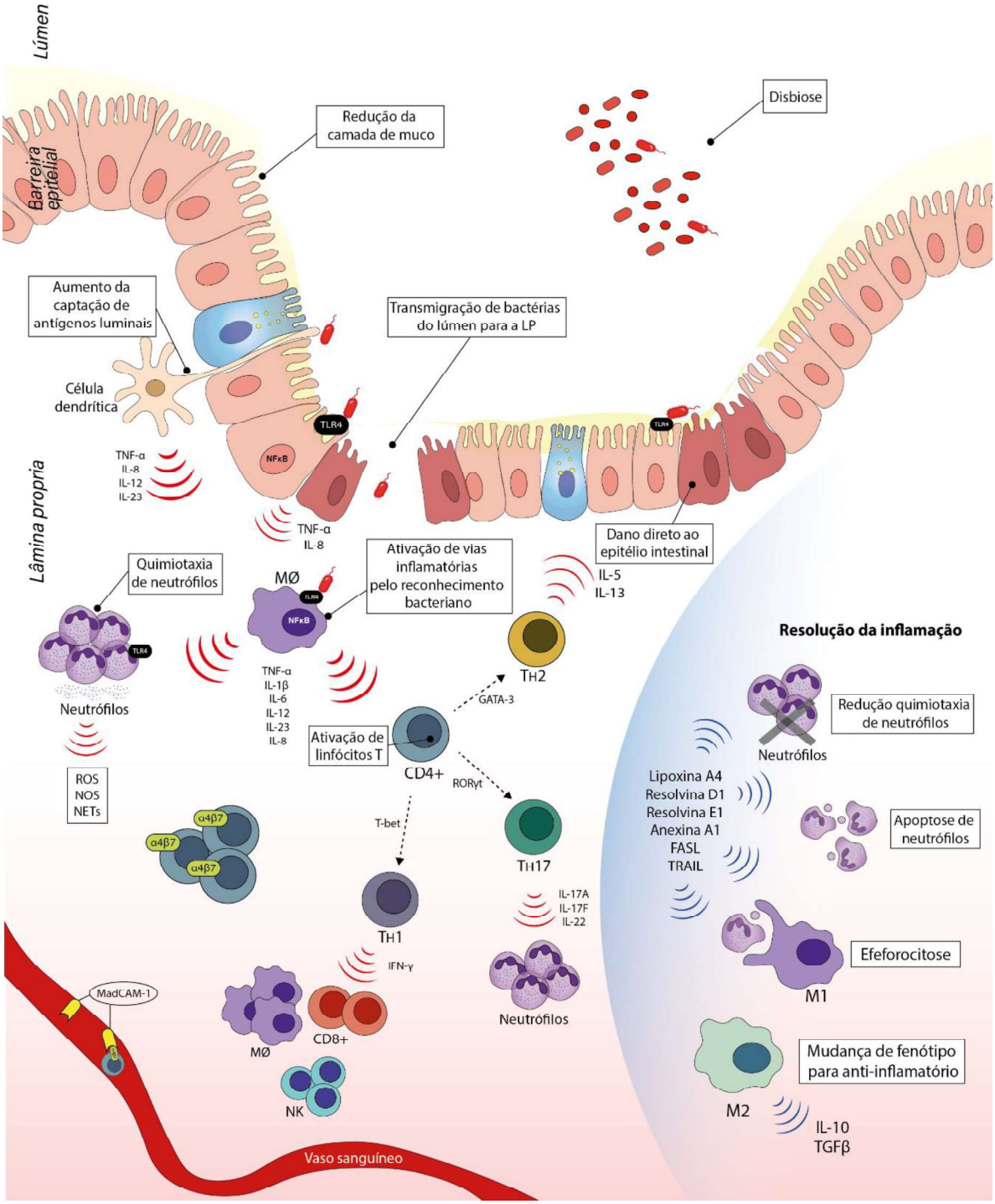

A figura representa os diversos eventos celulares promovem o estabelecimento da resposta inflamatória (esquerda) e a resolução do processo inflamatório relacionada principalmente ao papel dos macrófagos (direita). Fonte: o autor.

Terapias atuais e suas limitações

O tratamento das DIIs é baseado em principalmente em terapias que tentam controlar o processo inflamatório. A determinação da classe medicamentosa a ser utilizada é individualmente avaliada entre cada paciente e escolhida com base nos sintomas clínicos e estadiamento do grau da doença. A utilização de apenas uma das opções encontradas atualmente não resolve de forma efetiva os danos durante a fase ativa da doença, e a intervenção terapêutica precoce pode alterar o curso natural da doença e prevenir complicações irreversíveis (IM et al., 2018). Inicialmente, em casos considerados leves a moderados, as estratégias terapêuticas utilizadas são aminosalicilatos, como o 5-ASA, e corticosteroides. Os aminosalicilatos são potentes na redução da inflamação e utilizados para manter a remissão da doença, sendo a sua utilização isolada muitas vezes ineficaz; ademais, estudos realizados na década de 90 já demonstravam seus efeitos adversos, como por exemplo, quadros de artrite, aplasia de medula, nefrotoxicidade, pancreatite e pericardite, os quais comprometem a utilização destes agentes para a terapêutica (LIN; HINE, 1994; WILLIAMS et al., 2011). (MAGRO et al., 2017).

Um estudo realizado por Miyoshi et al., (2018) avaliou pacientes em estado ativo da UC e pacientes em remissão, onde ambos os pacientes apresentaram agravamento dos sintomas da doença, principalmente de sangramento, fato esse observado na também na reexposição ao fármaco, sugerindo o aminosalicilato como agravador da doença. A associação de 5-ASA e corticoides com medicamentos da classe das tiopurinas, como a azatioprina, também é protocolo de tratamento. Tiopurinas atuam como “antimetabólitos”, incorporados aos ácidos nucleicos e inibem vários genes da inflamação intestinal e do tráfego de leucócitos para o intestino (MIELE et al., 2020; NEURATH, 2010). No entanto, o uso de tiopurinas apresenta diversos efeitos adversos, como intolerância gastrointestinal, mielossupressão, hepatite, pancreatite e síndrome semelhante à gripe (CHAPARRO et al., 2013; CUFFARI et al., 1996). Ainda, a utilização de corticoides, como a prednisolona, dexametasona e budesonida, para o uso crônico é limitada devido a imunossupressão global que ocorre em tratamentos de longo prazo e outros numerosos efeitos adversos sistêmicos, como osteorporose, catarata e síndrome de Cushing (BUCHMAN, 2001).

O desenvolvimento das terapias biológicas revolucionou o tratamento das DIIs. Como mencionado anteriormente, a presença de TNFα está intimamente ligada a progressão da UC. Desta forma, estratégias terapêuticas surgiram visando neutralizar tal citocina através dos medicamentos biológicos (RIZZO, 2014). Essa abordagem é inserida nos casos considerados graves, onde os principais tratamentos empregados na UC, são os agentes anti-TNFα (infliximabe, adalimumabe e certolizumabe) que, na maioria das vezes, reduzem a necessidade de cirurgia e hospitalização e melhoraram a qualidade de vida dos pacientes ao mudar o curso da doença. Os anti-TNFα impedem a interação da citocina a seus receptores específicos na membrana celular e a consequente redução na ativação de células imunes e epiteliais (GUO; LU; BAI, 2013; KOBAYASHI et al., 2020; SOKOL; SEKSIK; COSNES, 2014). No entanto, parte dos doentes não são responsivos às terapias biológicas (VINCENT et al., 2013). Embora ainda sejam a principal opção de tratamento disponível tanto para RCU quanto DC, os tratamentos biológicos estão associados a reações de infusão, imunossupressão, infecções oportunistas e redução de sua eficácia com consequente atenuação ou perda de eficácia ao longo do tempo, secundária à produção de autoanticorpos (CLARK et al., 2007; STRIK et al., 2016).

Como já salientado, linfócitos T possuem papel crucial na patogênese das DIIs e contribuem para a instalação do processo inflamatório intestinal. A migração dessas células é dependente da liberação de diversas citocinas, selectinas e moléculas de adesão. Atualmente uma série de anticorpos monoclonais que atuam sobre essas proteínas já são utilizados na prática clínica enquanto outros com grande potencial ainda esão em fase clínica de testes (KOBAYASHI; HIBI, 2023). No que diz respeito aos utilizados clinicamente destaca-se o vedolizumabe (Entyvio; Takeda Pharmaceuticals) é um anticorpo monoclonal específico contra a integrina α4β7, uma molécula de adesão que participa do processo de migração de linfócitos (WYANT; FEDYK; ABHYANKAR, 2016). Vedolizumabe é utilizado em casos moderados a graves e como segunda linha de tratamento para pacientes que não respondem a terapias anti-TNFα, ou como primeira linha de bilógicos para pacientes que possuem limitações ao uso de anti-TNFα. Ainda a sua combinação com essa classe de aniticorpos monoclonais anti-TNF como o adalimumabe demosntrou resultados superiores ao uso isolado de ambas as terapias (SANDS et al., 2019). Outros anticorpos monoclonais utilizados no tratamentos de DIIs são os direcionados as citocinas IL-12 e IL-23 e suas subunidades. Ustekinumabe, por exemplo, um anticorpo

monoclonal que atua inibindo a via de sinalização dessas citocinas, responsáveis por induzir a diferenciação de linfócitos T CD4+ em T_H1 e T_H17 (LUO et al., 2010; SANDS et al., 2022).

O eixo microbiota/sistema imune é considerado um fator chave na patogênese das DIIs e um importante alvo farmacológico. A modulação do microbioma intestinal tem ganhado destaque como método alternativo e adjunto às terapias existentes. Pacientes com DIIs apresentam microbiota menos diversificada e descontrole da produção de metabólitos funtamentais para a regulação do sistema imune. Novas terapias incluem probióticos, prebioticos, simbióticos e, até mesmo transplante de microbiota fecal (PARAMSOTHY et al., 2017; AKUTKO; STAWARSKI, 2021). Neste caso, são relaizadas combinações sintéticas de bactérias específicas e terapias personalizadas baseadas em perfis de microbiomas individuais de cada paciente e regulação de ácidos biliares secundários (YANG et al., 2021; ZHOU et al., 2022).

Considerando que as DIIs são caracterizadas por uma natureza crônica e ausência de cura definitiva, os pacientes podem enfrentar abordagens terapêuticas contínuas ao longo de suas vidas. O principal objetivo desses tratamentos é estabilizar o curso da doença, reduzindo, assim, o risco a longo prazo de intervenções cirúrgicas e perda de funções intestinais. Embora os agentes biológicos tenham representado avanços significativos na gestão das DIIs, promovendo mudanças substanciais nas estratégias terapêuticas, é importante observar que uma parcela considerável de pacientes ainda enfrenta a necessidade de adotar terapias alternativas. Isso decorre tanto de falhas na resposta aos tratamentos existentes quanto da ocorrência de efeitos adversos, ressaltando a complexidade do manejo clínico dessas condições e a importância contínua da pesquisa para aprimorar opções terapêuticas mais eficazes e personalizadas (AL-HORANI; SPANUDAKIS; HAMAD, 2022; HIGASHIYAMA; HOKARI, 2023).

Anexina A1 e Ac2-26

A AnxA1 é uma proteína de 37 kDa, pertencente a superfamília das anexinas que inclui 13 moléculas com estruturas similares e com diferentes funções biológicas (BLACKWELL et al., 1980; ROTHHUT et al., 1983). As anexinas são caracterizadas estruturalmente por dois domínios terminais, onde uma pequena região N-terminal difere entre as isoformas e é responsável pelas atividades biológicas pela ligação da proteína a seus receptores na presença de Ca^{2+} (CROMPTON; MOSS; CRUMPTON, 1988) (Figura 4). Em condições basais, a AnxA1 é expressa de forma mais expressiva no citoplasma de neutrófilos, monócitos, macrófagos, eosinófilos, mastócitos, em algumas células tumorais, epitélios e, de forma mínima, em células T (GAVINS; HICKEY, 2012; RESCHER; GERKE, 2004). A síntese de AnxA1 é induzida por mediadores endógenos, sendo regulada principalmente pela ação de glicocorticoides e citocinas (BLACKWELL et al., 1980; PERRETTI; D'ACQUISTO, 2009a; SOLITO et al., 2003).

Figura 4. Estrutura proteica da Anexina A1 e seu peptídeo mimético derivado da região N-terminal, o Ac2-26.

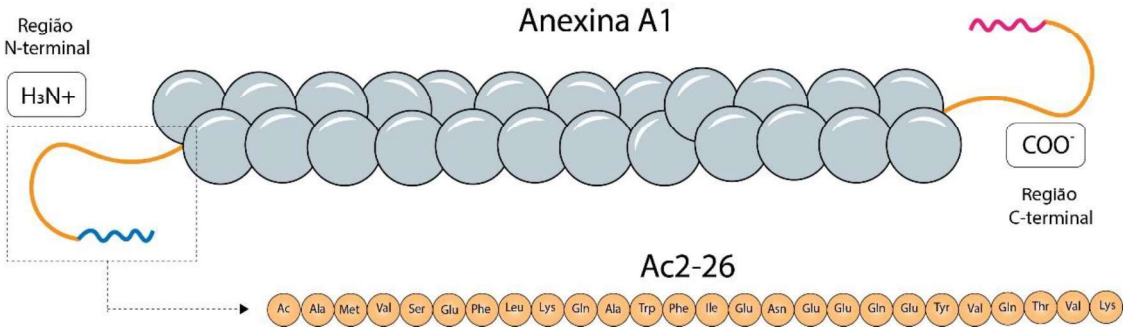

Fonte: o autor

Em condições de ativação celular, a AnxA1 é rapidamente mobilizada do citoplasma para o meio extracelular. Pelo menos três mecanismos de secreção são propostos, sendo variáveis de acordo com o tipo celular, a saber: pela ativação de transporte dependente de ATP (ATP-*binding cassette*); pela fosforilação de serina amino terminal e subsequente passagem por domínios lipídicos da membrana para porção extracelular (PERRETTI; D'ACQUISTO, 2009; VONG et al., 2012) e; pela fusão e eliminação de vesículas contendo AnxA1 diretamente pela membrana

plasmática (DALLI et al., 2008; LEONI et al., 2015a; NOVIZIO et al., 2020; PESSOLANO et al., 2019). Ao ser liberada no meio extracelular, a AnxA1 secretada no microambiente inflamado pode atuar de forma autócrina, parácrina e justácrina. A AnxA1 fosforilada se liga aos receptores de peptídeos formilados 1, 2 e 3 (FPR1, FPR2 e FPR3), ativando vias de sinalização intracelular dependentes de ERK1/2 e MAPK para atuar sobre as células (HAYHOE et al., 2006; MCARTHUR et al., 2020b; PERRETTI; D'ACQUISTO, 2009). Os FPRs são receptores acoplados a proteína G e são expressos em diversos tipos celulares; a ligação ao FPR1 e FPR2 são as mais descritas para a modulação anti-inflamatória da AnxA1. Ainda, os peptídeos miméticos derivados da região N-terminal da AnxA1, como o Ac2-26, composto de 24 aminoácidos; Ac2-12, composto de 10 aminoácidos; Ac2-50, composto de 46 aminoácidos; Ac9-12, composto de 3 aminoácidos, também são capazes de se ligar ao receptor FPR2 e promover resposta celular similar a AnxA1. O peptídeo mimético mais relatado pela literatura é o Ac2-26 capaz de induzir a ativação não somente de FPR2, mas também de FPR1(HAYHOE et al., 2006; LEONI et al., 2013, 2015a; LICE et al., 2022; PERRETTI et al., 2001, 2017; SUGIMOTO et al., 2016).

No que diz respeito ao seu papel anti-inflamatório, a AnxA1 age como regulador negativo na imunidade inata, atuando na transmigração e ativação de neutrófilos, monócitos e macrófagos (CHATTERJEE et al., 2005; GETTING; FLOWER; PERRETTI, 1997). Em animais geneticamente deficientes de AnxA1 ou tratados com bloqueadores de FPR2, a resposta inflamatória inata é exacerbada (BABBIN et al., 2008; LOCATELLI et al., 2014; MCARTHUR et al., 2020a; PERRETTI; GAVINS, 2003) e o tratamento com AnxA1 recombinante ou com seus peptídeos miméticos reverte a exacerbação da inflamação em animais deficientes de AnxA1 (GIROL et al., 2013a; QIN et al., 2015; VITAL et al., 2016). Anexina A1 (AnxA1), é inibidor da fosfolipase A2 (PLA2) de membrana. Essa ação inibitória tem implicações significativas na cascata do ácido aracdônico, uma vez que a PLA2 está envolvida na liberação desse precursor crucial. O ácido araquidônico, por sua vez, desencadeia a produção de eicosanoides, como a prostaglandina e outros mediadores lipídicos da inflamação (FLOWER; ROTHWELL, 1994; LIM et al., 1998). Sabe-se que a proteína é capaz de reduzir a diapedese de neutrófilos por meio da redução da expressão de moléculas de adesão celular responsáveis pelo rolamento e firme adesão dos leucócitos à parede vascular, que prejudica a subsequente migração destes para o foco de lesão (GETTING;

FLOWER; PERRETTI, 1997); modular a síntese de citocinas inflamatórias e anti-inflamatórias (CHIANG; SERHAN, 2006), além de atuar como mediador da ação anti-inflamatória do sulfito de hidrogênio (BRANCALEONE et al., 2014) e reduz a promoção da inflamação pela proteína translocadora (TSPO) (PANTALEÃO et al., 2018).

Além de modular o influxo de leucócitos para o foco de inflamação, em especial de neutrófilos e monócitos, a AnxA1 modula positivamente os processos de resolução da inflamação e reparo tecidual (PERRETTI; D'ACQUISTO, 2009). Estudos *in vivo* e *in vitro* mostram que a AnxA1 induz a apoptose de neutrófilo no foco de lesão e a subsequente fagocitose dos mesmos pelos macrófagos residentes e pela polarização de macrófagos para o fenótipo M2 (MCARTHUR et al., 2020; SCANNELL et al., 2007; SOLITO et al., 2003). Este mecanismo, que, em conjunto, é chamado de eferocitose é fundamental para a resolução da inflamação e sua indução é alvo na pesquisa e desenvolvimento de anti-inflamatórios (AIKAWA et al., 2018). Ademais, a AnxA1 endógena e exógena modula a angiogênese, a proliferação de fibroblastos e a secreção de citocinas anti-inflamatórias no modelo de regeneração tecidual, confirmando sua ação efetiva nos mecanismos de reparo. De fato, a literatura mostra, em modelos experimentais, que a AnxA1 é uma ferramenta como potencial na implantação de transplantes (COORAY et al., 2013; LACERDA et al., 2018).

Pelos mecanismos anti-inflamatórios e de reparo tecidual da AnxA1 citados acima, seu efeito benéfico em doenças inflamatórias tem sido amplamente demonstrado em modelos experimentais (BROERING et al., 2022; HARIDAS et al., 2019; LI et al., 2019a; LICE et al., 2022; MCARTHUR et al., 2020b). A AnxA1 emerge como um mediador crucial em condições de inflamação, desempenhando um papel resolutivo na recuperação tecidual. A expressão local de AnxA1 é essencial para a restauração do tecido afetado (LEONI et al., 2013; VERGNOLLE; COMERA; BUENO, 1995), especialmente na DC (REISCHL et al., 2020; SENA et al., 2013). Estudos recentes sugerem que níveis reduzidos de AnxA1 na DC estão associados a inflamação descontrolada, perpetuando a doença, e que análises diferenciais de AnxA1 podem indicar padrões de gravidade da doença (DE PAULA-SILVA et al., 2016a; SENA et al., 2015a; VERGNOLLE et al., 2004). Além disso, foi observada a expressão marcada de AnxA1 no cólon de pacientes com DC e que alcançaram remissão após o uso de infliximabe. No entanto, a falta de AnxA1 endógeno demonstrou ser prejudicial na progressão da colite experimental, resultando em piores

desfechos clínicos e histológicos, e uma taxa de mortalidade mais elevada. Esses resultados também indicam que a falta de AnxA1 pode impactar negativamente o tratamento com infliximabe (DE PAULA-SILVA et al., 2021).

De modo geral, a literatura indica que a secreção de AnxA1 é desencadeada durante os períodos de atividade da DII. Deficiências nesse mecanismo exacerbam a gravidade e prolongam a duração da doença. Da mesma maneira, intervenções terapêuticas capazes de potencializar os níveis de AnxA1 demonstram resultados mais eficazes (LEONI; NUSRAT, 2016). O uso do tripeptídeo MC12, derivado da estrutura da AnxA1, como tratamento na colite experimental em modelo de dimetil sulfóxido (DSS) e ácido trinitrobenzeno sulfônico (TNBS), ambos modelos que mimetizam a colite que atinge a mucosa e a região trans mural, respectivamente. MC12 demonstrou eficácia em reduzir parâmetros clínicos e inibir a ativação do fator de transcrição NF-κB (OUYANG et al., 2012).

Apesar de diferentes tipos celulares secretarem AnxA1 no cólon inflamado, a descoberta das vesículas extracelulares contendo AnxA1 secretadas por neutrófilos e células epiteliais intestinais proporcionaram o aprimoramento de um novo mecanismo de aplicação para a AnxA1 no tratamento da colite. O desenvolvimento de tecnologias com grande potencial de entrega direcionada capazes de regular negativamente o processo inflamatório e melhorar a cicatrização tecidual pode ser observado pelos resultados encontrados por Leoni et al. (2015), que utilizou nanopartículas poliméricas revestidas com colágeno IV contendo o peptídeo mimético Ac2-26 (Ac2-26-Col-IV) e aplicadas diretamente na mucosa intestinal ou intraperitoneal para o tratamento na colite experimental. Ainda, avaliando o potencial da mesma nanopartícula sobre a colite, Reischl et al. (2021) administrou de forma intraperitoneal Ac2-26-Col-IV para terapia perioperatória, que consistiu de avaliar a regeneração tecidual após excisão de parte do intestino. O modelo foi baseado em casos de pacientes que necessitam de remoção de parte do intestino resultante da cronificação do processo inflamatório e consequente necrose tecidual.

Apesar de apresentarem resultados promissores, a utilização de uma via de administração não invasiva é considerada de suma importância para a aderência do tratamento pelo paciente. Baseado nessa premissa, Li et al. (2019), desenvolveram um sistema de entrega capaz de liberar o peptídeo Ac2-26 em resposta a altas concentrações de ROS, atingindo o cólon inflamado de maneira específica, visto que

altas concentrações de ROS são encontradas em sítios inflamatórios. O tratamento promoveu regeneração tecidual e redução da resposta inflamatória gerada na colite experimental. Baseado no exposto acima, é clara a participação da AnxA1 como mediador para as DIIs, tanto na fase ativa da doença como potencial tratamento para essas enfermidades crônicas e sem tratamento efetivo.

Nanotecnologia

A nanotecnologia, uma das áreas mais promissoras do século 21, combina o estudo da nanociência com avanços tecnológicos para a produção de materiais em nanoescala, ou seja, produtos cujas dimensões estão na ordem de mil milionésimos de um metro (10^{-9} m) (DEAN; MANSOORI; FAUZI SOELAIMAN, 2005; MALIK; MUHAMMAD; WAHEED, 2023). As nanopartículas (NPs) são estruturas unidimensionais em nanoescala, com tamanhos variando de 1 a 100 nm. É importante observar que nanopartículas com dimensões superiores podem receber denominações específicas, como nanocápsulas ou nanorods. Essas estruturas podem ser compostas por diversos materiais, como polímero-lipídeo, polímero-metal, grafeno-metal, sílica-metal, ou podem consistir em apenas um componente, como polímero, lipídeo, sílica, metal ou carbono. A variação na dispersão e interação de seus componentes resulta em diferentes arranjos e composições, destacando a versatilidade dessas nanopartículas na aplicação de diversas tecnologias e campos, desde a medicina até a eletrônica (VERT et al., 2012).

Essa diferença dimensional confere às nanopartículas propriedades únicas que as tornam especialmente relevantes em áreas como diagnósticos avançados e terapêutica direcionada. Além disso, é importante destacar que as nanopartículas apresentam uma grande área superficial, uma característica intrínseca decorrente de suas dimensões reduzidas. Essa grande área superficial contribui para a notável capacidade de interação com uma variedade de componentes biológicos, como proteínas intracelulares e de membrana, enzimas e barreiras biológicas (ERDOĞAR; AKKIN; BILENSOY, 2019; FARAJI; WIPF, 2009; ZOLNIK et al., 2010). Devido à sua meticulosa engenharia que otimiza características físicas, químicas e mecânicas, as NPs diferem significativamente de materiais maiores, resultando em uma gama de novas aplicações, especialmente no campo biomédico (DENG et al., 2016; ZHANG et al., 2008).

As pesquisas relacionadas a administração de NPs têm sido direcionadas à diminuição dos efeitos adversos de certos fármacos, à otimização de doses e, entrega direcionada de determinadas subtâncias (BERNARDI et al., 2012; DIMER et al., 2013). Nesse sentido, nanocapsulas constituídas de polímeros biodegradáveis têm se mostrado mais promissoras, além de melhorar a aplicabilidade terapêutica e reduzir a toxicidade identificada em outros tipos de NPs (BEGINES et al., 2020; GIRON et al., 2019; POHLMANN et al., 2013), como por exemplo, a deposição de partículas metálicas em órgãos filtrantes, muitas vezes proveniente da interação das NPs com o sistema reticulo endotelial (YAO et al., 2019). Em relação à administração oral, as nanocapsulas poliméricas podem ajudar a ultrapassar a barreira gastrointestinal para moléculas com limitações de absorção por via oral (FRIEDRICH et al., 2014; RODRIGUES et al., 2016).

No contexto das DIIs, NPs de diferentes composições têm sido aplicadas para otimizar o uso dos tratamentos usuais das DIIs, os quais muitas vezes promovem efeitos sistêmicos indesejados, além de degradação da maior parte do medicamento no TGI. Estudos demonstraram que a nanoencapsulação de NPs contendo 5-ASA reduziu a degradação do medicamento e seus efeitos sistêmicos relacionados ao uso da medicação, sendo até 80% absorvido no cólon (MLADENOVSKA et al., 2007; VARSHOSAZ; JAFFARIAN DEHKORDI; GOLAFSHAN, 2006). Efeitos semelhantes foram encontrados com a nanoencapsulação de budesonida ligada a NPs de PLGA/Eudragit®S100, capaz de liberar o corticoide no cólon em concentrações efetivas (ZHOU; QIAN, 2018).

Em relação aos tratamentos com biológicos, foi descrito recentemente pelo grupo de Kim et al. (2020) um lipossoma revestido com Eudragit®-S100 contendo infliximab. Os lipossomas são principalmente compostos de fosfolipídios, e a taxa de liberação depende do número de bicamadas fosfolipídicas, podendo interagir de forma eficiente com o tecido intestinal. O estudo demonstrou que a entrega do fármaco ocorreu de forma direcionada no cólon, promovendo redução da ação do TNFα de forma mais eficiente do que pelo tratamento com infliximab de forma clássica e, ainda, reduziu os efeitos adversos (KIM et al., 2020). Outros compostos não utilizados na prática clínica também demonstraram eficácia quando encapsulados. Neste sentido, o ácido glicirrízico foi encapsulado em nanocarreadores de PLGA- Eudragit®-S100,

responsivos ao pH, que promoveu entrega eficiente no cólon e cicatrização da mucosa em curto prazo (ZEESHAN et al., 2019).

As pesquisas com NCs de núcleo lipídico tiveram início em meados dos anos 2000, quando um híbrido de NCs biodegradável, foi desenvolvido pelo grupo das professoras Adriana Pohlmann e Silvia Guterres, da Universidade Federal do Rio Grande do Sul (UFRGS). Alterações supramoleculares das partículas foram realizadas, como a adição do lipídeo sólido, monoestearato de sorbitano disperso no núcleo lipídico líquido das NCs (GUTERRES; ALVES; POHLMANN, 2007; JÄGER et al., 2009; VENTURINI et al., 2011). A estrutura supramolecular proposta para as nanocapsulas de núcleo lipídico (LNCs) consiste de um núcleo com característica organogel, e uma parede polimérica situada na pseudointerface óleo-água (POLETTO et al., 2012). Além disso, o desenvolvimento de uma estratégia de formação de camadas pela interação eletrostática das substâncias, permitiu a transformação da natiureza aniônica para catiônica pela adição e revestimento com quitosana, formando a nanocápsula de núcleo lipídico multicamadas (*multiwall lipid nanocapsules* - MLNC). A formação da MLNC se baseia da interação eletrostática entre o grupo amônio da quitosana e grupos carregados negativamente na superfície da LNC (BENDER et al., 2012).

A partir da MLNC, Bender et al., (2014) desenvolveram uma estrutura composta pelo complexo ligante metal-quitosana-lecitina, usando zinco (Zn^{2+}) para funcionalizar a superfície das nanocápsulas biodegradáveis. Esse metal reage com grupamentos de histidina da proteína, permitindo a complexação a estrutura da nanocapsula. As substâncias ativas, de acordo com suas características físico-químicas, podem localizar-se na fase dispersante, adsorvida na parede polimérica, particionada entre a fase dispersante e o nanocarreador, ou ainda no interior lipofílico da partícula. Dessa forma, as LNCs apresentam capacidade de controlar a velocidade de liberação de uma substância encapsulada (JÄGER et al., 2009), a rigidez particular e a capacidade de penetração em tecido biológico (FIEL et al., 2011, 2013).

Diversos estudos têm evidenciado que as nanocápsulas são uma opção promissora para otimizar a terapêutica de doenças (FRANK et al., 2015; GIRON et al., 2019; SMITH et al., 2020). Em um trabalho utilizando LNC, contendo indometacina carreada no núcleo, utilizadas no tratamento de glioblastoma *in vivo* por via oral, foi observada a capacidade da LNC de atravessar a barreira gastrointestinal e hematoencefálica de forma passiva, demonstrando maior acúmulo e retenção desses

fármacos encapsulados no tecido cerebral. Além disso, foi observada que tanto a administração pela via oral, quanto intraperitoneal não apresentaram diferenças na concentração do fármaco do tecido cerebral, destacando que não há impedimento na eficácia dos tratamentos NPs quando administrados por diferentes vias (RODRIGUES et al., 2016). Ainda, trabalhos que avaliaram o potencial antiproliferativo de tratamentos associados a MLNC sobre células cancerosas observaram efeitos consideravelmente maiores sobre a redução da proliferação de células de cancer de mama *in vitro* para MLNC-bromelina, quando comparado a bromelina não conjugada (OLIVEIRA et al., 2017) e de células de melanoma *in vivo* e *in vitro* utilizando LNC contendo acetileugenol no núcleo (DREWES et al., 2017). Além disso, a administração via oral e intraperitoneal de LNC contendo tracrolimos, um medicamento utilizado como profilaxia para transplante de órgãos sólidos, demonstrou redução significativa no número de leucócitos migrados, sendo sua efetividade equivalente em ambas as vias utilizadas e capaz de atravessar o trato gastrointestinal (TGI) sem ser degradado (FRIEDRICH et al., 2014).

Embora as LNCs permitam o carreamento de compostos ativos no seu núcleo lipídico, a plataforma desenvolvida permite a funcionalização e o carreamento de substâncias também ligadas a parede polimérica da nanocápsula, como por exemplo, os anticorpos direcionados a fração eletronegativa de lipoproteína de baixa densidade (LDL), utilizado por Cavalcante et al. (2021) e anticoporpo específico para molécula de adesão celular endotelial plaquetária (anti-Pecam-1), utilizado por De Castro Leão et al. (2021), ambas MLNCs direcionadas para tratamento intravenoso da aterosclerose. Com base na formulação da MLNC, que possibilita a funcionalização da estrutura com proteínas biologicamente ativas, e visando o potencial terapêutico associado à AnxA1 para controlar o processo inflamatório, surgiu a perspectiva promissora de combinar a plataforma MLNC conjugando-a à AnxA1 como um potencial tratamento para as DIIs.

Micropartícula mesoporosa ordenada

O avanço na combinação de diferentes materiais com potencial terapêutico tem viabilizado a criação de novas abordagens terapêuticas (ANSELMO; MITRAGOTRI, 2016; LIN; HURLEY; HAYNES, 2012). Nos últimos 10 a 15 anos, progressos

significativos foram alcançados na adaptação de estruturas em mesoescala. Dentre esses avanços, a organização de materiais mesoporosos se destaca como um exemplo representativo. Até os anos 1980, os materiais em mesoescala apresentavam poros que limitavam-se a 1,2 nm. A motivação para a pesquisa desses elementos surgiu da necessidade de desenvolver materiais com mesoporos de maior dimensão, capazes de atender às demandas práticas. A partir da descoberta da modelagem desses componentes surgiram as micropartículas mesoporosas. Esse material apresenta uma extensa área superficial composta por nanoporos de tamanhos ajustáveis que possibilitam a adsorção eficiente, carregamento de moléculas e íons-alvo, proporcionando acesso e difusão eficientes à superfície (DAVIS, 2002; KRESGE et al., 1992; YANAGISAWA et al., 1990; ZHAO et al., 1998a). O primeiro material da classe das sílicas mesoporosas a ser obtido com sucesso foi MCM-41 (*Mobil Composition of Matter*) e sua aplicação era primordialmente para catalise de reações. Desde então, nas últimas duas décadas, houve a incorporação de materiais de sílica mesoporosa para o desenvolvimento dessas estruturas em novos formatos, e ajuste do tamanho dos poros apenas controlando a estrutura e o tamanho das moléculas de surfactante na reação (BECK et al., 1992; KRESGE et al., 1992).

A sílica mesoporosa do tipo SBA-15 (*Santa Barbara Amorphous No. 15*) foi proposta inicialmente em 1998, apresentando características melhores do que a MCM-41. Com o objetivo de fornecer alta resistência térmica, hidrotermal e mecânica, a síntese desses materiais mesoporosos acontece por um processo denominado modelagem por cristal líquido, a qual utiliza como base o treta-etil ortosilicato (TEOS). Considerada um marco na síntese das micropartículas mesoporosa, a SBA-15 adquire um alto grau de ordenação resultante da utilização de um molde polimérico, que em meio ácido, aliado à hidrólise de TEOS, resulta na condensação dos complexos SiO_2 para formar redes tridimensionais de SiO2 sobre a estrutura de micelas formadas pelo molde polimérico (LAN; ZHAO, 2022; ZHAO et al., 1998a, 1998b). A estrutura da SBA-15 apresenta um grande número de grupos silanol (Si-OH) que são importantes para a ligação de proteínas na superfície da sílica, além de excelentes propriedades, como estrutura hexagonal altamente ordenada, mesoporos grandes e ajustáveis (8–50 nm) e alta estabilidade térmica e mecânica como resultado da grande espessura da parede de sílica (YIU; WRIGHT; BOTTING, 2001; ZHAO et al., 1998a, 1998b).

A utilização biológica da sílica mesoporosa demanda características específicas, como um tamanho de poro moderado (inferior a 200 nm) e uma ampla

área superficial, favorecendo o contato eficaz com tecidos biológicos. Essas características fornecem a SBA-15 grande potencial para aplicação em entrega de substâncias. Ainda, a funcionalização de SBA-15 com grupos como amina, tiol, nitrila, fenila e cloro para a imobilização de proteínas na sílica mesoporosa (YIU; WRIGHT; BOTTING, 2001). Observando as características como tamanho, formato, superfície e presença de surfactantes, além de outros fatores como dose e via de administração, que são cruciais para se obter um perfil seguro de uso, tomam a SBA-15 um material com grande capacidade de biocompatibilidade e baixa toxicidade *in vivo* (HUDSON et al., 2008; SOUID et al., 2012).

A utilização de SBA-15 como um sistema de entrega controlada de substâncias de diferentes propriedades químicas é extensivamente estudada (GKILIOPOULOS et al., 2022; PROKOPOWICZ et al., 2019; XU; RIIKONEN; LEHTO, 2013). A estrutura de sílica mesoporosa pode contribuir para o carreamento seguro de estruturas proteicas, sendo capaz de proteger essas substâncias contra a degradação pelo pH e ações enzimáticas (PERDEW; BURKE; ERNZERHOF, 1996; ZHANG et al., 2019). Neste sentido, Wang et al. (2012) carrearam soro o antígeno soro albumina bovina (BSA) em nanopartículas de sílica mesoporosa (MSN) com diferentes tamanhos de partícula (130 nm, 450 nm e 1-2μm) e a administração de MSN-BSA por via oral à camundongos promoveu desenvolvimento de resposta imune produzindo IgG1 e IgG2, contribuindo para as pesquisas sobre a aplicação da SBA-15 como adjuvante para vacinação por via oral. Outro trabalho observou efeito semelhante quando administrado SBA-15, contendo antígeno específico de *Mycoplasma hyopneumoniae* por via oral em porcos. A administração oral foi capaz de produzir resposta imune específica para a bactéria, sendo observado aumento de anticorpos apenas nos animais que receberam a vacina por via oral (MECHLER-DREIBI et al., 2021b). Ainda, o tratamento adjuvante mostrou que camundongos imunizados pela via oral com as partículas purificadas da proteína viral HbsAg, o principal componente da vacina contra hepatite B, conjugado em SBA-15 apresentaram aumento na resposta imune, reportando aumento nos títulos de IgA e IgG específicas para o vírus (SCARAMUZZI et al., 2011).

Quanto a toxicidade associada a SBA-15, um estudo que administrou por via oral 40 mg/kg de sílica mesoporosa de área superficial em nanoescala, demonstrou rápida excreção nas fezes e urina. Nenhuma anormalidade histológica foi observada quando

avaliadas a histologia do fígado, baço, pulmões e coração. No entanto, foram observados efeitos tóxicos aos rins, apresentando necrose tubular renal e hemorragia e congestão vascular no interstício renal para todos os camundongos tratados nanoparticulas mesoporosas. Vale ressaltar que nanopartículas mesoporosas têm maior absorção pela mucosa intestinal e consequentemente maior excreção renal, podendo ultrapassar o limite de filtração glomerular e causar lesões renais (LI et al., 2015). Sugere-se então que a SBA-15 possa ser absorvida pela mucosa intestinal de acordo com suas características físicas, no entanto por apresentar grande área superficial, pode ser majoritariamente excretada nas fezes (ZHAO et al., 1998b). Além disso, um estudo de toxicidade intestinal utilizando diferentes tipos de sílica mesoporosa tratadas oralmente, demonstrou que a SBA-15 não gerou toxicidade intestinal na dose de 50 mg/kg administrados por 7 dias por via oral (YU et al., 2021). Apesar do tratamento por via oral ser promissor e seguro, outras vias de administração como a subcutânea e intravenosa necessitam de mais estudos para aferir a segurança e efeito. Choi et al. (2015) demonstrou que a SBA-15 aplicada via subcutânea observou a formação de nódulos na região dorsal de camundongos. Esse resultado foi associado à baixa absorção do material por essa via.

Devido as suas características físicas e químicas, a SBA-15 apresenta potencial promissor para o desenvolvimento de sistema de entrega controlado e cólon específico, permitindo o carreamento de fármacos e proteínas de alto peso molecular. Do exposto acima fica evidente que a implementação de novas tecnologias e estudos experimentais são necessários para a implementação de abordagens terapêuticas inovadora, de forma que o planejamento cuidadoso desses sistemas de entrega em relação ao alvo e a via de administração possa resolver alguns dos problemas enfrentados pelas novas classes de moléculas ativas, e otimizando o tratamento de diversas doenças, em especial as DIIs.

Métodos alternativos para o estudo de DIIs

Apesar da aplicação de diversas abordagens terapêuticas no tratamento das DIIs, muitas delas enfrentam desafios que resultam frequentemente em falhas terapêuticas. É notável que diversos fatores podem estar associados a falhas terapêuticas, e muitos deles poderiam ser identificados por meio de estudos prévios. De fato, entre 40 a 50% dos medicamentos falham durante a fase clínica devido à

ausência de efeito comprovado das substâncias. Nesse contexto, para aprimorar as terapias existentes e não apenas introduzir novas moléculas terapêuticas, torna-se crucial a busca por métodos de análise inovadores. Esses métodos visam avaliar tanto a segurança quanto a eficácia dessas abordagens em ensaios clínicos. A implementação de análises mais robustas e estudos aprofundados pode contribuir não apenas para a compreensão das causas das falhas terapêuticas, mas também para otimizar o desenvolvimento de tratamentos mais eficazes e personalizados para pacientes com diferentes tipos de doenças crônicas como o câncer e até mesmo as DIIs (KIRIIRI; NJOGU; MWANGI, 2020; SUN et al., 2022; TEBON et al., 2023).

Os modelos tradicionais de estudos *in vivo* das DIIs compreendem, principalmente, a indução química da doença em modelos de DSS ou ácido 2,4,6-trinitrobenzeno sulfônico (TNBS), além do desenvolvimento de animais geneticamente modificados com deficiências no sistema imune inato e sistema e adaptativo (BAYDI et al., 2021; CHASSAING et al., 2014; NEURATH; FUSS; STROBER, 2000). Estes modelos são vantajosos no sentido de replicar o sistema fisiológico e todas as interações que ocorrem durante a doença, sendo indispensáveis para o estudo destas doenças. Porém, a indução química da colite apresenta limitações como a heterogeneidade no desenvolvimento da doença, que se desenvolve de forma diferente daquela observada em humanos, além do fato de as DIIs serem doenças com mecanismos celulares e moleculares muitas vezes específicos da espécie, características que dificultam a associação desses resultados para humanos (GOULD; JUNTTILA; DE SAUVAGE, 2015). Além disso, o uso de células humanas imortalizadas, como Caco-2, T84 e HT-29, tem sido amplamente utilizado para compreender a permeabilidade intestinal e compreender os mecanismos de reparação tecidual, mas são limitadas quanto às interações complexas que ocorrem *in vivo* (JIMINEZ et al., 2015; O'CONNELL; WINTER; AHERNE, 2021; SOLLID; JOHANSEN, 2008).

No cenário atual, o desenvolvimento de culturas celulares tridimensionais (3D) utilizando células-tronco adultas ou progenitoras para recriar tecidos *in vitro* surge como uma alternativa para superar as limitações das culturas 2D. Denominadas organoides, essas estruturas teciduais compartilham características semelhantes às dos órgãos, destacando-se como uma ferramenta valiosa para contornar as restrições dos modelos *in vitro* de células em monocamada. Tornam-se, assim, uma opção eficaz

para estudos de toxicidade, modelos de doenças e avanços na medicina personalizada, reproduzindo as funções estruturais, funcionais e genotípicas de órgãos específicos (JENSEN; TENG, 2020; KIM; KOO; KNOBLICH, 2020; RODRIGUEZ-GARCIA et al., 2020).

Os organoides podem originar-se de dois tipos de células com capacidade de diferenciação e auto-organização que refletem a origem do órgão: (1) células-tronco embrionárias pluripotentes e (2) células-tronco adultas (CLEVERS, 2016). A formação dessas estruturas baseia-se no rearranjo estrutural e morfogênico, resultante da interação física entre diferentes tipos celulares, considerando características como adesão, tensão, motilidade e contratilidade célula-célula (SASAI, 2013). A compreensão da sinalização celular que ocorre *in vivo* nas criptas intestinais tornou possível o desenvolvimento dos organoides. O gradiente de substâncias responsáveis pelas fases de proliferação e diferenciação celular é controlado pela adição de inibidores ou componentes necessários para a manutenção das células-tronco (CLEVERS, 2016).

A evolução dos diversos tipos de organoides proporciona uma compreensão mais aprofundada da organogênese e da fisiopatologia de diversas doenças. Na abordagem das DIIs, por exemplo, a criação de "mini-órgãos" tem se destacado como um modelo mais acessível em comparação com o uso de animais. Além disso, essa abordagem possibilita discernir a contribuição relativa de diferentes componentes teciduais para processos morfogenéticos complexos, oferecendo uma visão mais precisa das características específicas da doença (CALÀ et al., 2023; KRETZSCHMAR; CLEVERS, 2016; LI et al., 2014; NADAULD et al., 2014).

Organoides intestinais em 3D são capazes de manter as características e funções da célula original por longos períodos, mesmo em cultura, sendo capazes de sobreviverem por períodos mais prolongados *in vitro*, o que representa uma vantagem significativa em comparação com a capacidade limitada de propagação das células primárias (DOTTI et al., 2017; WANG et al., 2021). Essa abordagem inovadora baseada em células-tronco resulta no desenvolvimento de organoides 3D, tanto murinos quanto humanos. A diferenciação *in vitro* das células-tronco Lgr5+ possibilita a diferenciação em todos os tipos de células epiteliais do cólon, assemelhando-se ao intestino (CLEVERS, 2016; SATO et al., 2009). Dadas essas características, o modelo de organoides intestinais 3D permite a investigação do impacto de agentes tóxicos ambientais na integridade da barreira intestinal (SHARMA et al., 2021), explorar a

patogênese de patógenos intestinais (SAYED et al., 2020a, 2020b), e avaliar a eficácia de intervenções terapêuticas potenciais contra a DIIs (SAHOO et al., 2021).

A utilização de organoides na modelagem de doenças tem revelado *insights* cruciais em diversos aspectos, incluindo a importância da microbiota intestinal, interações do sistema imunológico e o desenvolvimento de tratamentos personalizados. No contexto da DII, onde os tratamentos visam predominantemente a regulação da resposta imune, o desenvolvimento de organoides a partir de células obtidas por biópsias de pacientes se mostra uma ferramenta valiosa de triagem (SARVESTANI et al., 2021), permitindo avaliar de forma mais confiável e específica a abordagem farmacológica para cada paciente (ANGUS et al., 2020; BAR-EPHRAIM; KRETZSCHMAR; CLEVERS, 2020; O'CONNELL; WINTER; AHERNE, 2021). Estudos comparativos entre organoides de pacientes com DII e saudáveis destacaram características distintas nos pacientes com a doença, como fenótipo inflamatório, aumento da morte celular e alterações nas junções celulares, que responderam aos tratamentos comuns, como anti-TNF e glicocorticoides (D'ALDEBERT et al., 2020).

Essa abordagem avançada não apenas amplia nossa compreensão das interações entre agentes tóxicos, patógenos e a barreira intestinal, mas também oferece uma plataforma promissora para o desenvolvimento de intervenções terapêuticas específicas para DII. Ao prolongar a viabilidade *in vitro* dos organoides e ao utilizar o modelo de "intestino em placa de cultura", conseguimos simular de maneira mais precisa o ambiente colônico humano, proporcionando um contexto relevante para estudos de toxicidade, investigação de patógenos e pesquisa terapêutica direcionada à DII. Este avanço, portanto, representa um passo significativo na melhoria da modelagem *in vitro* e no desenvolvimento de estratégias terapêuticas mais eficazes para doenças gastrointestinais (BASAK et al., 2017; SATO et al., 2011; TIAN et al., 2023).

Objetivos

O objetivo desse projeto foi formular e realizar a caracterização físico-quimica de novas estratégias terapêuticas sobre a colite experimental induzida pelo DSS utilizando a AnxA1 e seu peptídeo mimético Ac2-26, e avaliar a sua eficácia por diferentes vias de administração em camundongos.

Materiais e métodos

Síntese e obtenção da MLNC contendo AnxA1

A síntese das nanocapsulas foi realizada com o auxílio do grupo de pesquisa da Profa. Dra. Adriana Raffin Pohlmann, do Instituto de Química, e da Profa. Dra. Silvia Stanisçuaski Guterres, da Faculdade de Farmácia, ambas da Universidade Federal do Rio Grande do Sul, além do auxílio do aluno de doutorado Matheus de Castro Leão, aluno da Profa. Inar Castro, do Programa de Ciências dos Alimentos da Faculdade de Ciências Farmacêuticas da USP.

As suspensões de LNC utilizadas neste trabalho foram preparadas conforme método já descrito, chamado deposição interfacial de polímero pré-formado (JÄGER et al., 2009; MÜLLER C.R et al., 2001; VENTURINI et al., 2011). A fase orgânica foi preparada pela dissolução do componente oleoso, um triglicerídeo de cadeia média (TCM), a lecitina, o monoestearato de sorbitano e a blenda polimérica de poli (epsiloncaprolactona) (PCL) em um volume de 25 mL de acetona e 5 mL de éter. Esta foi suspensão mantida sob agitação e aquecimento a 40ºC por 2 horas. Em um frasco separado, o polissorbato 80 (tensoativo de caráter hidrofílico) foi disperso em água ultrapura, permanecendo sob agitação, a 40ºC por 2 horas (Tabela 1). Após a completa dissolução dos componentes de ambas as fases, a orgânica foi injetada na fase aquosa utilizando-se um funil. A suspensão resultante foi mantida sob agitação moderada (125 rpm) por 10 minutos, permanecendo sob agitação, a 40ºC. A suspensão foi concentrada a um volume final de 10 mL em evaporador rotatório, para eliminação dos solventes orgânicos e concentração da suspensão.

Tabela 1. Componentes da fase orgânica e fase aquosa da LNC.

Fase orgânica		**Fase aquosa**	
Matéria-prima	**Volume**	**Matéria-prima**	**Volume**
PCL	0,100 g	Água MilliQ®	60mL
TCM	120 µL	PS80	0,080g
Acetona	25 mL		
Lecitina	0,090 g		
Etanol	5 mL		
Monoesterato de sorbitano	0,040 g		

Fonte: o autor.

Para revestir a LNC, uma solução de quitosana (7 mg/mL) foi preparada por meio da dissolução do polissacarídeo em uma solução aquosa contendo 1% de ácido acético. Uma proporção de 10% desta solução foi adicionada por gotejamento à solução de LNC, sendo preparada comumente uma solução contendo 4,5 mL de LNC e 0,5 mL de quitosana. A solução foi mantida por 2 horas em agitação, a temperatura ambiente. Ao final deste período obteve-se a MLNC.

Para a funcionalização da MLNC com AnxA1 foi necessária a complexação de íons zinco (Zn^{2+}) na MLNC. Para tanto, uma solução de acetato de zinco (25 µg/mL diluídos com água MilliQ®) foi preparada e incorporada ao complexo da MLNC. Em seguida, a AnxA1 foi incorporada à estrutura polimérica da MLNC na concentração de 200 µg/mL (Figura 5). A AnxA1 recombinante (rAnxA1) foi cedida pelo Dr. Chris Reutlelinsgperger da Universidade de Maastrich, Holanda.

Figura 5. Representação gráfica do rearranjo estrutural de LNC, MLNC e MLNC-AnxA1

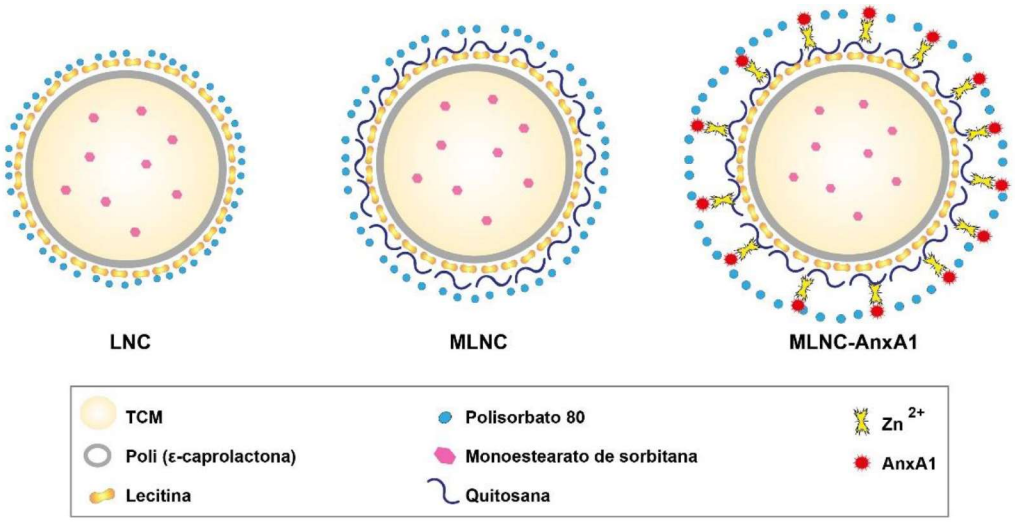

TCM: Triglicerídeo de cadeia média. Zn^{2+}: zinco. AnxA1: Anexina A1. LNC: Nanocapsula de núcleo lipídico. MLNC: nanocapsula multiparede de núcleo lipídico. MLNC-AnxA1: nanocapsula multiparede de núcleo lipídico conjugada com AnxA1. Fonte: o autor.

Análise físico-química das nanocapsulas

Espectroscopia de correlação de fótons potencial zeta

A curva de distribuição de tamanho de partícula, diâmetro hidrodinâmico médio (DLS) e índice de polidispersão (PDI) de todas as formulações foram determinados por espectroscopia de correlação de fótons (PCS), usando um Zetasizer® Nano ZS (Malvern, Reino Unido). Cada amostra foi diluída (500x) em água ultrapura (MilliQ®) filtrada (Millipore®, 0,45 µm), conforme descrito por Cé et al. (2016).

Potencial zeta

O potencial Zeta de todas as formulações foi determinado a partir da mobilidade eletroforética determinada por espalhamento de luz eletroforética em Zetasizer Nano ZS (Malvern, Reino Unido). Cada amostra foi diluída (500x) em solução aquosa filtrada (Millipore®, 0,45 µm) de NaCl (10 mmol/L) e o resultado expresso em milivolt (mV).

Análise de rastreamento de NPs (NTA)

A medição da distribuição de tamanho e a concentração das formulações foram determinadas por NTA (NanoSight LM10 & NTA 2.0 Analytical Software, NanoSight Ltd). Foram obtidas informações visuais da luz espalhada pela partícula em solução. As imagens de vídeo de luz espalhada pela partícula em movimento browniano foram seguidas em uma câmera vídeo CCD em tempo real. As formulações foram diluídas 20.000 vezes e cada videoclipe foi capturado por 60 segundos. O software analítico NTA 2.0 (NanoSight ®) foi usado para os cálculos. A análise foi realizada pela Dra. Aline Alves em colaboração com o grupo da Profas. Adriana Pohllmann e Silvia Guterres da Universidade Federal do Rio Grande do Sul.

Análise de pH

O valor de pH das formulações foi medido em potenciômetro (DM-22, Digimed, Brasil), calibrado com tampão fosfato (pH 4,01 e pH 6,86) em cada amostra sem diluição prévia. As medidas foram obtidas com sensibilidade ≥ 99%

Microscopia eletrônica de transmissão (MET)

As nanoformulações foram submetidas à análise morfológica em microscópio eletrônico de transmissão operando a 80kV. Amostras de nanocápsulas (100 µL) foram diluídas em água (1:10, v/v) e 20 µL da diluição foram depositados em grades de cobre (300 mesh) revestidas com filmes de carbono. Em seguida, um contraste negativo (solução de acetato de uranila 2%) foi adicionado à grade e mantido em dessecador a vácuo por 24 horas. As fotomicrografias foram posteriormente realizadas por técnicos treinados. A análise foi realizada pela Dra. Aline Alves em colaboração com o grupo da Profas. Adriana Pohllmann e Silvia Guterres da Universidade Federal do Rio Grande do Sul.

Quantificação de AnxA1 conjugada a MLNC

O rendimento da complexação de AnxA1 na superfície da nanocápsula foi determinado por um método indireto. Para isolar a fração não ligada de AnxA1, as nanocápsulas vetorizadas foram colocadas em unidades de ultrafiltração-centrifugação (100 kDa; Merck KGaA) e centrifugadas a 1840 × g durante 5 min (Sigma® 1-14; SIGMA Laborzentrifugen GmbH, Alemanha). A fração não ligada de AnxA1 nas formulações foi quantificada por um método colorimétrico (QuantiProTM BCA Assay Kit, Sigma-Aldrich, St. Louis, MO, EUA). De acordo com as instruções do fabricante, uma curva de calibração foi preparada usando diluições de BSA e AnxA1 (3 a 27 µg/mL). A absorbância do produto da reação foi registrada em um leitor de placas a 562 nm (Spectramax, Molecular Devices, Sunnyvale, CA, USA) onde o índice de correlação foi de 0,9917.

Síntese e caracterização da SBA-15 contendo Ac2-26

Obtenção da SBA-15-Ac2-26

A micropartícula SBA-15 foi sintetizada no Instituto de Física da Universidade de São Paulo, Brasil, pelo pesquisador Luis Carlos Cides de acordo com trabalho anterior (MATOS et al., 2001). Para a síntese da SBA-15 foram utilizandos 4 g de Pluronic P123 ($PEO_{20}PPO_{70}PEO_{20}$) (BASF, Alemanha), o qual foi dissolvido em 122 g de solução de HCl 2M e mantido sob agitação magnética e mecânica por 1 hora.

Foram adicionados 8,6 g de tetraetilortossilicato (Sigma-Aldrich; St. Louis, EUA) e a solução foi mantida sob agitação por 24 horas. Após esse processo, a mistura foi submetida a tratamento hidrotérmico por 48 horas a 100 °C em autoclave, posteriormente lavada com água deionizada e seca em temperatura ambiente. O molde de polímero foi então removido por calcinação a 540 °C em N_2 por 2 horas e ao ar por 4 horas.

O peptídeo A2-26 foi adquirido da empresa Proteinmax - São Paulo, Brasil. A incorporação de Ac2-26 resultou da dissolução do peptídeo em água MilliQ; em seguida foi realizada a mistura de SBA-15:Ac2-26 (1:1), onde 1 mg/mL de Ac2-26 foi adicionado a 1 mg de SBA-15. A mistura foi seca em estufa a 35°C até secagem completa. Para o revestimento com Eudragit® L30-D55 (Evonik Industries AG - Rellinghauser Straße – Essen Germany) foi adicionada uma proporção de 1:2 de SBA-15-Ac2-26 e Eudragit®. O material foi seco em estufa a 35°C por 4 horas e depois armazenado em congelador a -20°C.

Caracterização por DLS do peptídeo Ac2-26

A medição do espalhamento dinâmico de luz para analisar o tamanho de partícula foi realizada à temperatura ambiente, utilizando o equipamento Brookhaven DM-5000 (Brookhaven Instruments, NY, EUA) com comprimento de onda de 635 nm. A análise dos dados foi realizada utilizando o software BIC fornecido com a equipamento. A amostra foi diluída para 1 mg/mL para mitigar a influência da interação interpartículas no coeficiente de difusão das partículas e, consequentemente, nos dados obtidos. Estas análises foram realizadas pelo grupo da Profa. Marcia Fantini, do Instituto de Física da Universidade de São Paulo.

Espalhamento de raios X de pequeno ângulo - Small-angle X-ray Scattering (SAXS)

A análise por SAXS e adsorção de nitrogêgio foram realizadas no Intituto de Física da USP pelos pesquisadores e Pedro Leonidas Oseliero Filho e Luis Carlos Cides. A análise por SAXS foi realizada em um instrumento Nanostar (Bruker, Buffalo, EUA) equipado com um sistema microfoco Genix 3D (Xenocs, Massachusetts, EUA) e um detector Pilatus 300k (Dectris, Baden Suíça). A distância amostra-detector foi de ~667 mm, o que forneceu uma faixa efetiva do módulo do vetor de momento de transferência, $q = 4\pi\sin(\theta)/\lambda$ (onde 2θ é o ângulo de espalhamento e $\lambda = 1{,}5418$ Å é

o X- comprimento de onda do raio), de 0,015 a 0,30 Å-1. Para os experimentos, a água deionizada (utilizada no preparo da amostra) e a mesma amostra dos ensaios DLS foram medidas, em temperatura ambiente, em capilar de quartzo reutilizável com 1,5 mm de diâmetro montado em caixas de aço inoxidável. Amostras em pó de SBA-15 e SBA-15 adicionado ao peptídeo foram colocadas em um porta-amostras entre duas folhas de mica. Um conjunto de folhas de mica também foi medido para fins de correção de *backgroung*. O tratamento dos dados, que inclui integração azimutal, subtração de fundo e normalização de escala absoluta (para a amostra líquida), foi realizado utilizando o software XSACT fornecido pela Xenocs.

A determinação da isoterma de adsorção de nitrogênio (*Nitrogen Adsorption Isotherm*, NAI) foram obtidas no equipamento ASAP2020 (Micromeritics®, Atlanta, EUA) utilizando gás nitrogênio. Nessa técnica, nitrogênio é adsorvido pelos poros (ou seja, o gás entra e preenche os poros) e posteriormente dessorvido (ou seja, o gás sai dos poros) em temperatura constante. Estas análises foram realizadas pelo grupo da Profa. Marcia Fantini, do Instituto de Física da Universidade de Universidade de São Paulo.

Conjugação de SBA-15 e Ac2-26 a corantes fluorescentes

Para aplicação de SBA-15 e Ac2-26 em ensaios de rastreio da micropartícula/peptídeo *in vivo* e internalização celular *in vitro,* a micropartícula SBA-15 e o peptídeo Ac2-26 foram funcionalizados com fluorórofos. A SBA-15 foi funcionalizada previamente com 3-aminopropiltrimetoxissilano (APTES), o que permitiu a ligação de grupos amina presentes na estrutura do fluoróforo isotiocianato de fluoresceína (FITC)(Sigma-Aldrich; St. Louis, EUA). A conjugação foi realizada conforme protocolo descrito por Appiah-Ntiamoah et al. (2015). Após marcação, a SBA-15-FITC foi analisada por medidas SAXS para confirmação da conjugação do fluoróforo. A SBA-15-FITC foi então armazenada em congelador a -20 °C.

A conjugação do peptídeo foi realizada em colaboração com o laboratório do Professor Marco Antônio Stephano, FCF, USP. O peptídeo Ac2-26 foi conjugado com o corante Cianina 5.5 (Cy5.5 - Lumiprobe Corporation, Hunt Valley, USA). Ac2-26 foi dissolvido em tampão salina de fosfato (PBS) (pH de 7,4) para atingir uma concentração de 1,0 mg/mL. Simultaneamente, 1 mg de corante Cy5.5 foi dissolvido

em 1 mL de DMSO 1 mM. O peptídeo e o corante Cy5.5 foram misturados na proporção molar de 1:10, e qualquer excesso de corante foi removido por diálise usando uma membrana de 10 mm com ponto de corte de 500 Da. O peptídeo marcado com Cy5 foi purificado com Sephadex G-25 e depois liofilizado. A análise por espectrofotometria a 215 nm (Shimadzu Scientific, Marlborough, EUA) confirmou o sucesso do processo de rotulagem. O rendimento do peptídeo marcado com Cy5.5 foi de dez frascos, cada um contendo 450 µg.

Estabilidade de Eudragit-SBA-15-Ac2-26

Foram preparadas diferentes soluções mimetizando o pH estomacal e intestinal. A solução gástrica foi preparada utilizando NaCl (0,2 g) e HCl (0,7 mL) e o volume completado para 100 mL e o pH ajustado para 1,2. Já a solução intestinal foi preparada com KH_2PO_4 (0,68 g), NaOH (2N – 7,7 mL), o volume completado para 100 mL de H_2O e o pH ajustado para 6,8 (Mariano-Neto 2014). A solução de Eud-SBA-15-Ac2-26 (5 mg) foi misturada à solução tampão e a quantificação da concentração de peptídeo liberado foi analisada em diferentes tempos. Para quantificar o peptídeo liberado foi utilizado O QuantiPro™ BCA Assay Kit (Sigam-Aldrich) capaz de detectar proteínas nas concentrações de 0,5 to 30 µg/mL.

Experimentação animal

Animais

Foram utilizados camundongos C57Bl/6, machos com 8 a 10 semanas e pesando de 20 a 25 g. Os animais foram fornecidos pelo Biotério da Universidade Federal do Estado de São Paulo (UNIFESP) e mantidos em ciclo de 12 horas claro/escuro, temperatura de 20 a 25°C, com água e ração *ad libitum.* A execução do presente estudo foi aprovada pela Comissão de Ética no Uso de Animais da Faculdade de Ciências Farmacêuticas da Universidade de São Paulo. CEUA/FCF/USP - Protocolo nº 598 - MLNC-AnxA1 (Anexo 1 e 2). CEUA/FCF/USP - Protocolo nº 653 – SBA-15-Ac2-26 (Anexo 3).

Colite experimental

A colite experimental foi induzida pela ingestão de dextram sulfato de sódio (DSS - MW 40,000, Dextran Products Limited, Ontario, Canadá) veiculado na água dos animais durante 6 dias, sendo trocado a cada dois dias para que os animais recebessem doses constantes. Os tratamentos foram veiculados aos animais do 6º dia ao 9º dia de experimento (Figura 6). No 10º dia de experimento, os animais foram anestesiados e o sangue coletado pela aorta abdominal após abertura ventral. Em seguida, o cólon foi removido a partir da junção ileocecal até a proximidade do ânus, lavado com solução isotônica e avaliado macroscopicamente (peso e comprimento). Finalmente, o órgão foi fragmentado para análises histológicas (cólon distal), celulares (cólon médio) e de citocinas pró e anti-inflamatórias (cólon proximal). Ainda, parâmetros clínicos (peso corpóreo, diarreia e sangramento retal) foram avaliados diariamente (Dia 0 ao dia 10), para análise da evolução da doença e o Índice de Atividade da Doença (IAD) calculado a partir da soma dos parâmetros avaliados.

Figura 6. Cronograma de indução da colite experimental e tratamentos

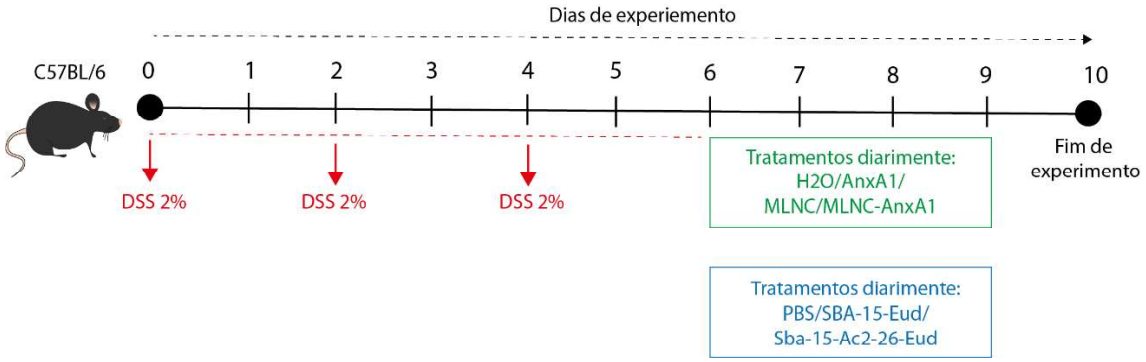

No dia 0 foram realizadas as coletas de fezes e aferição do peso, e o iniciou da indução da doença pela adição de 2% de DSS à água dos animais. A coleta de fezes e aferição do peso foi realizada diariamente durante os 10 dias de experimento. O DSS foi removido no 6º dia de experimentação e os tratamentos foram inciados no mesmo dia, seguindo-se até o 9º dia. No 10º dia os animais foram eutanasiados. Fonte: o autor.

Tratamentos

MLNC-AnxA1

Os tratamentos com MLNC-AxA1 foram administrados via oral, intravenoso e intraperitoneal. No tratamento por via oral, os animais foram tratados com AnxA1 (100 µg/mL) ou MLNC-AnxA1 (100 µg/mL – $3,1x10^{12}$ partículas) em um volume final de 250

µL. O tratamento intravenoso foi realziado com AnxA1 (10 µg/mL), MLNC ($7,5x10^{10}$ partículas/mL) ou MLNC-AnxA1 (10 µg/mL – $7,5x10^{10}$ partículas/mL) em um volume final de 50 µL. O tratamento intraperitoneal foi conduzido com AnxA1 (12,5 µg/mL), MLNC ($9,6x10^{11}$ partículas/mL) ou MLNC-AnxA1 (12,5 µg/mL – $9,6x10^{11}$ partículas/mL) em um volume final de 200 µL. Os grupos controle, que receberam apenas DSS 2%, receberam os volumes equivalente a cada via de administração de água MilliQ (veículo utilizado na diluição e preparação dos outros grupos).

SBA-15-Ac2-26

Para o tratamento com SBA-15-Ac2-26, os animais foram divididos em quatro grupos: Naive, DSS, DSS+SBA-15-Eudragit (200 µg) e DSS+SBA-15-Ac2.26-Eudragit-SBA-15-Ac2.26 (200 µg/200 µg). Os tratamentos foram preprados em PBS pH 5 em um volume final de 400 µL/animal. O grupo DSS foi tratado com 400 µL de PBS pH 5. Os tratamentos foram realizados diariamente por via oral, entre os dias 6 e 9.

Processamento histológico

Fragmentos coletados da parte distal do cólon foram fixados por 24 horas de incubação em paraformaldeído a 4%. Posteriormente, foram desidratados em etanol graduado 100%, 90% e 70%, clarificados em xilol e embebidos em parafina para análises histopatológicas e imuno-histoquímicas de acordo com nossos manuscritos anteriores (De Paula Silva 2016, 2021; Da Rocha 2020).

A análise histopatológica foi realizada em cortes de 4 µm. As amostras foram coradas com solução de hematoxilina e eosina e analisadas com objetiva de alto aumento (40×) em AxioCam acoplada a microscópio Zeiss (Carl Zeiss, Jena, Alemanha). A análise do escore histopatológico foi realizada de forma cega por dois analistas conhecedores das características do tecido intestinal. O escore considerou: edema tecidual, displasia/histoarquitetura alterada, edema de cripta, infiltrados inflamatórios e ulcerações. A análise de escore histológico foi adaptada de de Paula-Silva, (2020) e (Geboes et al. (2000). Foram considerados valores de 0 a 4 onde: 0 = ausência total; 1 = discreta; 2 = moderada; 3 = intensa; 4 = total descaracterização do tecido. Dez fotos foram capturadas de cada corte histológico usando uma objetiva de alto aumento de 20× e as pontuações foram avaliadas em uma escala que varia de 0 a 4.

Imunohistoquímica

As secções de cólon foram desparafinizados, hidratados e incubados com tampão citrato de sódio (pH 6,0) a 96°C por 30 minutos. A atividade da peroxidase endógena foi bloqueada com peróxido de hidrogênio a 3%, lavado três vezes após cada 10 minutos de incubação. Em seguida, o bloqueio de sítios de ligação inespecíficos foi realizado com BSA,1% diluído em tampão salina Tris (TBS) por 1 hora. As secções obtidas foram incubadas com anticorpos descritos na Tabela 2, e mantidos a 4°C. No dia seguinte, as secções foram lavadas e incubadas com anticorpo secundário conjugados com HRP (Abcam, Cambridge, Reino Unido) (1 hora, em temperatura ambiente, ao abrigo da luz) e detectados com 3,3'-diaminobenzidina (DAB - Dako Omnis, Agilent, Santa Clara, California, EUA). Por fim, as secções foram contrastadas com hematoxilina e as lâminas montadas. A análise de marcação dos anticorpos foi realizada utilizando o microscópio Imager. A2 Zeiss (Carl Zeiss, Jena, Alemanha). A quantificação dos núcleos proliferativos, células MUC2+ e CD163+ foram avaliada pelas fotografias utilizando uma objetiva de 40× em dez campos da camada mucosa e quantificados para cada campo avaliado.

A porcentagem de área marcada de Claudina-1 e ZO-1 e a quantificação de células positivas para PCNA, Ki67, MUC-2 e CD163 foram obtidas utilizando o *software* ImageJ. Os resultados foram expressos como média ± erro padrão da média (EPM) de porcentagem da área marcada.

Tabela 2. Anticorpos utilizados para imunohistoquímica

Anticorpos	Diluição	Fabricante	Experimento
Claudina 1	1:50	Abcam	MLNC/SBA
ZO-1	1:50	Abcam	MLNC
PCNA	1:10	Santa Cruz	MLNC/SBA
Ki67	1:100	Abcam	MLNC
MUC-2	1:100	Invitrogen	SBA
CD163	1:100	Bioss Antibodies Inc	SBA

Fonte: o autor

Análise celular da lâmina própria

Após a coleta de material dos animais, fragmentos do cólon foram coletados e processados para extração das células de lâmina própria, conforme descrito previamente por Sena et al. (2015) e adaptado em nosso laboratório. Tecidos

adjacentes foram retirados e as amostras foram imersas em 5 mL de solução de PBS-gentamicina, em gelo. O conteúdo dos fragmentos intestinais foi aberto longitudinalmente para remoção do conteúdo fecal e colocado em tubo de 15 mL contendo solução de Hanks (isenta de Ca^{2+} e Mg^{2+}) e mantidas em gelo sob agitação durante 15 minutos, para remoção das células epiteliais de mucosa. Esse processo de lavagem foi repetido duas vezes e a solução de Hanks trocada entre as lavagens. O tecido foi lavado em PBS para e incubado com 2 mL de solução de colagenase II e IV, a 37ºC, sob agitação, por 20 minutos, sob agitação a cada 5 minutos. Em seguida, foram adicionados 2 mL de PBS contendo 10% de soro fetal bovino (SFB) em cada tubo, e as células extraídas separadas do restante do tecido com o auxílio de um *cell strainer*. Essa solução foi centrifugada a 1200 g, por 5 min, e o sobrenadante foi descartado. Por fim, as células foram ressuspendidas em 1 mL de PBS + 10% de SFB e mantido em gelo para início imediato da técnica de citometria de fluxo.

Células isoladas da lâmina própria foram contadas em câmara de Neubauer e a concentração de $1x10^6$ células foram utilizadas para análise de citometria de fluxo. As amostras foram incubadas em tampão FACS contendo os diferentes anticorpos (Tabela 3) anticorpos Ly6G (granulócitos), F4/80 (células apresentadoras de antígeno) e CD4 (linfócitos T). As concentrações e marcações foram feitas de acordo com as instruções do fabricante e analisadas em citômetro de fluxo BD Accuri™ C6. Para as análises, 50.000 células foram detectadas e quantificadas por porcentagem.

Tabela 3. Anticorpos conjugados com fluoróforos utilizados para citometria de fluxo

Anticorpos	Diluição	Fabricante	Fluoróforo
CD80	1:50	BD Bioscience	PE
CD206	1:25	BD Bioscience	FITC
F4/80	1:100	BD Bioscience	PerCP-Cy5.5
Ly6G	1:100	BD Bioscience	APC

CD: cluster of differentiation; PE: phycoerythrin FITC: fluorescein isothiocyanate; PerCP-Cy5.5: PerCP-Cyanine5.5; APC: Allophycocyanin.

Avaliação in vivo e ex vivo de SBA-15 e Ac2-26 no trato gastrointestinal

O rastreio da SBA-15 no trato gastrointestinal (TGI) foi avaliado por SBA-15-FITC revestido com Eudragit. Eudragit-FITC-SBA-15 (400 µg/400 µL) foi administrado

oralmente a camundongos saudáveis. Os animais foram eutanasiados 6 ou 18 horas após o tratamento para retirada do TGI. A distribuição de Eudragit-SBA15-Ac2-26Cy5.5 foi analisada após 3 horas e 8 horas e o TGI analisado *ex vivo* nos mesmos intervalos de tempo.

As imagens de fluorescência *ex vivo* foram adquiridas utilizando o equipamento IVIS ® Lumina LT Series III (Xenogen Corp., Alameda, CA, EUA), com as seguintes parâmetros para obtenção das imagens: excitação/emissão 465/520, tempo de exposição automático, F/stop 4 e binning de 4. Para análise de intensidade de fluorescência selecionamos uma região de interesse e normalizamos pelas áreas correspondentes. Os sinais adquiridos foram analisados utilizando o Living Image® Software versão 4.7.2 (PerkinElmer®) em unidades de fótons/s. As análsies foram realizadas no laboratório do Professor Lionel Fernel Gamarra, localizado no Instituto Israelita de Ensino e Pesquisa Albert Einstein.

Análises *in vitro*

Macrófagos murinos da linhagem celular Raw 267.7 e células Caco-2 (células epiteliais derivadas de intestino humano) foram obtidos do banco de célula do Rio de Janeiro (BCRJ®) e foram utilizados para realização dos ensaios de citotoxicidade pelo ensaio de redução do (3-(4,5-Dimethylthiazol-2-yl)-2,5-DiphenyltetrazoliumBr) (MTT), morte e captação celular. A linhagem celular de macrófagos de camundongo J774A.1 (ATCC®; Washington DC, EUA) também foi utilizada para ensaios de captação celular. As células Raw 264.7 e J774A.1 foram mantidas com meio de cultivo celular *Dulbecco's Modified Eagle Medium* (*DMEM*) (Gibco™, Estados Unidos) suplementado com 10% de SFB (Gibco™) e 1 mM de piruvato em estufa a 37°C com 5% de CO^2. Células Caco-2 foram cultivadas com meio *Dulbecco's Modified Eagle Medium* (*DMEM*) (Gibco™) suplementado com 20% de SFB (Gibco™). Para realização dos experimentos foram utilizadas as passagens celulares 8 a 15.

Ensaio de citotoxicidade por MTT

As células Raw 264.7 foram plaqueadas ($1x10^4$) em microplacas de 96 poços e mantidas a 37°C com 5% de CO_2. Após 24 horas, os tratamentos foram realizados de acordo com os parâmetros apresentados nas Tabelas 4 e 5, e analisados após 24 e

48 horas de incubação. Como controle positivo de citotoxicidade foi empregado dimetilsufóxido (DMSO) a 10%. O crescimento celular foi revelado pelo ensaio de MTT. Foram adicionados 10 µL de MTT (5 mg/mL) por poço e a placa mantida por 3 horas em estufa a 37°C e 5% CO_2. Ao término desse período, o sobrenadante foi retirado e adicionados 100 µL de DMSO para a dissolução dos cristais de formazan formados pela redução do MTT. A densidade óptica (DO) de cada poço foi determinada em espectrofotômetro de microplacas em 570 nm (Asxys Expert 34 Plus, Microplate Reader G020 150, Eugendorf, Salzburg, ÁUSTRIA).

Os resultados em densidade óptica (DO) realizados em triplicata foram analisados empregando como indicador a porcentagem de viabilidade.

Tabela 4. Tratamentos de MLNC utilizados no ensaio de MTT

	Concentração de partículas e AnxA1/mL			
	1	2	3	4
AnxA1	50 ng	500 ng	2500 ng	5000 ng
MLNC	$1,55x10^9$	$15x10^9$	$77,5x10^9$	$150x10^9$
MLNC-AnxA1	$1,55x10^9$	$15x10^9$	$77,5x10^9$	$150x10^9$

Fonte: o autor.

Tabela 5. Tratamentos de SBA-15 utilizados no ensaio de MTT

	Concentração de partículas e Ac2-26 (µg/mL)			
	1	2	3	4
Ac2-26	0,5	5	10	50
SBA-15	0,5	5	10	50
SBA-15-Ac2-26	0,5	5	10	50

Fonte: o autor.

Viabilidade e morte celular

Para analisar o tipo de morte gerada pelas MLNCs, células Raw 264.7 foram plaqueadas ($5x10^4$) em placas de 24 poços e tratadas apenas com as concentrações que apresentaram maior redução da atividade mitocondrial no ensaio de MTT. Assim, os tratamentos consistiram em: AnxA1 (5000 ng), MLNC ($150x10^9$ partículas/mL) e MLNC-AnxA1 ($77,5x10^9$ e $150x10^9$ partículas/mL). A morte celular foi aferida 24 e 48 após as incubações. Após os tratamentos, os sobrenadantes foram coletados e as

células que permaneceram aderidas foram removidas com a adição de solução de tripsina (Gibco™). Em seguida, foram centrifugadas a 1200g por 5 minutos, e ressuspendidas em 200µL de tampão de ligação para a marcação com Anexina V conjugada com aloficocianina (AnxV-APC) (diluição 1:20) e com 7-aminoactinomicina D (7-AAD) (diluição 1:200), ambos os anticorpos provenientes da BD Biosciences, Franklin Lakes, NJ, USA. As células foram incubadas por 30 minutos ao abrigo da luz e a temperatura ambiente. Em seguida, foi realizada a leitura por citometria de fluxo utilizando o equipamento Accuri C6 (BD Biosciences, Franklin Lakes, NJ, USA). Foram reportados 10 mil eventos e os resultados expressos em porcentagem (%). O grupo duplo negativo para marcação AnxV-7-AAD indica as células viáveis, marcação única com AnxV indica as células em apoptose, marcação única com 7-AAD indica as células em necrose e o grupo duplo positivo para AnxV-7-AAD indica gro upo de células em apoptose tardia.

Captação (Uptake) celular de MLNC e SBA-15-Ac2-26

MLNC

A análise da internalização de MLNCs por células Raw 264.7 foi realizada por microscopia hiperespectral de campo escuro (CytoViva®). Lamínulas livres de poeira e extra limpas (Nexterion Glass D # D263T; Schott) foram inseridas em placa de 6 poços. Na parte superior de cada lamínula, foram adicionados $8x10^4$ células/poço. Foram testadas apenas as maiores concentrações de MLNC ($15x10^9$ partículas/mL) e MLNC-AnxA1 ($15x10^9$ partículas/mL) que não alteraram a viabilidade celular, após incubação por 2 ou 24 horas. Um grupo controle foi mantido na presença de DMEM 10% SFB (não tratado [NT]). Em seguida, as células foram lavadas três vezes com solução de PBS suplementado com 5% de SFB. As lamínulas foram colocadas entre as lâminas livres de poeira e extra limpas (NexterionR Glass B; Schott, NY, EUA) e lamínulas (Nexterion Glass D # D263T; Schott). As células foram fotografadas usando o sistema de imagem CytoViva Ultra Resolution (CytoViva, Inc., AL, EUA) montado em um microscópio Olympus BX51 (ampliação de 1500 ×; Olympus Corporation, Tóquio, Japão), equipado com uma abertura numérica (NA) de fluorita 100 × óleo de íris de 0,6-1,30 objetiva e fonte de luz 75 W Xe. As imagens ópticas foram obtidas usando uma câmera Retiga EXi CCD de imagem Q (Olympus Corporation, PA, EUA) e câmera digital Dage XL CCD com software de processamento de imagem (DageR;

DAGE-MTI de MC, Inc., MI, EUA). As análises no microscópio foram conduzidas pelas Dra. Mayara Uchiyama, em colaboração com o grupo do Prof. Koiti Araki, do Instituto de Química da Universidade de São Paulo.

Liberação in vitro de SBA-15-FITC e SBA-15-Ac2-26-Cy5.5

O peptídeo Ac2-26 marcado com Cy5.5 foi incorporado a SBA-15 (seguindo o protocolo de incorporação) e empregado para testar a liberação do peptídeo nas células. A captação de SBA-15-Ac2-26Cy.5.5 e SBA-15-FITC foi medida por citometria de fluxo (BD, Accuri C6, Estados Unidos) em macrófagos de camundongo Raw 264.7 e células Caco-2. A presença do peptídeo Ac2-26-Cy5.5 foi analisada após 30 minutos, 2, 6 e 24 horas de incubação com SBA-15-Ac2-26Cy.5.5. Células Caco-2 foram utilizadas para medir a absorção de SBA-15-FITC após 4 e 24 horas de incubação. Após o período de tratamentos, as células foram recolhidas, lavadas duas vezes e ressuspendidas em PBS. Para quantificar a porcentagem de células positivas, foram coletados pelo menos 10.000 eventos. Os eventos foram coletados com a delimitação da população principal de células saudáveis, e o percentual foi definido em relação à condição não tratada.

Células J774A.1 foram semeadas em placas de 24 poços como descrito anteriormente. A citocalasina D (20 µM) foi adicionada por 1 hora e removida antes do tratamento com SBA-15-FITC (10 µg/mL). A captação celular foi verificada 4 e 24 horas após o tratamento, utilizando imagem celular (CELENA ® Logos Biosystem, EUA) e dez campos para cada condição experimental foram analisados. A porcentagem de células fagocíticas foi quantificada utilizando o software ImageJ.

Polarização de macrófagos derivados da medula-óssea pela MLNC-AnxA1

O experimento foi realizado de acordo com o método previamente estabelecido por Ying et al. (2013). Inicialmente, camundongos C57Bl/6 foram anestesiados e eutanasiados para coleta dos fêmures esquerdo e direito para coleta do lavado medular, utilizando uma solução de PBS gelado contendo 2% de SFB. Em seguida o *pool* de medulas foi ressuspendido utilizando agulhas de 21G para dissociar as células e passá-las através de *cell strainer* de 70 µm para remoção de outros tecidos. As células foram lavadas com solução de NH_4Cl 0,8% e incubas em gelo para remoção das células vermelhas. Após centrifugação por 5 minutos, 500 x g a 4°C, as células

foram ressuspendidas com meio BMDM, composto por meio IMDM (Iscove's Modified Dulbecco's Media) (Gibco™, Grand Island, New York, USA), 20% de sobrenadante de cultura de células L929, o qual é rico em fator de crescimento de monócitos (M-CSF) e 10% de SFB. As células foram contadas e plaqueadas na concentração de $5x10^5$ células/poço em placa de 24 poços e mantidas no meio BMDM por 7 dias para diferenciação celular. Após a padronização da diferenciação e obtenção de 90% de macrófagos diferenciados em cultura (dados não apresentados), as células foram tratadas com LPS de *Escherichia coli* O111:B4 (Sigma-Aldrich Co, Saint Louis, MO, USA (100 ng/mL) e mantidas por 24 horas nessa condição para diferenciação em macrófagos M1. Após esse período foram realizados os tratamentos com dexametasona (500 ng/mL), AnxA1 (500 ng/mL), MLNC ($15x10^9$ partículas/mL) ou MLNC-AnxA1($15x10^9$ partículas/mL contendo 500 ng de AnxA1).Como controle positivo para polarização foi utilizado o corticóide dexametasona (500 ng/mL) (Aché Laboratórios Farmacêuticos S.A., Brasil). Após 48 horas de tratamentos, o sobrenadante foi retirado e armazenado para análise das citocinas interleucina-10 (IL-10) (BD OptEIA™ - BD, Becton Dickinson, New Jersey, EUA) e (TGFβ) (eBioscience™, California, EUA) por ensaio de ligação enzimática (Enzyme Linked Immuno Sorbent Assay – ELISA) de acordo com o manual de cada fabricante. A caracterização do fenótipo celular foi realizada pela marcação de anticorpos conjugados a fluoróforos previamente listados na Tabela 3. As células foram removidas e marcadas com os anticorpos F4/80, CD80 e CD206 para diferenciação de macrófagos M1 e M2. A análise foi realizando utilizando o equipamento Accuri C6 (BD Biosciences, Franklin Lakes, NJ, USA). A porcentagem de cada população celular foi reportada utilizando pelo menos dez mil eventos por amostra.

Organoides intestinais

Produção e cultura de organoides de cólon murino

Camundongos C57BL/6 foram mantidos de acordo com o protocolo *Institutional Animal Care and Use Committee* (IACUC) da Universidade de Massachusetts Lowell, Estados Unidos. Os organoides foram desenvolvidos a partir do cólon de camundongos (n = 3), conforme descrito em estudos prévios (SAYED et al., 2020b, 2021; SAYED; CHAKRABORTY; DAS, 2023). Os tecidos foram digeridos

pela enzima colagenase, a 37°C durante 20-30 minutos. As células foram então filtradas e cultivadas em meio condicionado (CM) a 50%, o qual proporciona a proliferação das células-tronco adultas extraídas do tecido. Para o desenvolvimento dos organóides é necessário a adição de uma solução que mimetiza a matriz extracelular. Para isso foi utilizado Matrigel® (Corning) para cultivo de organoides. Meio CM fresco a 50% foi adicionado a cada 2-3 dias e os organoides utilizados nos experimentos estavam em passagens iniciais (p2-p8).

Desenvolvimento de monocamadas polarizadas diferenciadas em suportes permeáveis de 96 poços

Organóides cultivados saudáveis foram tripsinizados em células únicas e diferenciados em monocamadas polarizadas derivadas de enteroides (EDMs), conforme descrito anteriormente com pequenas modificações (SAYED et al., 2020b, 2021; SAYED; CHAKRABORTY; DAS, 2023). Os suportes permeáveis de 96 poços (HTS Transwell®, Corning Incorporated©, EUA) foram revestidos com Matrigel® (Corning Incorporated©, EUA) diluído (1:40). Cerca de $5x10^4$ células foram suspensas em meio condicionado a 5% e semeadas no transwell. A diferenciação das células em EDMs ocorreu em 2-3 dias e as céluals foram então utilizadas nos experimentos.

Tratamento das EMDs diferenciados com LPS e AnxA-1 ou Ac2-26

As EDMs diferenciados foram desafiados ou não (não tratados) com LPS (*E. coli*, O111:B4, Sigma-Aldrich) na concentração de 500 ng/mL nos compartimentos basolateral e apical por 24 horas. AnxA1 e Ac2-26, na concentração de 50 ng/mL, foram adicionados com o LPS durante todo o tempo experimental. As células foram monitoradas microscópicamente quanto à morfologia e viabilidade.

Mensuração da resistência elétrica transepitelial (TEER) e avaliação do ensaio de permeabilidade transepitelial FITC-Dextran

A permeabilidade nas células epiteliais intestinais diferenciadas foi medida por duas abordagens: o ensaio de permeabilidade de FITC-dextram e TEER. Para as medidas de TEER, foi utilizado o medidor de resistência epitelial Voltímetro Millicel-ERS (Millipore®, ©Merck, Alemanha) para medir o valor de TEER em diferentes momentos. Os valores de TEER foram expressos como Ohm x cm^2. Para o ensaio de permeabilidade transepitelial FITC-Dextram, utilizamos isotiocianato de fluoresceína

conjugado ao dextram (peso molecular médio 40.000, ©Sigma-Aldrich). Ao final do experimento, 100 µL de FITC-dextram (1 mg/mL) foram adicionados ao compartimento apical do *transwell*, os meios foram recolhidos do compartimento basolateral após 1 hora e a fluorescência mensurada a 490 nm (excitação) e 520 nm (emissão) por leitor de placas Tecan (Tecan Trading AG, Suíça).

Quantificação de citocinas liberadas das EDMs

Os sobrenadantes foram coletados da parte basolateral das EDMs desafiados ou não com LPS +/-, AnxA1 ou Ac2-26. A concentração de ligante 1 de quimiocina (CXCL-1) de camundongo foi medido usando CXCL1/KC DuoSet™ ELISA de camundongo (©R&D Systems, EUA) de acordo com as instruções do fabricante. As concentrações de citocinas CXCL-1 foram comparadas nos EDMs +/- LPS +/- ANXA1 ou Ac2-26.

Quantificação dos níveis de RNA por RT-qPCR

Após desafio com LPS +/-, as EDMs tratadas com Anxa1 ou Ac2-26 foram lisados e o RNA isolado utilizando o kit Quick-RNA MicroPrep (©Zymo Research Corporated, EUA) de acordo com as instruções do fabricante. O RNA foi então utilizado para sintetizar DNA complementar (cDNA) usando qScript cDNA SuperMix (©Quantabio, EUA) de acordo com as instruções do fabricante. O RT-qPCR foi realizado usando 2x SYBR Green qPCR Master Mix em um equipamento Bio-Rad CFX Opus 96 Real-Time PCR System (©Bio-Rad, EUA) usando os primers listados na Tabela 6.

Tabela 6. Sequencia de primers utilizados nesse estudo

Primers	Forward primer (3'- 5')	Reverse primer (3'- 5')
18S rRNA	GTAACCCGTTGAACCCCATT	CCATCCAATCGGTAGTAGCG
Mouse GAPDH	CATCACTGCCACCCAGAAGACTG	ATGCCAGTGAGCTTCCCGTTCAG
Mouse ZO-1	GGGAGGGTCAAATGAAGACA	GGCATTCCTGCTGGTTACAT
Mouse Occludin	CCTCCAATGGCAAAGTGAAT	CTCCCCACCTGTCGTGTAGT
Mouse Claudin-1	CCCCCATCAATGCCAGGTATG	AGAGGTTGTTTTCCGGGGAC
Mouse Claudin-2	CCTTCGGGACTTCTACTCGC	TCACACATACCCAGTCAGGC
Mouse Cadherin	AACCCAAGCACGTATCAGGG	GAGTGTTGGGGGCATCATCA
Mouse MCP-1	AAGTGCAGAGAGCCAGACG	TCAGTGAGAGTTGGCTGGTG
Mouse IL-10	ATTTGAATTCCCTGGGTGAGAAG	CACAGGGGAGAAATCGATGACA
Mouse Fpr1	CATTTGGTTGGTTCATGTGCAA	AATACAGCGGTCCAGTGCAAT
Mouse Fpr2	GAGCCTGGCTAGGAAGGTG	TGCTGAAACCAATAAGGAACCTG

Fonte: o autor

O *cycle threshol* (ct) foi determinado e normalizado para o gene endógeno (18S rRNA e GAPDH). O método ΔΔCt foi utilizado para o cálculo. A alteração relativa de duplicação do nível de transcrição foi calculada (*Fold change*).

Avaliação das proteínas de integridade de TJ por microscopia confocal

As EDM foram plaqueadas em suportes *transwell* de 96 poços e o fundo dos suportes removidos e fixados em metanol a 100% (-20°C durante 20 minutos) ou paraformaldeído a 4% (PFA, ©Sigma-Aldrich) à temperatura ambiente durante 15-20 minutos. As EDMs fixadas em PFA foram incubados à temperatura ambiente durante 10 minutos com glicina 100 mM. Após a fixação, todos as EDMs foram lavados com PBS, permeabilizados com saponina a 0,1% à temperatura ambiente durante 10 minutos e bloqueados com tampão de bloqueio (saponina a 0,1% e BSA a 2%) durante 1 hora. As células foram marcadas utilizando anticorpo anti-ZO-1 (1:500) (©Proteintech Group, EUA) ou anti-claudina-2 (1:100, ©Abcam) diluídos em BSA a 1%, saponina 0,05 % e mantidas por 16 horas, a 4°C. Após as etapas de lavagem, as células foram incubadas com anticorpo secundário IgG Alexa Fluor 594 (1: 500,

Thermo Fisher) e DAPI (1:1000, Sigma-Aldrich) para coloração nuclear durante 1 hora à temperatura ambiente. As membranas EDM foram colocadas em uma lâmina de vidro, montadas com solução para montagem ProLong™ Glass (©Thermo Fisher Scientific, EUA) e cobertas com uma lamínula. As imagens foram tiradas com objetiva de 40x usando um microscópio confocal de varredura a laser Leica SP8 II (©Leica Microsystems, EUA). A intensidade da coloração foi avaliada pelo software ImageJ.

Análise estatística

As análises estatísticas foram realizadas com o software GraphPad Prism Software 10.1. As análises clínicas *in vivo* foram avaliadas por ANOVA Two-Way seguido de pós-teste de Bonferroni. Os resultados obtidos para RT-PCR foram comparados usando um Teste *t* de Student bicaudal. Para as demais análises, foram utilizados One-way ANOVA seguido dos pós-teste de Tukey. Os valores de $p<0,05$ foram considerados significantivos. Os resultados foram expressos como média ± EPM.

Resultados

MLNC-AnxA1 como plataforma de entrega da AnxA1

Formulação da MLNC-AnxA1

Inicialmente, para padronização foram preparados 3 lotes individuais de LNC, MLNC e MLNC-AnxA1, os quais foram avaliados para os parâmetros de polidispersão (PDI), tamanho (nm), potencial zeta (ζ – mV) e pH. As soluções de nanocápsulas foram avaliadas macroscópicamente e ambas as soluções apresentaram aspecto homogêneo, branco opalescente. Quando comparados, os tamanhos das nanocapsulas, MLNC (152,4 nm ±3,89) e MLNC-AnxA1 (162,8 nm ±11,61), apresentaram diâmetro médio superior a LNC (129,5 nm ±3,57), sendo estatisticamente significativo ($p<0,05$). A dispersão das partículas, representado pelo PDI, foi significativamente maior nos grupos MLNC e MLNC-AnxA1 quando comparadas ao grupo LNC (0,114 ±0,01); no entanto, a dispersão de partículas no grupo MLNC-AnxA1 (0,216 ±0,02) foi reduzida quando comparado ao grupo MLNC (0,269 ±0,01). O potencial zeta da LNC (-12,5 mV ±1,37) apresentou valor negativo, e positivo para MLNC (15,5 mV ±0,70) e MLNC-AnxA1 (16,2 mV ±1,71), não sendo observada diferença entre as nanocapsulas contendo quitosana. A adição de quitosana à estrutura da LNC causou redução significativa do pH quando comparados aos demais grupos ($p<0,01$). A análise de concentração de partículas por mL foi realizada no equipamento NanoSight e demonstrou que a concentração de partículas por mL foi reduzida significativamente quando comparados os grupos LNC ($3,6x10^{13}$ part/mL $\pm 6,5x10^{12}$) e MLNC-AnxA1 ($1,5x10^{13}$ part/mL $\pm 4,8x10^{12}$) (Tabela 6).

Tabela 7. Análise físico-química das nanocápsulas

	Nanocápsulas		
Parâmetros	**LNC**	**MLNC**	**MLNC-AnxA1**
D*h*	129 ± 3.57	152 ± 3.89 *	163 ± 11.61 **
PDI	0.11 ± 0.01	0.27 ± 0.01 ***	0.22 ± 0.01 *** §
mV	-12.5 ± 1.37	15.5 ± 0.70 ***	16.2 ± 1.71 ***
pH	4.52 ± 0.02	4.24 ± 0.09 **	4.23 ± 0.03 **
PND ($\times 10^{13}$/mL^{-1})	3.63 ± 0.66	2.75 ± 0.65	1.55 ± 0.48 *

Valores expressos em erro padrão da média ± SEM (n = 3). * $p < 0.05$, ** $p < 0.01$, *** $p < 0.001$ vs LNC. § $p<0.05$ vs MLNC.

Ademais, a análise de rastreamento de NPs realizada no equipamento NanoSight demonstrou que as nanocapsulas funcionalizadas com AnxA1 sobrepõem às revestidas com quitosana (Figura 7), demonstrando que ocorre conjugação com a proteína de forma eficiente. Em relação a eficiência de encapsulação, ou seja, quanto de AnxA1 foi conjugada a MLNC, a suspensão apresentou 92,22% (±1,47) para a AnxA1 após realizada ultra filtração-centrifugação da MLNC-AnxA1.

Figura 7. Sobreposição das NPs funcionalizadas com AnxA1 sobre as nanocápsulas revestidas com quitosana

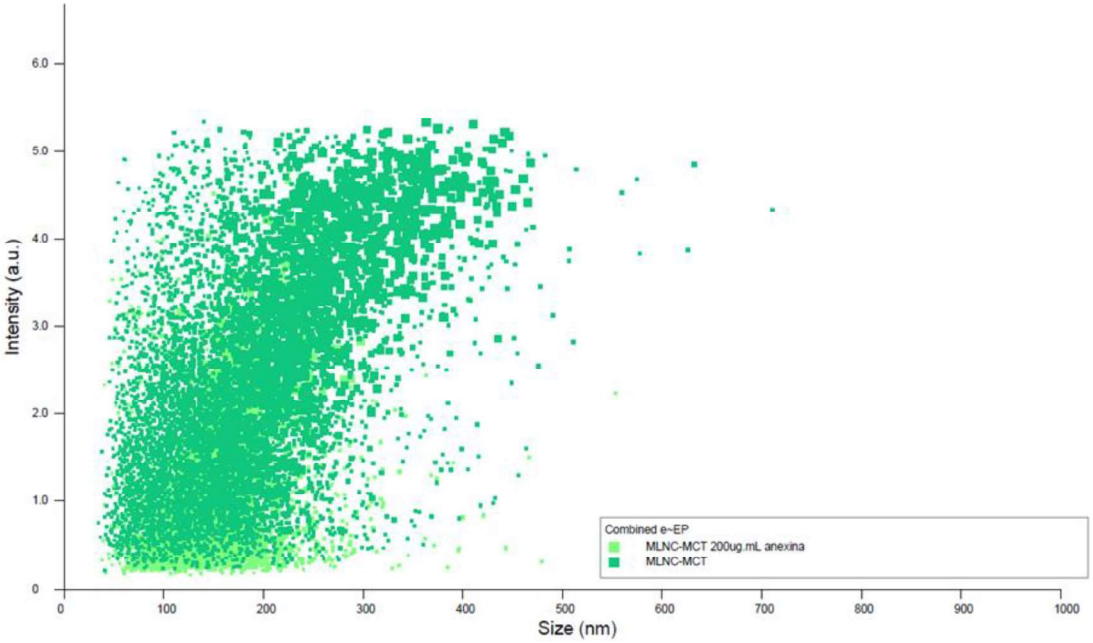

Gráfico obtido do equipamento NTA e processada com o software NTA 2.0 Analytical Software (NanoSight ®).

Utilizando a solução de MLNC-AnxA1, foram obtidas imagens de microscopia eletrônica de transmissão (MET) em diferentes aumentos. As imagens demonstraram que MLNC-AnxA1 manteve o formato esférico quando comparada a imagens de

micrografia realizadas em trabalhos anteriores (BENDER et al., 2014; CÉ et al., 2016) com a LNC e MLNC (20k, 50k, 100k e 300k) (Figura 8).

Figura 8. Análise de microscopia eletrônica de transmissão

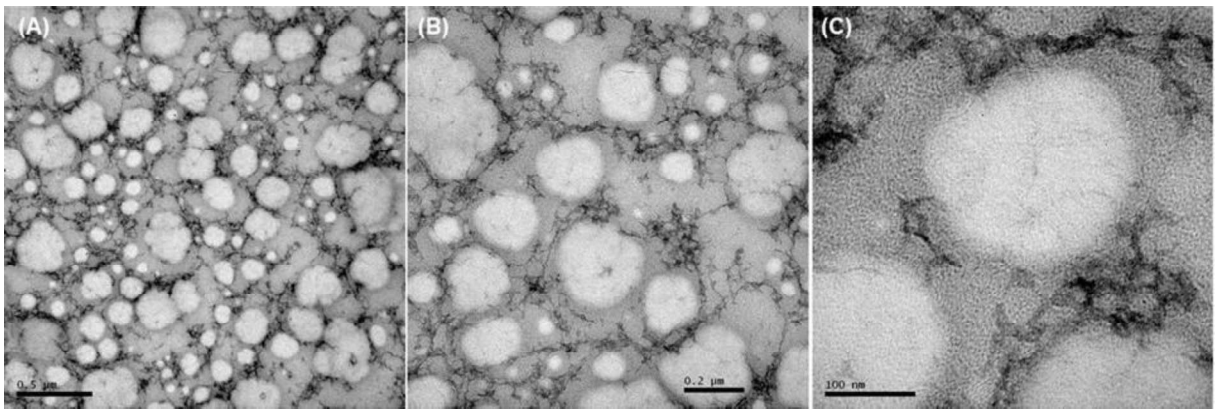

As nanocápsulas MLNC-AnxA1 foram analisadas utilizando diferentes ampliações. (A) 50x barra = 500 nm; (B) 100x barra = 200 nm; e (C) 300x barra = 100 nm.

Administração oral da MLNC-AnxA1 não apresentou eficácia terapêutica para a colite ulcerativa experimental

Após a caracterização físico-química da MLNC-AnxA1, a eficácia terapêutica das nanocápsulas foi investigada no modelo experimental de colite. Os camundongos receberam DSS 2% durante 6 dias para indução da colite e a partir do 6º dia, os animais receberam tratamento por via oral com AnxA1 (100 µg/mL) ou MLNC-AnxA1 (100 µg/mL – $3{,}1 \times 10^{12}$ partículas). Como esperado, a ingestão de DSS foi capaz de induzir colite como observado pelos parâmetros clínicos de perda de peso, escore de consistência das fezes, de presença de sangue nas fezes, comprimento do intestino e índice de atividade da doença, os quais foram similares aos dados obtidos anteriormente (DE PAULA-SILVA et al., 2016b; SENA et al., 2015b). De acordo com a Figura 9 (A-E), os tratamentos com AnxA1 ou MLNC-AnxA1 por via oral não foram capazes de alterar os danos causados na colite quando comparados com o grupo controle.

Figura 9. Tratamento com MLNC-AnxA1 por via oral após colite experimental induzida pelo DSS.

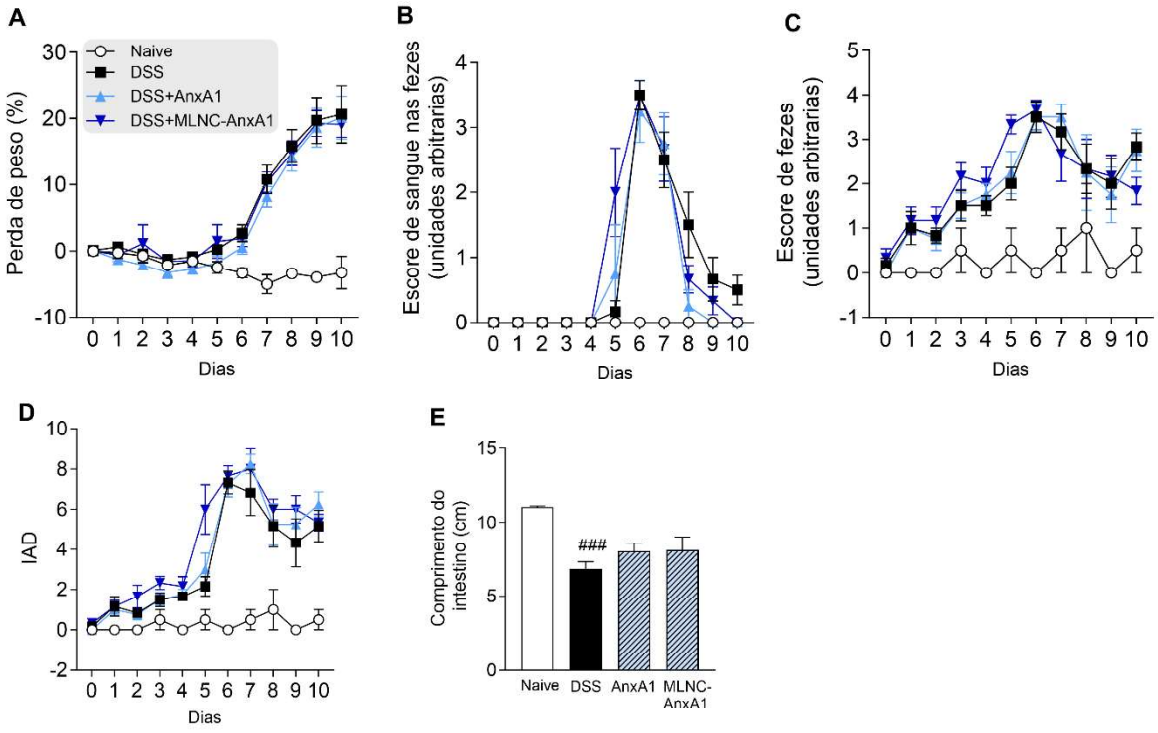

(A) Porcentagem de perda de peso; (B) Escore de sangue; (C) Escore de fezes; (D) IAD; (E) Comprimento do intestino. Os dados são expressos como ± erro padrão da média de 5 animais por grupo. ## p < 0,01 vs *naive*. v.o: via oral. Naive: nenhum tratamento.

Para analisar os efeitos dos tratamentos sobre a estrutura do intestino, foram realizadas análises histopatológicas. Os animais tratados tanto com MLNC-AnxA1, quanto com AnxA1 apresentaram dano tecidual semelhante ao grupo que recebeu apenas o DSS. Pela análise do corte histológico, foi possível observar displasia (seta preta fina), edema (seta vermelha), degeneração das criptas (seta preta cheia), ulcerações na mucosa (seta amarela) e intenso infiltrado inflamatório (seta verde) nos 3 grupos de animais (DSS, DSS+MLNC-AnxA1, ou AnxA1), quando comparados com o grupo *naive* (Figura 10).

Figura 10. Micrografia histológica obtida da região distal do intestino.

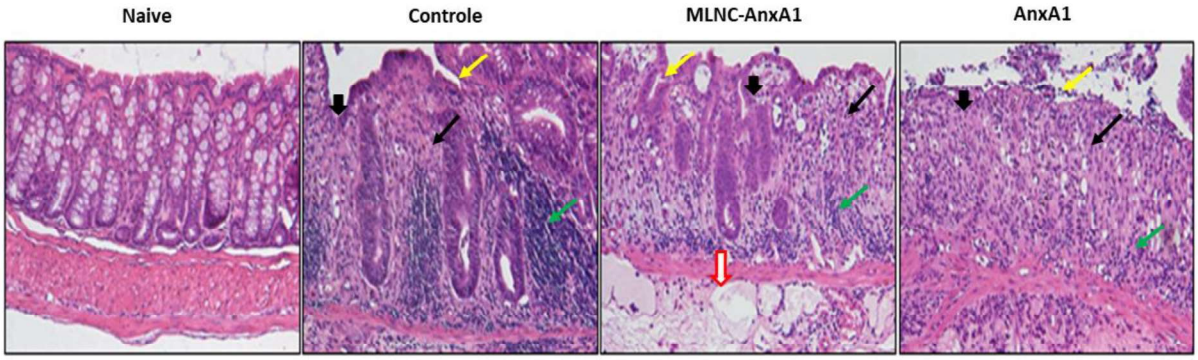

Secções histológicas com 4 µm de espessura, coradas com hematoxilina e eosina e observadas em um aumento de 10x demonstram a ausência de efeito terapêutico de MLNC-AnxA1 e AnxA1 sobre o intestino inflamado. Displasia (seta preta fina), edema (seta vermelha), degeneração das criptas (seta preta cheia), ulcerações na mucosa (seta amarela) e intenso infiltrado inflamatório (seta verde).

Administração intraperitoneal, mas não intravenosa, de MLNC-AnxA1 foi eficaz no tratamento da colite experimental

Dada a falta de eficácia terapêutica da administração oral do tratamento com MLNC-AnxA1 na colite experimental, optou-se por explorar outras vias de administração, incluindo intravenosa (i.v.) e intraperitoneal (i.p.). Foram estabelecidos cinco grupos experimentais, abrangendo diferentes condições: o grupo naive, sem DSS e tratamentos; o grupo controle, que recebeu apenas DSS; DSS+MLNC-AnxA1 (i.v.), DSS+MLNC-Anxa1 (i.p.) e DSS+AnxA1 (i.v.). Os protocolos de tratamento seguiram o mesmo cronograma previamente utilizado para a administração oral. Dentre os parâmetros clínicos analisados, observou-se redução significativa nos escores de fezes, de sangue e no IAD nos animais tratados com MLNC-AnxA1 (i.p.), quando comparados ao grupo controle que recebeu apenas DSS. O comprimento do intestino nos animais tratados com MLNC-AnxA1 (i.p.) foi equivalente ao grupo naive e significativamente maior do que nos animais que receberam apenas DSS, sugerindo que o tratamento com MLNC-AnxA1 i.p. favoreceu a recuperação tecidual após o dano causado pelo DSS. Surpreendentemente, a administração tanto de MLNC-AnxA1 quanto de AnxA1 via i.v. não apresentou diferenças significativas em nenhum dos parâmetros clínicos avaliados em comparação com o grupo controle (Figura 11A-F).

Figura 11. Painel clínico do tratamento i.p. e i.v. de MLNC-AnxA1.

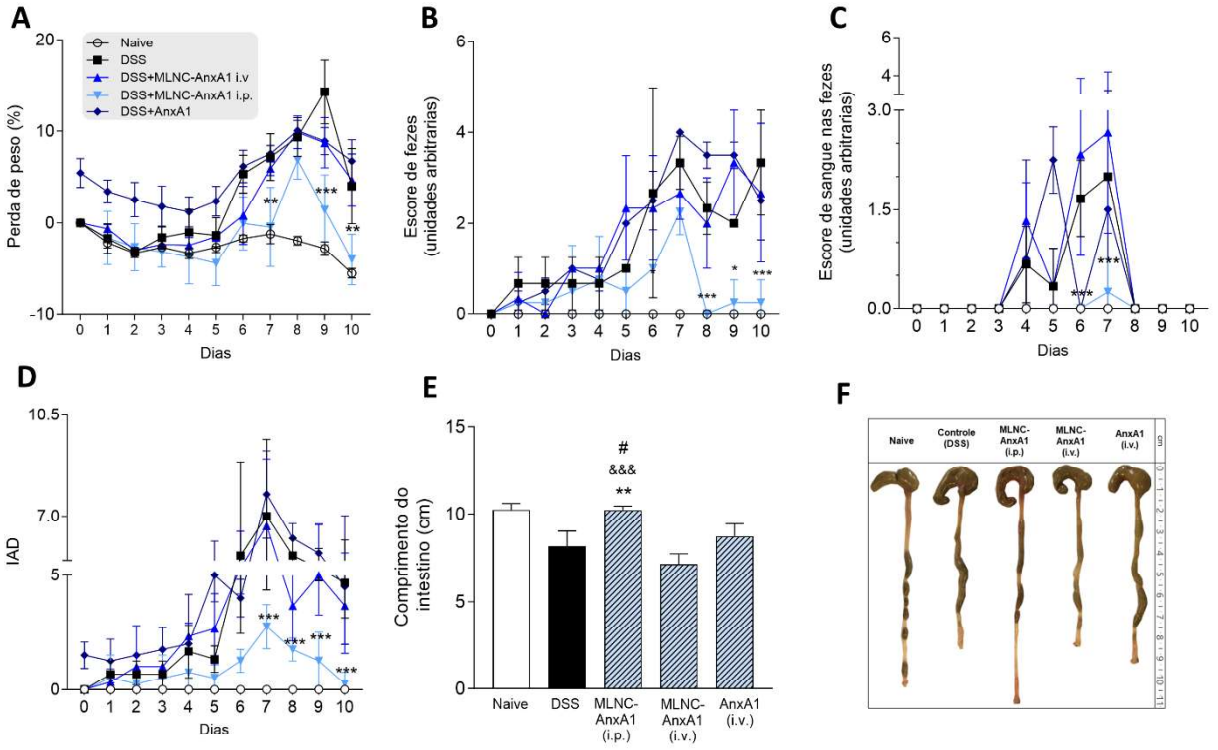

(A) Porcentagem de perda de peso; (B) Escore de fezes; (C) Escore de sangue; (D) IAD; (E) comprimento do intestino; (F) Imagens capturadas dos intestinos coletados no dia da eutanásia, comparando o comprimento entre cada grupo. Os dados são expressos como ± erro padrão da média de 6 animais por grupo *p < 0,05, **p <0,01, ***p<0,001 vs controle. $^{\&\&\&}$p<0,001 vs MLNC-AnxA1(i.v). $^{\#}$ p<0,05, $^{\#\#}$ p<0,01 vs naive.

Com base nos resultados previamente obtidos, um novo experimento de colite foi realziado com o intuito confirmar a efetividade do tratamento via i.p. e analisar o perfil celular da lâmina própria. O tratamento i.p. com MLNC-AnxA1 foi eficaz na redução dos sintomas da colite. Observou-se redução significativa na perda de peso, na diarreia e no índice de atividade da doença (Figura 12A-D), bem como a restauração da integridade estrutural do cólon, evidenciada pela recuperação do comprimento intestinal no 10º dia após a ingestão de DSS (Figura 12E-F).

Figura 12. Papel da terapia com MLNC-AnxA1 na atividade da colite induzida por DSS e na estrutura intestinal.

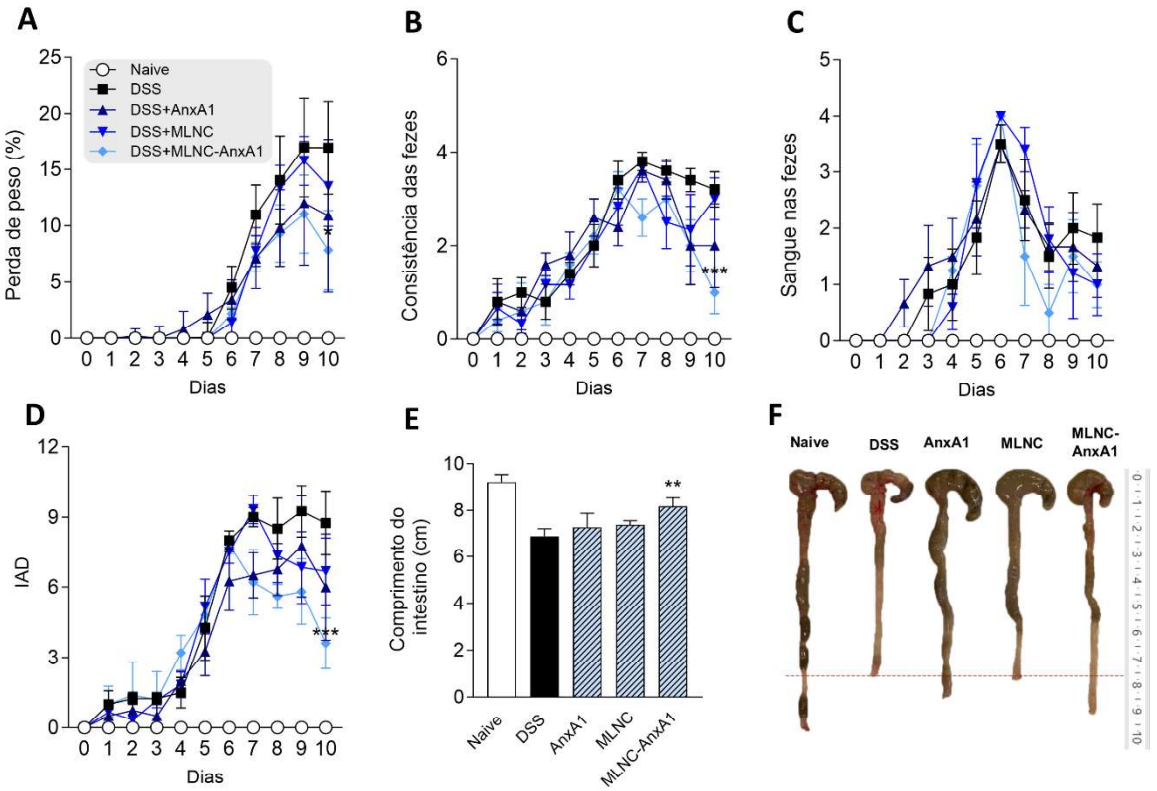

Os camundongos foram tratados com DSS 2% para desenvolver colite e foram tratados com rAnxA1 (12,5 µg/mL), MLNC (9,6x1011 partículas) ou MLNC-AnxA1 (9,6x1011 partículas/12,5 µg) entre os dias 6 e 9. (A) Percentual de perda de peso corporal; (B) Escore de diarreia; (C) Escore de sangue oculto; (D) DAI; (E) Comprimento intestinal; (F) Avaliação anatômica do cólon. n = 6 camundongos/grupo. *p < 0,05, **p < 0,01, ***p < 0,001 vs DSS.
LNC, nanocápsula com núcleo lipídico; MLNC, nanocápsula com núcleo lipídico multiparede; MLNC-AnxA1, nanocápsula de núcleo lipídico multiparede de complexo metálico; DAI, índice de atividade da doença.

A partir dos leucócitos extraídos da lâmina própria foi possível observar que a ingestão de DSS aumentou significativamente a porcentagem de neutrófilos ($Ly6G^+$; Figura 13A) e macrófagos (F4/80+; Figura 13B), refletindo aumento na quantidade de macrófagos do tipo M1 (F4/80/CD80+; Figura 13C). Nenhum dos tratamentos reduziu a quantidade de neutrófilos e macrófagos (Figura 13A e 13B); no entanto, o tratamento com MLNC-AnxA1 reduziu a quantidade de macrófagos do tipo M1 (F4/80/CD80+; Figura 13C), e tanto os tratamentos com AnxA1 quanto MLNC-AnxA1 aumentaram a quantidade de macrófagos do tipo M2 (F4/80/CD206+; Figura 13D).

Figura 13. MLNC-AnxA1 regula positivamente a polarização de macrófagos M2 na lâmina própria.

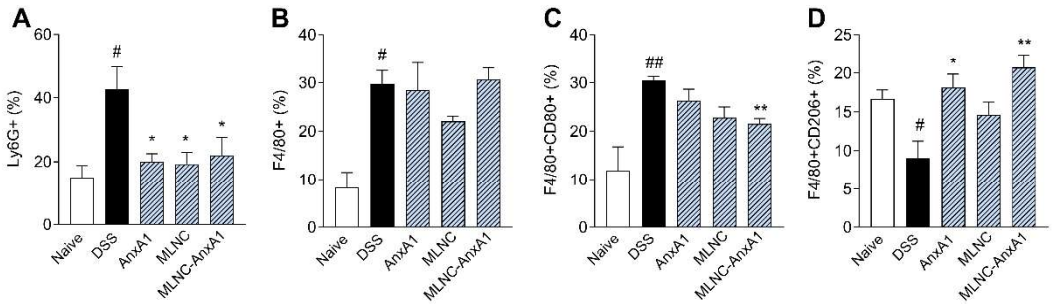

As células foram dissociadas por atividade enzimática da matriz extracelular e $2x10^5$ células foram utilizadas para marcação de anticorpos. (A) Ly6G+, (B) F4/80+, (C) F4/80+CD80, (D)+. F4/80+CD206+, n = 6 camundongos/grupo. *p<0,05, **p<0,01 vs DSS. #p <0,05, ##p <0,01 vs Naive.

O tratamento intraperitoneal com MLNC-AnxA1 recuperou a histoarquitetura e proteínas relacionadas à proliferação e estrutura epitelial

A ingestão de DSS causou danos severos ao tecido colônico de camundongos e atingiram a pontuação histológica mais alta em todos os parâmetros (Figura 14A): edema tecidual (linha pontilhada), displasia/alteração da histoarquitetura (seta preta), edema de cripta (seta amarela), infiltrados inflamatórios (seta branca) e úlceras (seta preta). Os camundongos tratados com MLNC apresentaram pontuações histológicas elevadas, semelhantes às do grupo DSS (Figuras 14G e H), enquanto o tratamento com AnxA1 promoveu melhorias nas pontuações histológicas, reduzindo alguns parâmetros como edema e displasia/alteração da histoarquitetura (Figura 14E e F). No entanto, apenas o tratamento com MLNC-AnxA1 levou à recuperação da histoarquitetura colônica durante a colite, diminuindo o edema de cripta, infiltrados inflamatórios e úlceras, em comparação ao grupo DSS (Figuras 14I e J). O grupo naive apresentou histoarquitetura normal, como esperado (Figura 14B).

Figura 14. Análise histopatológica da região proximal do cólon.

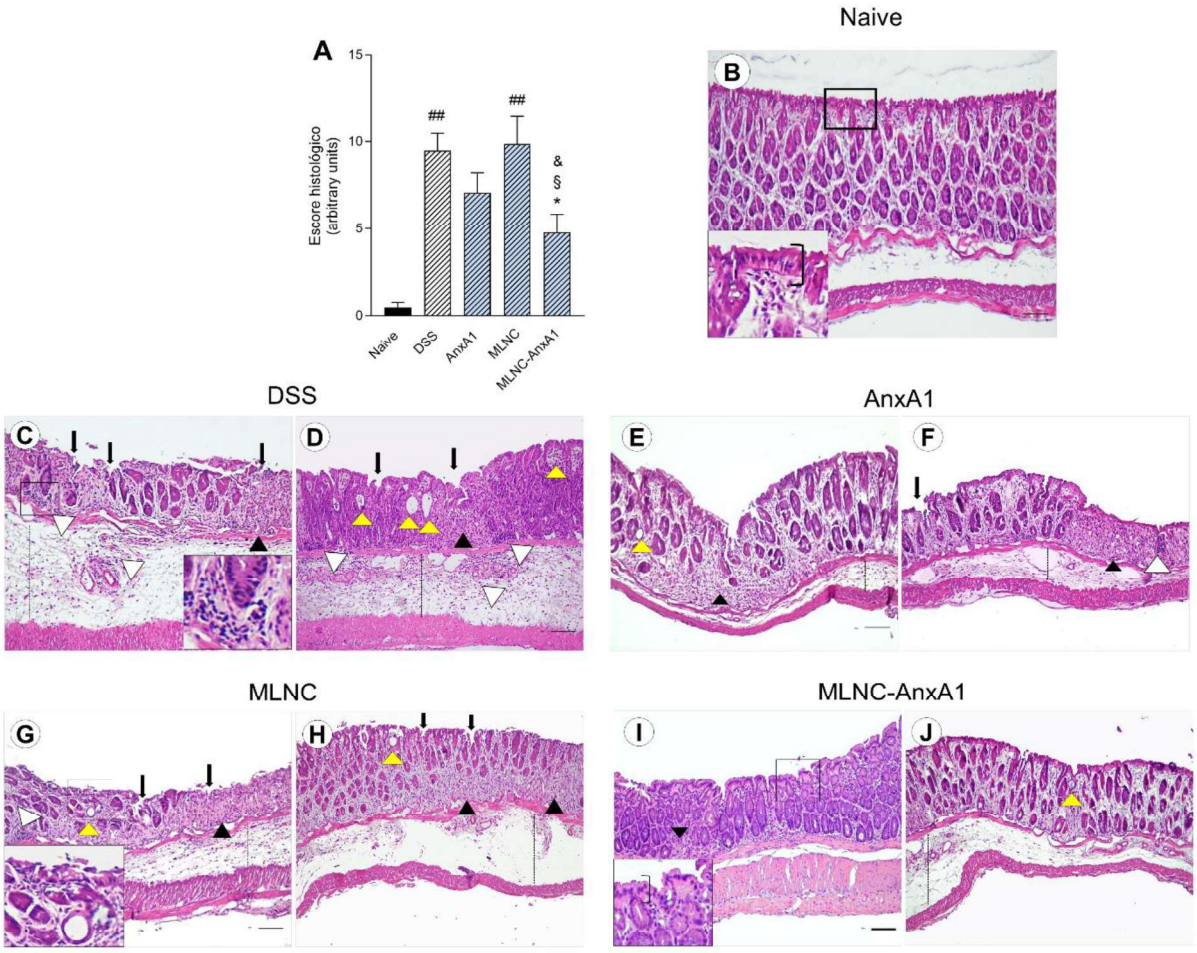

(A) Pontuação histopatológica representada por unidades arbitrárias. As secções foram avaliados cegamente e as alterações consideradas foram destacadas. Edema tecidual (linha pontilhada), displasia/histoarquitetura alterada (ponta de seta preta), edema de cripta (ponta de seta amarela), infiltrados inflamatórios (ponta de seta branca) e ulcerações (seta preta). (B) Naive apresentando histoarquitetura normal, com epitélio cilíndrico simples (quadrado preto); (C e D) grupo DSS; (E e F) grupo AnxA1; (G e H) grupo MLNC; (I e J) grupo MLNC-AnxA1. n = 6 camundongos/grupo. Barra de escala: 50 µm. Seções: 4 µm. Aumento óptico de 20x. *$p<0,05$ vs DSS. §$p<0,05$ vs AnxA1. &$p<0,05$ vs MLNC. ##$p<0,01$ vs Naive.

Ademais, a área marcada para as proteínas de junção epitelial Claudina-1 e ZO-1 foi reduzida nos camundongos DSS (Figura 15B e G) em comparação com o grupo naive (Figura 15A e F). Os tratamentos com AnxA1 e MLNC-AnxA1 restauraram a expressão de Claudina-1 (Figura 5H e J) e apenas MLNC-AnxA1 restaurou a expressão de ZO-1 (Figura 5E) em tecidos inflamados. O tratamento com MLNC apresentou o mesmo resultado que o DSS para a expressão de Claudina-1 (Figura 15I).

Figura 15. Efeitos do tratamento com MLNC-AnxA1 nas junções epiteliais.

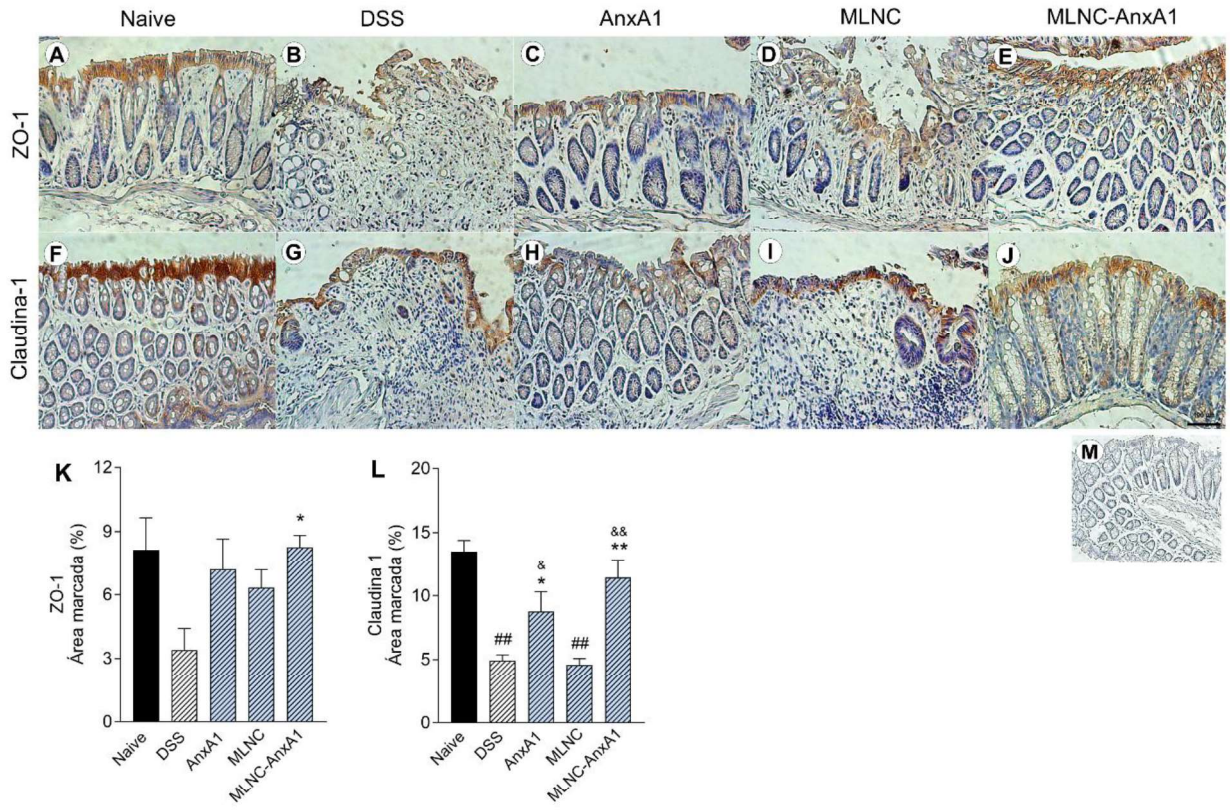

As secções da primeira linha representam a expressão de ZO-1 e as secções da segunda linha representam a expressão de Claudina 1 no tecido do cólon. (A e F) Grupo Naive; (B e G) grupo DSS; (C e H) grupo AnxA1; (D e I) grupo MLNC; (E e J) grupo MLNC-AnxA1. Os gráficos representam a porcentagem (%) de área marcada para ZO-1 (K) e Claudina1 (L). (M) Seção de controle. n=6 camundongos/grupo. Fotos: aumento óptico 40x. Secções: 4 µm. Barra de escala: 100 µm. *p<0,05, **p<0,01 vs DSS. &p <0,05, &&p <0,01 vs. #p<0,05, ##p<0,01 vs Naive.

Adicionalmente, o número de núcleos proliferativos na camada mucosa foi avaliado contando células positivas para PCNA e Ki67 (Figura 16F e L). Para ambos os alvos, apenas o tratamento com MLNC-AnxA1 aumentou o número de núcleos positivos, principalmente na região basal, o que juntamente com os demais resultados é indicativo de epitélio regenerativo (Figura 16E e K). Nos outros grupos de tratamento houve um baixo número e desorganização estrutural de células positivas para PCNA (Figura 16G, H, I e J) e Ki67 (Figura 16A, B, C e D), que se distribuíram irregularmente por toda a extensão das células epiteliais. Além disso, foi encontrada coloração aumentada na zona apical do tecido nos grupos tratados com DSS, AnxA1 ou MLNC, o que pode ser indicativo de áreas de displasia.

Figura 16. Efeitos do tratamento com MLNC-AnxA1 na regeneração e renovação epitelial no cólon danificado pela colite induzida por DSS.

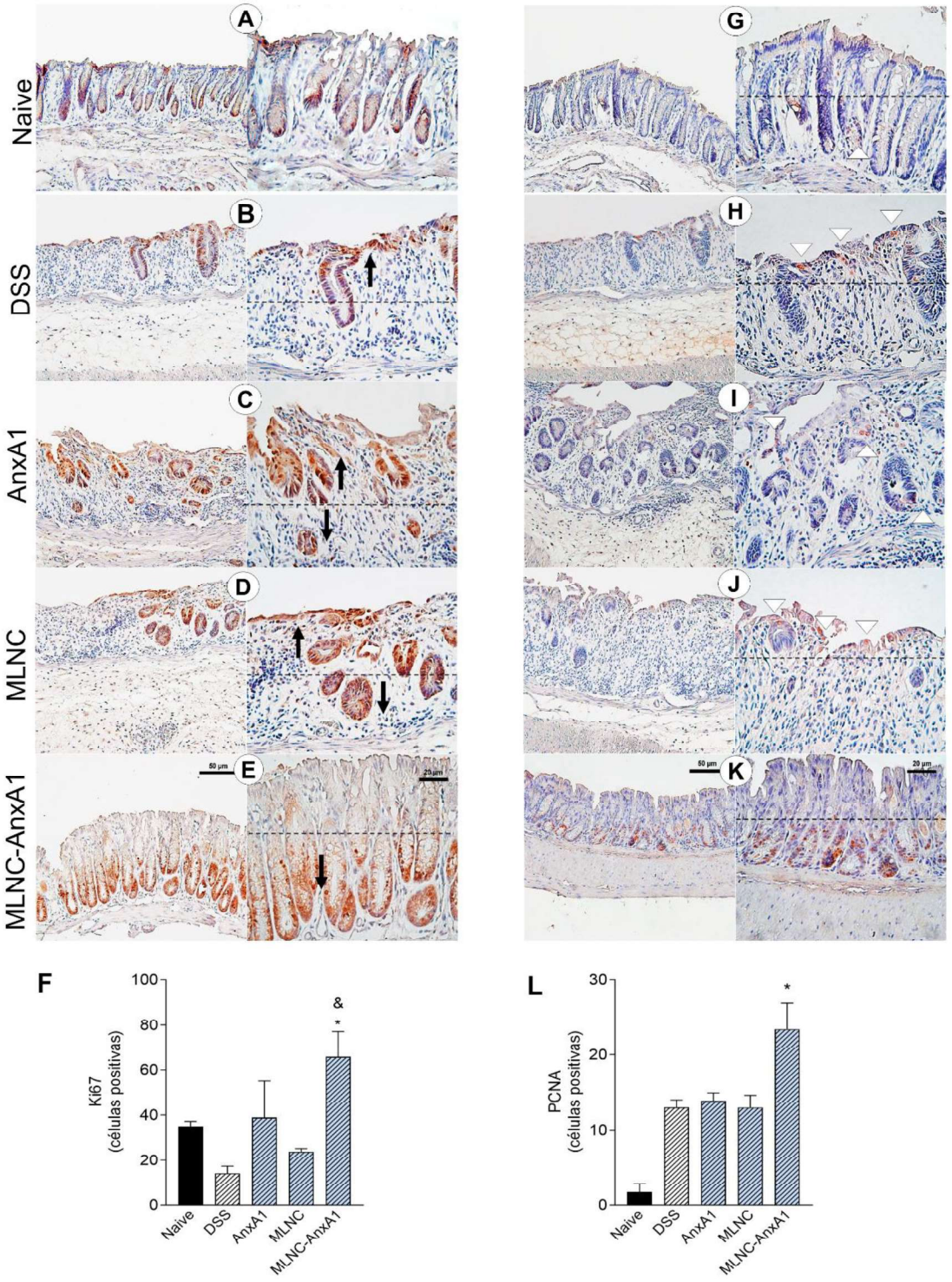

Ki67 e PCNA são representados em objetivas de 20x e 40x. (A e G) Grupo Naive; (B e H) grupo DSS; (C e I) grupo AnxA1; (D e J) grupo MLNC; (E e K) grupo MLNC-AnxA1. A quantificação dos núcleos proliferativos corados com Ki67 (F) e PCNA (L) são apresentadas nos gráficos. n=6 camundongos/grupo. Secções: 4 µm. Barras: 50 µm e 20 µm. * p<0,05 vs DSS. & p <0,05 vs MLNC.

MLNC-AnxA1 apresentou baixa citotoxicidade para macrófagos in vitro

Com base nos resultados *in vivo*, foram iniciados experimentos *in vitro* para elucidar o papel da MLNC e MLNC-AnxA1 sobre macrófagos murinos. Foram utilizadas células Raw 264.7 e, incialmente, foram realizados ensaios para verificar a viabilidade celular frente aos tratamentos. O ensaio de MTT, o qual avalia a função mitocondrial, foi utilizado como teste de triagem da viabilidade. Os resultados obtidos demonstraram que as concentrações de MLNC $68x10^9$ e $136x10^9$ e de MLNC-AnxA1 $77,5x10^9$ e $150x10^9$ apresentam atividade mitocondrial inferior a 75% após 48 horas, sugerindo efeito citotóxico. As reduções estão mostradas nas barras 3 e 4 da Figura 12, para os tratamentos com MNLC e MLNC+AnxA1. Os demais tratamentos com MLNC, MLNC-AnxA1 e AnxA1 apresentaram atividade mitocondrial superior a 75% em todos os tempos de tratamento (Figura 17).

Figura 17. Viabilidade celular relacionando a atividade mitocondrial pela técnica de redução do MTT

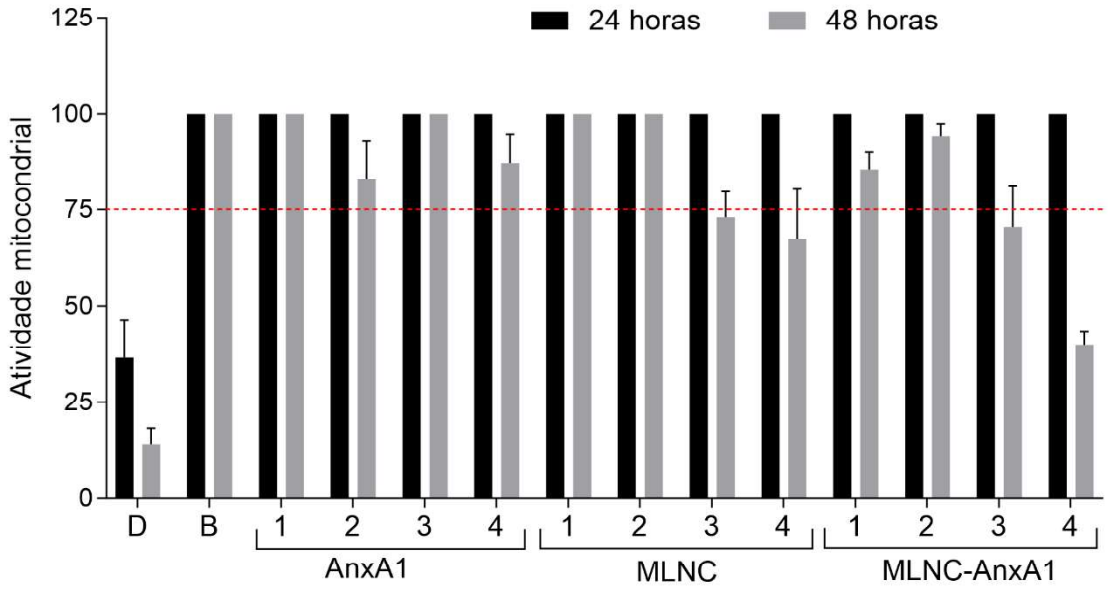

Os tratamentos da célula Raw 264.7 foram feitos com diferentes concentrações de AnxA1 (1) 50, (2) 500, (3) 2500 e (4) 5000 ng/mL; MLNC (1) $1,3x10^9$, (2) $13x10^9$, (3) $68x10^9$ e (4) $136x10^9$ partículas/mL) e MLNC-Anxa1 (1) $1,55x10^9$, (2) $15x10^9$, (3) $77,5x10^9$ e (4) $150x10^9$ partículas/mL) mantidas por três tempos: 24 e 48 horas. Como controle positivo para dano mitocondrial foi utilizado o DMSO (D) 5%. Como controle negativo foi utilizado PBS para resultado basal (B). Os dados são expressos como ± erro padrão da média de 4 experimentos individuais.

Para identificar o impacto na viabilidade celular, células Raw 264.7 foram tratadas com MLNC e MLNC-AnxA1 apenas nas concentrações que causaram menor

atividade mitocondrial no ensaio de MTT e com a maior concentração de AnxA1. Como marcadores de citotoxicidade foram utilizadas a dupla marcação de Anexina V e 7-AAD, e como marcador de célula viável foi utilizada a calceína 0,01 M. Observou-se viabilidade superior a 75% apenas no grupo que recebeu AnxA1 em todos os tempos analisados, enquanto os demais tratamentos com MLNC e MLNC-AnxA1 apresentaram redução da viabilidade celular. Os tratamentos com MLNC ($136x10^9$ partículas/mL (barra 3)) e MLNC-AnxA1 ($77,5x10^9$ (barra 3) e $50x10^9$ (barra 4) partículas/mL contendo, respectivamente, 2500 e 5000 ng/mL de AnxA1 na LMNC aumentaram significativamente a frequência de células necróticas e em apoptose tardia após incubação de 72 h (Figura 18).

Figura 18. MLNC e MLNC-AnxA1 promoveram aumento de células necróticas e em apoptose tardia após 72 horas de incubação.

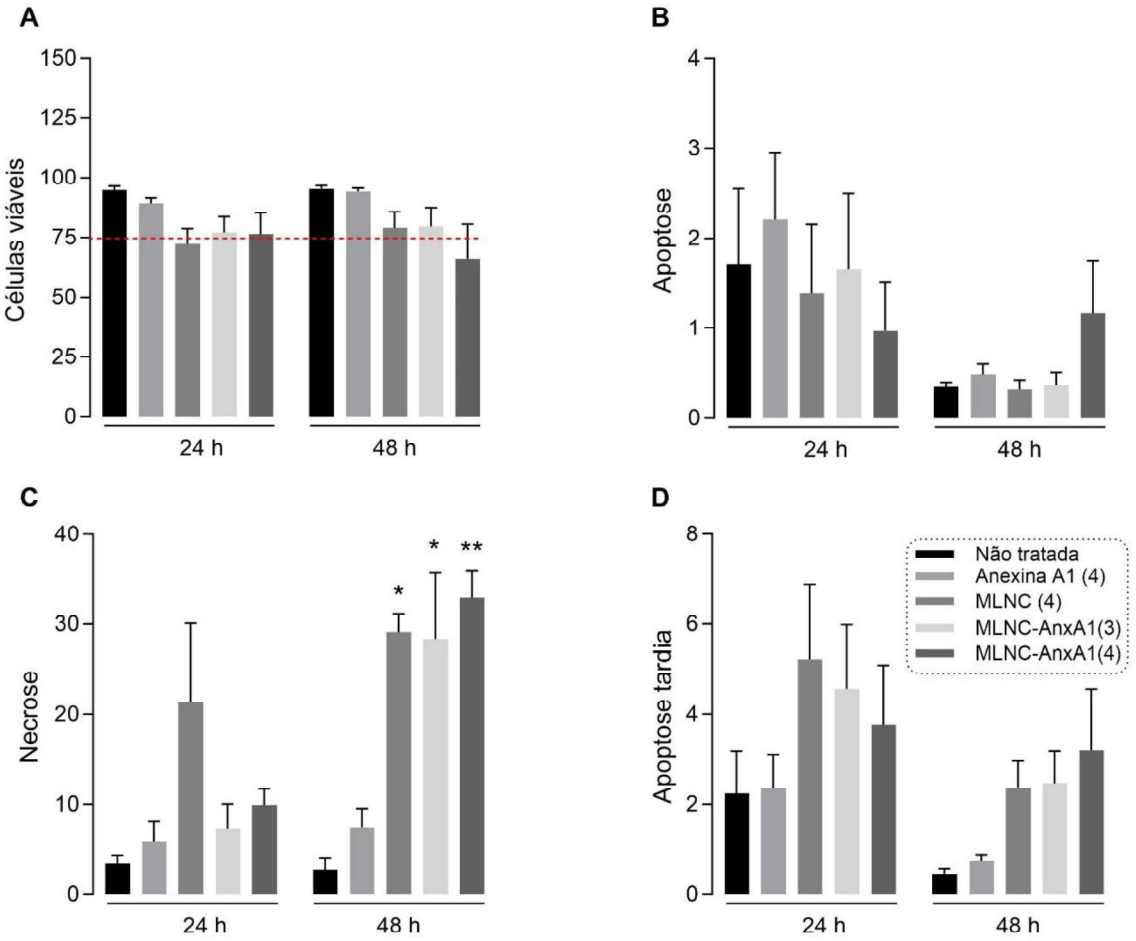

Células Raw 264.7 foram tratadas AnxA1, MLNC ou MLNC-AnxA1 e analisadas em diferentes tempos. (A) Porcentagem de células viáveis marcadas com calceína 0,01M; (B) Porcentagem de células em apoptose marcadas com Anexina V; (C) Porcentagem de células em necrose marcadas com 7-AAD;

(D) Porcentagem de células em apoptose tardia identificadas pela dupla marcação com anexina V e 7-AAD. *p<0,05 vs não tratado e **p<0,01 vs não tratado. N experimental = 4.

MLNC-AnxA1 foi internalizada por macrófagos e promoveu resposta anti-inflamatória

Os resultados obtidos no ensaio de citotoxicidade indicaram duas concentrações seguras para análise pelos ensaios de captação celular. As concentrações empregadas para avaliação da capacidade de captação celular foram de MLNC ($13x10^9$ partículas/mL) e MLNC-AnxA1 ($13x10^9$ partículas/mL). Utilizando a técnica de microscopia confocal de campo escuro de alta resolução, que demonstra maior refringência no interior celular é possível observar a presença de NPs no citoplasma celular, que ocorre pelo aumento da absorção de luz por essas NCs. As imagens obtidas demonstram internalização em células Raw 264.7 de MLNC após 2 horas de incubação, enquanto não foi observado internalização de MLNC-AnxA1 neste mesmo tempo de incubação. Após incubação com 24 horas foi possível perceber que ambas, MLNC e MLNC-AnxA1, se encontravam no interior celular, demonstrando que a presença de AnxA1 na estrutura da nanocápsula aumentou o tempo para captação celular (Figura 19).

Figura 19. Análise de uptake celular em células Raw 264.7 por CytoViva®

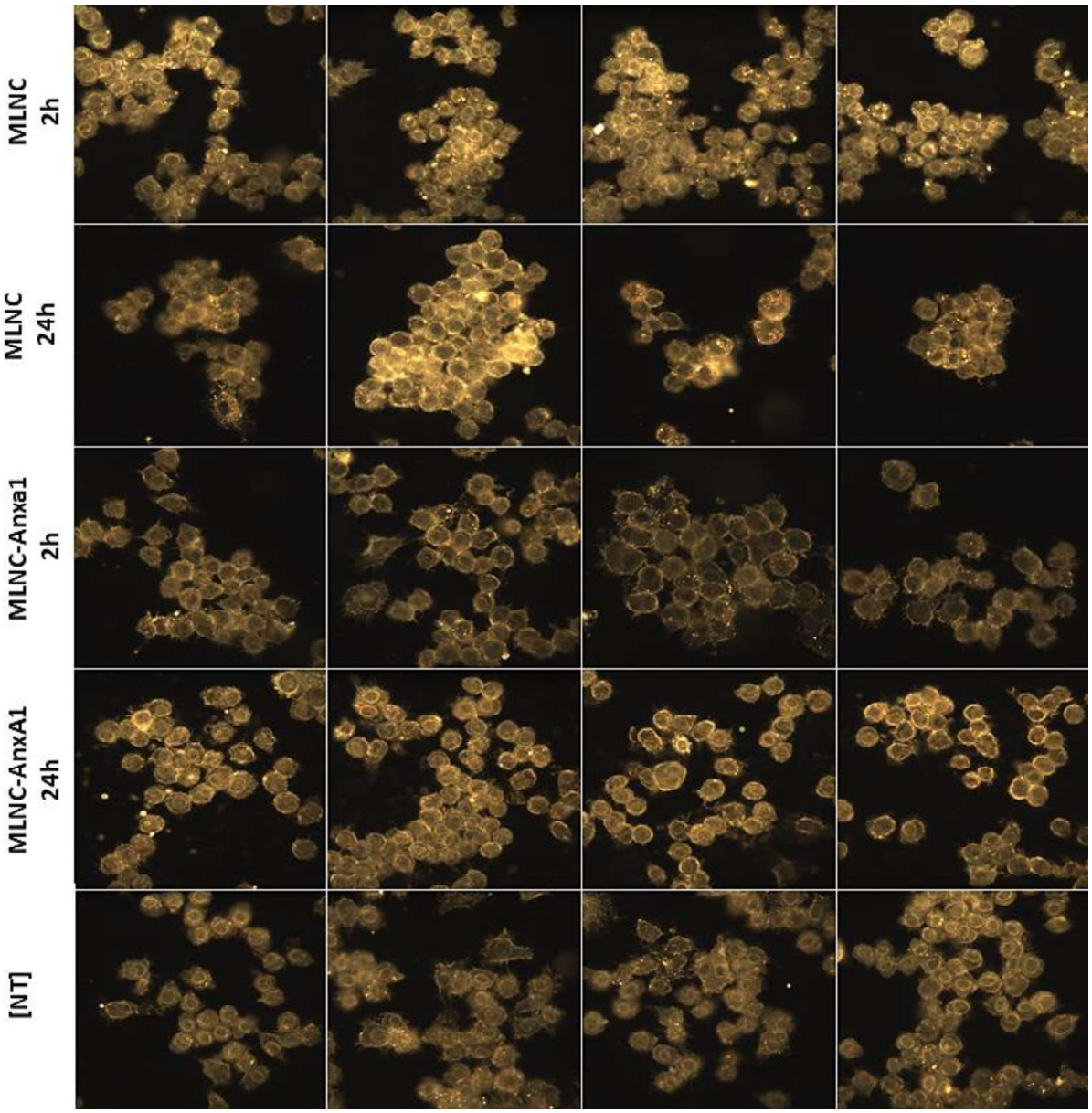

Células Raw 264.7 foram plaqueadas na concentração de $8x10^4$ células/poço e tratadas nos tempos de 2 e 24 horas com MLNC ($13x10^9$ partículas/mL) e MLNC-AnxA1 ($13x10^9$ partículas/mL). As células foram fotografadas usando o sistema de imagem CytoViva Ultra Resolution (CytoViva, Inc., AL, EUA) montado em um microscópio Olympus BX51 (ampliação de 1500 ×; Olympus Corporation, Tóquio, Japão) equipado com uma abertura numérica (NA) de fluorita 100 × óleo de íris de 0,6-1,30 objetiva e fonte de luz 75 W Xe e as imagens comparadas com o grupo não tratado ([NT]).

Com base nos resultados *in vivo* que nos conduziram para um efeito mais pronunciado do tratamento da MLNC-AnxA1 sobre macrófagos, foram realizados experimentos *in vitro* para elucidar o papel da MLNC e MLNC-AnxA1 sobre a polarização destas células. Macrófagos primários obtidos de medula óssea de camundongos C57Bl/6 foram diferenciados primeiramente em macrófagos pró-

inflamatório M1 pela adição de LPS (100 ng/mL). Após 48h de tratamento com AnxA1, MLNC ou MLNC-AnxA1, apenas MLNC-AnxA1 aumentou a porcentagem de células F4/80^{+}CD206^{+}, com fenótipo M2 (Figura 20A). Foi observada diminuição da porcentagem de células F4/80^{+}CD80^{+} apenas no tratamento com AnxA1 (500ng/mL) (Figura 20B). Ainda, o tratamento com MLNC-AnxA1 sobre macrófagos M1 foi capaz de aumentar significativamente a concentração de TGFβ (Figura 20C). Ademais, não houve diferença na concentração de IL-10 no sobrenadante celular (Figura 20D).

Figura 20. 3 MLNC-AnxA1 estimula a polarização de macrófagos com fenótipo M2

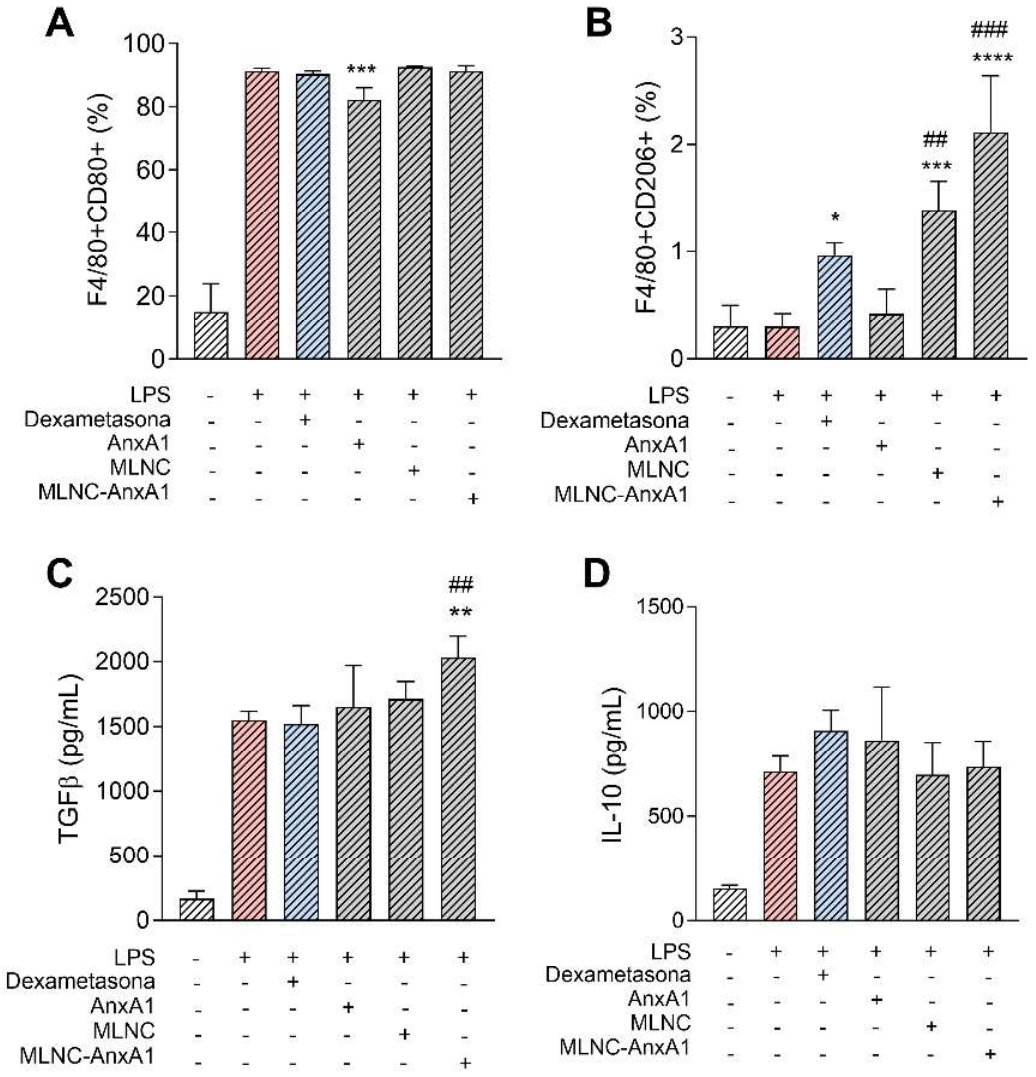

(A) Macrófagos F4/80+CD80+, (B) Macrófagos F4/80+CD206+, (C) TGFβ no sobrenadante de cultura, (D) IL-10 no sobrenadante de cultura. *p<0,05, **p<0,01 e ***p<0,001 vs LPS (100 ng/mL). #p<0,05 e ##p<0,01 vs Dexametasona (500 ng/mL).

Concluíndo, os dados apresentados acima mostraram a MLNC foi capaz de carrear a rAnxA1, e que a MLNC-AnxA1 foi efetiva para tratar a colite experimental pela via i.p. sendo que os efeitos observados foram mais significativos que os desencadeados pela rAnxA1 livre. No entanto, o projeto tinha como propósito carrear a AnxA1 ou seu peptídeo mimético Ac2-26 por via oral, como uma propsota de um tratamento não invasivo. Abaixo seguem os resultados das estratégias empregadas para atingir este objetivo e as eficácias terapêuticas obtidas.

SBA-15 funcionou como plataforma de entrega do peptídeo Ac-2-26 por via oral

A solução Ac2-26 é composta por partículas semelhantes a bastonetes

Ac2-26 foi disperso com sucesso em água deionizada a uma concentração de 6 mg/mL, permitindo experimentos futuros que poderiam exigir concentrações mais elevadas. É interessante observar que a amostra foi mais viscosa que a água pura e levemente turva, o que indicou a provável existência de grandes agregados, sendo essas características atenuadas após a diluição. Para analisar tais agregados, foram realizados ensaios de DLS. A Figura 21A mostra a função de autocorrelação obtida (círculos preenchidos em preto), C (τ) foi ajustado com um metodo adequado para o modelo (no caso, *Non-Negatively constrained Least Squares*, NNLS). A partir do ajuste satisfatório, avaliou-se a distribuição de tamanho ponderada por intensidade, volume e número (inseridos na Figura 1A). A intensidade espalhada é diretamente proporcional ao quadrado do volume da particula (ou, de maneira equivalente, ao seu raio/diametro elevado a sexta potencia). Conforme observado, existem três populações de partículas com tamanhos (23 ± 1) nm, (109 ± 28) nm e (58 ± 18) μm, sendo a primeira a mais numerosa.

Considerando os resultados, nenhum desses conjuntos corresponde ao peptídeo sozinho, com apenas 3.089,46 Da de peso molecular, conforme informado pelo fabricante, mas sim à sua estrutura supramolecular automontada e até mesmo agregados. Para confirmar esta característica, foram realizados experimentos SAXS na mesma amostra usada para DLS.

Figura 21. Parâmetros físicos de SBA-15, Ac2-26 e SBA-16-Ac2-26

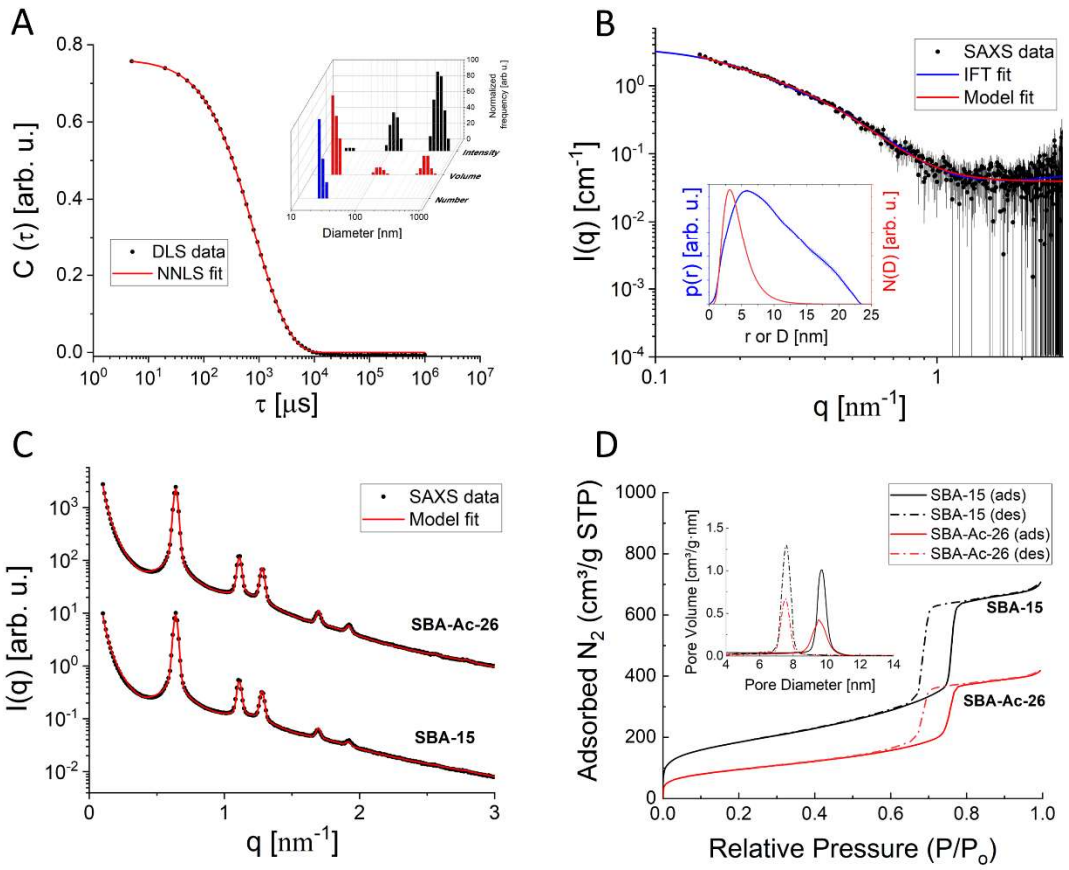

(A) Função de autocorrelação (círculos pretos preenchidos) ajustada pelo método NNLS (linha contínua). Inserção: Distribuições de diâmetro hidrodinâmico do peptídeo ponderadas por número, volume e intensidade. (B) Dados SAXS do peptídeo em solução (círculos preenchidos) ajustados pelo método IFT (linha contínua azul) e o modelo do cilindro (linha contínua vermelha). Inserção: A função p(r) obtida, do IFT, e a função de distribuição de tamanho do raio do cilindro, N(D), do ajuste do modelo. (C) Dados de SAXS (círculos pretos preenchidos) de SBA-15 pura e de SBA-15 incorporada com Ac2-26 (amostra SBA15-Ac2-26) ajustado pelo modelo SBA-15 (linha contínua vermelha). As curvas foram deslocadas verticalmente para uma visualização mais clara. (D) Dados de NAI de SBA-15 pura e SBA-15 incorporado com Ac2-26 (amostra SBA-Ac-26). Inserção: Distribuição do tamanho dos poros (PSD, adsorção e dessorção).

Os dados obtidos a partir da análise de SAXS estão mostrados na Figura 21B (círculos preenchidos em preto) e foram ajustados pela *Indirect Fourier Transform* (IFT), que permite obtermos informações da partícula no espaco real, representado pela função de distribuição de distância de pares, implementada no software WIFT (GLATTER, 1977). A partir do ajuste (linha contínua azul), foi obtida a chamada distribuição de distâncias de pares, p(r), (inserção da Figura 21B, linha contínua azul), que fornece o maior comprimento da partícula de ~23 nm (onde p(r) ≈ 0), compatível com os resultados do DLS relativos à população com os menores objetos. Além disso, a distribuição de distâncias de pares, p(r), sugeriu a presença de partículas alongadas,

com formato de bastonete. Neste contexto, foi realizado um teste no qual os dados de SAXS foram ajustados a um modelo de cilindro simples. Também foi utilizada uma distribuição de tamanho log normal para os valores dos raios, como em trabalhos anteriores (Pinto Oliveira, 2011). O ajuste satisfatório obtido (Figura 21B, linha contínua vermelha), corroborou a hipótese do formato cilíndrico. Neste caso, os objetos possuem raio médio de ~3 nm, de acordo com a distribuição de tamanho obtida (inserção da Figura 21B, linha vermelha contínua) e comprimento de ~80 nm. O primeiro valor ficou fora do comprimento da escala definido pelo valor mínimo da faixa q, portanto não pode ser determinado com precisão. Assim, o valor determinado pela função p(r), ~23 nm, foi assumido como o comprimento do cilindro. Em suma, os resultados de SAXS e DLS sugerem arranjo do peptídeo em partículas em forma de bastonete com comprimento de 23 nm e diâmetro de 6 nm, aproximadamente.

Micropartícula mesoporosa SBA-15 foi eficiente para ancorar o Ac2-26

A incorporação do peptídeo a SBA-15 foi de cerca de 88,8% ± 1,2 (n=4), medida pelo método de ligação ao corante de Bradford. As medições de SAXS foram realizadas em amostras seca de SBA-15 e SBA-15-Ac2-26 (Figura 21C). Para descrever quantitativamente sua nanoestrutura e eventuais diferenças, procedemos à análise dos dados utilizando o modelo totalmente detalhado por Losito et al 2021a. Os principais parâmetros de ajuste, bem como seus valores, estão resumidos na Tabela 8, e seu significado é explicado a seguir: R e T correspondem ao raio do núcleo e à espessura da parede, respectivamente, do cilindro núcleo-parede que modela os mesoporos, sendo σ_{rel} o desvio padrão compartilhado da distribuição de tamanho log-normal de R e T. O parâmetro $\frac{\Delta\rho_{núcleo}}{\Delta\rho_{parede}}$ informa sobre a densidade eletrônica de contraste do núcleo em relação à parede. Para idealmente "vazio", $\frac{\Delta\rho_{core}}{\Delta\rho_{shell}} = 0$. Diferente de, $\frac{\Delta\rho_{core}}{\Delta\rho_{shell}} \neq 0$ é um indício da existência de algum material no interior dos mesoporos. a é o parâmetro de rede e σ_a quantifica a distorção da rede em relação a uma rede hexagonal 2D ideal (para uma rede ideal , $\sigma_a = 0$). Por fim, AP é o fator de Porod (proporcional a q^{-4} lei decadente) e monitora a presença de grandes agregados, enquanto o fator $R_{G_{polymer}}$ analisa o contraste de densidade eletrônica relativa e quantifica a presença de material dentro dos mesoporos. Como esperado, ambas as curvas possuem parâmetros estruturais com valores próximos, exceto o

parâmetro AP. Em comparação ao SBA-15 puro, seu valor aumentou 3 vezes com a adição do peptídeo, o que sugere a presença de material na macroporosidade do SBA-15. Além disso, o parâmetro $\Delta\rho_{núcleo}/\Delta\rho_{parede}$ aumentou ligeiramente com a incorporação do peptídeo, indicando que uma fração do material está dentro dos mesoporos. Considerando que a porcentagem de ancoragem peptídica foi de 88%, conforme discutido anteriormente, possivelmente a maior parte do Ac2-26, em sua forma agregada/automontada, está na macroporosidade SBA-15.

Para obter mais informações sobre o preenchimento dos poros de SBA-15 pelo peptídeo, foram realizados experimentos NAI. Os resultados de sorção relacionados às amostras de SBA-15, puras e carregadas com Ac2-26 (peptídeo:sílica, 1:35% em peso), são mostrados na Figura 21D. A isoterma de ambas as amostras mostra *loops* de histerese com ramificações acentuadas de adsorção e dessorção, o que indica uma estreita distribuição de tamanho de poros. As distribuições de tamanho dos poros tanto para a adsorção quanto para a dessorção foi obtido com base nos métodos Brunauer–Emmett–Teller (BET) e Barrett–Joyner–Halenda (BJH) (inserção da Figura 21D) juntamente com outros parâmetros resumidos na Tabela 7. Embora a distribuição do tamanho dos poros de ambas as amostras seja muito semelhante, os dados apresentados na Tabela 7 mostram uma redução de cerca de 55% na área superficial (mesopicroporosidade interna x macroporosidade externa) após a incorporação do peptídeo na SBA-15. Considerando também a redução de ~62% no volume disponível dos mesoporos, o que pode indicar seu preenchimento ou bloqueio da entrada dos poros. Podemos concluir assim que o peptídeo está localizado dentro da porosidade da sílica (mesoporos e/ou macroporos).

Tabela 8. Propriedades estruturais e texturais das amostras de SBA-15

Técnica	Parâmetro físico avaliado em cada técnica	Amostras	
		SBA-15	SBA-Ac2-26
SAXS	$R\ [nm]$	4.37(1)	4.37(9)
	$T\ [nm]$	2.56(3)	2.53(2)
	$\sigma_{rel}\ [\%]$	7.2(2)	7.8(9)
	$\frac{\Delta\rho_{core}}{\Delta\rho_{shell}}$	0.000(1)	0.006(1)
	$a\ [nm]$	11.33(1)	11.33(1)
	$\sigma_a\ [nm]$	0.044(6)	0.041(4)
	$AP \times 10^{-8}$	7.2(7)	20.8(2)
	$R_{G_{polymer}}$ [Å]	6.7(6)	8.1(5)
NAI	BET área superficial $[m^2/g]$	768 (1)	342 (1)
	Diminuição área superficial [%]	***	55
	BJH Volume do mesoporo $[cm^3/g]$	1.74 (1)	0.65 (1)
	Preenchimento do poro [%]	***	62
	Diâmetro médio dos poros(ads) $[nm]$	9.4 (1)	9.5 (1)
	Diâmetro médio dos poros(des) $[nm]$	7.5 (1)	7.6 (1)
	Espessura da parede $[nm]$	1.9 (1)	1.8 (1)

Amostra SBA-15 e SBA-15 incorporada com Ac2-26 (amostra SBA-Ac-26) obtida pelas técnicas SAXS e NAI. O erro está apresentado entre parênteses.

Em conjunto com os resultados do SAXS, a hipótese de que provavelmente a maior parte do peptídeo estava na macroporosidade SBA-15 foi reforçada. Além disso, ficou evidente a possibilidade de aumento da concentração do peptídeo, com o cuidado de preservar uma distribuição homogênea, uma vez que ainda existia “espaço livre” na porosidade do SBA-15.

SBA-15 não causou citotoxicidade e liberou Ac2-26

A marcação com fluoróforo foi empregada para investigar a captação de SBA-15 e a liberação do Ac2-26 pelo SBA-15 nas células. A medição SAXS mostrou a incorporação do fluoróforo ao SBA-15 sem alterações robustas no perfil de espalhamento do SBA-15 (Figura 22).

Figura 22. Dados de análise de SAXS para SBA15-FITC

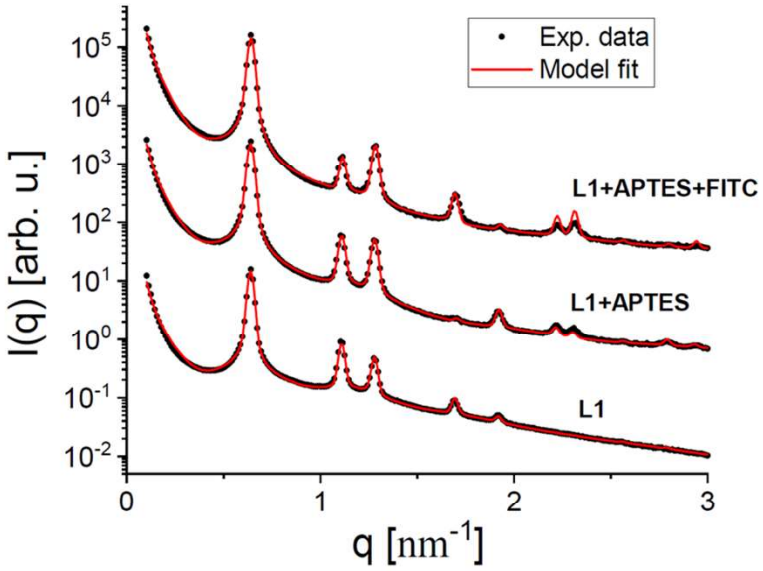

Dados de SAXS (círculos pretos preenchidos) de SBA-15 pura e de SBA-15 incorporada com FITC (amostra SBA-FITC) ajustado pelo modelo SBA-15 (linha contínua vermelha). L1:corresponde ao nome do lote de SBA-15 utilizado. APTES: 3-aminopropiltrimetoxissilano

A captação de SBA-15 por células epiteliais colônicas diferenciadas demonstrou baixa potencial de internalização de micropartículas (Figura 23A e D) bem como em organoides colônicos 3D (Figura 23B), que indicam que SBA-15 pode ser pouco absorvido no intestino. Além disso, análises adicionais de citometria de fluxo confirmaram esses dados (dados não apresentados). No entanto, o aumento da permeabilidade epitelial ou mesmo a ruptura da barreira epitelial que ocorre durante a inflamação intestinal pode favorecer o influxo de micropartículas para o tecido.

Os dados apresentados na Figura 23C mostraram que os macrófagos murinos J774 internalizaram a micropartícula por fagocitose, uma vez que a porcentagem de ingestão foi bloqueada pela citocalasina D com uma concentração de 20 µM. A captação de micropartículas aumentou com o tempo (Figura 23E e F) e não causou citotoxicidade até 48 horas de incubação (Figura 23G).

Para avaliar a entrega de Ac2-26 por SBA-15, as células epiteliais Caco-2 foram incubadas com SBA-15 marcado com Ac2-26-Cy5.5. O ensaio de citometria de fluxo detectou fluorescência emitida por Ac2-26-Cy5.5 nas células epiteliais após 30 minutos de incubação, que aumentou progressivamente após 6 horas de incubação (Figura 23H). Além disso, dados semelhantes foram encontrados em macrófagos Raw 264.7, o que também evidencia a capacidade do SBA-15 de entregar o peptídeo em fagócitos (Figura 23H).

Figura 23. Internalização de SBA-15-FITC e SBA-15-Ac2-26-Cy5.5

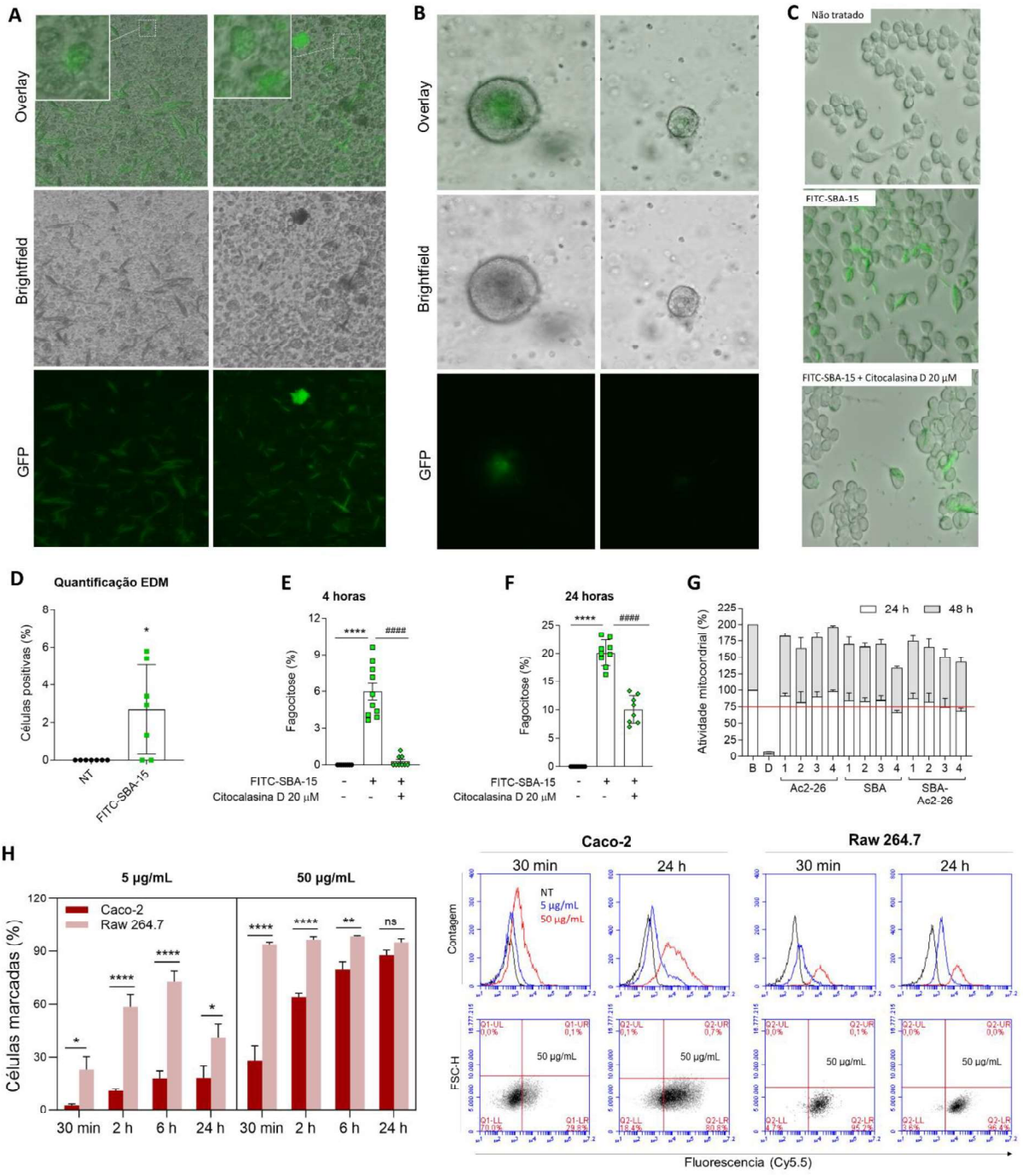

(A) Fotos representativas de EDMs diferenciados tratados com FITC-SBA por 24 horas. (D) A porcentagem de absorção de micropartículas foi determinada. (B) Imagens representativas mostraram organoides murinos 3D desafiados com micropartículas e cultivados por 6 dias. (C) Imagens representativas mostraram macrófagos J774 desafiados ou não com micropartículas por 24 horas na presença ou ausência de inibidores de fagocitose (citocalasina D). (E) e (F) representam a quantificação da captação de FITC-SBA após 4 horas (4h) e 24 horas (24h) após o tratamento. G Em todas as imagens, o verde dentro da célula representa a internalização das micropartículas. Citotoxicidade por ensaio MTT utilizando macrófagos murinos Raw 264.7. Concentrações de Ac2-26, SBA e Ac2-26-SBA 1, 2, 3 e 4 correspondentes a 0,5, 5, 10 e 50 µg/mL, respectivamente. H Gráfico representativo mostrando a porcentagem de células Caco-2 ou Raw 264.7 positivas para Ac2-26-Cy5 em diferentes momentos: 30 minutos (30min), 2 horas, 6 horas e 24 horas. O lado inferior esquerdo representa a mediana do histograma Caco-2 e Raw 264.7 de fluorescência (linha superior) e a porcentagem usando

altura de dispersão direta (FSC-H) versus emissão de fluorescência para Cy5. Os dados foram obtidos do software de citometria de fluxo Accuri C6 após 30 min e 24 horas. D conforme determinado pelo teste t de Student paramétrico. E e F conforme determinado por ANOVA unidirecional e comparações múltiplas de Tukey. H determinou comparações múltiplas de ANOVA Two-Way e Tukey. *<p 0,05, **<p 0,01 e ****p< 0,0001. ####p< 0,0001.

Eudragit-SBA-15 foi distribuído no trato gastrointestinal (TGI) e entregou o peptídeo Ac2-26 no intestino

A análise de dissolução *in vitro* mostrou que o peptídeo Ac2-26 foi liberado do Eudragit-SBA-15 em uma solução de pH próximo ao encontrado no duodeno (Figura 25).

Figura 24. Ensaio de liberação do peptídeo em diferentes pH

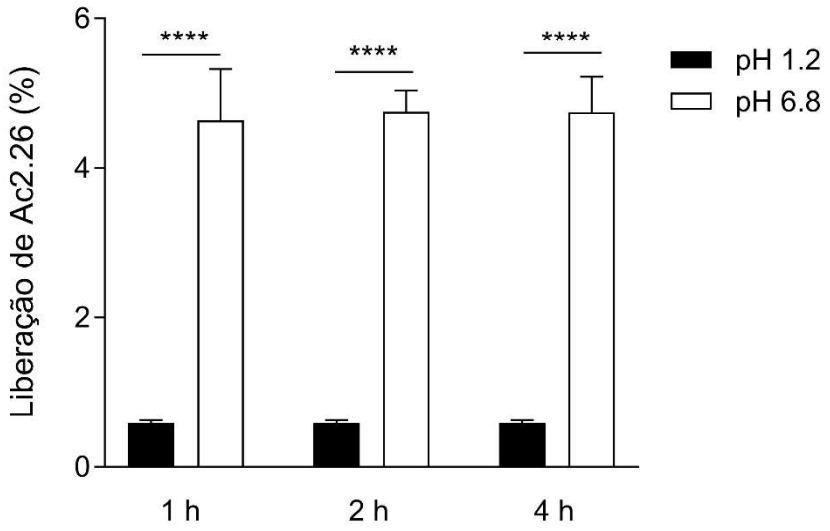

Eud-SBA-15-Ac2-26 foi colocado em solução com diferentes pH e a liberação de Ac2-26 pela SBA-15 quantificada. O resultado está expresso em porcentagem de liberação de peptídeo em relação a concentração inicial de 2 mg. **** p< 0,0001 vs pH 1,2.

Para confirmar se o peptídeo foi entregue no intestino, Eudragit-SBA-15-Ac2-26-Cy.5.5 foi administrado por via oral, e a intensidade da fluorescência foi alcançada no TGI após 3 horas de administração, permanecendo por até 8 horas de análise (Figura 25A).

Para avaliar o trânsito de Eudragit-FITC-SBA-15 nas condições do TGI e a capacidade de atingir o intestino grosso, rastreamos o tratamento por 6 e 18 horas após a administração oral em camundongos. A medição dos sinais detectou o Eudragit-FITC-SBA-15 nos intestinos delgado e grosso às 6 horas e 18 horas após a administração, respectivamente (Figura 26B). Os dados obtidos mostraram que o

Eudragit-SBA-15 permanece no TGI durante pelo menos 18 horas, o que pode levar à libertação sustentada do peptídeo no intestino, o que pode ser um fator relevante e desejado para a eficácia terapêutica do Eudragit-SBA-15-Ac2-26 por via oral em DII.

Figura 25. Biodistribuição ao longo do TGI de Eudragit-SBA15-Ac2-26Cy5.5 Eudragit-FITC-SBA-15

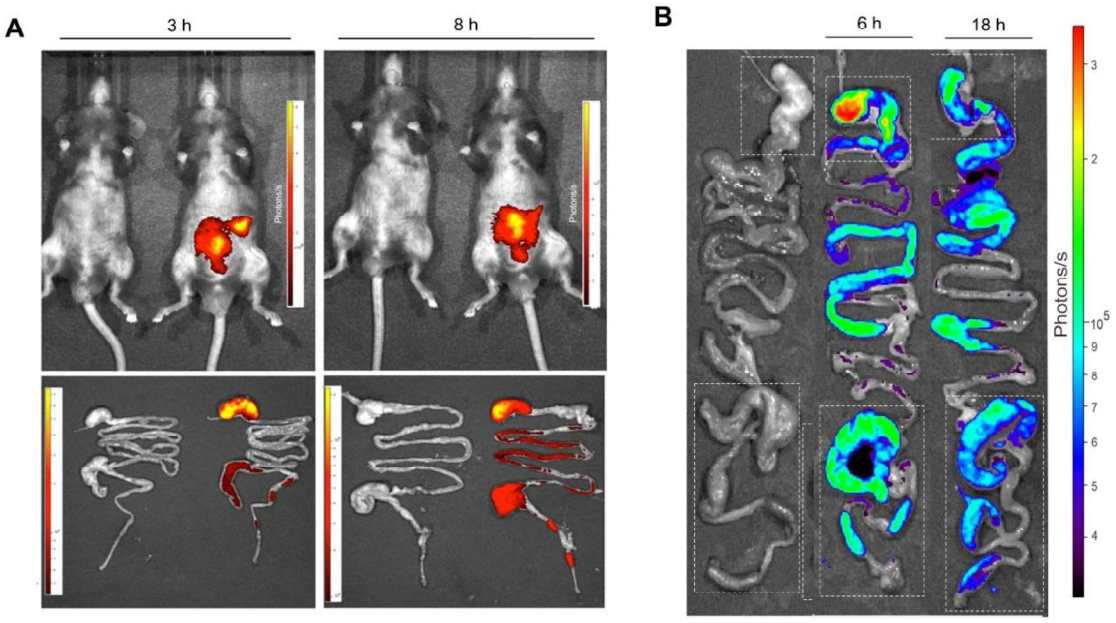

Os camundongos foram tratados por via oral e a intensidade da distribuição é representada por fótons/s. (A) distribuição de Eudragit-SBA15-Ac2-26Cy5.5 foi analisada após 3 horas e 8 horas *in vivo* (parte superior) e o TGI analisado separadamente *ex vivo* (parte inferior) nos mesmos tempos. A cor amarela representa a maior intensidade no tecido. (B) Biodistribuição de Eudragit-FITC-SBA-15 *ex vivo* ao longo do TGI após 6 horas e 18 horas. A cor vermelha representa a maior intensidade no tecido.

Administração oral do Eudragit-SBA15-Ac2-26 reduziu sintomas clínicos e inflamação no intestino

A administração de DSS por via oral desencadeou o pico da doença no dia 6, e a retirada do DSS resulta na recuperação inicial do tecido a partir do dia 10. Assim, o tratamento oral com Eudragit-SBA-15-Ac2-26 começou no pico da doença (dia 6) e foi mantida até o início da fase de recuperação (dia 10). Os dados obtidos mostraram que a administração oral de Eudragit-SBA-15-Ac2-26 preveniu a perda de peso e induziu a recuperação do comprimento do cólon, levando a um menor DAI, apesar de não alterar a consistência e sangue nas fezes (Figura 26A-F).

Figura 26. Perfil clínicode camundongos com colite induzida por DSS tratados com Eudragit-SBA-15 ou Eudragit-SBA15-Ac2-26

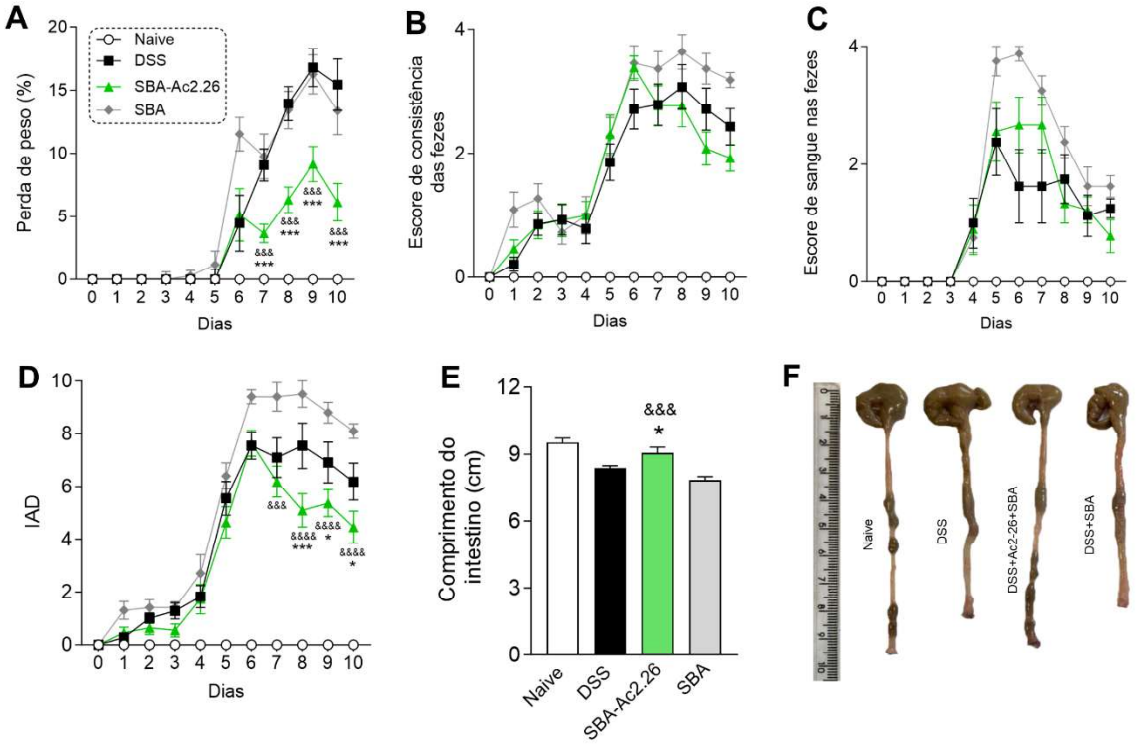

(A) Porcentagem de perda de peso corporal; (B) Escore de consistência das fezes; (C) Escore de sangue nas fezes; (D) IAD; (E) Medida de comprimento do cólon; (F) Avaliação anatômica do cólon. n = 10 animais/grupo. * p<0,05, ** p < 0,01, *** p< 0,001 vs DSS. & p<0.05, && p<0,01, &&& p< 0.001 vs Eudragit-SBA-15.

Ainda, o tratamento inibiu o influxo de neutrófilos e macrófagos para o intestino inflamado (Figura 27A e B), reduziu a secreção das citocinas inflamatórias TNFα e CXCL-1 e aumentou a secreção da citocina anti-inflamatória IL-10 (Figura 27C-E). Os efeitos benéficos do tratamento foram devidos à carga de Ac2-26, uma vez que o tratamento com Eudragit-SBA-15 não preveniu sintomas clínicos e parâmetros de inflamação (Figura 26A-F).

Figura 27. Perfil celular e secretório do cólon

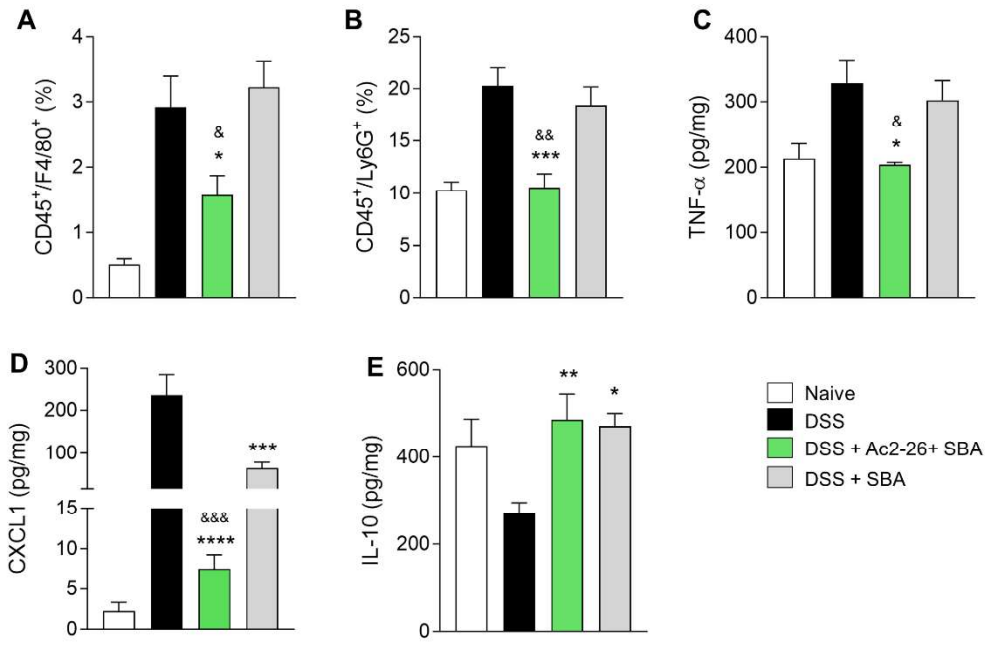

(A) Porcentagem de macrófagos isolados da lamina propria ($CD45^+/F4/80^+$); (B) Porcentagem de neutrófilos isolados da lâmina propria ($CD45^+/Ly6G^+$); (C) TNF-α; (D) CXCL-1; (E) IL-10. n = 10 animais/grupo. * p<0.05, **p<0.01, ***p< 0.001, ****p<0,0001 vs DSS. $^{\&}$p<0,05, $^{\&\&}$p<0,01, $^{\&\&\&}$p<0,001 vs Eudragit-SBA-15.

Administração oral do Eudragit-SBA15-Ac2-26 recuperou a histoarquitetura intestinal

A análise histológica do tecido mostrou que a administração de DSS induziu úlceras, abscessos nas criptas, degeneração hidrópica vacuolar, edema submucoso e infiltrado maciço de células inflamatórias na mucosa/submucosa. Essas alterações foram reduzidas e a arquitetura histológica do cólon foi recuperada pelo tratamento oral com Eudragit-SBA-15-Ac2-26 (Figura 28A).

Para descrever os mecanismos envolvidos na proteção da arquitetura intestinal causada pelo tratamento com Eudargit-SBA-15-Ac2-26, a expressão de marcadores de regeneração tecidual foi realizada por imuno-histoquímica. A administração de DSS levou a uma menor expressão de claudina-1, um componente importante das junções epiteliais, essencial para a integridade da barreira intestinal; redução do marcador mucina-2, associado às células caliciformes, levando à secreção prejudicada de muco; reduziu a proliferação de células epiteliais e reduziu a quantidade de macrófagos M2 anti-inflamatórios no tecido. O tratamento oral com

Eudragit-SBA-15-Ac2-26 resgatou todos estes prejuízos na arquitetura do tecido causada pela administração do DSS (Figura 28B-E).

Figura 28. Histopatologia e imunohistoquímica da região proximal do cólon

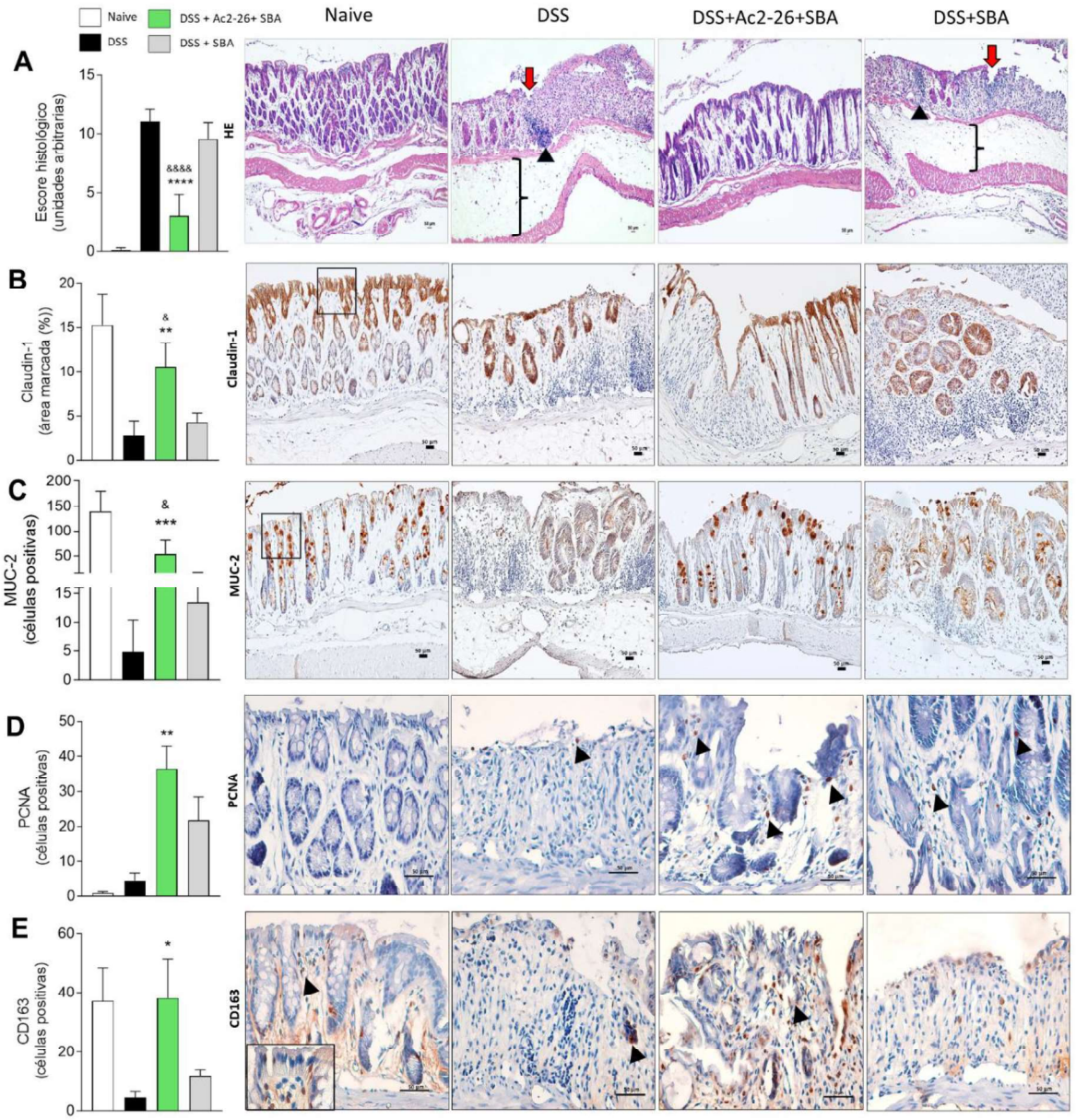

(A) Escore histopatológico representado por unidades arbitrárias. As secções foram avaliadas cegamente e as alterações consideradas foram destacadas. Edema tecidual (colchetes), infiltrados inflamatórios (ponta de seta preta) e ulcerações (seta vermelha). Grupo naive apresentando histoarquitetura normal. Secções de cólon de camundongos submetidas ao IHC. (B) Seções representativas e porcentagem (%) de área marcada para marcador Claudina-1. (C) Seções representativas e número de células positivas por campo para marcador MUC-2. (D) Secções representativas e número de células positivas por corte para o marcador PCNA. (E) Seções representativas e número de células positivas por campo para o marcador CD163. n = 10 animais/grupo. Barra de escala: 50 µm. Seções: 4 µm. *p < 0,05, **p < 0,01, ***p < 0,001, ****p < 0,0001 vs DSS; $^{\&}$p < 0,05, $^{\&\&\&\&}$p < 0,0001 vs DSS + Eudragit-SBA-15.

Associados, o conjuto de dados físico-químicos da caracterização da incorporação do peptídeo ao SBA-15, da cinética de transito do SBA-15 in vivo e da liberação do peptídeo Ac2-26 tanto in vivo como in vitro, bem como da efeicácia terapêutica por administração oral forneceram dados promissores para a utilziação da plataforma SBA-15- Eudragit para entrega do peptídeo no intestino inflamado.

Análise em Organoides Intestinais: Impacto de rAnxA1 e Ac2-26 nas Junções Epiteliais

Anxa1 aumentou TEER e suprimiu o comprometimento da integridade da barreira causado pelo tratamento com LPS

Para avaliar o efeito da rAnxA1 nas TJs epiteliais da barreira intestina, desenvolvemos organoides 3D baseados em células-tronco do cólon murino. Resumidamente, as células-tronco foram isoladas do cólon do camundongo através de tratamentos com colagenase e depois cultivadas como organoides 3D. Os enteroides foram, então, diferenciados em monocamadas epiteliais intestinais polarizadas que se assemelham aos diferentes tipos de enterócitos e colonócitos *in vivo* (Figura 29A). As células epiteliais polarizadas foram desafiadas com LPS para induzir o modelo intestinal inflamado e o efeito da rAnxA1 foi avaliado (Figura 29B; A50= rAnxA1. 50 ng/mL) Utilizamos duas abordagens para avaliar a permeabilidade da barreira intestinal: a resistência elétrica transepitelial (TEER) e o ensaio de permeabilização FITC-dextram. Primeiro, observamos que rAnxA1 (aumentou o TEER dos EDMs não inflamados em comparação com os não tratados (Figura 29C). Como esperado, o tratamento com LPS alterou as TJs epiteliais intestinais, levando à redução no TEER (Figura 29C, 1E) e aumento na permeabilização do FITC-dextrano (Figura 29F). Os efeitos anteriores sobre a integridade da barreira causados pleo LPS foram suprimidos e revertidos na presença de rAnxA1 (Figura 29C, 1E e 1F).

Figura 29. O tratamento com ANXA1 diminui a permeabilidade intestinal mediada por LPS em EDMs

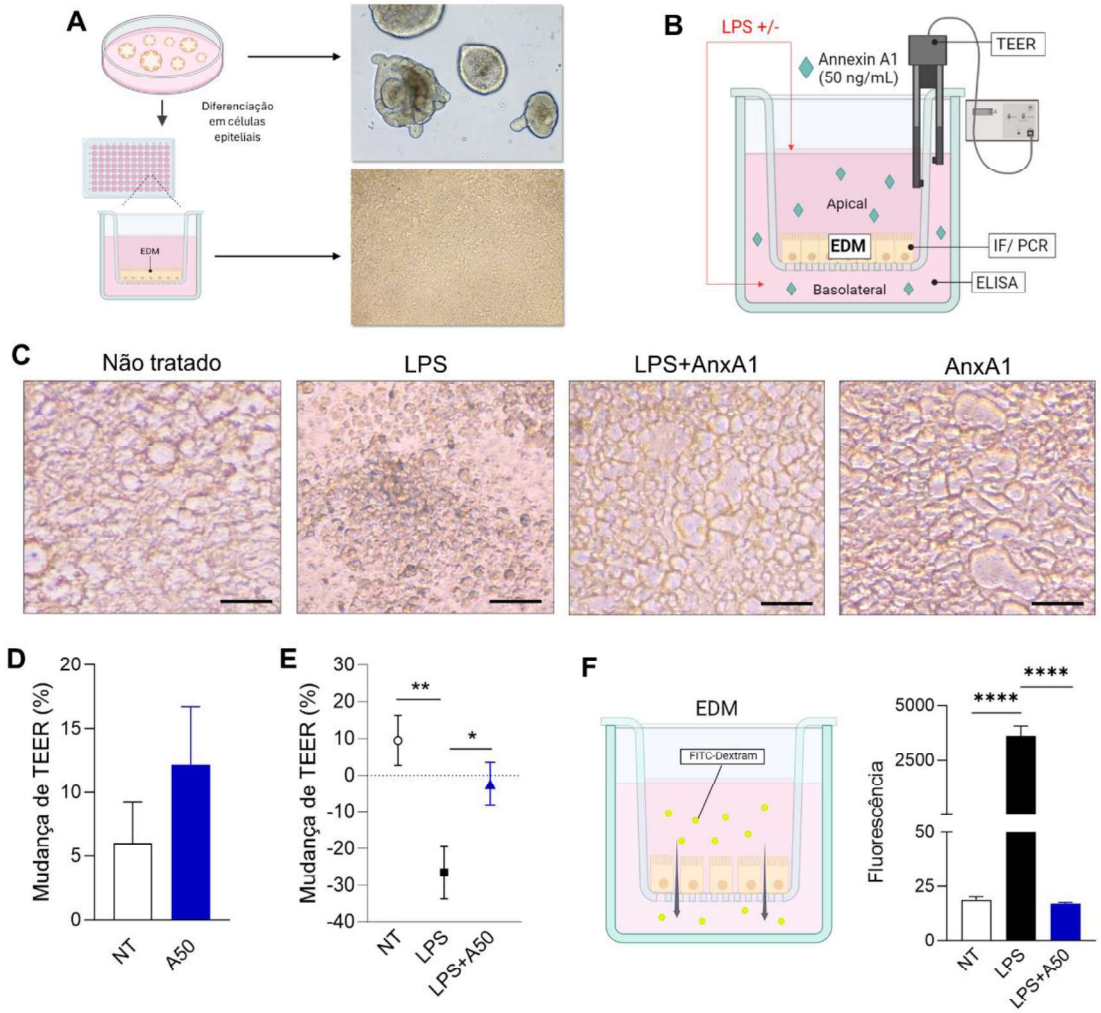

(A) Fluxograma mostrando o desenvolvimento de organoides murinos 3D do cólon de camundongos. Os organoides foram divididos em células únicas que são diferenciadas in vitro em células epiteliais polarizadas em uma placa de 96 poços.(B) Diagrama mostrando o desenho experimental. Os EDMs polarizados foram tratados ou não com rAnxA1 (A50; 50ng/mL) e desafiados com LPS. A integridade da barreira intestinal foi avaliada por TEER, as células foram utilizadas para PCR e IF, e os sobrenadantes foram coletados para ensaios de ELISA. (C) Imagens representativas de microscopia de EDMs não tratados, EDMs desafiados com LPS, EDMs desafiados com LPS e tratados com rAnxA1 e EDMs tratados com AnxA1. A ampliação é de 20x, barra de escala de 50 µm. (D) Alteração percentual no TEER em EDMs não tratados ou tratados com rrANXA1 por 24 horas. (E) Alteração percentual no TEER em EDMs desafiados com LPS e tratados ou não com AnxA1. *p<0,05, **p<0,01 conforme determinado pelo Teste *t* de Student. (F) (Esquerda) Diagrama mostrando o princípio do ensaio de permeabilização FITC-dextram. (Direita) As medições de fluorescência da permeabilização de FITC-dextrano em EDMs na mesma condição descrita em (E). **** p<0,0001 conforme determinado pelo teste One-Way ANOVA. NT, não tratado. EDM, *enteroid derived monolayer.*

O tratamento com rAnxA1 modificou a transcrição das proteínas juncionais epiteliais intestinais

Estudos anteriores relataram que ZO-1, ocludina, claudina-1 e claudina-2 são bons marcadores para TJs epiteliais intestinais no modelo EDMs (Sharma et al., 2021). Desta forma, os efeitos do tratamento com rAnxA1 na transcrição desses marcadores após o desafio com o LPS foram avaliados (Figura 30A) . Como esperado, o LPS reduziu o nível de transcrição de TJs epiteliais, como ocludina e ZO-1 (Figura 30B e C), e o tratamento com rAnxA1 reverteu esses efeitos do LPS. O nível de mRNA de claudina-2 foi regulado positivamente nos EDMs desafiados por LPS e o tratamento com rAnxA1 diminuíu os níveis de mRNA para esta molécula de junção epitelial (Figura 30D). Não houve diferença significativa na transcrição de claudina 1 (Figura 30E). Em relação à proteína de junção aderente, o nível de transcrição da caderina (CDH1) foi regulado negativamente nos EDMs desafiados por LPS, que foi protegido na presença de rAnxA1 (Figura 30F). Os efeitos anteriores do LPS e AnxA1 em vários transcritos de junções epiteliais não foram correlacionados com aumento nas expressões dos receptores AnxA1: FPR1 e FPR2 (Figura 30G e H).

Figura 30. AnxA1 reverte as alterações mediadas por LPS na transcrição de proteínas de TJs e de junção aderente

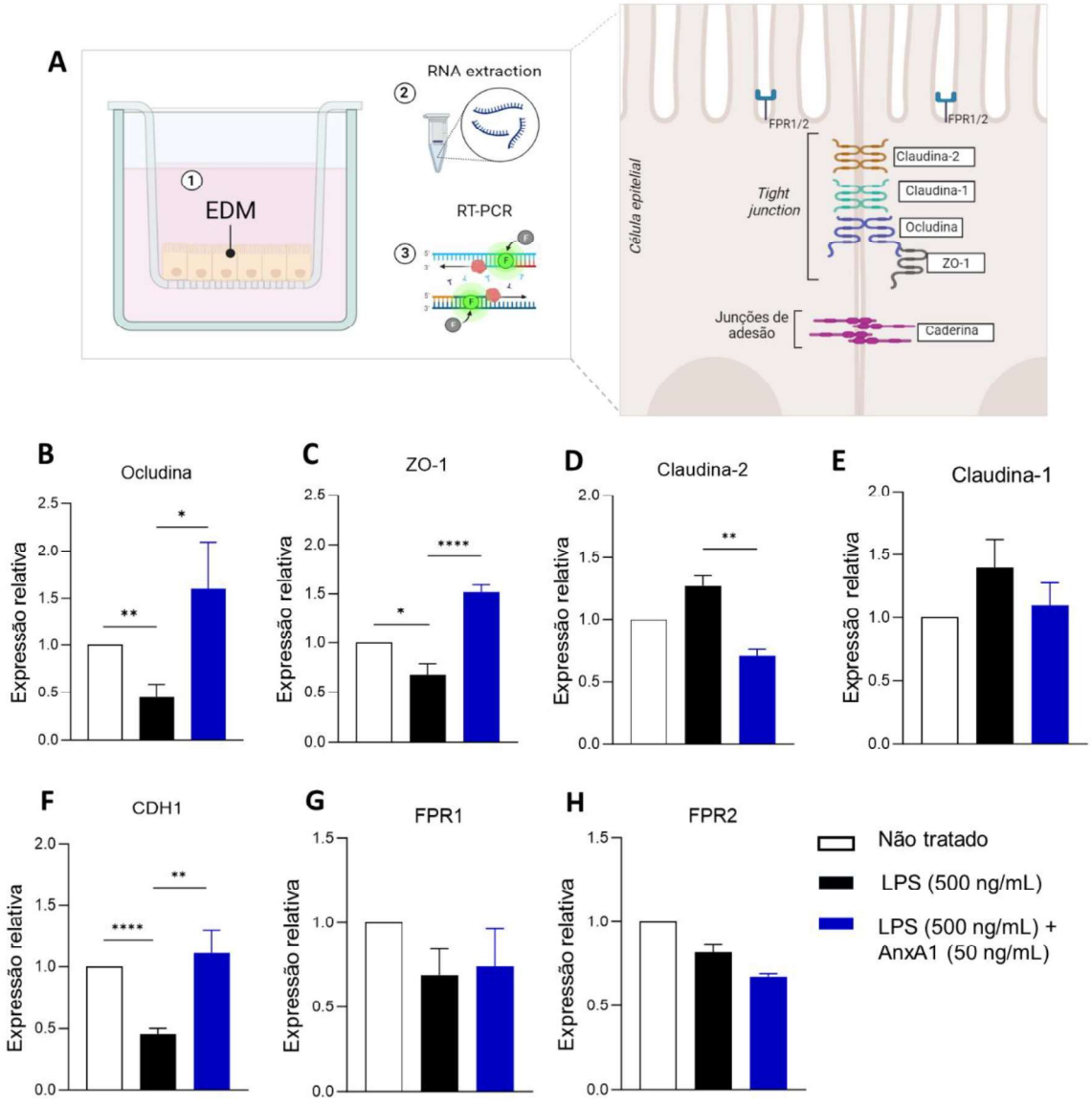

(A) Diagrama mostrando os principais alvos do ensaio RT-qPCR. Os níveis de transcrição das proteínas TJs (ZO-1, ocludina, claudina-1 e claudina-2) e junção aderente (caderina). A expressão gênica relativa de ocludina (B), ZO-1 (C), claudina-2 (D), claudina-1 (E), caderina (F), FPR1 (G) e FPR2 (H) foi comparada em EDMs nãu tratadas (branco), EDMs +LPS (preto) e EDMs + LPS+ AnxA1 (azul). *, ** e **** os valores médios de p são inferiores a 0,05, 0,01 e 0,0001, respectivamente, conforme determinado pelo Teste *t* de Student.

Em seguida, avaliamos a intensidade da coloração de ZO-1 e claudina-2 por microscopia confocal nos EDMs expostos a LPS. A intensidade do ZO-1 foi menor nos EDMs desafiados com LPS do que nos EDMs não tratados, enquanto o tratamento

com rAnxA1 aumentou a intensidade da coloração com ZO-1, confirmando os níveis de mRNA (Figura 31).

Figura 31. O tratamento com AnxA1 reverte o dano causado pelo LPS na proteína de integridade da barreira intestinal ZO-1

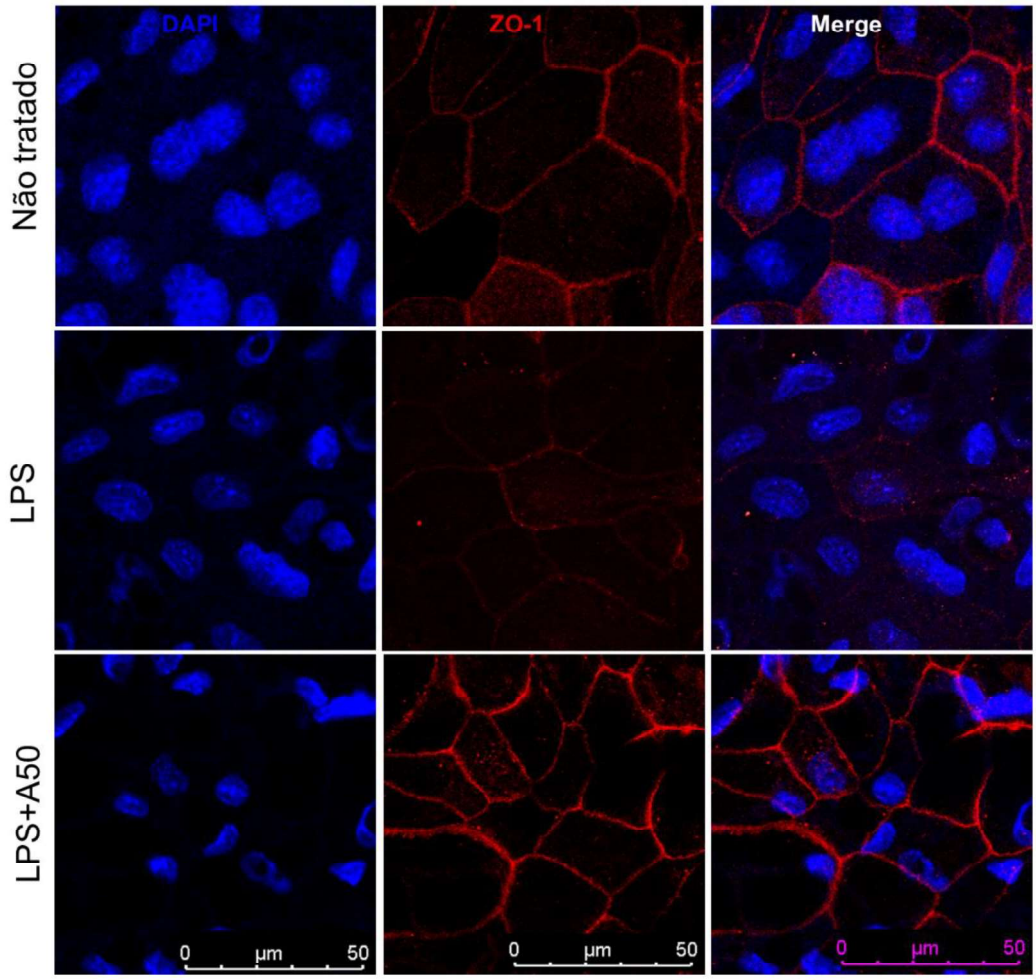

EDMs (não tratados), desafiados com LPS (LPS), desafiados com LPS e tratados com ANXA1 (LPS+A50), foram corados para ZO-1 (vermelho, e examinados por microscopia confocal . DAPI foi usado para coloração de núcleos. Imagens tiradas (40x) e barra de escala de 50 µm.

Além disso, a expressão da proteína formadora de poros, claudina-2, foi baixa nos EDMs não desafiados e aumentou após a estimulação com LPS. O tratamento com rAnxA1 reduziu a intensidade de claudina 2 nos EDMs desafiados por LPS (Figura 32). Coletivamente, os dados obtidos mostraram que o desafio com LPS mediou a ruptura das TJs epiteliais intestinais através da supressão dos marcadores de TJs (ZO-1) e aumentou o marcador claudina-2, associado ao aumento da permeabilidade da barreira, tanto na transcrição quanto na expressão da proteína (Figura 31 e Figura 32).

Figura 32. O tratamento com AnxA1 reverte a expressão da proteína de formação de poros na barreira intestinal Claudina-2

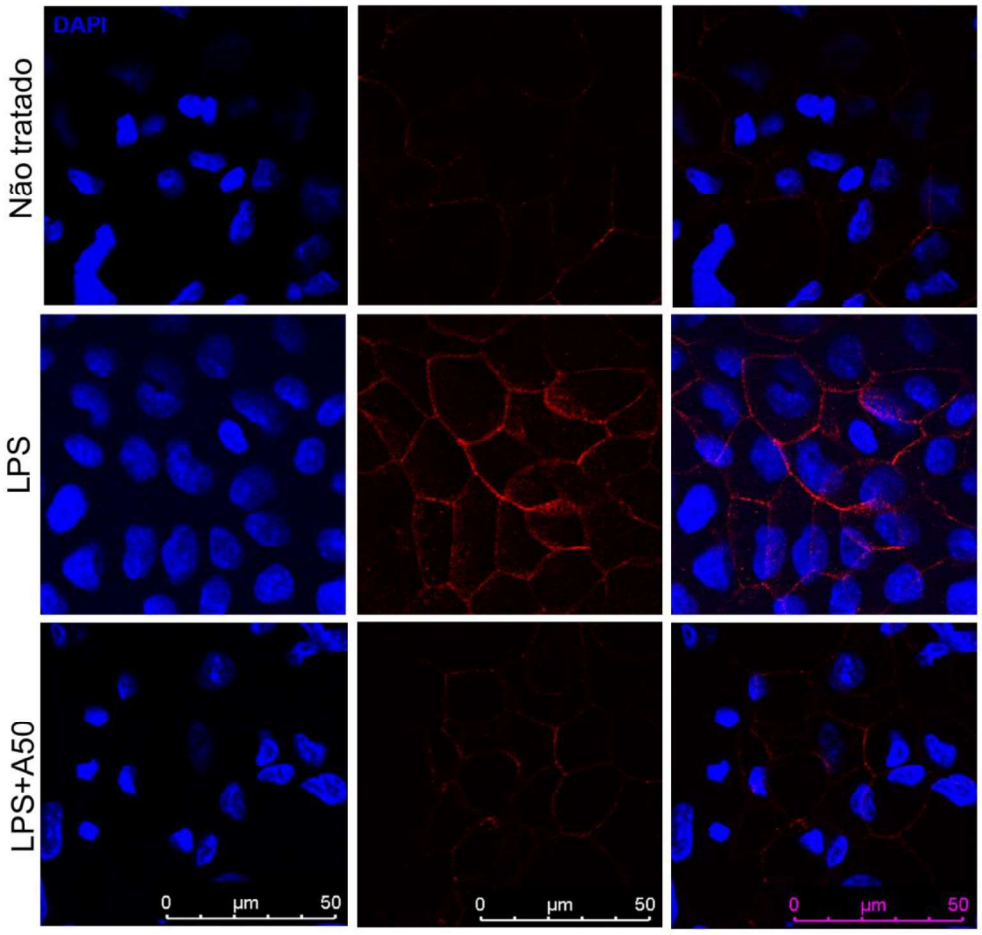

EDMs (não tratados), desafiados com LPS (LPS), desafiados com LPS e tratados com ANXA1 (LPS+A50), foram corados para Claudina-2 (vermelho, e examinados por microscopia confocal . DAPI foi usado para coloração de núcleos. Imagens tiradas (40x) e barra de escala de 50 µm.

O tratamento com rANXA1 afetou as citocinas inflamatórias mediadas pelo LPS

Em seguida, avaliamos o efeito do tratamento com rAnxA1 na produção de citocinas inflamatórias. O sobrenadante e lisado celular de EDMs desafiados com LPS e tratados ou não com rAnxA1 foram coletados para análises. O LPS aumentou a liberação de CXCL-1 e o nível de transcrição de MCP-1 (Figura 33A e B); e os tratamentos com rAnxA1 reverteram os efeitos anteriores. Em seguida, observamos que o tratamento com rAnxA1 aumentou o nível de transcrição de IL-10 (Figura 33C).

Figura 33. O tratamento com AnxA1 diminui as citocinas inflamatórias em células epiteliais

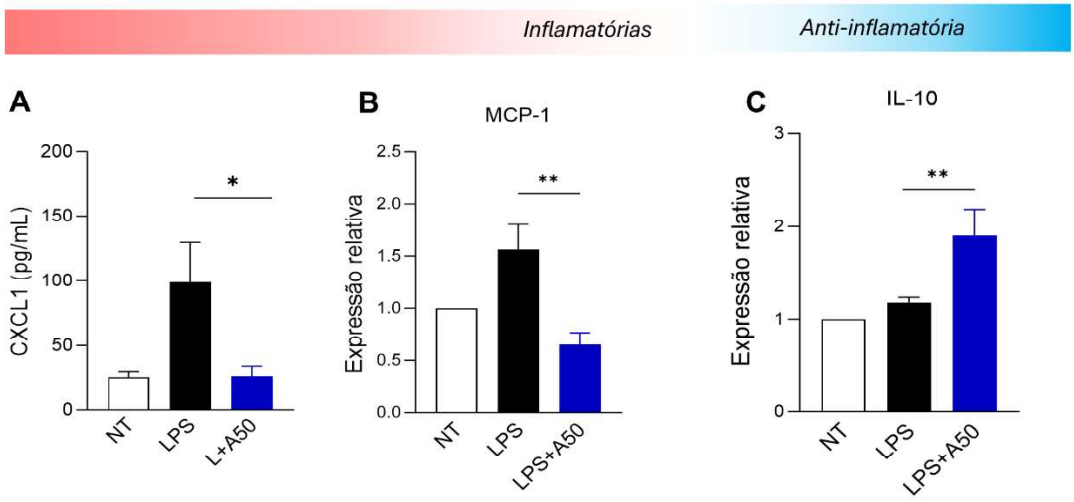

(A) O nível de CXCL-1 no sobrenadante foi medido por ELISA. (B) O nível de mRNA de MCP-1 foi medido no lisado celular por RT-qPCR bem como o de IL-10 (C). A expressão de mRNA na célula não tratada foi colocada como 1. * $p<0,05$, ** $p<0,01$.

O peptídeo Ac2-26 mimetizou os efeitos do tratamento com rAnxA1 no modelo EDM

O peptídeo Ac2-26 representa o N-terminal da proteína ANXA1 e inclui 26 aminoácidos (Figura 34A). Para avaliar o efeito do Ac2-26 na integridade da barreira intestinal e na resposta inflamatória, tratamos a inflamação mediada por LPS nos EDMs com Ac2-26 e depois avaliamos o efeito do Ac2-26 na integridade da barreira intestinal. O tratamento com o peptídeo Ac2-26 reduziu significativamente a queda no TEER mediada pelo LPS (Figura 34B). O efeito anterior foi mediado pelo aumento dos níveis de transcrição de TJs e proteínas de junção aderentes (ocludina, ZO-1 e caderina) e pela supressão da expressão de claudina-2 (Figura 34 C-F). Além disso, o Ac2-26 restaurou o efeito prejudicial do LPS nas junções epiteliais, aumentando a expressão e distribuição do ZO-1 (Figura 34G). Em relação ao efeito sobre a expressão gênica das citocinas, o tratamento com peptídeo Ac2-26 regulou negativamente de forma significativa a expressão de citocinas inflamatórias (CXCL-1 e MCP-1) e regulou positivamente a expressão da citocina anti-inflamatória, IL-10 (Figura 34H-J).

Figura 34. Ac2-26 mantém a integridade da barreira intestinal e tem efeito antiinflamatório

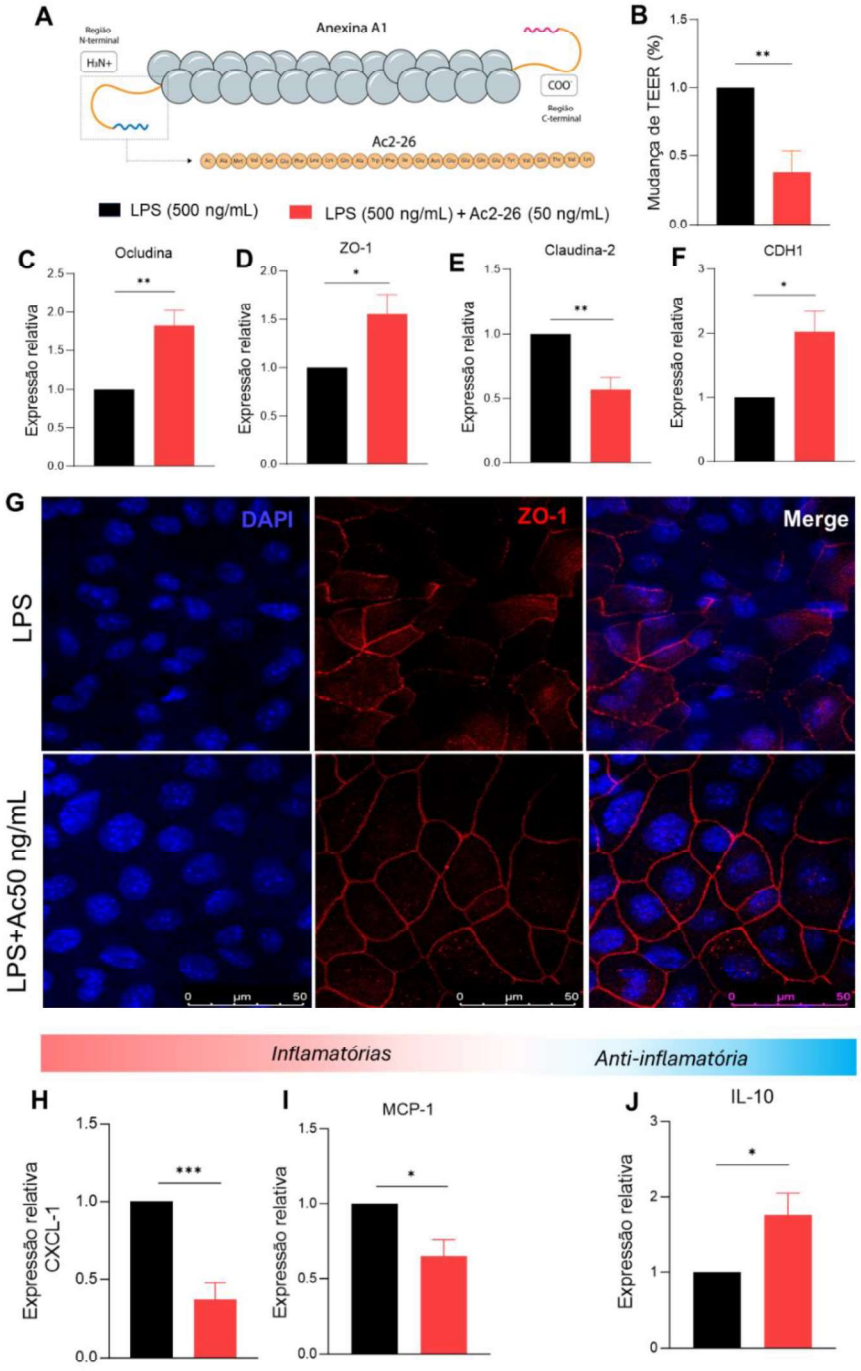

(A) Esquema mostrando do peptídeo Ac2-26. B) Efeito do peptídeo Ac2-26 no TEER de EDMs desafiados ou não com LPS. A queda relativa do TEER foi calculada em relação ao TEER dos EDMs não tratadoscom Ac2-26, expressos como como 1. O nível de mRNA de TJs e proteínas aderentes, como ocludina (C), ZO-1 (D), claudina-2 (E) e caderina (F) foi avaliado por RT-qPCR em EDMs desafiados por LPS tratados ou não com Ac2-26. A expressão gênica relativa foi calculada, em relação as EDMs desafiados com LPS, expressos como 1. (G) A integridade das EDMs foram analisadas para marcação com ZO-1 (vermelho) e DAPI (azul) foi usado para coloração de núcleos. (H) O nível de CXCL-1 no sobrenadante de EDMs desafiados com LPS e peptídeo LPS+Ac2-26 foi medido por ELISA e o valor relativo de CXCL-1 calculado. (I) O nível de mRNA de MCP-1 foi medido no lisado de EDMs

por RT-qPCR. O nível de transcrição de MCP-1 nos EDM desafiados por LPS foi expresso como 1. (J) O nível de mRNA de IL-10 foi medido no lisado de EDMs por RT-qPCR. * p<0,05, **p<0,01, ***p<0,001.

Discussão

O avanço no tratamento das DIIs representa uma colaboração global entre pesquisadores, considerando a complexidade da gênese da doença, natureza crônica e recorrente das enfermidades, resposta inadequada dos pacientes às farmacoterapias existentes e os sintomas físicos e psicossociais, que, associados, oneram os sistemas de saúde. A via oral é a preferida para administração de medicamentos no tratamento da DII, pois não é invasiva, permite alta adesão do paciente e flexibilidade no ajuste da dose, e entrega o medicamento diretamente na região do cólon. A nanotecnologia oferece uma alternativa inovadora medicamentos, entre os quais os anti-inflamatórios, principalmente por possibilitar o carreamento de substâncias diretamente ao local de inflamação, evitando efeitos sistêmicos (GIRON et al., 2019; HUA et al., 2015; IRVING; VICTORIA, 2007; MUDSHINGE et al., 2011). A veiculação de moléculas de proteínas de baixo peso molecular e peptídeos não é trivial, uma vez que estas são alvos de enzimas presentes nos diferentes compartimentos do organismo (HUA, 2020; LOU et al., 2023). Considerando que as estruturas da AnxA1 e do peptídeo Ac2-26, o projeto foi idealizado para desenvolver formulações farmacêuticas para veiculação dos mesmos para o tratamento de DIIs. Demonstramos a funcionalização eficiente da AnxA1 em MLNC e a incorporação do peptídeo Ac2-26 em SBA-15, e as eficácias terapêuticas dos mesmos na colite induzida em camundongos.

As LNCs tem demosntrado alta efetividade no carreamento de substâncias e tem como principal vantagem seu alto grau de estabilidade, além de possuírem duas interfaces para alocar substâncias de diferentes características de solubilidade, sendo o núcleo capaz de alocar substâncias lipossolúveis e a superfície polimérica capaz de ancorar proteínas e outras substâncias de caráter hidrossolúvel (POHLMANN et al., 2013; VENTURINI et al., 2011). As suspensões de LNC utilizadas neste trabalho foram preparadas conforme método já descrito (JÄGER et al., 2009; MÜLLER C.R et al., 2001; VENTURINI et al., 2011), chamado deposição interfacial de polímero pré-formado. A formação da MLNC se baseia da interação eletrostática entre o grupo amônio da quitosana e grupos carregados negativamente na superfície da LNC, indicando a interação da quitosana com a lecitina na interface partícula-água (MOSQUEIRA et al., 2000; VENTURINI et al., 2011).

O potencial eletrocinético de um sistema coloidal é medido por meio do potencial zeta, o qual expressa a diferença de potencial entre o meio de dispersão e a camada estacionária de fluido ligada à partícula (RABINOVICH-GUILATT et al.,

2004). O potencial zeta pode afetar principalmente a captação celular das NPs. A membrana celular é composta de proteoglicanos sulfatados negativamente, a interação eletrostática dessa superfície celular aniônica à NPs catiônicas resulta em uma ligação altamente iônica que facilita a captação celular (SAHAY; ALAKHOVA; KABANOV, 2010; WILHELM et al., 2003).

A mudança de polaridade da LNC para a MLNC observada no potencial zeta é atribuída a interação dos componentes lecitina, composta principalmente de fosfatidilserina que apresenta característica dipolar, que interage com a quitosana, carregada positivamente. Assim, a formação da MLNC se baseia na interação eletrostática entre o grupo amônio da quitosana e grupos carregados negativamente na superfície da LNC, indicando a interação da quitosana com a lecitina na interface partícula-água (MOSQUEIRA et al., 2000; PATTNI; TORCHILIN, 2015). A principal técnica utilizada para análise do potencial zeta é o espalhamento de luz eletroforético, sendo esse parâmetro considerado um importante ponto de estabilidade de NPs em suspensão (KATHE; HENRIKSEN; CHAUHAN, 2014). Os valores observados para LNC e MLNC correspondem aos encontrados em trabalhos anteriores que utilizaram nanocápsulas revestidas com os mesmos materiais (BENDER et al., 2012; CÉ et al., 2016) e a adição de AnxA1 a nanocápsula não alterou a polaridade da mesma

Além do potencial zeta, que dita o potencial de interação de par´ticulas com células e tecidos, o tamanho dessas partículas presentes em cada solução é outro parâmetrdo que ativa os mecanismos de internalização celular de NPs (BAHARI; HAMISHEHKAR, 2016; DANAEI et al., 2018; RENNICK; JOHNSTON; PARTON, 2021). Alguns nanocarreadores se acumulam em tecidos alvo ou sofrem agregação e, como consequência afeta a distribuição do tamanho das partículas ou índice de heterogeneidade na solução, identificado pelo PDI. O valores de PDI podem variar de 0 a 1, sendo os valores próximos de 0 são considerados monodispersos e indicam que a NP terá absorção pela célula, enquanto que valores de PDI maiores que 0,7 indicam que a amostra tem uma distribuição de tamanho de partícula ampla, o que dificulta a interação com as células (STETEFELD; MCKENNA; PATEL, 2016). Os valores obtidos pela MLNC foi 0,22 e semelhante a estudos prévios que empregaram LNC, MLNC e MLNC conjugada com proteína (BENDER et al., 2014; CAVALCANTE et al., 2021; CÉ et al., 2016; DE CASTRO LEÃO et al., 2021; VENTURINI et al., 2011).

As propriedades fisico-quimicas da MLNC-AnxA1 proporcionaram a continuidade para os estudos in vivo, sendo que o primeiro objetivo seria avaliar a eficácia da MLNC-AnxA1 pela administração oral. Em trabalho prévio do nosso grupo de pesquisa, Rodrigues et al. (2016) mostrou que a LNC é resistente ao pH estomacal e de ser capaz de atravessar barreiras endógenas. Ademais, os resultados obtidos no trabalho publicado por Michalowski et al., (2020), indicavam que a estrutura supramolecular obtida pela parede múltipla e a ligação covalente da proteína ao metal seriam suficientemente robustas para proteger a Anexina A1 da degradação nos compartimentos gastrointestinais. No entanto, a administração oral de MLNC-AnxA1 não foi efeicaz sobre os sintomas da colite, sugerindo que as ações *in vivo* dos componentes fisiológicos no TGI possam ter deslocado a proteína da estrutura supramolecular, com consequente inativação da AnxA1.

A nanotecnologia vem ganhado espaço na pesquisa e desenvolvimento de estratégias terapêuticas para as DII, sendo a administração realizada, principalmente, pelas vias oral ou intravenosa (GIRON et al., 2019; YANG; MERLIN, 2019). Apesar da administração via oral possuir as vantagens de ser menos invasiva e de fácil adesão a terapias, muitas vezes a via intraperitoneal é utilizada como um método alternativo à via oral para evitar a degradação de biofármacos pelo TGI e aumentar a absorção de formulações em suspenção (AL SHOYAIB; ARCHIE; KARAMYAN, 2020). Nosso estudo demonstrou que a administração intravenosa de MLNC-AnxA1 e rAnxA1 não inibiu a sintomatologia da colite induzida em camundongos, Embora, não desvendamos o que possa ter ocorrido com MNLC-AnxA1 no compartimento central, supomos que a nanocapsula utilizada não foi capaz de ser distribuída para o tecido inflamado, ou a rAnxA1 foi deslocada da MNLC e até mesmo degradada pelas enzimas plasmáticas. . No entanto, o tratamento intraperitoneal com MLNC-AnxA1 foi capaz de reduzir de forma eficiente os sintomas clínicos da doença e inibir resposta inflamatória e promover regeneração tecidual.

A administração de NPs pela via intraperitoneal pode aumentar a resposta farmacológica e reduzir a toxicidade de medicamentos em diversos casos (BRANQUINHO et al., 2017; DENG et al., 2016; MOSQUEIRA et al., 2004). A cavidade peritoneal é formada por um líquido composto de água, eletrólitos e outras substâncias provenientes do interstício. Possui uma quantidade significativa de leucócitos, sendo principalmente macrófagos, seguido de uma pequena quantidade de linfócitos do tipo B1 e B2 produtores de imunoglobulinas do tipo IgA (BAIN et al.,

2016; BLACKBURN; STANTON, 2014). Essas células são abundantes no omento, um tecido adiposo localizado logo abaixo das células mesoteliais, que recobre os órgãos peritoneais, tornando esse local ideal para gerar respostas imunológicas a antígenos ou patógenos na cavidade peritoneal (MIRONOV; GUSEV; BARADI, 1979; WILKOSZ et al., 2005). Além de possuir uma grande rede de capilares sanguíneos, vasos e nódulos linfáticos que se juntam ao sistema circulatório venoso através do ducto torácico e do ducto linfático direito, o peritônio visceral é composto por camada única de células mesoteliais escamosas com microvilosidades, que contêm grande número de vesículas pinocíticas que facilitam a absorção das moléculas (ISHIGURO et al., 2018; VAN BAAL et al., 2017).

Durante a resposta inflamatória, as células mesoteliais e estromais são responsáveis pela secreção de citocinas e quimiocinas, promovendo a quimiotaxia de leucócitos do peritôneo e da circulação, com acúmulo principalmente de neutrófilos e macrófagos M1 (BÉNÉZECH et al., 2015; MEZA-PEREZ; RANDALL, 2017). Diante de uma resposta inflamatória exacerbada, característica da colite, destaca-se o incremento acentuado de citocinas e quimiocinas na parede intestinal. Essas substâncias, produzidas pelas células na lâmina própria em resposta ao dano tecidual e à invasão da microbiota residente, desencadeiam a quimiotaxia de leucócitos da circulação. Esse fenômeno, por sua vez, sugere um possível aumento do contingente de células imunes na região peritoneal. Notavelmente, os nossos dados, indicam que a eficácia do mecanismo de entrega da rAnxA1 é otimizada quando administrada intraperitonealmente por nanocápsulas, as quais podem atuar sobre células do peritôneo ou sobre as células da parede intestinal. Há indícios de que essas nanocápsulas podem ser internalizadas pelas células do mesotélio visceral, agindo diretamente sobre o intestino inflamado (SINIS et al., 2018).

É importante ressaltar que a administração i.p. de todas os tratamentos MLNC; AnxA1 ou MLNC-AnxA1 inibiram o recrutamento de neutrófilos para a lâmina própria, o que não seria esperado para a MLNC, uma vez que se conhece que a AnxA1 inibe o recrutamento de neutrófios para foco de lesão inflamado (HAYHOE et al., 2006; SUGIMOTO et al., 2016). Resulatdos anteriores do nosso grupo mostraram que tratamentos com LNCs contendo poli ε-caprolactona apresentaram redução da capacidade migratória de leucócitos. Os resultados obtidos mostraram que os efeitos anti-inflamatórios das nanocápsulas foram dependentes da inibição da via de MAP-

quinase e da mobilização e influxo de cálcio intracelular (SANDRI et al., 2019)(SANDRI et al., 2019).Desta forma, o resultado obtido com a MLNC sugere investigações adicionais sobre a super-estrutura nanométrica sobre funções de neutrófilos. No entanto, a administração de MLNC-AnxA1 induziu a polarização de macrófagos para o perfil M2 da eferocitose, tanto in vivo quanto in vitro, induziu também a secreção de TGFbeta, e teve papel altamente benéfico na estruturação tecidual. Os resultados evocados pela LMNC-AnxA1 foram superiores ao induzido pela própria AnxA1 livre, o que demonstra que maior efetividade da foram nanaoestruturada.

A administração oral de medicamentos é considerada menos invasiva e permite alta adesão do paciente e flexibilidade no ajuste da dose. No entanto, pequenas moléculas e proteínas apresentam baixa biodisponibilidade por via oral e requerem abordagens técnicas farmacêuticas adequadas para resistir ao ambiente propício para a degradação de substâncias, uma vez que os desafios se encontram na presença de bactérias, enzimas e aos diferentes pHs no TGI (YUN; CHO; PARK, 2013). Com base nas ações benéficas robustas de AnxA1 sobre DIIs e nos resultados obtidos para o tratamento de colite experimental induzida por DSS com MLNC-AnxA1 pela via intraperitoneal, inferimos aqui que o peptídeo mimético Ac2-26 de AnxA1 poderia ser incorporado em um sistema de entrega colon-específico. Assim, o Ac2-26 foi conjugado na micropartícula de sílica mesoporosa ordenada SBA-15 e revestido com um polímero Eudragit® L30 D55, o qual apresenta resistencia a pHs inferiores a 7 e poderia proteger o SBA-15-Ac2-26 dos danos indesejados do TGI para fornecer Ac2-26 na área inflamada do cólon.

A SBA-15 apresenta estrtutura de alta resistência térmica, hidrotérmica e mecânica (ZHAO et al., 1998a), conferindo sua capacidade de resistir ao pH e às ações enzimáticas (MARIANO-NETO et al., 2014). Os componentes estruturais da SBA-15 contêm muitos grupos silanol essenciais (Si-OH) (ZHAO et al., 1998a, 1998b) para ligar substâncias em sua estrutura. SBA-15 também apresenta alta área superficial, grande volume de poros e distribuição de tamanho de nanoporos e mesoporosos, em torno de 10 nm. Juntas, essas propriedades permitem o transporte seguro de pequenas moléculas através do TGI (LU et al., 2010; MECHLER-DREIBI et al., 2021a; ROSENHOLM; SAHLGREN; LINDÉN, 2010; SARKAR et al., 2023; SCARAMUZZI et al., 2011; XU; LEI; YU, 2019). De fato, através da modelação dos dados SAXS, em combinação com os resultados do NAI, foi possível concluir que

grande parte do peptídeo Ac2-26 adicionados é carregada nos mesoporos de SBA-15. Em contraste, a concentração remanescente está, de alguma forma, na superfície da sílica, cenário semelhante ao observado em estudos anteriores nos quais os autores carregaram proteínas, em vez de peptídeos (LOSITO et al., 2021; TREZENA et al., 2022). Conforme sugerido por Rasmussen et al. (2019), em estudo que avaliou o potencial da SBA-15 como veículo para a anatoxina diftérica (dANA), focalizando sua aplicação em vacinas orais. Os resultados indicaram que a estrutura da dANA permaneceu estável após o processo de secagem. A liberação no ambiente intestinal mimético em pH 6,8, monitorada por SAXS, foi gradual, com destaque após 6 horas. A imunização oral de camundongos com SBA-dANA resultou na produção significativa de anticorpos específicos, destacando o SBA-15 como um adjuvante promissor para vacinas orais. Essa abordagem sugere uma plataforma viável para o desenvolvimento eficaz de vacinas orais e macroporosidade SBA-15 são capazes de proteger o conteúdo biológico adsorvido frente a condições ambientais adversas, como o TGI.

Pela indicação de que havia Ac2-26 na superfície da sílica, SBA-15-Ac2-26 foi revestida com Eudragit®, um copolímero aniônico responsivo ao pH produzido a partir de metacrilato de metila e ácido metacrílico. Apresenta características de solubilidade dependentes do pH, permanecendo estável sob condições ácidas, mas dissolvendo-se em pH básico (pH> 7,0) para facilitar a liberação do medicamento, que em condições fisiológicas pode começar na porção íleo distal (THAKRAL; THAKRAL; MAJUMDAR, 2013). Eudragit é um carreador de medicamento eficiente em pH ácido, pois carrega carga negativa significativa permitindo sua absorção preferencialmente em locais de inflamação (BARBOSA et al., 2019; HOLMÉN LARSSON et al., 2009; LI et al., 2020). A análise da tomografia de imagem corroborou que o Eudragit-SBA-15 administrado por via oral permaneceu no TGI por um período prolongado, adequado para a entrega de medicamentos ao intestino. Além disso, a absorção de Eudragit-SBA-15 pelas células epiteliais intestinais *in vitro* em modelos celulares bidimensionais ou tridimensionais foi deficiente, reforçando a hipótese de que o SBA-15 não é absorvido no intestino e pode ser excretado pelas fezes (ZHAO et al., 1998a). Dados adicionais abordaram o Eudragit-SBA-15 como uma plataforma adequada para entregar o peptídeo no intestino, já que Ac2-26 foi detectado no epitélio (células Caco-2) após incubação *in vitro* com SBA-15-Ac2-26, e Eudragit-SBA-15 entregou Ac2-26 no intestino após administração oral.

Os efeitos benéficos do Ac2-26 na sintomatologia da DII estão relacionados à sua ligação ao FPR1 no epitélio inflamado (LEONI et al., 2013, 2015b)(Leoni 2013; Leoni 2015). Ainda, o Ac2-26 atua como AnxA1, ligando-se a ambos os receptores para promover efeitos anti-inflamatórios e reparo tecidual (COORAY et al., 2013). É muito bem estabelecido que o Ac2-26 liga-se a FPR2 em neutrófilos e macrófagos, inibindo o desenvolvimento de inflamações inatas e facilitando a resolução do processo (DALLI et al., [s.d.]; RÜGER et al., 2020; ZHENG et al., 2023). Nas DIIs, AnxA1 é expressa e liberada por neutrófilos e macrófagos na lâmina própria e medeia a eferocitose via ligação ao receptor FPR2 (DE PAULA-SILVA et al., 2016, 2021). Com base nos conceitos bem estabelecidos do Ac2-26 na inflamação e na DII, bem como na distribuição do Ac2-26 in vivo após administração oral da Eudragit-SBA-15-Ac2-26 no intestino, podemos supor que o tratamento promoveu efeito benéfico de forma rápida, detectados pela acentuada redução da perda de peso 24 horas após o primeiro tratamento, que se manteve nas três administrações seguintes uma vez ao dia durante a fase de recuperação da doença.

A eficácia do tratamento oral da colite não pôde ser comparada à administração livre de Ac2-26 devido à baixa biodisponibilidade dos peptídeos por ingestão oral (LANGGUTH et al., 1997). No 10º dia de doença, o tratamento inibiu o influxo de neutrófilos e monócitos no tecido inflamado e reduziu os níveis de citocinas pró-inflamatórias secretadas no tecido. Este último efeito poderia refletir o menor número de células inflamatórias. Os níveis da citocina anti-inflamatória e pró-resolução IL-10 foram aumentados pelo tratamento e podem ser relacionados à alta quantidade de macrófagos CD163, marcador de macrófagos M2, no tecido dos camundongos tratados. De fato, o Ac2-26 apresenta efeito semelhantemente a AnxA1, limitando o tráfego de macrófagos e neutrófilos para locais inflamados (GIROL et al., 2013b; HAYHOE et al., 2006; LIM; PERVAIZ, 2007) e inibe a secreção de citocinas pró-inflamatórias pelas vias transcricional e pós-transcricional (REISCHL et al., 2021b; WALTHER; RIEHEMANN; GERKE, 2000).

Ac2-26 é um peptídeo de resolução reconhecido, que polariza macrófagos M2 e induz a apoptose de neutrófilos para eferocitose adicional por macrófagos (GIROL et al., 2013b; HAYHOE et al., 2006; LI et al., 2019b; LIM; PERVAIZ, 2007; MCARTHUR et al., 2020b; REISCHL et al., 2021b). Nossos resultados corroboram outro estudo que utilizou o tratamento local de NPs de PLGA-Colágeno IV como carreadores do peptídeo Ac2-26 via intra mucosal e observaram resposta clínica

semelhante ao nosso, além de aumento da regeneração tecidual e redução da resposta inflamatória promovendo resolução da inflamação de forma mais rápida após uma única injeção da nanopartícula de Ac2-26 (LEONI et al., 2015; REISCHL et al., 2021). Ainda, a entrega alvo-específica utilizando as características químicas do órgão também foram utilizadas por Li et al., (2019). Ao utilizar o revestimento polimérico sinsível a ROS, visto que altas concentrações de ROS são encontradas em sítios inflamatórios, o tratamento com NPs contento Ac2-26 apresentou resultados anti-inflamatórios promissores similares aos encontrados em nosso trabalho.

A complexidade dos mecanismos celulares e moleculares da regeneração tecidual nas DII envolve uma ampla diversidade de alvos como marcadores do processo. Optamos por quantificar o perfil de células imunes na lâmina propria, a expressão de moléculas de junção epitelial (*tight junctions* - TJ) e marcadores de proliferação celular. Macrófagos são células amplamente identificadas em todos os tecidos do organismo e possuem uma grande plasticidade celular, permitindo alterar seu fenótipo dependendo do microambiente e da fase da infamação (MOSSER; EDWARDS, 2009). O aumento da resposta anti-inflamatória induzida tanto por MLNC-AnxA1 quanto SBA15-Ac2-26 foi observado em nossos resultados, com o aumento do número celular de macrófagos M2 anti-inflamatórios na lamina própria. Esse resultado sobre a polarização de macrófagos *in vivo* corroborou os efeitos anti-inflamatórios já elucidados para a AnxA1 e reforçam a importância dessa proteína no controle da resolução da inflamação (MCARTHUR et al., 2020; MORAES et al., 2017).

Os resultados obtidos para o experimento de polarização de macrófagos utilizando células primárias obtidas de medula de camundongos demonstraram que MLNC-AnxA1 proporcinou aumento na porcentagem de macrófagos com fenótipo M2 (CD206+), bem como o aumento da produção de TGFβ, ambos resultados indicativos de resposta anti-inflamatória. Embora, mostramos que o tratamento com MLNC-AnxA1 polarizou os macrófagos de M1 para M2, nos surpreendemos com o fato de a AnxA1 não apresentar esse efeito. A literatura abrange diversos trabalhos que demonstram esse papel para a proteína, como mencionado anteriormente. No entanto, quando observadas as concentrações utilizadas, nos deparamos com concentrações muito maiores do que a por nós utilizada. Como visto no trabalho de McArthur et al. (2020) que utilizou 10 nM para polarizar macrófagos, quando comparado ao nosso estudo, que utilizou 500 ng/mL, que resultou em solução 0,075

nM de AnxA1, podemos concluir que a encapsulação da AnxA1 otimizou a resposta da proteína em macrófagos em concentração muito menor do que as utilizadas na literatura (LI et al., 2011; LOCATELLI et al., 2014; XU et al., 2021), sendo este dado inédito para a MLNC e AnxA1 e demonstra a importância de integrar a nanotecnologia com a farmacologia, como visto reduzindo a utilização de compostos e obtendo-se resultados farmacológicos consistentes (ZHANG et al., 2018).

As TJ são proteínas responsáveis por controlar a polarização de células epiteliais e endoteliais, bem como a sua formação morfológica e funcional, controlando a permeabilidade paracelular por meio da seletividade de carga e tamanho das moléculas em contato. O conjunto de proteínas que formam esse eixo celular pode ser dividido em proteínas transmebrana e citosólicas . Zonula Occludens-1 (ZO-1) é uma proteína TJ citosólica reguladora e essencial para a polimerização de outra TJ, a Claudina 1. A hemostasia gastrointestinal é dependente da função dessas proteínas, e alterações no ZO-1 afetam a expressão e funções de outros TJ. Portanto, níveis dinâmicos estáveis dessas proteínas são fundamentais para o funcionamento normal da barreira epitelial (HOROWITZ et al., 2023; UMEDA et al., 2006). Ambos tratamentos com MLNC-AnxA1 e SBA15-Ac2-26 interferiram na expressão das junções epiteliais. A expressão de ZO-1 foi reduzida no epitélio de camundongos com colite induzida por DSS, sendo essa expressão recuperada a níveis normais após o tratamento com MLNC-AnxA1. Esse resultado pode estar associado também a composição da MLNC a qual contém quitosana em sua estrutura. A administração oral de doses mais elevadas de do polissacarídeo quitosana durante a fase resolutiva da inflamação melhorou a recuperação dos parâmetros clínicos e histológicos, incluindo a expressão de ZO-1(SOMMER et al., 2021).

A Claudina 1, desempenha um papel relevante na homeostase intestinal, devido a sua localização transmembranar nas células epiteliais intestinais (ČUŽIĆ et al., 2021; POPE et al., 2014). Em nosso modelo de colite, a expressão de Claudina 1 foi reduzida e localizada no epitélio danificado do grupo de camundongos DSS. Os tratamentos com MLNC-AnxA1 e SBA15-Ac2-26 recuperaram a expressão de claudina-1 no tecido, especialmente em criptas reorganizadas. Portanto, os dados aqui mostrados evidenciam que tanto a AnxA1 quanto Ac2-26 liberados pela MLNC e SBA-15, respectivamente, promovem a expressão de proteínas TJ sendo capaz de reestabelecer a estrutura da cripta.

Efetivamente, a ação fisiológica da AnxA1 sobre as junções celulares foi evidenciada em células endoteliais da barreira hematoencefálica, conforme demonstrado por Cristante et al. (2013). Nesse cenário, a deficiência na expressão dessa proteína está associada à origem de doenças neurodegenerativas. É relevante destacar que, em situações assim, o tratamento agudo com rAnxA1 foi capaz de restaurar a expressão das junções celulares, contribuindo para a redução do desenvolvimento de doenças cerebrais. Além disso, evidenciou-se que o tratamento *in vitro* com rAnxA1 resulta no aumento da expressão de Claudina 1 e ZO-1 no epitélio uterino durante a fase de fixação dos blastocistos (HEBEDA et al., 2020). Associados, estes dados sustentam a AnxA1 como uma proteína essencial para a estabilização das TJ, e aqui mostramos, pela primeira vez, o efeito da AnxA1 funcionalizada no rearranjo das TJs no epitelio intestinal durante a colite. Explorando os efeitos promissores da AnxA1 na expressão de TJ, buscamos uma abordagem para elucidar o papel da AnxA1 e de seu peptídeo mimético Ac2-26 de forma específica sobre células epiteliais intestinais. Para evitar a interferência do sistema imune, optamos por empregar o modelo 2D de monocamada derivada de enteroides. Esse modelo, também denominado “intestino em placa de cultura”, é capaz de mimetizar a barreira intestinal devido a capacidade de diferenciação celular das células-tronco adultas, as quais são utilizadas para o desenvolvimento de organóides.

Vários mecanismos estão associados à perda da barreira intestinal, como diminuição da expressão de TJs e proteínas de junção aderente, mudança na expressão de claudinas e modulação do citoesqueleto (LECHUGA; IVANOV, 2017). O mecanismo de mudança de expressão de claudina ocorre pela regulação positiva de claudinas formadoras de poros no epitélio inflamado, especialmente a claudina 2 (IVANOV; NAYDENOV, 2013). A regulação positiva de claudina 2 é identificada em vários cenários de inflamação intestinal e proporciona o aumento da permeabilidade da barreira (SAHOO et al., 2021; WEI et al., 2021; ZHANG et al., 2013). O aumento da permeabilidade intestinal leva à translocação de bactérias e endotoxinas (LPS) através da mucosa danificada para a circulação, causando inflamação sistêmica (LECHUGA; IVANOV, 2017; LI et al., 2023). A presença de LPS no intestino e na circulação ativa várias vias de sinalização por meio da ligação do receptor TLR4-4 e da estimulação do fator de transcrição NF-κB, levando à liberação de citocinas inflamatórias (FITZGERALD et al., 2003). Neste estudo, desafiamos os EDMs com

LPS para induzir a ruptura de TJ nas camadas epiteliais, como mostrado por um aumento na queda de TEER e na permeabilização do dextrano FITC nos EDMs desafiados por LPS ao longo do tempo. A ruptura na integridade da barreira intestinal pode ter ocorrido pela diminuição na expressão de ocludina, ZO-1 e caderina e a um aumento na expressão da proteína TJ formadora de poros, claudina 2. Os tratamentos AnxA1 e Ac2-26 reverteram todos os efeitos prejudiciais mediados por LPS sobre as EDMs expostos. Estas descobertas sugerem que AnxA1 e Ac2-26 têm um efeito protetor direto no epitélio intestinal, afetando a transcrição de várias proteínas de junção epitelial.

Em seguida, avaliamos o efeito de AnxA1 e Ac2-26 nas citocinas inflamatórias liberadas pelas células epiteliais após estímulo inflamatório. Para este fim, avaliamos o nível de CXCL-1 e MCP-1 como as principais citocinas pró-inflamatórias liberadas pelas células epiteliais intestinais no modelo intestinal 2D [Sayed et al., 2020a; Sayed et al., 2020b]. AnxA1 e Ac2-26 reduziram as citocinas pró-inflamatórias mediadas pelo LPS e aumentaram o nível da citocina anti-inflamatória IL-10. Embora os linfócitos e macrófagos sejam as principais fontes de IL-10 no intestino, as células epiteliais também secretam IL-10 (NGUYEN; ALJAMAEI; STADNYK, 2021).

A IL-10 atua sobre as células epiteliais intestinais e contribui para vários papéis na homeostase intestinal, como regular a liberação de citocinas, para manter a integridade da barreira intestinal e promover a tolerância do epitélio e afetar as ações celulares (Nguyen et al., 2021). Curiosamente, a IL-10 é uma citocina importante para a barreira intestinal e o TEER, uma vez que regula a expressão das TJs, principalmente reduzindo a expressão de claudina 2 (ZHENG et al., 2017), aumentando a expressão da junção de adesão E-caderina e do componente dos desmossomos, desmogleína 2 (XUE et al., 2016). Nossos dados *in vivo* em modelo de colite experimental já indicavam a relação da AnxA1 e IL-10, no entanto em um microambiente com a presença de células imunes. Estudos anteriores mostraram que os efeitos anti-inflamatórios de AnxA1 e Ac2-26 são decorrentes, principalmente, de ações em células do sistema imunológico, incluindo a diminuição da migração de células do sistema imunológico para a área inflamada e o aumento da apoptose dos neutrófilos (LEONI; NUSRAT, 2016; PERRETTI; D'ACQUISTO, 2009a). Como já salientado, as ações anti-inflamatórias da AnxA1 são mediadas pelos receptores e FPR1 e 2 presentes nas membranas celulares. Aqui, relatamos que um possível efeito anti-inflamatório de Anxa1 e Ac2-26 é mediado pelas células epiteliais.

A reorganização epitelial que ocorre na fase de regeneração tecidual na colite experimental é dependente de vias de sinalização de proliferação celular, alterações morfológicas e diferenciação celular. PCNA e Ki67 são proteínas nucleares envolvidas nesses procesos. PCNA participa das vias de síntese e reparo de DNA, enquanto Ki67 está envolvido na proliferação celular e na transcrição de RNA ribossômico (MROUJ et al., 2021; RANDALL-DEMLLO et al., 2016). Corroborando a reorganização das criptas visualizadas em animais tratados com MLNC-AnxA1, foi também observado aumento da proliferação celular na região da base da cripta intestinal, região essa onde estão localizadas as células células-tronco e as células em diferenciação, e constituem um centro de sinalização fundamental para a formação da barreira celular intestinal (HSU; LI; FUCHS, 2014). Além disso, o tratamento com AnxA1 funcionalizado por MLNC reduziu a proliferação de células que se estende a região apical. Este efeito é observado no crescimento desorganizado e células proliferadas em aproximadamente dois terços do comprimento da cripta podem ser indicativos de displasia celular (JURÍKOVÁ et al., 2016; RANDALL-DEMLLO et al., 2016). O tratamento com SBA15-Ac2-26 proporcionou o aumento do número de células positivas para PCNA. Apesar da distribuição das células PCNA+ ocorrer de forma desorganizada, percorrendo a cripta em direção a parte apical, a combinação desse resultado com a histologia, o escore histológico e os sintomas clínicos do grupo tratado com SBA15-Ac2-26 indicam proliferação não associada a displasia e sim a regeneração tecidual. No estanto, para confirmar essa hipótese seria necessário a utilização de outro marcador de proliferação celular.

A formulação da nanocápsula de PCL é considerada biocompatível e biodegradável (POHLMANN et al., 2013), no entanto, alguns de seus compostos podem interferir em funções celulares e alterar a resposta celular fisiológica, promovendo efeitos tóxicos (IVANOV, 2008). O ensaio de MTT, o qual avalia a função mitocondrial, foi utilizado como teste de triagem para viabilidade e demonstrou que as concentrações (3) e (4) de MLNC e MLNC-AnxA1 (Tabela 3), após incubação de 48 horas apresentam atividade mitocondrial inferior a 75%. A citotoxicidade observada pode estar relacionada a alguns componentes da estrutura da nanocápsula, como o surfactante Tween 20. Como observado em um trabalho realizado por Eskandani et al. (2013) que utilizou o MTT para avaliar o crescimento celular, o Tween 20 foi capaz de reduzir o crescimento de células HUVEC e A549 de forma concentração

dependente, além de causar danos ao DNA, fragmentação de cromatina e induzir as células a apoptose. Outro trabalho avaliando a citotoxicidade de LNCs sobre células Raw 264.7, identificou que o componente surfactante com funç emulsificantes e solubilizantes, Solutol®, presente na estrutura da nanocápsula, também causava efeitos tóxicos, sendo que este foi o único componente identificado como tóxico, e quando testada a LNC completa (contendo o surfactante), não foram observados efeitos tóxicos quando comparado com o surfactante isolado (LE ROUX et al., 2017).

De acordo com as características do sistema coloidal empregado no presente trabalho, a análise de citotoxicidade por um método colorimétrico que utiliza a dispersão de luz, como o MTT, não é considerada a melhor alternativa para análise. Além disso, o resultado pode estar associado a alteração do metabolismo mitocondrial, e não a ausência de viabilidade diretamente (DE CRISTO SOARES ALVES et al., 2020; STEPANENKO; DMITRENKO, 2015). Células viáveis e com membranas celulares integras apresentam um conjunto de enzimas denominadas esterases que atuam de forma eficiente. Dessa forma, outra alternativa para análise direta de viabilidade é a marcação com calceína. Por se tratar de um método bem padronizado na literatura, apresenta alta sensibilidade. Essa substância incolor reage com as esterases, que removem os grupos éster e tornam a molécula fluorescente, ficando retida no citoplasma celular de células integras (BRATOSIN et al., 2005; LICHTENFELS et al., 1994). Foi observado que o tratamento com MLNC ou MLNC-AnxA1 reduziu o a porcentagem de células viáveis após 48 horas, diferentemente da AnxA1 que não causou toxicidade. Os resultados observados demonstraram que a toxicidade de MLNC e MLNC-AnxA1 na maior concentração de partículas apresenta diferença significativa na porcentagem de células em necrose após 48 horas de tratamento. Esse resultado corrobora com outros estudos que utilizaram a nanocápsula de PCL e observaram aumento de apoptose e necrose quando comparados os grupos MLNC contendo anticorpos em relação ao anticorpo livre (BRUINSMANN et al., 2020; DE CRISTO SOARES ALVES et al., 2020). Esse resultado sugere que o efeito tóxico encontrado no ensaio de morte celular é relativo a nanocápsula, e não a AnxA1.

A citotoxicidade de SBA-15 é extensivamente reportada pela literatura em diferentes tipos celulares, dentre eles a célula epitelial intestinal Caco-2 e células endoteliais HUVEC Ainda, as concentrações utilizadas nesses estudos são pelo menos quatro vezes maiores do que as utilizada em no presente trabalho (ALMÁŠI et

al., 2020; HEIKKILÄ et al., 2010; ZHAO et al., 2021). Nossos resultados demonstraram que 50 ng/mL de SBA-15 não apresentou efeitos tóxicos para macrófagos e células Caco-2 (dados não apresentados) sendo concentração de SBA-15 testada foi baseada nas concentrações de Ac2-26 utilizadas na literatura.

As NPs podem interagir de diferentes formas com células do sistema imune e serem captadas por diferentes mecanismos de endocitose de acordo com o tipo celular estudado e as características físico-químicas da NP utilizada (FARACE et al., 2016; GILLERON et al., 2013). A capacidade de internalização ou captação de NPs pelas células é o principal critério a ser levado em consideração antes da sua utilização *in vivo*, em especial o diâmetro e o PDI atributos a nanocarreadores lipídicos, que podem alterar a internalização celular, estabilidade, eficiência do encapsulamento, o perfil de liberação do medicamento, a biodistribuição e a mucoadesão (AZHAR; BAHARI; HAMISHEHKAR, 2016). Sabe-se que o *uptake* celular ocorre de forma quase exclusiva via endocitose, que é o processo de transporte ativo de materiais para o interior da célula. Esse processo ocorre principalmente por (1) endocitose dependente de clatrina e dinamina, (2) endocitose independente de clatrina, mas dependente de dinamina para endocitose rápida conduzida por ligante de proteínas de membrana específicas, (3) endocitose independente de clatrina e dinamina, (4) macropinocitose e (5) fagocitose.

Nosso resultado demonstrou que MLNC foi internalizada por macrófagos após 2 horas de tratamento, no entanto MLNC-AnxA1 necessitou de um tempo superior, sugerindo que a presença da proteína AnxA1 em sua estrutura possa estar alterando o mecanismo de endocitose, sendo necessário um tempo superior a 2 horas de tratamento para internalização. Esse resultado corrobora outros estudos que utilizaram LNC e observaram *uptake* da nanocápsulas em diferentes tipos celulares, como células de melanoma e endoteliais (DREWES et al., 2017b; PEREIRA et al., 2018; SANDRI et al., 2019). Ainda, um estudo realizado por Cavalcante et al. (2016), utilizando células Raw 264.7 tratadas com a MLNC funcionalizada com anticorpo reportou internalização celular após 3 horas de tratamento, corroborando nosso resultado o qual demonstrou ser necessário um tempo superior a 2 horas para a endocitose da MLNC-AnxA1. O estudo também avaliou os mecanismos de endocitose das NCs e concluiu que o mecanismo responsável pela internalização das NCs ocorre por meio de pinocitose, principalmente via macropinocitose e com pequena

participação de vias dependentes de dinamina. Por se tratar da mesma NC utilizada em nosso trabalho e também possuir uma proteína em sua camada polimérica, sugere-se que a MLNC-AnxA1 foi internalizada por mecanismo semelhante. No entanto, estudos utilizando bloqueadores de endocitose são necessários para confirmar essa hipótese.

Usualmente partículas com tamanho superior a 500 nm são internalizadas via fagocitose (MORENO-MENDIETA et al., 2022). De acordo com os resultados obtidos para as análises físicas de SBA-15, investigamos o mecanismo de captação dessas partículas por macrófagos J774A.1 e Raw 264.7. Macrófagos foram capazes de internalizar SBA-15 epós 4 horas de incubação, sendo esse resultado mais proeminente em 24 horas. A fagocitose foi confirmada como mecanismo responsável pela internalização da SBA-15 pela pré-incubação das células com o inibidor de fagocitose, citocalasina B. Ainda, nossos resultados demonstraram baixa internalização de SBA-15 sobre células epiteliais intestinais, resultado este confirmado pelos modelos de EDM e citometria de fluxo (dados não apresentados). Esse resultado corrobora a literatura que descreve a SBA-15 como um veículo para liberação rápida de substâncias, sendo sua absorção intestinal baixa (LI et al., 2015; ZHAO et al., 1998a).

Apesar da baixa internalização de SBA-15 por células epiteliais intestinais, nossos resultados demonstraram que o Ac2-26 foi propriamente liberado, sendo detectado tanto em macrófagos quanto células Caco-2. Este resultado sugere que a SBA-15-Ac2-26-Eud pode ser considerada um veículo promissor para o tratamento da colite, oferecendo um mecanismo eficaz de liberação local do peptídeo. Essa descoberta destaca o potencial terapêutico dessa formulação no contexto do tratamento da colite, abrindo caminho para investigações mais aprofundadas e desenvolvimento clínico.

Conclusões

Os resultados obtidos no presente trabalho revelam que as plataformas MLNC e SBA-15 desenvolvidas foram eficazes para a incorporação de rAnxA1 (92%) e Ac2-26 (88%) em MLNC e SBA-15, respectivamente. A funcionalização do MLNC demonstrou ser uma ferramenta eficaz para a entrega, via intraperitoneal, de moléculas hidrofílicas, oferecendo ações anti-inflamatórias e pró-resolução na reparação de tecidos danificados nos distúrbios intestinais. A reversão dos sintomas da colite experimental, associados a recuperação tecidual, ressaltou o potencial terapêutico da micropartícula SBA-15 revestida por polímero pela via oral. Embora ambas as abordagens apresentem resultados experimentais promissores, é crucial salientar a necessidade contínua de investigações mais aprofundadas para avaliar integralmente os riscos e benefícios dessas estratégias terapêuticas para doenças inflamatórias intestinais.

Referências bibliográficas

A JERSMANN, H. P. et al. Bacterial Lipopolysaccharide and Tumor Necrosis Factor Alpha Synergistically Increase Expression of Human Endothelial Adhesion Molecules through Activation of NF-B and p38 Mitogen-Activated Protein Kinase Signaling Pathways. **INFECTION AND IMMUNITY**, v. 69, n. 3, p. 1273–1279, 2001.

AGACE, W. W. T-cell recruitment to the intestinal mucosa. **Trends in Immunology**, v. 29, n. 11, p. 514–522, nov. 2008.

AHMAD, R. et al. Targeted colonic claudin-2 expression renders resistance to epithelial injury, induces immune suppression, and protects from colitis. 2014.

AIKAWA, M. et al. Mechanisms and Consequences of Defective efferocytosis in Atherosclerosis. **Article**, v. 4, p. 1, 2018.

AKUTKO, K.; STAWARSKI, A. Probiotics, Prebiotics and Synbiotics in Inflammatory Bowel Diseases. **Journal of Clinical Medicine**, v. 10, n. 11, p. 2466, 2 jun. 2021.

AL-HORANI, R.; SPANUDAKIS, E.; HAMAD, B. The market for ulcerative colitis. **Nature Reviews Drug Discovery**, v. 21, n. 1, p. 15–16, 23 jan. 2022.

AL SHOYAIB, A.; ARCHIE, S. R.; KARAMYAN, V. T. Intraperitoneal Route of Drug Administration: Should it Be Used in Experimental Animal Studies? **Pharmaceutical Research**, v. 37, n. 1, 2020.

ALMÁŠI, M. et al. Cytotoxicity study and influence of SBA-15 surface polarity and pH on adsorption and release properties of anticancer agent pemetrexed. **Materials Science and Engineering: C**, v. 109, p. 110552, abr. 2020.

ANGUS, H. C. K. et al. Intestinal Organoids as a Tool for Inflammatory Bowel Disease Research. **Frontiers in Medicine**, v. 6, 17 jan. 2020.

ANSELMO, A. C.; MITRAGOTRI, S. Nanoparticles in the clinic. **Bioengineering & Translational Medicine**, v. 1, n. 1, p. 10–29, 3 mar. 2016.

APPIAH-NTIAMOAH, R.; CHUNG, W. J.; KIM, H. A highly selective SBA-15 supported fluorescent “turn-on” sensor for the fluoride anion. **New Journal of Chemistry**, v. 39, n. 7, p. 5570–5579, 2015.

AZHAR, L.; BAHARI, S.; HAMISHEHKAR, H. The Impact of Variables on Particle Size of Solid Lipid Nanoparticles and Nanostructured Lipid Carriers; A Comparative Literature Review. **Tabriz University of Medical Sciences**, v. 6, n. 2, p. 143–151, 2016.

BABBIN, B. A. et al. Annexin A1 Regulates Intestinal Mucosal Injury, Inflammation, and Repair. **The Journal of Immunology**, v. 181, n. 7, p. 5035–5044, 2008.

BAHARI, L. A. S.; HAMISHEHKAR, H. **The impact of variables on particle size of**

solid lipid nanoparticles and nanostructured lipid carriers; A comparative literature reviewAdvanced Pharmaceutical Bulletin, 2016.

BAIN, C. C. et al. Resident and pro-inflammatory macrophages in the colon represent alternative context-dependent fates of the same Ly6Chi monocyte precursors. **Mucosal Immunology**, v. 6, n. 3, p. 498–510, maio 2013.

BAIN, C. C. et al. Constant replenishment from circulating monocytes maintains the macrophage pool in the intestine of adult mice. **Nature Immunology**, v. 15, n. 10, p. 929–937, 24 out. 2014.

BAIN, C. C. et al. Long-lived self-renewing bone marrow-derived macrophages displace embryo-derived cells to inhabit adult serous cavities. **Nature Communications**, v. 7, n. 1, 13 set. 2016.

BAR-EPHRAIM, Y. E.; KRETZSCHMAR, K.; CLEVERS, H. **Organoids in immunological researchNature Reviews Immunology**, 2020. Disponível em: <https://doi.org/10.1038/>

BARBOSA, J. A. C. et al. Using zeta potential to study the ionisation behaviour of polymers employed in modified-release dosage forms and estimating their pKa. **International Journal of Pharmaceutics: X**, v. 1, p. 100024, dez. 2019.

BARKER, N. et al. Identification of stem cells in small intestine and colon by marker gene Lgr5. **Nature**, v. 449, n. 7165, p. 1003–1007, 14 out. 2007.

BARKER, N. Adult intestinal stem cells: critical drivers of epithelial homeostasis and regeneration. **Nature Reviews Molecular Cell Biology**, v. 15, n. 1, p. 19–33, 11 jan. 2014.

BASAK, O. et al. Induced Quiescence of Lgr5+ Stem Cells in Intestinal Organoids Enables Differentiation of Hormone-Producing Enteroendocrine Cells. **Cell Stem Cell**, v. 20, n. 2, p. 177- 190.e4, fev. 2017.

BAYDI, Z. et al. An Update of Research Animal Models of Inflammatory Bowel Disease. **The Scientific World Journal**, v. 2021, p. 1–12, 13 dez. 2021.

BECK, J. S. et al. A new family of mesoporous molecular sieves prepared with liquid crystal templates. **Journal of the American Chemical Society**, v. 114, n. 27, p. 10834–10843, 1 dez. 1992.

BEGINES, B. et al. Polymeric Nanoparticles for Drug Delivery: Recent Developments and Future Prospects. **Nanomaterials**, v. 10, n. 7, 19 jul. 2020.

BENDER, E. A. et al. Hemocompatibility of poly(ε-caprolactone) lipid-core

nanocapsules stabilized with polysorbate 80-lecithin and uncoated or coated with chitosan. **International Journal of Pharmaceutics**, v. 426, n. 1–2, p. 271–279, 2012.

BENDER, E. A. et al. New strategy to surface functionalization of polymeric nanoparticles: One-pot synthesis of scFv anti-LDL(-)-functionalized nanocapsules. **Pharmaceutical Research**, v. 31, n. 11, p. 2975–2987, 2014.

BÉNÉZECH, C. et al. Inflammation-induced formation of fat-associated lymphoid clusters. **Nature Immunology**, v. 16, n. 8, 29 ago. 2015.

BERNARDI, A. et al. Indomethacin-loaded lipid-core nanocapsules reduce the damage triggered by Aβ1-42 in Alzheimer’s disease models. **International Journal of Nanomedicine**, set. 2012.

BERNINK, J. H. et al. Human type 1 innate lymphoid cells accumulate in inflamed mucosal tissues. **Nature Immunology**, v. 14, n. 3, p. 221–229, 20 mar. 2013.

BJERG BENNIKE, T. et al. Neutrophil Extracellular Traps in Ulcerative Colitis: A Proteome Analysis of Intestinal Biopsies. 2015.

BLACKBURN, S. C.; STANTON, M. P. Anatomy and physiology of the peritoneum. **Seminars in Pediatric Surgery**, v. 23, n. 6, dez. 2014.

BLACKWELL, G. J. et al. Macrocortin: a polypeptide causing the anti-phospholipase effect of glucocorticoids. **Nature**, v. 287, n. 5778, set. 1980.

BOURGONJE, A. R. et al. Patients With Inflammatory Bowel Disease Show IgG Immune Responses Towards Specific Intestinal Bacterial Genera. **Frontiers in Immunology**, v. 13, 25 maio 2022.

BRANCALEONE, V. et al. Annexin a1 mediates hydrogen sulfide properties in the control of inflammation. **Journal of Pharmacology and Experimental Therapeutics**, v. 351, n. 1, p. 96–104, 2014.

BRANQUINHO, R. T. et al. Biodegradable Polymeric Nanocapsules Prevent Cardiotoxicity of Anti-Trypanosomal Lychnopholide OPEN. **Nature Publishing Group**, 2017.

BRATOSIN, D. et al. Novel fluorescence assay using calcein-AM for the determination of human erythrocyte viability and aging. **Cytometry Part A**, v. 66, n. 1, p. 78–84, 2005.

BRINKMANN, V. Neutrophil Extracellular Traps Kill Bacteria. **Science**, v. 303, n. 5663, 5 mar. 2004.

BRITTON, G. J. et al. Microbiotas from Humans with Inflammatory Bowel Disease Alter the Balance of Gut Th17 and RORγt+ Regulatory T Cells and Exacerbate Colitis in

Mice. **Immunity**, v. 50, n. 1, p. 212- 224.e4, jan. 2019.

BROERING, M. F. et al. Development of Annexin A1-surface-functionalized metal-complex multi-wall lipid core nanocapsules and effectiveness on experimental colitis. **European Journal of Pharmaceutics and Biopharmaceutics**, v. 181, n. June, p. 49–59, 2022.

BROWN, S. B.; SAVILL, J. Phagocytosis Triggers Macrophage Release of Fas Ligand and Induces Apoptosis of Bystander Leukocytes. **The Journal of Immunology**, v. 162, n. 1, p. 480–485, 1 jan. 1999.

BRUINSMANN, F. A. et al. Erlotinib-Loaded Poly(ε-Caprolactone) Nanocapsules Improve In Vitro Cytotoxicity and Anticlonogenic Effects on Human A549 Lung Cancer Cells. **AAPS PharmSciTech**, v. 21, n. 6, 2020.

BUCHMAN, A. L. Side Effects of Corticosteroid Therapy. **Journal of Clinical Gastroenterology**, v. 33, n. 4, out. 2001.

CALÀ, G. et al. Primary human organoids models: Current progress and key milestones. **Frontiers in Bioengineering and Biotechnology**, v. 11, 3 mar. 2023.

CAMPBELL, D. J.; BUTCHER, E. C. Rapid Acquisition of Tissue-specific Homing Phenotypes by CD4 + T Cells Activated in Cutaneous or Mucosal Lymphoid Tissues. **The Journal of Experimental Medicine**, v. 195, n. 1, p. 135–141, 7 jan. 2002.

CAVALCANTE, M. F. et al. scFv-Anti-LDL(-)-Metal-Complex Multi-Wall Functionalized-Nanocapsules as a Promising Tool for the Prevention of Atherosclerosis Progression. **Frontiers in Medicine**, v. 8, n. April, p. 1–14, 2021.

CÉ, R. et al. Chitosan-coated dapsone-loaded lipid-core nanocapsules: Growth inhibition of clinical isolates, multidrug-resistant Staphylococcus aureus and Aspergillus ssp. **Colloids and Surfaces A: Physicochemical and Engineering Aspects**, 2016.

CHANG, J. T.; WHERRY, E. J.; GOLDRATH, A. W. Molecular regulation of effector and memory T cell differentiation. **Nature Immunology**, v. 15, n. 12, p. 1104–1115, 14 dez. 2014.

CHAPARRO, M. et al. Safety of Thiopurine Therapy in Inflammatory Bowel Disease: Long-term Follow-up Study of 3931 Patients. 2013.

CHASSAING, B. et al. Dextran sulfate sodium (DSS)-induced colitis in mice. **Current Protocols in Immunology**, 2014.

CHATTERJEE, B. E. et al. Annexin 1-deficient neutrophils exhibit enhanced

transmigration in vivo and increased responsiveness in vitro. **Journal of Leukocyte Biology**, v. 78, n. 3, set. 2005.

CHELAKKOT, C.; GHIM, J.; RYU, S. H. Mechanisms regulating intestinal barrier integrity and its pathological implications. **Experimental and Molecular Medicine**, v. 50, n. 8, 2018.

CHIANG, N.; SERHAN, C. N. Cell-Cell Interaction in the Transcellular Biosynthesis of Novel ω-3-Derived Lipid Mediators. In: **Cell-Cell Interactions in Health and Disease**. New Jersey: Humana Press, 2006. v. 341.

CHOI, Y. et al. A Biodegradation Study of SBA-15 Microparticles in Simulated Body Fluid and *in Vivo*. **Langmuir**, v. 31, n. 23, p. 6457–6462, 16 jun. 2015.

CLARK, M. et al. American Gastroenterological Association Consensus Development Conference on the Use of Biologics in the Treatment of Inflammatory Bowel Disease, June 21–23, 2006. **Gastroenterology**, v. 133, n. 1, jul. 2007.

CLEVERS, H. Modeling Development and Disease with Organoids. **Cell**, v. 165, n. 7, p. 1586–1597, jun. 2016.

COLOMBEL, J. F.; NARULA, N.; PEYRIN-BIROULET, L. Management Strategies to Improve Outcomes of Patients With Inflammatory Bowel Diseases. **Gastroenterology**, 2017.

COORAY, S. N. et al. Ligand-specific conformational change of the G-protein-coupled receptor ALX/FPR2 determines proresolving functional responses. **Proceedings of the National Academy of Sciences**, v. 110, n. 45, 5 nov. 2013.

CRISTANTE, E. et al. Identification of an essential endogenous regulator of blood–brain barrier integrity, and its pathological and therapeutic implications. **Proceedings of the National Academy of Sciences**, v. 110, n. 3, p. 832–841, 15 jan. 2013.

CROMPTON, M. R.; MOSS, S. E.; CRUMPTON, M. J. Diversity in the lipocortin/calpactin family. **Cell**, v. 55, n. 1, out. 1988.

CUFFARI, C. et al. 6-Mercaptopurine metabolism in Crohn's disease: correlation with efficacy and toxicity. **Gut**, v. 39, p. 401–406, 1996.

CUNNINGHAM, K. E.; TURNER, J. R. Myosin light chain kinase: pulling the strings of epithelial tight junction function. **Annals of the New York Academy of Sciences**, v. 1258, n. 1, p. 34–42, 25 jul. 2012.

ČUŽIĆ, S. et al. Claudins: Beyond Tight Junctions in Human IBD and Murine Models. **Frontiers in Pharmacology**, v. 12, 17 nov. 2021.

D'ALDEBERT, E. et al. Characterization of Human Colon Organoids From

Inflammatory Bowel Disease Patients. **Frontiers in Cell and Developmental Biology**, v. 8, 4 jun. 2020.

DALLI, J. et al. Annexin A1 regulates neutrophil clearance by macrophages in the mouse bone marrow. **The FASEB Journal • Research Communication**, [s.d.].

DALLI, J. et al. Annexin 1 mediates the rapid anti-inflammatory effects of neutrophil-derived microparticles. **Blood**, v. 112, n. 6, p. 2512–2519, 15 set. 2008.

DANAEI, M. et al. Impact of particle size and polydispersity index on the clinical applications of lipidic nanocarrier systems. **Pharmaceutics**, v. 10, n. 2, p. 1–17, 2018.

DAVIS, M. E. Ordered porous materials for emerging applications. **Nature**, v. 417, n. 6891, p. 813–821, jun. 2002.

DE CASTRO LEÃO, M. et al. Docosahexaenoic acid nanoencapsulated with anti-PECAM-1 as co-therapy for atherosclerosis regression. **European Journal of Pharmaceutics and Biopharmaceutics**, v. 159, fev. 2021.

DE CRISTO SOARES ALVES, A. et al. Chitosan-Coated Lipid-Core Nanocapsules Functionalized with Gold-III and Bevacizumab Induced In Vitro Cytotoxicity against C6 Cell Line and In Vivo Potent Antiangiogenic Activity. **Pharmaceutical Research**, v. 37, n. 6, 2020.

DE PAULA-SILVA, M. et al. Role of the protein annexin A1 on the efficacy of anti-TNF treatment in a murine model of acute colitis. **Biochemical Pharmacology**, 2016a.

DE PAULA-SILVA, M. et al. Role of the protein annexin A1 on the efficacy of anti-TNF treatment in a murine model of acute colitis. **Biochemical Pharmacology**, v. 115, p. 104–113, 2016b.

DE PAULA-SILVA, M. et al. Role of the protein annexin A1 on the efficacy of anti-TNF treatment in a murine model of acute colitis. **Biochemical Pharmacology**, v. 115, p. 104–113, set. 2016c.

DE PAULA-SILVA, M. et al. Formyl Peptide Receptors and Annexin A1: Complementary Mechanisms to Infliximab in Murine Experimental Colitis and Crohn's Disease. **Frontiers in Immunology**, v. 12, 17 set. 2021.

DE SOUSA E MELO, F.; DE SAUVAGE, F. J. Cellular Plasticity in Intestinal Homeostasis and Disease. **Cell Stem Cell**, v. 24, n. 1, p. 54–64, jan. 2019.

DEAN, S.; MANSOORI, G.; FAUZI SOELAIMAN, T. Nanotechnology — An Introduction for the Standards Community. **Journal of ASTM International**, v. 2, n. 6, 2005.

DENG, Y. et al. Improved i.p. drug delivery with bioadhesive nanoparticles. **Proceedings of the National Academy of Sciences**, v. 113, n. 41, p. 11453–11458, 11 out. 2016.

DIAMOND, J. M. Channels in epithelial cell membranes and junctions. **Federation proceedings**, v. 37, n. 12, p. 2639–43, out. 1978.

DIMER, F. A. et al. Impactos da nanotecnologia na saúde: produção de medicamentos. **Quimica Nova**, 2013.

DOTTI, I. et al. Alterations in the epithelial stem cell compartment could contribute to permanent changes in the mucosa of patients with ulcerative colitis. **Gut**, v. 66, n. 12, p. 2069–2079, dez. 2017.

DREWES, CARINE et al. role of poly(ε-caprolactone) lipid-core nanocapsules on melanoma-neutrophil crosstalk. **International Journal of Nanomedicine**, p. 12–7153, 2017a.

DREWES, C. C. et al. Role of poly(ε-caprolactone) lipid-core nanocapsules on melanoma-neutrophil crosstalk. **International Journal of Nanomedicine**, 2017b.

ERDOĞAR, N.; AKKIN, S.; BILENSOY, E. Nanocapsules for Drug Delivery: An Updated Review of the Last Decade. **Recent Patents on Drug Delivery & Formulation**, 2019.

ESKANDANI, M.; HAMISHEHKAR, H.; DOLATABADI, J. E. N. Cyto/genotoxicity study of polyoxyethylene (20) sorbitan monolaurate (tween 20). **DNA and Cell Biology**, v. 32, n. 9, p. 498–503, 2013.

FARACE, C. et al. Immune cell impact of three differently coated lipid nanocapsules: Pluronic, chitosan and polyethylene glycol. **Scientific Reports**, v. 6, n. November 2015, p. 1–14, 2016.

FARACHE, J. et al. Luminal Bacteria Recruit CD103+ Dendritic Cells into the Intestinal Epithelium to Sample Bacterial Antigens for Presentation. **Immunity**, v. 38, n. 3, p. 581–595, mar. 2013.

FARAJI, A. H.; WIPF, P. Nanoparticles in cellular drug delivery. **Bioorganic & Medicinal Chemistry**, v. 17, n. 8, abr. 2009.

FARQUHAR, M. G.; PALADE, G. E. JUNCTIONAL COMPLEXES IN VARIOUS EPITHELIA. **The Journal of Cell Biology**, v. 17, n. 2, p. 375–412, 1 maio 1963.

FEUERSTEIN, J. D. et al. Meta-analysis of dye-based chromoendoscopy compared with standard- and high-definition white-light endoscopy in patients with inflammatory bowel disease at increased risk of colon cancer. **Gastrointestinal Endoscopy**, v. 90,

n. 2, p. 186- 195.e1, ago. 2019.

FIEL, L. A. et al. Diverse deformation properties of polymeric nanocapsules and lipid-core nanocapsules. **Soft Matter**, v. 7, n. 16, 2011.

FIEL, L. A. et al. Variable temperature multiple light scattering analysis to determine the enthalpic term of a reversible agglomeration in submicrometric colloidal formulations: A quick quantitative comparison of the relative physical stability. **Colloids and Surfaces A: Physicochemical and Engineering Aspects**, v. 431, ago. 2013.

FITZGERALD, K. A. et al. LPS-TLR4 Signaling to IRF-3/7 and NF-κB Involves the Toll Adapters TRAM and TRIF. **The Journal of Experimental Medicine**, v. 198, n. 7, p. 1043–1055, 6 out. 2003.

FLOWER, R. J.; ROTHWELL, N. J. Lipocortin-1: cellular mechanisms and clinical relevance. **Trends in Pharmacological Sciences**, v. 15, n. 3, p. 71–76, mar. 1994.

FRANK, D. N. et al. Molecular-phylogenetic characterization of microbial community imbalances in human inflammatory bowel diseases. **Proceedings of the National Academy of Sciences**, v. 104, n. 34, p. 13780–13785, 21 ago. 2007.

FRANK, L. A. et al. Improving drug biological effects by encapsulation into polymeric nanocapsules. **Wiley Interdisciplinary Reviews: Nanomedicine and Nanobiotechnology**, 2015.

FRIEDRICH, R. B. et al. Nanoencapsulation of Tacrolimus in Lipid-Core Nanocapsules Showed Similar Immunosuppressive Activity After Oral and Intraperitoneal Administrations. **Journal of Biomedical Nanotechnology**, v. 10, n. 8, 1 ago. 2014.

FUJINO, S. Increased expression of interleukin 17 in inflammatory bowel disease. **Gut**, v. 52, n. 1, p. 65–70, 1 jan. 2003.

FUSS, I. J. et al. Nonclassical CD1d-restricted NK T cells that produce IL-13 characterize an atypical Th2 response in ulcerative colitis. **Journal of Clinical Investigation**, v. 113, n. 10, 15 maio 2004.

GAUDIER, E. et al. Butyrate specifically modulates *MUC* gene expression in intestinal epithelial goblet cells deprived of glucose. **American Journal of Physiology-Gastrointestinal and Liver Physiology**, v. 287, n. 6, p. G1168–G1174, dez. 2004.

GAVINS, F. N. E.; HICKEY, M. J. Annexin A1 and the regulation of innate and adaptive immunity. **Frontiers in Immunology**, v. 3, n. NOV, p. 1–11, 2012.

GEBOES, K. et al. A reproducible grading scale for histological assessment of inflammation in ulcerative colitis. **Gut**, v. 47, p. 404–409, 2000.

GETTING, S. J.; FLOWER, R. J.; PERRETTI, M. **Inhibition of neutrophil and monocyte recruitment by endogenous and exogenous lipocortin 1.** [s.l: s.n.].

GILLERON, J. et al. Image-based analysis of lipid nanoparticle–mediated siRNA delivery, intracellular trafficking and endosomal escape. **Nature Biotechnology**, 2013.

GIROL, A. P. et al. Anti-Inflammatory Mechanisms of the Annexin A1 Protein and Its Mimetic Peptide Ac2-26 in Models of Ocular Inflammation In Vivo and In Vitro. **The Journal of Immunology**, v. 190, n. 11, 1 jun. 2013a.

GIROL, A. P. et al. Anti-Inflammatory Mechanisms of the Annexin A1 Protein and Its Mimetic Peptide Ac2-26 in Models of Ocular Inflammation In Vivo and In Vitro. **The Journal of Immunology**, v. 190, n. 11, p. 5689–5701, 1 jun. 2013b.

GIRON, F. et al. Nanotechnology in the treatment of inflammatory bowel disease. **Inflammatory Bowel Diseases**, v. 25, n. 12, p. 1871–1880, 2019.

GKILIOPOULOS, D. et al. SBA-15 Mesoporous Silica as Delivery Vehicle for rhBMP-2 Bone Morphogenic Protein for Dental Applications. **Nanomaterials**, v. 12, n. 5, p. 822, 28 fev. 2022.

GLATTER, O. Data evaluation in small angle scattering: calculation of the radial electron density distribution by means of indirect Fourier transformation. **Acta Physica Austriaca**, v. 47, n. 1–2, p. 83–102, 1977.

GOULD, S. E.; JUNTTILA, M. R.; DE SAUVAGE, F. J. Translational value of mouse models in oncology drug development. **Nature Medicine**, v. 21, n. 5, p. 431–439, 7 maio 2015.

GRAHAM, D. B.; XAVIER, R. J. Pathway paradigms revealed from the genetics of inflammatory bowel disease. **Nature**, v. 578, n. 7796, p. 527–539, 27 fev. 2020.

GROOTJANS, J. et al. Ischaemia-induced mucus barrier loss and bacterial penetration are rapidly counteracted by increased goblet cell secretory activity in human and rat colon. **Gut**, v. 62, n. 2, p. 250–258, fev. 2013.

GROSS, M.; SALAME, T.-M.; JUNG, S. Guardians of the Gut â€“ Murine Intestinal Macrophages and Dendritic Cells. **Frontiers in Immunology**, v. 6, 2 jun. 2015.

GÜNZEL, D.; YU, A. S. L. CLAUDINS AND THE MODULATION OF TIGHT JUNCTION PERMEABILITY. 2013.

GUO, Y.; LU, N.; BAI, A. Clinical Use and Mechanisms of Infliximab Treatment on Inflammatory Bowel Disease: A Recent Update. **BioMed Research International**, v. 2013, 2013.

GUTERRES, S. S.; ALVES, M. P.; POHLMANN, A. R. Polymeric Nanoparticles, Nanospheres and Nanocapsules, for Cutaneous Applications. **Drug Target Insights**, 2007.

HARHAJ, N. S.; ANTONETTI, D. A. Regulation of tight junctions and loss of barrier function in pathophysiology. **The International Journal of Biochemistry & Cell Biology**, v. 36, n. 7, p. 1206–1237, jul. 2004.

HARIDAS, V. et al. Reciprocal regulation of pro-inflammatory Annexin A2 and anti-inflammatory Annexin A1 in the pathogenesis of rheumatoid arthritis. **Molecular Biology Reports**, v. 46, n. 1, 13 fev. 2019.

HART, A. L. et al. Characteristics of Intestinal Dendritic Cells in Inflammatory Bowel Diseases. **Gastroenterology**, v. 129, n. 1, jul. 2005.

HAYHOE, R. P. G. et al. Annexin 1 and its bioactive peptide inhibit neutrophil-endothelium interactions under flow: indication of distinct receptor involvement. **Blood**, v. 107, n. 5, p. 2123–2130, 1 mar. 2006.

HEBEDA, C. B. et al. Annexin A1/Formyl Peptide Receptor Pathway Controls Uterine Receptivity to the Blastocyst. **Cells**, v. 9, n. 5, p. 1188, 11 maio 2020.

HEIKKILÄ, T. et al. Cytotoxicity study of ordered mesoporous silica MCM-41 and SBA-15 microparticles on Caco-2 cells. **European Journal of Pharmaceutics and Biopharmaceutics**, v. 74, n. 3, p. 483–494, mar. 2010.

HELLER, F. et al. Epithelial apoptosis is a prominent feature of the epithelial barrier disturbance in intestinal inflammation: effect of pro-inflammatory interleukin-13 on epithelial cell function. **Mucosal Immunology**, v. 1, n. S1, 15 nov. 2008.

HIGASHIYAMA, M.; HOKARI, R. New and Emerging Treatments for Inflammatory Bowel Disease. **Digestion**, v. 104, n. 1, p. 74–81, 2023.

HOLMÉN LARSSON, J. M. et al. A complex, but uniform O-glycosylation of the human MUC2 mucin from colonic biopsies analyzed by nanoLC/MSn. **Glycobiology**, v. 19, n. 7, p. 756–766, jul. 2009.

HOROWITZ, A. et al. Paracellular permeability and tight junction regulation in gut health and disease. **Nature Reviews Gastroenterology & Hepatology**, v. 20, n. 7, p. 417–432, 25 jul. 2023.

HOWE, K. L. et al. Transforming Growth Factor-β Regulation of Epithelial Tight Junction Proteins Enhances Barrier Function and Blocks Enterohemorrhagic Escherichia coli O157:H7-Induced Increased Permeability. **The American Journal of**

Pathology, v. 167, n. 6, p. 1587–1597, dez. 2005.

HSU, Y.-C.; LI, L.; FUCHS, E. Transit-Amplifying Cells Orchestrate Stem Cell Activity and Tissue Regeneration. 2014.

HUA, S. et al. Advances in oral nano-delivery systems for colon targeted drug delivery in inflammatory bowel disease: Selective targeting to diseased versus healthy tissue. **Nanomedicine: Nanotechnology, Biology, and Medicine**, v. 11, n. 5, p. 1117–1132, 2015.

HUA, S. Advances in Oral Drug Delivery for Regional Targeting in the Gastrointestinal Tract - Influence of Physiological, Pathophysiological and Pharmaceutical Factors. **Frontiers in Pharmacology**, v. 11, 28 abr. 2020.

HUDSON, S. P. et al. The biocompatibility of mesoporous silicates. **Biomaterials**, v. 29, n. 30, p. 4045–4055, out. 2008.

HWANG, J. M.; VARMA, M. G. Surgery for inflammatory bowel disease. **World Journal of Gastroenterology**, v. 14, n. 17, p. 2678, 2008.

IM, J. P. et al. Changing treatment paradigms for the management of inflammatory bowel disease. **The Korean Journal of Internal Medicine**, v. 33, n. 1, 1 jan. 2018.

IRVING, B.; VICTORIA, N. **Nanoparticle Drug Delivery Systems**. [s.l: s.n.].

ISHIGURO, H. et al. The Peritoneum: Beyond the Tissue – A Review. **Front. Physiol**, v. 9, p. 738, 2018.

IVANOV, A. I. Pharmacological Inhibition of Endocytic Pathways: Is It Specific Enough to Be Useful? In: [s.l: s.n.].

IVANOV, A. I.; NAYDENOV, N. G. Dynamics and Regulation of Epithelial Adherens Junctions. In: [s.l: s.n.]. p. 27–99.

JÄGER, E. et al. Sustained Release from Lipid-Core Nanocapsules by Varying the Core Viscosity and the Particle Surface Area. **Journal of Biomedical Nanotechnology**, v. 5, n. 1, 1 fev. 2009.

JENSEN, C.; TENG, Y. Is It Time to Start Transitioning From 2D to 3D Cell Culture? **Frontiers in Molecular Biosciences**, v. 7, 6 mar. 2020.

JIMINEZ, J. A. et al. Animal models to study acute and chronic intestinal inflammation in mammals. **Gut Pathogens**, v. 7, n. 1, p. 29, 10 dez. 2015.

JOHANSSON, M. E. V et al. Bacteria penetrate the normally impenetrable inner colon mucus layer in both murine colitis models and patients with ulcerative colitis. **Gut**, v. 63, n. 2, p. 281–291, fev. 2014.

JURÍKOVÁ, M. et al. Ki67, PCNA, and MCM proteins: Markers of proliferation in the

diagnosis of breast cancer. **Acta Histochemica**, v. 118, n. 5, p. 544–552, jun. 2016.

KAPLAN, G. G.; JESS, T. The Changing Landscape of Inflammatory Bowel Disease: East Meets West. **Gastroenterology**, v. 150, n. 1, jan. 2016.

KAPLAN, G. G.; NG, S. C. Understanding and Preventing the Global Increase of Inflammatory Bowel Disease. **Gastroenterology**, v. 152, n. 2, jan. 2017.

KATHE, N.; HENRIKSEN, B.; CHAUHAN, H. Physicochemical characterization techniques for solid lipid nanoparticles: principles and limitations. **Drug Development and Industrial Pharmacy**, v. 40, n. 12, 25 dez. 2014.

KIM, J.; KOO, B.-K.; KNOBLICH, J. A. Human organoids: model systems for human biology and medicine. **Nature Reviews Molecular Cell Biology**, v. 21, n. 10, p. 571–584, 7 out. 2020.

KIM, J. M. et al. Nanocomposites-based targeted oral drug delivery systems with infliximab in a murine colitis model. **Journal of Nanobiotechnology**, v. 18, n. 1, 15 dez. 2020.

KIRIIRI, G. K.; NJOGU, P. M.; MWANGI, A. N. Exploring different approaches to improve the success of drug discovery and development projects: a review. **Future Journal of Pharmaceutical Sciences**, v. 6, n. 1, p. 27, 23 dez. 2020.

KOBAYASHI, K. S. et al. Nod2-Dependent Regulation of Innate and Adaptive Immunity in the Intestinal Tract. **Science**, v. 307, n. 5710, p. 731–734, 4 fev. 2005.

KOBAYASHI, T. et al. Ulcerative colitis. **Nature Reviews Disease Primers**, v. 6, n. 1, 2020.

KOBAYASHI, T.; HIBI, T. Improving IBD outcomes in the era of many treatment options. **Nature Reviews Gastroenterology & Hepatology**, v. 20, n. 2, p. 79–80, 12 fev. 2023.

KRESGE, C. T. et al. Ordered mesoporous molecular sieves synthesized by a liquid-crystal template mechanism. **Nature**, v. 359, n. 6397, p. 710–712, out. 1992.

KRETZSCHMAR, K.; CLEVERS, H. Organoids: Modeling Development and the Stem Cell Niche in a Dish. **Developmental Cell**, v. 38, n. 6, p. 590–600, set. 2016.

KURMAEVA, E. et al. T cell-associated α4β7 but not α4β1 integrin is required for the induction and perpetuation of chronic colitis. 2014.

KUWADA, T. et al. Identification of an Anti–Integrin αvβ6 Autoantibody in Patients With Ulcerative Colitis. **Gastroenterology**, v. 160, n. 7, p. 2383- 2394.e21, jun. 2021.

LACERDA, J. Z. et al. Annexin A12–26 Treatment Improves Skin Heterologous

Transplantation by Modulating Inflammation and Angiogenesis Processes. **Frontiers in Pharmacology**, v. 9, 10 set. 2018.

LAMB, C. A. et al. αEβ7 Integrin Identifies Subsets of Pro-Inflammatory Colonic CD4+ T Lymphocytes in Ulcerative Colitis. **Journal of Crohn's and Colitis**, p. jjw189, 20 out. 2016.

LAMB, C. A. et al. Gut-Selective Integrin-Targeted Therapies for Inflammatory Bowel Disease. **Journal of Crohn's and Colitis**, v. 12, n. suppl_2, p. S653–S668, 22 ago. 2018.

LAN, K.; ZHAO, D. Functional Ordered Mesoporous Materials: Present and Future. **Nano Letters**, v. 22, n. 8, p. 3177–3179, 27 abr. 2022.

LANGGUTH, P. et al. The challenge of proteolytic enzymes in intestinal peptide delivery. **Journal of Controlled Release**, v. 46, n. 1–2, p. 39–57, maio 1997.

LE ROUX, G. et al. Cytotoxicity and genotoxicity of lipid nanocapsules. **Toxicology in Vitro**, v. 41, p. 189–199, 2017.

LECHUGA, S.; IVANOV, A. I. Disruption of the epithelial barrier during intestinal inflammation: Quest for new molecules and mechanisms. **Biochimica et Biophysica Acta (BBA) - Molecular Cell Research**, v. 1864, n. 7, p. 1183–1194, jul. 2017.

LEE, S. H.; KWON, J. EUN; CHO, M. LA. **Immunological pathogenesis of inflammatory bowel diseaseIntestinal Research**, 2018.

LEONI, G. et al. Annexin A1, formyl peptide receptor, and NOX1 orchestrate epithelial repair. **Journal of Clinical Investigation**, v. 123, n. 1, p. 443–454, 2013.

LEONI, G. et al. Annexin A1'containing extracellular vesicles and polymeric nanoparticles promote epithelial wound repair. **Journal of Clinical Investigation**, v. 125, n. 3, p. 1215–1227, 2015a.

LEONI, G. et al. Human neutrophil formyl peptide receptor phosphorylation and the mucosal inflammatory response. **Journal of Leukocyte Biology**, v. 97, n. 1, p. 87–101, 2015b.

LEONI, G. et al. Annexin A1–containing extracellular vesicles and polymeric nanoparticles promote epithelial wound repair. **Journal of Clinical Investigation**, v. 125, n. 3, p. 1215–1227, 2 mar. 2015c.

LEONI, G.; NUSRAT, A. Annexin A1: Shifting the balance towards resolution and repair. **Biological Chemistry**, v. 397, n. 10, p. 971–979, 2016.

LI, C. et al. A Proresolving Peptide Nanotherapy for Site-Specific Treatment of Inflammatory Bowel Disease by Regulating Proinflammatory Microenvironment and

Gut Microbiota. **Advanced Science**, v. 6, n. 18, 2019a.

LI, C. et al. A Proresolving Peptide Nanotherapy for Site-Specific Treatment of Inflammatory Bowel Disease by Regulating Proinflammatory Microenvironment and Gut Microbiota. **Advanced Science**, v. 6, n. 18, p. 1900610, set. 2019b.

LI, L. et al. Biodistribution, excretion, and toxicity of mesoporous silica nanoparticles after oral administration depend on their shape. **Nanomedicine: Nanotechnology, Biology, and Medicine**, v. 11, n. 8, p. 1915–1924, 2015.

LI, Q. et al. Gut Barrier Dysfunction and Bacterial Lipopolysaccharides in Colorectal Cancer. **Journal of Gastrointestinal Surgery**, v. 27, n. 7, p. 1466–1472, 27 jul. 2023.

LI, X. et al. Oncogenic transformation of diverse gastrointestinal tissues in primary organoid culture. **Nature Medicine**, v. 20, n. 7, p. 769–777, 25 jul. 2014.

LI, X. et al. Site-specific targeted drug delivery systems for the treatment of inflammatory bowel disease. **Biomedicine & Pharmacotherapy**, v. 129, p. 110486, set. 2020.

LI, Y. et al. Pleiotropic regulation of macrophage polarization and tumorigenesis by formyl peptide receptor-2. **Oncogene**, v. 30, n. 36, p. 3887–3899, 2011.

LICE, I. et al. Effects of Formyl Peptide Receptor Agonists Ac9-12 and WKYMV in In Vivo and In Vitro Acute Inflammatory Experimental Models. **Cells**, v. 11, n. 2, p. 228, 11 jan. 2022.

LICHTENFELS, R. et al. CARE-LASS (calcein-release-assay), an improved fluorescence-based test system to measure cytotoxic T lymphocyte activity. **Journal of Immunological Methods**, v. 172, n. 2, p. 227–239, 1994.

LIM, L. H. K. et al. Promoting detachment of neutrophils adherent to murine postcapillary venules to control inflammation: Effect of lipocortin 1. **Proceedings of the National Academy of Sciences of the United States of America**, v. 95, n. 24, p. 14535–14539, 1998.

LIM, L. H. K.; PERVAIZ, S. Annexin 1: the new face of an old molecule. **The FASEB Journal**, v. 21, n. 4, p. 968–975, 10 abr. 2007.

LIN, A. G.; HINE, K. R. Drug points: Fever, vasculitic rash, arthritis, pericarditis, and pericardial effusion after mesalazine. **BMJ**, v. 308, n. 6921, 8 jan. 1994.

LIN, Y.-S.; HURLEY, K. R.; HAYNES, C. L. Critical Considerations in the Biomedical Use of Mesoporous Silica Nanoparticles. **The Journal of Physical Chemistry Letters**, v. 3, n. 3, p. 364–374, 2 fev. 2012.

LINDEN, S. K. et al. Mucins in the mucosal barrier to infection. **Mucosal Immunology**, v. 1, n. 3, p. 183–197, 2008.

LOCATELLI, I. et al. Endogenous Annexin A1 Is a Novel Protective Determinant in Nonalcoholic Steatohepatitis in Mice. 2014.

LOPES, R. L. et al. IL-10 is required for polarization of macrophages to M2-like phenotype by mycobacterial DnaK (heat shock protein 70). **Cytokine**, v. 85, p. 123–129, set. 2016.

LOSITO, D. W. et al. Biocomposites based on SBA-15 and papain: Characterization, enzymatic activity and cytotoxicity evaluation. **Microporous and Mesoporous Materials**, v. 325, p. 111316, out. 2021.

LOU, J. et al. Advances in Oral Drug Delivery Systems: Challenges and Opportunities. **Pharmaceutics**, v. 15, n. 2, p. 484, 1 fev. 2023.

LU, J. et al. Biocompatibility, Biodistribution, and Drug-Delivery Efficiency of Mesoporous Silica Nanoparticles for Cancer Therapy in Animals. **Small**, v. 6, n. 16, p. 1794–1805, 16 ago. 2010.

LUO, J. et al. Structural Basis for the Dual Recognition of IL-12 and IL-23 by Ustekinumab. **Journal of Molecular Biology**, v. 402, n. 5, p. 797–812, out. 2010.

MA, H.; TAO, W.; ZHU, S. T lymphocytes in the intestinal mucosa: defense and tolerance. **Cellular & Molecular Immunology**, v. 16, n. 3, p. 216–224, 20 mar. 2019.

MAGRO, F. et al. Journal of Crohn's and Colitis. p. 649–670, 2017.

MALIK, S.; MUHAMMAD, K.; WAHEED, Y. Nanotechnology: A Revolution in Modern Industry. **Molecules**, v. 28, n. 2, p. 661, 9 jan. 2023.

MALOY, K. J.; POWRIE, F. Intestinal homeostasis and its breakdown in inflammatory bowel disease. **Nature**, v. 474, n. 7351, p. 298–306, 15 jun. 2011.

MANTOVANI, A.; BONECCHI, R.; LOCATI, M. Tuning inflammation and immunity by chemokine sequestration: decoys and more. **Nature Reviews Immunology**, v. 6, n. 12, p. 907–918, 1 dez. 2006.

MARIANO-NETO, F. et al. Physical properties of ordered mesoporous SBA-15 silica as immunological adjuvant. **Journal of Physics D: Applied Physics**, v. 47, n. 42, p. 425402, 22 out. 2014.

MCARTHUR, S. et al. Annexin A1 drives macrophage skewing to accelerate muscle regeneration through AMPK activation. **Journal of Clinical Investigation**, v. 130, n. 3, p. 1156–1167, 2020a.

MCARTHUR, S. et al. Annexin A1 drives macrophage skewing to accelerate muscle

regeneration through AMPK activation. **Journal of Clinical Investigation**, v. 130, n. 3, p. 1156–1167, 4 fev. 2020b.

MCGOVERN, D. P. B. et al. Fucosyltransferase 2 (FUT2) non-secretor status is associated with Crohn's disease. **Human Molecular Genetics**, v. 19, n. 17, p. 3468–3476, 1 set. 2010.

MCGRATH, E. E. et al. TNF-related apoptosis-inducing ligand (TRAIL) regulates inflammatory neutrophil apoptosis and enhances resolution of inflammation. **Journal of Leukocyte Biology**, v. 90, n. 5, p. 855–865, 11 maio 2011.

MECHLER-DREIBI, M. L. et al. Oral vaccination of piglets against Mycoplasma hyopneumoniae using silica SBA-15 as an adjuvant effectively reduced consolidation lung lesions at slaughter. **Scientific Reports**, v. 11, n. 1, p. 22377, 17 nov. 2021a.

MECHLER-DREIBI, M. L. et al. Oral vaccination of piglets against Mycoplasma hyopneumoniae using silica SBA-15 as an adjuvant effectively reduced consolidation lung lesions at slaughter. **Scientific Reports**, v. 11, n. 1, p. 22377, 17 dez. 2021b.

MEDZHITOV, R. Inflammation 2010: New Adventures of an Old Flame. **Cell**, v. 140, n. 6, p. 771–776, mar. 2010.

MEENAN, J. et al. Altered expression of alpha 4 beta 7, a gut homing integrin, by circulating and mucosal T cells in colonic mucosal inflammation. **Gut**, v. 40, n. 2, p. 241–246, 1 fev. 1997.

MEZA-PEREZ, S.; RANDALL, T. D. Immunological Functions of the Omentum. **Trends in Immunology**, v. 38, n. 7, jul. 2017.

MICHALOWSKI, C. B. et al. pharmaceutics Oral Treatment of Spontaneously Hypertensive Rats with Captopril-Surface Functionalized Furosemide-Loaded Multi-Wall Lipid-Core Nanocapsules. **Pharmaceutics**, v. 12, p. 80, 2020.

MIELE, E. et al. Safety of Thiopurine Use in Paediatric Gastrointestinal Disease. **Journal of Pediatric Gastroenterology & Nutrition**, v. 71, n. 2, ago. 2020.

MIRONOV, V. A.; GUSEV, S. A.; BARADI, A. F. **Cell and Tissue Research Mesothelial Stomata Overlying Omental Milky Spots: Scanning Electron Microscopic StudyCell Tissue Res.** [s.l: s.n.].

MIYOSHI, J. et al. 5-Aminosalicylic acid aggravates colitis mimicking exacerbation of ulcerative colitis. **Intestinal Research**, v. 16, n. 4, 30 out. 2018.

MLADENOVSKA, K. et al. Colon-specific delivery of 5-aminosalicylic acid from chitosan-Ca-alginate microparticles. **International Journal of Pharmaceutics**, v. 342,

n. 1–2, set. 2007.

MOLODECKY, N. A.; KAPLAN, G. G. **Environmental Risk Factors for Inflammatory Bowel DiseaseGastroenterology & Hepatology**. [s.l: s.n.].

MORAES, L. A. et al. Annexin-A1 enhances breast cancer growth and migration by promoting alternative macrophage polarization in the tumour microenvironment. **Scientific Reports**, v. 7, n. 1, p. 17925, 20 dez. 2017.

MORENO-MENDIETA, S. et al. Understanding the Phagocytosis of Particles: the Key for Rational Design of Vaccines and Therapeutics. **Pharmaceutical Research**, v. 39, n. 8, p. 1823–1849, 23 ago. 2022.

MOSQUEIRA, V. C. F. et al. Poly(D,L-Lactide) nanocapsules prepared by a solvent displacement process: Influence of the composition on physicochemical and structural properties. **Journal of Pharmaceutical Sciences**, 2000.

MOSQUEIRA, V. C. F. et al. Efficacy and Pharmacokinetics of Intravenous Nanocapsule Formulations of Halofantrine in Plasmodium berghei-Infected Mice. **ANTIMICROBIAL AGENTS AND CHEMOTHERAPY**, v. 48, n. 4, p. 1222–1228, 2004.

MOSSER, D. M.; EDWARDS, J. P. Nihms84393. **Nat Rev Immunology**, v. 8, n. 12, p. 958–969, 2009.

MROUJ, K. et al. Ki-67 regulates global gene expression and promotes sequential stages of carcinogenesis. **Proceedings of the National Academy of Sciences**, v. 118, n. 10, 9 mar. 2021.

MUDSHINGE, S. R. et al. Nanoparticles: Emerging carriers for drug delivery. **Saudi Pharmaceutical Journal**, v. 19, n. 3, jul. 2011.

MUKHERJEE, T. et al. NOD1 and NOD2 in inflammation, immunity and disease. **Archives of Biochemistry and Biophysics**, v. 670, p. 69–81, jul. 2019.

MÜLLER C.R et al. Spray-dried diclofenac-loaded poly(epsilon-caprolactone) nanocapsules and nanospheres. Preparation and physicochemical characterization. **Pharmazie (Berlin)**, v. 56, n. 11, p. 864–867, 2001.

NADAULD, L. D. et al. Metastatic tumor evolution and organoid modeling implicate TGFBR2as a cancer driver in diffuse gastric cancer. **Genome Biology**, v. 15, n. 8, p. 428, 27 ago. 2014.

NEURATH, M. **Thiopurines in IBD: What Is Their Mechanism of Action?Gastroenterology & Hepatology**. [s.l: s.n.].

NEURATH, M.; FUSS, I.; STROBER, W. TNBS-Colitis. **International Reviews of Immunology**, v. 19, n. 1, p. 51–62, 10 jan. 2000.

NGUYEN, H. D.; ALJAMAEI, H. M.; STADNYK, A. W. The Production and Function of Endogenous Interleukin-10 in Intestinal Epithelial Cells and Gut Homeostasis. **Cellular and Molecular Gastroenterology and Hepatology**, v. 12, n. 4, p. 1343–1352, 2021.

NIKOLAUS, S.; SCHREIBER, S. Diagnostics of Inflammatory Bowel Disease. **Gastroenterology**, v. 133, n. 5, p. 1670–1689, nov. 2007.

NOVIZIO, N. et al. Annexin A1 Released in Extracellular Vesicles by Pancreatic Cancer Cells Activates Components of the Tumor Microenvironment, through Interaction with the Formyl-Peptide Receptors. **Cells**, v. 9, n. 12, p. 2719, 18 dez. 2020.

O'CONNELL, L.; WINTER, D. C.; AHERNE, C. M. The Role of Organoids as a Novel Platform for Modeling of Inflammatory Bowel Disease. **Frontiers in Pediatrics**, v. 9, 17 fev. 2021.

OLIVEIRA, C. P. et al. Bromelain-Functionalized Multiple-Wall Lipid-Core Nanocapsules: Formulation, Chemical Structure and Antiproliferative Effect Against Human Breast Cancer Cells (MCF-7). **Pharmaceutical Research**, v. 34, n. 2, 15 fev. 2017.

OUYANG, N. et al. MC-12, an Annexin A1-Based Peptide, Is Effective in the Treatment of Experimental Colitis. **PLoS ONE**, v. 7, n. 7, p. e41585, 23 jul. 2012.

PALLONE, F. et al. Genetic and pathogenetic insights into inflammatory bowel disease. **Current Gastroenterology Reports**, v. 5, n. 6, dez. 2003.

PANTALEÃO, L. et al. Connections of annexin A1 and translocator protein-18 kDa on toll like receptor stimulated BV-2 cells. **Experimental Cell Research**, v. 367, n. 2, jun. 2018.

PARAMSOTHY, S. et al. Multidonor intensive faecal microbiota transplantation for active ulcerative colitis: a randomised placebo-controlled trial. **The Lancet**, v. 389, n. 10075, p. 1218–1228, mar. 2017.

PARIKH, K. et al. Colonic epithelial cell diversity in health and inflammatory bowel disease. **Nature**, v. 567, n. 7746, p. 49–55, 7 mar. 2019.

PARK, K. T. et al. Leading Off The Cost of Inflammatory Bowel Disease: An Initiative From the Crohn's & Colitis Foundation. **Inflamm Bowel Dis •**, v. 26, n. 1, 2020.

PATTNI, B. S.; TORCHILIN, V. P. **Targeted Drug Delivery : Concepts and Design**. [s.l: s.n.].

PERDEW, J.; BURKE, K.; ERNZERHOF, M. Generalized Gradient Approximation Made Simple. **Physical review letters**, Phys. Rev. Lett. (USA). v. 77, n. 18, p. 3865–

3868, 1996.

PEREIRA, N. R. C. et al. Mechanisms of the effectiveness of poly(ε-caprolactone) lipid-core nanocapsules loaded with methotrexate on glioblastoma multiforme treatment. **International Journal of Nanomedicine**, v. 13, p. 4563–4573, 2018.

PERRETTI, M. et al. Involvement of the Receptor for Formylated Peptides in the in Vivo Anti-Migratory Actions of Annexin 1 and its Mimetics. **The American Journal of Pathology**, v. 158, n. 6, p. 1969–1973, jun. 2001.

PERRETTI, M. Editorial: To resolve or not to resolve: Annexin A1 pushes resolution on track. **Journal of Leukocyte Biology**, v. 92, n. 2, p. 245–247, 1 ago. 2012.

PERRETTI, M. et al. Characterizing the anti-inflammatory and tissue protective actions of a novel Annexin A1 peptide. **PLOS ONE**, v. 12, n. 4, p. e0175786, 13 abr. 2017.

PERRETTI, M.; D'ACQUISTO, F. **Annexin A1 and glucocorticoids as effectors of the resolution of inflammationNature Reviews Immunology**, 2009a.

PERRETTI, M.; D'ACQUISTO, F. **Annexin A1 and glucocorticoids as effectors of the resolution of inflammationNature Reviews Immunology**, 2009b.

PERRETTI, M.; D'ACQUISTO, F. **Annexin A1 and glucocorticoids as effectors of the resolution of inflammationNature Reviews Immunology**, jan. 2009c.

PERRETTI, M.; GAVINS, F. N. E. Annexin 1: An endogenous anti-inflammatory protein. **News in Physiological Sciences**, v. 18, n. 2, p. 60–64, 2003.

PESSOLANO et al. Annexin A1 Contained in Extracellular Vesicles Promotes the Activation of Keratinocytes by Mesoglycan Effects: An Autocrine Loop Through FPRs. **Cells**, v. 8, n. 7, p. 753, 19 jul. 2019.

PICKARD, J. M. et al. Gut microbiota: Role in pathogen colonization, immune responses, and inflammatory disease. **Immunological Reviews**, v. 279, n. 1, p. 70–89, 30 set. 2017.

POE, S. L. et al. STAT1-regulated lung MDSC-like cells produce IL-10 and efferocytose apoptotic neutrophils with relevance in resolution of bacterial pneumonia. **Mucosal Immunology**, v. 6, n. 1, p. 189–199, jan. 2013.

POHLMANN, A. R. et al. Poly(ε-caprolactone) microcapsules and nanocapsules in drug delivery. **Expert Opinion on Drug Delivery**, 2013.

POLETTO, F. S. et al. Fluorescent-Labeled Poly(ε-caprolactone) Lipid-Core Nanocapsules: Synthesis, Physicochemical Properties and Macrophage Uptake. **Journal of Colloid Science and Biotechnology**, v. 1, n. 1, p. 89–98, 1 jun. 2012.

POPE, J. L. et al. Claudin-1 regulates intestinal epithelial homeostasis through the

modulation of Notch-signalling. **Gut**, v. 63, n. 4, p. 622–634, abr. 2014.

PROKOPOWICZ, M. et al. Surface-Activated Fibre-Like SBA-15 as Drug Carriers for Bone Diseases. **AAPS PharmSciTech**, v. 20, n. 1, p. 17, 20 jan. 2019.

QIN, C. et al. Cardioprotective potential of annexin-A1 mimetics in myocardial infarction. **Pharmacology & Therapeutics**, v. 148, abr. 2015.

RABINOVICH-GUILATT, L. et al. Extensive surface studies help to analyse zeta potential data: the case of cationic emulsions. **Chemistry and Physics of Lipids**, v. 131, n. 1, ago. 2004.

RANDALL-DEMLLO, S. et al. Characterisation of colonic dysplasia-like epithelial atypia in murine colitis Basic Study. **World J Gastroenterol**, v. 22, n. 37, p. 8334–8348, 2016.

RASMUSSEN, M. K. et al. 3D visualisation of hepatitis B vaccine in the oral delivery vehicle SBA-15. **Scientific Reports**, v. 9, n. 1, p. 6106, 15 abr. 2019.

REISCHL, S. et al. Annexin A1 Expression Capacity as a Determinant for Disease Severity in Crohn's Disease. **Digestive Diseases**, v. 38, n. 5, p. 398–407, 2020.

REISCHL, S. et al. Ac2-26-Nanoparticles Induce Resolution of Intestinal Inflammation and Anastomotic Healing via Inhibition of NF-κB Signaling in a Model of Perioperative Colitis. **Inflammatory Bowel Diseases**, v. 27, n. 9, p. 1379–1393, 19 ago. 2021a.

REISCHL, S. et al. Ac2-26-Nanoparticles Induce Resolution of Intestinal Inflammation and Anastomotic Healing via Inhibition of NF-κB Signaling in a Model of Perioperative Colitis. **Inflammatory Bowel Diseases**, v. 27, n. 9, p. 1379–1393, 19 ago. 2021b.

RENNICK, J. J.; JOHNSTON, A. P. R.; PARTON, R. G. Key principles and methods for studying the endocytosis of biological and nanoparticle therapeutics. **Nature Nanotechnology**, v. 16, n. 3, p. 266–276, 2021.

RESCHER, U.; GERKE, V. Annexins - Unique membrane binding proteins with diverse functions. **Journal of Cell Science**, v. 117, n. 13, p. 2631–2639, 2004.

RESCIGNO, M. The intestinal epithelial barrier in the control of homeostasis and immunity. **Trends in Immunology**, v. 32, n. 6, jun. 2011.

RIZZO, G. Anti-TNF alpha in the treatment of ulcerative colitis: A valid approach for organ-sparing or an expensive option to delay surgery? **World Journal of Gastroenterology**, v. 20, n. 17, 2014.

RODRIGUES, S. F. et al. Lipid-core nanocapsules act as a drug shuttle through the blood brain barrier and reduce glioblastoma after intravenous or oral administration.

Journal of Biomedical Nanotechnology, v. 12, n. 5, p. 986–1000, 2016.

RODRIGUEZ-GARCIA, A. et al. 3D *In Vitro* Human Organ Mimicry Devices for Drug Discovery, Development, and Assessment. **Advances in Polymer Technology**, v. 2020, p. 1–41, 10 ago. 2020.

ROSENHOLM, J. M.; SAHLGREN, C.; LINDÉN, M. Towards multifunctional, targeted drug delivery systems using mesoporous silica nanoparticles – opportunities & challenges. **Nanoscale**, v. 2, n. 10, p. 1870, 2010.

ROTHHUT, B. et al. Further characterization of the glucocorticoid-induced antiphospholipase protein “Renocortin”. **Biochemical and Biophysical Research Communications**, v. 117, n. 3, dez. 1983.

RÜGER, M. et al. The formyl peptide receptor agonist Ac2-26 alleviates neuroinflammation in a mouse model of pneumococcal meningitis. **Journal of Neuroinflammation**, v. 17, n. 1, p. 325, 29 dez. 2020.

SAHAY, G.; ALAKHOVA, D. Y.; KABANOV, A. V. Endocytosis of nanomedicines. **Journal of Controlled Release**, v. 145, n. 3, ago. 2010.

SAHOO, D. et al. Artificial intelligence guided discovery of a barrier-protective therapy in inflammatory bowel disease. **Nature Communications**, v. 12, n. 1, p. 4246, 12 dez. 2021.

SANDBORN, W. J.; HANAUER, S. B. Antitumor Necrosis Factor Therapy for Inflammatory Bowel Disease: A Review of Agents, Pharmacology, Clinical Results, and Safety. **Inflammatory Bowel Diseases**, v. 5, n. 2, maio 1999.

SANDRI, S. et al. Direct effects of poly(ϵ-caprolactone) lipid-core nanocapsules on human immune cells. **Nanomedicine**, v. 14, n. 11, p. 1429–1442, 2019.

SANDS, B. E. et al. Vedolizumab versus Adalimumab for Moderate-to-Severe Ulcerative Colitis. **New England Journal of Medicine**, v. 381, n. 13, p. 1215–1226, 26 set. 2019.

SANDS, B. E. et al. Ustekinumab versus adalimumab for induction and maintenance therapy in biologic-naive patients with moderately to severely active Crohn’s disease: a multicentre, randomised, double-blind, parallel-group, phase 3b trial. **The Lancet**, v. 399, n. 10342, p. 2200–2211, jun. 2022.

SARKAR, S. et al. Mesoporous Silica Nanoparticles: Drug Delivery Vehicles for Antidiabetic Molecules. **ChemBioChem**, v. 24, n. 7, 3 abr. 2023.

SARVESTANI, S. K. et al. Induced organoids derived from patients with ulcerative colitis recapitulate colitic reactivity. **Nature Communications**, v. 12, n. 1, p. 262, 11

jan. 2021.

SASAI, Y. Cytosystems dynamics in self-organization of tissue architecture. **Nature**, v. 493, n. 7432, p. 318–326, 17 jan. 2013.

SATO, T. et al. Single Lgr5 stem cells build crypt-villus structures in vitro without a mesenchymal niche. **Nature**, v. 459, n. 7244, p. 262–265, 29 maio 2009.

SATO, T. et al. Long-term Expansion of Epithelial Organoids From Human Colon, Adenoma, Adenocarcinoma, and Barrett's Epithelium. **Gastroenterology**, v. 141, n. 5, p. 1762–1772, nov. 2011.

SAYED, I. M. et al. The DNA Glycosylase NEIL2 Suppresses Fusobacterium-Infection-Induced Inflammation and DNA Damage in Colonic Epithelial Cells. **Cells**, v. 9, n. 9, p. 1980, 28 ago. 2020a.

SAYED, I. M. et al. Host engulfment pathway controls inflammation in inflammatory bowel disease. **The FEBS Journal**, v. 287, n. 18, p. 3967–3988, 20 set. 2020b.

SAYED, I. M. et al. Functional assays with human patient-derived enteroid monolayers to assess the human gut barrier. **STAR Protocols**, v. 2, n. 3, p. 100680, set. 2021.

SAYED, I. M.; CHAKRABORTY, A.; DAS, S. Assays with Patient-Derived Organoids to Evaluate the Impact of Microbial Infection on Base Excision Repair (BER) Enzymes. In: [s.l: s.n.]. p. 157–172.

SCANNELL, M. et al. Annexin-1 and Peptide Derivatives Are Released by Apoptotic Cells and Stimulate Phagocytosis of Apoptotic Neutrophils by Macrophages. **The Journal of Immunology**, v. 178, n. 7, 1 abr. 2007.

SCARAMUZZI, K. et al. Nanostructured SBA-15 silica as an adjuvant in immunizations with hepatitis B vaccine. **Einstein (São Paulo)**, v. 9, n. 4, p. 436–441, dez. 2011.

SCHETT, G.; NEURATH, M. F. Resolution of chronic inflammatory disease: universal and tissue-specific concepts. **Nature Communications**, v. 9, n. 1, p. 3261, 15 ago. 2018.

SENA, A. et al. Dysregulation of Anti-Inflammatory Annexin A1 Expression in Progressive Crohns Disease. **PLoS ONE**, v. 8, n. 10, p. e76969, 10 out. 2013.

SENA, A. A. et al. Lack of TNFRI signaling enhances annexin A1 biological activity in intestinal inflammation. **Biochemical Pharmacology**, v. 98, n. 3, p. 422–431, 2015a.

SENA, A. A. et al. Lack of TNFRI signaling enhances annexin A1 biological activity in intestinal inflammation. **Biochemical Pharmacology**, 2015b.

SERHAN, C. N.; SAVILL, J. Resolution of inflammation: the beginning programs the

end. **Nature Immunology**, v. 6, n. 12, p. 1191–1197, 17 dez. 2005.

SHAOUL, R. et al. Colonic Expression of MUC2, MUC5AC, and TFF1 in Inflammatory Bowel Disease in Children. **Journal of Pediatric Gastroenterology and Nutrition**, v. 38, n. 5, p. 488–493, maio 2004.

SHARMA, A. et al. E-cigarettes compromise the gut barrier and trigger inflammation. **iScience**, v. 24, n. 2, p. 102035, fev. 2021.

SHARMA, A. et al. The crosstalk between microbial sensors ELMO1 and NOD2 shape intestinal immune responses. **Virulence**, v. 14, n. 1, 31 dez. 2023.

SHI, W. et al. Analysis of genes involved in ulcerative colitis activity and tumorigenesis through systematic mining of gene co-expression networks. **Frontiers in Physiology**, v. 10, n. MAY, p. 1–14, 2019.

SHIVASHANKAR, R. et al. Incidence and Prevalence of Crohn's Disease and Ulcerative Colitis in Olmsted County, Minnesota From 1970 Through 2010. **Clinical Gastroenterology and Hepatology**, v. 15, n. 6, jun. 2017.

SILVERBERG FRCPC, M. S. et al. **Toward an integrated clinical, molecular and serological classification of inflammatory bowel disease: Report of a Working Party of the 2005 Montreal World Congress of GastroenterologyCan J Gastroenterol**. [s.l: s.n.].

SIMONI, Y. et al. Human Innate Lymphoid Cell Subsets Possess Tissue-Type Based Heterogeneity in Phenotype and Frequency. **Immunity**, v. 46, n. 1, p. 148–161, jan. 2017.

SINIS, S. I. et al. Carbon Nanotubes and Other Engineered Nanoparticles Induced Pathophysiology on Mesothelial Cells and Mesothelial Membranes. **Frontiers in Physiology**, v. 9, 29 mar. 2018.

SMITH, T. et al. Application of smart solid lipid nanoparticles to enhance the efficacy of 5-fluorouracil in the treatment of colorectal cancer. **Scientific Reports**, v. 10, n. 1, 12 dez. 2020.

SOKOL, H.; SEKSIK, P.; COSNES, J. Complications and surgery in the inflammatory bowel diseases biological era. **Current Opinion in Gastroenterology**, v. 30, n. 4, jul. 2014.

SOLITO, E. et al. A novel calcium-dependent proapoptotic effect of annexin 1 on human neutrophils. **The FASEB Journal**, 2003.

SOLLID, L. M.; JOHANSEN, F.-E. Animal Models of Inflammatory Bowel Disease at the Dawn of the New Genetics Era. **PLoS Medicine**, v. 5, n. 9, p. e198, 30 set. 2008.

SOMMER, K. et al. Intestinal Mucosal Wound Healing and Barrier Integrity in IBD–Crosstalk and Trafficking of Cellular Players. **Frontiers in Medicine**, v. 8, 23 mar. 2021.

SOUID, A.-K. et al. In vitro biocompatibility of calcined mesoporous silica particles and fetal blood cells. **International Journal of Nanomedicine**, p. 3111, ago. 2012.

STEEL, A. W. et al. Increased proportion of CD16+ NK cells in the colonic lamina propria of inflammatory bowel disease patients, but not after azathioprine treatment. **Alimentary Pharmacology & Therapeutics**, v. 33, n. 1, jan. 2011.

STEPANENKO, A. A.; DMITRENKO, V. V. Pitfalls of the MTT assay: Direct and off-target effects of inhibitors can result in over/underestimation of cell viability. **Gene**, v. 574, n. 2, dez. 2015.

STETEFELD, J.; MCKENNA, S. A.; PATEL, T. R. **Dynamic light scattering: a practical guide and applications in biomedical sciencesBiophysical Reviews**, 2016.

STRIK, A. S. et al. **Optimization of anti-TNF therapy in patients with Inflammatory Bowel DiseaseExpert Review of Clinical Pharmacology**, 2016.

SUGIMOTO, M. A. et al. **Annexin A1 and the Resolution of Inflammation: Modulation of Neutrophil Recruitment, Apoptosis, and ClearanceJournal of Immunology Research**, 2016. Disponível em: <http://dx.doi.org/10.1155/2016/8239258>

SUGIMOTO, M. A. et al. Mediators of the Resolution of the Inflammatory Response. **Trends in Immunology**, v. 40, n. 3, p. 212–227, mar. 2019.

SUN, D. et al. Why 90% of clinical drug development fails and how to improve it? **Acta Pharmaceutica Sinica B**, v. 12, n. 7, p. 3049–3062, jul. 2022.

TEBON, P. J. et al. Drug screening at single-organoid resolution via bioprinting and interferometry. **Nature Communications**, v. 14, n. 1, p. 3168, 6 jun. 2023.

THAKRAL, S.; THAKRAL, N. K.; MAJUMDAR, D. K. Eudragit®: a technology evaluation. **Expert Opinion on Drug Delivery**, v. 10, n. 1, p. 131–149, 26 jan. 2013.

TIAN, C. et al. Stem cell-derived intestinal organoids: a novel modality for IBD. **Cell Death Discovery**, v. 9, n. 1, p. 255, 21 jul. 2023.

TREZENA, A. G. et al. Adjuvant effect of mesoporous silica SBA-15 on anti-diphtheria and anti-tetanus humoral immune response. **Biologicals**, v. 80, p. 18–26, out. 2022.

UDERHARDT, S. et al. 12/15-Lipoxygenase Orchestrates the Clearance of Apoptotic

Cells and Maintains Immunologic Tolerance. **Immunity**, v. 36, n. 5, p. 834–846, maio 2012.

UMEDA, K. et al. ZO-1 and ZO-2 Independently Determine Where Claudins Are Polymerized in Tight-Junction Strand Formation. **Cell**, v. 126, n. 4, p. 741–754, ago. 2006.

UTECH, M. et al. Mechanism of IFN-γ-induced Endocytosis of Tight Junction Proteins: Myosin II-dependent Vacuolarization of the Apical Plasma Membrane. **Molecular Biology of the Cell**, v. 16, n. 10, p. 5040–5052, out. 2005.

VAN BAAL, J. O. A. . et al. The histophysiology and pathophysiology of the peritoneum. **Tissue and Cell**, v. 49, n. 1, fev. 2017.

VARSHOSAZ, J.; JAFFARIAN DEHKORDI, A.; GOLAFSHAN, S. Colon-specific delivery of mesalazine chitosan microspheres. **Journal of Microencapsulation**, v. 23, n. 3, 8 jan. 2006.

VENTURINI, C. G. et al. Formulation of lipid core nanocapsules. **Colloids and Surfaces A: Physicochemical and Engineering Aspects**, 2011.

VERGNOLLE, N. et al. Annexin 1 Is Secreted in Situ During Ulcerative Colitis in Humans. **Inflammatory Bowel Diseases**, v. 10, n. 5, p. 584–592, set. 2004.

VERGNOLLE, N.; COMERA, C.; BUENO, L. Annexin 1 is Overexpressed and Specifically Secreted During Experimentally Induced Colitis in Rats. **European Journal of Biochemistry**, v. 232, n. 2, p. 603–610, set. 1995.

VERT, M. et al. Terminology for biorelated polymers and applications (IUPAC Recommendations 2012). **Pure and Applied Chemistry**, v. 84, n. 2, 11 jan. 2012.

VINCENT, F. B. et al. Antidrug antibodies (ADAb) to tumour necrosis factor (TNF)-specific neutralising agents in chronic inflammatory diseases: a real issue, a clinical perspective. **Annals of the Rheumatic Diseases**, v. 72, n. 2, fev. 2013.

VITAL, S. A. et al. Formyl-Peptide Receptor 2/3/Lipoxin A $_4$ Receptor Regulates Neutrophil-Platelet Aggregation and Attenuates Cerebral Inflammation. **Circulation**, v. 133, n. 22, 31 maio 2016.

VONG, L. et al. Up-Regulation of Annexin-A1 and Lipoxin A4 in Individuals with Ulcerative Colitis May Promote Mucosal Homeostasis. **PLoS ONE**, v. 7, n. 6, p. e39244, 18 jun. 2012.

WALTHER, A.; RIEHEMANN, K.; GERKE, V. A Novel Ligand of the Formyl Peptide Receptor. **Molecular Cell**, v. 5, n. 5, p. 831–840, maio 2000.

WANG, F. et al. Interferon-γ and Tumor Necrosis Factor-α Synergize to Induce

Intestinal Epithelial Barrier Dysfunction by Up-Regulating Myosin Light Chain Kinase Expression. **The American Journal of Pathology**, v. 166, n. 2, p. 409–419, fev. 2005.

WANG, L. et al. Advances in reconstructing intestinal functionalities in vitro: From two/three dimensional-cell culture platforms to human intestine-on-a-chip. **Talanta**, v. 226, p. 122097, maio 2021.

WANG, R. et al. Global, regional and national burden of inflammatory bowel disease in 204 countries and territories from 1990 to 2019: a systematic analysis based on the Global Burden of Disease Study 2019. **BMJ Open**, v. 13, n. 3, p. e065186, 28 mar. 2023.

WANG, T. et al. Enhanced mucosal and systemic immune responses obtained by porous silica nanoparticles used as an oral vaccine adjuvant: Effect of silica architecture on immunological properties. **International Journal of Pharmaceutics**, v. 436, n. 1–2, p. 351–358, out. 2012.

WEI, M. et al. Claudin-2 promotes colorectal cancer growth and metastasis by suppressing NDRG1 transcription. **Clinical and Translational Medicine**, v. 11, n. 12, 29 dez. 2021.

WILHELM, C. et al. Intracellular uptake of anionic superparamagnetic nanoparticles as a function of their surface coating. **Biomaterials**, v. 24, n. 6, mar. 2003.

WILHELM, S. M.; LOVE, B. L. Management of patients with inflammatory bowel disease: Current and future treatments. **Clinical Pharmacist**, 2017.

WILKOSZ, S. et al. A comparative study of the structure of human and murine greater omentum. 2005.

WILLIAMS, C. et al. Optimizing clinical use of mesalazine (5-aminosalicylic acid) in inflammatory bowel disease. **Therapeutic Advances in Gastroenterology**, v. 4, n. 4, 16 jul. 2011.

WLODARSKA, M. et al. Indoleacrylic Acid Produced by Commensal Peptostreptococcus Species Suppresses Inflammation. **Cell Host & Microbe**, v. 22, n. 1, p. 25- 37.e6, jul. 2017.

WOLFSON, D. M. et al. Granulomas do not affect postoperative recurrence rates in Crohn's disease. **Gastroenterology**, v. 83, n. 2, p. 405–9, ago. 1982.

WYANT, T.; FEDYK, E.; ABHYANKAR, B. An Overview of the Mechanism of Action of the Monoclonal Antibody Vedolizumab. **Journal of Crohn's and Colitis**, v. 10, n. 12, p. 1437–1444, dez. 2016.

XU, C.; LEI, C.; YU, C. Mesoporous Silica Nanoparticles for Protein Protection and Delivery. **Frontiers in Chemistry**, v. 7, 1 maio 2019.

XU, W.; RIIKONEN, J.; LEHTO, V.-P. Mesoporous systems for poorly soluble drugs. **International Journal of Pharmaceutics**, v. 453, n. 1, p. 181–197, ago. 2013.

XU, X. et al. Annexin A1 protects against cerebral ischemia–reperfusion injury by modulating microglia/macrophage polarization via FPR2/ALX-dependent AMPK-mTOR pathway. **Journal of Neuroinflammation**, v. 18, n. 1, 2021.

XUE, Y. et al. Metformin Improves Ileal Epithelial Barrier Function in Interleukin-10 Deficient Mice. **PLOS ONE**, v. 11, n. 12, p. e0168670, 21 dez. 2016.

YANAGISAWA, T. et al. The Preparation of Alkyltrimethylammonium–Kanemite Complexes and Their Conversion to Microporous Materials. **Bulletin of the Chemical Society of Japan**, v. 63, n. 4, p. 988–992, 1 abr. 1990.

YANG, C.; MERLIN, D. Nanoparticle-mediated drug delivery systems for the treatment of IBD: Current perspectives. **International Journal of Nanomedicine**, v. 14, p. 8875–8889, 2019.

YANG, M. et al. Bile Acid–Gut Microbiota Axis in Inflammatory Bowel Disease: From Bench to Bedside. **Nutrients**, v. 13, n. 9, p. 3143, 9 set. 2021.

YAO, Y. et al. The toxicity of metallic nanoparticles on liver: The subcellular damages, mechanisms, and outcomes. **International Journal of Nanomedicine**, v. 14, p. 8787–8804, 2019.

YING, W. et al. Investigation of Macrophage Polarization Using Bone Marrow Derived Macrophages. **Journal of Visualized Experiments**, n. 76, 23 jun. 2013.

YIU, H. H. .; WRIGHT, P. A.; BOTTING, N. P. Enzyme immobilisation using SBA-15 mesoporous molecular sieves with functionalised surfaces. **Journal of Molecular Catalysis B: Enzymatic**, v. 15, n. 1–3, p. 81–92, set. 2001.

YOO, J.-S.; OH, S. F. Unconventional immune cells in the gut mucosal barrier: regulation by symbiotic microbiota. **Experimental & Molecular Medicine**, v. 55, n. 9, p. 1905–1912, 11 set. 2023.

YU, Y. et al. Short-Term Oral Administration of Mesoporous Silica Nanoparticles Potentially Induced Colon Inflammation in Rats Through Alteration of Gut Microbiota. 2021.

YUN, Y.; CHO, Y. W.; PARK, K. Nanoparticles for oral delivery: Targeted nanoparticles with peptidic ligands for oral protein delivery. **Advanced Drug Delivery Reviews**, v. 65, n. 6, p. 822–832, jun. 2013.

ZEESHAN, M. et al. Glycyrrhizic acid-loaded pH-sensitive poly-(lactic-co-glycolic acid) nanoparticles for the amelioration of inflammatory bowel disease. **Nanomedicine**, v. 14, n. 15, p. 1945–1969, 2019.

ZEISSIG, S. et al. Changes in expression and distribution of claudin 2, 5 and 8 lead to discontinuous tight junctions and barrier dysfunction in active Crohn's disease. **Gut**, v. 56, n. 1, 1 jan. 2007.

ZENG, B. et al. ILC3 function as a double-edged sword in inflammatory bowel diseases. **Cell Death & Disease**, v. 10, n. 4, p. 315, 8 abr. 2019.

ZHANG, F. et al. Mesoporous Silica Nanoparticles for Protein Protection and Delivery. **Frontiers in Chemistry | www.frontiersin.org**, v. 1, p. 290, 2019.

ZHANG, F. X. et al. Bacterial Lipopolysaccharide Activates Nuclear Factor-κB through Interleukin-1 Signaling Mediators in Cultured Human Dermal Endothelial Cells and Mononuclear Phagocytes. **Journal of Biological Chemistry**, v. 274, n. 12, mar. 1999.

ZHANG, L. et al. Nanoparticles in Medicine: Therapeutic Applications and Developments. **Clinical Pharmacology & Therapeutics**, v. 83, n. 5, 24 maio 2008.

ZHANG, R. X. et al. Importance of integrating nanotechnology with pharmacology and physiology for innovative drug delivery and therapy – an illustration with firsthand examples. **Nature Publishing Group**, v. 39, p. 825–844, 2018.

ZHANG, Y. et al. Salmonella Infection Upregulates the Leaky Protein Claudin-2 in Intestinal Epithelial Cells. **PLoS ONE**, v. 8, n. 3, p. e58606, 11 mar. 2013.

ZHAO, D. et al. Triblock Copolymer Syntheses of Mesoporous Silica with Periodic 50 to 300 Angstrom Pores. **Science**, v. 279, n. 5350, p. 548–552, 23 jan. 1998a.

ZHAO, D. et al. Nonionic Triblock and Star Diblock Copolymer and Oligomeric Surfactant Syntheses of Highly Ordered, Hydrothermally Stable, Mesoporous Silica Structures. **Journal of the American Chemical Society**, v. 120, n. 24, p. 6024–6036, 1 jun. 1998b.

ZHAO, J. et al. Cytotoxicity of mesoporous silica modified by amino and carboxyl groups on vascular endothelial cells. **Environmental Toxicology**, v. 36, n. 7, p. 1422–1433, 25 jul. 2021.

ZHENG, L. et al. Microbial-Derived Butyrate Promotes Epithelial Barrier Function through IL-10 Receptor–Dependent Repression of Claudin-2. **The Journal of Immunology**, v. 199, n. 8, 15 out. 2017.

ZHENG, Y. et al. Annexin A1 (Ac2-26)-dependent Fpr2 receptor alleviates sepsis-

induced acute kidney injury by inhibiting inflammation and apoptosis in vivo and in vitro. **Inflammation Research**, v. 72, n. 2, p. 347–362, 22 fev. 2023.

ZHOU, H.; QIAN, H. Preparation and characterization of ph-sensitive nanoparticles of budesonide for the treatment of ulcerative colitis. **Drug Design, Development and Therapy**, p. 12–2601, 2018.

ZHOU, J. et al. Programmable probiotics modulate inflammation and gut microbiota for inflammatory bowel disease treatment after effective oral delivery. **Nature Communications**, v. 13, n. 1, p. 3432, 14 jun. 2022.

ZOLNIK, B. S. et al. Minireview: Nanoparticles and the immune system. **Endocrinology**, v. 151, n. 2, p. 458–465, 2010.

Anexos

Anexo 1. Aprovação da Comissão de Ética para Uso de Animais (CEUA/FCF) para o projeto MLNC-AnxA1

UNIVERSIDADE DE SÃO PAULO
FACULDADE DE CIÊNCIAS FARMACÊUTICAS
Comissão de Ética no Uso de Animais - CEUA

CEUA/FCF **071.2019-P598**

CERTIFICADO

Certificamos que a proposta intitulada **Efeitos da nanocápsula de núcleo lípidico contendo anexina A1 em modelo de colite ulcerativa induzida em camundongos**, registrada com o nº **598**, sob a responsabilidade do(a) pesquisador(a) **Milena Fronza Broering**, sob orientação da **Profa. Dra. Sandra Helena Poliselli Farsky** – que envolve produção ou manutenção ou utilização de animais pertencentes ao filo Chordata, subfilo Vertebrata (exceto humanos), para fins de pesquisa científica – encontra-se de acordo com os preceitos da Lei Federal nº 11.794, de 8 de outubro de 2008, do Decreto Federal nº 6.899, de 15 de julho de 2009, e das normas editadas pelo Conselho Nacional de Controle de Experimentação Animal (CONCEA), e foi aprovada pela Comissão de Ética no Uso de Animais (CEUA) da Faculdade de Ciências Farmacêuticas da Universidade de São Paulo (FCF/USP), em reunião de **04 de outubro de 2019.**

Finalidade	Pesquisa Científica
Vigência da autorização	04/10/2019 a 28/02/2022
Espécie/linhagem/raça	***Camundongo C57BL/6 WT***
Número de animais	**84**
Sexo	Macho
Peso/Idade	6-10 semanas – 20-25g
Origem	Biotérios UNIFESP
Espécie/linhagem/raça	**Camundongo C57BL/6$^{-/-}$**
Número de animais	**48**
Sexo	Macho
Peso/Idade	6-10 semanas – 20-25g
Origem	Biotério FCF/IQ/USP
Total de animais	**132**

Conforme a legislação vigente, deverá ser apresentado, no encerramento do projeto de pesquisa, o respectivo **relatório final**.

Ressaltamos que após o período de término do projeto de pesquisa, nenhum ensaio poderá ser realizado.

São Paulo, 04 de outubro de 2019.

Profa. Dra. Neuza Mariko Aymoto Hassimotto
Coordenadora CEUA/FCF/USP

Av. Prof. Lineu Prestes, 580, Bloco 13 A, Cidade Universitária, CEP 05508-900, São Paulo, SP
Telefone: (11) 3091 3622 - e-mail: ceuafcf@usp.br

Anexo 2. Aprovação da Comissão Interna de Biossegurança (CIBio)

UNVERSIDADE DE SÃO PAULO
FACULDADE DE CIÊNCIAS FARMACÊUTICAS
Comissão Interna de Biossegurança

Of.CIBio/0282019/FCF

São Paulo, 19 de setembro de 2019.

Senhora Professora,

Conforme parecer favorável do relator, informo a Vossa Senhoria que em reunião da Comissão Interna de Biossegurança da Faculdade de Ciências Farmacêuticas realizada nesta data., o Projeto *"Efeitos das nanocápsulas de núcleo lipídico contendo Anexina A1 em modelo de colite ulcerativa induzida em camundongos"* foi aprovado.

Atenciosamente,

Prof. Dr. JOÃO CARLOS MONTEIRO DE CARVALHO
Presidente da CIBio

Ilma. Sra.
Profa. Dra. **SANDRA HELENA POLISELLI FARSKY**
Departamento de Análises Clínicas e Toxicológicas da FCF-USP
NESTA

Av. Prof. Lineu Prestes, nº 580, Bloco 13 A - Cidade Universitária - CEP 05508-900 - São Paulo - SP
Fone (011) 3091-3042 - e-mail: atadfcf.usp.br

Anexo 3. Aprovação da Comissão de Ética para Uso de Animais (CEUA/FCF) para o projeto SBA-15-Ac2-26.

UNIVERSIDADE DE SÃO PAULO
Faculdade de Ciências Farmacêuticas
Comissão de Ética no Uso de Animais - CEUA

CEUA/FCF **048.2023 – P 653**

CERTIFICADO

Certificamos que a proposta intitulada " **EFEITOS DA MICROPARTÍCULA MESOPOROSA SBA-15 CONTENDO Ac2-26 REVESTIDA COM POLÍMERO EUDRAGIT EM MODELO DE COLITE EXPERIMENTAL INDUZIDA EM CAMUNDONGOS"** da Pesquisadora Luana Filippi Xavier, registrada com o nº 653, que envolve produção ou manutenção ou utilização de animais pertencentes ao filo *Chordata*, subfilo *Vertebrata* (exceto humanos), para fins de pesquisa científica – encontra-se de acordo com os preceitos da Lei Federal nº 11.794, de 8 de outubro de 2008, do Decreto Federal nº 6.899, de 15 de julho de 2009, e das normas editadas pelo Conselho Nacional de Controle de Experimentação Animal (CONCEA), e foi aprovada pela Comissão de Ética no Uso de Animais (CEUA) da Faculdade de Ciências Farmacêuticas da Universidade de São Paulo (FCF/USP), em reunião de **30 de junho de 2023.**

Finalidade	**Pesquisa Científica**
Vigência da autorização	**21/08/2023 a 31/12/2024**
Espécie/linhagem/raça	***Camundongo - (Mus musculus) - C57BL/6J***
Número de animais	**40**
Sexo	**Macho**
Peso/Idade	**20 a 25 gramas / 05 a 08 semanas**
Origem	**Biotério FCF - IQ**
Total de animais	**40**

Av. Prof. Lineu Prestes, 580, Bloco 13 A, Cidade Universitária, CEP 05508-900, São Paulo, SP
Telefone: (11) 3091 3622 - e-mail: ceuafcf@usp.br

Anexo 4. Artigos publicados entre 2019 e 2024

Co-autoria – 2020

Journal of Photochemistry & Photobiology, B: Biology 212 (2020) 112018

Contents lists available at ScienceDirect

Journal of Photochemistry & Photobiology, B: Biology

journal homepage: www.elsevier.com/locate/jphotobiol

Red light-emitting diode treatment improves tissue recovery in DSS-induced colitis in mice

Marina de Paula-Silva[a], Milena Fronza Broering[a], Pablo Scharf[a], Gustavo Henrique Oliveira da Rocha[a], Sandra Farsky[a], Adriana Lino-dos-Santos-Franco[b,*]

[a] Faculty of Pharmaceutical Sciences, University of São Paulo, Brazil
[b] Post-Graduate Program in Biophotonics Applied to Health Sciences, University Nove de Julho (UNINOVE), São Paulo, Brazil

ARTICLE INFO

Keywords:
Inflammatory bowel disease
Epithelial proliferation
Tight junctions
Resolution of inflammation
Annexin A1

ABSTRACT

Inflammatory bowel diseases are debilitating illnesses characterized by severe inflammation of the gastrointestinal tract. Treatments currently available are expensive and ineffective. We here investigated the role of red-light emitting diode (LED) on dextran sodium sulfate (DSS)-induced colitis. DSS was added to the drinking water of male mice at days 0, 2, 4 and withdrawn at day 6. LED irradiation was performed daily for 90s from day 6 to 9 on the right and left sides of the ventral surface and beside the external anal region. LED treatment decreased the amount of crypt dysplasia/edema, inflammatory infiltrates and ulcers, attenuated apoptosis and increased proliferation of crypt cells. Also, LED treatment induced expression of annexin A1 in the damaged epithelium, preserved the organization of claudin-1 and skewed cytokine profiling towards a more anti-inflammatory status. Thus, LED treatment promotes structural protection and modulates the inflammatory response, constituting a potential non-invasive and low-cost combined therapy to help patients achieve disease remission.

1. Introduction

Inflammatory bowel diseases (IBDs) are illnesses characterized by severe gastrointestinal inflammation leading to debilitating symptoms, such as abdominal pain, bloody diarrhea and pronounced loss of body weight [1]. From 1990 to 2016, the highest prevalence of IBDs worldwide was reported in the United States and Europe, but the incidence in emerging countries from Africa, Asia and South America has also increased. In 2017, IBDs affected 1.6 million people in the United States alone, representing a great burden to public health care [2].

The pathogenesis of IBDs emerges from a multifactorial background. Genetically predisposed individuals when exposed to environmental factors, such as unhealthy diet, smoking, pollution, hygiene conditions, intake of drugs, among others, suffer a loss of gut epithelial barrier function, compromising its tolerogenic relationship with gut microbiota [3,4]. As a result, the translocation of microorganisms to the intestinal tissue activates and recruits inflammatory cells to the injured site. This inflammatory infiltrate is characterized mainly by T lymphocytes, macrophages and neutrophils. T cells induce interferon-gamma (IFN-γ)-mediated proinflammatory actions. Macrophages secrete IL-6 and tumor necrosis factor-alpha (TNF-α), which prevent apoptosis of lymphocytes and induce macrophage activation and immune cell recruitment/transmigration, amplifying the inflammatory response. Neutrophils, once in the infiltrated tissue, release IL-6, IL-1β and TNF-α [4,5]. Together, all these effects sustain inflammation and halt tissue repair. Counter-regulatory mechanisms involve actions of endogenous pro-resolution mediators; however, anti-inflammatory mechanisms are often insufficient to halt the progression of this inflammatory process, which then leads to chronic tissue damage [6].

The two main types of IBDs - ulcerative colitis (UC) and Crohn's disease (CD) - have similar symptomatology, but they can compromise distinct regions of the gastrointestinal tract and affect its histoarchitecture differently [7]. Due to the complexity of these illnesses, some patients can show mixed symptoms and misleading histopathological features, compromising diagnosis; the condition of these patients can even be diagnosed as unclassified-IBD, making the choice of correct therapies difficult [8].

After diagnosis, IBD patients are usually subjected to a "step-up" therapeutic approach; treatment strategies start with amino salicylates, which are then substituted by corticosteroids, followed by immunosuppressants and finally by biological therapies should the previously used drugs cause adverse effects, fail to induce remission or the

* Corresponding author at: Post Graduate Program in Biophotonics Applied to Health Sciences, University Nove de Julho (UNINOVE), Vergueiro st., 239/245, São Paulo, SP CEP 01504-000, Brazil.
E-mail address: alsantosfranco@gmail.com (A. Lino-dos-Santos-Franco).

https://doi.org/10.1016/j.jphotobiol.2020.112018
Received 4 December 2019; Received in revised form 25 July 2020; Accepted 2 September 2020
Available online 05 September 2020
1011-1344/

Journal of Photochemistry & Photobiology, B: Biology 212 (2020) 112018

Contents lists available at ScienceDirect

Journal of Photochemistry & Photobiology, B: Biology

journal homepage: www.elsevier.com/locate/jphotobiol

Red light-emitting diode treatment improves tissue recovery in DSS-induced colitis in mice

Marina de Paula-Silva[a], Milena Fronza Broering[a], Pablo Scharf[a], Gustavo Henrique Oliveira da Rocha[a], Sandra Farsky[a], Adriana Lino-dos-Santos-Franco[b,*]

[a] Faculty of Pharmaceutical Sciences, University of São Paulo, Brazil
[b] Post-Graduate Program in Biophotonics Applied to Health Sciences, University Nove de Julho (UNINOVE), São Paulo, Brazil

ARTICLE INFO

Keywords:
Inflammatory bowel disease
Epithelial proliferation
Tight junctions
Resolution of inflammation
Annexin A1

ABSTRACT

Inflammatory bowel diseases are debilitating illnesses characterized by severe inflammation of the gastrointestinal tract. Treatments currently available are expensive and ineffective. We here investigated the role of red-light emitting diode (LED) on dextran sodium sulfate (DSS)-induced colitis. DSS was added to the drinking water of male mice at days 0, 2, 4 and withdrawn at day 6. LED irradiation was performed daily for 90s from day 6 to 9 on the right and left sides of the ventral surface and beside the external anal region. LED treatment decreased the amount of crypt dysplasia/edema, inflammatory infiltrates and ulcers, attenuated apoptosis and increased proliferation of crypt cells. Also, LED treatment induced expression of annexin A1 in the damaged epithelium, preserved the organization of claudin-1 and skewed cytokine profiling towards a more anti-inflammatory status. Thus, LED treatment promotes structural protection and modulates the inflammatory response, constituting a potential non-invasive and low-cost combined therapy to help patients achieve disease remission.

1. Introduction

Inflammatory bowel diseases (IBDs) are illnesses characterized by severe gastrointestinal inflammation leading to debilitating symptoms, such as abdominal pain, bloody diarrhea and pronounced loss of body weight [1]. From 1990 to 2016, the highest prevalence of IBDs worldwide was reported in the United States and Europe, but the incidence in emerging countries from Africa, Asia and South America has also increased. In 2017, IBDs affected 1.6 million people in the United States alone, representing a great burden to public health care [2].

The pathogenesis of IBDs emerges from a multifactorial background. Genetically predisposed individuals when exposed to environmental factors, such as unhealthy diet, smoking, pollution, hygiene conditions, intake of drugs, among others, suffer a loss of gut epithelial barrier function, compromising its tolerogenic relationship with gut microbiota [3,4]. As a result, the translocation of microorganisms to the intestinal tissue activates and recruits inflammatory cells to the injured site. This inflammatory infiltrate is characterized mainly by T lymphocytes, macrophages and neutrophils. T cells induce interferon-gamma (IFN-γ)-mediated proinflammatory actions. Macrophages secrete IL-6 and tumor necrosis factor-alpha (TNF-α), which prevent apoptosis of lymphocytes and induce macrophage activation and immune cell recruitment/transmigration, amplifying the inflammatory response. Neutrophils, once in the infiltrated tissue, release IL-6, IL-1β and TNF-α [4,5]. Together, all these effects sustain inflammation and halt tissue repair. Counter-regulatory mechanisms involve actions of endogenous pro-resolution mediators; however, anti-inflammatory mechanisms are often insufficient to halt the progression of this inflammatory process, which then leads to chronic tissue damage [6].

The two main types of IBDs - ulcerative colitis (UC) and Crohn's disease (CD) - have similar symptomatology, but they can compromise distinct regions of the gastrointestinal tract and affect its histoarchitecture differently [7]. Due to the complexity of these illnesses, some patients can show mixed symptoms and misleading histopathological features, compromising diagnosis; the condition of these patients can even be diagnosed as unclassified-IBD, making the choice of correct therapies difficult [8].

After diagnosis, IBD patients are usually subjected to a "step-up" therapeutic approach; treatment strategies start with amino salicylates, which are then substituted by corticosteroids, followed by immunosuppressants and finally by biological therapies should the previously used drugs cause adverse effects, fail to induce remission or the

* Corresponding author at: Post Graduate Program in Biophotonics Applied to Health Sciences, University Nove de Julho (UNINOVE), Vergueiro st., 239/245, São Paulo, SP CEP 01504-000, Brazil.
E-mail address: alsantosfranco@gmail.com (A. Lino-dos-Santos-Franco).

https://doi.org/10.1016/j.jphotobiol.2020.112018
Received 4 December 2019; Received in revised form 25 July 2020; Accepted 2 September 2020
Available online 05 September 2020
1011-1344/

patient becomes unresponsive after a long-term use. Ultimately, patients suffering from severe disease that do not respond to any medication undergo surgical procedures, but their quality of life is permanently reduced [1,9,10]. All such therapeutic failures contribute to a scenario of pharmacoeconomic overwhelming that can cost the patient up to US$ 26,555 just in the first year after diagnosis [11]. For these reasons, it is urgent to propose novel therapeutic strategies that can either achieve disease remission faster or prolong remission periods while also being cost-effective so more individuals can benefit from them [12].

In the last few years, studies have demonstrated the beneficial effects of photobiomodulation therapy on cellular and molecular processes [13–15]. In humans, it is already used for aesthetic purposes to sustain morphological cutaneous homeostasis and has already been demonstrated to be safe [16]. Nowadays, different lasers and low-level light therapies emitting wavelengths in the spectrum of the visible light have been emerging as potential options to treat a diversity of human diseases, including neurodegenerative disorders [17]. Based on recent successful studies in humans and on a plethora of results obtained in experimental animals, several clinical trials have been already proposed aiming to investigate the role of photobiomodulation on treatment of human disorders [18,19]. Recently, our group demonstrated the beneficial effects of LED treatment on experimental models of pulmonary inflammatory diseases, decreasing neutrophil influx and secretion of pro-inflammatory cytokines in the inflamed tissue [15] while also promoting secretion of pro-resolving mediators that favor tissue homeostasis [13].

Therapies able to induce early resolution of inflammation and tissue recovery can dramatically improve the quality of life of IBD patients. Here, we provide evidence that LED therapy protects intestinal histoarchitecture by preserving epithelial tight junctions, stimulating the expression of proliferative and resolutive mediators and attenuating inflammatory responses. These benefits of LED treatment, accompanied by a low-cost and ease of manipulation, allow us to suggest it can be combined with other therapies in order to help patients more easily achieve disease remission.

2. Methods

2.1. Animals

Male C57BL6 wild-type (WT) mice, aged 8–10 weeks and weighting 20–25 g were bred under pathogen-free conditions in the Faculty of Pharmaceutical Sciences of the University of São Paulo. Animals were kept in a 12-h light/dark cycle at temperatures ranging from 20 to 25 °C while having access to water and feed ad libitum. All experiments were performed in accordance with Brazilian laws of animal ethics; this study was approved by the Ethics Committee of Animal Use of the Faculty of Pharmaceutical Sciences of the University of São Paulo (CEUA/FCF/USP), protocol n° 596.

3. Colitis Model and LED Treatment

Mice were divided into four groups ($n = 5$ animals/group): Control, LED, DSS and DSS + LED. Control groups (Control and LED) received autoclaved water with no additives, while colitic groups (DSS and DSS + LED) received autoclaved water containing Dextran Sulfate Sodium (DSS, MW 40,000, Dextran Products Limited, Canada) at a concentration of 2%. DSS solutions were replenished every two days (Days 0, 2 and 4) so DSS received by the animals would be uniform. DSS was withdrawn on Day 6; up to Day 10, mice received water with no additives.

Between days 6 and 9, healthy and DSS treated mice (LED and DSS + LED, respectively) were irradiated with red LED during 90 s on both right and left sides of the ventral surface and beside the external anal region. Control and DSS groups were handled the same way as LED-treated animals but with the LED emitting device turned off in order to standardize exposure stress among groups.

The parameters of LED irradiation were chosen based on earlier studies (Costa et al. 2017), described as follows:

Wavelength	Potency	Energy density	Potency density	Area	Total energy	Time
660 nm	100 mW	5 J/cm^2	33.3 mW/cm^2	2.8cm^2	15 J	90s

Clinical parameters (body weight, diarrhea and rectal blood) were observed and registered daily and the Disease Activity Index (DAI) was calculated from the sum of these parameters. On day 10, animals were euthanized after inhalation of isoflurane anesthetic (2-chloro-2- (difluoromethoxy)-1,1,1-trifluoroethane). The colon was removed from the ileocecal junction up to the proximity of the anus, washed and macroscopically evaluated (weight and length). Finally, the colon was fragmented for histological (distal colon), enzymatic and protein (mid/proximal colon) analyzes.

4. Histopathological Analysis

Samples from the distal portion of the colon were fixed in 4% paraformaldehyde for 24 h, dehydrated in graded ethanol, cleared in xylene and embedded in paraffin for histopathological and immunohistochemical analyses. For histopathological analysis, 5 μm sections were stained with hematoxylin and eosin (EasyPath) and analyzed using a high-power objective (40×) on an AxioCam coupled to a Zeiss microscope (Carl Zeiss, Jena, Germany).

5. Immunohistochemical Staining and Analysis

Colon sections were deparaffinized, hydrated and incubated with sodium citrate buffer (pH 6.0) at 96 °C for 30 min for antigen retrieval. Endogenous peroxidase activity was blocked with 3% hydrogen peroxide used for three 10 min rounds. Next, blocking of unspecific binding sites was carried out with 10% BSA diluted in Tris-buffer saline (TBS) for one hour. Then, sections were incubated with anti-AnxA1, anti-claudin-1, anti-PCNA or anti-ZO antibodies overnight at 4 °C. Sections were then washed and incubated with a secondary antibody conjugated with HRP (1 h, room temperature). The staining was detected using 3,3′-diaminobenzidine (DAB substrate; Invitrogen, USA). Finally, sections were counterstained with hematoxylin and mounted.

Quantificction of proliferative nuclei. Five fields of the mucosal layer from PCNA-stained sections were photographed using a 40× high-power objective and the number of positive nuclei was quantified for each field assessed. Results were expressed as mean ± S.E.M. of proliferative nuclei.

6. TUNEL Assay

TUNEL staining was used to reveal apoptotic cells in tissues. Positive cells were detected using in situ Apoptosis Detection Kit (Abcam), according to manufacturer's instructions.

7. Quantification of Tissue Myeloperoxidase

The amount of neutrophils and macrophages infiltrated in the colonic tissue was indirectly measured by myeloperoxidase (MPO) colorimetric assay as previously described (de Paula Silva et al., 2016). Briefly, fragments from the middle colon were homogenized in a 5% EDTA/NaCl buffer (pH 4.7) with the aid of a homogenizing apparatus (Ultra-turrax) and centrifuged at 10,000 rpm at 4 °C for 15 min. The tissue pellet was resuspended in a 0.2% NaCl, 1.6% NaCl-5% glucose

and 0.5% hexadecyl trimethyl ammonium bromide (pH 5.4) solution. The samples were then frozen in liquid nitrogen and thawed at 37 °C three times. Finally, 50 μL of the supernatants were incubated with tetramethylbenzidine at 1:1 (TMB, Millipore, USA) and MPO activity was measured at 450 nm using a spectrophotometer. Results were expressed as mean ± S.E.M. of the optical density (O.D.) corrected by the weight of each sample (O.D./mg).

8. Quantification of pro-and Anti-Inflammatory Mediators in the Intestinal Tissue

Proximal colon samples were homogenized in RIPA buffer containing 0.1% of a protease inhibitor solution using an ultra-turrax apparatus. Next, samples were centrifuged at 12,000 rpm at 4 °C for 10 min. Cytokines (IFN-γ, IL-1β, IL-6, IL-10 and TNF-α) were analyzed from the supernatants by ELISA according to manufacturer's instructions (BD Biosciences). The concentrations obtained in pg/mL were corrected by the total amounts of protein of each sample, as measured by Bradford assay.

8.1. Statistical Analysis

Kolmogorov-Smirnov test was used to determine whether distributions of data sets were parametric or non-parametric. Then, one-way ANOVA tests followed by Tukey's (parametric) or Dunn's post-test (non-parametric) were carried out to compare differences between means. Probability values of $p < 0.05$ were considered statistically significant and results were expressed as mean ± SEM.

9. Results

9.1. LED Therapy Attenuates Disease Activity and Gut Alterations Induced by DSS

DSS administration was effective in inducing colitis; animals had higher DAI values characterized by increased weight loss, diarrhea, occult blood in feces and colon shortening (Fig. 1). LED treatment was initiated at Day 6, when the disease was at the peak of its course, and was carried out up to Day 9, spanning the chronification phase of the model. Data obtained showed LED treatment did not improve weight loss, diarrhea and fecal blood parameters individually, (Fig. 1A-C) but this treatment significantly reduced disease activity index at Day 8 (Fig. 1D) and prevented loss of colonic structure integrity (Fig. 1E-G). It is worthy mentioning that LED treatment, in healthy animals, did not cause any alterations in the parameters mentioned above.

10. LED Therapy Promotes Histological Recovery by Stimulating Epithelial Renovation

The significant effect of LED therapy on large intestine anatomy suggests it can induce recovery responses in the damaged tissue. Indeed, LED treatment protected colonic histoarchitecture during colitis, decreasing the frequency of crypts dysplasia/edema and reducing inflammatory infiltrates and ulcerations in comparison with non-treated mice (Fig. 2A-D). Possible mechanisms that could explain these interesting effects on epithelial protection were assessed by staining using Proliferating Cell Nuclear Antigen (PCNA) (Fig. 2F-I) and Terminal deoxynucleotidyl transferase dUTP nick end labeling (TUNEL) (Fig. 2K-O) to determine, respectively, proliferation and apoptosis.

PCNA is a 36 kDa acidic non-histone nuclear protein that allows DNA polymerase to initiate leading strand DNA replication and, as proliferating cells remain longer in G1-S phase, is also a marker of proliferation [20]. As expected, PCNA was normally expressed at the base of intestinal crypts of control mice, where undifferentiated cells are constantly proliferating to renovate the epithelial barrier (Fig. 2F). TUNEL assay did not reveal an evident staining of apoptotic cells in these mice (Fig. 2K). However, healthy animals treated with LED showed PCNA immunostained nuclei also in the migratory region of glands (Fig. 2G) and a more pronounced TUNEL staining in apical barrier cells (Fig. 2L), indicating that LED treatment by itself stimulates epithelial renovation. Similarly to LED-treated mice, DSS mice showed PCNA-positive cells throughout the extension of the glands (Fig. 2H), indicating that the damaged tissue is being induced towards recovery; however, this effect is not enough to fully revert the extensive ulcerations resulting from cell apoptosis at the apical epithelium (Fig. 2M). DSS + LED mice showed a significant increase in proliferative epithelial cells throughout the extension of the glands compared to untreated mice (Fig. 2I-J) and epithelial apoptosis was not detected (Fig. 2N). These effects contributed to preservation of the epithelial barrier.

Finally, both DSS and DSS + LED mice showed increased MPO activity in the colon, indicating these tissues have more infiltrated neutrophils and macrophages [21]. When relativized by MPO levels, the number of TUNEL-positive phagocytes in the colon of colitic mice was higher after LED therapy (data not show).

11. LED Therapy Induces Expression of Proteins Related to Integrity of Epithelial Structure

Epithelial integrity is maintained by the interaction of anchoring molecules expressed in cell-cell and cell-membrane interfaces, which not only allows physical binding, but also signaling of intracellular pathways which control the necessary cell metabolism responsible for keeping such epithelial integrity [22]. Based on our previous data, claudin-1 and *zonula occludens*-1 (ZO-1) were assessed via immunohistochemistry; these proteins are pivotal paracellular molecules in the intestinal barrier. No differences regarding ZO-1 and claudin-1 expressions were observed between groups (Fig. 3A-E and F-J, respectively). However, the structural organization of claudin-1 was altered by DSS, which became irregularly distributed throughout the extension of epithelial cells (Fig. 3H - detail). Mice treated with LED showed preserved claudin-1 organization in the epithelial barrier (Fig. 3I), evidencing LED treatment acts specifically on control of claudin-1 organization rather than on its expression.

Annexin A1 (AnxA1) is an anti-inflammatory and pro-resolutive protein expressed and secreted by epithelial and inflammatory cells. In the same manner as PCNA, AnxA1 is expressed in the epithelial barrier of mice undergoing DSS-induced colitis and is linked to homeostatic mechanisms which involve wound closure and down-regulation of inflammatory responses [23]. It has been fully demonstrated that colitis is aggravated in AnxA1-knockout mice [25]. In colitic mice treated with LED, higher expression of AnxA1 was detected in epithelial cells at damaged areas (Figs. 3K-3N, 3O) and increased overall expression in tissue homogenates was confirmed by ELISA (Fig. 3P), suggesting this could be another mechanism of tissue repair induced by LED therapy.

12. LED Therapy Induces Expression and Secretion of Cytokines Responsible for Tissue Recovery

Further quantification of cytokines secreted by gut tissue contributed towards a better understanding of the link between disease stage and actions of LED therapy. Although TNF-α levels are very low in the tissue of DSS mice (Fig. 4A), increased levels of IL-1β and IL-6 (Figured 4B−4C) and reduced levels of IL-10 (Figured 4D) indicate active disease. LED therapy attenuated the inflammatory process by preventing the increase of IL-1β and IL-6 levels caused by DSS (Figured 4B−4C) and accelerated its resolution by markedly increasing IFN-γ and TGF-β levels (Figs. 4E-4F).

13. Discussion

IBDs are debilitating diseases of complex pathogenesis and it often takes time after initial diagnosis for proper individualized therapeutic

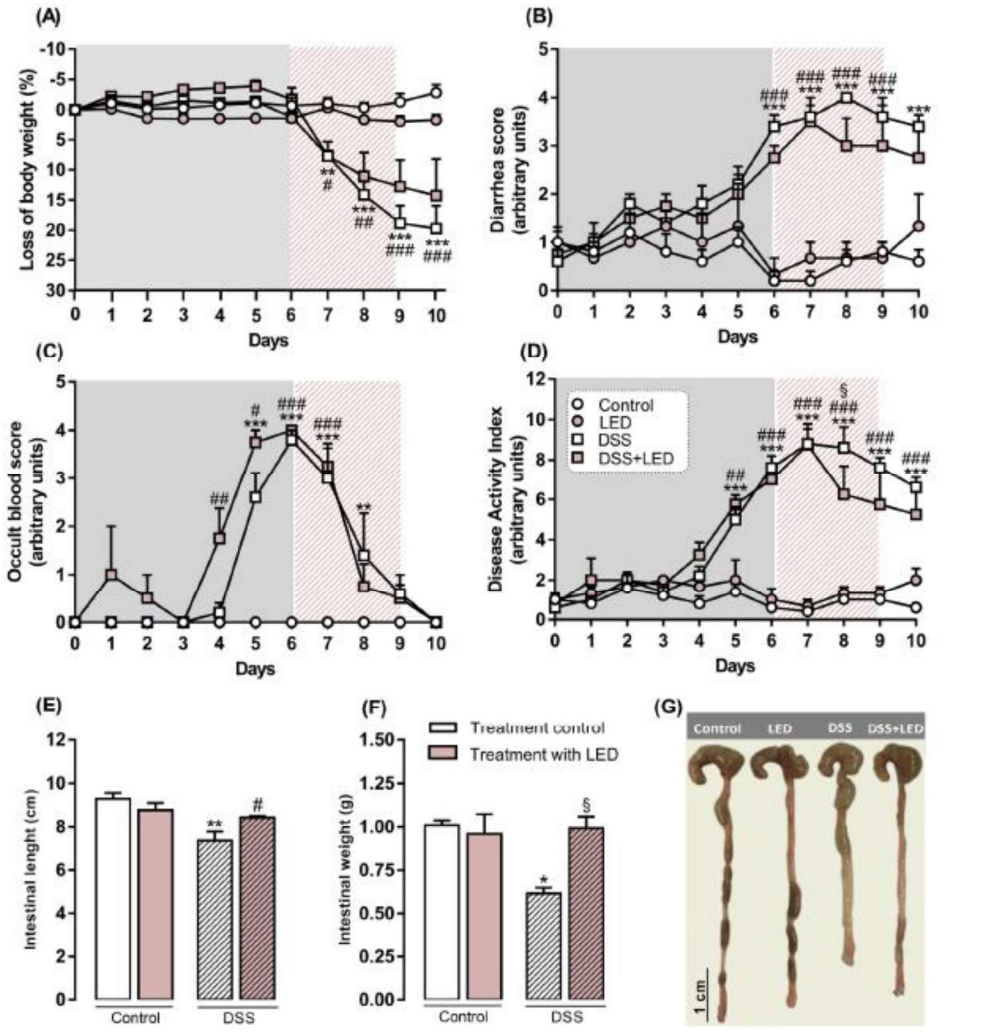

Fig. 1. Roles of LED therapy on DSS-induced colitis activity and colonic structure. (A) Percentage of body weight loss. (B) Diarrhea score. (C) Occult blood score. (D) Disease activity Index (DAI). (E) Intestinal length. (F) Intestinal weight. (G) Anatomic evaluation of the colon. $n = 5$ mice/group. * $p < 0.05$, ** $p < 0.01$, *** $p < 0.001$ vs Control; # $p < 0.05$, ## $p < 0.01$, ### $p < 0.001$ vs LED; § $p < 0.05$ vs DSS.

approaches to be decided upon. The currently available therapies are cost-intensive and pose great burdens to health care systems [11]. Here we demonstrate the beneficial actions of a non-invasive, low-cost LED therapy on a DSS-induced colitis model, focusing on its promising protective actions on the epithelial barrier.

IBDs are autoimmune diseases heavily influenced by both environment and immune/genetic background of patients [4]. Although DSS-induced colitis as a model does not address all intrinsic characteristics of IBDs genesis, it is a useful experimental tool used to determine the efficacy of novel therapies in a complex organism affected by intestinal inflammation. DSS causes lesions in the intestinal epithelium allowing translocation of microbiota components into the underlying tissue, which then initiates an immune response leading to tissue damage [26]. In our model, DSS induced clinical manifestations equivalent to those observed in IBD patients, and LED treatment at days 7–9 of the disease had a subtle but certain protective role, considering especially intestinal morphology. Intestine shortening and reduction of intestinal weight are common occurrences in DSS-induced colitis [26]; although there are no final explanations in scientific literature as to what exactly causes such severe anatomical changes, it is known that intestinal length in humans is correlated with body weight [28]. Thus, it is possible to suggest that loss of body weight decreases intestinal length, which is accompanied by a decrease of intestinal weight, as we here demonstrate. Also, the intestine damaged by inflammation initiates a response towards homeostasis that involves tissue remodeling; in this process, intestinal cells can either accumulate or degrade extracellular matrix (ECM)

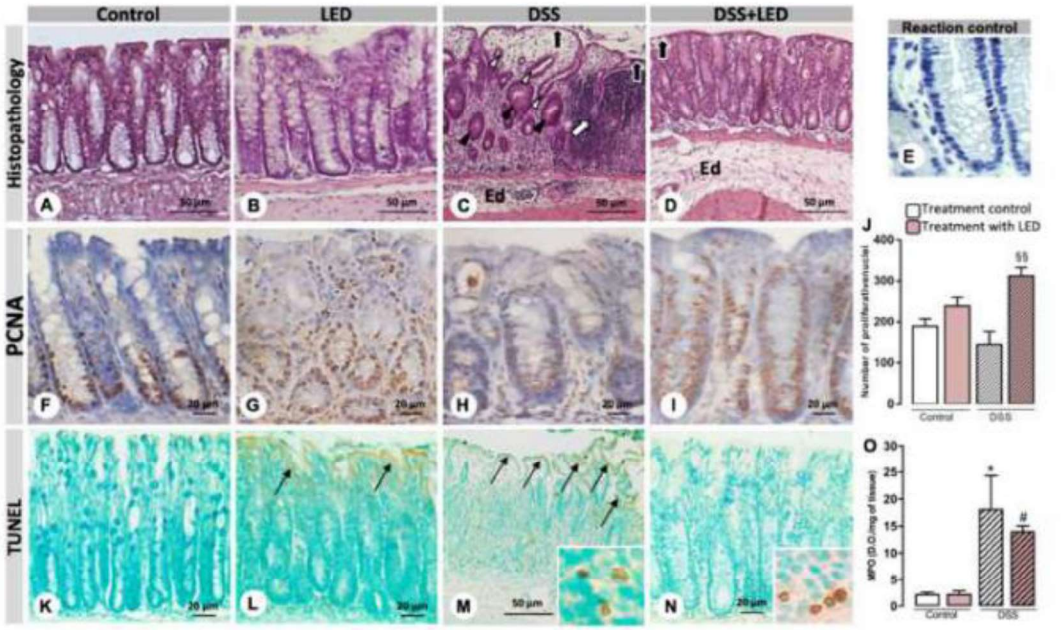

Fig. 2. Effects of LED treatment on epithelial regeneration and renovation in the colon damaged by DSS-induced colitis. (A-D) Histopathological analyses. Ulcers (black arrows). Inflammatory infiltrate (white arrows). Dysplastic crypts (white arrowheads). Crypts edema (black arrowheads). Ed (submucosal edema). (F–I) Proliferative nuclei marked with PCNA. (K–N) Apoptotic cells labeled with TUNEL (thin arrows). Apoptotic phagocytes (details). (E) Reaction control. (J) Mean of PCNA-positive nuclei in colonic glands. (O) MPO levels in the intestinal tissue. $n = 4$ mice/group. Sections: 3 μm. Bars: 20 μm (F–I, K, L, N), 50 μm (A-D, M). Staining: Hematoxylin-Eosin (A-D). Counterstaining: Hematoxylin (F–I), Methyl green (K–N). * $p < 0.05$ vs Control; # $p < 0.05$ vs LED; §§ $p < 0.01$ vs DSS. (For interpretation of the references to colour in this figure legend, the reader is referred to the web version of this article.)

components on its walls, which could evolve to either fibrosis or structural rupture [25]. As these events impact intestinal anatomy and function, the protection exerted by LED therapy upon intestine weight might be a consequence of a more complex beneficial effect on gut structure and could play a role on clinical improvement.

Indeed, further histological data corroborated the effects of LED treatment on tissue recovery, as it increased proliferation of epithelial cells and prevented their apoptosis, contributing to wound closure. Downregulating inflammatory responses is another strategy to protect the epithelial barrier, as the accumulation of inflammatory cells and mediators in the damaged site prolongs tissue injury [3]. Our research group had previously demonstrated LED therapy decreases MPO activity in bronchoalveolar lavage in an acute lung injury model in mice [27]. Here, LED treatment did not affect MPO activity, but slightly increased apoptosis of transmigrated phagocytes (data not shown). Although the number of apoptotic neutrophils/macrophages corrected by MPO levels for each mouse of the DSS + LED treated group was not statistically significant when compared to the DSS group, this is evidence that at the final day of the experimental model LED therapy starts the resolution of the immune response. This process protects the epithelial barrier from further damage and helps ceasing the translocation of microbiota components to the intestinal tissue, attenuating disease progression [25].

Alongside epithelial cell death, disruption of tight junctions constitutes an important mechanism linked to epithelial barrier damage [30]. Claudin-1 belongs to a family of 26 proteins and composes the backbone of tight junction strands in simple epithelial cells, directly controlling their barrier functions [31]. Claudin-1 is down-expressed in myeloid differentiation protein 2 knockout mice, and when these mice are subjected to DSS-induced colitis, the disease develops in a more severe manner than in wild-type strains [32]. Furthermore, several pharmacological approaches aimed at treating IBDs induce the expression of claudin-1, resulting in an improvement of epithelial barrier integrity in UC patients [33,34]. Claudin-1 also activates intracellular signaling pathways that include metalloproteinase-9 and p-ERK, activating Notch-signaling and leading to epithelial proliferation [34]. In the present investigation, we observed immunostaining for Claudin-1 was "unorganized" in the DSS group, while LED treated mice showed a strong and more spread immunostaining. We also detected a higher expression of AnxA1 in the epithelial barrier of DSS + LED mice compared to DSS mice. AnxA1 is a 37 kDa phospholipid binding protein expressed by inflammatory and epithelial cells under a diversity of stimuli, and this mediator exerts pivotal control on the development of the innate immune response, on resolution of inflammation and on tissue repair [35]. Existing evidence on the role of AnxA1 in IBD experimental models is robust. AnxA1 is highly expressed by epithelial cells during the resolution phase of disease, and clinical symptoms of colitis are worse in AnxA1 knockout mice than in WT animals [25,36]. In biopsies from CD patients, decreased expression of AnxA1 is correlated with inflammatory activity and poor response to anti-TNF-α treatments [37]. Also, in the sera of UC patients, increased amounts of secreted AnxA1-containing extracellular vesicles were detected, suggesting the release of AnxA1 in vesicles constitutes a systemic manner of activating wound repair responses [24]. In the cells that compose the blood-brain-barrier (BBB), endogenous AnxA1 regulates cytoskeleton structure and stabilizes tight junctions, being expressed at higher levels

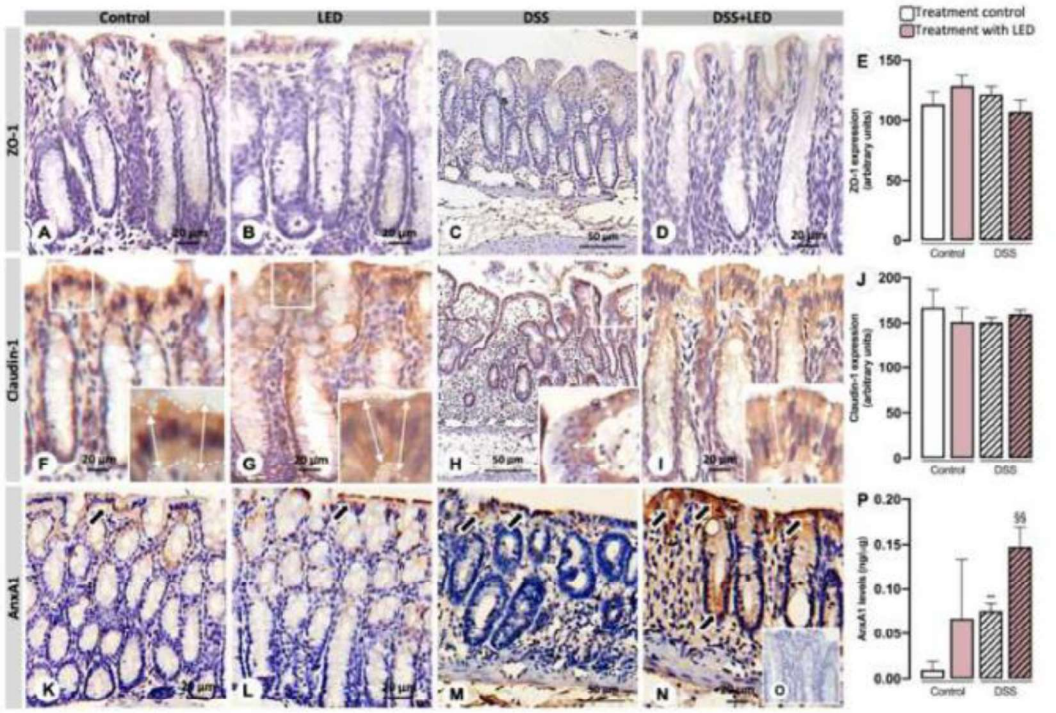

Fig. 3. Expression of tissue integrity-related proteins in the epithelial barrier of DSS-induced colitis mice treated with LED. (A-D and E) ZO-1 localization and expression. (F–I and J) Claudin-1 localization (white arrows) and expression. (K–N and P) AnxA1 localization (black arrows) and tissue levels. (O) Reaction control. $n = 3$ mice/group. Sections: 3 μm. Bars: 20 μm (A, B, D; E, F, H; I, J, L), 50 μm (C, G, K). Counterstaining: Hematoxylin.** $p < 0.01$ vs Control; §§ $p < 0.01$.

in cell-cell contact sites [38]; indeed, AnxA1-knockout mice show decreased organization of tight junctions in these same structures [39]. Our data indicate the increased expression of AnxA1 induced by LED therapy in epithelial cells might have a potential effect on claudin-1 organization during DSS-induced colitis.

Besides its structural functions, AnxA1 also plays several roles as an anti-inflammatory and pro-resolutive mediator. This protein was first described as an inhibitor of phospholipase A2 activity in cell membranes, impairing the production of lipid pro-inflammatory mediators [40]. Up-regulation and down regulation of pro- and anti-inflammatory mediators are, respectively, hallmarks of colitis. Here, we observed the intestinal tissue collected from LED treated mice produced lower amounts of IL-1β and IL-6 while producing higher levels of IFN-γ. The later effect is unexpected as IFN-γ is an important mediator for the pathogenesis of IBDs [3,41]. However, IFN-γ also plays a role in the resolution of colitis by evoking the expression of the IL-10 receptor on intestinal epithelium and inducing the polarization of anti-inflammatory macrophages [42]. Other investigations have pointed out the roles of IFN-γ in inhibiting leukocyte transmigration into inflamed lung tissue and in limiting inflammation at injured sites [43]. We have already showed LED treatment on an acute lung injury model induced by LPS increases the levels of IFN-γ in bronchoalveolar lavage [29]. Hence, the increased secretion of IFN-γ emerges as a potential pro-resolutive mechanism of action promoted by LED therapy and, at later phases of colitis, might contribute to anti-inflammatory effects and tissue reorganization. Finally, LED treatment increased the levels of TGF-β, a down-modulator of mucosal inflammation and promoter of epithelial repair [43]. Interestingly, levels of TNF-α and IL-10 were low and equivalent in all groups of animals studied, suggesting that these cytokines do not play a relevant role at Day 10 of DSS-induced colitis model in mice.

IBDs are complex processes characterized by secretion of a plethora of proteins by a diversity of cells, which exert pleiotropic actions and can exert either deleterious or benefic actions on different phases of the disease. Targeting a specific cell or mediator not always leads to conclusive results. Data here obtained demonstrate the beneficial actions of LED therapy on the intestinal mucosa damaged by DSS. Due to its non-invasive delivery and low-cost applicability, LED therapy and its anti-inflammatory effects might be used as promising tools to be combined with other drugs in order to accelerate remission in IBD patients.

Author contributions statement

Study conception and design: S.F. and A.L.S.F.
Drafting of manuscript: S.F., A.L.S.F., M.P.S.
Critical revision: S.F. and A.L.S.F.
Experimental analysis: M.P.S., M.F.B., P.S., G.H.O.R.
Acquisition of data: M.P.S., M.F.B., P.S., G.H.O.R.
Analysis and interpretation of data: M.P.S., M.F.B., P.S., G.H.O.R., S.F. and A.L.S.F.

Declaration of Competing Interest

The authors declare no competing interests.

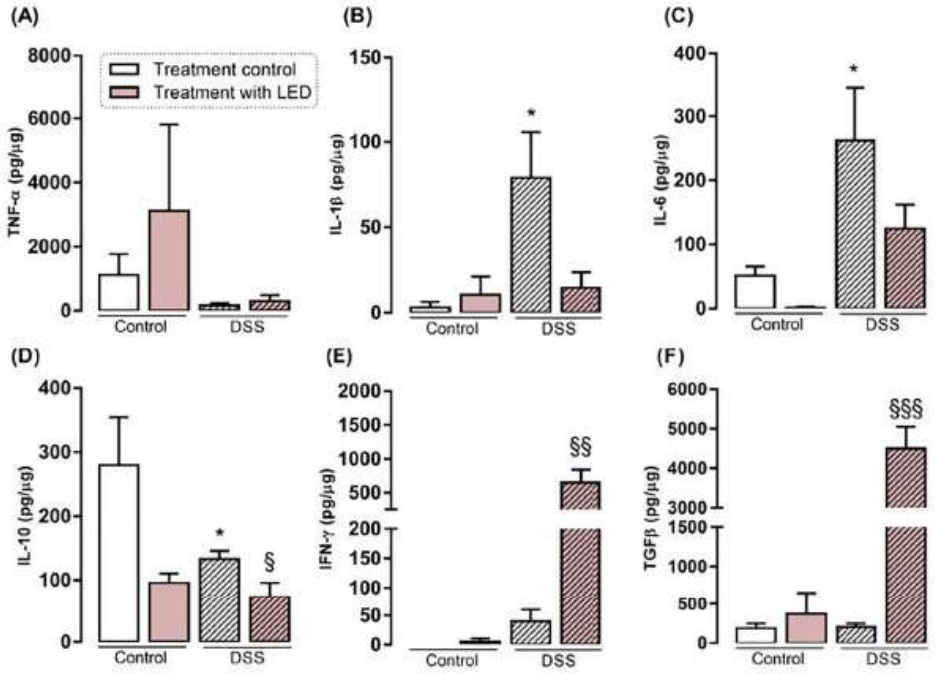

Fig. 4. Cytokine alterations induced by LED treatment. (A) TNF-α. (B) IL-1β. (C) IL-6. (D) IL-10. (E) IFN-γ. (F) TGF-β. $n = 2$ (LED); $n = 4$ mice/group. * $p < 0.05$ vs Control; § $p < 0.05$, §§ $p < 0.01$, §§§ $p < 0.001$ vs DSS.

Acknowledgements

This work was supported by the São Paulo Research Foundation (Fundação de amparo a pesquisa do estado de são Paulo (FAPESP) – Brazil, Grant 2014/07328-4). Dextran Sulfate Sodium was kindly gifted by Dextran Products Limited (Canada). The authors thank Vitoria Larissa F. Villas Boas for drawing the graphical abstract.

References

[1] S.M. Wilhelm, B.L. Love, Management of patients with inflammatory bowel disease: current and future treatments, Clin. Pharm. 9 (3) (2017) 1–24, https://doi.org/10.1211/CP.2017.20202316.

[2] S.C. Ng, H.Y. Shi, N. Hamidi, F.E. Underwood, W. Tang, E.I. Benchimol, R. Panaccione, S. Ghosh, J.C.Y. Wu, F.K.L. Chan, J.J.Y. Sung, G.G. Kaplan, Worldwide incidence and prevalence of inflammatory bowel disease in the 21st century: a systematic review of population-based studies, Lancet. 390 (2017) 2769–2778, https://doi.org/10.1016/S0140-6736(17)32448-0.

[3] M.F. Neurath, Cytokines in inflammatory bowel disease, Nat. Rev. Immunol. 14 (5) (2014) 329–342, https://doi.org/10.1038/nri3661.

[4] S.H. Lee, J. Eun Kwon, M. La Cho, Immunological pathogenesis of inflammatory bowel disease, Intest. Res. 16 (1) (2018) 26, https://doi.org/10.5217/ir.2018.16.1.26.

[5] C. Abraham, R. Medzhitov, Interactions between the host innate immune system and microbes in inflammatory bowel disease, Gastroenterology. 140 (6) (2011) 1729–1737, https://doi.org/10.1053/j.gastro.2011.02.012.

[6] G. Rogler, Resolution of inflammation in inflammatory bowel disease, Lancet Gastroenterol. Hepatol. 2 (7) (2017) 521–530, https://doi.org/10.1016/S2468-1253(17)30031-6.

[7] Y.R. Yu, J.R. Rodriguez, Clinical presentation of Crohn's, ulcerative colitis, and indeterminate colitis: symptoms, extraintestinal manifestations, and disease phenotypes, Semin. Pediatr. Surg. 26 (6) (2017) 349–355, https://doi.org/10.1053/j.sempedsurg.2017.10.003.

[8] Å.H. Everhov, M.C. Sachs, P. Malmborg, C. Nordenvall, P. Myrelid, H. Khalili, M. Elmberg, A. Ekbom, J. Askling, G. Jakobsson, J. Halfvarson, J.F. Ludvigsson, O. Olén, Changes in inflammatory bowel disease subtype during follow-up and over time in 44,302 patients, Scand. J. Gastroenterol. 54 (1) (2019) 55–63, https://doi.org/10.1080/00365521.2018.1564361.

[9] Ole Haagen Nielsen, Mark Andrew Ainsworth, Tumor necrosis factor inhibitors for inflammatory bowel disease, N. Engl. J. Med. 368–8 (2013) 754–762, https://doi.org/10.1056/NEJMct1209614.

[10] C. Steenholdt, J. Brynskov, O.Ø. Thomsen, L.K. Munck, J. Fallingborg, L.A. Christensen, G. Pedersen, J. Kjeldsen, B.A. Jacobsen, A.S. Oxholm, J. Kjellberg, K. Bendtzen, M.A. Ainsworth, Individualised therapy is more cost-effective than dose intensification in patients with Crohn's disease who lose response to anti-TNF treatment: a randomised, controlled trial, Gut 63 (6) (2014), https://doi.org/10.1136/gutjnl-2013-305279 929–927.

[11] K.T. Park, O.G. Ehrlich, J.I. Allen, P. Meadows, E.M. Szigethy, K. Henrichsen, S.C. Kim, R.C. Lawton, S.M. Murphy, M. Regueiro, D.T. Rubin, N.M. Engel-Nitz, C.A. Heller, The cost of inflammatory bowel disease: an initiative from the Crohn's & colitis foundation, Inflamm. Bowel Dis. (2019), https://doi.org/10.1093/ibd/izz104.

[12] J.F. Colombel, N. Narula, L. Peyrin-Biroulet, Management strategies to improve outcomes of patients with inflammatory bowel diseases, Gastroenterology. 152 (2) (2017) 351–361, https://doi.org/10.1053/j.gastro.2016.09.046.

[13] M. Palma-Cruz, R.F. da Silva, D. Monteiro, H.M.M.A. Rehim, C.C. Grabulosa, A.P.L. de Oliveira, A. Lino-dos-Santos-Franco, Photobiomodulation modulates the resolution of inflammation during acute lung injury induced by sepsis, Lasers Med. Sci. 34 (1) (2019) 191–199, https://doi.org/10.1007/s10103-018-2668-1.

[14] S.E. Aragona, F.R. Grassi, G. Nardi, J. Lotti, G. Mereghetti, E. Canavesi, E. Equizi, A.M. Puccio, G. Gianazza, T. Lotti, I. Morisi, Photobiomodulation with polarized light in the treatment of cutaneous & mucoeal ulcerative lesions, J. Biol. Regul. Homeost. Agents 31 (2) (2017) 213–218.

[15] S.A.P. Costa, G.P. Florezi, G.E. Artes, J.R. da Costa, R.T. Gallo, P.M. de Freitas, A.L. Witzel, The analgesic effect of photobiomodulation therapy (830 nm) on the masticatory muscles: a randomized, double-blind study, Braz. Oral Res. 31 (2017) 1–10, https://doi.org/10.1590/1807-3107bor-2017.vol31.0107.

[16] A. Yadav, A. Gupta, Noninvasive red and near-infrared wavelength-induced photobiomodulation: promoting impaired cutaneous wound healing, Photodermatol. Photoimmunol. Photomed. 33 (1) (2017) 4–13, https://doi.org/10.1111/phpp.12282.

[17] R. Zomorrodi, G. Loheswaran, A. Pushparaj, L. Lim, Pulsed near infrared Transcranial and intranasal Photobiomodulation significantly modulates neural oscillations: a pilot exploratory study, Sci. Rep. 9 (1) (2019) 6309, https://doi.org/10.1038/s41598-019-42693-x.

[18] A.P.J. Isabella, J.T.C. Silva, T. da Silva, M.F.S.D. Rodrigues, A.C.R.T. Horliana,

L.J. Motta, S.K. Bussadori, C. Pavani, F.T. da Silva, Effect of irradiation with intravascular laser on the hemodynamic variables of hypertensive patients: Study protocol for prospective blinded randomized clinical trial, Medicine (Baltimore) 98 (14) (2019) e1511, https://doi.org/10.1097/MD.0000000000015111.

[19] J.C. Milan-Mattos, C. de Oliveira Francisco, A.M. Ferroli-Fabrício, V. Minatel, A.C.A. Marcondes, A. Porta, T. Beltrame, N.A. Parizotto, C. Ferraresi, V.S. Bagnato, A.M. Catai, Acute effect of photobiomodulation using light-emitting diodes (LEDs) on baroreflex sensitivity during and after constant loading exercise in patients with type 2 diabetes mellitus, Lasers Med. Sci. (2019) 1–8, https://doi.org/10.1007/s10103-019-02815-3.

[20] W. Strzalka, A. Ziemienowicz, Proliferating cell nuclear antigen (PCNA): a key factor in DNA replication and cell cycle regulation, Ann. Bot. 107 (7) (2011) 1127–1140, https://doi.org/10.1093/aob/mcq243.

[21] F. Shaeib, S.N. Khan, M. Thakur, H.R. Kohan-Ghadr, S. Drewlo, G.M. Saed, S. Pennathur, H.M. Abu-Soud, The impact of myeloperoxidase and activated macrophages on metaphase II mouse oocyte quality, PLoS One 11 (3) (2016) e0151160, , https://doi.org/10.1371/journal.pone.0151160.

[22] A.A. Bhat, S. Uppada, I.W. Achkar, S. Hashem, S.K. Yadav, M. Shanmugakonar, H.A. Al-Naemi, M. Haris, S. Uddin, Tight junction proteins and signaling pathways in cancer and inflammation: a functional crosstalk, Front. Physiol. 9 (2019) 1–19, https://doi.org/10.3389/fphys.2018.01942.

[23] G. Leoni, A. Alam, P. Alexander Neumann, J.D. Lambeth, G. Cheng, J. McCoy, R.S. Hilgarth, K. Kundu, N. Murthy, D. Kusters, C. Reutelingsperger, M. Perretti, C.A. Parkos, A.S. Neish, A. Nusrat, Annexin A1, formyl peptide receptor, and NOX1 orchestrate epithelial repair, J. Clin. Invest. 123 (1) (2013) 443–454, https://doi.org/10.1172/JCI65831.

[24] G. Leoni, P.A. Neumann, N. Kamaly, M. Quiros, H. Nishio, H.R. Jones, R. Sumagin, R.S. Hilgarth, A. Alam, G. Fredman, I. Argyris, E. Rijcken, D. Kusters, C. Reutelingsperger, M. Perretti, C.A. Parkos, O.C. Farokhzad, A.S. Neish, A. Nusrat, Annexin A1-containing extracellular vesicles and polymeric nanoparticles promote epithelial wound repair, J. Clin. Invest. 125 (3) (2015) 1215–1227, https://doi.org/10.1172/JCI76693.

[25] M. de Paula-Silva, B.E. Barrios, L. Macció-Maretto, A.A. Sena, S.H.P. Farsky, S.G. Correa, S.M. Oliani, Role of the protein annexin A1 on the efficacy of anti-TNF treatment in a murine model of acute colitis, Biochem. Pharmacol. 115 (2016) 104–113, https://doi.org/10.1016/j.bcp.2016.06.012.

[26] D.D. Richele, K.K. Kharbanda, Dextran sodium sulfate colitis murine model: an indispensable tool for advancing our understanding of inflammatory bowel diseases pathogenesis, World J. Gastroenterol. 23 (33) (2017) 6016, https://doi.org/10.3748/wjg.v23.i33.6016.

[27] A.A. Sena, L.P. Pedrotti, B.E. Barrios, H. Cejas, D. Balderramo, A. Diller, S.G. Correa, Lack of TNFRI signaling enhances annexin A1 biological activity in intestinal inflammation, Biochem. Pharmacol. 98 (3) (2015) 422–431, https://doi.org/10.1016/j.bcp.2015.09.009.

[28] G. Hounnou, C. Destrieux, J. Desmé, P. Bertrand, S. Velut, Anatomical study of the length of the human intestine, Surg. Radiol. Anat. 24 (5) (2002) 290–294, https://doi.org/10.1007/s00276-002-0057-y.

[29] S.G. Costa, E. Barioni, A. Ignácio, J. Albuquerque, N.O.S. Câmara, C. Pavani, L.B. Vitoretti, A.S. Damazo, S.H.P. Farsky, A. Lino-Dos-Santos-Franco, Beneficial effects of Red Light-Emitting Diode treatment in experimental model of acute lung injury induced by sepsis, Sci. Rep. 7 (1) (2017) 12670, https://doi.org/10.1038/s41598-017-13117-5.

[30] F. Wang, B.T. Schwarz, W.V. Graham, Y. Wang, L. Su, D.R. Clayburgh, C. Abraham, J.R. Turner, IFN-γ-induced TNFR2 expression is required for TNF-dependent intestinal epithelial barrier dysfunction, Gastroenterology. 131 (4) (2006) 1153–1163, https://doi.org/10.1053/j.gastro.2006.08.022.

[31] V. García-Hernández, M. Quirós, A. Nusrat, Intestinal epithelial claudins: expression and regulation in homeostasis and inflammation, Ann. N. Y. Acad. Sci. 1397 (1) (2017) 66, https://doi.org/10.1111/nyas.13360.

[32] M. Han, Y.S. Jung, J.H. Cheon, S. Park, Regional variations in the use of biologics and immunomodulators among Korean patients with inflammatory bowel diseases, J. Gastroenterol. Hepatol. 34 (2019) 1166–1174, https://doi.org/10.1111/jgh.14609.

[33] A. Fischer, M. Gluth, F. Weege, U.F. Pape, B. Wiedenmann, D.C. Baumgart, F. Theuring, Glucocorticoids regulate barrier function and claudin expression in intestinal epithelial cells via MKP-1, Am. J. Physiol. - Gastrointest. Liver Physiol. 306 (3) (2014) G218–G228, https://doi.org/10.1152/ajpgi.00095.2013.

[34] J.L. Pope, A.A. Bhat, A. Sharma, R. Ahmad, M. Krishnan, M.K. Washington, R.D. Beauchamp, A.B. Singh, P. Dhawan, Claudin-1 regulates intestinal epithelial homeostasis through the modulation of notch-signalling, Gut. 64 (4) (2014) 622–634, https://doi.org/10.1136/gutjnl-2012-304241.

[35] M. Perretti, F. D'Acquisto, Annexin A1 and glucocorticoids as effectors of the resolution of inflammation, Nat. Rev. Immunol. 9 (1) (2009) 62, https://doi.org/10.1038/nri2470.

[36] B.A. Babbin, M.G. Laukoetter, P. Nava, S. Koch, W.Y. Lee, C.T. Capaldo, E. Peatman, E.A. Severson, R.J. Flower, M. Perretti, C.A. Parkos, A. Nusrat, Annexin A1 regulates intestinal mucosal injury, inflammation, and repair, J. Immunol. 181 (7) (2008) 5035–5044, https://doi.org/10.4049/jimmunol.181.7.5035.

[37] A. Sena, I. Grishina, A. Thai, L. Goulart, M. Macal, A. Fenton, J. Li, T. Prindiville, S.M. Oliani, S. Dandekar, L. Goulart, S. Sankaran-Walters, Dysregulation of anti-inflammatory Annexin A1 expression in progressive Crohns disease, PLoS One 8 (10) (2013) 1–13, https://doi.org/10.1371/journal.pone.0076969.

[38] E. Cristante, S. McArthur, C. Mauro, E. Maggioli, I.A. Romero, M. Wylezinska-Arridge, P.O. Couraud, J. Lopez-Tremoleda, H.C. Christian, B.B. Weksler, A. Malaspina, E. Solito, Identification of an essential endogenous regulator of blood-brain barrier integrity, and its pathological and therapeutic implications, Proc. Natl. Acad. Sci. U. S. A. 110 (3) (2013) 832–841, https://doi.org/10.1073/pnas.1209362110.

[39] M.H. Sheikh, E. Solito, Annexin A1: uncovering the many talents of an old protein, Int. J. Mol. Sci. 19 (4) (2018) 1045, https://doi.org/10.3390/ijms19041045.

[40] L. Parente, E. Solito, Annexin 1: more than an anti-phospholipase protein, Inflamm. Res. 53 (4) (2004) 125–132, https://doi.org/10.1007/s00011-003-1235-z.

[41] D.J. Kominsky, E.L. Campbell, S.F. Ehrentraut, K.E. Wilson, C.J. Kelly, L.E. Glover, C.B. Collins, A.J. Bayless, B. Saeedi, E. Dobrinskikh, B.E. Bowers, C.F. MacManus, W. Müller, S.P. Colgan, D. Bruder, IFN-γ-mediated induction of an apical IL-10 receptor on polarized intestinal epithelia, J. Immunol. 192 (3) (2014) 1267–1276, https://doi.org/10.4049/jimmunol.1301757.

[42] L. Nie, W. Wu, Z. Lu, G. Zhu, J. Liu, CXCR3 may help regulate the inflammatory response in acute lung injury via a pathway modulated by IL-10 secreted by CD8 + CD122 + regulatory T cells, Inflammation. 39 (2) (2016) 526–533, https://doi.org/10.1007/s10753-015-0276-0.

[43] F. Chen, W. Yang, X. Huang, A.T. Cao, A.J. Bilotta, Y. Xiao, M. Sun, L. Chen, C. Ma, X. Liu, C.-G. Liu, S. Yao, S.M. Dann, Z. Liu, Y. Cong, Neutrophils promote Amphiregulin production in intestinal epithelial cells through TGF-β and contribute to intestinal homeostasis, J. Immunol. 201 (8) (2018) 2492–2501, https://doi.org/10.4049/jimmunol.1800003.

Co-autoria 2020

International Journal of
Molecular Sciences

MDPI

Review

Cellular and Molecular Mechanisms of Environmental Pollutants on Hematopoiesis

Pablo Scharf, Milena Fronza Broering, Gustavo Henrique Oliveira da Rocha and Sandra Helena Poliselli Farsky *

Department of Clinical and Toxicological Analyses, Faculty of Pharmaceutical Sciences, University of São Paulo, São Paulo, SP 005508-000, Brazil; scharfpablo@gmail.com (P.S.); milenafbroering@gmail.com (M.F.B.); gustavohorocha@gmail.com (G.H.O.d.R.)
* Correspondence: sfarsky@usp.br; Tel.: +55-(11)-30911193

Received: 26 August 2020; Accepted: 21 September 2020; Published: 23 September 2020

check for updates

Abstract: Hematopoiesis is a complex and intricate process that aims to replenish blood components in a constant fashion. It is orchestrated mostly by hematopoietic progenitor cells (hematopoietic stem cells (HSCs)) that are capable of self-renewal and differentiation. These cells can originate other cell subtypes that are responsible for maintaining vital functions, mediate innate and adaptive immune responses, provide tissues with oxygen, and control coagulation. Hematopoiesis in adults takes place in the bone marrow, which is endowed with an extensive vasculature conferring an intense flow of cells. A myriad of cell subtypes can be found in the bone marrow at different levels of activation, being also under constant action of an extensive amount of diverse chemical mediators and enzymatic systems. Bone marrow platelets, mature erythrocytes and leukocytes are delivered into the bloodstream readily available to meet body demands. Leukocytes circulate and reach different tissues, returning or not returning to the bloodstream. Senescent leukocytes, specially granulocytes, return to the bone marrow to be phagocytized by macrophages, restarting granulopoiesis. The constant high production and delivery of cells into the bloodstream, alongside the fact that blood cells can also circulate between tissues, makes the hematopoietic system a prime target for toxic agents to act upon, making the understanding of the bone marrow microenvironment vital for both toxicological sciences and risk assessment. Environmental and occupational pollutants, therapeutic molecules, drugs of abuse, and even nutritional status can directly affect progenitor cells at their differentiation and maturation stages, altering behavior and function of blood compounds and resulting in impaired immune responses, anemias, leukemias, and blood coagulation disturbances. This review aims to describe the most recently investigated molecular and cellular toxicity mechanisms of current major environmental pollutants on hematopoiesis in the bone marrow.

Keywords: environmental pollutants; xenobiotics; hematopoiesis; myelotoxicity

1. Hematopoiesis Overview

1.1. Hematopoiesis and Hematopoietic Hierarchy

Hematopoiesis is a continuous, albeit complex, process that aims to generate blood cell subtypes in a steady manner. Hematopoietic stem cells (HSCs) represent a small population of pluripotent, self-renewing cells responsible for initiating the renewal of blood cells by giving rise to other cell progenitors. In humans, such cells are $CD34^{+}CD38^{-}$ [1].

In bone marrow (BM), HSCs initially give rise to multipotent progenitors (MPPs), which can also be considered pluripotent. These cells have limited self-renewal capabilities, yet possess full-lineage differentiation potential [2]. These cells remain mostly quiescent at the G0 phase of the cell cycle [2,3],

but through signaling mediated by intrinsic and extrinsic factors, this population initiates cell cycle entry and starts differentiating [4,5]. MPPs give rise to common myeloid precursors (CMPs) and lymphoid precursors (CLPs) through cytokine signaling and the activation of several transcription factors [6]. MPPs differentiated into CLPs originate lymphocytes and natural killer cells that rely mainly on activation of PU.1, Ikaros and GATA-3 transcription factors [7]. Soluble factors such as IL-7 and its receptor (CD127) actively participate in CLP maturation and development, as IL-7 and CD127 deficiencies disrupt production of B and T cells. On the other hand, MPP fate-decision differentiation into CMP, which originates granulocyte-macrophage (GMP) and megakaryocyte-erythrocyte progenitors (MEPs), is modulated by PU.1 and GATA-1 [7–9].

GMP differentiation is dependent on secretion of granulocyte-macrophage-colony-stimulating factor (GM-CSF), after which macrophage-colony-stimulating factor (M-CSF) modulates the differentiation of monocytes/macrophages and granulocyte-colony-stimulating factor (G-CSF) modulates the differentiation of neutrophils, basophils, and eosinophils; the latter in a process known as granulopoiesis. MEP, under erythropoietin modulation (EPO), initiates erythropoiesis originating erythrocytes and, under thrombopoietin (TPO) effects, MEP originates megakaryocytes and platelets [6,10]. During erythropoiesis, MEP differentiates into burst-forming unit erythroid (BFU-E) and, finally, into colony-forming unit erythroid (CFU-E); this whole process is tightly modulated by soluble mediators such as erythropoietin (EPO), stem cell factor (SCF), and IL-3 and -6. At a molecular level, activation of GATA-1, STAT-5, and Kruppel-like factor-1 (KLF-1) pathways ensures that erythroid differentiation and maturation take place. Disruption of these molecular pathways leads to anemia and myeloproliferative syndromes [6,11,12].

1.2. HSC Quiescence

The functionality of HSCs depend on the balance between quiescence and activation. Reduced ability of HSCs to leave quiescence results in insufficient blood cell production; on the other hand, greater amounts of HSCs leaving quiescence or failing to return to quiescence after activation exhaust the HSC pool, leading to BM failure, which favors the onset of malignant diseases [13,14]. Proper response by hematopoietic progenitors to regulatory stimuli and adequate control of cell-signaling pathways that culminate in controlling DNA damage are essential for avoiding exhaustion of the HSC pool [15].

Quiescent HSCs eventually become senescent and lose the ability to proliferate. The fine-tuning between proliferative, quiescent, and senescent cells is vital for the homeostasis of the hematopoietic environment [16]. In specific areas of BM, approximately 80% of HSCs remain quiescent throughout an average human lifespan, ensuring their "stemness" when needed. HSCs can leave quiescent states and become proliferative in a transient manner in response to external stimuli, such as injuries or infections, then become quiescent again [17]. The modulation of proliferation, differentiation, and migration capabilities of HSCs is essential for control of their quiescence. The hematopoietic microenvironment is fundamental for such regulation, fine-tuning the balance required for overall homeostasis [13].

1.3. HSC Niches

HSCs are spatially distributed in BM in highly organized niches composed of several cell subpopulations that maintain HSC quiescence. Interactions with several stromal adjacent cell populations such as fibroblasts, osteoblasts, macrophages, and endothelial cells, in addition to the actions of soluble factors released by these cell groups, ensure the preservation of the HSC pool and modulate proliferation and quiescence of these cells [18].

A significant amount of HSCs is also associated with sinusoidal endothelial cells, from where they are able to readily enter the peripheral blood [19,20]. The release of these cells into the bloodstream and their subsequent migration and return to BM are physiological processes pivotal for homeostasis [21,22].

HSCs are located both in the endosteal and vascular niches. The endosteal niche is a complex structure that includes several components, such as progenitor and stromal cells, growth factors,

and extracellular matrix molecules that participate in the regulation of hematopoiesis [23]. The endosteal niche is interposed between the bone and BM, and includes bone-forming osteoblasts and bone resorption osteoclasts alongside other cells, such as fibroblasts, macrophages, and endothelial cells located near the endosteum [23,24]. The anatomical location of the endosteal niche also supports the modulation of HSCs, as the endosteum provides a microenvironment containing low levels of oxygen, which is an important factor for HSC quiescence [25]. Osteoblastic cells present in the endosteal niche secrete chemical mediators that activate cell signaling cascades and regulate HSCs [26,27]. The secretion of TPO and angiopoietin (Ang-1) leads to the expression of adhesion molecules in HSCs (β1-integrin and *N*-cadherin) and increases quiescence of these cells [26,27]. Osteoblasts also secrete Notch receptor ligands and soluble Jagged factors; the activation of Notch receptors in HSCs inhibits differentiation of these cells and increases their self-renewal capacity under either stress or physiological conditions [27,28].

In the vascular niche, hematopoiesis occurs in the extravascular spaces between the sinuses. The medullary vascular sinuses are lined with endothelial cells and are surrounded by adventitious cells, also called CXCL12 abundant reticular (CAR) cells [29]. CAR cells are the major producers of cytokines that modulate HSC behavior, such as CXCL12 and SCF [29]. The proximity between sinusoidal endothelial cells and HSCs is very important for the maturation of the latter and, therefore, for the hematopoietic process [30]. The vascular niche is essential for the production of factors essential for the mobilization, homing, and engraftment of HSCs. The interaction between mature cells and the vascular niche is required for the release of these cells into the bloodstream. The expression of adhesion molecules by endothelial cells, such as vascular cell-adhesion molecule-1 (VCAM-1), associated with chemokine factors, mediates the maturation of megakaryocytes and the release of platelets into the bloodstream [31].

BM shelters several populations of progenitor cells other than HSCs that are essential for homeostasis, such as mesenchymal stem cells (MSCs). These cells provide a supportive microenvironment for HSCs and display high regenerative capabilities with a therapeutic potential, arising from several cell lines such as adipocytes, chondrocytes, and osteocytes [32]. The therapeutic effects associated with paracrine mechanisms linked to MSCs are extremely complex and include diverse cytokines and growth factors as well as other related receptors and signaling molecules with a wide range of biological functions [33]. MSCs and their derivatives are also essential for maintaining hematopoiesis, and for the maturation of hematopoietic lineages [34,35].

Endothelial progenitor cells (EPCs) can also be found in BM; EPCs and HSCs share hemangioblasts as common progenitors [36]. EPCs are recruited in response to ischemia and initiate angiogenesis, leading to the formation of new blood vessels, connecting fibronectin, and forming colonies and/or colony-forming units [37,38]. EPCs resemble embryonic angioblasts, which are anchorage-independent cells capable of proliferating, migrating, and differentiating into mature ECs [39]. EPCs express mainly cluster of differentiation 34 (CD34) and fetal liver kinase 1 (FLK1), although other markers have also already been identified, such as vascular endothelial growth factor receptor 2 (VEGFR2) and CD146 [40]. EPC mobilization into the bloodstream occurs depending on different disease conditions, such as tumor and cardiovascular disorders, and is mediated by a plethora of chemical mediators, with VEGF being the most well-known [41].

A schematic overview of HSC niches is illustrated in Figure 1A.

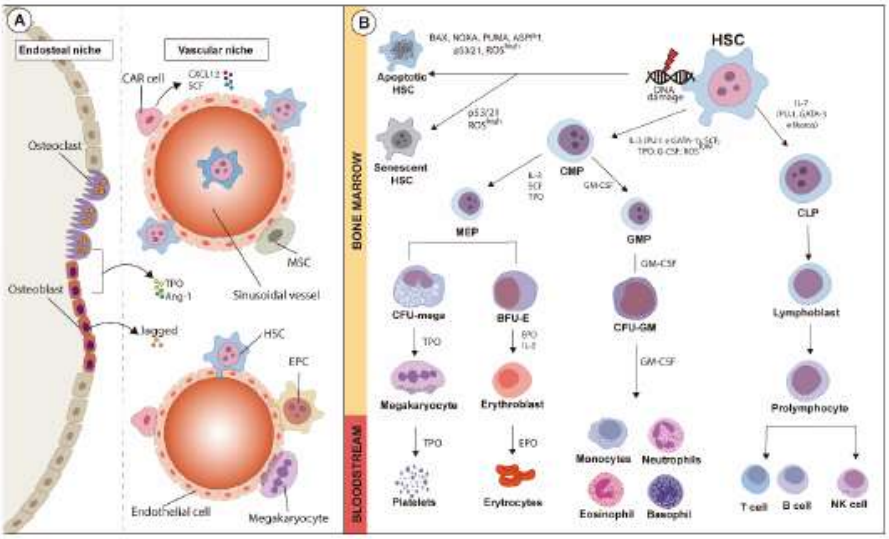

Figure 1. Schematic overview of HSC niches and fate-decision of hematopoietic lineages during hematopoiesis, along with the major transcription factors and cytokines involved. (**A**) HSC niches comprise endosteal and vascular regions containing several cell types. In the endosteal niche, osteoclasts and osteoblasts, as well as other cell types, support the vascular niche where mesenchymal stromal cells (MSCs), hematopoietic stem cells (HSCs) and CXCL12-abudant (CAR) cells are anchored. The maturation of hematopoietic lines is modulated by the fine balance between both niches. (**B**) Hematopoietic stem cells (HSCs) can undergo either apoptosis or senescence after suffering oxidative stress or DNA damage, which might or might not activate apoptotic pathways. Under physiological status, activation of GATA-1 and PU.1, low levels of reactive oxygen species (ROSs), and modulation exerted by soluble factors such as IL-3, SCF, TPO and G-CSF in HSCs give rise to common myeloid progenitors (CMPs), which then originate neutrophils, eosinophils, basophils and monocytes. On the other hand, common lymphoid progenitors (CLPs), under influence of IL-7, are modulated by the activation of GATA-2, Ikaros, and PU.1. CMPs originate erythrocytes and platelets after the maturation of intermediary precursors, and CLPs mature into B and T lymphocytes and natural killer cells.

1.4. HSC Mobilization

The recruitment of hematopoietic stem cells and progenitors (HSPCs) from BM into peripheral blood is a process known as mobilization that occurs either under physiological or stressful conditions, such as acute inflammation and chemotherapy [42,43]. Mobilization occurs based on the interplay between HSPCs and BM niche components, as well as resulting from the interaction between chemokines and their receptors. Adhesion molecules, proteases, and activation of intracellular signaling pathways also play roles in cell mobilization [42].

Indeed, the inactivation of stromal cell-derived factor-1 (SDF-1) and interleukin-8 (IL-8) alongside the enzymatic actions of proteases such as elastase, cathepsin G, and metalloproteinases (MMP-2 and MMP-9) modulate the SDF-1/C-X-C receptor 4 (CXCR4) axis and promote the release of BM-resident progenitor cells to peripheral tissues [44,45]. The SDF-1/CXCR4 axis is crucial for the maintenance, retention, and mobilization of HSPCs under homeostatic conditions or after an injury [46], as HSPCs that express CXCR4 are attracted to the highly expressing SDF-1 endosteal niche. Also, upregulation of adhesion molecules such as vascular cell adhesion molecule-1 (VCAM-1), very late antigen 4 (VLA-4), and leukocyte function antigen 1 (LFA-1) are important for the retention of HSCPs in BM; in turn,

downregulation of these molecules and of other chemokines is closely related to the mobilization of progenitors into the bloodstream [42].

HSPCs are endowed with a great therapeutic potential and, as with most of BM transplants, rely on the use of HSPCs isolated from peripheral blood after the mobilization of progenitors has been induced. The modulation of the aforementioned mechanisms mobilizes HSPCs, and this practice is widely used in clinical practice [47]. G-CSF is one of the most effective mobilizing agents [47], and repetitive G-CSF stimulation accelerates myeloid hematopoiesis, enhancing HSPC motility and migration into peripheral areas of the body [45]. Also, G-CSF induces the release of proteases, cathepsin G, and MMP-9, which downregulate levels of adhesion molecules, favoring the mobilization of HSPCs [48].

Increased release of progenitor cells and mature leukocytes from BM is part of the immune response leading to inflammatory processes. Depending on the severity of the inflammatory response, immature cells are also delivered into the bloodstream [49]. A broad range of molecules such as leukotrienes, resolvins, annexin A1, cytokines, and chemokines, among others, are involved in modulating inflammation and returning HSPCs to BM [50–53]. After an injury, such as exposure to radiation, stromal cells in BM release high amounts of SDF-1, which is responsible for inducing homing and modulating the repopulation capabilities of HSPCs [54].

1.5. DNA Damage, ROS Generation and Hypoxia in the Control of HSC

The mechanisms underlying the transformation of normal cells into malignant phenotypes are not yet fully understood. In order to better understand such mechanisms, the cell cycle of hematopoietic cells has been extensively investigated, as aging processes are closely linked to the accumulation of DNA damage and telomerase shortening in quiescent cells [4,55]. Such accumulated DNA damage in quiescent HSCs leads to the activation of DNA repair mechanisms only when these cells leave the G0 phase of the cell cycle; failures of DNA repair machineries, however, allow such accumulation of genomic damage to deregulate further cell cycle processes, and this is a key mechanism for leukemogenesis [15,56,57]. Still, in order to avoid malignant changes and to sustain homeostasis, hematopoietic progenitors are capable of tolerating some DNA damage due to protective mechanisms, such as DNA translesion synthesis (TLS) [58,59].

The accumulation of DNA damage and the insufficient activation of repair mechanisms leads to the exhaustion of progenitors, driving them to senescence or apoptosis. Activation of apoptotic pathways in HSCs aims to avoid a proliferation of compromised cells that have suffered irreparable DNA damage, preventing the development of malignancies. The main pro-apoptotic factor activated is the tumor suppressor protein p53. Activation of p53 leads to quiescence via activation of its downstream effector and cell cycle inhibitor p21, causing damaged cells to cease proliferation and become senescent [60,61]. Induction of apoptosis is linked to pathways involving BAX, NOXA, and PUMA in addition to activation of the ASPP1 protein, a p53 cofactor that selectively promotes or inhibits p53-mediated apoptosis. The process of controlling apoptosis and activation of HSCs, while complex, is crucial for preserving the HSC pool [61–63].

DNA damage also activates other protective intracellular mechanisms, such as autophagy. Autophagy is a catabolic process marked by the lysosomal degradation of damaged organelles and proteins, and is essential for maintaining hematopoiesis and HSC differentiation and quiescence by suppressing cell metabolism [64–66]. In response to stressors, HSCs induce autophagy to prevent cell death, mitigate the increase of reactive oxygen species (ROS) levels and promote activation of DNA repair machineries [67,68]. Mice lacking the autophagy related gene 7 (atg7) are more susceptible to oxidative stress, accumulation of DNA damage and loss of function of HSCs after irradiation [69].

Much like apoptosis, generation of ROSs also plays a protective role and induces autophagy. However, oxidative stress, when excessive, becomes one of the main causes of DNA damage. Excessive production of ROSs and the resulting imbalance of enzymatic mechanisms that constitute redox signaling leads to oxidative stress, resulting in oxidative-induced damage [70]. Uncontrolled ROS production is responsible for damaging DNA and macromolecules such as lipids and proteins [71,72].

Several studies associate high levels of ROS and oxidative damage as factors for the initiation and progression of hematological diseases, such as leukemias [73–76]. Still, ROS generation is essential for the functionality and modulation of HSC phenotypes and their progenitors, as the generation of ROSs regulates the self-renewal and differentiation of adult stem cells [77]. At low levels, ROSs ensure that precursors remain pluripotent, but at excessive levels, ROSs can impair the functionality of these populations, even leading to BM failure under extreme circumstances [78,79].

Aiming to avoid excessive oxidative stress, antioxidant proteins act quickly in the face of high levels of ROSs. Among them, superoxide dismutase (SOD), catalase, and glutathione peroxidase are the most important; reduced glutathione (GSH), which also exists in the cell in its oxidized form (GSSG), is perhaps the most abundant of enzymatic antioxidants [80,81].

The enzymatic machinery responsible for keeping ROS levels low in hematopoietic progenitor cells is also aided by the microenvironment of hematopoietic niches [25,78]. As the generation of ROSs is closely linked to oxygen demand, several transcription factors are involved with the regulation of low levels of oxygen in HSCs. Hypoxia-inducible factor 1 (HIF-1) is the main transcription factor responsible for allowing cells to adapt to low oxygen levels; the expression of its inducible subunit, HIF-1α, is linked to the maintenance of ROSs at homeostatic levels. Lacking activity of HIF-1α in progenitor cells leads to the exacerbated generation of ROS, culminating in increased cell proliferation and loss of self-renewal capacity [82,83]. Activation of fork-head O transcription factor (FoxO) subunits also plays a crucial role in keeping low the levels of ROSs in HSCs, thus playing a protective role upon oxidative stress. The deletion of heterodimers of the FoxO's family in hematopoietic cells substantially decreases the number of HSCs, leading to increased cell cycle activation, and this effect appears to be dependent on oxidative stress, as treatment with n-acetylcysteine, a potent antioxidant, is able to restore homeostatic cell-cycling conditions [84,85]. Activation of p38 mitogen-activated protein kinase (MAPK), a transcription factor, in response to ROS generation, is also important for regulating HSCs in the face of oxidative stress. MAPK activation limits the lifespan of progenitor cells, and inhibition of p38 pathways protects the self-renewal capabilities of HSCs, avoiding their exhaustion and thus being a potential therapeutic target for improving the "stemness" of HSCs [79,86].

These reports highlight the complexity of the processes responsible for regulating HSC physiology in hematopoiesis and how fragile this vital system is. Moreover, the maturation and differentiation of hematopoietic precursor cells leading to the delivery of mature cells into the bloodstream also involves fine-tuning mechanisms, which can be easily disrupted. Disturbances on HSC biology and functions and on the delivery of precursors into the bloodstream are mechanisms of blood and vascular diseases. The hematopoietic hierarchy alongside indications of HSC damage leading to senescence and apoptosis is summarized in Figure 1B.

2. Cellular and Molecular Mechanisms of Toxicity on Hematopoiesis

The amount of pollutants in the environment has increased in the modern era. Air pollution before industrialization mainly originated from the burning of organic materials used for house-heating and cooking. Such pollution resulted in increased releases of carbon monoxide and particulate matter, which by then already affected the health of populations [87]. Since industrialization, the amount and diversity of pollutants in the air have increased, and alarming levels of pollutants have been quantified in several countries worldwide, regardless of them being developing or having already been developed [88,89]. Consequently, hazardous effects for both the environment and human health have led to public health concerns worldwide. The complexity of hematopoiesis and of the fine-tuning mechanisms that control functions of blood components such as host defense, oxygen supply for tissues, and bloodstream rheology makes the hematopoietic system a suitable target for the actions of xenobiotics, including those released to the environment. Blood is also a pivotal matrix used for the assessment of xenobiotic levels and biological end points during intoxications. Below is described the most relevant data on the cellular and molecular actions of current environmental pollutants on the BM hematopoietic system in mammals.

2.1. Benzene and Its Metabolites

Benzene (BZ) is a volatile liquid aromatic hydrocarbon solvent, a byproduct of petroleum refinement. It used to be widely employed as an industrial chemical, either as a solvent or as a starting material for the synthesis of other chemicals, until its severe toxicity to occupationally exposed humans, especially by inducing hematological disorders and cancer, was described [90,91]. While the relationship between BZ exposure and leukemia had already been reported at the beginning of the 20th century in industry workers [91], BZ was classified as an environmental carcinogen in 1982 due to its BM toxicity [92]. Nowadays, even though the use of BZ in working environments is controlled around the world [93], alarming levels of this solvent are frequently found in the air of both developing and developed countries [94,95]. BZ, alongside toluene and xylene, is a contaminant of gasoline and diesel, thus being a common pollutant in high-traffic cities [96,97]. Smokers are also exposed to high amounts of BZ and its metabolite hydroquinone (HQ), which are compounds of cigarettes [98,99].

BZ is extensively metabolized after absorption via lungs, mouth, and skin, and the resulting metabolites are responsible for its harmful effects. BZ is initially converted to benzene oxide by cytochrome P450 enzymes, mainly CYP2E1, in the lungs and liver; benzene oxide is then rearranged into phenol, which is subsequently metabolized to HQ, catechol, and 1,4-benzoquinone (1,4-BQ) by action of CYP2E1 enzymes, especially in the liver. HQ is transported to the BM and metabolized to the highly reactive BQ by oxidative enzymes, such as myeloperoxidases (MPOs) [100]. Benzene oxide can also be hydrolyzed generating catechol and 1,2-BQ, or it can be metabolized by glutathione S-transferases forming the less-toxic metabolite *S*-phenylmercapturic acid. Benzene oxide can also have its aromatic ring opened, resulting in reactive muconaldehydes and *E,E*-muconic acid [100], which are quantified in urine as intoxication end-points. Detoxification by redox systems in BM, such as NADPH–quinone oxidoreductase 1 (NQO1), reduces the local levels of oxidative toxic agents generated by BZ metabolism [100,101], but prolonged exposure to BZ leads to lasting high levels of BZ and accumulation of BQ, which lead to toxic effects in BM. The role of redox systems on BZ toxicity has been evidenced by several reports as lower and higher hematotoxicity caused by BZ in CYP450 and NQO1 knockout mice, respectively [102,103]. NQO1 polymorphism is associated with increased hematotoxicity in humans exposed to BZ [104], and administration of the major compounds of garlic, diallyl di and trisulfide reduces BZ hematotoxicity in mice by deactivating CYP2E1 and MPO and activating GSH and NQO1 [105].

BZ exposure affects BM by interfering with different hematopoiesis pathways due to actions of its multiple metabolites, mainly HQ and BQ. This leads to failures in the BM environment, which result in decreased peripheral counts of erythrocytes, leukocytes, platelets, pancytopenia, aplastic anemia, myelodysplasia, and myelogenous leukemia [90,100,106,107]. Robust studies carried out over the years have evidenced that BZ exposure affects BM cells by causing chromosomal aberrations, gene mutations, oxidative stress, apoptosis, epigenetic deregulation, impairment of DNA repair, modification of protein secretion, and suppression of immune systems [90,91]. It is worth mentioning that toxic effects are not due to direct actions of BZ and its metabolites only, as these are also powerful inducers of ROS generation, and high ROS levels also mediate the harmful effects of BZ intoxication [90].

It is worrisome that there are no described safe levels for BZ exposure regarding hematopoiesis. BZ toxicity is influenced by different genetic profiles and living conditions; blood cell functions and their production and delivery processes are very intricate and offer a great number of targets for BZ metabolites to act upon [101,108]. Novel toxic mechanisms exerted upon hematological parameters by BZ exposure have been continuously reported, especially for exposures at levels considered sub-toxic [108,109].

As the overall population should not be exposed to high levels of BZ, elucidating how BZ exposures of low frequency and low doses disturb cell pathways is a goal of current investigations. Indeed, gene alterations in human HSCs have been fully demonstrated after low-dose exposures to BZ (lesser than 1 ppm, the threshold level), resulting in aberrant expression of downstream genes, malignant transformations, and HSC dysfunction [110–112]. Exposure of HSCs to non-cytotoxic doses

of BZ have caused ruptures of DNA structures at breakpoint hot stops in the leukemia-related genes MLL and CBFB similar to those found in leukemia patients [113]. DNA breaking within the MLL gene leads to rearrangement of over 120 other partner genes, resulting in acute leukemia with poor prognostics [114], and DNA breakings within the CBFB gene is the cause for about 10% of acute myeloid leukemia cases [115]. Enhanced autophagy is another mechanism elicited by lower levels of BZ exposure, as reported in BM mononuclear cells from patients exposed to BZ and in mice cells exposed to HQ. Autophagy is regulated by post-translational modifications such as phosphorylation, ubiquitination, and acetylation. BZ exposure reportedly decreases acetylation of autophagy components by inhibiting the activity of acetyltransferases such as p300 [116]. Hematopoietic cells collected from workers exposed to low doses of BZ or incubated with 1,4 BZ have shows increased apoptosis and autophagy rates, dependent on expression of the long-non-coding RNA cRNAVNN3 triggered by BZ or 1,4 BZ-induced oxidative stress; cRNAVNN3-enhanced phosphorylation of Bcl-2 and beclin-1 led to cell death [117]. Physiological autophagy levels are required for maintaining stable cell homeostasis under stress conditions, while exacerbated autophagy induces uncontrolled cell death. Therefore, depending on the intensity of the aggressive stimuli, autophagy can be either beneficial or harmful, playing either a protective role on cell death or contributing to it [118].

HIF-1α is a transcription factor involved in the harmful effects of BZ on HSC niches. HIF-1α controls the hypoxic microenvironment of such niches as to maintain quiescence, survival, and metabolic phenotypes of cells by increasing anaerobic glycolysis and reducing ROS generation [78,82,119]. Recent evidence has demonstrated that exposure to BZ can inhibit HIF-1α, as mice exposed to BZ showed high levels of ROSs alongside lower levels of HIF-1α in niches of stem cells [120]. HIF-1α binds to DNA in the hypoxia-response-element (HRE) DNA domain, and several genes such as those responsible for the expression of vascular endothelial growth factor (VEGF) and erythropoietin (among others) contain HRE binding sites in their sequences and are thus targets for the actions of HIF-1α. It has been demonstrated that treatment of BM cells from mice with BZ downregulated expression of genes containing the HRE domain, impairing expression of genes involved with self-renewal, cell cycle, differentiation, and apoptosis pathways of HSCs [121]. In accordance, overexpression of HIF-1α in a myelogenous leukemia (CML) K562 cell line reduced apoptosis and ROS levels induced by 1,4-BQ by targeting Nox4, Bcl-2, and key glycolytic enzymes [122].

Reduction of the number of circulating red blood cells is also a clinical symptom of low intensity BZ toxicity [123]. It has been demonstrated that damage caused to erythroid burst-forming units (BFU-E) in workers exposed to BZ is dose-dependent, and that erythroid cell differentiation is more sensitive to the harmful effects of BZ or HQ exposure than other hematopoietic precursor cells [124,125]. It has also recently been reported that BZ inhibited erythroid cell differentiation by downregulating the expression of miRNA-451a and miRNA486-5p [126]; miRNA-451a positively modulates the terminal differentiation of erythroid cells protecting red cells against oxidative stress [127,128] and miRNA486-5p regulates the differentiation and growth of erythroid cells [129].

Another topic of BZ toxicity that is yet to be fully elucidated is whether hematopoiesis disturbances caused by BZ exposures of low frequency and dose are reverted after exposure ceases. It has been demonstrated that exposure to BZ in mice impaired frequency and colony formation of HSC SCA-1^{+}c-kit^{+} cells (LSK) and reduced mRNA levels of Notch-1 and p53 in BM cells collected 10 months after the end of BZ exposure. This provides evidence that molecular and cellular alterations affecting the self-renewal of HSCs are long-lasting after exposure to BZ, and may allow pre-leukemic clones to evade elimination, leading to an increased risk of development of transforming neoplasia [130]. In the same vein, exposure of rats to BZ at low doses for 14 days impaired erythropoiesis, which partially recovered 56 days after exposure has ceased as reduced numbers of reticulocytes in the bloodstream and reduced phagocytosis ability in macrophages collected from mature erythroblastic islands could be observed after this period [131].

The modulation of the cytosolic transcription factor aryl hydrocarbon receptor (AhR) linked to BZ toxicity on BM and blood cells has recently been investigated. AhR is a ligand-activated transcription

factor expressed in hematopoietic progenitor cells, lymphocytes, neutrophils, and splenocytes [132–134]. The connection between BZ exposure and AhR was first demonstrated by studies that provided evidence that hematopoietic toxicity induced by BZ was not observed in AhR knockout mice, but that toxicity would take place when the BM of animals was repopulated with cells from wild-type mice. Accordingly, BZ-induced hematotoxicity in irradiated wild-type mice repopulated with AhR knockout BM cells was not observed, as measured by granulo-macrophage-colony-forming units assay [135–137].

AhR expression is also essential for the differentiation and activation of Th17 cells in the pathogenesis of rheumatoid arthritis [138,139]. Solid experimental and clinical data show a correlation between exposure to cigarette smoking and the induction and aggravation of rheumatoid arthritis [140,141]; there is also increased AhR expression in the synovial membrane of smokers [142]. Cigarette smoke is an important source of BZ and HQ, as each stick delivers about 72.2 and 100 µg of BZ and HQ, respectively [99,143]. The connection between HQ exposure and AhR to rheumatoid arthritis was recently tested in mice and rats exposed to HQ by inhalation following an experimental design of low-dose exposures. Although HQ-exposed animals had no alterations in BM or blood cell numbers, disease symptoms worsened, with a high frequency of AhR^+ neutrophils and Th17 lymphocytes in the inflamed synovia. Accordingly, rheumatoid arthritis symptoms were not observed in AhR knockout mice exposed to HQ [133,134] (Heluany et al., under review). These data evidence that exposure to BZ metabolites worsens rheumatoid arthritis involving HQ actions through AhR on blood cells, and that both BZ and HQ are cigarette compounds involved with the harmful effects on the evolution of the disease as a result of cigarette smoking.

Although scientific studies regarding hematotoxicity evoked by BZ exposure have been published extensively in scientific literature over the last 50 years, the broad actions of BZ and its metabolites upon the complex hematopoietic phenomena and resulting effects to the immune system in exposed subjects, especially those exposed to low concentrations, constitute a still-vast area for investigations with a meaningful impact on public health.

2.2. *Engineered Nanoparticles*

Nanotechnology as a field has grown at a fast pace over the last 20 years, and has been responsible for the development of materials with useful properties for a plethora of industrial and biological applications in the engineering, communication, food, and textile industries, to name a few. Nanomaterials also have bioenvironmental applications, and can act as reliable drug carriers [144]. Nanoparticles (NPs) are sized less than 100 nm, and are characterized by an increased surface area and unique physicochemical properties, which make them extensively employed in several fields. Due to NPs being such a recent breakthrough, the number of studies focusing on subjects occupationally exposed to NPs is still low, but increasing. The impact of NPs on occupational health and safety is currently difficult to predict, halting advances on the risk assessment of NPs [145]. The main factors that determine the toxicological effects of NPs are exposure conditions such as route, concentration, and duration; the individual characteristics of exposed subjects; and the intrinsic characteristics of NPs, including ability to bind to or coat surface species, surface area, composition, and catalytic activity, among others [146]. Moreover, NP pharmacokinetics differ from those of common bulk materials, which is another barrier to advances on understanding their toxicological potential [147].

Current nanomaterial research has mostly focused on nanotechnology applications, whereas there is little information regarding occupational and environmental exposure assessment and risk characterization associated with NPs. As airborne NPs are mainly absorbed by respiratory routes, some of the toxic effects of NPs on lungs have been described in both humans and experimental animals, being characterized mostly by inducible inflammatory reactions [144]. Still, inhaled NPs have a very small size and can be arrested from alveoli into other tissues by the bloodstream, which may lead to systemic harmful effects [148]. Indeed, it has been demonstrated that pulmonary instillation of titanium dioxide (TiO2) NPs has resulted in increased plaque deposits in atherosclerosis-prone apolipoprotein E-deficient mice [149]. In addition, environmental exposure to TiO2 NPs has affected

the biology of circulating angiogenic cells (EPCs), which contribute to the harmful vascular effects of NPs [150]. After birth, EPCs circulate in the peripheral blood until being recruited and incorporated into sites of active neovascularization, being then committed to vascular repair [37,151].

No clear evidence is available regarding the effects of occupational or environmental exposure to NPs on hematopoiesis in BM. Nevertheless, alterations in the number and functions of circulating immune cells have been described in addition to those induced by the inflammatory response by itself as a result of exposure to NPs. Magnetic NPs have been extensively used as contrasting agents in magnetic resonance imaging; assessment of toxic effects due to the inhalation of manufactured magnetic NPs has revealed these NPs to be highly distributed to different tissues and to increase hematopoiesis in the spleen, where there are increased numbers of erythroid and myeloid cells in the red pulp [152].

Although studies available on the harmful effects of engineered nanotechnology products on the hematopoietic system are scarce, the systemic toxic effects of NPs that unintentionally reach complex tissues (such as the central nervous system [153]) have shown evidence that further investigations on the toxic potential of NPs on BM could provide valuable data for risk assessment studies.

2.3. Incidental Environmental Nanoparticles and Particulate Matter

Exposure to NPs or particulate matter (PM) found in polluted air causes systemic harmful effects, which have been extensively described in humans, and exposure to associations of NPs and PM can lead to the onset of diseases as well [154–156]. PM comprises a heterogeneous mixture of particles of different sizes and chemical compositions. The severity of toxic systemic effects is closely linked to particle size, as both NPs and PM 2.5 (smaller than 2.5 μm) can reach the bloodstream from alveoli and be distributed into tissues causing systemic effects [157–160]. Particles can also contain harmful airborne microorganisms and metals, which greatly increase their toxicity [161,162]. The World Health Organization estimates 92% of the global population lives in areas where the levels of fine PM 2.5 exceed the recommended annual average air concentration limit of 10 $\mu g/m^3$. Recent findings have shown that exposure to PM 2.5 can pose hazards to public health at low levels, even below those recommended by regulatory agencies [154,163–167].

Local and systemic inflammation, especially linked to chronic exposures, is a common hallmark of exposure to airborne NPs and MPs [160,168]. Cytokines secreted at inflammation sites reach BM and alter HSC niches, affecting maturation and differentiation phases of leukocytes and delivery of cells into the bloodstream. Both acute and chronic in vivo exposure to PM are reported to cause lung inflammation and leukocytosis due to an increased release of immature granulocytes into circulation [169]. This effect was evidenced by increased numbers of band neutrophils found in the bloodstream and a reduced monocyte transit time in BM after lung instillation of PM 10 in rabbits; this effect was also observed in rabbits instilled with supernatant culture medium of alveolar macrophages incubated with PM 10, but not in rabbits instilled with supernatant collected from alveolar macrophages incubated with inert carbon [169,170]. Thus, PM 10 actions depend on activation of lung macrophages, followed by secreted chemical mediators reaching BM and inducing neutrophil and monocyte delivery into the bloodstream [171,172].

The association between PM 2.5 exposure and cardiovascular morbidity and mortality has been extensively demonstrated in epidemiological and experimental studies [173,174]. Both direct and indirect actions of these particles on BM have been shown. Toxic effects on the cardiovascular system caused by MP 2.5 are characterized by alterations on blood rheology and endothelial cells of blood vessels, mostly associated with endothelial oxidative stress and inflammation [175,176]. Moreover, it a tracheal instillation of PM 2.5 from diesel exhaust in mice was reported to have increased the mobilization of neutrophils from BM, and the resulting neutrophilia led to myocardial oxidative stress [177]. Solid evidence has demonstrated that in vivo exposure to PM 2.5 affects BM by limiting the inherent functionality and mobilization of EPCs into the bloodstream, as acute exposure of humans or mice to PM 2.5 has been negatively correlated with plasma levels of EPCs [178,179]. In addition,

EPCs from the BM of mice exposed to PM 2.5 have displayed reduced proliferation and tube formation capabilities that were not due to cell death, but rather dependent on the downregulation of genes that support cell proliferation and the cell cycle of BM EPCs. These effects were absent in overexpressing extracellular superoxide dismutase ecSOD-Tg mice exposed to PM 2.5, resulting in reduced oxidative stress and higher nitric oxide bioavailability even upon exposure to PM 2.5. GSH levels were also reduced in BM cells obtained from PM 2.5 exposed mice [179]. Therefore, harmful effects on BM EPCs caused by exposure to PM 2.5 may comprise likely mechanisms for its toxic effects linked to cardiovascular morbidity and mortality.

Other studies further evidenced the toxic effects of PM on BM cells, as incubation of PM 2.5 or PM 10 collected from polluted air impaired proliferation of human HSCs in a concentration-dependent manner, increased expression of cytokine genes associated with inflammation (e.g., TNF-α and IL-6), and impaired expression of the cell cycle regulator gene p53 [180].

Recent studies have described associations between exposure to PM 2.5 during pregnancy and effects on HSCs in the BM of offspring. Pups from female mice exposed to PM 2.5 via respiration during pregnancy suffered from lung inflammation and oxidative stress, which lasted until adulthood. Although offspring aged two and six months had normal leucograms, the two-months-old offspring showed increased BM oxidative stress, inflammation, and osteoclast activity. Damage done to BM evolved and six-months-old offspring exhibited senescent phenotypes of BM HSCs, demonstrated by reduced clonogenic formation, donor-cell-derived reconstitution and self-renewal, increased levels of mitochondrial ROSs, NrF2 expression, cyclin-dependent kinase inhibitors, and increased p38 phosphorylation and DNA double-strand breaking. Considering that no effects were observed on the BM of exposed dams, it is likely that offspring from mothers exposed to PM 2.5 have less efficient anti-oxidant mechanisms in their BM than their mothers [181].

Although scientific studies assessing exposure to PM and BM effects are not plentiful, this only reifies that the BM microenvironment should be considered for risk assessment studies. BM is a direct target for the actions of PM, especially PM 2.5, enduring impairments on cell proliferation, lifespan, and functionality due to systemic oxidative stress and inflammation.

2.4. Dioxins and Polychlorinated Biphenyls (PCBs)

Dioxins are persistent organic pollutants (POPs) released to the atmosphere as undesired byproducts of an anthropogenic and natural origin. These compounds can originate as byproducts from combustion processes, such as the incineration of solid waste, the chlorine bleaching of paper and wood-pulp, the burning of coal in power plants, and forest wildfires [182]. These pollutants also occur as contaminants in several pesticides, herbicides, and fungicides [183]. Among POPs, dioxins are considered the most hazardous to human health, with their major toxic effects being linked to binding to the aryl hydrocarbon receptor (AhR) in several cell types.

PCBs make up a class of 209 volatile, structurally related organochlorine compounds used for different industrial and commercial applications, which were mass-produced until the 1970s. Since then, PCBs have been identified as carcinogens, and their global commercial production was banned by signatory nations in the Stockholm Convention on Persistent Organic Pollutants in 2001 [184,185]. Nevertheless, PCBs continue to pose a significant risk to human health through exposure sources such as the continuous release from hazardous waste sites, PCB-contaminated equipment that is still in use, and contact with construction materials used in buildings erected prior to the PCB production ban. In addition, non-legacy PCB congeners have also been detected in paint and industrial pigments [186]. PCBs are still considered among the most important groups of food contaminants, and food and agricultural authorities strictly monitor the PCB contamination of foods. As air pollutants and contaminants of extensively used organochlorine pesticides, PCBs contaminate foods in the same manner as described above, by being byproducts of industrial processes, the combustion of certain materials, or accidental fires. Recycling and the production of certain minerals can also produce PCBs [187]. Depending on the position of chlorine atoms in the biphenyl backbone, PCBs can be

of planar or non-planar geometry. Non-chlorine substitution in the ortho position determines non co-planar geometry, while substitution of one to four chlorine molecules in the ortho position determines varying degrees of co-planar ring geometry. Co-planar congeners bind to AhR and are therefore called dioxin-like PCBs. Among 209 known PCB congeners, 12 can bind to AhR [188]. Long degradation half-life and high liposolubility contribute to the bioaccumulation of dioxin and PCBs in biological organisms [189].

AhR is a cytoplasmic basic helix-loop-helix/PAS transcription factor that, upon activation by ligands, can lead to either physiological or toxic effects. AhR has traditionally been described as a central regulator of responses to environmental factors and of xenobiotic metabolism. First studies on the toxic effects of dioxins and AhR evidenced 2,3,7,8-tetrachlorodibenzo-p-dioxin (TCDD, dioxin) can bind to AhR, leading to several toxic effects [190,191]. Under homeostatic conditions, AhR remains predominantly in the cytoplasm as part of a protein complex linked to molecular chaperone heat shock protein 90 (HSP90), p23, and XAP2 [192]. Several stressors can drive AhR activation and evoke its conformational transition, resulting in its nuclear translocation [193]. AhR then dissociates from HSP90 and binds to the AhR nuclear translocator (ARNT), and the AhR/ARNT complex binds to promoter regions in the DNA known as AhR-responsive DNA elements or xenobiotic response elements (XREs), which leads to an increased expression of target genes (e.g., cytochrome P450 (CYP) 1A1, CYP1A2 and CYP1B1) [193,194]. This canonical pathway for AhR activation mediates several toxic responses, including liver damage, chloracne, teratogenesis, cancer, and immunosuppression [195,196].

In recent years, research has demonstrated that AhR-null mice suffer from developmental impairments, evidencing AhR as a crucial homeostasis modulator in several tissues and biological processes, including hematopoiesis [197,198]. AhR modulation on HSC self-renewal, proliferation, cell cycle, and senescence has been demonstrated by the in vivo gene deletion of the AhR exon 3. HSCs from AhR knockout mice abandon quiescence and become hyperproliferative, revealing that AhR is likely a negative regulator of excessive or unnecessary proliferation [197–199]. AhR also affects the maturation of HSCs by acting on progenitor strains. AhR deletion in human embryonic stem cells, or blocking of these cells with AhR antagonists, leads to increased differentiation into $CD34^+$, $CD45^+$, and $CD31^+$ EPCs [200,201]. Conversely, in later maturation phases, AhR deletion favors the proliferation of myeloid colonies [201].

Epidemiologic studies have demonstrated associations between 2,3,7,8-tetrachlorodibenzo-p-dioxin (TCDD), the most toxic member of the polychlorinated dibenzodioxins (PCDD) family, and onco-hematologic diseases, particularly non-Hodgkin lymphomas, chronic lymphocytic leukemia, and multiple myeloma [202–204]. Indeed, the BM of adult mice exposed to acute doses of TCDD becomes hypocellular, with a significant decrease in the total number of HSCs—effects that are not due to cell death, but rather to direct AhR modulation [205].

Exposure to TCDD impairs humoral responses, and it has been determined that such exposure can lead to B-cell disorders and increased incidence of B-cell-derived cancers [206,207]. Mice exposed to TCDD have shown a reduced number of B-cell progenitors [208] and skewed HSC differentiation favoring myeloid progenitors to the detriment of lymphoid progenitors, giving rise to mature B cells [110,209]. It has also been reported that HSCs treated with TCDD are not able to repopulate the BM of irradiated mice [210,211]. Gene analysis of HSCs revealed that TCDD treatment modified the transcription of genes linked to both migration—such as CD184 (CXCR4) and CD44—and the development and function of the hematological system (e.g., Fos, JunB, Egr1, Ptgs2, and CXCL2) [212].

TCDD is not only toxic to HSC, and its effects on BM stromal cells can also contribute to decreased B-cell numbers. Exposure to TCDD downregulates IL-6 gene transcription in stromal cells, inhibiting the growth of early B-cell progenitors in a NF-kB-dependent manner [213]. Inefficient humoral responses in offspring from mothers exposed to TCDD and dioxin-like PCBs has led to the reprogramming of hematopoietic stem and progenitor cells during development [214].

The toxic effects of dioxins upon the hematological system demonstrate the importance of AhR on the control of proliferation, function, and migration of hematological progenitor cells in BM.

Even though dioxin-like xenobiotics are capable of strongly binding to AhR, and of causing severe toxic effects in humans, the harmful effects caused to the hematological system, mainly impairing humoral responses, are suitable end points for the risk assessment of dioxin exposure.

2.5. Heavy Metals

The number of individuals exposed to has metals increased throughout history in accordance with industrial and urban growth, eventually leading to researchers investigating correlations between exposure to metals and the onset of diseases [215]. Heavy metals (HMs) are raw materials of great importance for the steel cutting, welding, electroplating, plastics, and automobile industries [216]. HMs are classified by their atomic number, atomic weight, density, and toxicity, of which chromium (Cr), lead (Pb), mercury (Hg), cadmium (Cd), arsenic (As), copper (Cu), manganese (Mn), nickel (Ni), zinc (Zn), and silver (Ag) are the most relevant for human exposure and toxicity [217]. Among these HMs, Pb, Cd, As, and Hg have been described as harmful to BM, causing anemia and immune deficiencies, as evidenced by epidemiological and clinical studies and by experimental models of intoxications caused by these HMs.

Levels of HM in the atmosphere, in the occupational environment, and in biological samples can all be used to measure the impact of HM exposure on the health of workers and of the general populations residing in industrial areas [215]. Acute exposure to HMs can severely damage lungs, liver, kidneys, and the central nervous system (ATSDR, 2004). Long-term exposure can lead to HM bioaccumulation not only in humans, but also in crops, soil, and wildlife used as food sources, indirectly affecting humans [218,219]. While acute exposures to HMs knowingly causes severe toxic effects, concerns by public health authorities are currently focused on chronic, low-dose exposures, which can lead to cumulative effects. Even exposures to HMs at levels lower than those assigned for "safe" threshold values are potentially toxic, resulting in cancer, neurological damage, and infertility, among other effects [220–222].

Exposure to HMs can cause disturbances in the hematological system and can be used as biological end-points for assessing HM exposure; HM intoxications cause immunosuppression, anemias, and leukemias and disrupt coagulation [223–226]. While HM exposure can directly impact circulating blood cells, several toxic effects occur in the BM environment and affect hematopoiesis.

2.5.1. Lead (Pb)

Exposure to Pb reduces the number of blood cells, including both erythrocytes and leukocytes. Toxic effects on BM due to Pb exposure have been described even at lower levels in humans under occupational exposures or in animal experimental intoxication models [227]. In this context, mice exposed to Pb have displayed reduced numbers of colony-forming units in their BM [228], and exposure to Pb impaired differentiation of CMPs, resulting in decreased numbers of mature myeloid cells [229]. Mechanisms associated with these effects involve higher expressions of interferon regulatory factor-8 (IRF8), which blocks C/EBPα and modulates neutrophil differentiation [230]. Recent evidence shows that exposure to Pb at occupational levels can result in lower numbers of innate lymphoid cells (ILCs) in the blood of mice, with this effect being dependent on activation of Janus Kinase-1 leading to an inability of BM CLP progenitors to become mature and be delivered into the bloodstream [231]. CLPs differentiate into innate lymphoid cell-restricted progenitors via transcription factor ID2, which further differentiate into mature ILC 1, 2, and 3 [232]. Under stimulation, mature ILC 1, 2, and 3 are activated and exert functions similar to those exerted by Th1, Th2, and Th17 cells, respectively [233,234]. These functions play roles during the innate immune response occurring in certain scenarios, such as during asthma, tumors, and tissue remodeling [235,236], all of which are aggravated due to Pb exposure.

Pb intoxication also interferes with erythropoiesis, as evidenced by aplastic anemia. High levels of reactive oxygen species seem to be the mediators of this effect, as children with aplastic anemia are reported to show higher levels of Pb in the blood alongside increased markers of oxidative stress [237].

2.5.2. Cadmium (Cd)

Humans are exposed to Cd derived from occupational activities, cigarette smoking, Cd-contaminated dust and ingestion of contaminated food [238]. Cd is extensively distributed to other tissues and has a long half-life (approximately 10 years), contributing to its high toxicity [239]. Much like Pb exposure, Cd exposure affects the differentiation and functionality of HSCs in BM. It has been reported that mice exposed to Cd showed increased myelopoiesis to the detriment of lymphopoiesis, there being higher numbers of neutrophils and lower numbers of B and T lymphocytes in the bloodstream and in secondary lymphoid tissues. Cd exposure is also harmful to HSC niches in BM, as transplantation of normal HSCs to Cd-exposed and lethally irradiated mice did not repopulate the BM, whereas HSCs from Cd-exposed mice partially reconstituted the hematopoietic system of non-exposed and lethally irradiated mice [240]. A recent study carried out in mice further demonstrated that Cd exposure impaired the HSC ability to repopulate the BM of lethally irradiated recipients, and this toxic effect upon HSCs is dependent on increased expression of cdc42, a small GTPAse crucial for HSC functions in mice. Indeed, pharmacological blocking of cdc42 restored the hematopoietic ability of HSCs from Cd-exposed mice [241].

2.5.3. Arsenic (As)

As is considered to be among the metals most capable of causing harmful effects to human health. Geologically distributed in pentavalent (As^{5+}, arsenate) and trivalent (As^{3+}, arsenite) forms in some regions of the world, its concentration in soil and water exceeds in up to 10 times allowed levels, according to the World Health Organization [242]. The most common form of contact with As is through contaminated water consumed either directly or through food. Absorption via inhalation also occurs during the handling of pesticides, fungicides and paints. Arsenic metabolism determines its toxicity, as trivalent arsenic, either methylated or not, easily reacts with thiol groups in proteins and is thus more toxic than pentavalent arsenicals [243].

Studies using murine models have found that exposure to arsenic in drinking water can result in anemia and impaired immune responses elicited by mononuclear cells [244–248]. These effects have also been confirmed in humans [249]. As can be easily distributed to several tissues through the bloodstream, reaching BM where it causes toxic effects. Indeed, arsenic trioxide (As_2O_3) administered to mice severely damages the BM microenvironment, making stromal cells unable to form a healthy matrix to support hematopoietic progenitors [250].

Epidemiological studies carried out in Bangladesh and Romania, areas characterized by geogenic contamination of underground drinking water, correlated chronic As exposure with anemia [251–254]. A case report demonstrated pronounced histological alterations in the BM of a patient suffering from arsenic poisoning, characterized by marked nuclear aberrations involving nucleus shape, chromatin distribution, and nuclear envelope [255]. In vitro analyses showed that the molecular mechanism for toxicity of arsenic trioxide in erythroleukemic cell lines and on normal hemopoietic progenitor cells (HPCs) involves several pathways, such as inhibition of Stat5 activation and reduced expression of target genes Bcl-X(L) and glycophorin-A; activation of apoptotic mechanisms leading to cleaving of erythroid transcription factors Tal-1 and GATA-1, whose integrity is required for erythroid cell survival and differentiation; and reduced expression of heat shock protein 70, which is required for maintaining GATA-1 integrity [256]. In vivo, exposure to arsenite also impaired the formation of burst-forming unit-erythroid (BFU-E) colonies and the differentiation of erythroblasts into further stages in mice [257].

2.5.4. Mercury (Hg)

Mercury intoxications usually occur due to acute exposures to its natural form during extraction of fossil fuels, burning of biomass, forest fires, and deforestation [258]. However, exposure to small concentrations, which occurs during contact with dental amalgams, consumption of fish and other

seafood from contaminated regions, and occupational exposure (e.g., farming, industrial activities, and gold mining), can also affect human health [259]. Hg is toxic to virtually every human organ; due to its affinity for sulfhydryl groups, Hg alters tertiary and quaternary structures of proteins and disrupts membrane permeability [259]. Disturbance of hematopoietic systems is also a hallmark of Hg intoxication, characterized mainly by anemia and lymphocytopenia [223,260].

The harmful effects of Hg on BM were first demonstrated in patients with BM hypoplasia [261]. Exposure of mice BM cells to inorganic and organic Hg inhibited colony formation [262], and exposure to Hg in rat BM cells inhibited activities of acetylcholinesterase, glutathione reductase, and glucose-6-phosphate [263,264]. Even though absorbed Hg reaches BM (Dabrowski et al., 1983), in vivo toxicity seems to be dependent on higher exposure doses and on frequent exposures, as low dose exposures caused only minor and transient impairments on lymphocyte production in mice [265,266]. Recently, toxic mechanisms associated with long lasting exposure to Hg in mice have been linked to a decreased proliferation of HSC, which is dependent on reduced levels of interferon gamma in BM [225].

Intoxications caused by HM, especially Pb, Cd, As, and Hg, have severe harmful effects on the hematopoietic systems, leading to anemia and immune deficiencies, and it is intriguing that mechanisms linked to such toxic effects have not yet been more thoroughly assessed. These metals reach BM and easily interact with proteins, affecting several hematopoietic pathways. Further studies on cellular and molecular mechanisms linked to the toxic actions of metals in BM should investigate additional toxic effects arising from such interactions.

3. Conclusions

Exposure of living beings to environmental pollutants has increased, influencing public health policy-making even in scenarios where exposures are below thresholds considered safe. Simultaneous exposure to different air pollutants also certainly contributes to the increase of alarming data, which has been evidenced in epidemiological studies. Hematopoiesis is pivotal for hemostasis and host defense, and disturbances on this process lead to severe outcomes, as summarized in Figure 2. Advances in scientific knowledge regarding hematopoiesis mechanisms have evidenced novel targets for actions of xenobiotics not yet described, hence further studies on hematopoiesis are needed for improving environmental pollutant risk assessment.

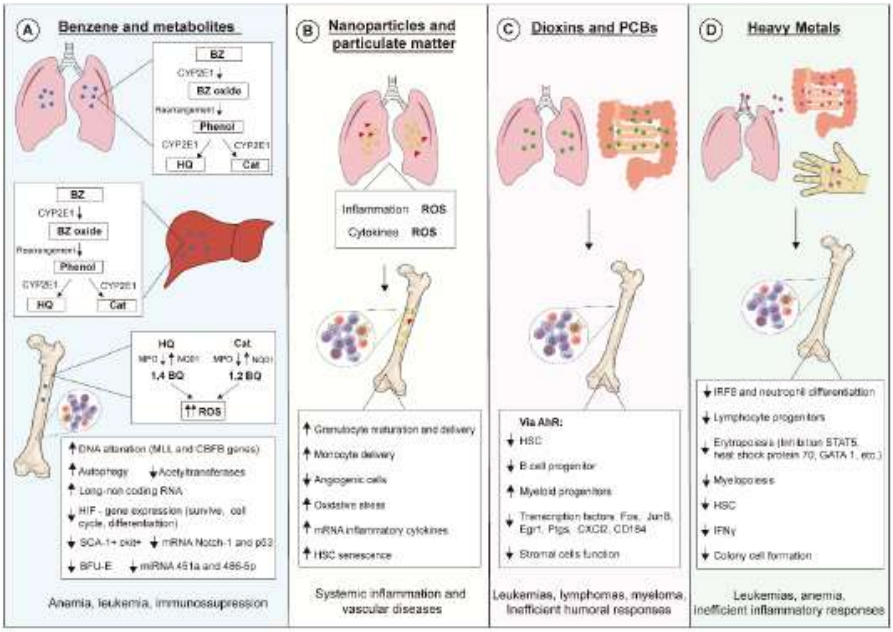

Figure 2. Molecular and cellular mechanisms linked to toxic effects of environmental pollutants on hematopoiesis. (**A**) Benzene (BZ) is metabolized by CYP2E1 in liver and lung generating hydroquinone (HQ) and catechol (Cat), which are then transformed into benzoquinone (BQ). These metabolites exert myelotoxic actions upon several hematopoietic progenitors mainly by increasing levels of reactive oxygen species (ROSs), leading to oxidative DNA damage. (**B**) Nanoparticles and particulate matter induce generation of ROSs and secretion of inflammatory cytokines that affect the behavior of several hematopoietic cell lineages. (**C**) Dioxins and PCBs bind to and activate the aryl hydrocarbon receptor (AhR) in mucosal tissues, modulating the hematopoietic stem cell (HSC) pool and triggering both immunosuppressive effects and myelodysplastic and malignant abnormalities. (**D**) Heavy metals can enter the body via several contact routes, their toxic effects being responsible for impairing inflammatory responses and triggering leukemias and anemias.

Funding: The authors thank the Fundação de Amparo à Pesquisa do Estado de Sao Paulo (FAPESP; research grants nr. 2014/07328-4, approval date 30 November 2014 and 2019/19573-7, approval date 20 May 2020) for providing funding support to MFB (2018/26383-7, approval date 1 April 2019) and GHOR (2017/05430-4, approval date 1 October 2017) and also thank the Conselho Nacional de Desenvolvimento Científico e Tecnológico (CNPq) for providing funding support to PS (130090/2019-0, approval date 16 January 2019).

Conflicts of Interest: The authors declare no conflict of interest.

References

1. Orkin, S.H.; Zon, L.I. Hematopoiesis: An Evolving Paradigm for Stem Cell Biology. *Cell* **2008**, *132*, 631–644. [CrossRef] [PubMed]
2. Seita, J.; Weissman, I.L. Hematopoietic stem cell: Self-renewal versus differentiation. *Wiley Interdiscip. Rev. Syst. Biol. Med.* **2010**, *2*, 640–653. [CrossRef]
3. Cheshier, S.H.; Morrison, S.J.; Liao, X.; Weissman, I.L. In vivo proliferation and cell cycle kinetics of long-term self-renewing hematopoietic stem cells. *Proc. Natl. Acad. Sci. USA* **1999**, *96*, 3120–3125. [CrossRef]
4. Rossi, D.J.; Jamieson, C.H.; Weissman, I.L. Stems Cells and the Pathways to Aging and Cancer. *Cell* **2008**, *132*, 681–696. [CrossRef] [PubMed]

27. Lilly, A.J.; Johnson, W.E.; Bunce, C. The Haematopoietic Stem Cell Niche: New Insights into the Mechanisms Regulating Haematopoietic Stem Cell Behaviour. *Stem Cells Int.* **2011**, *2011*, 1–10. [CrossRef] [PubMed]
28. Butler, J.M.; Nolan, D.J.; Vertes, E.L.; Varnum-Finney, B.; Kobayashi, H.; Hooper, A.T.; Seandel, M.; Shido, K.; White, I.A.; Kobayashi, M.; et al. Endothelial Cells Are Essential for the Self-Renewal and Repopulation of Notch-Dependent Hematopoietic Stem Cells. *Cell Stem Cell* **2010**, *6*, 251–264. [CrossRef]
29. Omatsu, Y.; Sugiyama, T.; Kohara, H.; Kondoh, G.; Fujii, N.; Kohno, K.; Nagasawa, T. The Essential Functions of Adipo-osteogenic Progenitors as the Hematopoietic Stem and Progenitor Cell Niche. *Immunity* **2010**, *33*, 387–399. [CrossRef]
30. Li, B.; Bailey, A.S.; Jiang, S.; Liu, B.; Goldman, D.C.; Fleming, W.H. Endothelial cells mediate the regeneration of hematopoietic stem cells. *Stem Cell Res.* **2010**, *4*, 17–24. [CrossRef]
31. Psaila, B.; Lyden, D.; Roberts, I. Megakaryocytes, malignancy and bone marrow vascular niches. *J. Thromb. Haemost.* **2012**, *10*, 177–188. [CrossRef]
32. Pontikoglou, C.; Deschaseaux, F.; Sensebé, L.; Papadaki, H.A. Bone Marrow Mesenchymal Stem Cells: Biological Properties and Their Role in Hematopoiesis and Hematopoietic Stem Cell Transplantation. *Stem Cell Rev. Rep.* **2011**, *7*, 569–589. [CrossRef]
33. Parekkadan, B.; Milwid, J.M. Mesenchymal Stem Cells as Therapeutics. *Annu. Rev. Biomed. Eng.* **2010**, *12*, 87–117. [CrossRef]
34. Le Blanc, K.; Samuelsson, H.; Gustafsson, B.; Remberger, M.; Sundberg, B.; Arvidson, J.; Ljungman, P.; Lönnies, H.; Nava, S.; Ringdén, O. Transplantation of mesenchymal stem cells to enhance engraftment of hematopoietic stem cells. *Leukemia* **2007**, *21*, 1733–1738. [CrossRef] [PubMed]
35. Lazar-Karsten, P.; Dorn, I.; Meyer, G.; Lindner, U.; Driller, B.; Schlenke, P. The influence of extracellular matrix proteins and mesenchymal stem cells on erythropoietic cell maturation. *Vox Sang.* **2010**, *101*, 65–76. [CrossRef]
36. Yin, T.; Li, L. The stem cell niches in bone. *J. Clin. Investig.* **2006**, *116*, 1195–1201. [CrossRef] [PubMed]
37. Asahara, T.; Murohara, T.; Sullivan, A.; Silver, M.; Van Der Zee, R.; Li, T.; Witzenbichler, B.; Schatteman, G.; Isner, J.M. Isolation of Putative Progenitor Endothelial Cells for Angiogenesis. *Science* **1997**, *275*, 964–966. [CrossRef] [PubMed]
38. Urbich, C.; Dimmeler, S. Endothelial progenitor cells: Characterization and role in vascular biology. *Circ. Res.* **2004**, *95*, 343–353. [CrossRef]
39. Slukvin, I.I.; Kumar, A. The mesenchymoangioblast, mesodermal precursor for mesenchymal and endothelial cells. *Cell. Mol. Life Sci.* **2018**, *75*, 3507–3520. [CrossRef]
40. Yang, J.; Ii, M.; Kamei, N.; Alev, C.; Kwon, S.-M.; Kawamoto, A.; Akimaru, H.; Masuda, H.; Sawa, Y.; Asahara, T. $CD34^+$ Cells Represent Highly Functional Endothelial Progenitor Cells in Murine Bone Marrow. *PLoS ONE* **2011**, *6*, e20219. [CrossRef]
41. Moccia, F.; Guerra, G. Ca^{2+} Signalling in Endothelial Progenitor Cells: Friend or Foe? *J. Cell. Physiol.* **2015**, *231*, 314–327. [CrossRef]
42. Marquez, L.A.; Turner, A.R.; Sridharan, S.; Ratajczak, M.Z.; Janowska-Wieczorek, A. The Ins and Outs of Hematopoietic Stem Cells: Studies to Improve Transplantation Outcomes. *Stem Cell Rev. Rep.* **2010**, *7*, 590–607. [CrossRef]
43. Schuettpelz, L.G.; Link, D.C. Regulation of Hematopoietic Stem Cell Activity by Inflammation. *Front. Immunol.* **2013**, *4*, 204. [CrossRef]
44. Jin, F.; Zhai, Q.; Qiu, L.; Meng, H.; Zou, D.; Wang, Y.; Li, Q.; Yu, Z.; Han, J.; Zhou, B. Degradation of BM SDF-1 by MMP-9: The role in G-CSF-induced hematopoietic stem/progenitor cell mobilization. *Bone Marrow Transplant.* **2008**, *42*, 581–588. [CrossRef]
45. Heissig, B.; Hattori, K.; Dias, S.; Friedrich, M.; Ferris, B.; Hackett, N.R.; Crystal, R.G.; Besmer, P.; Lyden, D.; Moore, M.A.; et al. Recruitment of Stem and Progenitor Cells from the Bone Marrow Niche Requires MMP-9 Mediated Release of Kit-Ligand. *Cell* **2002**, *109*, 625–637. [CrossRef]
46. Lapidot, T.; Kollet, O. The essential roles of the chemokine SDF-1 and its receptor CXCR4 in human stem cell homing and repopulation of transplanted immune-deficient NOD/SCID and NOD/SCID/B2mnull mice. *Leukemia* **2002**, *16*, 1992–2003. [CrossRef]

47. Giralt, S.A.; Costa, L.; Schriber, J.; DiPersio, J.; Maziarz, R.; Mccarty, J.; Shaughnessy, P.; Snyder, E.; Bensinger, W.; Copelan, E.; et al. Optimizing Autologous Stem Cell Mobilization Strategies to Improve Patient Outcomes: Consensus Guidelines and Recommendations. *Biol. Blood Marrow Transplant.* **2014**, *20*, 295–308. [CrossRef]
48. Levesque, J.-P.; Takamatsu, Y.; Nilsson, S.K.; Haylock, D.; Simmons, P.J. Vascular cell adhesion molecule-1 (CD106) is cleaved by neutrophil proteases in the bone marrow following hematopoietic progenitor cell mobilization by granulocyte colony-stimulating factor. *Blood* **2001**, *98*, 1289–1297. [CrossRef]
49. Rosales, C. Neutrophil: A Cell with Many Roles in Inflammation or Several Cell Types? *Front. Physiol.* **2018**, *9*, 113. [CrossRef]
50. Bautz, F.; Denzlinger, C.; Kanz, L.; Möhle, R. Chemotaxis and transendothelial migration of $CD34^+$hematopoietic progenitor cells induced by the inflammatory mediator leukotriene D4 are mediated by the 7-transmembrane receptor CysLT1. *Blood* **2001**, *97*, 3433–3440. [CrossRef]
51. Chung, J.W.; Kim, G.-Y.; Mun, Y.-C.; Ahn, J.-Y.; Seong, C.-M.; Kim, J.-H. Leukotriene B4 pathway regulates the fate of the hematopoietic stem cells. *Exp. Mol. Med.* **2005**, *37*, 45–50. [CrossRef] [PubMed]
52. Pietras, E.M. Inflammation: A key regulator of hematopoietic stem cell fate in health and disease. *Blood* **2017**, *130*, 1693–1698. [CrossRef] [PubMed]
53. Machado, I.D.; Spatti, M.; Hastreiter, A.; Santin, J.R.; Fock, R.A.; Gil, C.D.; Oliani, S.M.; Perretti, M.; Farsky, S.H.P. Annexin A1 Is a Physiological Modulator of Neutrophil Maturation and Recirculation Acting on the CXCR4/CXCL12 Pathway. *J. Cell Physiol.* **2016**, *231*, 2418–2427. [CrossRef]
54. Ponomaryov, T.; Peled, A.; Petit, I.; Taichman, R.S.; Habler, L.; Sandbank, J.; Arenzana-Seisdedos, F.; Magérus-Chatinet, A.; Caruz, A.; Fujii, N.; et al. Induction of the chemokine stromal-derived factor-1 following DNA damage improves human stem cell function. *J. Clin. Investig.* **2000**, *106*, 1331–1339. [CrossRef]
55. Wang, L.; Xiao, H.; Zhang, X.; Wang, C.; Huang, H. The role of telomeres and telomerase in hematologic malignancies and hematopoietic stem cell transplantation. *J. Hematol. Oncol.* **2014**, *7*, 61. [CrossRef]
56. Mohrin, M.; Bourke, E.; Alexander, D.; Warr, M.R.; Barry-Holson, K.; Le Beau, M.M.; Morrison, C.; Passegué, E. Hematopoietic Stem Cell Quiescence Promotes Error-Prone DNA Repair and Mutagenesis. *Cell Stem Cell* **2010**, *7*, 174–185. [CrossRef]
57. Sherman, M.H.; Bassing, C.H.; Teitell, M.A. Regulation of cell differentiation by the DNA damage response. *Trends Cell Biol.* **2011**, *21*, 312–319. [CrossRef]
58. Pilzecker, B.; Buoninfante, O.A.; Berk, P.V.D.; Lancini, C.; Song, J.-Y.; Citterio, E.; Jacobs, H. DNA damage tolerance in hematopoietic stem and progenitor cells in mice. *Proc. Natl. Acad. Sci. USA* **2017**, *114*, E6875–E6883. [CrossRef]
59. Pilzecker, B.; Buoninfante, O.A.; Jacobs, H. DNA damage tolerance in stem cells, ageing, mutagenesis, disease and cancer therapy. *Nucleic Acids Res.* **2019**, *47*, 7163–7181. [CrossRef]
60. Insinga, A.; Cicalese, A.; Faretta, M.; Gallo, B.; Albano, L.; Ronzoni, S.; Furia, L.; Viale, A.; Pelicci, P.G. DNA damage in stem cells activates p21, inhibits p53, and induces symmetric self-renewing divisions. *Proc. Natl. Acad. Sci. USA* **2013**, *110*, 3931–3936. [CrossRef]
61. Yamashita, M.; Nitta, E.; Suda, T. Aspp1 Preserves Hematopoietic Stem Cell Pool Integrity and Prevents Malignant Transformation. *Cell Stem Cell* **2015**, *17*, 23–34. [CrossRef]
62. Pietsch, E.C.; Sykes, S.M.; McMahon, S.B.; E Murphy, M. The p53 family and programmed cell death. *Oncogene* **2008**, *27*, 6507–6521. [CrossRef] [PubMed]
63. Jia, Y.; Peng, L.; Rao, Q.; Xing, H.; Huai, L.; Yu, P.; Chen, Y.; Wang, C.; Wang, M.; Mi, Y.; et al. Oncogene iASPP enhances self-renewal of hematopoietic stem cells and facilitates their resistance to chemotherapy and irradiation. *FASEB J.* **2014**, *28*, 2816–2827. [CrossRef] [PubMed]
64. Cao, Y.; Fang, Y.; Cai, J.; Li, X.; Xu, F.; Yuan, N.; Zhang, S.; Wang, J. ROS functions as an upstream trigger for autophagy to drive hematopoietic stem cell differentiation. *Hematology* **2016**, *21*, 1–6. [CrossRef]
65. Ho, T.T.; Warr, M.R.; Adelman, E.R.; Lansinger, O.; Flach, J.; Verovskaya, E.V.; Figueroa, M.E.; Passegué, E. Autophagy maintains the metabolism and function of young and old stem cells. *Nature* **2017**, *543*, 205–210. [CrossRef] [PubMed]

66. Orsini, M.; Chateauvieux, S.; Rhim, J.; Gaigneaux, A.; Cheillan, D.; Christov, C.; Dicato, M.; Morceau, F.; Han, B.W. Sphingolipid-mediated inflammatory signaling leading to autophagy inhibition converts erythropoiesis to myelopoiesis in human hematopoietic stem/progenitor cells. *Cell Death Differ.* **2018**, *26*, 1796–1812. [CrossRef]
67. Lin, W.; Yuan, N.; Wang, Z.; Cao, Y.; Fang, Y.; Li, X.; Xu, F.; Song, L.; Wang, J.; Zhang, H.; et al. Autophagy confers DNA damage repair pathways to protect the hematopoietic system from nuclear radiation injury. *Sci. Rep.* **2015**, *5*, 12362. [CrossRef] [PubMed]
68. Koschade, S.E.; Brandts, C.H. Selective Autophagy in Normal and Malignant Hematopoiesis. *J. Mol. Biol.* **2020**, *432*, 261–282. [CrossRef]
69. Mortensen, M.; Watson, A.S.; Simon, A.K. Lack of autophagy in the hematopoietic system leads to loss of hematopoietic stem cell function and dysregulated myeloid proliferation. *Autophagy* **2011**, *7*, 1069–1070. [CrossRef]
70. Finkel, T. Oxidant signals and oxidative stress. *Curr. Opin. Cell Biol.* **2003**, *15*, 247–254. [CrossRef]
71. Sohal, R.S. Role of oxidative stress and protein oxidation in the aging process. *Free. Radic. Biol. Med.* **2002**, *33*, 37–44. [CrossRef]
72. Nita, M.; Grzybowski, A. The Role of the Reactive Oxygen Species and Oxidative Stress in the Pathomechanism of the Age-Related Ocular Diseases and Other Pathologies of the Anterior and Posterior Eye Segments in Adults. *Oxidative Med. Cell. Longev.* **2016**, *2016*, 1–23. [CrossRef] [PubMed]
73. Hole, P.S.; Darley, R.L.; Tonks, A. Do reactive oxygen species play a role in myeloid leukemias? *Blood* **2011**, *117*, 5816–5826. [CrossRef] [PubMed]
74. Irwin, M.E.; Valle, N.R.-D.; Chandra, J. Redox Control of Leukemia: From Molecular Mechanisms to Therapeutic Opportunities. *Antioxid. Redox Signal.* **2013**, *18*, 1349–1383. [CrossRef] [PubMed]
75. Sillar, J.R.; Germon, Z.P.; De Iuliis, G.N.; Dun, M.D. The Role of Reactive Oxygen Species in Acute Myeloid Leukaemia. *Int. J. Mol. Sci.* **2019**, *20*, 6003. [CrossRef]
76. Samimi, A.; Khodayar, M.J.; Alidadi, H.; Khodadi, E. The Dual Role of ROS in Hematological Malignancies: Stem Cell Protection and Cancer Cell Metastasis. *Stem Cell Rev. Rep.* **2020**, *16*, 262–275. [CrossRef]
77. Ludin, A.; Gur-Cohen, S.; Golan, K.; Kaufmann, K.B.; Itkin, T.; Medaglia, C.; Lu, X.-J.; Ledergor, G.; Kollet, O.; Lapidot, T. Reactive Oxygen Species Regulate Hematopoietic Stem Cell Self-Renewal, Migration and Development, As Well As Their Bone Marrow Microenvironment. *Antioxid. Redox Signal.* **2014**, *21*, 1605–1619. [CrossRef]
78. Jang, Y.-Y.; Sharkis, S.J. A low level of reactive oxygen species selects for primitive hematopoietic stem cells that may reside in the low-oxygenic niche. *Blood* **2007**, *110*, 3056–3063. [CrossRef]
79. Prieto-Bermejo, R.; Romo-González, M.; Pérez-Fernández, A.; Ijurko, C.; Hernández-Hernández, Á. Reactive oxygen species in haematopoiesis: Leukaemic cells take a walk on the wild side. *J. Exp. Clin. Cancer Res.* **2018**, *37*, 125. [CrossRef]
80. Davies, K.P. Oxidative Stress, Antioxidant Defenses, and Damage Removal, Repair, and Replacement Systems. *IUBMB Life* **2000**, *50*, 279–289. [CrossRef]
81. Lü, J.-M.; Lin, P.H.; Yao, Q.; Chen, C. Chemical and molecular mechanisms of antioxidants: Experimental approaches and model systems. *J. Cell. Mol. Med.* **2009**, *14*, 840–860. [CrossRef] [PubMed]
82. Takubo, K.; Goda, N.; Yamada, W.; Iriuchishima, H.; Ikeda, E.; Kubota, Y.; Shima, H.; Johnson, R.S.; Hirao, A.; Suematsu, M.; et al. Regulation of the HIF-1α Level Is Essential for Hematopoietic Stem Cells. *Cell Stem Cell* **2010**, *7*, 391–402. [CrossRef]
83. Spencer, J.A.; Ferraro, F.; Roussakis, E.; Klein, A.; Wu, J.; Runnels, J.M.; Zaher, W.; Mortensen, L.; Alt, C.; Turcotte, R.; et al. Direct measurement of local oxygen concentration in the bone marrow of live animals. *Nature* **2014**, *508*, 269–273. [CrossRef] [PubMed]
84. Marinkovic, D.; Zhang, X.; Yalcin, S.; Luciano, J.P.; Brugnara, C.; Huber, T.; Ghaffari, S. Foxo3 is required for the regulation of oxidative stress in erythropoiesis. *J. Clin. Investig.* **2007**, *117*, 2133–2144. [CrossRef]
85. Tothova, Z.; Kollipara, R.; Huntly, B.J.; Lee, B.H.; Castrillon, D.H.; Cullen, D.E.; McDowell, E.P.; Lazo-Kallanian, S.; Williams, I.R.; Sears, C.; et al. FoxOs Are Critical Mediators of Hematopoietic Stem Cell Resistance to Physiologic Oxidative Stress. *Cell* **2007**, *128*, 325–339. [CrossRef]
86. Ito, K.; Hirao, A.; Arai, F.; Takubo, K.; Matsuoka, S.; Miyamoto, K.; Ohmura, M.; Naka, K.; Hosokawa, K.; Ikeda, Y.; et al. Reactive oxygen species act through p38 MAPK to limit the lifespan of hematopoietic stem cells. *Nat. Med.* **2006**, *12*, 446–451. [CrossRef] [PubMed]

frontiers in Pharmacology

ORIGINAL RESEARCH
published: 21 December 2020
doi: 10.3389/fphar.2020.591561

Pioglitazone-Mediated Attenuation of Experimental Colitis Relies on Cleaving of Annexin A1 Released by Macrophages

*Gustavo Henrique Oliveira da Rocha, Marina de Paula-Silva, Milena Fronza Broering, Pablo Rhasan dos Santos Scharf, Larissa Satiko Alcântara Sekimoto Matsuyama, Silvya Stuchi Maria-Engler and Sandra Helena Poliselli Farsky **

Department of Clinical and Toxicological Analyses, Faculty of Pharmaceutical Sciences, University of São Paulo, São Paulo, Brazil

OPEN ACCESS

Edited by:
Mireille Alhouayek, Catholic University of Louvain, Belgium

Reviewed by:
Makoto Makishima, Nihon University, Japan
Sumathi Sankaran, UC Davis Health, United States

***Correspondence:**
Sandra Helena Poliselli Farsky
sfarsky@usp.br

Specialty section:
This article was submitted to Inflammation Pharmacology, a section of the journal Frontiers in Pharmacology

Received: 23 September 2020
Accepted: 24 November 2020
Published: 21 December 2020

Citation:
da Rocha GHO, de Paula-Silva M, Broering MF, Scharf P, Matsuyama LSAS, Maria-Engler SS and Farsky SHP (2020) Pioglitazone-Mediated Attenuation of Experimental Colitis Relies on Cleaving of Annexin A1 Released by Macrophages. Front. Pharmacol. 11:591561. doi: 10.3389/fphar.2020.591561

Ulcerative colitis and Crohn's disease are chronic inflammatory bowel diseases (IBDs) which burden health systems worldwide; available pharmacological therapies are limited and cost-intensive. Use of peroxisome proliferator activated-receptor γ (PPARγ) ligands for IBD treatment, while promising, lacks solid evidences to ensure its efficacy. Annexin A1 (AnxA1), a glucocorticoid-modulated anti-inflammatory protein, plays a key role on IBD control and is a potential biomarker of IBD progression. We here investigated whether effects of pioglitazone, a PPARγ ligand, rely on AnxA1 actions to modulate IBD inflammation. Experimental colitis was evoked by 2% dextran sodium sulfate (DSS) in AnxA1 knockout (AnxA1$^{-/-}$) or wild type (WT) C57BL/6 mice. Clinical and histological parameters were more severe for AnxA$^{-/-}$ than WT mice, and 10 mg/kg pioglitazone treatment attenuated disease parameters in WT mice only. AnxA1 expression was increased in tissue sections of diseased WT mice, correlating positively with presence of CD68^{+} macrophages. Metalloproteinase-9 (MMP-9) and inactive 33 kDa AnxA1 levels were increased in the colon of diseased WT mice, which were reduced by pioglitazone treatment. Cytokine secretion, reactive oxygen species generation and MMP-9 expression caused by lipopolysaccharide (LPS) treatment in AnxA1-expressing RAW 264.7 macrophages were reduced by pioglitazone treatment, effects not detected in AnxA1 knockdown macrophages. LPS-mediated increase of AnxA1 cleaving in RAW 264.7 macrophages was also attenuated by pioglitazone treatment. Finally, pioglitazone treatment increased extracellular signal-regulated kinase (ERK) phosphorylation in AnxA1-expressing RAW 264.7 macrophages, but not in AnxA1-knockdown macrophages. Thus, our data highlight AnxA1 as a crucial factor for the therapeutic actions of pioglitazone on IBDs.

Keywords: inflammatory bowel disease, experimental colitis, pioglitazone, macrophage, annexin A1

INTRODUCTION

Ulcerative colitis and Crohn's disease comprise inflammatory bowel diseases (IBDs), which are widespread and pose burdens to healthcare systems worldwide (Mak et al., 2020). In 2016 in the United States alone, the prevalence of both maladies combined was last reported to be of one for every 209 people, and incidence increases steadily each year (Luther and Dave, 2020); also, the estimated loss of earnings due to IBDs were calculated as $31 billion in the same year (Xu et al., 2018). Patients suffer from diarrhea, anemia, fatigue and severe gut pain, among other symptoms, which become more intense during acute episodes, causing them to lose workdays and drastically reducing quality of life (Xu et al., 2018). Pharmacological options to treat these diseases are limited, as traditionally used drugs address only the major symptoms of inflammatory bowel diseases and fail to conduct patients to complete remission (Duijvestein et al., 2018). Biological therapies involving anti-TNFα antibodies, such as infliximab, while proven successful and better than conventional drugs, do not cause any response in about a third of patients and are very cost-intensive (Hossain et al., 2020). There is also a trend nowadays for new IBD therapies to aim for objective targets in an individualized manner rather than following pre-determined therapy paradigms (e.g., aim for mucosal healing rather than "overall remission"), and thus the understanding of new IBD biomarkers and of how new or already existing drugs work and with which other molecules they interact on intestinal tissue becomes a necessity (Im et al., 2018; Ho et al., 2020).

Annexin A1 (AnxA1), a 37 kDa protein modulated by the actions of glucocorticoids is one such molecule currently assessed as a potential target for therapy of not only IBDs, but of other inflammatory chronic diseases as well, playing roles on the inflammatory modulation of diseases such as asthma, type-2 diabetes, cystic fibrosis, rheumatoid arthritis, among others (Patel et al., 2012; Perretti and D'acquisto, 2009; Perucci et al., 2017; Sheikh and Solito, 2018). It is expressed by epithelial cells and monocytes, neutrophils and macrophages to a great extent (Perretti and D'acquisto, 2009). In IBD animal models, AnxA1 and its N-terminal mimetic peptides are known to attenuate disease progression and promote epithelial repair (Babbin et al., 2008; Ouyang et al., 2012; Zou et al., 2016), and when lacking halts disease remission caused by treatment with infliximab (de Paula-Silva et al., 2016). AnxA1 expression is increased in intestinal tissue of ulcerative colitis patients while decreased in Crohn's disease patients, evidencing these diseases deregulate AnxA1 actions leading to compromised anti-inflammatory responses (Vong et al., 2012; Sena et al., 2013). It has been reported AnxA1 also plays a role on healing of damaged intestinal epithelium on murine IBD models, and that its expression is correlated with better prognosis on Crohn's disease patients (Leoni et al., 2015; Reischl et al., 2020).

While seemingly a beneficial role player on downmodulating inflammation, AnxA1 can be cleaved into smaller 33 kDa fragments which are believed to be non-functional and even lead to pro-inflammatory effects, such as increased neutrophil transmigration via endothelium (Williams et al., 2010; Sugimoto et al., 2016); while this event has not yet been described in neither IBD patients nor in experimental colits animal models, it has been evidenced cleaved AnxA1 correlates with increased inflammatory damage in animal pleurisy models and in neutrophils recruited from animals treated with LPS (Vago et al., 2012; Vago et al., 2016).

In the search for new pharmacological targets to treat IBDs, in the same vein as AnxA1, peroxisome proliferator activated γ (PPARγ) has been explored as a potential transcription factor linked to modulation of IBD, and it has been evidenced its impaired expression is linked to disease progression in humans (Yamamoto-Furusho et al., 2011; Dou et al., 2015). PPARγ ligands such as thiazolidinediones have emerged as potential new anti-inflammatory candidates for IBD therapy, and first reviews on the efficacy of PPARγ ligands for treatment of IBDs date back 20 years ago (Wada et al., 2001). While traditionally used for treatment of diabetes, such ligands have been explored as anti-inflammatories in the past few years and shown as promising treatment options for several chronic inflammatory diseases, especially those that affect the central nervous system, such as Alzheimer's disease, Parkinson's disease and multiple sclerosis (Galimberti and Scarpini, 2017; Bonato et al., 2018). Pioglitazone, one such PPARγ ligand, is also effective in attenuating inflammation in alcoholic-induced cirrhosis livers and reducing specific histologic lesions in cancerous lungs of smokers (Chongmelaxme et al., 2019; Keith et al., 2019). On macrophages, pioglitazone is reported to induce M2 polarization, attenuate TNFα and IL-1ß expressions, reduce actions of CXCL1 and CCL2 and increase the expression of IL-10 and TGF-ß (Fernandez-Boyanapalli et al., 2010; Ahmadian et al., 2013; Pisanu et al., 2014). Most importantly, however, is pioglitazone role on attenuating the progression of IBDs, as demonstrated by experimental animal models, where treatment of animals induced to development of IBD causes prevention of weight loss, mucosal healing and epithelium restructuration via increase of ZO-1 and claudin-5; pioglitazone also attenuates overall inflammation by reducing NF-kB activation, secretion of cytokines (such as IL-2, TNFα and IL-17) and myeloperoxidase activity (Takagi et al., 2002; Takaki et al., 2006; Da Silva et al., 2018; El Awdan and Mostafa, 2018; Huang et al., 2020).

Even though several animal studies evidence the beneficial role of pioglitazone on treatment and remission of IBDs, the few studies involving pioglitazone and other PPARγ ligands on humans, while conducted to some success, at the end have failed to advance to further stages of clinical trials or relied only on *in silico* approaches (Liang and Ouyang, 2008; Abedi et al., 2015). AnxA1 expression is associated with progression of inflammation in both IBD models and in patients, and previous findings from our group evidenced AnxA1 plays a role on PPARγ activation and actions (da Rocha et al., 2019). Therefore, we aimed to investigate whether AnxA1 could play a role on pioglitazone-mediated resolution of inflammation in an IBD model in order to elucidate how pioglitazone ameliorates disease progression.

MATERIAL AND METHODS

In Vivo Experimentation

Animals Used

Wild type (WT) or knockout annexin A1 (AnxA1$^{-/-}$) male C57Bl/6 mice were obtained from the Center for Development of Experimental Models for Biology and Medicine, Federal University of São Paulo (CEDEME/UNIFESP). Animals were kept under 12 h light/dark cycles at 25°C and were given water and feed *ad libitum*. Experiments were carried in accordance with Ethical Principles for Animal Experimentation (COBEA) and were approved under protocol no. 577 by the Ethics Committee on Animal Use of the Faculty of Pharmaceutical Sciences of the University of São Paulo (CEUA/FCF/USP).

Experimental Colitis and Pharmacological Treatment

Acute colitis was induced by ingestion of dextran sodium sulfate (DSS) 40 kDa (Dextran Products Limited, Scarborough, ON, Canada) administered to the drinking water of mice. Throughout a period of 6 days mice consumed water containing 2% DSS 40 kDa, replaced every 2 days so DSS consumption would be homogeneous (de Paula-Silva et al., 2016).

WT and AnxA1$^{-/-}$ mice were divided in the following groups: 1) Control (driking water with no other additives), 2) DSS and 3) DSS + pioglitazone. All mice received daily injections of either pioglitazone (Sigma-Aldrich, St. Louis, MO, United States) at a dose of 10 mg/kg or its vehicle (0.9% sterile saline +0.5% carboxymethylcellulose, Sigma-Aldrich, St. Louis, MO, United States). Pioglitazone was prepared in vehicle suspension and sonicated in a sonic bath USC 800® (Unique, Indaiatuba, SP, Brazil) for 30 min. A volume of 200 µl of the pioglitazone suspension was injected intraperitoneally into mice. The experimental protocol was based on previous works from our research group (Santin et al., 2013; de Paula-Silva et al., 2016). A graphical representation of the experimental protocol is described in Supplementary Material (**Supplementary Figure S1**).

Evaluation of Clinical Parameters

Clinical parameters of animals were verified daily during induction and progression of colitis. Animals were weighted; consistency of feces was determined by collecting a piece of stool and pressing it with forceps in order to verify its softness/hardness; rectal blood was assessed on feces tested for occult blood. For detection of occult blood, a piece of stool was dispersed into 150 µl of 0.9% saline solution alongside 150 µl of a benzidine (Sigma-Aldrich, St. Louis, MO, United States) and hydrogen peroxide (Synth, Diadema, SP, Brazil) solution; the resulting greenish solution was scored according to its intensity. All mentioned parameters were scored from 0 to 4 as follows (0) weight loss inferior to 1%, solid feces, absence of occult blood (Mak et al., 2020); weight loss ranging from 1 to 5%, slightly softened feces, small amount of occult blood (Luther and Dave, 2020); weight loss ranging from 5 to 10%, softened feces, moderate amount of occult blood (Xu et al., 2018); weight loss ranging from 10 to 20%, pastry feces, considerable amount of occult blood (Duijvestein et al., 2018); weight loss superior to 20%, liquid feces, high amount of occult blood. Scores were summed at each day, resulting in the disease Activity Index (DAI) (Chassaing et al., 2014).

Euthanasia of Mice and Collection of Biological Material

At the end of the experimental model, mice were euthanized by inhalation of isoflurane (BioChimico, Itatiaia, RJ, Brazil) followed by cervical dislocation, as preconized by Norm no. 37 of the National Council for Control of Animal Experimentation (CONCEA). Only after complete inactivity of the animals biological material and tissues were collected. Colons of animals were removed from the ileocecal junction up to the anus, washed and measured; the material was then processed and fragmented, the distal colon being used for histological analyses and the medium/proximal colon being used for protein analyses (Geboes et al., 2000; de Paula-Silva et al., 2016).

Processing of Histological Sections

Distal colon fragments harvested from mice were kept overnight in 4% paraformaldehyde (Synth, Diadema, SP, Brazil) at −4°C. For processing, samples were placed in plastic cassettes and washed with decreasing polarity solutions for 1 h each for dehydrating as follows: 70% ethanol, 95% ethanol, absolute ethanol (3x) and xylol (2x) (Synth, Diadema, SP, Brazil). Afterward, samples were embedded in paraffin (Merck, Darmstadt, HE, Germany) pre-heated at 60°C. Then, 5 µm serial histological sections were obtained using a microtome (Leica Biosystems, Wetzlar, HE, Germany) and placed upon poly-lysine treated slides (Sigma-Aldrich, St. Louis, MO, United States). Prior to staining, slides were deparaffinized by pre-heating at 60°C, washed and rehydrated.

Histological Analyses of the Colon

Deparaffinated and hydrated slides were stained with filtered Harris hematoxylin (Sigma-Aldrich, St. Louis, MO, United States) for 2 min; slides were washed with 80% ethanol and then stained with filtered eosin for 1 min. After washing with distilled water, slides were dehydrated and mounted using a coverslip and Entelan® (Sigma-Aldrich, St. Louis, MO, United States).

For histological analysis, slides were assessed with a high-power objective (×40) in a Zeiss Axio Imager 2® microscope (Carl Zeiss, Oberkochen, WB, Germany) and the images obtained were processed using Zeiss Zen® software (Carl Zeiss, Oberkochen, WB, Germany). Histological evaluation was performed in a qualitative manner by comparing normal colon histology of control mice with that of DSS-treated animals. Histological parameters assessed were: epithelium integrity and ulceration, loss of crypt structure, presence of edema, hydropic vacuolar degeneration, crypt dysplasia, crypt abscess and presence of inflammatory infiltrate, both in lamina propria and submucosa (Chassaing et al., 2014; de Paula-Silva et al., 2016).

Immunohistochemical Detection of Annexin A1 and CD68

Deparaffinated and hydrated slides were placed in citrate buffer at 96°C for 30 min. Endogenous peroxidase activity was blocked with 12% hydrogen peroxide (Synth, Diadema, SP, Brazil) for 30 min. Blocking of unspecific epitopes and tissue permeabilization was carried out by incubating the sections with tris-buffered saline (Tris-HCl buffer 200 mM, sodium chloride 1.37 M, all from Synth, Diadema, SP, Brazil) containing 10% bovine serum albumin (Sigma-Aldrich, St. Louis, MO, United States) and 0.1% Tween-20 (Synth, Diadema, SP, Brazil) (TBS-BSA). Then, two serial sections of a same organ were incubated overnight at 4°C with either polyclonal primary anti-annexin A1 (Invitrogen, Waltham, MA, United States) or anti-CD68 (Abcam, Cambridge, CBE, United Kingdom) antibodies at dilutions of 1/250 and 1/25, respectively, diluted in TBS-BSA. Negative controls incubated only with TBS-BSA were also prepared. Then, slides were washed with TBS-BSA and incubated with anti-IgG secondary antibodies conjugated with horseradish peroxidase (HRP) (Invitrogen, Waltham, MA, United States) (Abcam, Cambridge, CBE, United Kingdom) at an 1/200 dilution for 1 h. The sections were washed with TBS-BSA and positive staining was detected using 3,3′-diaminobenzidine (DAB) (Sigma-Aldrich, St. Louis, MO, United States) for a period of 1.5 min. Then, sections were counterstained with hematoxylin (Sigma-Aldrich, St. Louis, MO, United States) and finally mounted with Entelan® (Sigma-Aldrich, St. Louis, MO, United States) under a coverslip.

Immunohistochemical analysis was carried out using a Zeiss Axio Imager 2® microscope (Carl Zeiss, Oberkochen, WB, Germany) and the images obtained were processed using Zeiss Zen® software (Carl Zeiss, Oberkochen, WB, Germany). First at a lower power magnification (×10) slides were screened for "hot spots" areas of $CD68^+$ cells, which were identified as brownish-yellow stained cells of monocyte/macrophage-like morphology. Using then higher power magnification (×100), these cells were counted in a total of twelve 0.2 mm^2 fields and averaged. Next, in corresponding areas in adjacent serial sections the intensity of DAB signal related to AnxA1 staining was determined in an arbitrary scale ranging from 0 to 255. Image processing, counting of cells and determination of intensity of DAB staining were carried out using ImageJ® software (Rueden et al., 2017).

Culturing of Explants and Quantification of Cytokines and MMP-9

Colonic tissue fragments obtained at the end of the experimental model were washed with sterile 0.9% saline solution so debris were removed and placed in 24-well plates in 1 ml of Dulbecco's Modified Eagle's Medium (DMEM) (Vitrocell Embriolife, Campinas, SP, Brazil) containing 10% of fetal bovine serum (FBS) (Vitrocell Embriolife, Campinas, SP, Brazil) and 0.1% of antibiotics (streptomycin, amphotericin and penicillin) (Vitrocell Embriolife, Campinas, SP, Brazil). Explants remained in culture at 37°C under controlled 5% CO_2 atmosphere for a 24 h period. Next, the supernatant culture medium was collected and used for quantification of TNFα, IL-10 and metalloproteinase-9 (MMP-9) via enzyme-linked immunoassay (ELISA). Analysis was carried out using BD Opteia® and DuoSet® commercial kits according to manufacturer instructions (BD Biosciences, Franklin Lakes, NJ, United States) (R&D Systems, Minneapolis, MN, United States).

Processing of Colonic Tissue and Western Blotting Analysis

Fragments of the colonic tissue collected at the end of the conducting of the experimental model were immersed in 200 µl of radioimmunoprecipitation assay (RIPA) buffer (Tris-HCl buffer 50 mM pH 7.4, sodium deoxycholate 0.5%, dodecyl sodium sulfate 0.1%, sodium chloride 150 mM, all from Synth, Diadema, SP, Brazil) containing protease inhibitors (Sigma-Aldrich, St. Louis, MO, United States) and then processed using a tissue homogenizer T10-Basic Ultra-Turrax® (IKA, Staufen, BW, Germany). The resulting suspensions were centrifuged at 5,000 g in a Sorvall ST 8R® centrifuge (Thermo Fisher Scientific, Waltham, MA, United States) for 5 min for removal of non-fragmented tissue. The resulting solutions were sonicated in a Vibra-Cell VCX 500® sonic bath (Sonics, Newtown, CT, United States) for complete cell lysis. The amount of protein in the homogenates was quantified via Bradford assay (Bradford, 1976). Protein homogenates were kept at −80°C until further Western Blotting tests were carried out.

Colon tissue homogenates were subjected to protein separation by sodium dodecyl sulfate polyacrylamide gel electrophoresis (SDS/PAGE) in 12% polyacrylamide gels at 100 V for 90 min; proteins were then transferred to a polyvinylidene fluoride (PVDF) membrane (Merck, Darmstadt, HE, Germany) at 400 mA for 120 min. Membranes were blocked with a solution of TBS containing 5% BSA (Sigma-Aldrich, St. Louis, MO, United States) and then incubated with either primary anti-AnxA1 antibody (Invitrogen, Waltham, MA, United States) or primary anti-PPARγ antibody (Thermo Fisher Scientific, Waltham, MA, United States), both at an 1/1,000 dilution, *overnight* at 4°C. The membranes were then washed with TBS and incubated with secondary anti-rabbit HRP conjugated antibody (Invitrogen, Waltham, MA, United States, Cat. NA9340V) at a 1/5,000 dilution for 120 min. Proteins were assessed by chemiluminescence using enhanced-chemiluminescent reagents WestPico SuperSignal® (Thermo Fisher Scientific, Waltham, MA, United States), in an Amershan Imager 600® (GE Healthcare, Chicago, IL, United States). Band intensities were quantified using ImageJ and are expressed as normalized optometric density units relative to ß-actin (Sigma-Aldrich, St. Louis, MO, United States) protein levels. All Western Blotting equipment used was from Bio-Rad (Bio-Rad, Hercules, CA, United States).

In Vitro Experimentation

Cell Lines Used

RAW 264.7 cells (immortalized murine macrophages) were obtained from the Rio de Janeiro Cell Bank (BCRJ, Rio de Janeiro, RJ, Brazil) and cultured in DMEM high glucose medium (4.500 pg/ml) containing 10% FBS and 1 mM sodium pyruvate (all from Vitrocell Embriolife, Campinas, SP, Brazil). Cells were kept at 37°C under controlled CO_2 atmosphere of 5%. Cell medium was changed every 2–3 days and cells were

subcultured every 4–5 days when cells were about to become fully confluent using trypsin 0.01% containing 0.02% ethylenediamine tetra acetic acid (EDTA) (all from Vitrocell Embriolife, Campinas, SP, Brazil).

Knockdown of AnxA1 Expression in Macrophages

Knockdown of AnxA1 on RAW 264.7 cells was carried out using commercial Mission® pLKO.1 plasmids (#Addgene 10,878) containing four different short-hairpin RNA (shRNA) sequences designed to be complementary to the 3′-UTR murine AnxA1 mRNA sequence (Sigma-Aldrich, St. Louis, MO, United States). Transformed *E. coli* purchased in glycerol stocks were grown according to manufacturer instructions (Sigma-Aldrich, St. Louis, MO, United States).

Plasmids were purified from culture medium containing transformed bacteria using the commercial kit PureLink® HiPure Plasmid Maxiprep (Thermo Fisher Scientific, Waltham, MA, United States), according to manufacturer instructions. After purification, plasmid concentration was assessed using a Nanodrop 2000® spectrophotometer (Thermo Fisher Scientific, Waltham, MA, United States).

HEK293FT cells (renal embryo cells, American Type Culture Collection, Manassas, VA, United States) were plated on 10 cm dishes at a density of 2 x 10^6 cells per plate and cultured with DMEM containing 10% FBS, 1 mM sodium pyruvate and 1 mM glutamine (Vitrocell Embriolife, Campinas, SP, Brasil) at 37°C under controlled CO_2 atmosphere of 5%. Once cells reached 80% confluence, they were washed and culture medium was renewed with medium containing 25 μM chloroquine (Sigma-Aldrich, St. Louis, MO, United States), which remained on the cells for 30 min. After this period, these cells were transfected by calcium phosphate precipitation. For such, 3 μg of each accessory plasmid (pRSV rev, pMDLg/pRRE and pHCMV-G), 0.5 μg of fluorescence reporter plasmid (pEGFP) and 8 μg of the control plasmids (pLKO.1 empty vector and a plasmid containing scrambled, non-functional sequence, used for mock-transfection) or shRNA plasmids (Mission® pLKO.1 AnxA1 shRNA plasmid, Sigma-Aldrich, St. Louis, MO, United States) were added to 500 μl of a 0.25 M $CaCl_2$ solution. After that, 500 μl of HEPES Buffer Saline 2X (280 mM NaCl, 1.5 mM Na_2HPO_4 and 50 mM HEPES; pH 7.0, all from Synth, Diadema, SP, Brazil) were added to the transfection mixture while vortexing and then allowed to rest for eration. HEK293FT cells were incubated for 6 h in culture medium containing 25 μM of chloroquine and the transfection mixture. At the end of this period, culture medium was renewed and the cells remained in incubator at 37°C under 5% CO_2 for further 42 h. Forty-eight hours after transfection, the supernatants containing lentiviral particles were harvested, centrifuged at (3,000 rpm for 15 min) and filtered using 0.45 μm filters. All procedures involving manipulation of lentiviral material were carried out following special safety regulations as preconized by Brazilian health and safety laws.

RAW 264.7 cells were previously plated in 6-well plates at a density of 2 x 10^5 cells per well for lentiviral transduction and cultured as described in item 2.2.1. These cells were incubated with a solution of renewed media, containing 1:3 (2 ml per well) diluted virus and supplemented with 10 μg/ml of polybrene (EMD Millipore, Billerica, MA, United States). RAW 264.7 cells were kept in incubation for 24 h at 37°C under controlled CO_2 atmosphere. Puromycin (Santa Cruz Biotechnology, Dallas, TX, United States) was added to the culture medium at a final concentration of 7 μg/ml for 48 h for selection of stable transduced cells.

After puromycin selection, a total of 5 x 10^5 cells were lyzed in 50 μl of RIPA buffer containing protease inhibitors; Western Blotting procedure for validation of AnxA1 knockdown was identical to the procedure described in item 2.1.9. Out of the four shRNA sequences tested, the one which led to most efficient AnxA1 knockdown was selected to be used for all further experiments. The growth of mock-transfected and AnxA1-knockdown cells was assessed daily by manual counting for 7 days and compared to the growth of wild type RAW 264.7 cells.

Information regarding shRNA sequences used, AnxA1 knockdown efficiency and cell growth rates are detailed in Supplementary Material (**Supplementary Figure S2**).

Cell Treatments

RAW 264.7 cells were cultured as described in item 2.2.1. For experimentation, cells were cultured in 24-well plates at a density of 2 x 10^5 cells/well (for flow cytometry and ELISA tests) or in 12-well plates at a density of 5 x 10^5 cells/well (for Western Blotting tests). After cells had adhered, the culture medium was replaced with fresh medium and cells were treated.

Cells were treated with pioglitazone, a specific PPARγ ligand, at a concentration of 10 μM (Sigma-Aldrich, St. Louis, MO, United States) for 24 h. *E. coli* lipopolysaccharide 026.B6 at a concentration of 1 μg/ml was added to the cells 1 h after pioglitazone was added. For specific experiments, cells were also treated with GW9662, a PPARγ antagonist, at a concentration of 10 μM (Tocris, Bristol, BRS, United Kingdom) for 30 min prior to treatment with pioglitazone. Control cells were treated only with the vehicle used for solubilization of pioglitazone, 0.1% dimethyl sulfoxide (DMSO) (Synth, Diadema, SP, Brazil).

At the end of each treatment, supernatants from the culture medium were collected and stored at −80°C until further ELISA tests and cells were washed with phosphate buffer saline (PBS) and harvested with trypsin 0.01% containing 0.02% EDTA (all from Vitrocell Embriolife, Campinas, SP, Brazil) for either flow cytometry or Western Blotting tests.

Details of the experimental protocol for cell treatment are graphically described in Supplementary Material (**Supplementary Figure S3**).

Assessment of Cytokine and MMP-9 Secretion

After treatments, cell supernatants were collected for assessment of cytokine and MMP-9 secretion via ELISA. Quantification was carried out using commercial ELISA kits following manufacturer instructions (BD Biosciences, Franklin Lakes, NJ, United States). TNFα and IL-10 cytokines were assessed.

Assessment of ROS Production and Expression of Surface Markers

After treatments, cells were collected and production of reactive oxygen species (ROS) and expression of adhesion molecules and

of formyl peptide receptors 1 and 2 (FPR1 and FPR2) on cell surface were assessed via flow cytometry. For assessment of reactive oxygen species (ROS) production, $5x10^4$ cells were separated from the total amount of treated cells, washed with PBS and incubated with 0.3 mM dichlorofluorescein diacetate (DCFH-DA) (Sigma-Aldrich, St. Louis, MO, United States) solution diluted in PBS. Cells were kept at 37°C under controlled CO_2 atmosphere of 5% for 30 min. After this incubation period, cold PBS was added to the cells. Lastly, cells were taken to an Accuri C6® flow cytometer (BD Biosciences, Franklin Lakes, NJ, United States) and a minimum of 10,000 events were acquired per sample. For assessment of cell surface adhesion molecules, 2 x 10^5 cells were plated, treated, collected, washed with PBS and incubated with phycoerythrin-labeled (PE) anti-CD54 (BD Biosciences, Franklin Lakes, NJ, United States, Cat. 553263) or PE-labeled anti-CD62L (BD Biosciences, Franklin Lakes, NJ, United States, Cat. 553151), both at a 1/100 dilution in PBS, for 30 min. The protocol was the same for assessment of FPR1 and FPR2, but cells were incubated with either fluorescein isothiocyanate (FITC) labeled anti-FPR2 antibody (Bioss, Woburn, MA, United States) for 30 min or primary anti-FPR1 antibody (CliniSciences, Nanterre, IDF, France) for 2 h, both at a 1/100 dilution; cells previously incubated with anti-FPR1 antibody were washed with PBS and incubated with PE-labeled anti-IgG secondary antibody (Abcam, Cambridge, CBE, United Kingdom) at a 1/200 dilution for 30 min. Lastly, cells were again washed and taken to an Accuri C6® flow cytometer (BD Biosciences, Franklin Lakes, NJ, United States) and a minimum of 10,000 events were acquired per sample.

Assessment of AnxA1 Expression and Cleaving and PPARγ Expression

For assessment of AnxA1 cleaving, cells were harvested after treatments as described in item 2.2.3 and cell lysates were prepared using RIPA buffer containing protease inhibitors; quantification of protein content via Bradford assay and Western Blotting analyses of quantification of AnxA1 and of assessment of AnxA1 cleaving were carried out as described in item 2.1.9.

For assessment of AnxA1 and PPARγ expression, cells were harvested, fixed with 4% paraformaldehyde for 30 min (Synth, Diadema, SP, Brazil), washed with 0.1 M glycin (Synth, Diadema, SP, Brazil) and permeabilized with 0.01% Triton-X for 30 min (Sigma-Aldrich, St. Louis, MO, United States). Cells were washed with PBS between all steps. Then, cells were incubated overnight with either primary anti-AnxA1 (BD Biosciences, Franklin Lakes, NJ, United States) or anti-PPARγ (Thermo Fisher Scientific, Waltham, MA, United States) antibodies in a 0.1% BSA and 0.01% sodium azide solution (Thermo Fisher Scientific, Waltham, MA, United States) at an 1/100 dilution for either. Cells were then washed and incubated with PE conjugated secondary anti-IgG antibody at a 1/200 dilution for 30 min. Cells were then taken to an Accuri C6® flow cytometer (BD Biosciences, Franklin Lakes, NJ, United States) and a minimum of 10,000 events were acquired.

Assessment of ERK Phosphorylation

Phosphorylation of extracellular signal-regulated kinase (ERK) proteins was carried out via flow cytometry. Mock-transfected and AnxA1-knockdown RAW 264.7 cells were harvested after treatments and processed the same manner as described in item 2.2.3. Cells were incubated overnight with primary anti-ERK1/2 and anti-pERK1(Thr202)/2(Thr185) antibodies (BD Biosciences, Franklin Lakes, NJ, United States) at 1/100 and 1/200 dilutions, respectively. Cells were then washed and incubated with FITC and PE conjugated secondary anti-IgG antibodies at dilutions 1/200 for 30 min. Finally, cells were taken to an Accuri C6® flow cytometer (BD Biosciences, Franklin Lakes, NJ, United States) and a minimum of 10,000 events were acquired.

Statistical Analysis

Data were analyzed using GraphPad Prism seven software (Graphpad Software®, San Diego, CA, United States). For analysis of clinical parameters two factor analysis of variance tests (Two-Way ANOVA) followed by Bonferroni post-hoc tests were performed. For comparison between number of stained macrophages and intensity of AnxA1 signal in DAB-stained tissue sections, linear regressions followed by Pearson's correlation tests were performed. For all other experiments performed, data were analyzed using when appropriate either Student's t tests or one factor analysis of variance (One-Way ANOVA) followed by Tukey post-hoc tests in order to assess differences between the evaluated groups. Differences between assessed means and correlation coefficients were considered statistically significant assuming $p < 0.05$. All results are shown as mean ± standard-error of the mean.

RESULTS

Pioglitazone Treatment Attenuates Dextran Sodium Sulfate-Induced Colitis Progression of Wild Type, but Not AnxA1$^{-/-}$ Mice

Clinical manifestations of DSS-induced colitis were assessed as body weight loss, rectal bleeding and consistency of feces, their sum resulting in a greater DAI in DSS-treated than control mice. All these disease parameters were even more pronounced in AnxA1$^{-/-}$ mice, confirming AnxA1$^{-/-}$ mice are more susceptible to damage caused by DSS (Babbin et al., 2008; Leoni et al., 2015; de Paula-Silva et al., 2016). The intraperitoneal administration of pioglitazone reduced body weight loss and increased feces consistency between days 2 and 4 of the disease in WT mice. Pioglitazone treatment did not attenuate clinical parameters of colitis in AnxA1$^{-/-}$ mice, and disease scores remained comparable to that of non-treated animals (**Figures 1A–D**). These data evidence pioglitazone attenuates the development of DSS-induced colitis in an AnxA1 dependent manner.

Also, in order to verify whether these beneficial clinical effects caused by pioglitazone treatment could be influenced or not by AnxA1 knockdown or by DSS intake due to changes in PPARγ expression, PPARγ expression was assessed in tissue homogenates from colon fragments. PPARγ expression in AnxA1$^{-/-}$ mice was

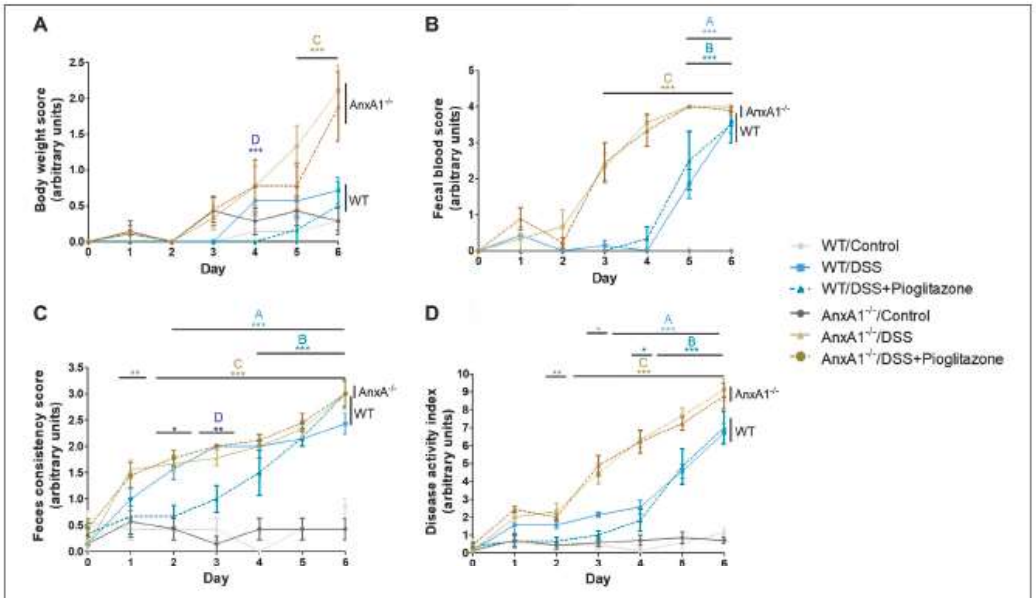

FIGURE 1 | Clinical parameters throughout progression of experimental colitis. Experimental colitis was induced in wild type or AnxA1$^{-/-}$ mice via ingestion of DSS and mice were treated with pioglitazone daily at a 10 mg/kg dose for a 6 days period. Throughout the development of the experimental model, loss of body weight **(A)**, rectal bleeding **(B)** and feces consistency **(C)** were assessed daily, resulting in the disease Activity Index **(D)**. *, **, ***$p < 0.05$, 0.01, 0.001 in comparison to another group as specified by the letters above each curve: A: WT/Control x WT/DSS; B: WT/Control x WT/DSS + Pioglitazone; C: AnxA1$^{-/-}$/Control x AnxA1$^{-/-}$/DSS and/or AnxA1$^{-/-}$/DSS + Pioglitazone; D: WT/DSS x WT/DSS + Pioglitazone. Data were statistically analyzed using Two-Way ANOVA followed by Bonferroni post-test ($n = 6$). Results are expressed as mean ± SE.

found to be at the same levels of WT mice, regardless of any treatments, thus showing any effects on clinical parameters (and on all other further effects described *in vivo*) caused by pioglitazone treatment in mice were likely not influenced by changes in PPARγ expression (**Supplementary Figure S4**).

Pioglitazone Treatment Preserves Colon Extension and Histoarchitecture of Wild Type, but Not AnxA1$^{-/-}$ Mice

The extension of large intestines of DSS-treated mice was significantly reduced in comparison to samples of control mice. Pioglitazone treatment attenuated such reduction only in WT mice, as intestines harvested from DSS treated AnxA1$^{-/-}$ mice treated with pioglitazone had the same extension as AnxA1$^{-/-}$ mice which received DSS only (**Figures 2A,B**). These data corroborate the findings related to assessment of clinical parameters confirming pioglitazone treatment halts DSS-induced colitis progression in WT but not in AnxA1$^{-/-}$ mice.

Histopathological analyses of intestines showed administration of DSS induced tissue injuries not observed in control mice, which resemble those found in human IBD (Perse and Cerar, 2012) (**Figures 2C–E**). DSS administration caused loss of tissue structure alongside ulcerations, loss of crypt structure, presence of edema and of inflammatory infiltrates, crypt abscesses, crypt dysplasia and vacuolar hydropic degeneration. Such effects were more pronounced in AnxA1$^{-/-}$ mice (**Figures 2F–H**). Pioglitazone treatment attenuated loss of tissue morphology in WT mice, as there was less edema and crypts were still preserved to some extension (**Figure 2E**). Beneficial effects of pioglitazone treatment were not observed in tissue sections of DSS-treated AnxA1$^{-/-}$ mice (**Figure 2H**). In association with clinical parameters, these findings show pioglitazone preserves colon histoarchitecture and reduces damage caused by DSS administration, the presence of AnxA1 being an important role player for such effects.

Inhibitory Effects of Pioglitazone on Secretion of Inflammatory Cytokines by Colon Tissue Is Modulated by AnxA1

Analysis of inflammatory cytokines evidenced increased secretion of TNFα and IL-10 from WT or AnxA1$^{-/-}$ inflamed colon explants. Treatment with pioglitazone reduced the secretion of both cytokines from colon explants of WT mice, but not from colon explants of AnxA1$^{-/-}$ mice, suggesting pioglitazone relies on expression of AnxA1 to attenuate the secretion of inflammatory cytokines (**Figures 3A–D**). These data, altogether with those describing assessment of clinical parameters, intestine extension and colon

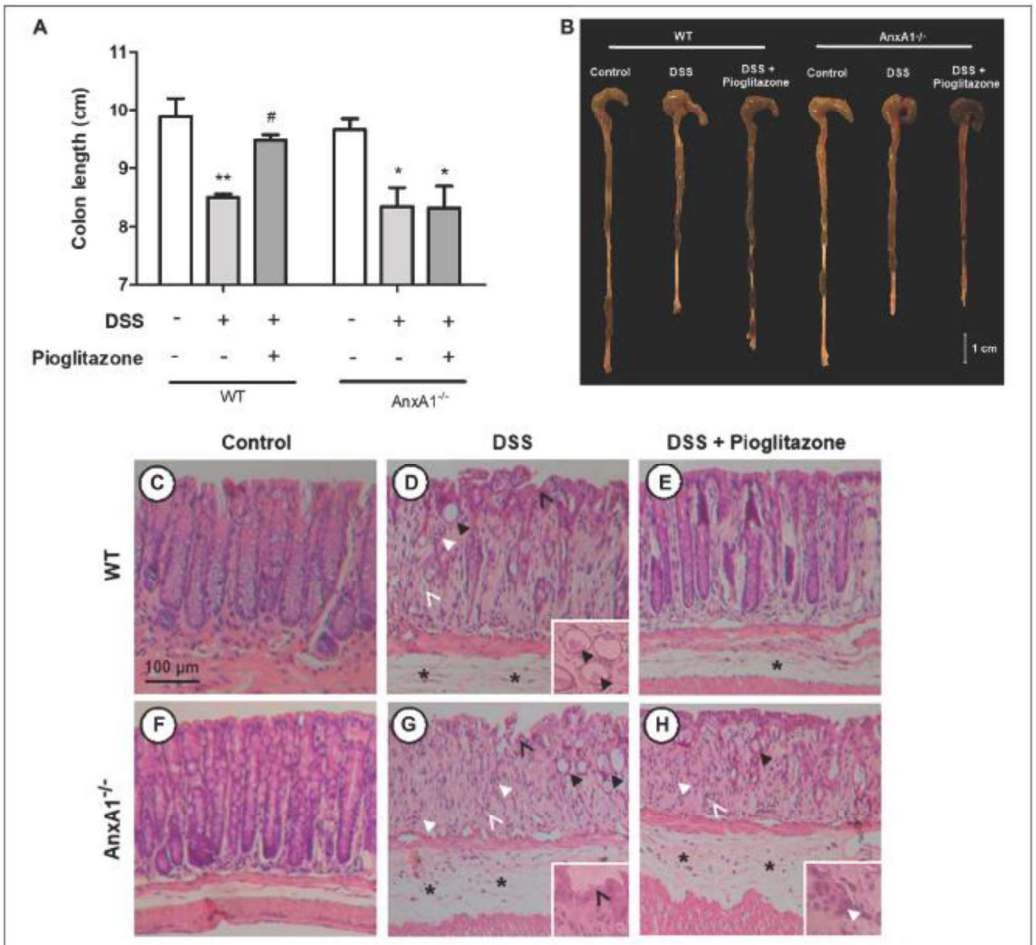

FIGURE 2 | Large intestine extension and colon histoarchitecture on tissue sections. Wild type and AnxA1$^{-/-}$ mice were euthanized at the end of the experimental model; large intestines were harvested and their extensions measured **(A,B)**. Paraffin-embedded sections were prepared from distal colon fragments and HE-stained; tissue histoarchitecture and presence of DSS lesions were evaluated via optical microscopy for both wild type **(C–E)** and AnxA$^{-/-}$ mice **(F–H)** ($n = 6$). Asterisks in histological images indicate edema; thicker black arrows indicate dysplastic crypts (crypt abscess in the detail in D); thinner black arrows indicate epithelium ulceration; thicker white arrows indicate leukocyte infiltration; thinner white arrows indicate hydropic vacuolar degeneration. *, **$p < 0.05$, 0.01 in comparison to respective control group; #$p < 0.05$ in comparison to respective DSS-treated group. Data were statistically analyzed using One-Way ANOVA followed by Tukey's post-test ($n = 6$). Results are expressed as mean ± SE.

histoarchitecture, evidence pioglitazone treatment modulates the development of DSS induced colitis in an AnxA1 dependent manner.

Pioglitazone Prevents Cleaving of AnxA1 in Colon Tissue

As it was evidenced AnxA1 is necessary for the anti-inflammatory effects of pioglitazone on DSS-induced colitis, its expression and cleaving status were assessed in WT mice. DSS administration increased expression of AnxA1 in the inflamed colon, regardless of treatment with pioglitazone (**Figure 4A**; **Supplementary Figures S5A–D**). However, pioglitazone treatment prevented AnxA1 cleaving into non-functional 33 kDa fragments, preserving whole the functional 37 kDa protein (**Figure 4B**; **Supplementary Figures S5A–D**). Also, while DSS-treatment increased the expression of MMP-9 as assessed in colon tissue homogenates, treatment with

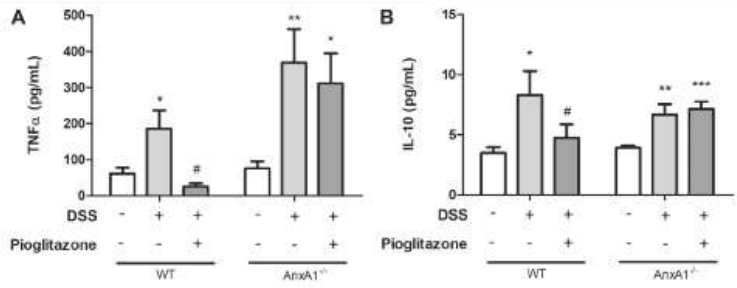

FIGURE 3 | Cytokines from tissue explants. Wild type and AnxA1$^{-/-}$ mice were euthanized at the end of the experimental model; large intestines were harvested and a fragment of the colon was cultured; after 24 h, supernatants were collected and secretion of TNFα **(A)** and IL-10 **(B)** was assessed via ELISA. *, **, ***$p < 0.05$, 0.01, 0.001 in comparison to the control group; #$p < 0.05$ in comparison to the DSS-treated group. Data were statistically analyzed using One-Way ANOVA followed by Tukey's post-test ($n = 6$). Results are expressed as mean ± SE.

pioglitazone decreased such expression (**Figure 4C**). These data demonstrate pioglitazone treatment preserves the structure of full length 37 kDa AnxA1 and decreases the expression of MMP-9 induced by DSS, which was previously shown to be involved with AnxA1 cleaving in mice intestinal epithelial cells (Leoni et al., 2015).

Dextran Sodium Sulfate-Induced Colitis Promotes Recruitment of AnxA1-Releasing Macrophages Regardless of Pioglitazone Treatment

Analysis of colon sections showed higher number of CD68 $^{+}$ macrophages in the colon of DSS-treated mice in comparison to control mice, regardless of treatment with pioglitazone (**Figures 5A–C,G**). Corresponding areas in serial sections assessed for AnxA1 staining evidenced a greater presence of this protein in tissue sections from DSS-treated mice in comparison to tissue sections from control mice; such increased staining corresponding to AnxA1 also was not influenced by pioglitazone treatment (**Figures 5D–F,H**). Correlation analysis associated AnxA1 expression with increased number of CD68 $^{+}$ macrophages (**Figures 5I–K**). These findings allow us to suggest DSS colitis leads to recruitment of AnxA1-releasing CD68 $^{+}$ macrophages and also increases AnxA1 secretion, and such events are unaffected by pioglitazone treatment.

Lipopolysaccharide-Induced Inflammatory Parameters Are Attenuated by Pioglitazone in RAW 264.7 Macrophages Relying on AnxA1 Expression

The generation of AnxA1 knockdown RAW 264.7 cells and further stimulation with LPS was the strategy employed to investigate the role of AnxA1 on pioglitazone-mediated anti-inflammatory effects and the actions of pioglitazone on cleaving of AnxA1 in macrophages. LPS treatment increased the generation of ROS and secretion of TNFα and IL-10 by RAW 264.7 macrophages. These parameters were attenuated in mock-transfected cells treated with pioglitazone, but not in AnxA1-knockdown transfected cells (**Figures 6A–C**). LPS treatment also increased surface expression of CD54 and CD62L, which was reversed by treatment with pioglitazone in mock-transfected cells but not in AnxA1-knockdown cells (**Supplementary Figures S6A,B**). Thus, these data evidence AnxA1 is key for the anti-inflammatory effects of pioglitazone on macrophages, corroborating our *in vivo* data in an isolated *in vitro* system.

Following a similar rationale as investigated in mouse tissue, PPARγ expression was verified as to assess whether changes on it would influence anti-inflammatory outcomes exerted by pioglitazone treatment. Unlike the results seen in mouse tissue, PPARγ expression increased due to LPS treatment, regardless of actions of pioglitazone, but only in mock-transfected RAW 264.7 cells (**Supplementary Figure S7A**). Further analysis under non-inflammatory conditions revealed pioglitazone induced PPARγ expression as expected in mock-transfected cells but not in AnxA1-knockdown cells (**Supplementary Figure S7B**). These findings evidence that functional expression of AnxA1 is required for pioglitazone to exert its actions and induce PPARγ expression.

Pioglitazone Prevents the Cleaving of AnxA1 in RAW 264.7 Macrophages

In the same vein as seen *in vivo*, inflammation caused by LPS increased AnxA1 expression in wild type RAW 264.7 cells, effect not reversed by treatment with pioglitazone (**Figure 7A**). LPS also caused AnxA1 cleaving into 33 kDa fragments, while pioglitazone prevented such cleaving (**Figure 7B**; **Supplementary Figures S8A–J**). LPS treatment also increased MMP-9 expression, and pioglitazone treatment did prevent such increase (**Figure 7C**). Thus, corroborating our *in vivo* data, pioglitazone is unable to control AnxA1 expression in inflammatory conditions, but can modulate its functionality by preventing its cleaving.

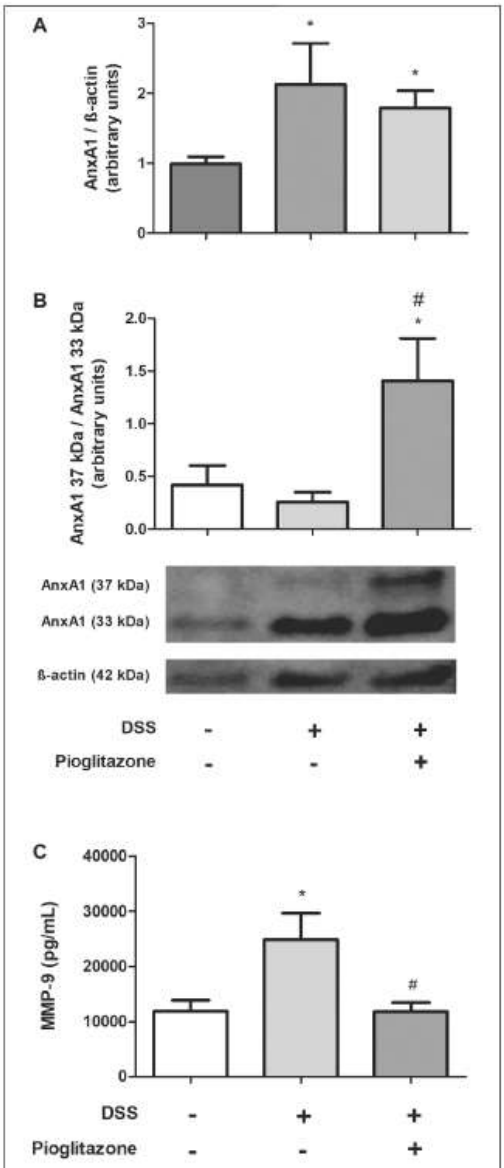

FIGURE 4 | Cleaving of AnxA1 in colon tissue. Wild type and AnxA1$^{-/-}$ mice were euthanized at the end of the experimental model; large intestines were harvested and protein homogenates were prepared; expression and cleaving of AnxA1 were assessed via *Western Blotting* **(A,B)** and MMP-9 expression was assessed via ELISA **(C)**. *$p < 0.05$ in comparison to the control group; #$p < 0.05$ in comparison to the DSS-treated group. Data were statistically analyzed using One-Way ANOVA followed by Tukey's post-test ($n = 6$). Results are expressed as mean ± SE.

Pioglitazone Actions Are PPARγ-Dependent in RAW 264.7 Macrophages

As it was determined PPARγ expression increased due to treatment with pioglitazone in mock-transfected cells, we investigated whether anti-inflammatory effects seen so far in AnxA1-expressing RAW 264.7 cells would be abrogated due to blocking of PPARγ. Increased levels of TNFα and MMP-9 induced by LPS were attenuated by treatment with pioglitazone, but not when cells have been previously treated with GW9662 (**Supplementary Figures S9A,B**). This evidences the anti-inflammatory actions of pioglitazone, at least those here assessed, are likely dependent on PPARγ activation.

AnxA1 Is Required for ERK Phosphorylation Induced by Pioglitazone in RAW 264.7 Macrophages

ERK phosphorylation is a *downstream* pathway event following AnxA1 binding to its receptors and pioglitazone can induce ERK phosphorylation. Hence, we investigated ERK phosphorylation as a possible factor connecting the anti-inflammatory actions of pioglitazone and AnxA1. Indeed, ERK phosphorylation was increased in mock-transfected RAW 264.7 cells treated with pioglitazone, but not in AnxA1-knockdown cells, meaning *downstream* signaling after PPARγ activation requires expression of functional AnxA1 (**Figure 8A**). Expressions of FPR1 and FPR2, G-protein coupled receptors known to bind to AnxA1 and exert downstream signaling, of which FPR2 is the better described for anti-inflammatory effects of AnxA1, did not change due to treatment with pioglitazone in either mock-transfected or AnxA1-knockdown cells, but FPR2 expression was overall higher in AnxA1-knockdown cells, likely as a cell response to low levels of AnxA1 (**Figures 8B,C**). Thus, while pioglitazone does not necessarily modulate FPR2 expression, the lack of AnxA1, which is needed for ERK activation via FPR2, induces its expression.

DISCUSSION

Research on IBD therapy has advanced on the past few years, and inflammatory cytokines or specific cellular pathways such as JAK/STAT and phosphodiesterase-4 have all been explored as potential targets for IBD treatment (Pekow, 2017). Still, it is unlikely that a significant number of such newly-developed drugs aimed at interacting with the aforementioned targets will reach clinical practice, as several of these compounds do not display satisfactory remission rates or lead to severe adverse effects, such as increased risk for infection, malignancies or immunological disorders in larger clinical trials (Pekow, 2017; Click and Regueiro, 2019).

Thus, the search for drugs for treatment of IBDs has taken scientists to explore molecules beyond those designed to specifically treat IBDs and reassess drugs originally developed to treat other maladies (Lloyd et al., 2019; Kostoff et al., 2020). Such is the case of thiazolidinediones, PPARγ ligands originally

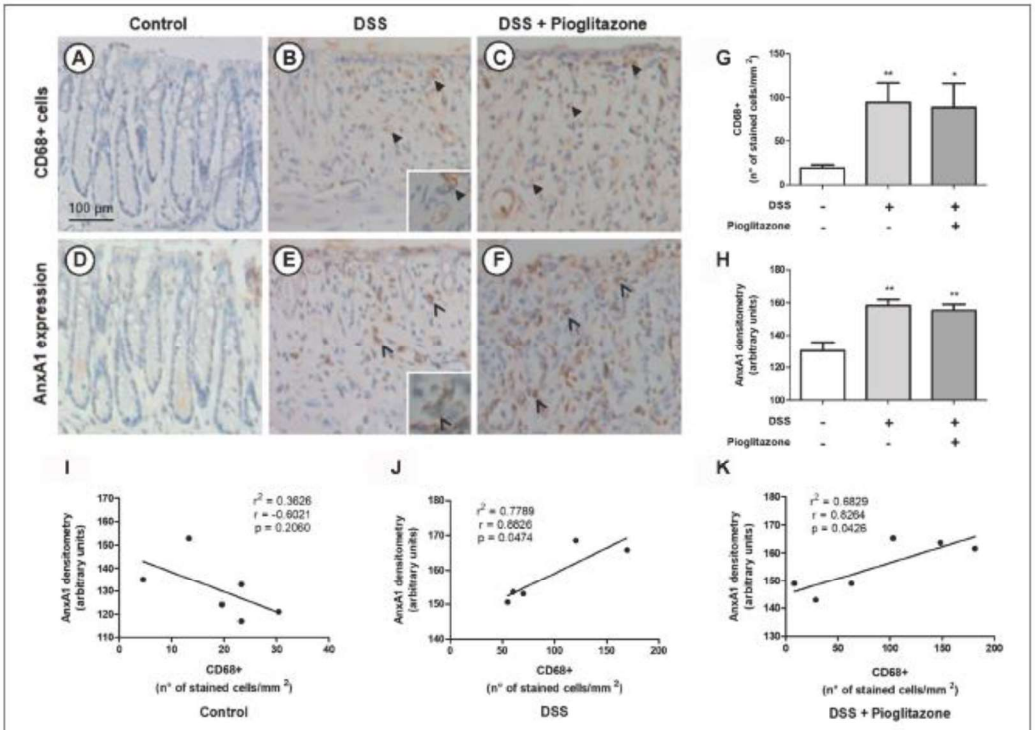

FIGURE 5 | Expression of AnxA1 and presence of CD68$^+$ macrophages in tissue sections. Wild type and AnxA1−/− mice were euthanized at the end of the experimental model; large intestines were harvested and colon paraffin-embedded sections were prepared. Number of CD68$^+$ macrophages and staining intensity corresponding to AnxA1 were assessed via DAB-staining in serial sections **(A–F)** (thicker black arrows indicate CD68$^+$ cells; thinner black arrows indicate staining corresponding to AnxA1 in macrophage-like cells), quantified **(G,H)** and correlated **(I–K)**. *, **$p < 0.05$, 0.01 in comparison to the control group. Data were statistically analyzed using One-Way ANOVA followed by Tukey's post-test ($n = 6$). Results are expressed as mean ± SE. Corresponding areas in each serial section were analyzed using Pearson's correlation test.

developed for treatments of diabetes, which have been explored to some success for treatment of IBDs. While clinical trials on PPARγ ligands seem somewhat promising, obtaining of conclusive results which could take research steps further on drug repurposing has been elusive so far (Lewis et al., 2008; Liang and Ouyang, 2008; Abedi et al., 2015).

While mechanisms unveiling how thiazolidinediones ameliorate IBD progression are yet to be completely understood, data on AnxA1 roles on IBD suggest it might be a promising player on the actions of PPARγ ligands leading to anti-inflammatory effects. Indeed, our research group has evidenced AnxA1 is vital for infliximab actions on murine IBD models (de Paula-Silva et al., 2016) and that AnxA1 is a promising biomarker for assessing responsiveness to infliximab in human IBD patients (unpublished observations). We have also shown both exogenous and endogenous AnxA1 are required for pioglitazone to induce BV2 microglia cells to phagocytize apoptotic cells, and that AnxA1 can modulate PPARγ expression in such cells (da Rocha et al., 2019). Data here obtained confirm the connection between pioglitazone and AnxA1 on treatment of experimental colitis, evidencing the inhibition of AnxA1 cleaving into its inactive form as a mechanism of action of pioglitazone; therefore, we suggest AnxA1 is as a key player required for the anti-inflammatory actions of pioglitazone and thus possibly other PPARγ ligands.

Data here obtained corroborated other studies which already evidenced the beneficial actions of pioglitazone in murine models of colitis (Saubermann et al., 2002; Takagi et al., 2002; Shah et al., 2007; Huang et al., 2020) and evidenced the lack of pioglitazone effects on AnxA1$^{-/-}$ mice demonstrating the pivotal role of AnxA1 for pioglitazone anti-inflammatory actions. However, these data do not rule out the effects of pioglitazone and AnxA1 are independent; inflammation exerted when lacking endogenous AnxA1 could be exceedingly exacerbated, overwhelming any attempts of PPARγ-activation linked mechanisms to halt disease progression. Indeed, DSS-colitis in

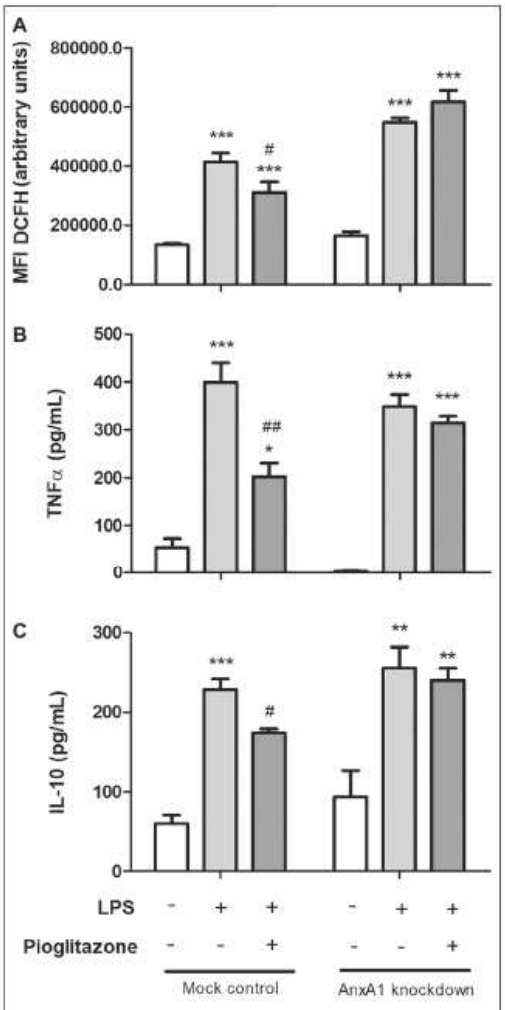

FIGURE 6 | Secretion of inflammatory cytokines and ROS production by transfected RAW 264.7 macrophages. Mock-transfected and AnxA1-knockdown RAW 264.7 cells were plated and treated with 10 μM pioglitazone for 1 h followed by 1 μg/ml LPS for 24 h. Cells were harvested and ROS production was assessed via DFCH-DA via flow cytometry **(A)**; supernatants were collected and secretion of TNFα **(B)** and IL-10 **(C)** was assessed via ELISA. *, **, ***$p < 0.05$, 0.01, 0.001 in comparison to the control group; #, ##$p < 0.05$, 0.01 in comparison to the LPS-treated group. Data were statistically analyzed using One-Way ANOVA followed by Tukey's post-test ($n = 3$). Results are expressed as mean ± SE.

AnxA1$^{-/-}$ mice is more pronounced and leads to increased mortality (Babbin et al., 2008; de Paula-Silva et al., 2016) and AnxA1 expression in the colon of WT mice increased regardless of treatment with pioglitazone. However, we here show pioglitazone prevented cleaving of AnxA1 whole 37 kDa form into smaller 33 kDa fragments, which are supposedly non-functional and induce inflammation, as evidenced in other models where AnxA1 cleaving correlates with increased inflammatory status in neutrophils (Vong et al., 2007; Williams et al., 2010; Vago et al., 2012; Sugimoto et al., 2016; Vago et al., 2016). AnxA1 can be cleaved at different cells and tissues, such as in neutrophils, adipose tissue and melanomas; non-functional 33-kDa peptides released promote inflammation facilitating cell transmigration to inflamed areas, inducing adipogenesis and causing skin tumors to become more aggressive (Williams et al., 2010; Boudhraa et al., 2014; Pietrani et al., 2018). Pioglitazone treatment also reduced MMP-9 expression in the inflamed gut of WT mice. Metalloproteinases such as MMP-9 induce inflammatory damage on tissues by cleaving extracellular matrix proteins, and that by itself can aggravate ulcerative colitis (Marshall et al., 2015; Chen et al., 2017). In this context, MMP-9 also cleaves AnxA1 into inactive 33 kDa proteins under inflammatory conditions (Zamilpa et al., 2010; Sugimoto et al., 2016). It must be noted that PPARγ expression suffered no changes due to DSS treatment or to lack of AnxA1, meaning pioglitazone could bind to its target in colon tissue at similar levels for all experimental conditions. This is in accordance with other authors who also reported PPARγ levels suffer little to no variances in colon tissue throughout the development of DSS colitis (Huang et al., 2020).

Thus, our data suggest that pioglitazone might indeed be linked to AnxA1 in order to exert its anti-inflammatory actions during the progression of DSS-induced colitis, but by modulating its functionality rather than its overall expression. Considering AnxA1 is a strong candidate for predictor of disease remission due to therapies on IBDs and AnxA1 expression levels tend to vary greatly in IBD patients, such information might aid elucidating why clinical trials investigating PPARγ ligands on IBDs tend to fail (Lewis et al., 2001; Lewis et al., 2008).

It is known that lamina propria residential macrophages play an important housekeeping role by phagocytosing apoptotic epithelial cells, clearing translocated bacteria and promoting epithelial stem cell maturation (Na et al., 2019). On the course of IBDs, residential macrophages and recruited monocytes become inflammatory M1 macrophages, which secrete inflammatory cytokines such as TNFα, IL-12, and IL-23 and induce Th1 responses (Bernardo et al., 2017; Na et al., 2019). However, during resolution phases of IBDs, lamina propria macrophages acquire a M2 phenotype and promote tissue repair due to releasing several anti-inflammatory factors such as IL-10 and AnxA1 (Na et al., 2019; Koelink et al., 2020). Macrophages are thus vital for both sustaining intestinal homeostasis and carrying intestinal inflammation, and evidence suggests AnxA1 released by these cells during resolutive phases of IBD can be responsible for attenuating disease progression (Vong et al., 2012; Quiros et al., 2017). Also, PPARγ in macrophages plays an important role on IBD physiopathology, as macrophage-specific PPARγ knockdown leads to pronounced colitis clinical effects, accumulation of TCD8+ lymphocytes in lamina propria, increase of CD40

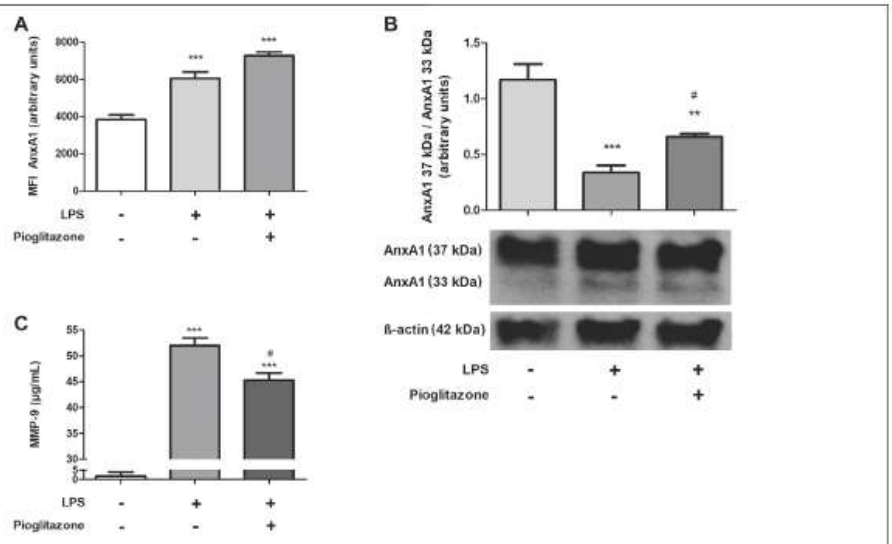

FIGURE 7 | Expression and cleaving of AnxA1 in RAW 264.7 macrophages. Non-transfected (wild-type) RAW 264.7 cells were plated and treated with 10 µM pioglitazone for 1 h followed by 1 µg/ml LPS for 24 h. Cells were harvested and AnxA1 expression via flow cytometry was assessed on part of them **(A)**; protein lysates were prepared from the remaining cells and AnxA1 cleaving was assessed via Western Blotting **(B)**. Culture supernatants were collected and MMP-9 secretion was assessed via ELISA **(C)**. *, ***$p < 0.05$, 0.001 in comparison to the control group; #$p < 0.05$ in comparison to the LPS-treated group. Data were statistically analyzed using One-Way ANOVA followed by Tukey's post-test ($n = 5$). Results are expressed as mean ± SE.

surface expression and secretion of inflammatory cytokines in the intestine (Shah et al., 2007; Hontecillas et al., 2011). Data here obtained show tissue sections from WT mice had a basal counting of CD68$^+$ macrophages which increased due to DSS administration, regardless of pioglitazone treatment, and indeed, corresponding areas on sections immunostained for AnxA1 evidenced there is a positive correlation between number of CD68$^+$ macrophages and AnxA1 expression, as both increased proportionally when mice were subjected to development of DSS-induced colitis. Thus, tissue inflammation caused by DSS led to recruitment of AnxA1 secreting monocytes in order to halt inflammation and evoke tissue repair (Steinbach and Plevy, 2014; Na et al., 2019). Other authors have reported increased number of CD68$^+$ macrophages in tissue sections either from biopsies specimens of Crohn's disease or ulcerative colitis patients or from intestines of DSS-treated mice, corroborating our data (Vong et al., 2012; Hong et al., 2014; Lissner et al., 2015; Reischl et al., 2020). However, studies correlating counting of CD68$^+$ macrophages with AnxA1 expression report seemingly contradicting evidence. It is reported by authors in biopsies from Crohn's disease patients that AnxA1 expression correlates only with myeloperoxidase-positive neutrophils excluding CD68$^+$ macrophages in lamina propria (Reischl et al., 2020), but others report the opposite by showing AnxA1 expression correlates with increased CD68$^+$ counting in tissue biopsies from ulcerative colitis and Crohn's disease patients, in agreement with our findings (Vong et al., 2012). Given the complexity of IBD as a disease, it is unsurprizing contradicting evidence would be found, and our work contributes in elucidating such ambiguities.

While the findings here described utilizing a murine model of experimental colitis so far evidence there is a connection between pioglitazone actions and AnxA1, assessment of AnxA1 as a marker of disease progression under pioglitazone treatment should still be considered in a preliminary manner and approached with due reservations in further studies involving humans. The immune system of mice is quite different from that of humans, and different immune responses in the gut can lead to different inflammatory processes being observed in both experimental colitis and human IBD which are not always similar, such as seen for activation of Treg cells, secretion of cytokines and infiltration of B lymphocytes (Del Prete et al., 1993; Stevceva et al., 2001; Mestas and Hughes, 2004; Gibbons and Spencer, 2011; Neurath, 2014; Wang et al., 2015; Do et al., 2017; Sun et al., 2017). Still, despite there being discrepancies, certain AnxA1 roles described in murine models of experimental colitis are corroborated in human IBD patients, such as infliximab treatment in AnxA1 knockout mice undergoing DSS colitis failing to attenuate disease progression, which links to other findings evidencing infliximab-responsive IBD patients show a greater expression of AnxA1 in colon tissue (Sena et al., 2013; de Paula-Silva et al., 2016). The same is true for PPARγ, as Crohn's disease-like ileitis is prevented in disease-susceptible SAMP/Fc mice crossbred with disease-resistant mice due to inheritance of

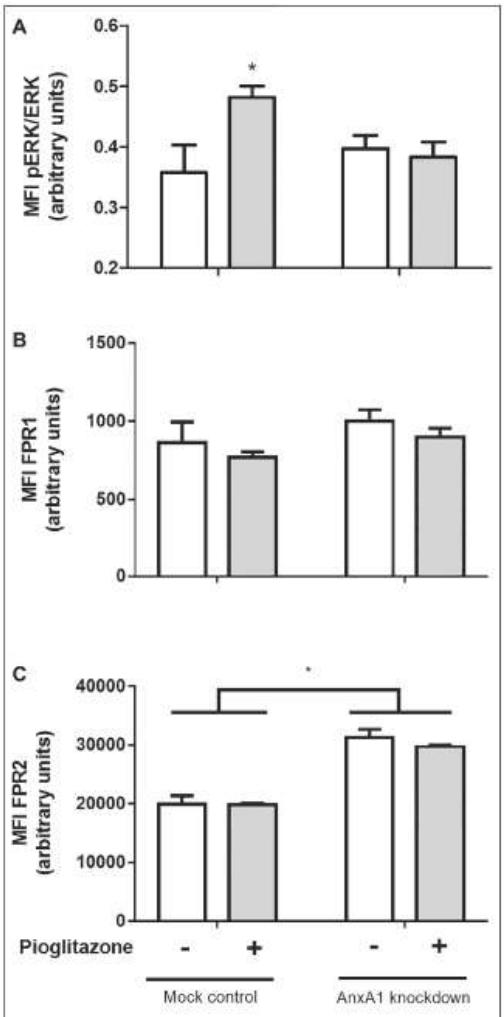

FIGURE 8 | Phosphorylation of ERK and expression of FPR1 and FPR2 in transfected RAW 264.7 macrophages. Mock-transfected and AnxA1-knockdown RAW 264.7 cells were plated and treated with 10 μM pioglitazone for 1 h. Cells were harvested and both ERK phosphorylation **(A)** and expression of FPR1 **(B)** and FPR2 **(C)** were assessed via flow cytometry. *$p < 0.05$ in comparison to the control group. Data were statistically analyzed using One-Way ANOVA followed by Tukey's post-test ($n = 4$). Results are expressed as mean ± SE.

functional PPARγ alleles, and certain polymorphisms in the PPARγ gene have been described as prevalent in Crohn's disease patients (Sugawara et al., 2005). In the same vein, a number of drugs used for treatment of IBD in humans have been successfully validated for use in experimental colitis models in mice (Melgar et al., 2008). Translation between mouse colitis models and human IBD is thus very feasible, but future assessment of mechanisms involving AnxA1 and pioglitazone as described in this work, when in human IBD patients, should therefore consider the aforementioned reservations.

In order to reinforce our *in vivo* data, an *in vitro* experimental protocol was carried out using the RAW 264.7 macrophage cell line. Using LPS to mimic an inflammatory environment, we found that LPS treatment increased secretion of TNFα and IL-10 and generation of ROS, effects abrogated due to treatment with pioglitazone. Corroborating our *in vivo* data, the anti-inflammatory effects of pioglitazone were only detected in mock-transfected cells, but not in AnxA1 knockdown cells, which evidences endogenous AnxA1 is vital for pioglitazone anti-inflammatory effects in macrophages. The same manner as seen in our *in vivo* data, pioglitazone did not modify AnxA1 expression. It has been reported that rosiglitazone and prostaglandin J2, both PPARγ ligands, increase AnxA1 expression, but such has been demonstrated in MDA-MB-231 and MCF-7 breast cancer cells to variable results and not at inflammatory conditions (Chen et al., 2017). LPS also increased AnxA1 expression by RAW 264.7 cells and expressed AnxA1 was cleaved into smaller, non-functional 33 kDa fragments, and regardless of the effects of pioglitazone on AnxA1 expression, it prevented AnxA1 cleaving and attenuated secretion of MMP-9. Control of MMP-9 secretion is a known anti-inflammatory effect of pioglitazone and other PPARγ ligands; they can modulate septin-2 in cancer cells preventing MMP-9 actions, and during the course of intestinal inflammations, down-modulation of PPARγ can make MMP-9 more stable (Kundu et al., 2014; Cao et al., 2015). Still, it had not yet been demonstrated that such effect could be linked to prevention of AnxA1 cleaving. As described previously, pioglitazone seems to attenuate inflammation by preventing AnxA1 cleaving rather than controlling its overall expression, and using our *in vitro* model we found evidence that so happens in macrophages, strengthening our *in vivo* data. Of note, contrary to what was seen *in vivo*, inflammatory conditions increased PPARγ expression in mock-transfected but not in AnxA1-knockdown macrophages. Under non-inflammatory conditions, pioglitazone by itself induced PPARγ expression, as expected due to it being a PPARγ ligand, but also only in mock-transfected cells. It is reported LPS activates PPARγ as a means of "desensitizing" macrophages attenuating responses to further inflammatory stimuli, and AnxA1 seems to be involved with such modulation of PPARγ in both inflammatory and non-inflammatory conditions (Von Knethen and Bernhard, 2001). Whether lack of AnxA1 prevents pioglitazone binding to PPARγ or prevents some sort of post-translational mechanism after interaction between PPARγ and a ligand was not assessed in our work, but the fact this interaction was seen in isolated macrophage cultures and not in mice tissue further reinforces the need for *in vitro* models to better investigate specific effects which might become hidden

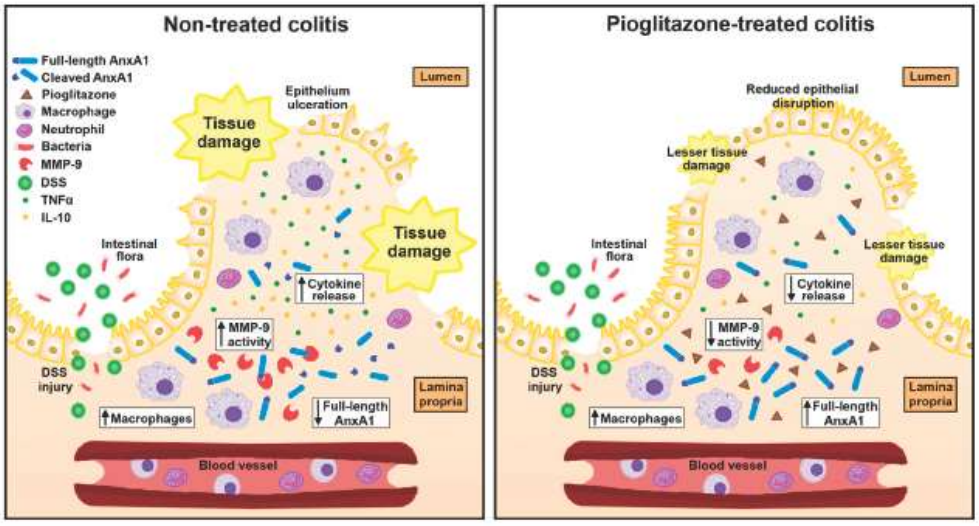

FIGURE 9 | Schematics of connections between pioglitazone effects and AnxA1 on experimental colitis. In experimental colitis induced by DSS, tissue injury exposes intestinal lamina propria to gut microorganisms triggering inflammation and increasing the number of AnxA1-releasing macrophages. AnxA1 released this way is cleaved into smaller, non-functional fragments by proteolytic enzymes such as MMP-9, which impairs its anti-inflammatory actions leading to greater secretion of cytokines such as TNFα and IL-10 and causing overall disruption of the intestinal tissue. Upon treatment with pioglitazone, MMP-9 expression decreases and causes AnxA1 released by macrophages to remain non-fragmented for longer, allowing it to promote its anti-inflammatory actions, decreasing cytokine secretion and reducing overall tissue disruption.

amid the myriad of simultaneous biological processes occurring *in vivo*. Indeed, PPARγ in colon tissue is expressed not only by lamina propria macrophages, but also at considerable levels by crypt epithelial cells (Su et al., 2007).

While pioglitazone showed its anti-inflammatory effects to be reliant on AnxA1, it is known pioglitazone has other effects that are PPARγ-independent, such as induction of migration of vascular smooth muscle cells and inhibition of proliferation of tumor cells (Emery et al., 2006; Li et al., 2008). By expanding some of the *in vitro* findings previously described, we evidenced some of the anti-inflammatory actions of pioglitazone are indeed PPARγ-dependent, as treatment of RAW 264.7 cells with the PPARγ antagonist GW9662 prevented the increased secretions of TNFα and MMP-9 to be attenuated by pioglitazone. To our knowledge, this effect has been previously described for TNFα in myocytes, but not in RAW 264.7 macrophages (Liu et al., 2009). This is relevant for prospective studies on PPARγ ligands and AnxA1, as knowing that inhibition of MMP-9 secretion is dependent on PPARγ makes it more likely that other PPARγ ligands studied for treatment of IBD would have the same effect in preventing AnxA1 cleaving.

As to further elucidate how AnxA1 could influence the anti-inflammatory effects of pioglitazone, we investigated whether AnxA1 knockdown of RAW 264.7 macrophages could affect pioglitazone-induced phosphorylation of extracellular regulator kinase (ERK). ERK is a signaling factor linked to several cell processes, such as cell survival, differentiation and migration, among others (Maurice et al., 2018; Li et al., 2019; Zhou et al., 2019), and it is known that pioglitazone can activate ERK1/2 phosphorylation leading to anti-inflammatory effects, as reported on ischemic cardiomyocytes and on different cell lines, including colon cell lines (Wang et al., 2012; Kole et al., 2016). Our data showed that pioglitazone did cause ERK phosphorylation, but such effect was not seen in AnxA1 knockdown cells, evidencing AnxA1 is required for pioglitazone-induced ERK phosphorylation to occur. ERK phosphorylation is also known to take place *downstream* to AnxA1 activation in a plethora of cells, including macrophages (Dufton et al., 2010; Bena et al., 2012). As we evidenced lacking AnxA1 prevents ERK phosphorylation, it can be inferred that AnxA1 might be the sole activator of ERK phosphorylation *downstream* to PPARγ activation in this scenario, being an intermediate molecule connecting pioglitazone actions and ERK phosphorylation, which is allowed to activate ERK by pioglitazone by remaining functional and non-cleaved for longer. In addition, increased FPR2 expression, but not FPR1, in AnxA1-knockdown cells suggests there is a cell response under absence of AnxA1 which aims to increase FPR2-mediated downstream signaling, which is known to involve ERK phosphorylation (Bena et al., 2012) leading to most anti-inflammatory effects of AnxA1, such

as reduction of inflammatory cytokines and of neutrophil activation in different murine models of inflammation (Ding et al., 2020; Machado et al., 2020). Pioglitazone, by preserving full length-AnxA1, thus possibly increases the likelihood for AnxA1 to bind to FPR2 leading to ERK phosphorylation.

Overall, our main findings evidence pioglitazone relies on AnxA1 expressed by macrophages to exert its anti-inflammatory actions throughout the course of experimental colitis, and that it does so by preventing AnxA1 cleaving. A graphical representation of such findings is depicted in **Figure 9**.

CONCLUSION

Data obtained in the present work evidence pioglitazone attenuates inflammation *in vivo* in a murine colitis model, and prevention of AnxA1 cleaving seems to be involved with such effect. Data obtained *in vitro* show that this process occurs in macrophages, and that pioglitazone effects rely on ERK phosphorylation, which requires AnxA1. This sum of evidence allows us to suggest that the beneficial effects of pioglitazone on the treatment of IBDs are connected to AnxA1 cleaving rather than its expression. As AnxA1 has been increasingly targeted as a potential predictor of IBD progression and treatment-induced remission, this evidence is of value for future clinical trials investigating PPARγ ligands for treatment of IBDs, as biomarkers which might indicate more accurately how therapeutic success on patients is more likely to be achieved, such as AnxA1, can be more thoroughly assessed.

DATA AVAILABILITY STATEMENT

The raw data supporting the conclusions of this article will be made available by the authors, without undue reservation.

ETHICS STATEMENT

The animal study was reviewed and approved by Ethics Committee on Animal Use of the Faculty of Pharmaceutical Sciences, University of São Paulo.

AUTHOR CONTRIBUTIONS

GdR and SF designed the study and wrote the final manuscript. GdR, MdP-S, MB, PS, and LM performed experiments. LM and SM-E provided expertize on cell transfection protocols.

FUNDING

This work received financial support from the National Council for Scientific and Technological Development (CNPq, no. 130090/2019-0) and from the São Paulo Research Foundation (FAPESP, nos. 2014/07328-4, 2016/19682-2, 2017/05430-4 and 2018/26383-7), which also provided funds for open access publication fees.

ACKNOWLEDGMENTS

The authors acknowledge Dextran Products Ltd. (ON, Canada), who kindly donated dextran sodium sulfate used in this work.

SUPPLEMENTARY MATERIAL

The Supplementary Material for this article can be found online at: https://www.frontiersin.org/articles/10.3389/fphar.2020.591561/full#supplementary-material.

REFERENCES

Abedi, V., Lu, P., Hontecillas, R., Verma, M., Vess, G., Philipson, C. W., et al. (2015). Phase III placebo-controlled, randomized clinical trial with synthetic crohn's disease patients to evaluate treatment response computational modeling-based discovery of novel classes of anti-inflammatory drugs that target lanthionine synthetase C-like protein emerging trends in computational biology. *Bioinf. Systems Biol. Systems Appl.* 2 (79), 169

Ahmadian, M., Suh, J. M., Hah, N., Liddle, C., Atkins, A. R., Downes, M., et al. (2013). PPARγ signaling and metabolism: the good, the bad and the future. *Nat. Med.* 19 (5), 557–566. doi:10.1038/nm.3159

Babbin, B. A., Laukoetter, M. G., Nava, P., Koch, S., Lee, W. Y., Capaldo, C. T., et al. (2008). Annexin A1 regulates intestinal mucosal injury, inflammation, and repair. *J. Immunol.* 181 (7), 5035–5044. doi:10.4049/jimmunol.181.7.5035

Bernardo, D., Mora-Gutierrez, I., Marin, A., Díaz-Guerra, A., Caminero-Fernández, R., Caldas, M., et al. (2017). Characterization of human intestinal macrophage subsets in health and inflammatory bowel disease. *J. Crohn's Colitis* 11, S131. doi:10.1093/ecco-jcc/jjx002.236

Hontecillas, R., Horne, W. T., Climent, M., Guri, A. J., Evans, C., Zhang, Y., et al. (2011). Immunoregulatory mechanisms of macrophage PPAR-γ in mice with experimental inflammatory bowel disease. *Mucosal Immunol.* 4 (3), 304–313. doi:10.1038/mi.2010.75

Hossain, A., Lördal, M., Olsson, A. E., Storlåhls, A., Aleman, S., Eberhardson, M., et al. (2020). Sustained clinical benefit, improved quality of life, and reduced intestinal surgery from maintenance infliximab treatment in inflammatory bowel disease. *Scand. J. Gastroenterol.* 55 (2), 178–183. doi:10.1080/00365521.2020.1722738

Huang, Y., Wang, C., Tian, X., Mao, Y., Hou, B., Sun, Y., et al. (2020). Pioglitazone attenuates experimental colitis-associated hyperalgesia through improving the intestinal barrier dysfunction. *Inflammation* 43 (2), 568–578. doi:10.1007/s10753-019-01138-3

Bonato, J. M., Bassani, T. B., Milani, H., Vital, M. A. B. F., and de Oliveira, R. M. W. (2018). Pioglitazone reduces mortality, prevents depressive-like behavior, and impacts hippocampal neurogenesis in the 6-OHDA model of parkinson's disease in rats. *Exp. Neurol.* 300, 188–200. doi:10.1016/j.expneurol.2017.11.009

Boudhraa, Z., Merle, C., Mazzocut, D., Chezal, J. M., Chambon, C., Miot-Noirault, E., et al. (2014). Characterization of pro-invasive mechanisms and N-terminal cleavage of ANXA1 in melanoma. *Arch. Dermatol. Res.* 306 (10), 903–914. doi:10.1007/s00403-014-1517-z

Cao, L. Q., Shao, Z. L., Liang, H. H., Zhang, D. W., Yang, X. W., Jiang, X. F., et al. (2015). Activation of peroxisome proliferator-activated receptor-γ (PPARγ) inhibits hepatoma cell growth via downregulation of SEPT2 expression. *Cancer Lett.* 359 (1), 127–135. doi:10.1016/j.canlet.2015.01.004

Chen, L., Yuan, Y., Kar, S., Kanchi, M. M., Arora, S., Kim, J. E., et al. (2017). PPARγ ligand-induced annexin A1 expression determines chemotherapy response via deubiquitination of death domain kinase RIP in triple-negative breast cancers. *Mol. Cancer Ther.* 16 (11), 2528–2542. doi:10.1158/1535-7163.MCT-16-0739

Click, B., and Regueiro, M. (2019). A practical guide to the safety and monitoring of new IBD therapies. *Inflamm. Bowel Dis.* 25 (5), 831–842. doi:10.1093/ibd/izy313

da Rocha, G. H. O., Loiola, R. A., Pantaleão, Ld. N., Reutelingsperger, C., Solito, E., and Farsky, S. H. P. (2019). Control of expression and activity of peroxisome proliferated-activated receptor γ by Annexin A1 on microglia during efferocytosis. *Cell Biochem. Funct.* 37 (7), 560–568. doi:10.1002/cbf.3433

Da Silva, S., Keita, A. V., Mohlin, S., Pahlman, S., Theodorou, V., Pahlman, I., et al. (2018). A novel topical PPARgamma agonist induces PPARgamma activity in ulcerative colitis mucosa and prevents and reverses inflammation in induced colitis models. *Inflamm. Bowel Dis.* 24 (4), 792–805. doi:10.1093/ibd/izx079

de Paula-Silva, M., Barrios, B. E., Macció-Maretto, L., Sena, A. A., Farsky, S. H., Correa, S. G., et al. (2016). Role of the protein annexin A1 on the efficacy of anti-TNF treatment in a murine model of acute colitis. *Biochem. Pharmacol.* 115, 104–113. doi:10.1016/j.bcp.2016.06.012

Bradford, M. M. (1976). A rapid and sensitive method for the quantitation of microgram quantities of protein utilizing the principle of protein-dye binding. *Anal. Biochem.* 72 (1-2), 248–254. doi:10.1006/abio.1976.9999

Ding, Y., Flores, J., Klebe, D., Li, P., McBride, D. W., Tang, J., et al. (2020). Annexin A1 attenuates neuroinflammation through FPR2/p38/COX-2 pathway after intracerebral hemorrhage in male mice. *J. Neurosci. Res.* 98 (1), 168–178. doi:10.1002/jnr.24478

Dou, X., Xiao, J., Jin, Z., and Zheng, P. (2015). Peroxisome proliferator-activated receptor-γ is downregulated in ulcerative colitis and is involved in experimental colitis-associated neoplasia. *Oncol. Lett.* 10 (3), 1259–1266. doi:10.3892/ol.2015.3397

Dufton, N., Hannon, R., Brancaleone, V., Dalli, J., Patel, H. B., Gray, M., et al. (2010). Anti-inflammatory role of the murine formyl-peptide receptor 2: ligand-specific effects on leukocyte responses and experimental inflammation. *J. Immunol.* 184 (5), 2611–2619. doi:10.4049/jimmunol.0903526

Emery, M. N., Leontiou, C., Bonner, S. E., Merulli, C., Nanzer, A. M., Musat, M., et al. (2006). PPAR-gamma expression in pituitary tumours and the functional activity of the glitazones: evidence that any anti-proliferative effect of the glitazones is independent of the PPAR-gamma receptor. *Clin. Endocrinol.* 65 (3), 389–395. doi:10.1111/j.1365-2265.2006.02610.x

Von Knethen, A., and Bernhard, B. (2001). Delayed activation of PPARγ by LPS and IFN-γ attenuates the oxidative burst in macrophages. *FASEB J.* 15 (2), 535–544. doi:10.1096/fj.00-0187com

El Awdan, S., and Mostafa, R. E. (2018). Protective effects of pioglitazone against dextran sodium sulphate-induced colitis in rats. *Iran. J. Pharm. Sci.* 14 (3), 1–12

Duijvestein, M., Battat, R., Vande Casteele, N., D'Haens, G. R., Sandborn, W. J., Khanna, R., Khanna, R., et al. (2018). Novel therapies and treatment strategies for patients with inflammatory bowel disease. *Curr. Treat. Options Gastroenterol.* 16 (1), 129–146. doi:10.1007/s11938-018-0175-1

Galimberti, D., and Scarpini, E. (2017). Pioglitazone for the treatment of alzheimer's disease. *Expet Opin. Invest. Drugs* 26 (1), 97–101. doi:10.1080/13543784.2017.1265504

Geboes, K., Riddell, R., Öst, A., Jensfelt, B., Persson, T., and Löfberg, R. (2000). A reproducible grading scale for histological assessment of inflammation in ulcerative colitis. *Gut* 47 (3), 404–409. doi:10.1136/gut.47.3.404

Gibbons, D. L., and Spencer, J. (2011). Mouse and human intestinal immunity: same ballpark, different players; different rules, same score. *Mucosal Immunol.* 4 (2), 148–157. doi:10.1038/mi.2010.85

Fernandez-Boyanapalli, R., Frasch, S. C., Riches, D. W., Vandivier, R. W., Henson, P. M., and Bratton, D. L. (2010). PPARγ activation normalizes resolution of acute sterile inflammation in murine chronic granulomatous disease. *Blood* 116 (22), 4512–4522. doi:10.1182/blood-2010-02-272005

Ho, G. T., Cartwright, J. A., Thompson, E. J., Bain, C. C., and Rossi, A. G. (2020). Resolution of inflammation and gut repair in IBD: translational steps towards complete mucosal healing. *Inflamm. Bowel Dis.* 26 (8), 1131–1143. doi:10.1093/ibd/izaa045

Hong, K., Zhang, Y., Guo, Y., Xie, J., Wang, J., He, X., et al. (2014). All-trans retinoic acid attenuates experimental colitis through inhibition of NF-κB signaling. *Immunol. Lett.* 162 (1 Pt A), 34–40. doi:10.1016/j.imlet.2014.06.011

Keith, R. L., Blatchford, P. J., Merrick, D. T., Bunn, P. A., Bagwell, B., Dwyer-Nield, L. D., et al. (2019). A randomized phase II trial of pioglitazone for lung cancer chemoprevention in high-risk current and former smokers. *Cancer Prev. Res.* 12 (10), 721–730. doi:10.1158/1940-6207.CAPR-19-0006

Chongmelaxme, B., Phisalprapa, P., Sawanglit, R., Dilokthornsakul, P., and Chaiyakunapruk, N. (2019). Weight reduction and pioglitazone are cost-effective for the treatment of non-alcoholic fatty liver disease in thailand. *Pharmacoeconomics* 37 (2), 267–278. doi:10.1007/s40273-018-0736-0

Kostoff, R. N., Briggs, M. B., and Shores, D. R. (2020). Treatment repurposing for inflammatory bowel disease using literature-related discovery and innovation. *World J. Gastroenterol.* 26 (33), 4889–4899. doi:10.3748/wjg.v26.i33.4889

Kundu, P., Ling, T. W., Korecka, A., Li, Y., D'Arienzo, R., Bunte, R. M., et al. (2014). Absence of intestinal PPARγ aggravates acute infectious colitis in mice through a lipocalin-2-dependent pathway. *PLoS Pathog.* 10 (1), e1003887. doi:10.1371/journal.ppat.1003887

Liang, H. L., and Ouyang, Q. (2008). A clinical trial of combined use of rosiglitazone and 5-aminosalicylate for ulcerative colitis. *World J. Gastroenterol.* 14 (1), 114–119. doi:10.3748/wjg.14.114

Lissner, D., Schumann, M., Batra, A., Kredel, L. I., Kühl, A. A., Erben, U., et al. (2015). Monocyte and M1 macrophage-induced barrier defect contributes to chronic intestinal inflammation in IBD. *Inflamm. Bowel Dis.* 21 (6), 1297–1305. doi:10.1097/MIB.0000000000000384

Lu, Y. Q., Ngo, A., Hoffmann, P., Ferrante, A., and Hii, C. S. (2019). Regulation of endothelial cell survival and death by the MAP kinase/ERK kinase kinase 3 - glyceraldehyde-3-phosphate dehydrogenase signaling axis. *Cell. Signal.* 58, 20–33. doi:10.1016/j.cellsig.2019.03.002

Luther, J., and Dave, M. (2020). Rising inflammatory bowel disease prevalence highlights the need for effective, cost-effective therapies. *Inflamm. Bowel Dis.* 26 (4), 626–627. doi:10.1093/ibd/izz203

Ma, J. P., Ye, B. D., Kim, Y. S., and Kim, J. S. (2018). Changing treatment paradigms for the management of inflammatory bowel disease. *Korean J. Intern. Med.* 33 (1), 28–35. doi:10.3904/kjim.2017.400

Machado, M. G., Tavares, L. P., Souza, G. V. S., Queiroz-Junior, C. M., Ascenção, F. R., Lopes, M. E., et al. (2020). The Annexin A1/FPR2 pathway controls the inflammatory response and bacterial dissemination in experimental pneumococcal pneumonia. *FASEB J.* 34 (2), 2749–2764. doi:10.1096/fj.201902172R

Marshall, D. C., Lyman, S. K., McCauley, S., Kovalenko, M., Spangler, R., Liu, C., et al. (2015). Selective allosteric inhibition of MMP9 is efficacious in preclinical models of ulcerative colitis and colorectal cancer. *PLoS One* 10 (5), e0127063. doi:10.1371/journal.pone.0127063

Melgar, S., Karlsson, L., Rehnstrom, E., Karlsson, A., Utkovic, H., Janston, L., et al. (2008). Validation of murine dextran sulfate sodium-induced colitis using four therapeutic agents for human inflammatory bowel disease. *Int. Immunopharm.* 8 (6), 836–844. doi:10.1016/j.intimp.2008.01.036

Mestas, J., and Hughes, C. C. (2004). Of mice and not men: differences between mouse and human immunology. *J. Immunol.* 172 (5), 2731–2738. doi:10.4049/jimmunol.172.5.2731

Koelink, P. J., Bloemendaal, F. M., Li, B., Westera, L., Vogels, E. W. M., van Roest, M., et al. (2020). Anti-TNF therapy in IBD exerts its therapeutic effect through macrophage IL-10 signalling. *Gut* 69 (6), 1053–1063. doi:10.1136/gutjnl-2019-318264

Na, Y. R., Stakenborg, M., Seok, S. H., and Matteoli, G. (2019). Macrophages in intestinal inflammation and resolution: a potential therapeutic target in IBD. *Nat. Rev. Gastroenterol. Hepatol.* 16 (9), 531–543. doi:10.1038/s41575-019-0172-4

Neurath, M. F. (2014). Cytokines in inflammatory bowel disease. *Nat. Rev. Immunol.* 14 (5), 329–342. doi:10.1038/nri3661

Lewis, J. D., Lichtenstein, G. R., Stein, R. B., Deren, J. J., Judge, T. A., Fogt, F., et al. (2001). An open-label trial of the PPAR-gamma ligand rosiglitazone for active ulcerative colitis. *Am. J. Gastroenterol.* 96 (12), 3323–3328. doi:10.1111/j.1572-0241.2001.05333.x

Bena, S., Brancaleone, V., Wang, J. M., Perretti, M., and Flower, R. J. (2012). Annexin A1 interaction with the FPR2/ALX receptor: identification of distinct domains and downstream associated signaling. *J. Biol. Chem.* 287 (29), 24690–24697. doi:10.1074/jbc.M112.377101

Del Prete, G., De Carli, M., Almerigogna, F., Giudizi, M. G., Biagiotti, R., and Romagnani, S. (1993). Human IL-10 is produced by both type 1 helper (Th1) and type 2 helper (Th2) T cell clones and inhibits their antigen-specific proliferation and cytokine production. *J. Immunol.* 150 (2), 353–360.

Ouyang, N., Zhu, C., Zhou, D., Nie, T., Go, M. F., Richards, R. J., et al. (2012). MC-12, an annexin A1-based peptide, is effective in the treatment of experimental colitis. *PLoS One* 7 (7), e41585. doi:10.1371/journal.pone.0041585

Patel, H. B., Kornerup, K. N., Sampaio, A. L., D'Acquisto, F., Seed, M. P., Girol, A. P., et al. (2012). The impact of endogenous annexin A1 on glucocorticoid

control of inflammatory arthritis. *Ann. Rheum. Dis.* 71 (11), 1872–1880. doi:10.1136/annrheumdis-2011-201180

Pekow, J. (2017). IBD therapies: coming attractions. *Clin. Gastroenterology Inflammatory Bowel Dis.*, 183–204. doi:10.1007/978-3-319-53763-4_11

Perretti, M., and D'acquisto, F. (2009). Annexin A1 and glucocorticoids as effectors of the resolution of inflammation. *Nat. Rev. Immunol.* 9 (1), 62–70. doi:10.1038/nri2470

Perse, M., and Cerar, A. (2012). Dextran sodium sulphate colitis mouse model: traps and tricks. *J. Biomed. Biotechnol.* 2012, 718617. doi:10.1155/2012/718617

Perucci, L. O., Sugimoto, M. A., Gomes, K. B., Dusse, L. M., Teixeira, M. M., and Sousa, L. P. (2017). Annexin A1 and specialized proresolving lipid mediators: promoting resolution as a therapeutic strategy in human inflammatory diseases. *Expert Opin. Ther. Targets* 21 (9), 879–896. doi:10.1080/14728222.2017.1364363

Leoni, G., Neumann, P. A., Kamaly, N., Quiros, M., Nishio, H., Jones, H. R., et al. (2015). Annexin A1-containing extracellular vesicles and polymeric nanoparticles promote epithelial wound repair. *J. Clin. Invest.* 125 (3), 1215–1227. doi:10.1172/JCI76693

Pietrani, N. T., Ferreira, C. N., Rodrigues, K. F., Perucci, L. O., Carneiro, F. S., Bosco, A. A., et al. (2018). Proresolving protein Annexin A1: the role in type 2 diabetes mellitus and obesity. *Biomed. Pharmacother.* 103, 482–489. doi:10.1016/j.biopha.2018.04.024

Pisanu, A., Lecca, D., Mulas, G., Wardas, J., Simbula, G., Spiga, S., et al. (2014). Dynamic changes in pro- and anti-inflammatory cytokines in microglia after PPAR-gamma agonist neuroprotective treatment in the MPTPp mouse model of progressive parkinson's disease. *Neurobiol. Dis.* 71, 280–291. doi:10.1016/j.nbd.2014.08.011

Quiros, M., Nishio, H., Neumann, P. A., Siuda, D., Brazil, J. C., Azcutia, V., et al. (2017). Macrophage-derived IL-10 mediates mucosal repair by epithelial WISP-1 signaling. *J. Clin. Invest.* 127 (9), 3510–3520. doi:10.1172/JCI90229

Reischl, S., Troger, J., Jesinghaus, M., Kasajima, A., Wilhelm, D. F., Friess, H., et al. (2020). Annexin A1 expression capacity as a determinant for disease severity in crohn's disease. *Dig. Dis.* 38 (5), 398–407. doi:10.1159/000505910

Rueden, C. T., Schindelin, J., Hiner, M. C., DeZonia, B. E., Walter, A. E., Arena, E. T., et al. (2017). ImageJ2: ImageJ for the next generation of scientific image data. *BMC Bioinf.* 18 (1), 529. doi:10.1186/s12859-017-1934-z

Santin, J. R., Machado, I. D., Rodrigues, S. F., Teixeira, S., Muscará, M. N., Galdino, S. L., et al. (2013). Role of an indole-thiazolidine molecule PPAR pan-agonist and COX inhibitor on inflammation and microcirculatory damage in acute gastric lesions. *PLoS One* 8 (10), e76894. doi:10.1371/journal.pone.0076894

Saubermann, L. J., Nakajima, A., Wada, K., Zhao, S., Terauchi, Y., Kadowaki, T., et al. (2002). Peroxisome proliferator-activated receptor gamma agonist ligands stimulate a Th2 cytokine response and prevent acute colitis. *Inflamm. Bowel Dis.* 8 (5), 330–339. doi:10.1097/00054725-200209000-00004

Sena, A., Grishina, I., Thai, A., Goulart, L., Macal, M., Fenton, A., et al. (2013). Dysregulation of anti-inflammatory annexin A1 expression in progressive crohns disease. *PLoS One* 8 (10), e76969. doi:10.1371/journal.pone.0076969

Shah, Y. M., Morimura, K., and Gonzalez, F. J. (2007). Expression of peroxisome proliferator-activated receptor-γ in macrophage suppresses experimentally induced colitis. *Am. J. Physiol. Gastrointest. Liver Physiol.* 292 (2), G657–G66. doi:10.1152/ajpgi.00381.2006

Sheikh, M. H., and Solito, E. (2018). Annexin A1: uncovering the many talents of an old protein. *Int. J. Mol. Sci.* 19 (4), 1045. doi:10.3390/ijms19041045

Liu, J., Xia, Q., Zhang, Q., Li, H., Zhang, J., Li, A., et al. (2009). Peroxisome proliferator-activated receptor-gamma ligands 15-deoxy-delta(12,14)-prostaglandin J2 and pioglitazone inhibit hydroxyl peroxide-induced TNF-alpha and lipopolysaccharide-induced CXC chemokine expression in neonatal rat cardiac myocytes. *Shock* 32 (3), 317–324. doi:10.1097/SHK.0b013e31819c374c

Maurice, D., Costello, P., Sargent, M., and Treisman, R. (2018). ERK signaling controls innate-like CD8. *J. Immunol.* 201 (6), 1681–1691. doi:10.4049/jimmunol.1800704

Mak, W. Y., Zhao, M., Ng, S. C., and Burisch, J. (2020). The epidemiology of inflammatory bowel disease: east meets west. *J. Gastroenterol. Hepatol.* 35 (3), 380–389. doi:10.1111/jgh.14872

Steinbach, E. C., and Plevy, S. E. (2014). The role of macrophages and dendritic cells in the initiation of inflammation in IBD. *Inflamm. Bowel Dis.* 20 (1), 166–175. doi:10.1097/MIB.0b013e3182a69dca

Stevceva, L., Pavli, P., Husband, A. J., and Doe, W. F. (2001). The inflammatory infiltrate in the acute stage of the dextran sulphate sodium induced colitis: B cell response differs depending on the percentage of DSS used to induce it. *BMC Clin. Pathol.* 1 (1), 3. doi:10.1186/1472-6890-1-3

Su, W., Bush, C. R., Necela, B. M., Calcagno, S. R., Murray, N. R., Fields, A. P., et al. (2007). Differential expression, distribution, and function of PPAR-gamma in the proximal and distal colon. *Physiol. Genom.* 30 (3), 342–353. doi:10.1152/physiolgenomics.00042.2007

Sugawara, K., Okon, T. S., Moskaluk, C. A., Stevens, B. K., Hoang, S., Kozaiwa, K., et al. (2005). Linkage to peroxisome proliferator-activated receptor-gamma in SAMP1/YitFc mice and in human Crohn's disease. *Gastroenterology* 128 (2), 351–360. doi:10.1053/j.gastro.2004.11.001

Sugimoto, M. A., Vago, J. P., Teixeira, M. M., and Sousa, L. P. (2016). Annexin A1 and the resolution of inflammation: modulation of neutrophil recruitment, apoptosis, and clearance. *J. Immunol. Res.* 2016, 8239258. doi:10.1155/2016/8239258

Sun, X., He, S., Lv, C., Sun, X., Wang, J., Zheng, W., et al. (2017). Analysis of murine and human Treg subsets in inflammatory bowel disease. *Mol. Med. Rep.* 16 (3), 2893–2898. doi:10.3892/mmr.2017.6912

Takagi, T., Naito, Y., Tomatsuri, N., Handa, O., Ichikawa, H., Yoshida, N., et al. (2002). Pioglitazone, a PPAR-gamma ligand, provides protection from dextran sulfate sodium-induced colitis in mice in association with inhibition of the NF-kappaB-cytokine cascade. *Redox Rep.* 7 (5), 283–289. doi:10.1179/135100002125000802

Takaki, K., Mitsuyama, K., Tsuruta, O., Toyonaga, A., and Sata, M. (2006). Attenuation of experimental colonic injury by thiazolidinedione agents. *Inflamm. Res.* 55 (1), 10–15. doi:10.1007/s00011-005-0002-8

Vago, J. P., Nogueira, C. R., Tavares, L. P., Soriani, F. M., Lopes, F., Russo, R. C., et al. (2012). Annexin A1 modulates natural and glucocorticoid-induced resolution of inflammation by enhancing neutrophil apoptosis. *J. Leukoc. Biol.* 92 (2), 249–258. doi:10.1189/jlb.0112008

Vago, J. P., Tavares, L. P., Sugimoto, M. A., Lima, G. L., Galvao, I., de Caux, T. R., et al. (2016). Proresolving actions of synthetic and natural protease inhibitors are mediated by annexin A1. *J. Immunol.* 196 (4), 1922–1932. doi:10.4049/jimmunol.1500886

Kole, L., Sarkar, M., Deb, A., and Giri, B. (2016). Pioglitazone, an anti-diabetic drug requires sustained MAPK activation for its anti-tumor activity in MCF7 breast cancer cells, independent of PPAR-γ pathway. *Pharmacol. Rep.* 68 (1), 144–154. doi:10.1016/j.pharep.2015.08.001

Vong, L., D'Acquisto, F., Pederzoli-Ribeil, M., Lavagno, L., Flower, R. J., Witko-Sarsat, V., et al. (2007). Annexin 1 cleavage in activated neutrophils: a pivotal role for proteinase 3. *J. Biol. Chem.* 282 (41), 29998–30004. doi:10.1074/jbc.M702876200

Vong, L., Ferraz, J. G., Dufton, N., Panaccione, R., Beck, P. L., Sherman, P. M., et al. (2012). Up-regulation of Annexin-A1 and lipoxin A(4) in individuals with ulcerative colitis may promote mucosal homeostasis. *PLoS One* 7 (6), e39244. doi:10.1371/journal.pone.0039244

Wada, K., Nakajima, A., and Blumberg, R. S. (2001). PPARγ and inflammatory bowel disease: a new therapeutic target for ulcerative colitis and crohn's disease. *Trends Mol. Med.* 7 (8), 329–331. doi:10.1016/s1471-4914(01)02076-7

Wang, L., Ray, A., Jiang, X., Wang, J. Y., Basu, S., Liu, X., et al. (2015). T regulatory cells and B cells cooperate to form a regulatory loop that maintains gut homeostasis and suppresses dextran sulfate sodium-induced colitis. *Mucosal Immunol.* 8 (6), 1297–1312. doi:10.1038/mi.2015.20

Wang, H., Zhu, Q. W., Ye, P., Li, Z. B., Li, Y., Cao, Z. L., et al. (2012). Pioglitazone attenuates myocardial ischemia-reperfusion injury via up-regulation of ERK and COX-2. *Biosci. Trends* 6 (6), 325–332. doi:10.5582/bst.2012.v6.6.325

Williams, S. L., Milne, I. R., Bagley, C. J., Gamble, J. R., Vadas, M. A., Pitson, S. M., et al. (2010). A proinflammatory role for proteolytically cleaved annexin A1 in neutrophil transendothelial migration. *J. Immunol.* 185 (5), 3057–3063. doi:10.4049/jimmunol.1000119

Lewis, J. D., Lichtenstein, G. R., Deren, J. J., Sands, B. E., Hanauer, S. B., Katz, J. A., et al. (2008). Rosiglitazone for active ulcerative colitis: a randomized placebo-controlled trial. *Gastroenterology* 134 (3), 688–695. doi:10.1053/j.gastro.2007.12.012

Li, L., Gao, P. J., Xi, R., Wu, C. F., Zhu, D. L., Yan, J., et al. (2008). Pioglitazone inhibits homocysteine-induced migration of vascular smooth muscle cells through a peroxisome proliferator-activated receptor gamma-independent mechanism. *Clin. Exp. Pharmacol. Physiol.* 35 (12), 1471–1476. doi:10.1111/j.1440-1681.2008.05025.x

Lloyd, K., Papoutsopoulou, S., Smith, E., Stegmaier, P., Bergey, F., Morris, L., et al. (2019). Using systems medicine to identify a therapeutic agent with potential for repurposing in Inflammatory Bowel Disease. *bioRxiv*

Xu, F., Dahlhamer, J. M., Zammitti, E. P., Wheaton, A. G., and Croft, J. B. (2018). Health-risk behaviors and chronic conditions among adults with inflammatory bowel disease—united states, 2015 and 2016. *MMWR Morb. Mortal. Wkly. Rep.* 67 (6), 190. doi:10.15585/mmwr.mm6706a4

Chassaing, B., Aitken, J. D., Malleshappa, M., and Vijay-Kumar, M. (2014). Dextran sulfate sodium (DSS)-induced colitis in mice. *Curr. Protoc. Im.* 104, 15.25.1–15.25.14. doi:10.1002/0471142735.im1525s104

Yamamoto-Furusho, J. K., Penaloza-Coronel, A., Sanchez-Munoz, F., Barreto-Zuniga, R., and Dominguez-Lopez, A. (2011). Peroxisome proliferator-activated receptor-gamma (PPAR-gamma) expression is downregulated in patients with active ulcerative colitis. *Inflamm. Bowel Dis.* 17 (2), 680–681. doi:10.1002/ibd.21322

Zamilpa, R., Lopez, E. F., Chiao, Y. A., Dai, Q., Escobar, G. P., Hakala, K., et al. (2010). Proteomic analysis identifies *in vivo* candidate matrix metalloproteinase-9 substrates in the left ventricle post-myocardial infarction. *Proteomics* 10 (11), 2214–2223. doi:10.1002/pmic.200900587

Zhang, A., Reid, R. C., Lohman, R. J., Sweet, M. J., Fairlie, D. P., and Iyer, A. (2017). An HDAC6 inhibitor confers protection and selectively inhibits B-cell infiltration in DSS-induced colitis in mice. *J. Pharmacol. Exp. Ther.* 360 (1), 140–151. doi:10.1124/jpet.116.236711

Zhou, X., Li, T., Chen, Y., Zhang, N., Wang, P., Liang, Y., et al. (2019). Mesenchymal stem cellderived extracellular vesicles promote the *in vitro* proliferation and migration of breast cancer cells through the activation of the ERK pathway. *Int. J. Oncol.* 54 (5), 1843–1852. doi:10.3892/ijo.2019.4747

Zou, Z., Zuo, D., Yang, J., and Fan, H. (2016). The ANXA1 released from intestinal epithelial cells alleviate DSS-induced colitis by improving NKG2A expression of Natural Killer cells. *Biochem. Biophys. Res. Commun.* 478 (1), 213–220. doi:10.1016/j.bbrc.2016.07.066

Conflict of Interest: The authors declare that the research was conducted in the absence of any commercial or financial relationships that could be construed as a potential conflict of interest.

Co-autoria 2021

frontiers in Immunology

ORIGINAL RESEARCH
published: 17 September 2021
doi: 10.3389/fimmu.2021.714138

Formyl Peptide Receptors and Annexin A1: Complementary Mechanisms to Infliximab in Murine Experimental Colitis and Crohn's Disease

Marina de Paula-Silva[1,2], Gustavo Henrique Oliveira da Rocha[1], Milena Fronza Broering[1], Maria Luiza Queiroz[3], Silvana Sandri[1], Rodrigo Azevedo Loiola[1], Sonia Maria Oliani[4], Andrea Vieira[3], Mauro Perretti[2] and Sandra Helena Poliselli Farsky[1]

[1] Department of Clinical and Toxicological Analyses, University of São Paulo (USP), São Paulo, Brazil, [2] Centre for Biochemical Pharmacology, The William Harvey Research Institute, Barts and The London School of Medicine, Queen Mary University of London (QMUL), London, United Kingdom, [3] Gastroenterology Service, Irmandade da Santa Casa de Misericórdia de São Paulo, São Paulo, Brazil, [4] Department of Biology, São Paulo State University (UNESP), São José do Rio Preto, São Paulo, Brazil

OPEN ACCESS

Edited by:
Attila Mócsai, Semmelweis University, Hungary

Reviewed by:
Miguel Quiros, University of Michigan, United States
Áron Pánczél, Semmelweis University, Hungary

***Correspondence:**
Sandra Helena Poliselli Farsky
sfarsky@usp.br

Specialty section:
This article was submitted to Autoimmune and Autoinflammatory Disorders, a section of the journal Frontiers in Immunology

Received: 24 May 2021
Accepted: 16 August 2021
Published: 17 September 2021

Citation:
de Paula-Silva M, da Rocha GHO, Broering MF, Queiroz ML, Sandri S, Loiola RA, Oliani SM, Vieira A, Perretti M and Farsky SHP (2021) Formyl Peptide Receptors and Annexin A1: Complementary Mechanisms to Infliximab in Murine Experimental Colitis and Crohn's Disease. Front. Immunol. 12:714138. doi: 10.3389/fimmu.2021.714138

Non-responsiveness to anti-TNF-α therapies presents relevant rates in inflammatory bowel disease patients, presenting the need to find biomarkers involved in therapeutic efficacy. Herein, we demonstrate that higher levels of colonic formyl peptide receptor 1 and annexin A1 correlate with histological recovery in Crohn's disease patients under remission. Using the dextran sulfate sodium colitis model in mice, we suggest that infliximab induces annexin A1 expression and secretion in activated intestinal leukocytes. Conversely, this mechanism might stimulate epithelial formyl peptide receptors, inducing wound healing and consequent histological remission. Our data indicate that assessing intestinal expressions of formyl peptide receptors and annexin A1 might provide precious information on the disease activity and responsiveness to infliximab in inflammatory bowel disease patients.

Keywords: biomarkers, formyl peptide receptor, annexin A1, infliximab, Crohn's disease, dextran sodium sulfate

INTRODUCTION

Inflammatory bowel diseases (IBDs), mainly Crohn's disease (CD) and ulcerative colitis (UC), are characterized by severe gastrointestinal inflammation (1). Biological therapies, such as monoclonal antibodies and infliximab (IFX), are very effective in inducing remission for moderate-to-severe IBDs (2, 3). By binding soluble and transmembrane tumor necrosis factor alpha (TNF-α), IFX attenuates inflammation and decreases the need for surgery (2, 4, 5). However, side effects and non-responsiveness illuminate the relevance of validating biomarkers to assess therapeutic efficacy (6, 7).

We previously described a possible relationship between the response to IFX and the expression of annexin A1 (AnxA1) in mice with experimental colitis (8). AnxA1 is a resolutive mediator in human and experimental conditions such as cardiovascular diseases (9, 10), multiple sclerosis (11),

and rheumatoid arthritis (12). AnxA1 is produced by epithelial cells and secreted by infiltrating leukocytes in IBD patients (13). Local expression of AnxA1 is pivotal to tissue recovery in CD and experimental colitis (14–16). Recently, it has been suggested that low levels of AnxA1 in CD support the uncontrolled inflammation that perpetuates the disease and that differential expressions of AnxA1 might allow the identification of disease severity patterns (14, 17). After cell activation, AnxA1 is mobilized to the membrane, where it is able to trigger anti-inflammatory pathways through formyl peptide receptors (FPRs) (18). FPRs have been increasingly studied in IBD as they participate in antimicrobial and inflammatory processes. FPR expression in the gut correlates with pathology during acute inflammation, but plays a protective role in the chronic phases (19). FPR1 is a wound closure mediator (20, 21), whereas FPR2 induces mucosal healing by regulating the traffic of leukocytes into the inflamed tissue (22, 23).

This background provides valuable information about the roles of AnxA1 in IBD; however, only a couple of studies—including ours—have addressed the involvement of AnxA1 in the efficacy of IFX (8, 14). Also, none has explored the potential participation of the AnxA1–FPR axis. Herein, we describe some IFX mechanisms that are affected by the AnxA1–FPR axis and seek to explain how it could mediate distinct responses to anti-TNF-α.

MATERIALS AND METHODS

Patient Approach and Ethics Statement

CD patients from the Santa Casa School of Medical Sciences (São Paulo, Brazil) and donors with no IBD history willingly donated blood (12 ml). Medical records and paraffinized colon biopsies provided the CD Activity Index (CDAI) (24) and microscopic grading (25). This study was conducted in accordance with the Declaration of Helsinki and the ethics boards from Santa Casa and the University of São Paulo (protocol #07100819.3.0000.0067). Written consent was obtained.

Criteria for Patient Enrollment

The diagnosis of CD for patients participating in this study took into account endoscopic, histological, and clinical criteria assessed and interpreted by members of the medical staff from the Santa Casa School of Medical Sciences. Individuals younger than 18 years and/or with a diagnosis of an infectious disease (such as tuberculosis, chlamydia, and the common flu) were excluded.

Participants were divided into groups as follows:

Blood donors: Healthy individuals with no prior history of IBD provided control samples of blood matching the average age, gender, and ethnicity from CD groups. "Remission patients" reached clinical remission upon IFX treatment, while "Failure patients" were refractory to previous therapies and were not responding clinically to IFX at the moment of blood donation. One untreated CD patient provided active disease parameters and was receiving other medications (including immunosuppressants and corticosteroids), but not IFX.

Biopsy donors: Remission patients reached clinical and histological remission when treated with IFX. The Failure group was composed of patients who did not present improvement of clinical parameters and histological homeostasis upon IFX. "CD untreated" individuals were those with an active disease despite treatment administration of other medications (including immunosuppressants and corticosteroids), but not IFX.

It should be noted that all patients enrolled in this study had previously received or were receiving other medication classes at the time of our sample collection. The absence/interruption of responsiveness to other therapies followed by remission or non-remission upon IFX was the defining parameter for separating the Remission and Failure groups, respectively. Clinical parameters (mean and range of age, gender, and concomitant

TABLE 1 | Characteristics from CD[a] patients and healthy donors.

Parameters	Healthy donors	Blood			Tissue		
		CD patients					
		Untreated	Remission	Failure	Untreated	Remission	Failure
Average age (min.–max.)	32 (23–41)	24	35 (19–50)	39 (19–63)	28 (19–49)	43 (17–44)	38 (61–16)
Standard deviation (age)	10.11	0.00	12.14	14.65	13.96	3.51	31.81
Females	3	1	8	5	3	2	0
Males	2	0	4	7	1	1	2
Total	5	1	12	11	4	3	2
Medications							
Corticosteroids	–	–	–	3 (27.3%)	1 (25%)	–	1 (50%)
Mesalazine	–	1 (100%)	3 (25%)	6 (54.6%)	2 (50%)	2 (66.6%)	1 (50%)
Azathioprine	–	–	3 (25%)	4 (36.4%)	3 (75%)	–	2 (100%)
Anti-diarrheic	–	–	1 (8.3%)	1 (9.1%)	–	1 (33.3%)	–
Antidepressants	2 (40%)	–	2 (16.6%)	–	–	1 (33.3%)	1 (50%)
Antibiotics	–	–	–	2 (18.2%)	1 (25%)	–	–
Hepatics and pancreatics	–	–	–	3 (27.3%)	1 (25%)	–	1 (50%)
Hepatics and Hidrocortisone pre-IFX[b]	–	–	–	1 (9.1%)	–	–	–
Other	2 (40%)	1 (100%)	2 (16.6%)	4 (36.4%)	2 (50%)	1 (33.3%)	2 (100%)

[a]*CD, Crohn's disease;* [b]*IFX, infliximab.*

medications) from the Untreated CD, CD+IFX Remission, or CD+IFX Failure groups are presented in **Table 1**.

Isolation of Leukocytes and Detection of AnxA1 in the Blood of CD Patients

Blood from healthy donors ($n = 5$) and CD patients treated with IFX ($n = 23$) or not ($n = 1$) was used to isolate the following:

Plasma AnxA1: AnxA1 was detected in plasma samples using an ELISA kit (MyBioSource, San Diego, CA, USA).

Leukocytes: NH_4Cl (0.13 M) was added to the remaining cell fraction to lysate erythrocytes. Pellets were fixed in 1% paraformaldehyde (PFA) and incubated with anti-FPR1 (PE, R&D Systems, Minneapolis, MN, USA) and anti-FPR2 (FITC, Bioss, Woburn, MA, USA) antibodies. Readings were conducted using a BD Accuri Flow Cytometer (BD Biosciences, Franklin Lakes, NJ, USA) to acquire 10,000 events/sample. Positive populations were determined by labeling for each antibody separately.

Detection of AnxA1, FPR1 and FPR2 in CD Biopsies

Paraffin-embedded colon biopsies from CD untreated ($n = 4$) and treated positive ($n = 3$) or negative ($n = 2$) responders to IFX were permeabilized (0.01% Triton), retrieved (sodium citrate buffer), and blocked (20% fetal bovine serum, FBS). Samples were incubated with mouse anti-FPR1 (1:25, clone 5F1; BD Biosciences), anti-FPR2 (1:10, clone 2D8; Sigma-Aldrich, St. Louis, MO, USA), or anti-AnxA1 (1:50, clone 1B, 10 µg/ml). Incubation with 20% FBS provided the negative control. After incubation with anti-mouse Alexa Fluor 488 secondary antibody (1:200; Thermo Fisher, Waltham, MA, USA) and DAPI, the slides were mounted and five regions of interest (ROIs) per slide were photographed on a confocal microscope (Zeiss LSM800). Before acquiring images, the settings for gain, offset, and exposure time were adjusted based on the reaction control and standardized for each ROI from the stained samples. Acquired composite images (.czi format) were imported to Fiji (ImageJ Software, Bethesda, MD, USA) and split into blue and green channels. For densitometric analysis, the green channel (Alexa Fluor 488) was selected and modified to be displayed with a gray filter. Background pixel averages were then subtracted from the image pixels of interest to correct uneven illumination with the aid of the "Process > Math > Subtract" process. Fluorescence measures were performed manually by the selection of positive regions; average values were expressed in arbitrary units.

Ethics Statement and Animals

C57BL6 wild-type (WT) or AnxA1-null mice ($AnxA1^{-/-}$), males, 8–10 weeks old, were used to perform colitis. WT C57BL6, males, 16–18 weeks old, were used to provide intestinal immune cells to *ex vivo* experiments. Mice were obtained from the Federal University of São Paulo Animal House (Brazil), kept in 12:12-h light/dark cycle, and provided with food and water *ad libitum*. Experiments were performed in accordance with the Brazilian laws of protection and approved by the Committee on Ethics of Animal Experiments from the University of São Paulo.

Colitis Model and Clinical Analysis

Fresh 2% dextran sodium sulfate (DSS; weight/volume, 40 kDa; Dextran Products Limited, Scarborough, Ontario, Canada) was added to the drinking water of WT and $AnxA1^{-/-}$ mice (day 0) and replenished every other day up to day 6 (26). Control and non-treated DSS mice received vehicle (sterile saline 0.9% + DMSO 0.5%) intraperitoneally (i.p.) on days 0–9. DSS-treated groups received i.p. IFX (1 mg/kg; Remicade® Janssen-Cilag, Buenos Aires, Argentina) on day 1 and/or FPR antagonist Boc-2 (10 µg/kg; N-t-BOC-MET-LEU-PHE, MP Biomedicals, Irvine, CA, USA) on days 0–9. Body weight, diarrhea, and rectal bleeding were scored daily to provide the Disease Activity Index (DAI). On day 10, mice were euthanized by overexposure to nasal anaesthesia [isoflurane; 2-chloro-2-(difluoromethoxy)-1,1,1-trifluoro-ethane].

Dosage of Tissue MMP-9

Samples of medium colon were homogenized in RIPA buffer containing a protease inhibitor (1:100; Thermo Fisher) in an Ultra-Turrax homogenizer (T10-Basic-IKA). After 20 min on ice, the tissue debris were removed and matrix metalloproteinase 9 (MMP-9) was detected by ELISA (R&D Systems).

Histological Analysis *In Vivo*

Distal colons were fixed in 4% buffered PFA, dehydrated, and embedded in paraffin. Samples were analyzed using high-power objectives on the Imager.A2 Zeiss microscope (Zeiss, Oberkochen, Germany).

Histopathology

Histological grading was based on a previous report (8). The following features were analyzed by a blinded histologist: changes on crypts and histoarchitecture, edema, ulceration and immune cells at the epithelium, lamina propria, or submucosa. Grades of 0, 1, 2, 3, and 4 were respectively attributed to normal, mild, mild–moderate, moderate–severe, and severe conditions. Results were expressed as the mean of total grading.

Immunohistochemistry

After permeabilization (Triton 0.01%) and antigen retrieval (sodium citrate buffer, 10 mM, pH 6.0), peroxidase was inactivated with 3% hydrogen peroxide. Samples were blocked with 10% Tris-buffered saline–bovine serum albumin and incubated with the anti-AnxA1 antibody (1:500; Thermo Fisher). The reaction control was incubated with a blocking solution. The slides were finalized with an anti-rabbit horseradish peroxidase (HRP) antibody (Abcam, Cambridge, UK), 3,3-diaminobenzidine (DAB; Thermo Fisher), and hematoxylin counterstaining.

Immunofluorescence

Permeabilized samples were retrieved in sodium citrate buffer and blocked with 20% FBS. Antibodies were incubated overnight (4°C): polyclonal mouse anti-β-actin (1:200) and rabbit anti-villin (1:50; Abcam). After secondary antibodies (anti-mouse DyLight 549 and anti-rabbit FITC, 1:200; Vector Laboratories, Burlingame, CA, USA), the nuclei were stained with DAPI.

Isolation of Leukocytes From Lamina Propria and Flow Cytometry

Leukocytes from proximal colonic lamina propria were isolated after washes with 2 mM EDTA and digestion with collagenase V from *Clostridium histolyticum* (1 mg/ml; Sigma-Aldrich) (26). The cells were washed through 40-µm strainers (Corning, Corning, NY, USA) and stained with CD4 (FITC) and CD25 (APC) (1:100; BD Biosciences). Positive populations were determined by labeling with single antibodies. A minimum of 10,000 events per sample were acquired on a BD Accuri Flow Cytometer. The results were expressed as percentages of positive cells normalized by controls from each experiment.

Isolation of Colonic Lamina Propria Leukocytes and *Ex Vivo* Treatments

After euthanasia by overexposure to isoflurane, colons from C57BL6 mice were opened longitudinally and washed with supplemented phosphate-buffered saline (10,000 µg/ml penicillin/streptomycin and 50 µg/ml gentamycin). Under a sterile hood, the tissues were fragmented, washed in Hank's salt solution buffer without calcium/magnesium for 20 min (twice), and digested with collagenases from *C. histolyticum* (types II and IV, 0.5 mg/ml; Gibco, Waltham, MA, USA). The digested tissue was washed twice through 40-µm strainers (Corning) and the pellets were counted and resuspended at the Roswell Park Memorial Institute (RPMI + 1% FBS). Cells were seeded in a 96-well plate (2×10^5/well) and treated with 200 ng/ml lipopolysaccharide (LPS; Sigma-Aldrich) 30 min before IFX (0.1, 1.0, or 10.0 µg/ml). Controls were untreated or treated with those IFX doses. After 24 h, the supernatants were collected to dose secreted AnxA1 (MyBioSource) according to the manufacturer's instructions.

Statistical Analysis

To determine the parametric or non-parametric distributions, we used the Kolmogorov–Smirnov test. ANOVA followed by Tukey's was performed for parametric tests, and Kruskal–Wallis followed by Dunn's post-test was performed for non-parametric tests. To compare the two groups, we applied unpaired (single measures) or paired *t*-test (repeated measures). Pearson's correlation was performed for correlation analysis, providing the correlation coefficient r and the coefficient of determination R^2. Probabilities with $p < 0.05$ were considered significant. The results were expressed as the mean ± standard deviation (SD; human samples, individual variabilities) or standard error of the mean (SEM; *in vivo*/*ex vivo* assays, group variability). All statistical assessments were conducted using GraphPad Prism® software, version 9.1.2 (San Diego, CA, USA).

RESULTS

AnxA1 and FPR1 Are Differentially Expressed in the Colon of CD Patients Responsive to IFX

Recently, it has been suggested that differential expressions of AnxA1 might allow the identification of disease severity patterns in IBD (14, 17). Thus, we proposed screening the expression patterns of AnxA1 and its receptors, FPR1 and FPR2, in CD biopsies of colons from untreated and IFX-treated patients who either went into remission or did not. Information about the healthy volunteers and CD patients are listed in **Table 1**.

Hematoxylin/eosin-stained colon biopsies revealed ulcers, crypt alterations/abscesses, and prominent inflammatory infiltrates in untreated and IFX Failure patients (**Supplementary Figures 1A, C**). Based on the grading system (**Supplementary Table 1**), we confirmed lower histological damage for remittent (**Supplementary Figure 1B** and **Figure 1F**) rather than untreated CD individuals.

Subsequently, FPR1, FPR2, and AnxA1 were detected on the colon biopsies using confocal microscopy (**Figure 1**). For those three markers, the *Z*-scores were above the population mean for the IFX-induced remission group, contrasting with the lower levels in the untreated and IFX Failure groups (**Figure 1A**). Despite the increased fluorescence detected for FPR1 (**Figures 1C, G**) and FPR2 (**Figures 1D, H**) in remittent patients, only AnxA1 was significantly higher than that in the untreated group (**Figures 1E, I**). Epithelial cells from barrier, crypts, and leukocytes were the major sources of FPR1, FPR2, and AnxA1. Furthermore, colonic FPR1 and AnxA1 expressions presented a strong negative correlation with the histological grading (**Figures 1J, L**), which means that the decrease of these markers is associated with more tissue damage. For FPR2, a moderate correlation was detected ($r = -0.5355$), but this was not enough to characterize a significant association (**Figure 1K**). Based on this, we presume that the upregulation of colonic FPR1 and AnxA1 in CD positive responders to IFX provides a marker of differential expression for therapy efficacy.

Using the patients' medical histories, we calculated the CDAI (**Supplementary Table 2**). Despite the different intensities of disease activity among patients, no patterns for circulating FPR1, FPR2 (leukocytes), or AnxA1 (plasma) were observed for the healthy, remission, or failure groups (**Supplementary Figure 2A**). As expected, CDAI was significantly higher in IFX-unresponsive patients than in remission patients (**Supplementary Figure 2B**). Furthermore, FPR1, FPR2, and AnxA1 in blood did not correlate with CDAI, indicating that patients' circulating levels might not be reliable biomarkers for remission or failure after IFX treatment (**Supplementary Figures 2C–H**).

FPR Signaling Complements the Beneficial Effects of IFX on Colitis Symptomatology and Tissue Damage

After detecting the correlations between high expressions of FPR1/AnxA1 and histological recovery in CD, we wondered how the modulation of these markers would impact resolution after IFX. We have previously demonstrated the failure of IFX in treating acute colitis using AnxA1-null Balb/c mice (8). To explore the mechanisms involved in the efficacy of IFX, we performed DSS-induced colitis in WT and AnxA1$^{-/-}$ C57BL6 mice and followed up to the late phase of the disease (**Figure 2** and **Supplementary Figures 3, 4**). As expected, colitis induced significant weight loss and increased the DAI in both WT (**Figures 2A–C**) and AnxA1$^{-/-}$ strains (**Supplementary**

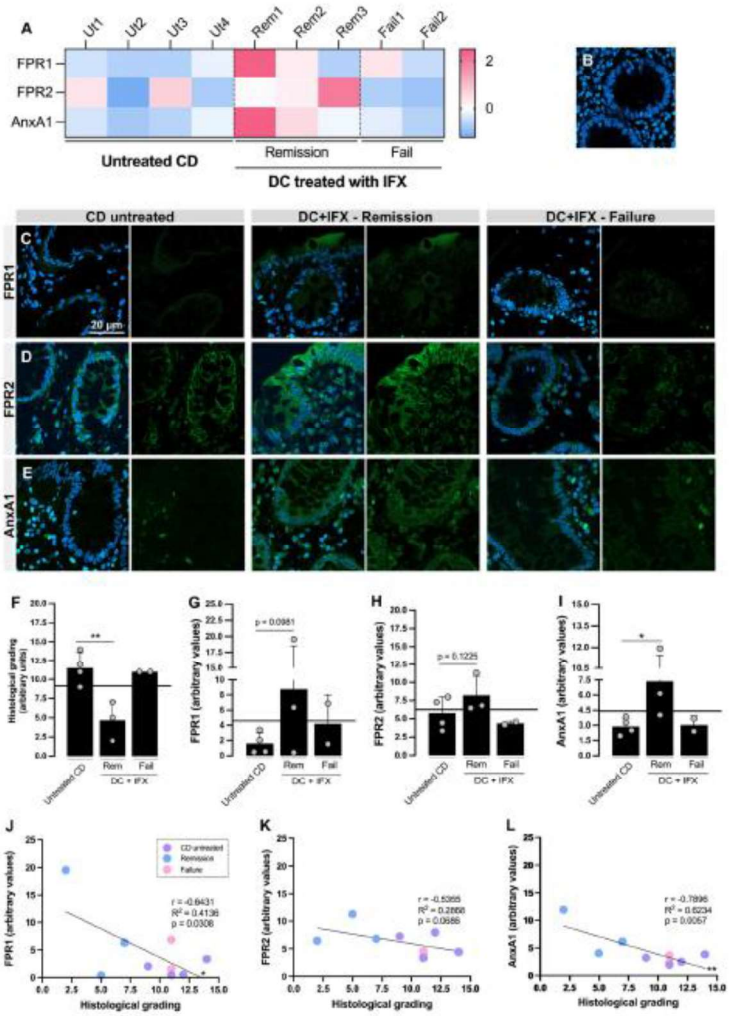

FIGURE 1 | Formyl peptide receptor 1 (FPR1), FPR2, and annexin A1 (AnxA1) are differentially expressed in the colon of Crohn's disease (CD) responders to infliximab (IFX) and correlate with histological homeostasis. **(A)** Heatmap based on the *Z*-scores of FPR1, FPR2, and AnxA1 expression values in the colon. **(B–E)** Confocal imaging: negative control of reaction **(B)**, FPR1 **(C)**, FPR2 **(D)**, and AnxA1 **(E)** tissue staining. Embedding, paraffin; sections, 3 µm. *Bar*, 20 µm. **(F)** Histological grading, calculated based on **Supplementary Table 1**. **(G–I)** Densitometric analysis of fluorescence: FPR1 **(G)**, FPR2 **(H)**, and AnxA1 **(I)**. **(J–L)** Correlation analysis between histological grading of biopsies and fluorescence intensity of staining: FPR1 **(J)**, FPR2 **(K)**, and AnxA1 **(L)**. $^{*}p < 0.05$, $^{**}p < 0.01$. $n = 4$ (CD untreated); $n = 3$ (Remission); $n = 2$ (Failure). Results are expressed as the mean ± SD.

Figures 4A, B). Anatomic and microscopic alterations were also produced by DSS, including colon shortening, MMP-9 increase, ulcers, altered crypt, crypt abscesses, vacuolar hydropic degeneration, submucosal edema, and mucosal/submucosal massive inflammatory infiltrates (**Figures 2D–H** and **Supplementary Figures 4E–I**). IFX attenuated body weight loss (days 9 and 10; **Figure 2A**) and DAI during the late phase of the disease (day 8; **Figures 2B, C**) in WT mice. Except for

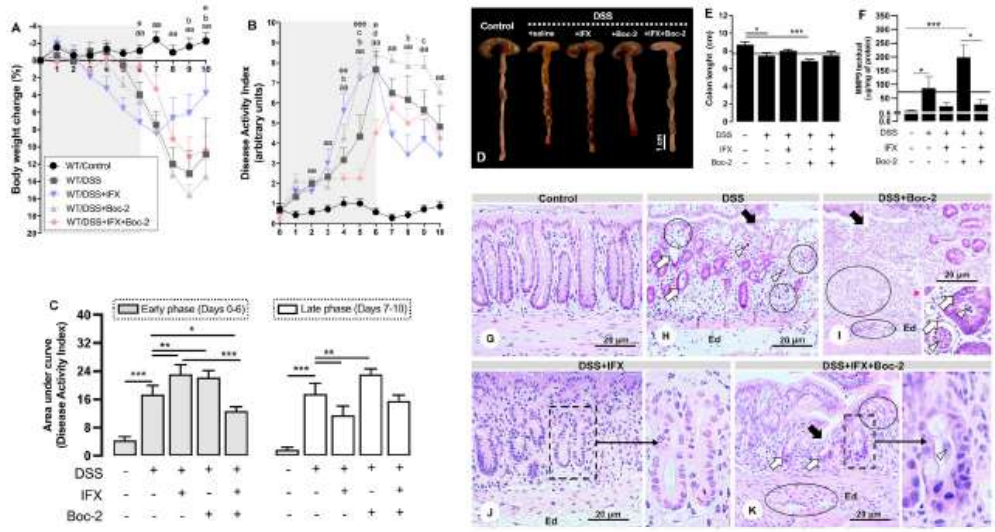

FIGURE 2 | Formyl peptide receptor (FPR) blockade impairs clinical and histological improvements induced by infliximab (IFX) during colitis. **(A)** Loss of body weight. **(B)** Disease Activity Index (DAI). **(C)** Area under the curve from DAI, early and late phases. **(D, E)** Colon length and anatomic changes. **(F)** Colonic MMP-9 levels. Mean of all samples (*continuous lines*). *Bar*, 1 cm. $^{aa}p < 0.01$ (DSS *vs.* Control); $^{b}p < 0.05$ (DSS+IFX *vs.* DSS); $^{c}p < 0.05$ (DSS+Boc-2 *vs.* DSS); $^{d}p < 0.05$ (DSS+IFX+Boc-2 *vs.* DSS); $^{a}p < 0.05$, $^{aa}p < 0.01$, $^{aaa}p < 0.001$ (DSS+IFX+Boc-2 *vs.* DSS+IFX). $^{*}p < 0.05$, $^{**}p < 0.01$, $^{***}p < 0.001$. $n = 4$–6 mice/group. Results are expressed as the mean ± SEM. **(G–K)** Histopathology in wild-type (WT) groups. Ulcer (*black arrows*), altered crypts (*white arrows*), crypt abscesses (*white arrowheads*), edema (*Ed*), and inflammatory infiltrate (*circles*). Staining, hematoxylin–eosin; embedding, paraffin; sections, 3 µm. *Bars*, 20 µm.

some remaining infiltrated leukocytes and submucosal edema, the colonic histological architecture was protected by IFX (**Figure 2J**). These improvements were not only absent in the AnxA1$^{-/-}$ group upon IFX treatment (**Supplementary Figures 4A, B, J**), but anti-TNF-α seemed to be harmful without endogenous AnxA1 as well: a 50% mortality rate was recorded (**Supplementary Figure 4C**). AnxA1-deficient mice had significant colon shortening (**Supplementary Figures 4E, F**) and a 200- to 300-fold increase in tissue MMP-9 with or without IFX treatment (**Supplementary Figure 4G**). Moreover, AnxA1$^{-/-}$/DSS+IFX mice had less intestinal T regulatory lymphocytes than did the mice in the respective WT group and the untreated group (AnxA1$^{-/-}$/DSS), reaffirming the relevance of AnxA1 to the downregulation of inflammation even when TNF-α is being blocked by IFX (**Supplementary Figure 4D**).

For the next step, we blocked the AnxA1 receptors, FPRs, to assess their potential involvement in the effects of IFX. The FPR blockade, by itself, confirmed their well-known role in wound healing (15, 27). FPR neutralization was detrimental to the clinical parameters in both early and late phases of disease (**Figures 2A–C**), intensified colon shortening (**Figures 2D, E**), and increased MMP-9 (**Figure 2F**). Microscopically, the FPR blockade with Boc-2 worsened the DSS damage, especially with regard to epithelial/glandular loss and infiltrated leukocytes (**Figure 2I**). When combined with IFX, blocking FPRs was detrimental to the clinical conditions in the late phase as the beneficial effects of IFX on body weight and DAI were lost (days 9 and 10 and day 8 in **Figures 2A, B**, respectively) (**Figure 2C**). Although the colon length and MMP-9 from IFX-treated mice were not affected by Boc-2 (**Figures 2D, E**), the cecum very consistently assumed a distorted morphology and paleness for this group (**Figure 2D**).

Finally, the histological parameters were analyzed. IFX-mediated preservation of the colonic histoarchitecture was partially impaired by an FPR blockade, with the presence of immune cells in the mucosa and punctual but persistent ulcerations (**Figure 2K**). The clearest histological alteration in this group was poor crypt recovery (details in **Figure 2K**). For this reason, we proceeded to explore the effects of halting the signaling through FPRs for the regeneration of crypts after IFX treatment.

Blocking FPRs Compromises the Effects of IFX on Crypt Regeneration

The relevance of FPRs for crypt regeneration was confirmed by structural protein immunostaining (**Figure 3**). In control mice, β-actin revealed the cylindric shape of enterocytes (**Figure 3A**, a1) with villin expressed on the apical surfaces of cells (**Figure 3A**, a2). A similar pattern was observed on crypts

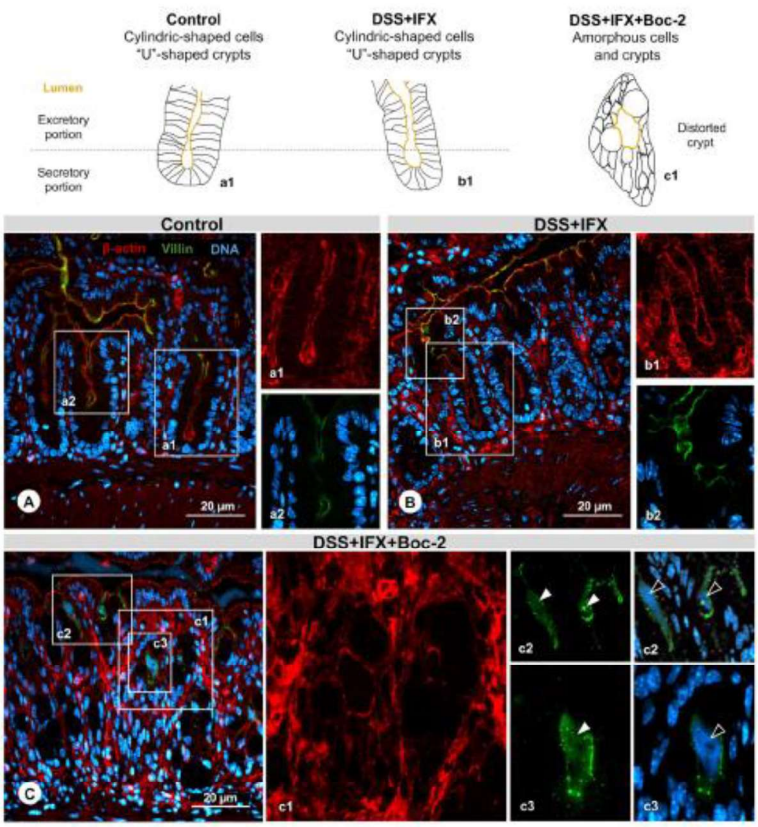

FIGURE 3 | Crypt regeneration mediated by infliximab (IFX) requires formyl peptide receptor (FPR) signaling. **(A)** Control: cylindrical-shaped cells forming a U-shaped crypt revealed by β-actin staining (*a1*, *red*). Presence of villin (*a2*, *green*) in the inner surface from the excretory part of the crypt lumen. Representation of a normal structure. **(B)** DSS+IFX: preserved crypt morphology resembling the control condition (*b1* and *b2*). **(C)** DSS+IFX+Boc-2: defects in crypt closure (*c1*); presence of villin (*c2* and *c3*, *white arrowheads*); and DNA residue (*c2* and *c3*, *black arrowheads*) in the crypt lumen. $n = 4$–6 mice/group. Embedding, paraffin; sections, 3 µm. Bars, 20 µm.

from DSS+IFX mice (**Figure 3B**, b1 and b2). In both groups, it is possible to identify the secretory and excretory portions from the mucosal glands, forming a U-shaped structure with a centered vertical lumen that opens to the intestinal wall, where the secretions produced by crypts are liberated.

Upon FPR inactivation, with or without IFX treatment, crypt cells assumed a deformed morphology lacking cylindric limits. The elongated shape from crypts gave place to an amorphous structure, many times with the lumen turned into a round form that was no longer connected with the epithelium surface (**Figure 3C**, c1). In this space, we observed residues of the shed villin (**Figure 3C**, *c2* and c3, green) that co-localized with DNA (**Figure 3C**, c2 and c3, blue). FPRs were associated with epithelial repair, migration, and wound healing before, but our results suggest that these roles are also required for the intestinal barrier homeostasis mediated by IFX. Considering that AnxA1 is an important FPR agonist and a pivotal mediator of tissue repair in IBD, our final step was to assess the possible kinds of interplay among AnxA1 expression, FPR activation, and IFX efficacy.

IFX Induces AnxA1 Expression and Secretion by Tissue Leukocytes During Inflammation

Intracellular and FPR-binding AnxA1 mediate inflammation resolution and tissue repair on experimental colitis (8, 28). In our model, we assessed the expression patterns for endogenous AnxA1 in the colon (**Figure 4**). The reaction control confirmed specificity (**Figure 4J**).

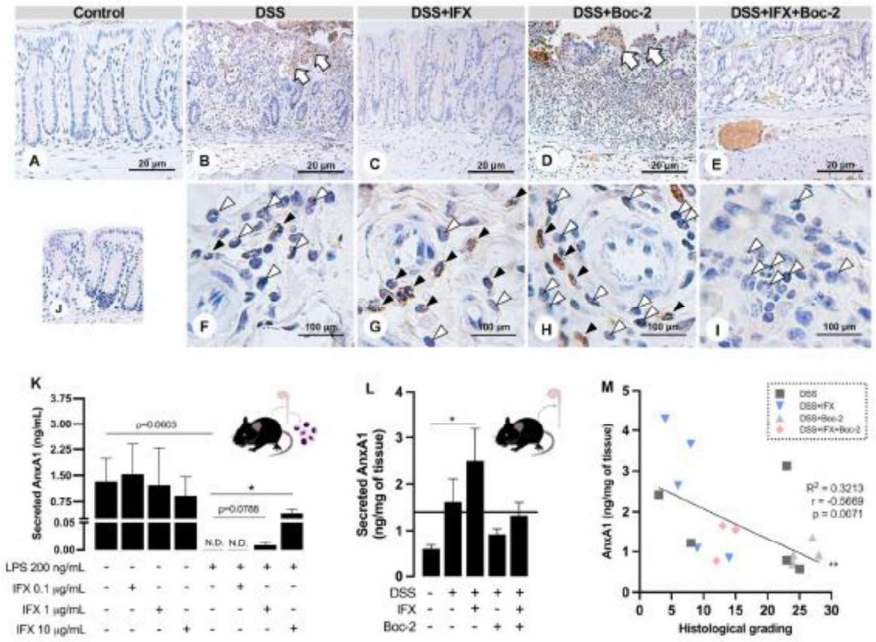

FIGURE 4 | Infliximab (IFX) induces annexin A1 (AnxA1) expression and secretion by infiltrated leukocytes during inflammation. **(A–E)** AnxA1 expression in the epithelial barrier from wild-type (WT) mice colon. AnxA1 concentrated on the wound bed (*white arrows*). **(F–I)** Immunostaining for AnxA1 in submucosal leukocytes. Tissue leukocytes positive (*black arrowheads*) or negative (*white arrowheads*) for AnxA1 staining. **(J)** Reaction control. Counterstaining, hematoxylin; embedding, paraffin; sections, 3 µm. *Bars*, 20 µm **(A–E)** and 100 µm **(F–I)**. **(K)** AnxA1 secreted by lamina propria leukocytes cultured *ex vivo*. **(L)** AnxA1 secreted by colon explants in culture. **(M)** Moderate negative correlation between AnxA1 secreted into the tissue and histological grading. *N.D.*, non-detected. $^{*}p < 0.05$, $^{**}p < 0.01$. n = 3–4 mice/group **(K)**; n = 4–6 mice/group **(L)**. Results are expressed as the mean ± SEM.

In the control epithelium, AnxA1 was weakly detected (**Figure 4A**). Colitis upregulated AnxA1 in the damaged epithelium from the DSS and DSS+Boc-2 groups (**Figures 4B, D**). Mice treated with IFX, with or without FPR signaling, presented epithelial AnxA1 similar to the control group (**Figures 4C, E**). In turn, AnxA1 was weakly detected in tissue leukocytes in non-treated colitis (**Figure 4F**). After IFX, a high number of infiltrated AnxA1-positive immune cells were observed (**Figure 4G**). AnxA1 was also detected in leukocytes under Boc-2 (**Figure 4H**). Interestingly, in mice treated with IFX and Boc-2, most tissue leukocytes were negative for AnxA1 (**Figure 4I**).

Because the intracellular expression of AnxA1 was upregulated in tissue leukocytes upon IFX, we hypothesized that transmigrated immune cells could be important sources of AnxA1 for the inflamed tissue treated with this anti-TNF-α. Using LPS *in vitro* assays, we simulated an inflammatory response in immune cells isolated from the colon of naive mice. When treated with increasing concentrations of IFX (0.1, 1.0, and 10 µg/ml), we detected a dose-dependent augmentation in AnxA1 secretion to the milieu (**Figure 4K**). This phenomenon was reproduced in the DSS-induced colitis treated with IFX, as colon explant supernatants had increased levels of AnxA1 compared to the control group (**Figure 4L**). Finally, we observed a moderate negative correlation between the secreted AnxA1 and the grading for histological damage of the colon (**Figure 4M**). These results suggest that IFX induces AnxA1 expression and secretion by tissue leukocytes, and this mechanism is linked to tissue repair.

DISCUSSION

Previously, we reported the relevance of AnxA1 in the efficacy of IFX during acute colitis in female Balb/c mice (8). Here, we corroborate it using mice of different strain and sex and focusing on the late phase of disease. On biopsies from CD patients, we further confirm that IFX modulates AnxA1 in positive responders. Moreover, we describe FPR1 as a potential marker of tissue homeostasis after IFX treatment. Our results suggest that IFX stimulates activated intestinal leukocytes to express and

secrete AnxA1 to the inflamed milieu, where it is free to bind to FPRs and promote tissue repair (29).

Although biologicals are the most successful drug class at inducing remission among the therapies classically used to treat IBD (30), they still burden patients with heterogeneous outcomes, including hypersensitivity, allergies, lack of responsiveness, or progressive loss of efficacy over the lifetime (31). Even clinically remittent patients may present remaining mucosal inflammation associated with severe mucosal disease activity (32). In response to this, the follow-up protocol for treated patients proposes the assessment of histological remission as a more reliable tool to predict a sustained and steroid-free clinical remission, with lower need for hospitalization and surgery (33). Herein, we observed a marked expression of AnxA1 in the colon of CD patients who underwent remission after IFX. For AnxA1 and FPR1, high tissue levels correlated with lower histological damage. In a general manner, the literature on IBD suggests that AnxA1 secretion is evoked during the active disease. Failures in this mechanism contribute to a more severe and prolonged disease (26, 34). Similarly, therapeutic interventions have a better outcome when capable of increasing AnxA1 levels (8, 14). In the inflamed site, AnxA1 binding to FPRs mediates the resolution of inflammation and mucosal homeostasis (16, 28). The data we present here support the mechanisms described above. Moreover, they suggest that tissue FPR1 and AnxA1 could constitute useful tools for following up the disease activity and the efficacy of IFX in CD patients.

Mucosal inflammation begins with the opening of the epithelial barrier after injury, which allows the translocation of microbial agents. Once the commensal microbiota is detected by the immune cells that patrol the tissue, an inflammatory response is assembled to contain the spreading of bacteria to the blood and other tissues. However, an unbalanced inflammation feed-forwards tissue damage and increases bacterial translocation (35). Upon injury or death, column-shaped intestinal epithelial cells can lose contact with each other, assuming a flat morphology. The organism responds by triggering a proliferation of basal crypt cells and epithelial migration, promoting wound closure (36). By binding FPRs, full-length AnxA1 and its peptide, Ac2-26, stimulate the migration of epithelial cells and wound healing (15, 16). Ac2-26 binding to FPR1 induces oxidative inactivation of phosphatase and tensin homolog protein and protein tyrosine phosphatase-PEST, phosphorylating focal adhesion kinase and paxillin, consequently stimulating cells to migrate (15). Additionally, endogenous AnxA1 acts as an anchor between cytoplasmic β-actin and the plasma membrane, whereas the AnxA1–FPR2 axis inhibits RhoA GTPase activity, stabilizing the cytoskeleton (37). Our results confirmed that the lack of endogenous AnxA1 is very detrimental to the progression of experimental colitis: AnxA1$^{-/-}$ mice had much worse clinical and histological outcomes, fewer intestinal regulatory T cell (Treg) counts, and a 25% mortality rate compared to WT mice. Preventing AnxA1 and other agonists from binding with FPRs *in vivo* was almost equally harmful as all clinical parameters were impaired and tissue damage was remarkable, especially considering crypt and epithelial loss. Interestingly, treatment with IFX did not compensate for the absence of endogenous AnxA1 or FPR signaling. The blockade of the AnxA1–FPR axis impaired crypt restitution, whereas a lack of AnxA1 impacted the ability of IFX to promote wound healing and to rebalance the immune response. Based on these data, we propose that protection of the epithelial barrier with IFX must be complemented by the downstream pathways resulting from the binding of AnxA1 (and other endogenous agonists) to FPRs (**Figure 5**).

It is well known that the use of IFX on chronic diseases modulates cellular pathways downstream of TNF receptors (TNFRs) by blocking soluble and transmembrane TNF-α (38, 39). Considering the complexity of the mechanisms evoked by IFX and the heterogeneous responses it produces, other endogenous players are likely to be involved in successful outcomes. Herein, we suggest that AnxA1 expression might be one mechanism induced by IFX, which may, in turn, regulate its effects at some level. This notion is supported by the modulation of intracellular and secreted AnxA1 after IFX treatment in colitic mice. In colonic mucosal and submucosal leukocytes activated by inflammatory mediators, IFX evoked AnxA1 expression. The same group had increased secretion of AnxA1, which was most likely being provided by those leukocytes. In line with this, increased levels of AnxA1 were secreted as higher doses of IFX were added to LPS-stimulated intestinal leukocytes *ex vivo*. These results seem to be translatable to the human condition because we also observed increased AnxA1 in biopsies from CD patients in association with histological remission. Indeed, the lack of TNF-α signaling through TNFR1 in mice during colitis favors tissue AnxA1 expression and increases the frequency of CD4$^+$ and CD8$^+$ T lymphocytes positive for AnxA1 (26). These data indicate that intestinal immune cells are the major sources of secreted AnxA1; this could be one resolutive mechanism of IFX that was not previously described. Interestingly, the Boc-2 groups had less secreted AnxA1 with or without IFX. This suggests a more complex mechanism of action for IFX, in which proper FPR signaling is required to induce AnxA1 secretion by leukocytes and, in turn, to mediate tissue repair and wound healing.

Obviously, FPR agonists other than AnxA1 could be involved in the efficacy of IFX. In the inflammatory milieu, FPR ligands can be found among endogenous metabolites, peptides, and damage- and pathogen-associated molecular patterns (DAMPs and PAMPs, respectively) (40). These include *N*-formyl-peptides from mitochondrial damage (41), the antimicrobial peptide LL-37 and lipoxin A4 (22). It should be noted that the bacterial-derived peptide formyl-methyl-leucine-phenylalanine (fMLP) can be present at high concentrations in the wounded intestinal tissue (42) and binds FPR1 with a strong affinity, triggering healing pathways on epithelial cells (20, 43). Despite that, this work addresses AnxA1 participation because of its pivotal roles in IBD. Our choice was also supported by the increased AnxA1 secretion upon IFX in experimental colitis and its correlation with tissue recovery. It is also important to point out that, although we argue that AnxA1 and FPRs contribute to

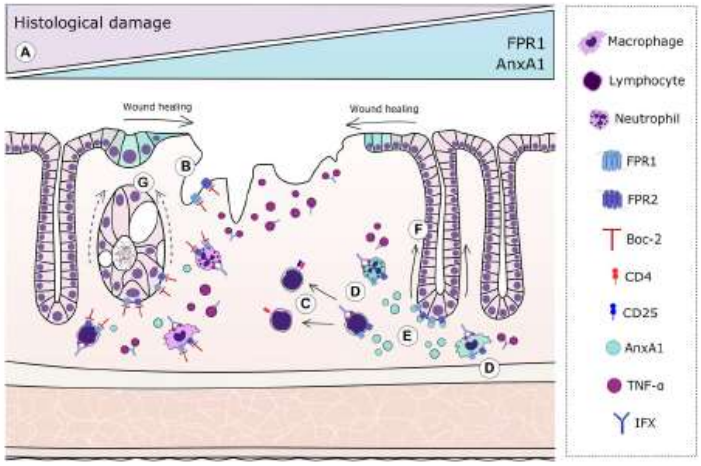

FIGURE 5 | Graphical representation of the resolutive effects of the annexin A1 (AnxA1)–formyl peptide receptor (FPR) axis complementary to infliximab (IFX) mechanisms. *In humans*: **(A)** Increased expressions of FPR1 and AnxA1 in colonic epithelial cells and lamina propria leukocytes correlate with histological remission after IFX. *In mice*: **(B)** AnxA1 expression is evoked in epithelial cells from damaged areas, but blockage of FPRs impairs proper re-epithelization. **(C)** In tissue T lymphocytes, the absence of endogenous AnxA1 skews cells to a more pro-inflammatory profile, resulting in the decreased number of regulatory T cells (Tregs). **(D)** Immune cells transmigrated to the intestinal tissue are important sources of AnxA1 after IFX. **(E)** IFX induces AnxA1 secretion to the inflammatory milieu, which correlates with histological recovery. **(F)** In IFX-treated colitis, proper signaling of FPRs is crucial to adequate crypt regeneration. **(G)** Blockade of FPRs impairs the ability of IFX to protect glandular cells and restore the characteristic U-shape of crypts, producing amorphous structures after loss of basal–apical orientation and β-actin/villin distribution.

the efficacy of IFX, it is possible that they might be involved in the effects of other therapies as well. We do not claim that this modulation is exclusive to IFX, but that it obtains for this specific therapy. We hope that our study encourages others to explore therapies that might be complemented by AnxA1–FPR, elucidating possible mechanisms of therapeutic failure in IBD. We believe that the data we presented here may contribute to the identification of poor responsiveness cases, leading to long-term remission based on the pivotal homeostatic roles of AnxA1 through FPRs.

DATA AVAILABILITY STATEMENT

The original contributions presented in the study are included in the article/**Supplementary Material**. Further inquiries can be directed to the corresponding author.

ETHICS STATEMENT

The studies involving human participants were reviewed and approved by the boards on ethics from Santa Casa and University of São Paulo. The patients/participants provided their written informed consent to participate in this study. The animal study was reviewed and approved by the Committee on Ethics of Animal Experiments, University of São Paulo.

AUTHOR CONTRIBUTIONS

MS and SF conceived the hypothesis, designed the study, interpreted the data, and prepared the manuscript. MS, GR, MB, SS, and RL designed and carried out the experiments. MS, MQ, and AV participated in patient approach and collecting samples and medical history. SO, MP, and SF provided scientific supervision, infrastructure, and essential tools to perform experiments. All authors contributed to the article and approved the submitted version.

FUNDING

This work was supported by Fundação de Amparo a Pesquisa do Estado de São Paulo, Brazil (grant nos. FAPESP 2014/07328-4, 2016/19682-2 and 2019/02806-9).

ACKNOWLEDGMENTS

The authors thank Dextran Products Limited (Canada) and Janssen-Cilag Pharmaceutics (Argentina) for kindly

providing DSS and Remicade®, respectively. We thank the medical and nursing staff from Santa Casa School of Medical Sciences (Brazil) for collecting the blood samples. Confocal analyses were supported by CMR Advanced Bio-Imaging Facility (UK).

REFERENCES

1. Abraham C, Medzhitov R. Interactions Between the Host Innate Immune System and Microbes in Inflammatory Bowel Disease. *Gastroenterology* (2011) 140:1729–37. doi: 10.1053/j.gastro.2011.02.012
2. Klotz U, Teml A, Schwab M. Clinical Pharmacokinetics and Use of Infliximab. *Clin Pharmacokinet* (2007) 46:645–60. doi: 10.2165/00003088-200746080-00002
3. Berns M, Hommes DW. Anti-TNF-α Therapies for the Treatment of Crohn's Disease: The Past, Present and Future. *Expert Opin Investig Drugs* (2016) 25:129–43. doi: 10.1517/13543784.2016.1126247
4. Costa J, Magro F, Caldeira D, Alarcão J, Sousa R, Vaz-Carneiro A. Infliximab Reduces Hospitalizations and Surgery Interventions in Patients With Inflammatory Bowel Disease: A Systematic Review and Meta-Analysis. *Inflamm Bowel Dis* (2013) 19:2098–110. doi: 10.1097/MIB.0b013e31829936c2
5. Fratila OC, Craciun C. Ultrastructural Evidence of Mucosal Healing After Infliximab in Patients With Ulcerative Colitis. *J Gastrointest Liver Dis* (2010) 19:147–53.
6. Veyrard P, Boschetti G, Nancey S, Roblin X. Predictive Models of Therapeutic Response to Vedolizumab: A Novel Step Into Personalized Medicine in Crohn's Disease? *Inflamm Bowel Dis* (2018) 24:1193–5. doi: 10.1093/ibd/izy033
7. Scaldaferri F, Pecere S. Emerging Mechanisms of Action and Loss of Response to Infliximab in Ibd: A Broader Picture. *Biochem Pharmacol Open Access* (2015) 05:1–9. doi: 10.4172/2167-0501.1000206
8. de Paula-Silva M, Barrios BE, Macció-Maretto L, Sena AA, Farsky SHP, Correa SG, et al. Role of the Protein Annexin A1 on the Efficacy of Anti-TNF Treatment in a Murine Model of Acute Colitis. *Biochem Pharmacol* (2016) 115:104–13. doi: 10.1016/j.bcp.2016.06.012
9. Ferraro B, Leoni G, Hinkel R, Ormanns S, Paulin N, Ortega-Gomez A, et al. Pro-Angiogenic Macrophage Phenotype to Promote Myocardial Repair. *J Am Coll Cardiol* (2019) 73:2990–3002. doi: 10.1016/j.jacc.2019.03.503
10. de Jong R, Leoni G, Drechsler M, Soehnlein O. The Advantageous Role of Annexin A1 in Cardiovascular Disease. *Cell Adhes Migr* (2017) 11:261–74. doi: 10.1080/19336918.2016.1259059
11. Colamatteo A, Maggioli E, Azevedo Loiola R, Hamid Sheikh M, Calì G, Bruzzese D, et al. Reduced Annexin A1 Expression Associates With Disease Severity and Inflammation in Multiple Sclerosis Patients. *J Immunol* (2019) 203:1753–65. doi: 10.4049/jimmunol.1801683
12. Headland SE, Jones HR, Norling LV, Kim A, Souza PR, Corsiero E, et al. Neutrophil-Derived Microvesicles Enter Cartilage and Protect the Joint in Inflammatory Arthritis. *Sci Transl Med* (2015) 7:1–25. doi: 10.1126/scitranslmed.aac5608
13. Kamal AM, Flower RJ, Perretti M. An Overview of the Effects of Annexin 1 on Cells Involved in the Inflammatory Process. *Mem Inst Oswaldo Cruz* (2005) 100:39–48. doi: 10.1590/S0074-02762005000900008
14. Sena A, Grishina I, Thai A, Goulart L, Macal M, Fenton A, et al. Dysregulation of Anti-Inflammatory Annexin A1 Expression in Progressive Crohns Disease. *PloS One* (2013) 8:1–13. doi: 10.1371/journal.pone.0076969
15. Leoni G, Alam A, Alexander Neumann P, Lambeth JD, Cheng G, McCoy J, et al. Annexin A1, Formyl Peptide Receptor, and NOX1 Orchestrate Epithelial Repair. *J Clin Invest* (2013) 123:443–54. doi: 10.1172/JCI65831
16. Leoni G, Neumann PA, Kamaly N, Quiros M, Nishio H, Jones HR, et al. Annexin A1-Containing Extracellular Vesicles and Polymeric Nanoparticles Promote Epithelial Wound Repair. *J Clin Invest* (2015) 125:1215–27. doi: 10.1172/JCI76693.dination
17. Reischl S, Troger J, Jesinghaus M, Kasajima A, Wilhelm DF, Friess H, et al. Annexin A1 Expression Capacity as a Determinant for Disease Severity in Crohn's Disease. *Dig Dis* (2020) 38:398–407. doi: 10.1159/000505910
18. Perretti M, D'Acquisto F. Annexin A1 and Glucocorticoids as Effectors of the Resolution of Inflammation. *Nat Rev Immunol* (2009) 9:62–70. doi: 10.1038/nri2470
19. Tsai YF, Yang SC, Hwang TL. Formyl Peptide Receptor Modulators: A Patent Review and Potential Applications for Inflammatory Diseases (2012-2015). *Expert Opin Ther Pat* (2016) 26:1139–56. doi: 10.1080/13543776.2016.1216546
20. Babbin BA, Jesaitis AJ, Ivanov AI, Kelly D, Laukoetter M, Nava P, et al. Formyl Peptide Receptor-1 Activation Enhances Intestinal Epithelial Cell Restitution Through Phosphatidylinositol 3-Kinase-Dependent Activation of Rac1 and Cdc42. *J Immunol* (2007) 179:8112–21. doi: 10.4049/jimmunol.179.12.8112
21. Wentworth CC, Jones RM, Kwon YM, Nusrat A, Neish AS. Commensal-Epithelial Signaling Mediated *via* Formyl Peptide Receptors. *Am J Pathol* (2010) 177:2782–90. doi: 10.2353/ajpath.2010.100529
22. Vong L, Ferraz JGPP, Dufton N, Panaccione R, Beck PL, Sherman PM, et al. Up-Regulation of Annexin-A1 and Lipoxin A4 in Individuals With Ulcerative Colitis may Promote Mucosal Homeostasis. *PloS One* (2012) 7:1–9. doi: 10.1371/journal.pone.0039244
23. Birkl D, O'Leary MN, Quiros M, Azcutia V, Schaller M, Reed M, et al. Formyl Peptide Receptor 2 Regulates Monocyte Recruitment to Promote Intestinal Mucosal Wound Repair. *FASEB J* (2019) 33:13632–43. doi: 10.1096/fj.201901163R
24. Best WR, Becktel JM, Singleton JW, Kern F, Kern F. Development of a Crohn's Disease Activity Index: National Cooperative Crohn's Disease Study. *Gastroenterology* (1976) 70:439–44. doi: 10.1016/S0016-5085(76)80163-1
25. Laharie D, Reffet A, Belleannée G, Chabrun E, Subtil C, Razaire S, et al. Mucosal Healing With Methotrexate in Crohns Disease: A Prospective Comparative Study With Azathioprine and Infliximab. *Aliment Pharmacol Ther* (2011) 33:714–21. doi: 10.1111/j.1365-2036.2010.04569.x
26. Sena AA, Pedrotti LP, Barrios BE, Cejas H, Balderramo D, Diller A, et al. Lack of TNFRI Signaling Enhances Annexin A1 Biological Activity in Intestinal Inflammation. *Biochem Pharmacol* (2015) 98:1–10. doi: 10.1016/j.bcp.2015.09.009
27. Alam A, Leoni G, Wentworth CC, Kwal JM, Wu H, Ardita CS, et al. Redox Signaling Regulates Commensal-Mediated Mucosal Homeostasis and Restitution and Requires Formyl Peptide Receptor. *Mucosal Immunol* (2014) 7:645–55. doi: 10.1038/mi.2013.84
28. Babbin B, Laukoetter M, Nava P, Koch S, Lee W, Capaldo C, et al. Annexin A1 Regulates Intestinal Mucosal Injury, Inflammation, and Repair. *J Immunol* (2008) 181:5035–44. doi: 10.4049/jimmunol.181.7.5035
29. Khau T, Langenbach SY, Schuliga M, Harris T, Johnstone CN, Anderson RL, et al. Annexin-1 Signals Mitogen-Stimulated Breast Tumor Cell Proliferation by Activation of the Formyl Peptide Receptors (FPRs) 1 and 2. *FASEB J* (2011) 25:483–96. doi: 10.1096/fj.09-154096
30. Magro F, Portela F. Management of Inflammatory Bowel Disease With Infliximab and Other Anti-Tumor Necrosis Factor Alpha Therapies. *BioDrugs* (2010) 24:3–14. doi: 10.2165/11586290-000000000-00000
31. Pichler WJ. Adverse Side-Effects to Biological Agents. *Allergy Eur J Allergy Clin Immunol* (2006) 61:912–20. doi: 10.1111/j.1398-9995.2006.01058.x
32. Baars JE, Nuij VJAA, Oldenburg B, Kuipers EJ, van der Woude CJ. Majority of Patients With Inflammatory Bowel Disease in Clinical Remission Have Mucosal Inflammation. *Inflamm Bowel Dis* (2012) 18:1634–40. doi: 10.1002/ibd.21925
33. Pineton de Chambrun G, Blanc P, Peyrin-Biroulet L. Current Evidence Supporting Mucosal Healing and Deep Remission as Important Treatment Goals for Inflammatory Bowel Disease. *Expert Rev Gastroenterol Hepatol* (2016) 10:915–27. doi: 10.1586/17474124.2016.1174064
34. Leoni G, Nusrat A. Annexin A1: Shifting the Balance Towards Resolution and Repair. *Biol Chem* (2016) 397:971–9. doi: 10.1515/hsz-2016-0180
35. Rogler G. Resolution of Inflammation in Inflammatory Bowel Disease. *Lancet Gastroenterol Hepatol* (2017) 2:521–30. doi: 10.1016/S2468-1253(17)30031-6

SUPPLEMENTARY MATERIAL

The Supplementary Material for this article can be found online at: https://www.frontiersin.org/articles/10.3389/fimmu.2021.714138/full#supplementary-material

36. Iizuka M, Konno S. Wound Healing of Intestinal Epithelial Cells. *World J Gastroenterol* (2011) 17:2161–71. doi: 10.3748/wjg.v17.i17.2161
37. Cristante E, McArthur S, Mauro C, Maggioli E, Romero IA, Wylezinska-Arridge M, et al. Identification of an Essential Endogenous Regulator of Blood-Brain Barrier Integrity, and Its Pathological and Therapeutic Implications. *Proc Natl Acad Sci USA* (2013) 110:832–41. doi: 10.1073/pnas.1209362110
38. Ten Hove T, Van Montfrans C, Peppelenbosch MP, Van Deventer SJH. Infliximab Treatment Induces Apoptosis of Lamina Propria T Lymphocytes in Crohn's Disease. *Gut* (2002) 50:206–11. doi: 10.1136/gut.50.2.206
39. Pedersen J, Coskun M, Soendergaard C, Salem M, Nielsen OH. Inflammatory Pathways of Importance for Management of Inflammatory Bowel Disease. *World J Gastroenterol* (2014) 20:64–77. doi: 10.3748/wjg.v20.i1.64
40. Migeotte I, Communi D, Parmentier M. Formyl Peptide Receptors: A Promiscuous Subfamily of G Protein-Coupled Receptors Controlling Immune Responses. *Cytokine Growth Factor Rev* (2006) 17:501–19. doi: 10.1016/j.cytogfr.2006.09.009
41. He HQ, Ye RD. The Formyl Peptide Receptors: Diversity of Ligands and Mechanism for Recognition. *Molecules* (2017) 22:1–33. doi: 10.3390/molecules22030455
42. Leoni G, Gripentrog J, Lord C, Riesselman M, Sumagin R, Parkos CA, et al. Human Neutrophil Formyl Peptide Receptor Phosphorylation and the Mucosal Inflammatory Response. *J Leukoc Biol* (2015) 97:87–101. doi: 10.1189/jlb.4A0314-153R
43. Wentworth CC, Alam A, Jones RM, Nusrat A, Neish AS. Enteric Commensal Bacteria Induce Extracellular Signal-Regulated Kinase Pathway Signaling *via* Formyl Peptide Receptor-Dependent Redox Modulation of Dual Specific Phosphatase. *J Biol Chem* (2011) 286:38448–55. doi: 10.1074/jbc.M111.268938

Conflict of Interest: The authors declare that the research was conducted in the absence of any commercial or financial relationships that could be construed as a potential conflict of interest.

Primeira autoria 2022

European Journal of Pharmaceutics and Biopharmaceutics 181 (2022) 49–59

Contents lists available at ScienceDirect

European Journal of Pharmaceutics and Biopharmaceutics

journal homepage: www.elsevier.com/locate/ejpb

Research paper

Development of Annexin A1-surface-functionalized metal-complex multi-wall lipid core nanocapsules and effectiveness on experimental colitis

Milena Fronza Broering [a], Matheus de Castro Leão [b], Gustavo Henrique Oliveira da Rocha [a], Pablo Scharf [a], Luana Fillipi Xavier [a], Aline de Cristo Soares Alves [c], Inar Castro [b], Chris Reutelingsperger [d], Mayara Klimuk Uchiyama [e], Koiti Araki [e], Sílvia Stanisçuaski Guterres [c], Adriana Raffin Pohlmann [c], Sandra Helena Poliselli Farsky [a,*]

[a] Department of Clinical & Toxicological Analyses, Faculty of Pharmaceutical Sciences, University of Sao Paulo, SP, Brazil
[b] Department of Food and Experimental Nutrition, Faculty of Pharmaceutical Sciences, University of Sao Paulo, SP, Brazil
[c] Postgraduate Program in Pharmaceutical Sciences, Faculty of Pharmaceutical Sciences, Federal University of Rio Grande do Sul, Porto Alegre, Brazil
[d] Faculty of Health, Medicine and Life Sciences, Part of Maastricht University Medical Center, Part of Maastricht University, 6211 LK Maastricht, the Netherlands
[e] Department of Fundamental Chemistry, Institute of Chemistry, University of Sao Paulo, SP, Brazil

ARTICLE INFO

Keywords:
Lipid core nanocapsules
C57BL/6 mice
Resolution of inflammation
Macrophages
Tight junctions
Cell proliferation

ABSTRACT

Annexin A1 (AnxA1), a 37KDa protein, is secreted by inflammatory and epithelial cells and displays anti-inflammatory and wound healing activities in intestinal bowel diseases. Herein, we aimed to functionalize recombinant AnxA1 (AnxA1) on multi-wall lipid core nanocapsules (MLNC) and investigate its effectiveness on experimental colitis. MLNC were prepared by covering lipid core nanocapsules (LNC) with chitosan, which coordinates metals to specific protein chemisorption sites. Therefore, MLNC were linked to Zn^{2+} and AnxA1 was added to form MLNC-AnxA1. LNC, MLNC and MLNC-AnxA1 presented average size of 129, 152 and 163 nm, respectively, and similar polydispersity indexes (0.xx); incorporation of chitosan inverted the negative potential zeta; the coordination efficiency of AnxA1 was 92.22 %, and transmission electron microscope photomicrograph showed MLNC-AnxA1 had a spherical shape. The effectiveness of MLNC-AnxA1 was measured in Dextran Sulfate Sodium (DSS)-induced colitis in male C57BL/6 mice. DSS (2 % solution) was administered from days 1–6; saline, LNC, MLNC, MLNC-AnxA1 or AnxA1 were administered, once a day, by oral or intraperitoneal (i.p.) routes, from days 6–9. Clinical parameters of the disease were measured from day 0–10 and gut tissues were collected for histopathology, immunohistochemistry and flow cytometry analyses. Only i.p. treatment with MLNC-AnxA1 reduced weight loss, diarrhea and disease activity index, and prevented loss of colonic structure integrity; induced the switch of macrophages into M2 phenotype in the lamina propria; recovered the colonic histo-architecture by decreasing dysplasia of crypts, inflammation and ulcerations; restored the expression of claudin-1 Zonna-occludens-1 tight junctions in the inflamed gut; and induced stem cell proliferation in intestinal crypts. Associated, data highlight the functionalization of MLNC with AnxA1 as a tool to improve the local actions of such protein in the inflamed gut by inducing resolution of inflammation and tissue repair.

1. Introduction

Inflammatory bowel diseases (IBDs) are chronic and multifactorial disorders characterized by an exacerbated and progressive immune response to homeostasis disruption of the intestinal epithelium [1]. IBDs comprise Crohn's disease (CD) and ulcerative colitis (UC) [2]. Lesions spread out at different parts of the intestine characterize CD, leading to inflammation at the transmural level [3]. UC, on the other hand, is typically limited to the colon, affecting the mucosal and submucosal layers [4–5]. The exact etiology of IBDs remains unclear; however, genetic variations in the immune system, alterations in the intestinal microbiota, and exposure to environmental pollutants are strongly associated with induction and development of IBDs [6]. Current pharmacotherapy on IBDs treats only symptoms of the disease all the while

* Corresponding author at: Department of Clinical and Toxicological Analyses, School of Pharmaceutical Sciences, University of São Paulo, Av. Prof. Lineu Prestes 580 Bl.13 B, Butantan, São Paulo 05508-000, Brazil.
E-mail address: sfarsky@usp.br (S.H.P. Farsky).

https://doi.org/10.1016/j.ejpb.2022.10.022
Received 8 June 2022; Received in revised form 27 October 2022; Accepted 28 October 2022

Table 1
Physicochemical analysis of nanoparticles.

Nanocapsules	Dh	PDI	mV	pH	PND ($\times 10^{13}$ nanocapsules mL^{-1})
LNC	129 ± 3.57	0.11 ± 0.01	−12.5 ± 1.37	4.52 ± 0.02	3.63 ± 0.66
MLNC	152 ± 3.89 *	0.27 ± 0.01 ***	15.5 ± 0.70 ***	4.24 ± 0.09 **	2.75 ± 0.65
MLNC-rAnxA1	163 ± 11.61 **	0.22 ± 0.01 *** §	16.2 ± 1.71 ***	4.23 ± 0.03 **	1.55 ± 0.48 *

Values are expressed as mean ± SEM (n = 3). * $p < 0.05$, ** $p < 0.01$, *** $p < 0.001$ vs LNC. § $p < 0.05$ vs MLNC. Abbreviations: LNC, lipid core nanocapsule; MLNC, multi wall lipid core nanocapsule; MLNC-AnxA1, metal-complex multi-wall lipid core nanocapsule; D_h, z-average diameter; PDI, polydispersity index; ZP, zeta potential; PND, particle number density.

being highly costly. Furthermore, patients may be unresponsive to available treatments. Hence, novel therapies for IBDs treatment are being constantly researched [7].

Inflammation is mediated by a diversity of pro-inflammatory mediators secreted in order to evoke an effective response against an aggressor. Nevertheless, such process cannot be exacerbated otherwise risking injuring host tissue, and for this reason anti-inflammatory mediators are secreted to halt and resolve the process. Annexin A1 (AnxA1) is a 37 KDa protein secreted by immune and epithelial cells, known as a blocker of neutrophil recruitment into lesioned areas and as an inducer of efferocytosis and tissue repair [8–9]. AnxA1 anti inflammatory actions occur due to binding to formyl-peptide receptors (FPRs) in cell membranes, and subsequent activation of downstream intracellular pathways [8,10–11].

Data obtained from samples collected from IBDs patients or experimental models of colitis show AnxA1 is highly expressed by epithelial and inflammatory cells during IBDs course, being associated with the protection of gastrointestinal mucosa and epithelial recovery by activating FPR1 and FPR2 [12–18]. AnxA1 has been claimed as a marker of IBD [14,18–19]. It was recently shown that AnxA1 mediates the actions of therapeutic drugs on treatment of IBD, such as infliximab, an anti-tumor necrosis factor (anti-TNF) antibody [19], and pioglitazone, an ligand of the peroxisome proliferator-activated receptor γ [13].

Lipid core nanocapsules (LNC) are biodegradable and efficiently load poorly water soluble molecules [20]. LNC enhance bioavailability and drive different lipophilic molecules to pharmacological targets, being capable of crossing biological barriers including the gastrointestinal and the blood–brain-barrier. Therefore, drug-loaded LNC represent potential formulations to treat inflammatory and cancer diseases [21–28]. More recently, LNC technology was improved to allow carrying of polar molecules, as proteins, enzymes and antibodies due to the development of multi-wall lipid core nanocapsules (MLNC) [29]. MLNC are built by adding chitosan-metal complexes in order to adsorb molecules containing heteroatoms in their chemical structure, including oxygen or nitrogen. The metal complex with Zn^{2+} provides better binding of proteins to the MLNC structure by interacting with histidine residues present in the C-terminal region of molecules [30]. Recent studies have demonstrated the higher bioavailability and therapeutic effectiveness of MLNC functionalized with hydrophilic molecules, including enzymes and proteins [31–33].

Considering the feasibility of MLNC to load proteins, we here developed MLNC functionalized with recombinant AnxA1 (AnxA1) and tested its effectiveness on experimental model of colitis in mice.

2. Material and methods

2.1. Materials

Protease inhibitor cocktail, poly(ε-caprolactone) (α,ω-dihydroxy telechelic PCL, Mw = 14,000 g mol^{-1}), sorbitan monostearate (SM, Span 60®), polysorbate 80 (Tween 80®), zinc acetate, low molecular weight chitosan (Mw = 50,000–190,000 g mol^{-1}, deacetylation degree: 75–85 %, viscosity: 20,000 cP) (Sigma-Aldrich Co, Saint Louis, MO, USA); soybean phosphatidylcholine (LPS75; 75 % pure; Lipoid® S75, Gerbras Química Farmacêutica Ltda, São Paulo, Brazil); medium chain triglyceride (MCT,- Nutrimed Ind. Ltda, São Paulo, Brazil). Recombinant AnxA1 (AnxA1) protein was purifted by a previously established method [34] and provided by Professor Chris Reutelingsperger, from Maastricht University; acetone and ethanol used were of analytical grade; dextran sulfate sodium (DSS, MW 40,000, Dextran Products Limited, Canada); anti-mouse CD206 and anti-mouse Zonna occludens-1 (ZO-1; Invitrogen®, Waltham, Massachusetts, USA); anti-mouse F4/80, anti-mouse CD80 (eBioscience™, San Diego, California, USA); anti-mouse Claudin-1 and secondary antibody anti-rabbit conjugated with HRP (Abcam Plc, Cambridge, United Kingdom); anti-mouse Ly6G (BD, Becton Dickinson, New Jersey, US); DAB Substrate Chromogen System (Dako Omnis, Agilent, Santa Clara, California, USA); anti-Ki67 (Cell Signaling Technologies, Danvers, Massachusetts, USA); anti- proliferating cell nuclear antigen (PCNA), Santa Cruz Biotechnology, Dallas, Texas, USA); Collagenase II and Collagenase IV from *Clostridium histolyticum* and bovine serum albumin (BSA) (Gibco™, Grand Island, New York, USA). Isoflurano (Critália Produto Químicos e Farmacêuticos Ltda, São Paulo, Brazil). Paraformaldehyde, xilene, sodium citrate, peroxide and tris (hydroxymethyl) aminomethane (Synth® - Labsynth Produtos para Laboratórios LTDA, São Paulo, Brazil).

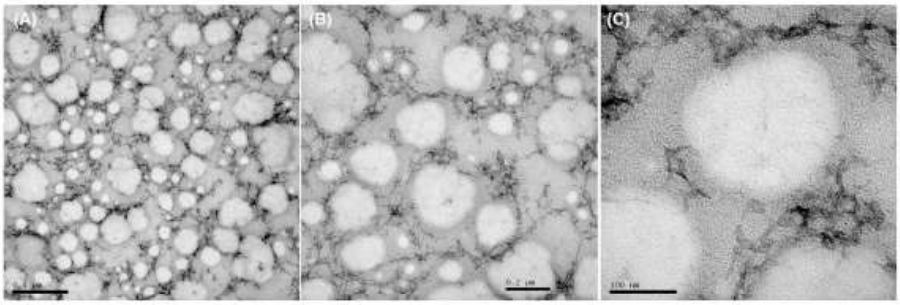

Fig. 1. Transmission electron microscopy analysis. The MLNC-AnxA1 nanocapsules were analyzed using different magnifications. (A) bar = 500 nm; (B) bar = 200 nm; and (C) bar = 100 nm. Abbreviations: LNC, lipid core nanocapsule; MLNC, multi wall lipid core nanocapsule; MLNC-AnxA1, metal-complex multi-wall lipid core nanocapsule.

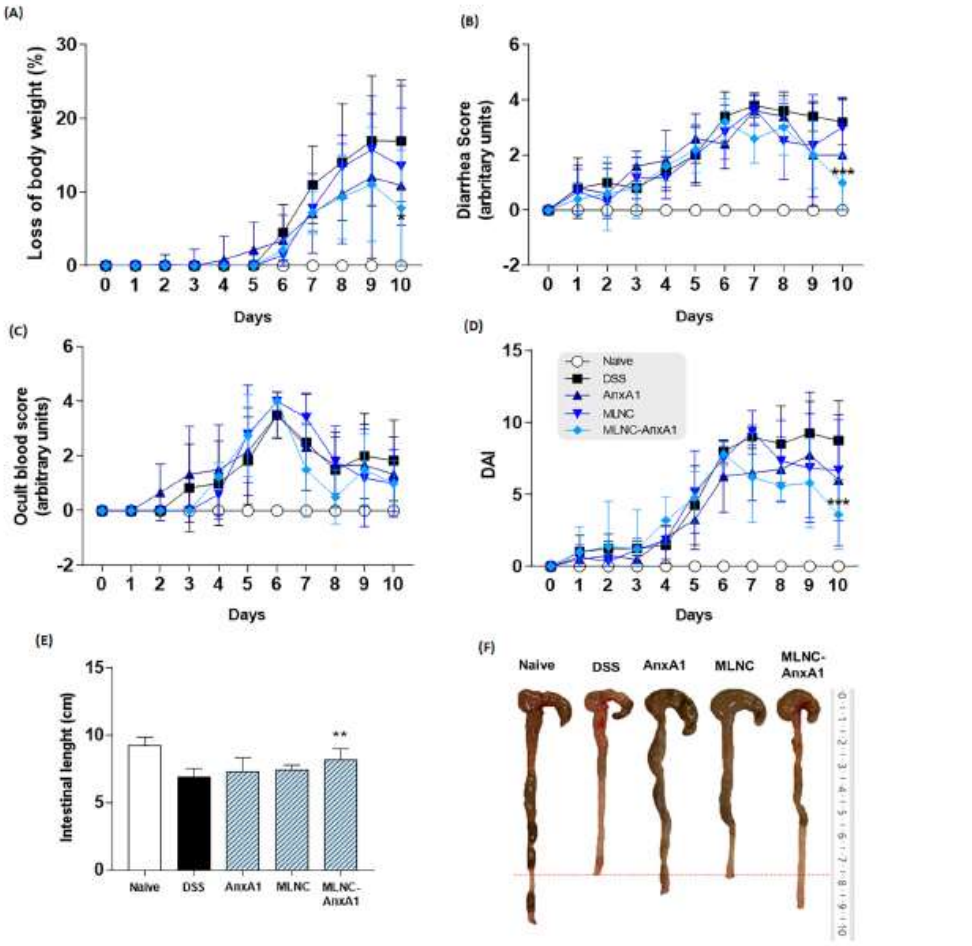

Fig. 2. Roles of MLNC-AnxA1 therapy on DSS-induced colitis activity and intestinal structure. Mice were treated with DSS 2 % in order to develop colitis and were treated with AnxA1 (12.5 μg/mL), MLNC ($9.6x10^{11}$ particles) or MLNC-AnxA1 ($9.6x10^{11}$ particles/ 12.5 μg) between days 6 and 9. (A) Percentage of body weight loss; (B) Diarrhea score; (C) Occult blood score; (D) DAI; (E) Intestinal length; (F) Anatomic evaluation of the colon. $n = 6$ mice/group. * $p < 0.05$, ** $p < 0.01$, *** $p < 0.001$ vs DSS. Abbreviations: LNC, lipid core nanocapsule; MLNC, multi wall lipid core nanocapsule; MLNC-AnxA1, metal-complex multi-wall lipid core nanocapsule; DAI, disease activity index.

2.2. Synthesis of the AnxA1-Surface-Functionalised Metal-Complex MLNC

The first step of the synthesis of nanocapsules consisted of the interfacial deposition of pre-formed polymer method, as previously described [21,29]. An organic solution was prepared by addition of PCL (0.100 g), SM (0.040 g), and MCT (120 μL) dissolved in acetone (25 mL). An additional organic solution was prepared by mixing 5 mL of ethanol with LPS75 (0.090 g). The organic solutions were maintained under magnetic stirring at 40 °C for 1 h. Afterwards, both solutions were mixed and maintained under agitation at 40 °C for 1 h. Another aqueous solution was prepared using distilled water (60 mL) with 0.080 g of nonionic surfactant Tween® 80, by mixing for 1 h at 40 °C. Afterwards, the final organic solution was injected into the aqueous solution and stirred for 10 min. The resulting translucid solution was evaporated to be concentrated to final volume of 9 mL, using a rotary evaporator under reduced pressure at 40 °C. The formulation consisted of lipid-core nanocapsules in aqueous dispersion (LNC). The volume of the final solution was adjusted to 10 mL using ultrapure water. The supramolecular structure is stabilized by weak forces (dipole–dipole and ion–dipole interactions).

Twenty-four hs later, 500 μL of a filtered (0.45 μm, Millipore, Merck Millipore, Darmstadt, Germany) aqueous solution of chitosan (0.3 %) was pipetted (1 drop every 10 s) into 4.5 mL of LNC solution. The mixture was maintained under magnetic stirring for 2 hs (second step of reaction consisting of interfacial ionic bonds). Next, a Zn^{2+} solution containing 28 mg of zinc acetate in ultrapure water (10 mL) was prepared. Thereafter, the third and fourth steps lead to the organometallic coordination, 12.5 μL of zinc acetate solution were added into 412.5 μL of the chitosan-coated lipid-core nanocapsules solution (MLNC) under

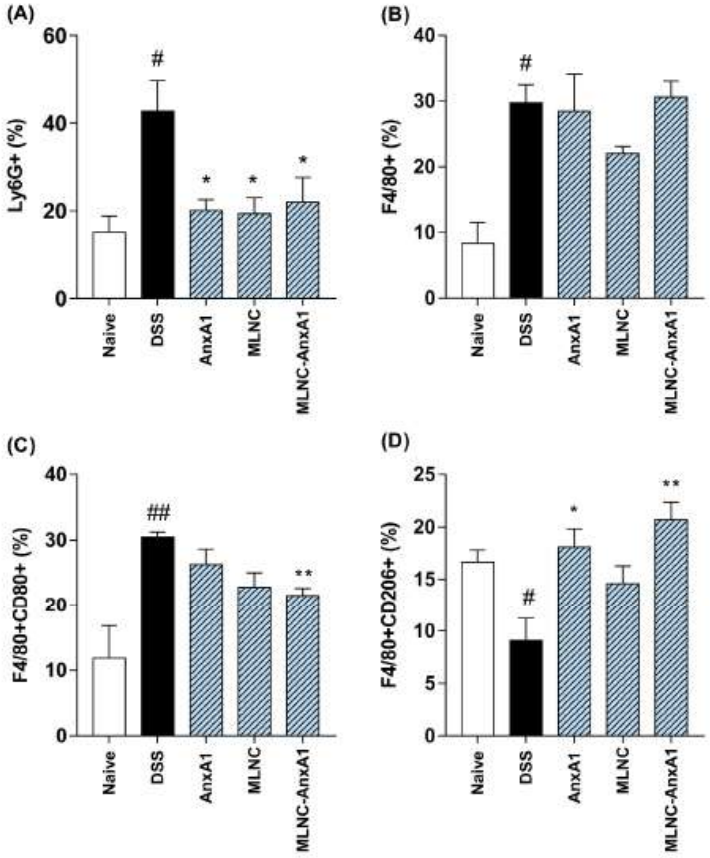

Fig. 3. MLNC-AnxA1 up-regulate M2 macrophage polarization in lamina propria. Cells were dissociated by enzymatic activity from extracellular matrix and $2x10^5$ cells were used for antibody labeling. (A) $Ly6G^+$, (B) $F4/80^+$, (C) $F4/80^+CD80$, (D) $^+$. $F4/80^+CD206^+$, $n = 6$ mice/group. * $p < 0.05$, ** $p < 0.01$ vs DSS. # $p < 0.05$, ## $p < 0.01$ vs Naïve.

magnetic stirring at 350 rpm. After 40 s, 75 μL of AnxA1 solution 1.33 mg mL^{-1}) were added into the same solution under magnetic stirring at 350 rpm. The AnxA1-Zn^{2+}-chitosan-coated lipid-core nanocapsules complex (MLNC-AnxA1) was maintained under magnetic stirring (350 rpm) for 20 min at room temperature (20 °C). At final formulation, the theoretical concentration of AnxA1 was 200 μg mL^{-1}. The four steps to obtain the intermediate formulations (LNC and MLNC) and the final formulation (MLNC-AnxA1) are represented in the Figure S1.

2.3. Physicochemical characterization of the nanocapsules

Initially, z-average hydrodynamic diameter and polydispersity index (PDI) values were calculated after determining the particle size distribution using dynamic light scattering at 25 °C (DLS; Zetasizer® Nano ZS, Malvern Instruments, Malvern, UK). The measurement was performed after dilution of samples (500 ×) in purified and previously filtered water (MilliQ®) (0.45 μm, Millipore®, Billerica, MA, USA). Zeta potential (ζ – mV) mean values were calculated using the electrophoretic mobility distribution (Zetasizer® Nano ZS, Malvern Instruments, Malvern) in formulation diluted (500 ×) in a pre-filtered (0.45 μm, Millipore®, Billerica, MA, USA) NaCl aqueous solution (10 mM). The quantifications of pH were carried out in the formulation using a calibrated potentiometer (DM-22, Digimed, São Paulo, Brazil). The concentration and size distribution quantification of the formulations (particle number density) were obtained by using nanocapsule tracking analysis (NTA) (NanoSight LM10 & NTA 2.0 Analytical Software, NanoSight® ltd). Quantification of AnxA1 bound to the nanocapsules was realized by an indirect method. The free AnxA1 in the formulations was quantified by a colorimetric method (QuantiProTM BCA Assay Kit, Sigma-Aldrich, St. Louis, MO, USA) according to manufacturer's instructions. To separate the free fraction of AnxA1, the MLNC-AnxA1 formulation was centrifugated in ultrafiltration units (100 kDa; Merck KGaA), using 1,840 xg for 5 min (Sigma® 1–14; SIGMA Laborzentrifugen GmbH, Germany). The obtained ultrafiltrate was quantified by colorimetric methods and the protein concentration was obtained using a calibration curve. The results were expressed in coordination efficiency. The morphology of the MLNC-AnxA1 formulation was visualized under a transmission electron microscope operating at 80 kV. Samples of nanocapsule (100 μL) were diluted in water (1:10, v/v). Only 10 μL of the diluted solution were deposited on copper grids (400 mesh), which were coated with carbon films. Afterwards, 2 % uranyl acetate solution, used as negative contrast, was added to the grid, and was kept in a

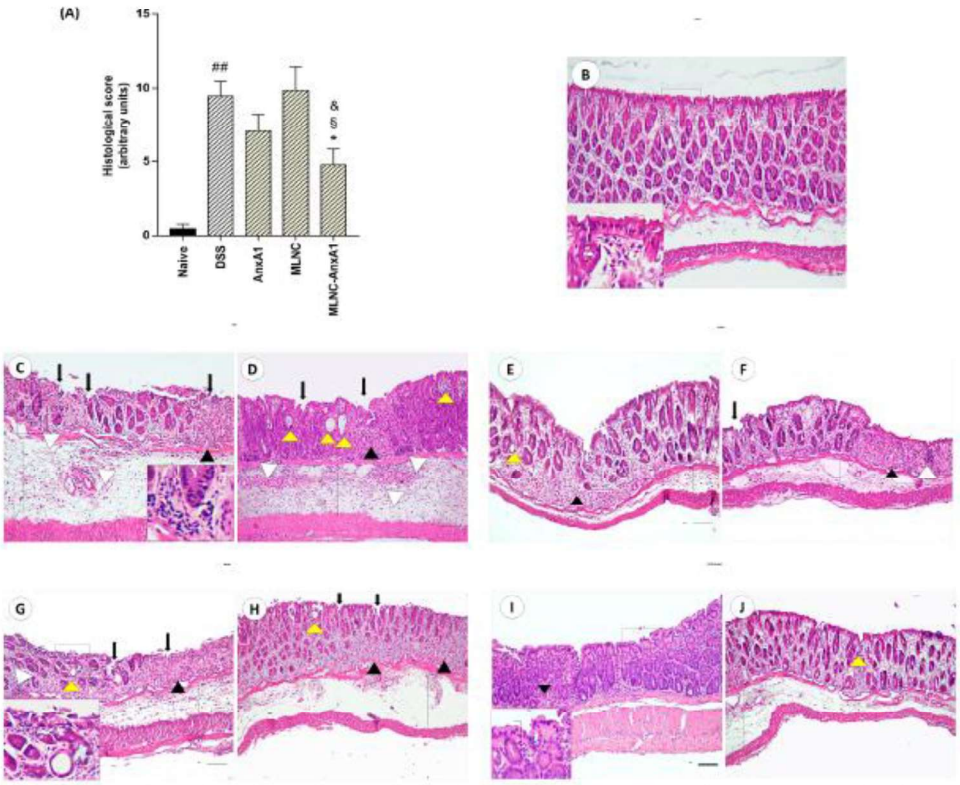

Fig. 4. Histopathological analyses. (A) Histopathological score represented by arbitrary units. The sections were blindly evaluated and considered alterations were highlighted. Tissue edema (dotted line), dysplasia/altered histoarchitecture (black arrow head), crypt edema (yellow arrow head), inflammatory infiltrates (white arrow head) and ulcerations (black arrow). (B) Naïve section presenting normal histoarchitecture, with simple cylindrical epithelium (black square); (C and D) DSS group; (E and F) AnxA1 group; (G and H) MLNC group; (I and J) MLNC-AnxA1 group. $n = 6$ mice/group. Scale bar: 50 μm. Sections: 4 μm. * $p < 0.05$ vs DSS. § $p < 0.05$ vs AnxA1. & $p < 0.05$ vs MLNC. ## $p < 0.01$ vs Naïve. Abbreviations: DSS, dimethyl sulfoxide. (For interpretation of the references to colour in this figure legend, the reader is referred to the web version of this article.)

vacuum desiccator for 24 h.

2.4. Animals

Male C57BL6 wild-type (WT) mice, aged 8–10 weeks and weighting 20–25 g were used. Animals, obtained from Faculty of Pharmaceutical Sciences of the University of São Paulo. They were maintained under pathogen-free conditions and in a 12-h light/dark cycle, at temperatures between 20 and 25 °C, with free access to water and food. The protocol of study was approved by the Ethics Committee of Animal Use of the Faculty of Pharmaceutical Sciences of the University of São Paulo (CEUA/FCF/ USP; protocol nº 598), following the Brazilian laws of animal ethics.

2.5. Colitis induction and treatments

Five groups of animals were employed (n = 6 animals/group), as follow: Naive, DSS, AnxA1, MLNC and MLNC-AnxA1. The naive group received just filtered water, colitic animals (DSS, AnxA1, MLNC and MLNC-AnxA1) received DSS solution (2 %) from day 1 to the day 6; the DSS solution was replaced with two days of intervals. On day 6, DSS was withdrawn and replaced with filtered water until day 10. Between days 6 and 9, the mice were treated once daily with different doses of AnxA1, MLNC, MLNC-AnxA1 or diluent solution (H_2O MilliQ®) according to the route of administration. Oral: AnxA1 (100 μg/mL) or MLNC-AnxA1 (100 μg/mL – $3.1x10^{12}$ particle/mL^{-1}); intraperitoneal (i.p.): AnxA1 (12.5 μg/mL), MLNC ($9.6x10^{11}$ particle/mL^{-1} or MLNC-AnxA1 (12.5 μg/mL – $9.6x10^{11}$ particles/mL^{-1}) in a final volume of 200 μL. Naive or DSS groups were manipulated as the other groups, but with the carrier solution H_2O only (MilliQ®).

Clinical parameters were achieved by measuring body weight, diarrhea and rectal blood. They were observed and registered daily and used to calculate the Disease Activity Index (DAI), as DAI was obtained by the the sum of these parameters. On day 10, animals were anaesthetized by inhalation of isoflurane anesthetic (2-chloro-2- (difluoromethoxy)- 1,1,1-trifluoroethane) and euthanized. Samples of the colon were collected from the ileocecal junction up to the proximity of the anus, to macroscopic evaluation. Furthermore, fragments of the colon were used to histological (distal colon), enzymatic and flow cytometry (mid/proximal colon) analyzes. Peritoneal lavage was collected using ice-cold PBS solution and cellularity was quantified by flow cytometry.

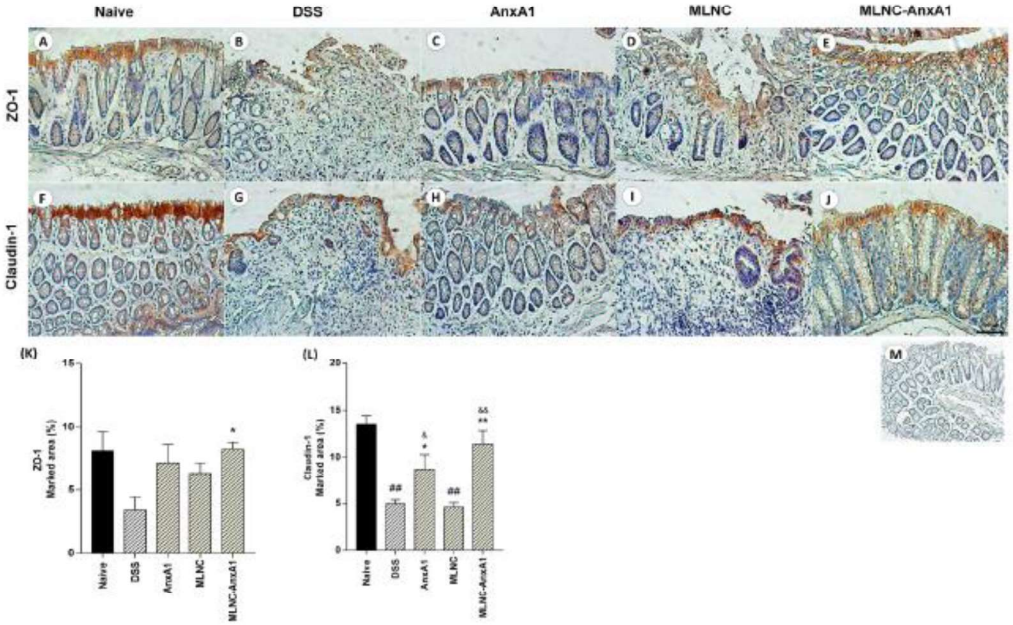

Fig. 5. Effects of MLNC-AnxA1 treatment on epithelial tight junctions in the colon damaged by DSS-induced colitis. First line sections represent ZO-1 expression and second line sections represent Claudin-1 expression in colonic tissue. (A and F) Naïve group; (B and G) DSS group; (C and H) AnxA1 group; (D and I) MLNC group; (E and J) MLNC-AnxA1 group. The quantification of ZO-1 stained area (K) and Claudin-1 (L) are presented in the graphs. (M) Control section. $n = 6$ mice/group. Pictures: high-power objective (40 x). Sections: 4 μm. Scale bar: 100 μm. * $p < 0.05$, ** $p < 0.01$ vs DSS. & $p < 0.05$, && $p < 0.01$ vs MLNC. # $p < 0.05$, ## $p < 0.01$ vs Naïve. Abbreviations: ZO-1, zonula occludens-1; DSS, dimethyl sulfoxide.

2.6. Histopathological and immunohistochemistry analysis

Fragments collected from the distal part of the colon were fixed by 24 h incubation in 4 % paraformaldehyde for 24 h. Afterwards, they were dehydrated in graded ethanol, cleared in xylene and embedded in paraffin for histopathological and immunohistochemistry analyses according to our previous manuscripts [13–14].

Histopathological analysis was performed in 4 μm sections. Samples were stained using hematoxylin and eosin solution and analyzed using a high-power objective (40 ×) on an AxioCam coupled to a Zeiss microscope (Carl Zeiss, Jena, Germany). The histopathological score analysis was performed blindly by two analysts knowledgeable on characteristics of intestinal tissue. The score was adapted [35] and considered: tissue edema, dysplasia/altered histoarchitecture, crypt edema, inflammatory infiltrates and ulcerations. Ten photos were taken of each histological section using a 20 × high power objective and scores were evaluated on a scale ranging from 0 to 4.

During immunohistochemistry measurements, colon sections was achieved were deparaffinized, hydratated and incubated with sodium citrate buffer (pH 6.0) at 96 °C for 30 min. Endogenous peroxidase activity was blocked with 3 % hydrogen peroxide, three times washed after each in 10 min of incubation. Next, blocking of unspecific binding sites was carried out with 1 % BSA diluted in Tris-buffer saline (TBS) for one h. Sections obtained were incubated with anti-Claudin-1, anti-ZO-1, anti-PCNA and anti-Ki67 antibodies overnight at 4 °C. Afterwards they were washed and incubated with a secondary antibody conjugated with HRP (1 h, room temperature), and detected using 3,3′-diaminobenzidine. Finally, sections were counterstained with hematoxylin and mounted. The sections were photographed using a 20 × high power objective and the percentage of marked area of claudin-1 and ZO-1 was quantified using ImageJ software. Results were expressed as mean ± S.E.M. of percentage of marked area.

The quantification of proliferative nuclei was evaluated by the photographs using a 40 × high power objective in ten fields of the mucosal layer from PCNA-stained and Ki67-stained sections and the number of positive nuclei was quantified for each field assessed. Results were expressed as mean ± S.E.M. of proliferative nuclei.

2.7. Isolation of Leukocytes from lamina propria and flow cytometry

Leukocytes from proximal colonic lamina propria were isolated after washes with 2 mM EDTA followed by digestion with collagenase II and IV from *Clostridium histolyticum* (1 mg/mL). The cells were washed through 40-μm strainers (Corning, Corning, NY, USA) and stained with Ly6G (PE), F4/80 (PerCpCy5.5), CD206 (FITC) and CD80 (PE). Positive populations were determined by labeling with single antibodies. A minimum of 10,000 events per sample was acquired on a BD Accuri C6 Flow Cytometer (BD, Becton Dickinson, New Jersey, US). The results were expressed as percentages of positive cells normalized by controls from each experiment.

2.8. Statistical analysis

Clinical parameters in experimental colitis were analyzed by Two-way ANOVA followed by Bonferroni post-test. For other analyses, One-way ANOVA was used followed by Tukey's post-test. Values of $p < 0.05$ were considered significant. Results were expressed as mean ± SEM. Statistical analyses were performed using GraphPad Prism Software 7.0.

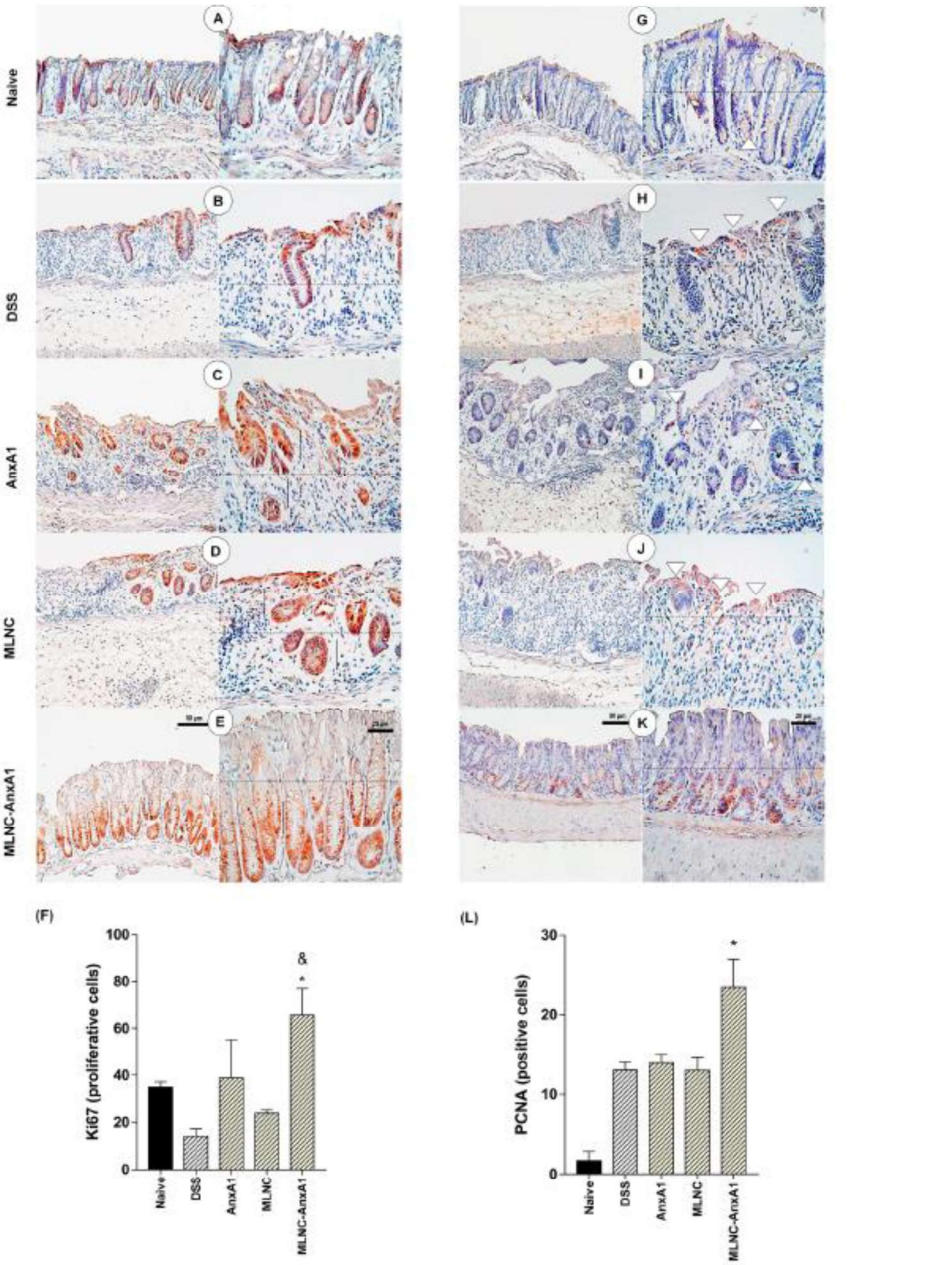

Fig. 6. Effects of MLNC-AnxA1 treatment on epithelial regeneration and renovation in the colon damaged by DSS-induced colitis. Ki67 and PCNA are represented in 20x and 40x high-power objective. (A and G) Naïve group; (B and H) DSS group; (C and I) AnxA1 group; (D and J) MLNC group; (E and K) MLNC-AnxA1 group. The quantification of proliferative nuclei stained with Ki67 (F) and PCNA (L) are presented in the graphs. $n = 6$ mice/group. Sections: 4 μm. Bars: 50 μm and 20 μm. * $p < 0.05$ vs DSS. & $p < 0.05$ vs MLNC. Abbreviations: PCNA, Proliferating Cell Nuclear Antigen.

3. Results

3.1. Development of nanocapsules

All formulations showed white-opalescent homogeneous macroscopic aspect, with no visible aggregation in storage vials. Three individual batches of LNC, MLNC or MLNC-AnxA1 were prepared. After the addition of chitosan, the z-average diameters of MLNC and MLNC-AnxA1 presented values greater than the mean diameter of LNC ($p < 0.05$ and $p < 0.01$ respectively) (Table 1; Fig. 1). PDI was significantly higher for the MLNC and MLNC-AnxA1 formulations (moderate polydispersity) when compared to the LNC (narrow polydispersity) ($p < 0.001$). Comparing MLNC and MLNC-AnxA1 formulations, the latter presented a lower polydispersity index ($p < 0.05$) (Table 1; Figure S2). PDI of the 3 formulations was lower than 0.3. The zeta potential was inverted after the addition of chitosan ($p < 0.001$), and no difference was observed between the chitosan-containing nanocapsules (MLNC and MLNC-AnxA1) (Table 1, Fig. 1). The addition of chitosan to the LNC structure caused a significant pH reduction when compared to the other groups ($p < 0.01$), an expected result since acetic acid is used to disperse the chitosan solution (Table 1).

Furthermore, using 2D plots (intensity of light scattering versus diameter), nanoparticle tracking analysis showed that MLNC-AnxA1 overlap MLNC (Figure S3), demonstrating that conjugation with the protein occurred efficiently, and no aggregation occurred after forming the organometallic complex. Coordination efficiency of AnxA1 (92.22 ± 1.47 %) was calculated after ultrafiltration-centrifugation and quantification of unconjugated protein. TEM photomicrographs (Fig. 1) demonstrated MLNC-AnxA1 spherically shaped. The aspect of those nanocapsules were similar to other chitosan-coated nanocapsule formulations previously published [30,37].

3.2. Intraperitoneal injection of MLNC-AnxA1 attenuates ulcerative colitis

DSS ingestion induced colitis as observed by clinical parameters weight loss, diarrhea score and occult blood in stool, bowel length and DAI. Treatments with AnxA1 or MLNC-AnxA1 by oral route did not attenuate the damage caused by DSS ingestion (Figure S4). Only i.p. treatment with MLNC-AnxA1 was effective in reducing the symptoms of ulcerative colitis. It was observed reduced weight loss, diarrhea and disease activity index (Fig. 2A-D), as well as restoration of the colonic structure integrity, as demonstrated by the intestine length recovery at day 10 after DSS ingestion (Fig. 2E-F).

3.3. MLNC-AnxA1 treatment modulates macrophage phenotype in intestinal lamina propria

The characterization of cells isolated from the lamina propria demonstrated that DSS ingestion markedly increased the number of neutrophils ($Ly6G^+$; Fig. 3A) and macrophages ($F4/80^+$; Fig. 3B), which reflected increased amount of M1 macrophages ($F4/80/CD80^+$; Fig. 3C). None of the treatments reduced the amounts of neutrophils and macrophages (Fig. 3A and 3B); nevertheless, MLNC-AnxA1 treatment reduced the amount of M1 macrophages ($F4/80/CD80^+$; Fig. 3C) and both AnxA1 and MLNC-AnxA1 treatments elevated the amount of M2 macrophages ($F4/80/CD206^+$; Fig. 3D).

Based on these results, we further investigated if MLNC or MLNC-AnxA1 were up-taken by macrophages. Data presented in Figure S5, obtained in CytoViva experiments, showed cultured Raw 264.7 cells taken up both nanocapsule preparations 24 hs after incubation. Moreover, to test the efficacy of taken up, we investigated the mice bone marrow macrophages polarization into M2 phenotype, as AnxA1 switches macrophage into M2 cells. As visualized in the Figure S6, dexamethasone (positive control of the experiment) and MNLC induced M2 polarization; nevertheless MLNC-AnxA1 effect was higher in comparison to those groups of cells. In addition, only MLNC-AnxA1 treated cells secreted higher amounts of TGF-β, a pro-resolution mediator secreted by M2 cells Figure S6). It is noteworthy to mention, AnxA1-treated cells did not switch cells into M2 profile, reinforcing the importance AnxA1 encapsulation in the MLNC.

3.4. MLNC-AnxA1 treatment improves histological recovery, expression of proteins related to epithelial proliferation and structure

DSS ingestion caused severe damage to the colonic tissue of mice; untreated mice reached the highest histological score (Fig. 4A, C and D) in all parameters: tissue edema (dotted line), dysplasia/altered histoarchitecture (black arrow head), crypt edema (yellow arrow head), inflammatory infiltrates (white arrow head) and ulcerations (black arrow). MLNC-treated mice showed high histological scores, similar to seen for the DSS group (Fig. 4G and H), while AnxA1 treatment elicited improvements on histological scores, reducing some parameters as edema and dysplasia/altered histoarchitecture (Fig. 4E and F). However, only MLNC-AnxA1 treatment led to recovery of the colonic histoarchitecture during colitis, decreasing crypt edema, inflammatory infiltrates and ulcerations, and restoring tissue histoarchitecture in comparison with the DSS group (Fig. 4I and J). Also, the naïve group showed a normal histoarchitecture as expected (Fig. 4B).

Moreover, the area stained for tight adhesion molecules claudin-1 and ZO-1 was reduced in DSS mice (Fig. 5B and G) when compared with naïve group (Fig. 5A and F) and treatments with AnxA1 and MLNC-AnxA1 restored the expression of Claudin-1 (Fig. 5H and J) and MLNC-AnxA1 treatment restored the expression of ZO-1 (Fig. 5E) in inflamed tissues. In addition, AnxA1 and MLNC did not restore the ZO-1 expression (Fig. 5C and D) and MLNC showed the same result as DSS to the expression of claudin-1 (Fig. 5I).

Additionally, the number of proliferative nuclei in the mucosal layer was assessed by counting PCNA and Ki67 positive cells (Fig. 6F and L). PCNA and Ki67 are nuclear proteins; PCNA participates in DNA synthesis and repair pathways, while Ki67 is involved in cell proliferation and ribosomal RNA transcription. For both targets, only treatment with MLNC-AnxA1 increased the number of positive nuclei, mostly in the basal region, indicating regenerative epithelium (Fig. 6E and K). In other treatment groups, there was a low number and structural disorganization of PCNA (Fig. 6G, H, I and J) and Ki67 (Fig. 6A, B, C and D) positive cells, which became irregularly distributed throughout the extension of epithelial cells. Moreover, increased staining in the apical zone of tissue was found in DSS, AnxA1 or MLNC treated groups, indicating areas of dysplasia.

4. Discussion

Development of novel approaches for treatment of IBDs is a collective effort of a massive number of researchers worldwide, considering chronicity and relapsing features of such diseases. Moreover, patients are not always responsive to current pharmacotherapy, and the physical and psychosocial symptoms associated with high costs of medication burdens health care systems [38]. Based on our previous data showing multi-wall LNC (MLNC) as effective tools to functionalize proteins [32,39], we here employed MLNC to functionalize recombinant Annexin A1 (AnxA1), a known anti-inflammatory and tissue repair protein secreted by inflammatory and epithelial cells during IBDs [19,14–16,40–42]. AnxA1 was efficiently functionalized onto MLNC, and MLNC-AnxA1 administered into the peritoneum of mice reduced disease symptoms and improved gut tissue recovery in mice-induced colitis. These effects were not evoked by non-functionalized AnxA1, highlighting the functionalization of AnxA1 into MNLC as a tool to improve local anti-inflammatory and repairing tissues properties of the protein.

The MLNC-AnxA1 supramolecular structure here employed comprises LNC containing polyester as the first wall, coated with a negative

layer of lecithin containing phosphatidic acid that is covered by a chitosan wall generating electrostatic interactions. The incorporation of chitosan was confirmed by the inversion of the zeta potential, by slightly enhancing values of z-average diameters comparing MLNC and MLNC-AnxA1 to LNC. Chitosan is pivotal for coordination of metals within specific protein chemisorption sites. Indeed, the unimodal nanometric profile after protein addition showed high affinity between AnxA1 and Zn^{2+}, and the efficiency of coordination of 92 % confirmed the protein chemisorption at the nanocapsule surface. Mean diameters lower than 200 nm, PDI lower than 0.3 and satisfactory TEM images ensure investigation of biological activity of MLNC-AnxA1 is feasible.

A pivotal challenge was to test the effectiveness of oral administration of MLNC-AnxA1 on colitis, as we hypothesized the supra molecular structure achieved by the multi wall and the covalent binding of the protein to the metal would be robust enough to protect AnxA1 from degradation inside the gastrointestinal compartments. Previous study using the same nanotechnology here employed showed high bioavailability of MLNC-captopril-furosemide by oral route, which was highly efficient in reducing hypertension in comparison to treatments with non-functionalized drugs [33]. Oral administration of MLNC-AnxA1 did not affect the symptoms of colitis. Therefore, it may be inferred *in vivo* actions of physiological components within the gastrointestinal compartments could have displaced the protein from the supra molecular structure and further inactivate it.

Conversely, i.p. administration of MLNC-AnxA1 inhibited the development of main colitis symptoms, the DAI being lower after four treatment doses. Histological analyses corroborated the higher effectiveness of MLNC-AnxA1 in causing tissue recovery. Non-functionalized AnxA1 was not so efficient in restituting epithelial membrane and crypt reorganization as MLNC-AnxA1. These data, alongside the recovery of gut length in MLNC-AnxA1 treated mice, suggest functionalized AnxA1 exerted mechanisms of wound healing.

The onset of epithelial healing in IBD is characterized by rapid migration of epithelial cells in order to reorganize rudimentary barriers, which is followed by influx of inflammatory cells into the lamina propria. Morphological changes of crypts, showing bifurcating/branching structures, and stem cell proliferation supports wound closure, characterized by restitution of the normal pattern of epithelial structure, cellular differentiation, and barrier function [43]. The complexity of cell and molecular mechanisms in wound healing in IBDs involves a broad diversity of targets as markers of the process. We here chose to quantify the profile of immune cells in the lamina propria, expression of tight junction (TJ) molecules involved with epithelial permeability, and markers of cell proliferation.

TJ are expressed at the top of the lateral membrane of intestinal epithelial cells keeping them together as a barrier, forming channels that allow passage between cells and also activate intracellular signaling [44]. Zonula Occludens-1 (ZO-1) is a pivotal regulatory TJ protein for gastrointestinal hemostasis, and alterations on ZO-1 affect expression and functions of other TJ [45]. Therefore, stable dynamic levels of ZO-1 protein are fundamental for normal function of the epithelial barrier. ZO-1 expression was reduced in epithelium of DSS-induced colitic mice, which was rescued to normal levels by MLNC-AnxA1 treatment. Although values were not significantly different, MLNC and Annexin A1 treatments also enhanced ZO-1 expression [46]. Indeed, it has been shown that oral administration of higher doses of chitosan during the resolutive phase of inflammation improved recovery of clinical and histological parameters, including expression of ZO-1 [42]. Claudin-1, also a TJ protein, plays a relevant role in intestinal homeostasis but regulation of its expression depends on type of IBD disease and in which stage it finds itself in regarding symptoms [44,47]. In our model of colitis under our schedule of treatments, claudin-1 expression was reduced and localized in the damaged epithelium of DSS mice group. MLNC-AnxA1 treatment increased the expression of claudin-1, especially in reorganized crypts. Therefore, data herein demonstrated evidence AnxA1, mainly the one released by MLNC, promotes expression of TJ proteins in order to reestablish crypt structure. In fact, the physiological actions of AnxA1 on TJ have been demonstrated in endothelial cells of the blood brain barrier [48], in which deficient expression of the protein is related to the genesis of neurodegenerative diseases. In these cases, acute treatment with AnxA1 rescues TJ expression and ameliorates the development of brain diseases [48–51]. Furthermore, *in vitro* AnxA1 treatment enhanced the expression of both claudin-1 and ZO-1 in uterine epithelium during blastocyte attachment [52]. Associated, these data support AnxA1 as a pivotal protein for stabilizing TJ, and here we show, for the first time, the effect of functionalized AnxA1 on rearrangement of gut epithelial TJ during colitis.

Corroborating the reorganization of crypts visualized in animals treated with MLNC-AnxA1, treatment with the functionalized AnxA1 enhanced the proliferation in the region where transit-amplifying cells and stem cells are localized, at the bottom of crypts and constitute a signaling center that is a pivotal factor for tissue growth [53]. In addition, the treatment with MLNC-functionalized AnxA1 reduced the proliferation of cells extends to the apical tissue. This effect is observed in disorganized growth and proliferated cells approximately-two-thirds of the crypt length can indicate dysplasia. It is also a favorable effect as proliferating cells in PCNA and Ki67 labeling in the damaged tissue indicate dysplasia [54–58].

Taken together, data here depicted highlight the functionalization of AnxA1 as a possible adjuvant to therapeutic approaches employed on IBDs treatment. Previous data had already shown the high effectiveness of nanoparticles loading AnxA1 mimetic peptide Ac2-26 on experimental colitis [16,59] validating further studies.

5. Conclusion

Experimental data provided in this study corroborated the ability of multi-wall LNC functionalization as a tool for delivery of hydrophilic molecules into target tissues. Moreover, the findings support the development of nanoparticles containing AnxA1 to drive it into damaged intestine areas, as it provides effective anti-inflammatory and pro-resolving actions in tissue repair. Short treatment period with area-focused low concentrations of AnxA1 may be an efficient strategy to improve tissue recovery during the relapsing acute inflammatory crisis in IBDs. Nevertheless, further studies must still be carried out to evaluate the risks and benefits of this approach.

Declaration of Competing Interest

The authors declare that they have no known competing financial interests or personal relationships that could have appeared to influence the work reported in this paper.

Data availability

Data will be made available on request.

Acknowledgements

The authors thank the Coordenação de Aperfeiçoamento de pessoal de ensino superior (CAPES); Conselho Nacional de Pesquisa e Desenvolvimento (CNPq) and Fundação de Amparo a Pesquisa do Estado de São Paulo (FAPESP #2014/07328-4).

Milena Fronza Broering (grant #2018/26383-7), Gustavo H. O. da Rocha (grant # 2017/05430-4), Pablo R. S. Scharf (grant # 2020/14368-3) are PhD fellow from FAPESP; Silvia S. Guterres, Adriana R. Pohlmann, and Sandra H. P. Farsky are CNPq researcher fellows.

Appendix A. Supplementary material

Supplementary data to this article can be found online at https://doi.org/10.1016/j.ejpb.2022.10.022.

References

[1] S.C. Ng, H.Y. Shi, N. Hamidi, et al., Worldwide incidence and prevalence of inflammatory bowel disease in the 21st century: a systematic review of population-based studies, Lancet. 390 (10114) (2017) 2769–2778, https://doi.org/10.1016/S0140-6736(17)32448-0.

[2] D.C. Baumgart, W.J. Sandborn, Inflammatory bowel disease: clinical aspects and established and evolving therapies, Lancet. 369 (9573) (2007) 1641–1657, https://doi.org/10.1016/S0140-6736(07)60751-X.

[3] F. Magro, P. Gionchetti, R. Eliakim, et al., Third European Evidence-based Consensus on Diagnosis and Management of Ulcerative Colitis. Part 1: Definitions, Diagnosis, Extra-intestinal Manifestations, Pregnancy, Cancer Surveillance, Surgery, and Ileo-anal Pouch Disorders, J Crohn's Colitis. 11 (6) (2017) 649–670, https://doi.org/10.1093/ecco-jcc/jjx008.

[4] J. Burisch, H. Vardi, D. Schwartz, et al., Health-care costs of inflammatory bowel disease in a pan-European, community-based, inception cohort during 5 years of follow-up: a population-based study, Lancet Gastroenterol Hepatol. 5 (5) (2020) 454–464, https://doi.org/10.1016/S2468-1253(20)30012-1.

[5] F. Gomollón, A. Dignass, V. Annese, et al., 3rd European Evidence-based Consensus on the Diagnosis and Management of Crohn's Disease 2016: Part 1: Diagnosis and Medical Management, J Crohn's Colitis. 11 (1) (2017) 3–25, https://doi.org/10.1093/ecco-jcc/jjw168.

[6] Graham DB, Xavier RJ. Pathway paradigms revealed from the genetics of inflammatory bowel disease. *Nature*. 2025;578. 10.1038/s41586-020-2025-2.

[7] K.O. Chudy-Onwugaje, K.E. Christian, F.A. Farraye, R.K. Cross, A State-of-the-Art Review of New and Emerging Therapies for the Treatment of IBD, Inflamm Bowel Dis. 25 (5) (2019) 820–830, https://doi.org/10.1093/ibd/izy327.

[8] M. Perretti, F. D'Acquisto, Annexin A1 and glucocorticoids as effectors of the resolution of inflammation, Nat Rev Immunol. 9 (1) (2009) 62–70, https://doi.org/10.1038/nri2470.

[9] M.H. Sheikh, E. Solito, Annexin A1: Uncovering the many talents of an old protein, Int J Mol Sci. 19 (4) (2018) 1–20, https://doi.org/10.3390/ijms19041045.

[10] X. Xu, W. Gao, L. Li, et al., Annexin A1 protects against cerebral ischemia–reperfusion injury by modulating microglia/macrophage polarization via FPR2/ALX-dependent AMPK-mTOR pathway, J Neuroinflammation. 18 (1) (2021) 119, https://doi.org/10.1186/s12974-021-02174-3.

[11] S. McArthur, G. Juban, T. Gobbetti, et al., Annexin A1 drives macrophage skewing to accelerate muscle regeneration through AMPK activation, J Clin Invest. 130 (3) (2020) 1156–1167, https://doi.org/10.1172/JCI124635.

[12] J. Cosnes, C. Gower-Rousseau, P. Seksik, A. Cortot, Epidemiology and Natural History of Inflammatory Bowel Diseases, Gastroenterology. 140 (6) (2011), https://doi.org/10.1053/j.gastro.2011.01.055.

[13] G.H.O. da Rocha, M. de Paula-Silva, M.F. Broering, et al., Pioglitazone-Mediated Attenuation of Experimental Colitis Relies on Cleaving of Annexin A1 Released by Macrophages, Front Pharmacol. 11 (December) (2020) 1–19, https://doi.org/10.3389/fphar.2020.591561.

[14] M. de Paula-Silva, B.E. Barrios, L. Macció-Maretto, et al., Role of the protein annexin A1 on the efficacy of anti-TNF treatment in a murine model of acute colitis, *Biochem Pharmacol*. Published online (2016), https://doi.org/10.1016/j.bcp.2016.06.012.

[15] G. Leoni, A. Alam, P. Alexander Neumann, et al., Annexin A1, formyl peptide receptor, and NOX1 orchestrate epithelial repair, J Clin Invest. 123 (1) (2013) 443–454, https://doi.org/10.1172/JCI65831.

[16] G. Leoni, P.A. Neumann, N. Kamaly, et al., Annexin A1'containing extracellular vesicles and polymeric nanoparticles promote epithelial wound repair, J Clin Invest. 125 (3) (2015) 1215–1227, https://doi.org/10.1172/JCI76693.

[17] S. Reischl, J.H. Lee, J.R.E. Miltschitzky, et al., Ac2-26-Nanoparticles Induce Resolution of Intestinal Inflammation and Anastomotic Healing via Inhibition of NF-κB Signaling in a Model of Perioperative Colitis, *Inflamm Bowel Dis*. Published online (January 29, 2021.), https://doi.org/10.1093/ibd/izab008.

[18] A. Sena, I. Grishina, A. Thai, et al., Dysregulation of Anti-Inflammatory Annexin A1 Expression in Progressive Crohns Disease, *PLoS One*. Published online (2013), https://doi.org/10.1371/journal.pone.0076969.

[19] M. de Paula-Silva, G.H.O. da Rocha, M.F. Broering, et al., Formyl Peptide Receptors and Annexin A1: Complementary Mechanisms to Infliximab in Murine Experimental Colitis and Crohn's Disease, Front Immunol. 12 (September) (2021) 1–12, https://doi.org/10.3389/fimmu.2021.714138.

[20] S. Calgaroto, L.E. Fauri, L.A. Frank, K. Paese, S.S. Guterres, A.R. Pohlmann, Chemical stability, mass loss and hydrolysis mechanism of sterile and non-sterile lipid-core nanocapsules: The influence of the molar mass of the polymer wall, React Funct Polym. 133 (2018) 161–172, https://doi.org/10.1016/J.REACTFUNCTPOLYM.2018.09.018.

[21] E. Jäger, C.G. Venturini, F.S. Poletto, et al., Sustained Release from Lipid-Core Nanocapsules by Varying the Core Viscosity and the Particle Surface Area, J Biomed Nanotechnol. 5 (1) (2009), https://doi.org/10.1166/jbn.2009.1004.

[22] C.G. Venturini, E. Jäger, C.P. Oliveira, et al., Formulation of lipid core nanocapsules. *Colloids Surfaces A Physicochem Eng Asp*, Published online (2011), https://doi.org/10.1016/j.colsurfa.2010.12.011.

[23] S.F. Rodrigues, L.A. Piel, A.L. Shimada, et al., Lipid-core nanocapsules act as a drug shuttle through the blood brain barrier and reduce glioblastoma after intravenous or oral administration, J Biomed Nanotechnol. 12 (5) (2016) 986–1000, https://doi.org/10.1166/jbn.2016.2215.

[24] N.R.C. Pereira, R.A. Loiola, S.F. Rodrigues, et al., Mechanisms of the effectiveness of poly(ε-caprolactone) lipid-core nanocapsules loaded with methotrexate on glioblastoma multiforme treatment, Int J Nanomedicine. 13 (2018) 4563–4573, https://doi.org/10.2147/IJN.S168400.

[25] S. Sandri, C.B. Hebeda, R.A. Loiola, et al., Direct effects of poly(ε-caprolactone) lipid-core nanocapsules on human immune cells, Nanomedicine. 14 (11) (2019) 1429–1442, https://doi.org/10.2217/nnm-2018-0484.

[26] Drewes carine, de cs alves aline, hebeda cristina B, et al. role of poly (ε-caprolactone) lipid-core nanocapsules on melanoma-neutrophil crosstalk. *Int J Nanomedicine*. Published online 2017:12-7153. 10.2147/IJN.S140557.

[27] C.P. Oliveira, W.A. Prado, V. Lavayen, et al., Bromelain-Functionalized Multiple-Wall Lipid-Core Nanocapsules: Formulation, Chemical Structure and Antiproliferative Effect Against Human Breast Cancer Cells (MCF-7), Pharm Res. 34 (2) (2017), https://doi.org/10.1007/s11095-016-2074-2.

[28] L.R. Zancan, F.A. Bruinsmann, K. Paese, et al., Oral delivery of ambrisentan-loaded lipid-core nanocapsules as a novel approach for the treatment of pulmonary arterial hypertension, Int J Pharm. (2021) 610, https://doi.org/10.1016/j.ijpharm.2021.121181.

[29] E.A. Bender, M.D. Adorne, L.M. Colomé, D.S.P. Abdalla, S.S. Guterres, A. R. Pohlmann, Hemocompatibility of poly(ε-caprolactone) lipid-core nanocapsules stabilized with polysorbate 80-lecithin and uncoated or coated with chitosan, Int J Pharm. 426 (1–2) (2012) 271–279, https://doi.org/10.1016/j.ijpharm.2012.01.051.

[30] E.A. Bender, M.F. Cavalcante, M.D. Adorne, et al., New strategy to surface functionalization of polymeric nanoparticles: One-pot synthesis of scFv anti-LDL (-)-functionalized nanocapsules, Pharm Res. 31 (11) (2014) 2975–2987, https://doi.org/10.1007/s11095-014-1392-5.

[31] Bruinsmann FA, de Cristo Soares Alves A, de Fraga Dias A, et al. Nose-to-brain delivery of simvastatin mediated by chitosan-coated lipid-core nanocapsules allows for the treatment of glioblastoma in vivo. *Int J Pharm*. 2022;616:121563. 10.1016/j.ijpharm.2022.121563.

[32] M.F. Cavalcante, M.D. Adorne, W.M. Turato, et al., scFv-Anti-LDL(-)-Metal-Complex Multi-Wall Functionalized-Nanocapsules as a Promising Tool for the Prevention of Atherosclerosis Progression, Front Med. (2021) 8, https://doi.org/10.3389/fmed.2021.652137.

[33] C.B. Michalowski, M.D. Arbo, L. Altknecht, et al., pharmaceutics Oral Treatment of Spontaneously Hypertensive Rats with Captopril-Surface Functionalized Furosemide-Loaded Multi-Wall Lipid-Core Nanocapsules, Pharmaceutics. 12 (2020) 80, https://doi.org/10.3390/pharmaceutics12010080.

[34] D.H.M. Kusters, M.L. Chatrou, B.A.G. Willems, et al., Pharmacological Treatment with Annexin A1 Reduces Atherosclerotic Plaque Burden in LDLR-/-Mice on Western Type Diet, Published online (2015), https://doi.org/10.1371/journal.pone.0130484.

[35] K. Geboes, R. Riddell, A. Öst, B. Jensfelt, T. Persson, R. Löfberg, A reproducible grading scale for histological assessment of inflammation in ulcerative colitis, Gut. 47 (2000) 404–409, https://doi.org/10.1136/gut.47.3.404.

[37] R. Cé, J.G. Marchi, V.Z. Bergamo, et al., Chitosan-coated dapsone-loaded lipid-core nanocapsules: Growth inhibition of clinical isolates, multidrug-resistant Staphylococcus aureus and Aspergillus ssp, Colloids Surfaces A Physicochem Eng Asp. 511 (2016) 153–161, https://doi.org/10.1016/j.colsurfa.2016.09.086.

[38] G.G. Kaplan, T. Jess, The Changing Landscape of Inflammatory Bowel Disease: East Meets West, Gastroenterology. 150 (1) (2016), https://doi.org/10.1053/j.gastro.2015.11.029.

[39] de Castro Leão M, Raffin Pohlmann A, de Cristo Soares Alves A, et al. Docosahexaenoic acid nanoencapsulated with anti-PECAM-1 as co-therapy for atherosclerosis regression. *Eur J Pharm Biopharm*. 2021;159. 10.1016/j.ejpb.2020.12.016.

[40] N. Vergnolle, Proteinase-activated receptor-2-activating peptides induce leukocyte rolling, adhesion, and extravasation in vivo, J Immunol. 163 (9) (1999) 5064–5069. http://www.ncbi.nlm.nih.gov/pubmed/10528212.

[41] N. Vergnolle, P. Pagès, R. Guimbaud, et al., Annexin 1 is secreted in situ during ulcerative colitis in humans, Inflamm Bowel Dis. 10 (5) (2004) 584–592, https://doi.org/10.1097/00054725-200409000-00013.

[42] B.A. Babbin, M.G. Laukoetter, P. Nava, et al., Annexin A1 Regulates Intestinal Mucosal Injury, Inflammation, and Repair, J Immunol. 181 (7) (2008) 5035–5044, https://doi.org/10.4049/jimmunol.181.7.5035.

[43] K. Sommer, M. Wiendl, T.M. Müller, et al., Intestinal Mucosal Wound Healing and Barrier Integrity in IBD–Crosstalk and Trafficking of Cellular Players, Front Med. (2021) 8, https://doi.org/10.3389/fmed.2021.643973.

[44] S. Čužić, M. Antolić, A. Ognjenović, et al., Claudins: Beyond Tight Junctions in Human IBD and Murine Models, Front Pharmacol. (2021) 12, https://doi.org/10.3389/fphar.2021.682614.

[45] H. Zhang, S. Zhang, J. Zhang, et al., ZO-1 expression is suppressed by GM-CSF via miR-96/ERG in brain microvascular endothelial cells, J Cereb Blood Flow Metab. 38 (5) (2018) 809–822, https://doi.org/10.1177/0271678X17702668.

[46] J. Wang, C. Zhang, C. Guo, X. Li, Chitosan Ameliorates DSS-Induced Ulcerative Colitis Mice by Enhancing Intestinal Barrier Function and Improving Microflora, Int J Mol Sci. 20 (22) (2019) 5751, https://doi.org/10.3390/ijms20225751.

[47] J.L. Pope, A.A. Bhat, A. Sharma, et al., Claudin-1 regulates intestinal epithelial homeostasis through the modulation of Notch-signalling, *Gut*. Published online (2014), https://doi.org/10.1136/gutjnl-2012-304241.

[48] Cristante E, McArthur S, Mauro C, et al. Identification of an essential endogenous regulator of blood-brain barrier integrity, and its pathological and therapeutic implications. *Proc Natl Acad Sci U S A*. Published online 2013. 10.1073/pnas.1209362110.

[49] J.C. Park, S.H. Baik, S.H. Han, et al., Annexin A1 restores Aβ1-42-induced blood–brain barrier disruption through the inhibition of RhoA-ROCK signaling pathway, Aging Cell. 16 (1) (2017) 149–161, https://doi.org/10.1111/acel.12530.

[50] M. Ries, H. Watts, B.C. Mota, et al., Annexin A1 restores cerebrovascular integrity concomitant with reduced amyloid-β and tau pathology, Brain. 144 (5) (2021) 1526–1541, https://doi.org/10.1093/brain/awab050.
[51] M.H. Sheikh, S.M. Henson, R.A. Loiola, et al., Immuno-metabolic impact of the multiple sclerosis patients' sera on endothelial cells of the blood-brain barrier, J Neuroinflammation. 17 (1) (2020), https://doi.org/10.1186/s12974-020-01810-8.
[52] C.B. Hebeda, S. Sandri, C.M. Benis, et al., Annexin A1/Formyl Peptide Receptor Pathway Controls Uterine Receptivity to the Blastocyst, Cells. 9 (5) (2020), https://doi.org/10.3390/cells9051168.
[53] Y.-C. Hsu, L. Li, E. Fuchs, Transit-Amplifying Cells Orchestrate Stem Cell Activity and Tissue Regeneration, Published online (2014), https://doi.org/10.1016/j.cell.2014.02.057.
[54] S. Randall-Demllo, S. Singh Sohal, D. Kunde, et al., Characterisation of colonic dysplasia-like epithelial atypia in murine colitis Basic Study, World J Gastroenterol. 22 (37) (2016) 8334–8348, https://doi.org/10.3748/wjg.v22.i37.8334.
[55] K. Mrouj, N. Andrés-Sánchez, G. Dubra, et al., Ki-67 regulates global gene expression and promotes sequential stages of carcinogenesis, Proc Natl Acad Sci U S A. 118 (10) (2021) 1–12, https://doi.org/10.1073/pnas.2026507118.
[56] Drewes CC, Alves A de CS, Hebeda CB, et al. Role of poly(ε-caprolactone) lipid-core nanocapsules on melanoma-neutrophil crosstalk. *Int J Nanomedicine*. Published online 2017. 10.2147/IJN.S140557.
[57] Araki. Increased apoptosis and decreased proliferation of colonic epithelium in dextran sulfate sodium-induced colitis in mice. Oncol. Rep. 2010;24(4). 10.3892/or.2010.869.
[58] M. Juríková, L. Danihel, Š. Polák, I. Varga, Ki67, PCNA, and MCM proteins: Markers of proliferation in the diagnosis of breast cancer, Acta Histochem. 118 (5) (2016) 544–552, https://doi.org/10.1016/j.acthis.2016.05.002.
[59] C. Li, Y. Zhao, J. Cheng, et al., A Proresolving Peptide Nanotherapy for Site-Specific Treatment of Inflammatory Bowel Disease by Regulating Proinflammatory Microenvironment and Gut Microbiota, Adv. Sci. 6 (18) (2019), https://doi.org/10.1002/advs.201900610.

Co-autoria 2023

Biomedicine & Pharmacotherapy 167 (2023) 115474

Contents lists available at ScienceDirect

Biomedicine & Pharmacotherapy

journal homepage: www.elsevier.com/locate/biopha

Effect of nanocapsules containing docosahexaenoic acid in mice with chronic inflammation

Matheus de Castro Leão [a], Isabella di Piazza [a], Sarah Jorge Caria [a], Milena Fronza Broering [b], Sandra Helena Poliselli Farsky [b], Mayara Klimuk Uchiyama [c], Koiti Araki [c], Kennedy Bonjour [d], Bruno Cogliati [d], Adriana Raffin Pohlmann [e], Silvia Stanisçuaski Guterres [f], Inar Alves Castro [a,*]

[a] Department of Food and Experimental Nutrition, Faculty of Pharmaceutical Sciences, University of São Paulo, São Paulo, São Paulo, Brazil
[b] Department of Clinical & Toxicological Analyses, School of Pharmaceutical Sciences, University of São Paulo, São Paulo, São Paulo, Brazil
[c] Department of Fundamental Chemistry, Institute of Chemistry, University of São Paulo, São Paulo, São Paulo, Brazil
[d] Department of Pathology, School of Veterinary Medicine and Animal Science, University of São Paulo, São Paulo, São Paulo, Brazil
[e] Department of Organic Chemistry, Institute of Chemistry, Federal University of Rio Grande do Sul, Porto Alegre, Rio Grande do Sul, Brazil
[f] Department of Production and Drugs Control, Pharmaceutical Faculty, Federal University of Rio Grande do Sul, Porto Alegre, Rio Grande do Sul, Brazil

ARTICLE INFO

Keywords:
Atherosclerosis
Nanocapsules
DHA
Inflammation
Omega 3
Cytokines

ABSTRACT

Background: Omega 3 fatty acids, such as docosahexaenoic acid (DHA) have been widely consumed as supplements to control chronic inflammation. Nanocapsules containing DHA (MLNC-DHA-a1) were developed and showed excellent stability. Thus, our objective was to evaluate the effect of MLNC-DHA-a1 nanocapsules on biomarkers of chronic inflammation.

Methods: Cells viability was determined by flow cytometry. The uptake of MLNC-DHA-a1 nanocapsules by macrophages and their polarization were determined. *In vivo*, *LDLr*$^{(-/-)}$ mice were fed a Western diet to promote chronic inflammation and were treated with MLNC-DHA-a1 nanocapsules, intravenously injected via the caudal vein once a week for 8 weeks.

Results: MLNC-DHA-a1 nanocapsules decreased the concentration of TNFα ($p = 0.02$) in RAW 264.7 cells compared to the non-treated group (NT), with no changes in IL-10 ($p = 0.29$). The nanocapsules also exhibited an increase in the M2 ($F4/80^+$ CD206) phenotype ($p < 0.01$) in BMDM cells. *In vivo*, no difference in body weight was observed among the groups, suggesting that the intervention was well tolerated. However, compared to the CONT group, MLNC-DHA-a1 nanocapsules led to an increase in IL-6 (90.45 ×13.31 pg/mL), IL-1β (2.76 ×1.34 pg/mL) and IL-10 (149.88 ×2.51 pg/mL) levels in plasma.

Conclusion: MLNC-DHA-a1 nanocapsules showed the potential to promote *in vitro* macrophage polarization and were well-tolerated *in vivo*. However, they also increased systemic pro-inflammatory cytokines. Therefore, considering that this immune response presents a limitation for clinical trials, further studies are needed to identify the specific compound in MLNC-DHA-a1 that triggered the immune response. Addressing this issue is essential, as MLNC-DHA-a1 tissue target nanocapsules could contribute to reducing chronic inflammation.

1. Introduction

Chronic inflammatory conditions lead to several diseases that collectively represent the leading causes of disability and mortality worldwide, such as cardiovascular disease, cancer, diabetes mellitus, chronic kidney disease, non-alcoholic fatty liver disease, autoimmune and neurodegenerative disorders [1–4]. In these examples, the long-lasting chronic inflammation is a result of the signaling promoted by cells of the innate and adaptive immune system, as response to the presence of damage-associated molecular patterns (DAMPs) in the blood stream or inside the host cells and tissues [1,5].

The reaction of the immune system cells to various types of DAMPs is complex and difficult of controlling. For this reason, in many cases, due to discomfort, pain or even risk of more severe complications, the

* Correspondence to: LADAF, Department of Food and Experimental Nutrition, Faculty of Pharmaceutical Sciences, University of São Paulo, Av. Lineu Prestes, 580, B14, Zip Code: - 05508–900, São Paulo, São Paulo, Brazil.
E-mail address: inar@usp.br (I.A. Castro).

https://doi.org/10.1016/j.biopha.2023.115474
Received 28 June 2023; Received in revised form 6 September 2023; Accepted 7 September 2023
Available online 21 September 2023

systemic inflammation is suppressed by drugs. However, non-steroidal anti-inflammatory drugs (NSAIDs) or glucocorticoids, have many adverse effects [6–10], and their continuous intake can increase the individual susceptibility to infections [11,12].

In this context, pharmacological strategies based on bioactive compounds could provide an interesting alternative to complement drug prescriptions, thereby improving the quality of life for patients. Among the bioactive lipids, it has been reported the anti-inflammatory effects attributed to omega-3 fatty acids, particularly eicosapentaenoic acid (C20:5 n3; EPA) and docosahexaenoic acid (C22:6 n3; DHA) [13]. EPA and DHA exert anti-inflammatory activity by replacing arachidonic acid (AA) in the phospoholipids, leading to produce less potent prostaglandins, prostacyclins, leukotrienes and thromboxanes after the activation of cyclooxigenases (COX) and lipoxygenases (LOX) [13,14]. In addition, EPA and DHA can inhibit the translocation of the nuclear factor NF-kappaB (NFkB) to the nucleus through Peroxisome proliferator-activated receptor gamma (PPARγ) depending mechanisms, reducing the expression of genes encoding pro-inflammatory molecules [14–16]. It has also been reported that EPA and DHA suppress the inflammasome pathway, decreasing the Interleukin 1β (IL1β) maturation and release, and they can also serve as substrates for the synthesis of specialized pro-resolving mediators (SPMs), such as resolvins, protectins and maresins, capable of resolving the inflammatory process [2,3,17–19]. In fact, EPA and DHA may posses preventive and therapeutic potential in managing chronic inflammatory diseases [16], and new-nanotechnology-based strategies have been developed to deliver omega − 3 fatty acids to target tissues [20].

On the other side, strategies involving general immunosuppression have shown some important limitations, because inflammation is essential to protect individuals also against pathogens–associated molecular patterns (PAMPs) and damage-associated molecular patterns (DAMPs) [1,2]. One example is a study published by Ridcker et al., in which patients with cardiovascular disease treated with Interleukin-1β monoclonal antibody showed a reduction of cardiovascular events, but had more infections caused by the systemic suppression of the immune system [21]. Thus, it is necessary to develop alternatives for reducing chronic inflammation without inhibiting the immune system's ability to protect the body against new infections. One alternative is the application of nanotechnology-based drug delivery systems to deliver anti-inflammatory compound straightly to the target tissue. Nanoparticle-mediated drug delivery systems have been used in anti-inflammatory therapies, reducing medical dosage and improving therapeutic effectiveness [22].

In a previous study carried out by our group [23], anti-PECAM-1-surface-functionalized metal-complex multi-wall nanocapsules containing DHA richer algae oil in their core (MLNC-DHA-a1) were developed, showed a 94.80% conjugation efficiency and did not show significant toxicity towards HUVEC cells. Thus, our hypothesis, as summarized in Fig. 1, is that MLNC-DHA-a1 nanocapsules could be engulfed by the macrophage as a DAMP, their lipid content hydrolyzed by lysosomal lipases, releasing non-esterified fatty acids (NEFA) such as DHA for generation of lipid mediators [24]. Upon Toll-like receptor 4 (TLR4) activation, there is a rapid decrease in the cellular content of polyunsaturated fatty acids due to increased phagocytic activity, endoplasmic reticulum enlargement and synthesis of oxylipins [25]. Thus, it is supposed that the DHA supplied by our nanocapsules can be rapidly oxidized by cyclooxygenase, 5-lipoxygenase and cytochrome P450 (CYP), leading to the synthesis of anti-inflammatory oxylipins, including Specialized Pro-Resolving Mediators (SPMs) [25,26]. SPMs modulate the phenotype conversion of M1 into M2 macrophages, contributing to the resolution of inflammation [27]. In addition, the increase of DHA/AA ratio can reduce the inflammation by other mechanisms [13].

Given the hypothesis outlined in Fig. 1, it is important to evaluate the cytotoxicity, determine the *in vitro* effect of these nanocapsules on macrophage uptake and polarization, and to evaluate the tolerance of the animals to the nanocapsules injections and their inflammatory

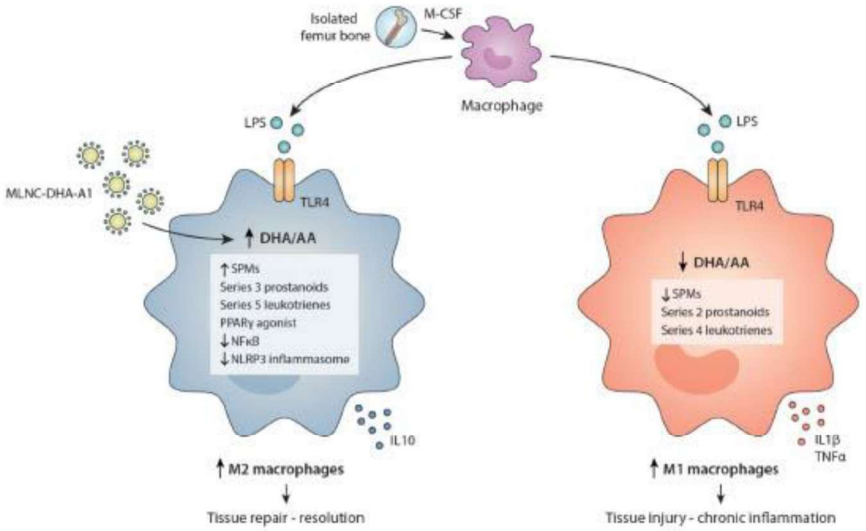

Fig. 1. Summary of the strategy proposed in this study. The surface-functionalized (anti-PECAM-1) metal-complex multi-wall nanocapsules containing algae oil as DHA source (MLNC-DHA-a1) could be internalized by the macrophages, promoting a higher DHA/AA ratio inside the cell compared with non-treated samples. As consequence, MLNC-DHA-a1 supplemented cells could show an anti-inflammatory condition associated to M2 polarization, leading to a higher plaque stability. Abbreviations: Macrophage colony-stimulating factor (M-CSF), Lipopolysaccharides (LPS), Tool Like Receptor 4 (TLR4), docosahexaenoic acid (DHA), arachidonic acid (AA), Interleukin 1β (IL 1β), Interleukin 10 (IL 10), Tumor necrosis factor-alpha (TNF-α), Peroxisome proliferator-activated receptor gamma (PPARγ), factor nuclear kappa B (NFkB), NOD-, LRR- and pyrin domain-containing protein 3 inflammasome (NLRP3) and Specialized pro-resolving mediators (SPMs).

response in plasma and liver after the treatment.

2. Material and methods

2.1. Materials

Lipid-core nanocapsules containing DHA (LNC-DHA), multi-wall nanocapsules containing DHA (MLNC-DHA) and the surface-functionalized (anti-PECAM-1) metal-complex multi-wall nanocapsules containing DHA (MLNC-DHA-a1) were prepared and characterized in our previous study [23] (Fig. S1). Algae oil applied in the oral supplementation (DHASCO™) was purchased from DSM (Heerlen, Netherlands). Medium-chain triacylglycerol (MCT) was purchased from Nutrimed Ind. Ltda (São Paulo, Brazil). Honey was supplied by Apis-Nutri Ltd. (Mandaguari, Brazil). The fatty acid composition of the algae oil and MCT were previously described in another study published by our group [23].

2.2. Methods

2.2.1. Cell culture

RAW 264.7 (immortalized murine macrophages) cells were obtained from the Rio de Janeiro Cell Bank (BCRJ, Rio de Janeiro, RJ, Brazil) and cultured in DMEM (Gibco, Grand Island, NY, USA) high glucose (4500 pg/mL) containing 10% FBS. Cells were kept at 37 °C under a controlled CO_2 atmosphere of 5%. Cell's culture medium was replaced every 2–3 days and the cells were trypsinized with 0.01% trypsin in EDTA buffer (Vitrocell Embriolife, Campinas, SP, Brazil).

2.2.2. Cell viability

The cytotoxicity of the nanocapsules was evaluated using a flow cytometer after culturing. Briefly, cells were seeded at 2.5×10^4 cells/well in 24-well microplates (Costar® Multiple Well Cell Culture Plates, Corning, Glendale, Arizona, USA) and kept at 37 °C for 24 h. Afterward, cells were treated with LNC-DHA; MLNC-DHA and MLNC-DHA-a1 (Fig. S1) at three concentrations: 0.14, 0.75 and 1.40×10^{11} nanoparticles/mL, and cultured for 24, 48 and 72 h. Isolated anti-PECAM-1 was also evaluated at a 200 μg/mL concentration. After that, cells were detached and washed twice in phosphate-buffered saline containing 1% bovine serum albumin. Next, cells were incubated with Annexin V (previously diluted (1:20) in Annexin V (Life Technologies, Carslabe, USA) binding buffer (10 mM N-2-hydroxyethylpiperazine-N′−2-ethanesulfonic acid, 140 mM NaCl, 25 mM $CaCl_2$, pH 7.4; BD Pharmingen, Franklin Lakes, NJ) during 20 min in the dark, at room temperature. After this, 200 μL Annexin V binding buffer and 7-AAD (1:200) were added. Data from 10,000 events were acquired in an Accuri C6 flow cytometer (BD Pharmingen), and the stained cells were analyzed. The negative double group for AnxV and 7-AAD-(non-apoptotic and non-necrotic) marking was plotted to quantify the cell viability (AnxV-, 7-ADD -), single marking with AnxV represented cells in apoptosis (AnxV+, 7-ADD -), single marking with 7-AAD indicated cells in necrosis (AnxV-, 7-ADD+), while the double group positive for AnxV-7-AAD denoted the group of cells in late apoptosis (AnxV+ , 7-ADD+). The results of triplicates were expressed as a percentage (%).

2.2.3. Real-time uptake of the nanocapsules by RAW 264.7 macrophages

The uptake of nanocapsules by macrophages was determined by enhanced dark-field hyperspectral microscopy (CytoViva®) as described by Sandri et al. [28]. First, RAW 264.7 murine macrophages (8×10^4 cells) were seeded in extra clean dust-free Nexterion® Glass D coverslips (#D263T; Schott, New York, NY, USA) present in 96-well plates (Corning, NY, USA). After adherence, cells were incubated with a medium containing MLNC-DHA and MLNC-DHA-a1 at 0.75×10^{11} nanoparticles/mL for 4 h at 37 °C under a 5% CO_2 atmosphere. A non-treated group (NT) was kept in DMEM 10% SFB. Immediately after incubation, cells were washed three times with 5% FBS-PBS, and the coverslip was placed on extra clean dust-free Nexterion® Glass B slides (NexterionR Glass B; Schott, NY, EUA) containing 10 μL of 5% FBS-PBS. Then, 10 μL of cell solution were set up using extra clean dust-free slides (NexterionR Glass B; Schott, NY, USA) and coverslips (Nexterion Glass D #D263T; Schott). RAW 264.7 murine macrophages were imaged using a CytoViva Ultra Resolution Imaging System (CytoViva, Inc., AL, USA) mounted on an Olympus BX51 microscope (x1500 magnification; Olympus Corporation, Tokyo, Japan) equipped with fluorite 100 × oil iris 0.6–1.30 numerical aperture (NA) objective and a 75 W Xe light source. Optical images were taken using a Dage XL CCD digital camera with Image Processing Software (Dage ®; DAGE-MTI of MC, Inc., MI, USA). ImageJ software, version 2.1.0/ 1.53c (2010–2022), was used to place the scale bars. One hundred cells from representative photomicrographs were randomly chosen for this measurement and each treatment.

2.2.4. Macrophage polarisation

The experiment was performed according to the method previously established by Ying et al. [29]. Initially, C57Bl/6 mice were anesthetized and euthanized to collect the left and right femurs for medullary washes collection, using an icy PBS solution containing 2% Fetal Bovine Serum (FBS). All animal experiments were conducted under the National Institutes of Health guidelines and were approved by the Institutional Animal Care and Use Committee of FCF/USP. Then the bone marrow pool was resuspended using 21 G needles to dissociate the cells and pass them through a 70 μm cell strainer to remove other tissues. The cells were washed with NH_4Cl 0.8% solution and incubated in ice for red cell removal. After centrifugation for 5 min, 500 x g at 4 °C, the cells were resuspended with bone marrow-derived macrophages (BMDM) medium, composed of IMDM (Iscove Modified Dulbecco Media), 20% L929 cell culture rich in monocyte growth factor (M-CSF) and 10% of FBS. The cells were counted and plated at the concentration of 5×10^5 cells/well in a 24-well plate and maintained in BMDM medium for 7 days for cell differentiation. After this period, and considering that this time provides 90% of macrophage differentiation, naive cells were exposed to *Escherichia coli* (LPS) 100 ng/mL and maintained for 24 h to generate the M1- inflammatory phenotype macrophage. Treatments were performed with dexamethasone (500 ng/mL), MLNC-DHA (0.75×10^{11} particles/mL) or MLNC-DHA-a1 (0.75×10^{11} particles/mL containing 200 μg/mL of Anti-PECAM-1). After 48 h, the supernatant was removed and cytokines were analyzed by ELISA assay according to the manufacturer's instructions. Single-cell suspensions were prepared at 2×10^7 cells/mL in staining buffer (10% FCS in PBS) and pre-incubated with 1 μg of the 2.4G2 antibodies for 5–10 min on ice prior to staining. About 50 μL of cell suspension (equal to 10^6 cells) were dispensed into each tube or well along with a previously determined optimal concentration of cell surface specific antibody against $F4/80^+$ CD80 and $F4/80^+$ CD206 for differentiation of M1 and M2 macrophages respectively, in 50 μL of staining buffer. Cell surface expression of these maturation markers was measured on BD opteia™ kits (BD Biosciences). The collected events were analyzed with FlowJo v7.6 (Treestar).

2.2.5. Animal protocol

Three-month-old male homozygous $LDLr^{(-/-)}$ mice in the C57BL/6 background were purchased from the Faculty of Pharmaceutical Sciences, University of São Paulo. The animals were divided into 5 groups and kept for 24 weeks under a Western diet *ad libitum*. After this period, one group (BASELINE) was euthanized (n = 10), and the diet of the other groups was replaced by AIN93M regular diet [30] for 8 weeks (Fig. S2). The animals were kept at 25 ± 2 °C and relative humidity of 55 ± 15% in an inverted cycle of 12 h light/12 h dark. Diet formulation and chemical composition is shown in Supplementary material (Table S1 and Table S2), respectively. Food intake and animal weight were weekly measured. During the last 8 weeks, DHA-D group (n = 9) was supplemented with algae oil by gavage. Algae oil (0.011 mL) was mixed with 0.094 mL of honey and 0.094 mL of soybean oil to reduce the gavage stress [31]. This mixture (0.20 mL) was given to each animal

once a week, and the dose was based on 1.8 g/day for humans [32]. CONT group (n = 11) had no supplementation. The MLNC-DHA-a1 group (n = 15) received 5.36×10^8 surface-functionalized (anti–PECAM-1) metal-complex multi-wall nanocapsules containing 12 μL algae oil/mL and LNC-MCT group (n = 15) received 1.09×10^8 lipid-core nanocapsules containing 12 μL MCT/mL, intravenously injected via caudal vein once a week. The body weight of the animals at the beginning of the intervention was 47.03 ± 0.62 g. Thus, the dose of DHA provided by diet or nanocapsules were 28.57 mg ≈ 10 mg DHA Kg bw/day and 0.0011 mg ≈ 0.0004 mg DHA Kg bw/day, respectively. After this second period, mice were anesthetized with isoflurane and euthanized. Blood samples were collected after the euthanasia, transferred to EDTA (1%) vacutainer tubes, and centrifuged at 3000 x g for 10 min at 4 °C. Tissues and plasma were frozen in liquid nitrogen and stored at − 80 °C for analysis.

2.2.6. Plasma metabolites

The concentration of plasma lipids, including total cholesterol (TC), triglycerides (TG), high-density lipoprotein (HDL), low-density lipoprotein (LDL), besides glucose, aspartate transaminase (AST) and alanine transaminase (ALT) was quantified using commercial kits from Labtest Diagnóstica SA (Lagoa Santa, Brazil).

2.2.7. Inflammatory and oxidative stress biomarkers

The cytokines concentration, including interleukin-6 (IL-6), tumor necrosis factor-alpha (TNF-α), interleukin-10 (IL-10) and interleukin 1β (IL-1β), was quantified in plasma and liver homogenate, using MILLIPLEX MAP Mouse Cytokine/Chemokine Magnetic Bead Panel (MCYTOMAG-70 K) (Millipore, St. Charles, MO, USA). The protein content of the homogenates was quantified by Bradford methodology. Malondialdehyde (MDA) concentration was determined by reverse phase HPLC according to Hong et al. [33] and analyzed using a Phenomenex reverse-phase C18 analytical column (250 mm × 4.6 mm; 5 mm; Phenomenex) with an LC8-D8 pre-column (Phenomenex AJ0- 1287) coupled to an HPLC (Agilent Technologies 1200 Series). A standard curve was prepared using 1,1,3,3-Tetraethoxypropane (TEP, T9889 Sigma-Aldrich), and data were expressed as nmol/mg protein.

2.2.8. Fatty acids proportion

Fatty acids were determined in the liver homogenates and plasma according to Shirai et al. [34] using a gas chromatography coupled with a triple quadrupole mass spectrometer (GC-MS Agilent 7890 A GC System, Agilent Technologies Inc., Santa Clara, USA). Fatty acids were separated on a fused silica capillary column (J&W DB-23 Agilent Inc. Santa Clara, USA). Compounds were identified by comparing the retention time of fatty acids in the samples with the retention time of standards (FAME 37 Component Mix Supelco 47885) and also based on a comparison of their mass spectra with those given in the spectral database of the National Institute of Standards and Technology (NIST, Gaithersburg, MD, USA). One analysis was carried out/animal, and the fatty acid/IS (C23:0, Fluka 91478) area ratio was applied to calculate the percentage of each fatty acid.

2.2.9. Statistical analysis

Data were presented as mean ± SEM. Treatments were compared using one-way ANOVA and Tukey HSD post-test or non-parametric Kruskal-Wallis ANOVA by Ranks, followed by Multiple Comparisons (2-tailed). T-test or Mann-Whitney test were applied to compare BASELINE and CONT groups. A p-value of 0.05 was adopted to reject the null hypothesis. Calculations will be performed using Statistica v.13 (TIBCO Software Round Road, TX, USA). Graphs were elaborated using R Studio and GraphPad Prism v9 (GraphPad Software, CA, USA).

3. Results

3.1. In vitro assays

The toxicity of the nanocapsules was determined using RAW 264.7 murine macrophages (Fig. 2). The results showed that the viability of the cells incubated with three concentrations of nanocapsules for 24 h (Fig. 2A), ranged from 52.36 ± 17.62% to 83.33 ± 1.59%, but did not differ among themselves ($p = 0.39$) (Fig. 2B). A similar trend was observed after 48 h (Fig. S3) and 72 h (Fig. S4). Although no statistically differences were observed, we opted to proceed with the concentration of 0.75×10^{11} nanocapsules/mL was for the subsequent assays to minimize any potential toxicological risk. Fig. 3 shows that all nanocapsules were internalized as a damage-associated molecular pattern (DAMP) by RAW 264.7 macrophages, according to the strategy proposed in our hypothesis (Fig. 1). In the next step, BMDM cells were applied to evaluate macrophage polarization. As shown in Fig. 4, internalization of MLNC-DHA and MLNC-DHA-a1, led to a reduction in TNF-α compared with NT cells ($p = 0.01$) (Fig. 4A), while no difference was observed to IL-10 ($p = 0.29$) (Fig. 4B). Regarding to macrophage polarization, treatments with dexamethasone or nanocapsules did not change the M1 phenotype ($p = 0.25$) (Fig. 4C). However, MLNC-DHA-a1 enhanced ($p < 0.01$) M2 phenotype compared with NT cells, while MLNC-DHA showed a trend to increase it ($p = 0.06$) (Fig. 4D), suggesting the beneficial effect of the nanocapsule in promoting macrophage switch phenotype.

3.2. In vivo assays

This is the first *in vivo* study that applies a surface-functionalized nanocapsule containing algae oil in the core. For this reason, our first challenge was to evaluate if weekly caudal injections could influence diet intake and, consequently, body weight gain of the animals. In our experimental protocol, all groups received a Western diet for 24 weeks. After, about two to three animals were selected from each group to compose the BASELINE (n = 10) group, while the remaining animals were divided into four groups (n = 9–15) and received a regular diet for 8 weeks. There was no difference among the groups at the beginning (25.74 ± 0.31 g, $p = 0.32$, $n = 57$), nor after 24 weeks under a Western diet containing about 36% lipids (47.03 ± 0.62 g, $p = 0.57$, $n = 56$). The same was observed among the 4 groups receiving a regular diet after 32 weeks (35.39 ± 0.65 g, $p = 0.49$, $n = 47$) (Fig. S5A). Neither Western diet (2.40 ± 0.04 g pc, $p = 0.96$) nor regular diet intake (3.02 ± 0.22 g pc, $p = 0.26$) changed according to the groups (Fig. S5B). The use of a Western diet in $LDL^{(-/-)}$ mice is a classical model for inducing inflammation and promoting lipid profile alteration. In our model, the Western diet caused the increase of TC, LDL, HDL, TG, ALT, IL-1β concentration in plasma, and TNFα ($p = 0.05$) in liver homogenate (Table S3). However, 8 weeks after discontinuing the stimulus, except for IL-1β, the other measured cytokines in plasma and liver did not change, suggesting a maladapted post-resolution condition.

After 24 weeks, the inflammatory stimulus was removed by replacing the Western diet with a regular diet, and the effect of the oral interventions with algae oil (DHA-D) and the functionalized nanocapsules (MLNC-DHA-a1) was compared in terms of lipid profile and oxidative stress. Table 1 describes the major fatty acids profiles determined in the animals after 32 weeks, both in liver homogenate and plasma. No important changes were observed in the proportion of fatty acids analyzed in plasma among the groups. In the liver, DHA-D group that received algae oil supplementation by gavage showed a higher proportion of DHA compared with CONT ($p = 0.02$), but not compared with MLNC-DHA-a1 ($p = 0.18$) (Table 1). This result suggests that some of the DHA from the surface-functionalized nanocapsules reached the liver, but it was not enough to increase DHA proportion compared to CONT ($p = 0.35$). Furthermore, no alteration was observed in the relative liver weight (0.04 ± 0.00%, $p = 0.45$).

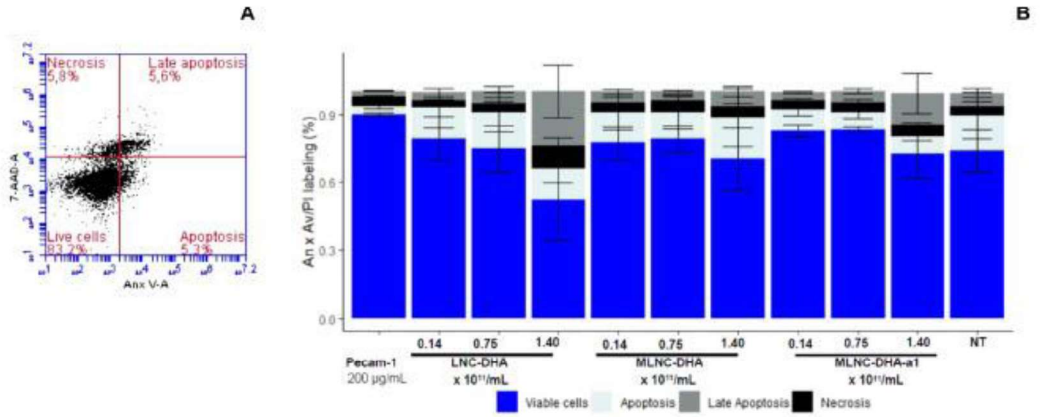

Fig. 2. RAW 264.7 murine macrophages viability, necrosis, apoptosis and late apoptosis as estimated by flow cytometry after culturing incubated with LNC-DHA, MLNC-DHA and MLNC-DHA-a1 at three concentrations (0.14×10^{11}, 0.75×10^{11} and 1.40×10^{11} /mL), also incubated without any nanocapsules (NT) and isolated anti-PECAM-1 at 200 µg/mL for 24 h. Fig. 2A: Flow cytometry colocalization of annexin-V binding and propidium iodine uptake for quantitation of RAW 264.7 murine macrophages incubated with MLNC-DHA-a1, as example. The horizontal axis depicts fluorescein-labeled annexin V; the vertical axis shows binding of propidium iodide fluorescence. Fig. 2B: Proportion of RAW 264.7 murine macrophages viability, necrosis, apoptosis and late apoptosis. Vertical bars are mean ± SEM ($n = 3$). No difference was observed among the samples according to cell viability ($p = 0.34$), necrosis ($p = 0.66$), apoptosis ($p = 0.75$) and late apoptosis ($p = 0.48$) by Kruskal Wallis analysis.

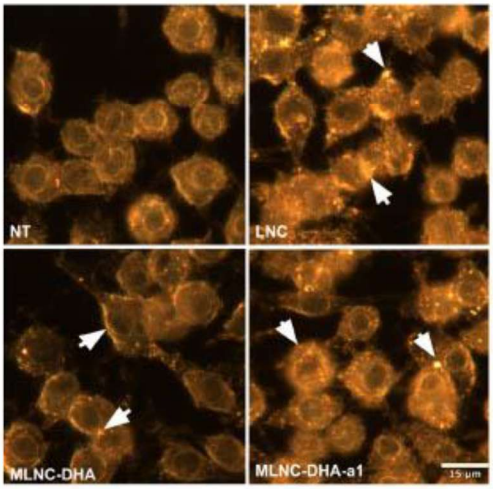

Fig. 3. Three-dimensional Cytoviva microscopy images of uptake performed in RAW 264.7 murine macrophages after 2 h of incubation with LNC-DHA, MLNC-DHA and MLNC-DHA-a1 at 0.75×10^{11} /mL, and also incubated without any nanocapsules (NT). Scale bar: 15 µm.

Given the higher proportion of polyunsaturated fatty acids in oral DHA supplementation, it was expected to potentially increase oxidative stress. However, in our model, no difference was observed in MDA concentration ($p = 0.47$) in the liver homogenate (Fig. S6). The other biomarkers measured in the groups at the end of 32 weeks did not show a significant difference (Table 2). In the subsequent analysis, a LNC-MCT group was included as a control of the MLNC-DHA-a1 group. The LNC-MCT group contained MCT instead of DHA in the lipid core. The effect of the intervention with the nanocapsules and oral supplementation on systemic cytokines is shown in Fig. 5. The MLNC-DHA-a1 group increased levels of IL-6 (Fig. 5A; $p < 0.01$), IL-1β (Fig. 5B; $p = 0.01$) but also increased IL-10 (Fig. 5C; $p < 0.01$) without altering TNFα (Fig. 5D; $p = 0.11$). No changes were observed in the cytokines determined in the liver (Table 2).

3.2.1. Discussion

Our data showed that lipid-core nanocapsules containing DHA (LNC-DHA), multi-wall nanocapsules containing DHA (MLNC-DHA) and the surface-functionalized (anti-PECAM-1) metal-complex multi-wall nanocapsules containing DHA (MLNC-DHA-a1) did not present toxicity when evaluated at 0.14 and 0.75 and 1.40×10^{11} nanocapsules/mL in RAW 264.7 cells, after 24, 48 and 72 h. The toxicity and ability to be phagocyted by immune system cells is a complex subject that depends on many factors, including carrier components, excipients, impurities, therapeutic content, shape, size, elasticity, surface chemistry, and charge [35]. The nanocapsules were composed of polycaprolactone, sorbitan monostearate, zinc acetate, low molecular weight chitosan and polysorbate 80, as previously described (Fig. S1) [23]. These materials have been widely applied to synthesize nanoparticles without reported toxicity, even using animal models [36–38]. Our results confirm that the material applied to build the capsule wall and the anti-PECAM-1 applied on the surface did not affect the cells viability at 0.75×10^{11} nanocapsules/mL. Moreover, the algae oil (DHASCO®, DSM) containing 35.13 ± 0.35 g/100 g of DHA, used to compose the lipid core, was not sterilized or depyrogenated due to its low oxidative stability. Thus, our results showed that although non-sterilized, the algae oil applied in our study can be considered relatively safe to prepare nanocapsules for further *in vivo* animal assays. However, extrapolating from *in vitro* data to *in vivo* behavior should be done cautiously [35].

Concerning phagocytosis and polarization, the shape and size of our nanocapsules may also have contributed to their internalization by RAW 264.7 macrophages. Our nanocapsules showed a spherical shape, with sizes ranging from 159.12 ± 1.25–163.50 ± 5.33 nm, and all absolute zeta potential values were below 14 mV, regardless of the negative or positive coating [23]. It has been reported that non-spherical and non-electrical charged carriers may circulate longer than similarly sized spheres, cationic or anionic nanoparticles, due to reduced recognition by

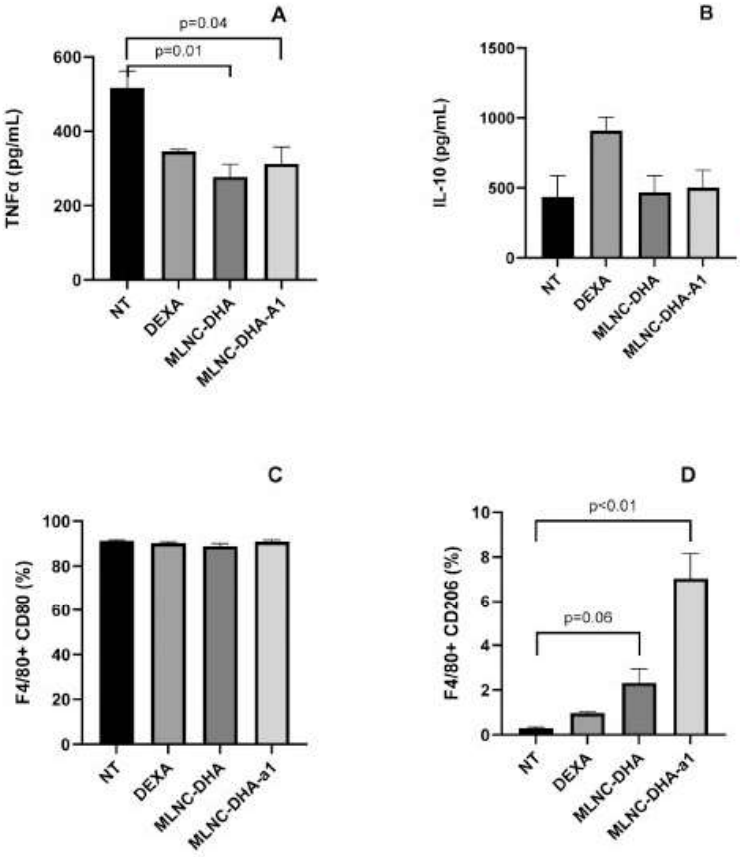

Fig. 4. Cytokines concentration and polarization in C57BL/6 mouse bone marrow-derived macrophages (BMDM). Assays were performed with dexamethasone (500 ng/mL) (DEXA), MLNC-DHA (0.75×10^{11} particles/mL), MLNC-DHA-a1 (0.75×1011 particles/mL containing 200 μg/mL of Anti-PECAM-1 and without any treatment (NT) for 48 h. Fig. 4A: TNFα (pg/mL); $p = 0.02$; Fig. 4 B: IL-10 (pg/mL); $p = 0.29$; Fig. 4C: Percentage of F4/80 + CD80 double positive cells (M1), ($p = 0.25$) and Fig. 4D: Percentage of F4/80 + and CD206 double positive cells (M2), ($p < 0.01$). Vertical bars are mean ± SEM (NT, n = 3; DEXA, n = 2; MLNC-DHA, n = 6 and MLNC-DHA-a1, n = 5 for cytokines and NT, n = 5; DEXA, n = 4; MLNC-DHA, n = 6 and MLNC-DHA-a1, n = 6 for polarization). Treatments were compared by One-way ANOVA and Tukey HSD or equivalent non parametric Kruskal Wallis analysis.

host defense cells [35,39]. The ability of RAW macrophages to engulf booth MLNC-DHA and MLNC-DHA-a1 nanocapsules, as shown in Fig. 3, may result from a balance between their spherical shape associated with non-ionic surface charge. This combination may influence their further *in vivo* application.

In our study using mice-derived BMDM cells, it was not observed any differences in the M1%, as measured using the F4/80 + CD80 marker (Fig. 4C) or in the IL-10 concentration (Fig. 4B), which is typically found in lower levels in M1 phenotype [40,41]. Taking into account the intense M2 polarization showed by MLNC-DHA-a1 (7.04%) compared with NT (0.30%), as measured using F4/80 + CD206 marker (Fig. 4D), followed by the reduced secretion of TNFα (Fig. 4A) observed to both MLNC-DHA and MLNC-DHA-a1, our results suggest that DHA present in the algae oil composing the lipid core of the nanocapsules has the potential to reduce the inflammatory microenvironment and improve macrophage functionality.

Based on these *in vitro* results, the nanocapsules were evaluated using an animal model. A limited number of *in vivo* studies has investigated the biological effects of omega-3 fatty acids-containing nanomaterials in cardiovascular diseases and cancer [20,42] and to the best of our knowledge, none of these studies has applied algae oil in the core of a nanocapsule surface-functionalized with anti-PECAM-1. For this reason, there was any previous information about a safe dose for intervention. Our data showed 5.36×10^8 surface-functionalized (anti-PECAM-1) metal-complex multi-wall nanocapsules containing 12 μL DHA/mL were well tolerated by $LDL^{(-/-)}$ mice, since all groups had similar diet intake and body weight gain, without no signs of local inflammation following caudal vein injections. Furthermore, data from fatty acids profile, relative weight and cytokines concentration suggested that our nanocapsules did not accumulate in the liver, causing any inflammatory reaction.

Conversely, MLNC-DHA-a1 nanocapsules promoted a modulation in the cytokine profile in the plasma, suggesting an inflammatory activation due to the increased release of IL-6 and IL-1β (Figs. 5A and 5B). However, there were no change observed in TNFα (Fig. 5C), while an increase was verified to anti-inflammatory IL-10 (Fig. 5C). It is important to note that several aspects of the nanocarriers can interact with the immune system, remembering that host defenses are the leading causes of nanocarriers side effects [35,43]. It has been reported that the size between 100 and 200 nm has the highest potential for prolonged circulation because this range is large enough to avoid the uptake by the liver, but small enough to avoid filtration in the spleen, thereby extending circulation and providing more opportunities for target engagement [43]. In a study reported by Deshpande et al. [44] flaxseed oil containing 17-β-estradiol was nanoencapsulated and functionalized with CREKA-peptides due to their specific binding affinity to

Table 1
Major fatty acid composition determined in plasma and liver homogenate of the experimental groups after 32 weeks of treatment.

	CONT	DHA-D	MLNC-DHA-a1	P[a] value
Plasma (%)				
C16:0	33.41 ± 1.86	32.49 ± 2.23	33.40 ± 1.19	*0.92*
C16:1 n7	2.56 ± 0.24	1.92 ± 0.09	2.29 ± 0.19	*0.15*
C17:0	0.02 ± 0.02	0.06 ± 0.06	ND	*0.35*
C18:0	17.09 ± 1.94	19.38 ± 2.24	19.53 ± 0.81	*0.44*
C18:1 n9	27.37 ± 2.65	24.02 ± 4.48	23.77 ± 1.34	*0.52*
C18:2 n6 (LNA)	14.73 ± 1.70	15.87 ± 1.20	14.88 ± 0.88	*0.83*
C18:3 n3 (ALA)	ND[a]	0.43 ± 0.05[b]	0.23 ± 0.05[ab]	*< 0.01*
C18:3 n6	0.15 ± 0.08	0.12 ± 0.08	0.20 ± 0.06	*0.66*
C20:3 n6	ND	0.12 ± 0.12	0.07 ± 0.07	*0.52*
C20:4 n6 (AA)	3.76 ± 0.71	3.78 ± 0.68	4.35 ± 0.41	*0.67*
C20:0	0.04 ± 0.02	0.03 ± 0.03	ND	*0.20*
C20:5 n3 (EPA)	0.03 ± 0.02	0.01 ± 0.01	ND	*0.19*
C22:6 n3 (DHA)	0.78 ± 0.37	1.78 ± 0.43	1.29 ± 0.24	*0.18*
Liver (%)				
C16:0	38.22 ± 2.81[a]	35.03 ± 0.62[ab]	32,22 ± 0.82[b]	*0.04*
C16:1 n7	1.43 ± 0.13[a]	2.01 ± 0.12[ab]	2.38 ± 0.22[b]	*0.01*
C18:0	19.81 ± 2.64	20.19 ± 1.39	18.76 ± 0.73	*0.78*
C18:1 n9	18.72 ± 3.04	20.48 ± 1.58	25.07 ± 0.92	*0.05*
C18:2 n6 (LNA)	16.14 ± 1.82	14.87 ± 1.03	15.19 ± 0.89	*0.78*
C18:3 n3 (ALA)	0.49 ± 0.29	0.26 ± 0.08	0.24 ± 0.05	*0.48*
C18:3 n6	0.23 ± 0.08	0.10 ± 0.07	0.20 ± 0.06	*0.48*
C20:4 n6 (AA)	4.03 ± 0.48	4.82 ± 0.62	4.45 ± 0.30	*0.67*
C22:6 n3 (DHA)	0.89 ± 0.40[a]	2.23 ± 0.29[b]	1.47 ± 0.22[ab]	*0.03*

[a] Values were expressed as mean ± SEM (CONT, n = 6; DHA-D, n = 5 and MLNC-DHA-a1, *n* = 9). Treatments were compared by One-way ANOVA and Tukey HSD or equivalent non parametric Kruskal Wallis analysis. P values refer to the comparison among the four groups. Values followed by the same letter do not differ ($p < 0.05$).

Table 2
Biochemical parameters observed in the experimental groups after 32 weeks of treatment.

	CONT	DHA-D	LNC-MCT	MLNC-DHA-a1	P value[a]
Plasma					
Glucose (mg/dL)	151.70 ± 19.50	190.50 ± 21.39	124.86 ± 15.56	148.20 ± 12.03	*0.08*
TC (mg/dL)	191.40 ± 18.35	230.25 ± 36.52	173.07 ± 13.54	195.40 ± 9.26	*0.74*
LDL (mg/dL)	92.40 ± 10.72	84.00 ± 8.71	78.43 ± 6.83	89.67 ± 5.52	*0.56*
HDL (mg/dL)	39.30 ± 2.51	43.50 ± 2.20	42.36 ± 3.02	44.60 ± 2.39	*0.57*
TG (mg/dL)	85.30 ± 12.42	101.25 ± 20.79	68.29 ± 5.17	85.33 ± 7.49	*0.39*
ALT (mg/dL)	69.20 ± 12.61	59.25 ± 9.21	44.00 ± 7.04	55.53 ± 6.31	*0.22*
AST (mg/dL)	168.80 ± 35.89	136.50 ± 17.79	117.64 ± 14.22	129.33 ± 14.46	*0.78*
Liver					
Relative weight (%)	0.04 ± 0.01	0.04 ± 0.01	0.04 ± 0.01	0.04 ± 0.01	*0.33*
Cytokines (liver)					
IL1β (pg/mL)	0.47 ± 0.07	0.57 ± 0.07	0.65 ± 0.05	0.61 ± 0.07	*0.29*
IL-6 (pg/mL)	4.70 ± 0.36	3.91 ± 0.34	4.97 ± 0.44	4.25 ± 0.33	*0.24*
IL-10 (pg/mL)	2.86 ± 0.38	2.26 ± 0.20	3.78 ± 0.43	3.16 ± 0.44	*0.05*
TNFα (pg/mL)	0.24 ± 0.03	0.25 ± 0.02	0.25 ± 0.02	0.23 ± 0.02	*0.90*

[a] *Values were expressed as mean ± SEM (CONT, n = 11; DHA-D, n = 9; LNC-MCT, n = 14 and MLNC-DHA-a1, n = 15).* Treatments were compared by One-way ANOVA and Tukey HSD or equivalent non parametric Kruskal Wallis analysis. P values refer to the comparison among the four groups.

atherosclerotic plaque. Similar to our protocol, the nanocapsules were intravenously injected in ApoE $^{(-/-)}$ mice fed a high-fat diet for 10 weeks, totalizing 10 doses at the end of the experiment. The authors observed that the weight gain of animals was not affected by the treatment, and plasma ALT and AST concentrations remained within the normal range. Sha et al. [42] developed a nanoparticle derived from macrophage membrane-coated liposome, aiming to improve efferocytosis in the arterial wall. They observed good compatibility, prolonged blood circulation time, and no cytotoxicity in MTT assays. Thus, the observed weight gain and dietary tolerance in our study may be attributed to a combination of MLNC-DHA-a1 size (164 nm), spherical shape and an adequate dose.

Under normal circumstances, opsonization by immunoglobulins and complement proteins begins immediately upon contact of the nanoparticles with plasma, followed by mechanical filtration in the spleen [43]. Although there is no data about pharmacokinetic and pharmacodynamics properties in our research, it is plausible that our nanocapsules infiltrated the inflamed endothelium, spleen or other tissue and cells that express PECAM-1 and have triggered the immune response observed in plasma.

The systemic inflammation observed in our study may be caused by the purity of algae oil in the lipid core, the antibody in the nanocapsule surface or the chitosan applied in the wall, since group LNC-MCT did not show the same behavior. In fact, LNC-MCT group was included in our protocol because there were previous studies reporting its safety when applied in animal models [38,45]. Platelet-Endothelial Cell Adhesion Molecule-1 (PECAM-1) is a protein widely expressed, to different degrees, on most leukocyte subtypes, platelets and endothelial cells, where its expression is primarily concentrated at junctions between adjacent cells [46]. It has been reported that under an inflammatory condition, such as those observed in atherosclerosis, PECAM-1 increases the junction permeability between the endothelial cells, facilitating the infiltration of immune cells into the inflamed intima [47]. However, the toxicity of anti-PECAM-1 has shown controversial results. Fig. 2 shows that 200 μg/mL of Anti-PECAM-1 did not reduce viability when evaluated in RAW 264.7 cells. In another study, PECAM-targeted polymer nanocarriers injected into mice did not show toxicity [48]. Despite this, it was observed a systemic release of pro-inflammatory cytokines after intravenous administration of anti-PECAM-1 [49]. This adverse result could be attributed to the fact that the engagement of the extracellular domains of PECAM-1 can compromise barrier function or lead to bidirectional signaling, with consequences toward cell survival, affecting junctional integrity and leukocytes and platelet adhesion. Thus, more studies involving anti-PECAM must be carried out to establish PECAM-1 targeted drugs safety, considering that nanoparticle binding can lead to unexpected biological consequences.

Conversely, chitosan has been considered non-toxic, biocompatible and biodegradable. However, caution should be taken regarding its interactions with biological systems, which depends on concentration, deacetylation degree and positive charge [50]. In a study involving algae oil, two samples obtained from Schizochytrium sp, were submitted to a battery of in vivo and in vitro genotoxicity tests. The results indicated that the oil was well tolerated and had no adverse effects at the highest dose of 3305 and 3679 mg/kg bw/day, for male and female rats, respectively [51], that is about 120 times higher than the dose applied in our study. According to the supplier, the algae oil applied in our nanocapsules contained DHA in the form of triacylglycerol along with ascorbyl palmitate (250 ppm) and tocopherol (250 ppm), being certified as safe for the intended use. However, considering the direct intravenous injection, a higher degree of purity than those approved for dietary use should be evaluated in further studies. Besides the purity, the amount of DHA injected in the plasma by the nanocapsules could trigger an immune system response. In our study, fatty acids were expressed as a percentage, and the proportion found in plasma similar to the proportion found in liver. It was estimated that each application of the nanocapsules provided about 2.8 μg DHA kg bw. Thus, quantitative

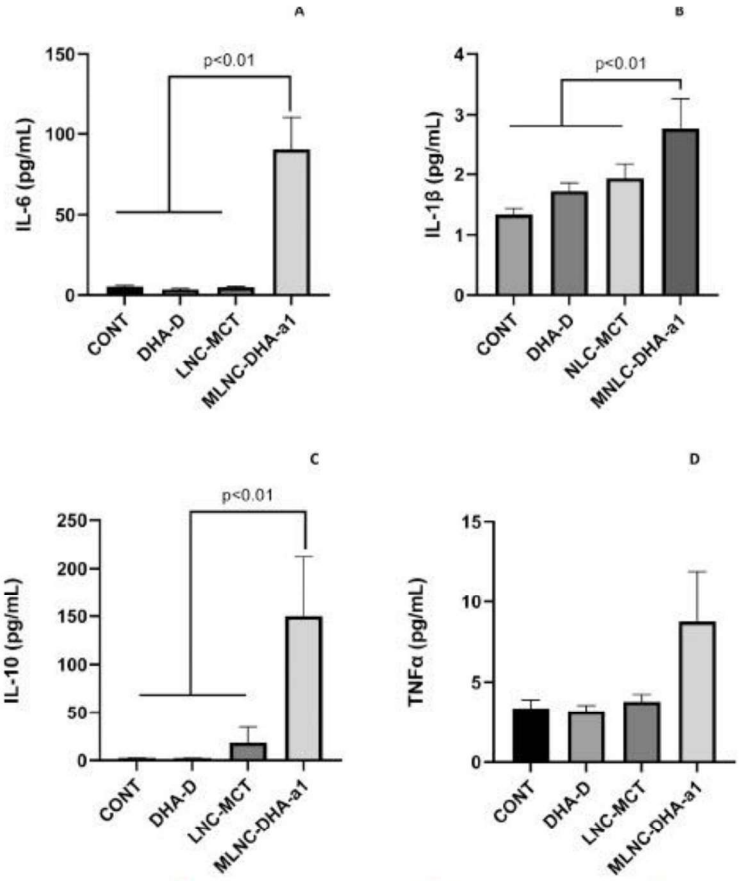

Fig. 5. Cytokines concentration analyzed in plasma. Fig. 5A: IL-6 concentration (pg/mL); Fig. 5B: IL-1β concentration (pg/mL); Fig. 5C: IL-10 concentration (pg/mL); and Fig. 5D: TNFα concentration (pg/mL). Vertical bars are mean ± SEM (CONT, n = 10; DHA, n = 8; LNC-MCT, n = 14 and MLNC-DHA-a1, n = 12). Treatments were compared by One-way ANOVA and Tukey HSD or equivalent non parametric Kruskal Wallis analysis.

determination of DHA in plasma should be done in the next studies.

Concerning the oral supplementation of algae oil, it was also expected that the replacement of AA by EPA and DHA in membrane phospholipids could promote a reduction in the substrate necessary to synthesize series 2 and 4 eicosanoids, able to facilitate acquired immunity and induce long-lasting immune inflammation [52]. However, there was no difference in cytokines concentration comparing DHA-D and CONT groups, suggesting that the supplementation was insufficient to reduce systemic inflammation once the stimulus was discontinued. Toko et al. [53] observed a suppression in the expression of pro-inflammatory cytokines in the heart of mice supplemented with EPA and DHA. However, it is also worth noting that they applied a dose much higher (1500.00 mg/kg. bw/day) than the dose used in our model (10.00 mg/kg.bw/say). In other study, C57BL/6 mice were supplemented with 200 mg/kg.bw of algae oil and intestinal damage was induced by Ceftriaxone sodium. After 8 days, the animals showed inhibition of the pro-inflammatory cytokine tumor necrosis factor (TNF)-α, interleukin (IL)– 6 and myeloperoxidase (MPO) activity [54]. Xu et al. [55] induced colitis in Male C57BL/6 mice using 2.5% DSS and followed them with 2 weeks of treatment with algal oil (250 or 500 mg/kg/day). The authors concluded that algal oil could be applied in the development of therapeutics for intestinal inflammation.

In fact, there is currently no evidence to suggest that the control of chronic inflammation is dose-related [56]. The solution applied in our study contained 1.34×10^{13} nanocapsules/mL with 12 μL/mL of algae oil (35.13 ± 0.35% DHA). This solution was injected at a rate of 40 μL/animal once a week for 8 weeks. This amount corresponded to 8.9×10^{-19} mols/animal/week, based on the Avogadro's number. The results showed that MLNC-DHA-a1 nanocapsules were well-tolerated *in vivo*, but activated an immune response, increasing the cytokines concentration in the plasma. Considering that this immune response is a limitation to clinical trials, future experiments should aim to identify which compound within the nanocapsules was responsible for activating the immune response.

4. Conclusion

Our findings suggest that algae oil with a higher DHA content, incorporated as part of the lipid core within the nanocapsules, appears to improve the macrophage phenotype, being a potential therapy for

controlling chronic inflammation However, MLNC-DHA-a1 nanocapsules increased pro-inflammatory cytokines in the plasma. Thus, further studies should identify which compounds triggered the immune response and to assess whether this effect might have adverse implications for susceptibility to infections.

Ethics approval and informed consent

All the protocols were approved by the Institutional Animal Care and Use Committee of the Faculty of Pharmaceutical Sciences, University of São Paulo (CEUA/FCF 555).

Funding

This study was supported by The State of São Paulo Research Foundation (FAPESP) (Scholarship and Research Grant 2019/21029–3, 2021/02021–1, 2021/08196–0) and National Council for Scientific and Technological Development (CNPq – Scholarship: 166541/2017–6).

CRediT authorship contribution statement

Conceptualization, I.A.C.; methodology, I.P.; S.J.C.; M.C.L.; A.R.P and S.S.G; formal analysis, I.P.; S.C.J.; K.B.; B.C.;M.K.U.; K.A.; resources, I.A.C.; writing, I.A.C; M.C.L.;I.P.; review and editing, I.P.; M.C.L. All authors have read and agreed to the published version of the manuscript.

Declaration of Competing Interest

The author reports no conflicts of interest in this work.

Data Availability

Data will be made available on request.

Appendix A. Supporting Information

Supplementary data associated with this article can be found in the online version at doi:10.1016/j.biopha.2023.115474.

References

[1] L. Chen, H. Deng, H. Cui, et al., Inflammatory responses and inflammation-associated diseases in organs, Oncotarget 9 (6) (2017) 7204–7218, https://doi.org/10.18632/oncotarget.23208.
[2] D. Furman, J. Campisi, E. Verdin, et al., Chronic inflammation in the etiology of disease across the life Span, Nat. Med 25 (12) (2019) 1822–1832, https://doi.org/10.1038/s41591-019-0675-0.
[3] A. Christ, M. Lauterbach, E. Latz, Western Diet and the Immune System: An Inflammatory Connection, Immunity 51 (5) (2019) 794–811, https://doi.org/10.1016/j.immuni.2019.09.020.
[4] P. Stenvinkel, M. Ketteler, R.J. Johnson, B. Lindholm, R. Pecoits-Filho, M. Riella, O. Heimbürger, T. Cederholm, M. Girndt, IL-10, IL-6, and TNF-α: Central factors in the altered cytokine network of uremia—The good, the bad, and the ugly, Kidney Int. 67 (4) (2005) 1216–1233, https://doi.org/10.1111/j.1523-1755.2005.00200.x.
[5] Hangai, S., Ao, T., Kimura, Y., Matsuki, K., Kawamura, T., Negishi, H., Nishio, J., Kodama, T., Taniguchi, T. and Yanai, H. (2016). PGE2 induced in and released by dying cells functions as an inhibitory DAMP. Proceedings of the National Academy of Sciences of the United States of America, [online] 113(14): 3844–3849. doi:10.1073/pnas.1602023113.
[6] M.D. Howard, E.D. Hood, B. Zern, V.V. Shuvaev, T. Grosser, V.R. Muzykantov, Nanocarriers for vascular delivery of anti-inflammatory agents, Annu. Rev. Pharmacol. Toxicol. 54 (2014) 205–226, https://doi.org/10.1146/annurev-pharmtox-011613-140002.
[7] T. Rhen, J.A. Cidlowski, Antiinflammatory action of glucocorticoids — new mechanisms for old drugs, N. Engl. J. Med 353 (2005) 1711–1723, https://doi.org/10.1056/NEJMra050541.
[8] H.E. Vonkeman, M.A.F.J. van de Laar, Nonsteroidal anti-inflammatory drugs: adverse effects and their prevention, Semin. Arthritis Rheum. 39 (2010) 294–312, https://doi.org/10.1016/j.semarthrit.2008.08.001.
[9] S. Wongrakpanich, A. Wongrakpanich, K. Melhado, J. Rangaswami, A comprehensive review of non-steroidal anti-inflammatory drug use in the elderly ([online]), Aging Dis. 9 (1) (2018) 143, https://doi.org/10.14336/ad.2017.0306.
[10] ANON.
[11] J.S. Chandan, D.T. Zemedikun, R. Thayakaran, N. Byne, S. Dhalla, D. Acosta-Mena, K.M. Gokhale, T. Thomas, C. Sainsbury, A. Subramanian, J. Cooper, A. Anand, K. O. Okoth, J. Wang, N.J. Adderley, T. Taverner, A.K. Denniston, J. Lord, G. N. Thomas, C.D. Buckley, Nonsteroidal antiinflammatory drugs and susceptibility to COVID-19, Arthritis Rheumatol. 73 (2021) 731–739, https://doi.org/10.1002/art.41593.
[12] W. Zhang, Y. Zhao, F. Zhang, Q. Wang, T. Li, Z. Liu, J. Wang, Y. Qin, X. Zhang, X. Yan, X. Zeng, S. Zhang, The use of anti-inflammatory drugs in the treatment of people with severe coronavirus disease 2019 (COVID-19): the perspectives of clinical immunologists from China, Clin. Immunol. 214 (2020), 108393, https://doi.org/10.1016/j.clim.2020.108393.
[13] P.C. Calder, Omega-3 fatty acids and inflammatory processes: from molecules to man, Biochem Soc. Trans. 45 (5) (2017) 1105–1115, https://doi.org/10.1042/BST20160474.
[14] P.C. Calder, Omega-3 fatty acids and inflammatory processes, Nutrients 2 (3) (2010) 355–374, https://doi.org/10.3390/nu2030355.
[15] R. Bosviel, L. Joumard-Cubizolles, G. Chinetti-Gbaguidi, D. Bayle, C. Copin, N. Hennuyer, I. Duplan, B. Staels, G. Zanoni, A. Porta, L. Balas, J.-M. Galano, C. Oger, A. Mazur, T. Durand, C. Gladine, DHA-derived oxylipins, neuroprostanes and protectins, differentially and dose-dependently modulate the inflammatory response in human macrophages: putative mechanisms through PPAR activation, Free Radic. Biol. Med. 103 (2017) 146–154, https://doi.org/10.1016/j.freeradbiomed.2016.12.018.
[16] H.Y. Chang, H.N. Lee, W. Kim, Y.J. Surh, Docosahexaenoic acid induces M2 macrophage polarization through peroxisome proliferator-activated receptor γ activation, Life Sci. 120 (2015) 39–47, https://doi.org/10.1016/j.lfs.2014.10.014.
[17] K.T. Feehan, D.W. Gilroy, Is resolution the end of inflammation? Trends Mol. Med 25 (3) (2019) 198–214, https://doi.org/10.1016/j.molmed.2019.01.006.
[18] B.E. Sansbury, M. Spite, Resolution of Acute Inflammation and the Role of Resolvins in Immunity, Thrombosis, and Vascular Biology, 24, Circ. Res 119 (1) (2016) 113–130, https://doi.org/10.1161/CIRCRESAHA.116.307308.
[19] Y. Yan, W. Jiang, T. Spinetti, A. Tardivel, R. Castillo, C. Bourquin, R. Zhou, Omega-3 fatty acids prevent inflammation and metabolic disorder through inhibition of NLRP3 inflammasome activation, Immunity 38 (6) (2013) 1154–1163, https://doi.org/10.1016/j.immuni.2013.05.015.
[20] S. Serini, R. Cassano, S. Trombino, G. Calviello, Nanomedicine-based formulations containing ω-3 polyunsaturated fattyacids: potential application in cardiovascular and neoplastic diseases, Int J. Nanomed. 14 (2019) 2809–2828, https://doi.org/10.2147/IJN.S197499.
[21] P.M. Ridker, B.M. Everett, T. Thuren, et al., Anti-inflammatory therapy with canakinumab for atherosclerotic disease, N. Engl. J. Med 377 (12) (2017) 1119–1131, https://doi.org/10.1056/NEJMoa1707914.
[22] H. Wang, Y. Zhou, Q. Sun, et al., Update on nanoparticle-based drug delivery system for anti-inflammatory treatment, Front Bioeng. Biotechnol. 17 (9) (2021), 630352, https://doi.org/10.3389/fbioe.2021.630352.
[23] M. de Castro Leão, A. Raffin Pohlmann, A. de Cristo Soares Alves, et al., Docosahexaenoic acid nanoencapsulated with anti-PECAM-1 as co-therapy for atherosclerosis regression, Eur. J. Pharm. Biopharm. 159 (2021) 99–107, https://doi.org/10.1016/j.ejpb.2020.12.016.
[24] S. Schlager, N. Vujic, M. Korbelius, et al., Lysosomal lipid hydrolysis provides substrates for lipid mediator synthesis in murine macrophages, Oncotarget 8 (25) (2017) 40037–40051, https://doi.org/10.18632/oncotarget.16673.
[25] L. Ménégaut, A. Jalil, C. Thomas, D. Masson, Macrophage fatty acid metabolism and atherosclerosis: The rise of PUFAs, Atherosclerosis 291 (2019) 52–61, https://doi.org/10.1016/j.atherosclerosis.2019.10.002.
[26] C.N. Serhan, B.D. Levy, Resolvins in inflammation: emergence of the pro-resolving superfamily of mediators, J. Clin. Invest 128 (7) (2018) 2657–2669, https://doi.org/10.1172/JCI97943.
[27] S.A. Amici, J. Dong, M. Guerau-de-Arellano, Molecular mechanisms modulating the phenotype of macrophages and microglia, Front Immunol. 8 (2017) 1520, https://doi.org/10.3389/fimmu.2017.01520. PMID: 29176977; PMCID: PMC5686097.
[28] S. Sandri, C.B. Hebeda, R.A. Loiola, et al., Direct effects of poly(ε-caprolactone) lipid-core nanocapsules on human immune cells, Nanomed. (Lond.) 14 (11) (2019) 1429–1442, https://doi.org/10.2217/nnm-2018-0484 W.
[29] W. Ying, P.S. Cheruku, F.W. Bazer, S.H. Safe, B. Zhou, Investigation of macrophage polarization using bone marrow derived macrophages, J. Vis. Exp. 76 (2013) 50323, https://doi.org/10.3791/50323.
[30] P.G. Reeves, F.H. Nielsen, G.C. Fahey, AIN-93 purified diets for laboratory rodents: final report of the American institute of nutrition ad hoc writing committee on the reformulation of the AIN-76A rodent diet, J. Nutr. 123 (11) (1993) 1939–1951, https://doi.org/10.1093/jn/123.11.1939.
[31] T. Küster, B. Zumkehr, C. Hermann, et al., Voluntary ingestion of antiparasitic drugs emulsified in honey represents an alternative to gavage in mice, J. Am. Assoc. Lab Anim. Sci. 51 (2) (2012) 219–223.
[32] P.M. Kris-Etherton, W.S. Harris, L.J. Appel, AHA nutrition committee. american heart association. Omega-3 fatty acids and cardiovascular disease: new recommendations from the american heart association, Arterioscler. Thromb. Vasc. Biol. 23 (2) (2003) 151–152, https://doi.org/10.1161/01.atv.0000057393.97337.ae.
[33] Y.-L. Hong, S.-L. Yeh, C.-Y. Chang, et al., Total plasma malondialdehyde levels in 16 taiwanese college students determined by various thiobarbituric acid tests and

an improved high-performance liquid chromatography-based method, Clin. Biochem 33 (8) (2000) 619–625, https://doi.org/10.1016/s0009-9120(00)00177-6.
[34] N. Shirai, H. Suzuki, S. Wada, Direct methylation from mouse plasma and from liver and brain homogenates, Anal. Biochem 343 (1) (2005) 48–53, https://doi.org/10.1016/j.ab.2005.04.037.
[35] H. Parhiz, M. Khoshnejad, J.W. Myerson, et al., Unintended effects of drug carriers: Big issues of small particles, Adv. Drug Deliv. Rev. 130 (2018) 90–112, https://doi.org/10.1016/j.addr.2018.06.023.
[36] M.F. Cavalcante, M.D. Adorne, W.M. Turato, et al., scPv-Anti-LDL(-)-metal-complex multi-wall functionalized-nanocapsules as a promising tool for the prevention of atherosclerosis progression, Front Med (Lausanne) 8 (2021), 652137, https://doi.org/10.3389/fmed.2021.652137.
[37] C.B. Michalowski, M.D. Arbo, L. Altknecht, et al., Oral treatment of spontaneously hypertensive rats with captopril-surface functionalized furosemide-loaded multi-wall lipid-core nanocapsules, Pharmaceutics 12 (1) (2020) 80, https://doi.org/10.3390/pharmaceutics12010080.
[38] F.A. Bruinsmann, A. de Cristo Soares Alves, A. de Praga Dias, et al., Nose-to-brain delivery of simvastatin mediated by chitosan-coated lipid-core nanocapsules allows for the treatment of glioblastoma in vivo, Int J. Pharm. 616 (2022), 121563, https://doi.org/10.1016/j.ijpharm.2022.121563.
[39] P.M. Glassman, J.W. Myerson, L.T. Ferguson, et al., Targeting drug delivery in the vascular system: Focus on endothelium, Adv. Drug Deliv. Rev. 157 (2020) 96–117, https://doi.org/10.1016/j.addr.2020.06.013.
[40] G. Chinetti-Gbaguidi, S. Colin, B. Staels, Macrophage subsets in atherosclerosis, Nat. Rev. Cardiol. 12 (1) (2015) 10–17, https://doi.org/10.1038/nrcardio.2014.173.
[41] M. de Gaetano, D. Crean, M. Barry, O. Belton, M1- and M2-type macrophage responses are predictive of adverse outcomes in human atherosclerosis, Front Immunol. 7 (2016) 275, https://doi.org/10.3389/fimmu.2016.00275.
[42] X. Sha, Y. Dai, L. Chong, M. Wei, M. Xing, C. Zhang, et al., Pro-efferocytic macrophage membrane biomimetic nanoparticles for the synergistic treatment of atherosclerosis via competition effect, J. Nanobiotechnol. 20 (1) (2022) 506, https://doi.org/10.1186/s12951-022-01720-2.
[43] R.A. Petros, J.M. DeSimone, Strategies in the design of nanoparticles for therapeutic applications, Nat. Rev. Drug Discov. 9 (8) (2010) 615–627, https://doi.org/10.1038/nrd2591.
[44] D. Deshpande, S. Kethireddy, D.R. Janero, M.M. Amiji, Therapeutic efficacy of an ω-3-fatty acid-containing 17-β estradiol nano-delivery system against experimental atherosclerosis, PLoS One 11 (2) (2016), e0147337, https://doi.org/10.1371/journal.pone.0147337.
[45] M.T.P. de Oliveira, D.S. Coutinho, S.S. Guterres, A.R. Pohlmann, PMRE Silva, M. A. Martins, A. Bernardi, Resveratrol-loaded lipid-core nanocapsules modulate acute lung inflammation and oxidative imbalance induced by LPS in mice, Pharmaceutics 13 (5) (2021) 683, https://doi.org/10.3390/pharmaceutics13050683. PMID: 34068619; PMCID: PMC8151102.
[46] A. Woodfin, M.-B. Voisin, S. Nourshargh, PECAM-1: a multi-functional molecule in inflammation and vascular biology, Arterioscler. Thromb. Vasc. Biol. 27 (12) (2007) 2514–2523, https://doi.org/10.1161/ATVBAHA.107.151456.
[47] J.R. Privratsky, P.J. Newman, PECAM-1: regulator of endothelial junctional integrity, Cell Tissue Res 355 (3) (2014) 607–619, https://doi.org/10.1007/s00441-013-1779-3.
[48] T.D. Dziubla, V.V. Shuvaev, N.K. Hong, et al., Endothelial targeting of semi-permeable polymer nanocarriers for enzyme therapies, Biomaterials 29 (2) (2008) 215–227, https://doi.org/10.1016/j.biomaterials.2007.09.023.
[49] R.Y. Kiseleva, C.F. Greineder, C.H. Villa, et al., Vascular endothelial effects of collaborative binding to platelet/endothelial cell adhesion molecule-1 (PECAM-1), Sci. Rep. 8 (1) (2018) 1510, https://doi.org/10.1038/s41598-018-20027-7.
[50] L.A. Frank, G.R. Onzi, A.S. Morawski, et al., Chitosan as a coating material for nanoparticles intended for biomedical applications, React. Funct. Polym. 147 (11) (2020), 104459, https://doi.org/10.2174/1389200218666170925122201.
[51] D. Schmitt, N. Tran, J. Peach, et al., Toxicologic evaluation of DHA-Rich algal oil: genotoxicity, acute and subchronic toxicity in rats, Food Chem. Toxicol. 50 (10) (2012) 3567–3576, https://doi.org/10.1016/j.fct.2012.07.054.
[52] T. Aoki, S. Narumiya, Prostaglandins and chronic inflammation, Trends Pharm. Sci. 33 (6) (2012) 304–311, https://doi.org/10.1016/j.tips.2012.02.004.
[53] H. Toko, H. Morita, M. Katakura, et al., Omega-3 fatty acid prevents the development of heart failure by changing fatty acid composition in the heart, Sci. Rep. 10 (1) (2020) 15553, https://doi.org/10.1038/s41598-020-72686-0.
[54] H. Zhang, Z. Xu, W. Chen, F. Huang, S. Chen, X. Wang, C. Yang, Algal oil alleviates antibiotic-induced intestinal inflammation by regulating gut microbiota and repairing intestinal barrier, Front Nutr. 9 (2023) 1081717, https://doi.org/10.3389/fnut.2022.1081717. PMID: 36726819; PMCID: PMC9884693.
[55] Z. Xu, H. Tang, F. Huang, et al., Algal Oil Rich in n-3 PUFA Alleviates DSS-induced colitis via regulation of gut microbiota and restoration of intestinal barrier, Front. Microbiol (2020) 16, https://doi.org/10.3389/fmicb.2020.615404.
[56] A.C. Skulas-Ray, P.M. Kris-Etherton, W.S. Harris, et al., Dose-response effects of omega-3 fatty acids on triglycerides, inflammation, and endothelial function in healthy persons with moderate hypertriglyceridemia, Am. J. Clin. Nutr. 93 (2) (2011) 243–252, https://doi.org/10.3945/ajcn.110.

Co-autoria 2023

cells

MDPI

Article

Role of Annexin A1 Secreted by Neutrophils in Melanoma Metastasis

Silvana Sandri [1], Cristina Bichels Hebeda [1,2], Milena Fronza Broering [1], Marina de Paula Silva [3], Luciana Facure Moredo [4], Milton José de Barros e Silva [4], André Sapata Molina [4], Clóvis Antônio Lopes Pinto [4], João Pedreira Duprat Neto [4], Chris P. Reutelingsperger [5], Cristiane Damas Gil [6] and Sandra Helena Poliselli Farsky [1,*]

[1] Department of Clinical and Toxicological Analyses, School of Pharmaceutical Sciences, University of Sao Paulo, São Paulo 05508-000, SP, Brazil
[2] NPCMed—Núcleo de Pesquisa em Ciências Médicas, Centro Universitário para o Desenvolvimento do Alto Vale do Itajaí—UNIDAVI, Rio do Sul 89160-932, SC, Brazil
[3] Center for Stem Cells & Regenerative Medicine, Kings College London, London WC2R 2LS, UK
[4] Skin Cancer Department, A.C. Camargo Cancer Center, São Paulo 01509-010, SP, Brazil
[5] Cardiovascular Research Institute Maastricht, Maastricht University Medical Center, Maastricht University, 6211 LK Maastricht, The Netherlands
[6] Department of Morphology and Genetics, Universidade Federal de São Paulo (UNIFESP), São Paulo 04023-900, SP, Brazil
* Correspondence: sfarsky@usp.br; Tel.: +55-(11)-3091-2197

Abstract: Annexin A1 (AnxA1) is highly secreted by neutrophils and binds to formyl peptide receptors (FPRs) to trigger anti-inflammatory effects and efferocytosis. AnxA1 is also expressed in the tumor microenvironment, being mainly attributed to cancer cells. As recruited neutrophils are player cells at the tumor sites, the role of neutrophil-derived AnxA1 in lung melanoma metastasis was investigated here. Melanoma cells and neutrophils expressing AnxA1 were detected in biopsies from primary melanoma patients, which also presented higher levels of serum AnxA1 and augmented neutrophil–lymphocyte ratio (NLR) in the blood. Lung melanoma metastatic mice (C57BL/6; i.v. injected B16F10 cells) showed neutrophilia, elevated AnxA1 serum levels, and higher labeling for AnxA1 in neutrophils than in tumor cells at the lungs with metastasis. Peritoneal neutrophils collected from naïve mice were co-cultured with B16F10 cells or employed to obtain neutrophil-conditioned medium (NCM; 18 h incubation). B16F10 cells co-cultured with neutrophils or with NCM presented higher invasion, which was abolished if B16F10 cells were previously incubated with FPR antagonists or co-cultured with AnxA1 knockout ($AnxA1^{-/-}$) neutrophils. The depletion of peripheral neutrophils during lung melanoma metastasis development (anti-Gr1; i.p. every 48 h for 21 days) reduced the number of metastases and AnxA1 serum levels in mice. Our findings show that AnxA1 secreted by neutrophils favors melanoma metastasis evolution via FPR pathways, addressing AnxA1 as a potential biomarker for the detection or progression of melanoma.

Keywords: neutrophil-depleted mice; melanoma patients; FPR antagonists; B16F10 cells; neutrophil–lymphocyte ratio (NLR)

check for updates

Citation: Sandri, S.; Hebeda, C.B.; Broering, M.F.; de Paula Silva, M.; Moredo, L.F.; de Barros e Silva, M.J.; Sapata Molina, A.; Lopes Pinto, C.A.; Duprat Neto, J.P.; Reutelingsperger, C.P.; et al. Role of Annexin A1 Secreted by Neutrophils in Melanoma Metastasis. *Cells* 2023, *12*, 425. https://doi.org/10.3390/cells12030425

Academic Editor: Luciana Tavares

Received: 15 December 2022
Revised: 16 January 2023
Accepted: 23 January 2023
Published: 27 January 2023

1. Introduction

The tumor microenvironment consists of a heterogeneous population of cancer cells and a variety of other cells including the resident and infiltrating host cells [1]. Infiltrating immune cells in the microenvironment distinctly influences the tumor progression. While T-cell-mediated anti-tumor immune response correlates with favorable disease outcomes and is the basis of cancer immunotherapy [2–5], the myeloid cells act as antigen-presenting cells to promote anti-tumor T-cell responses at the initial phases of tumorigenesis; however, lately, they have been effectors of the tumor progression [6–8].

Neutrophils are myeloid cells constantly produced in the bone marrow and released into the blood. During the host defense against aggressions, this pattern is exacerbated, leading to different neutrophil phenotypes with different half-lives and functions [9,10]. Neutrophilia is also detected in cancer patients, especially those with advanced-stage disease [11], and a high neutrophil-lymphocyte ratio (NLR) has been considered a biomarker of poor clinical outcomes in many types of cancer [12–15]. Neutrophils also represent a significant proportion of immune cells infiltrating in many types of cancer [16–18]. At the tumor site, tumor-associated neutrophils (TAN) are plastic cells that adapt to different microenvironments. In the early tumorigenesis phase, the N1 TAN phenotype stimulates antitumor immune response; however, under the continuous action of chemical mediators released in the tumor microenvironment, TAN changes to a N2 immunosuppressive phenotype and stimulates motility, migration, and invasion of tumor cells [19,20].

In melanoma, the most aggressive type of skin cancer, a body of research has emerged employing NLR in the prognostic of both localized and metastatic melanoma [21–25], as in immunotherapy monitoring in melanoma, being high in NLR was associated with poor outcomes [22,26]. It has been pointed out that circulating neutrophils stimulate angiogenesis and enhanced melanoma cell migration toward blood endothelial cells [27], allowing tumor cell invasion; TLR-4 activation in peripheral neutrophils promotes the metastatic spread of melanoma [28]; and neutrophils activated by complement-membrane-attack-complex release neutrophil extracellular traps (NETs), which open the endothelial barrier favoring melanoma cells to reach into the circulation and their systemic spread [29]. Furthermore, circulating neutrophils migrate to the tumor by actions of chemotactic mediators produced in the lung melanoma microenvironment [30–32], and immature neutrophils at the tumor-bearing lungs display pro-tumoral effects, such as the enhanced frequency of ROS-producing cells [33] and NET formation [34]; conversely, neutrophils expressing lower amounts of Wip-1, a negative regulator of p53, trigger anti-tumor effects [35], and high infiltration of phagocyting neutrophils evoked by intratumoral injection of vaccine-stimulating biodegradable polysaccharide favors the maturation of dendritic cells and the generation of immune memory [36].

Azurophil granules of neutrophils stock the anti-inflammatory protein Annexin A1 (AnxA1), and in inflammatory conditions, newly synthesized and AnxA1 stored in the neutrophil granules are released into the microenvironment, mainly in microvesicle contents [37]. Secreted AnxA1 is phosphorylated in a calcium-dependent manner and binds to G-protein-coupled receptors named formyl peptide receptors—FPR1 and FPR2—to downstream different intracellular signaling pathways [38,39]. The neutrophil AnxA1 actions are associated with the blockade of leukocyte migration activated at the early inflammation, efferocytosis, and tissue repair [40–42]. Moreover, a lower frequency of circulating neutrophil-AnxA1^{+} is associated with a reduction of the plasma levels of the protein, which is found in systemic inflammatory diseases [43], and impaired AnxA1 expression in neutrophils at the site of lesion exacerbates and lengthens the course of inflammation [44].

Many types of cancer cells also express AnxA1, and its effects are associated with cancer development by inducing proliferation, angiogenesis, stemness, and cell invasion in FPR-dependent pathways [45]. Previous studies demonstrated that melanoma cells expressed AnxA1 into the microenvironment, which is associated with angiogenesis, tumor cell invasiveness, and growth [46–48]. *In vitro* studies corroborating the expression of AnxA1 by melanoma cells is related to invasiveness behavior, depending, at least in part, on metalloproteinase-2 (MMP-2) expression [48]. The fine-tuned understanding of neutrophils on solid tumors is nowadays a remarkable goal to clarify the mechanisms of tumor progression and to point out a target for treatment. Hence, we here depicted the role of AnxA1 secreted by neutrophils in lung melanoma mice and melanoma patients and unveiled the fact that AnxA1 derived from the blood or tumor-site neutrophils displays pro-tumor invasiveness during lung melanoma development.

2. Materials and Methods

2.1. Patients

Eighteen-year-old or older patients with histological confirmation of nevus or melanoma by a pathologist were eligible for enrollment in the study. The patients recruited at A.C. Camargo Cancer Center, São Paulo, Brazil, donated blood (8 mL) and authorized access to biopsies for posterior analysis. Healthy donors were included as controls. The study was conducted under the Declaration of Helsinki and approved by the Ethics in Research Committee of the University of São Paulo and A.C. Camargo Cancer Center (CAAE 277951120.0000.0067 and 277951120.4.3001.5432, respectively). In total, 16 patients were included, and sample characteristics are depicted in Table 1.

Table 1. Characteristics of patient's sample. ***: absence. SLN: sentinel lymph node.

Characteristics								
Total Patients Enrolled (*n*) = 16								
Age (Years) (*Mean* ± *SD*) = 55.93 ± 15.25								
Patients	**Skin Phototype**	**Site**	**Diagnostic**	**Breslow Thickness (mm)**	**Ulceration**	**Inflammatory Infiltrate**	**SLN**	**Stage**
1	I	Left infra scapular	Melanoma	0.6	No	Slight	No	IA
2	NA	Left abdomen	Melanoma	14	No	Discrete	Yes	IV
3	NA	Right leg	Melanoma	0.6	No	Mild	No	IA
4	II	Right upper back	Melanoma	3.2	No	Discrete	No	IIA
5	II	Left flank	Compound nevus	0	No	Discrete	No	0
6	III	Right scapular	Melanoma (lentigo maligno)	0	No	0	No	0
7	III	Left inframammary	Compound nevus	0	No	***	No	0
8	-	Left thigh	Residual melanoma (lentigo maligno)	0	No	0	No	IB
9	III	Right thorax (breast)	Atypical nevus	0	No	0	No	0
10	II	Left lumbar	Melanoma	0.8	No	Discrete	No	IIIA
11	III	Right arm	Melanoma	2.5	No	Discrete	No	IIA
12	II	Right thoracolumbar	Melanoma (ES)	1.1	No	Slight	No	0
13	III	Left scapular	Melanoma	*in situ*	No	Intense	No	0
14	II	Right scapular	Dysplastic melanocytic nevus	0	No	***	No	0
15	II	Right lower abdomen	Dysplastic melanocytic nevus	0	No	***	No	0
16	II	Right axillary	Dysplastic junctional melanocytic nevus	0	No	***	No	0

2.2. Animals

Female C57BL/6 mice wild-type (AnxA1$^{+/+}$) or AnxA1-knockout mice (AnxA1$^{-/-}$) (25–30 g; 3–5 per group) were provided by the Central Animal House of the School of Pharmaceutical Sciences and the Chemistry Institute of the University of São Paulo. Mice were housed in polycarbonate cages (four animals per cage; Tecniplast, Buguggiate, Italy) at room temperature (22 °C ± 0.1 °C) and humidity (50% ± 10%) with a 12 h light/dark cycle, receiving standard food and water ad libitum. Animals were anesthetized with a combination of ketamine/xylazine solution (20:2 mg/kg, intraperitoneal (i.p.); xylazine

hydrochloride—Ceva Santé Animale; ketamine—Syntec do Brasil Ltda) before each experimental procedure. All procedures were approved by the Institutional Animal Care and Use Committee (IACUC) at the School of Pharmaceutical (CEUA FCF/USP 583).

2.3. Melanoma Cell Culture

The B16F10 malignant melanoma cell line was obtained from the Banco Células do Rio de Janeiro (BCRJ), Rio de Janeiro, Rio de Janeiro, Brazil. Cells were grown in culture dishes for 5–10 passages in Dulbecco's modified Eagle's medium (DMEM; #12100046 Gibco, Carlsbad, CA, USA) supplemented with 10% heat-inactivated fetal bovine serum (FBS; #2024-06 Gibco) and 100 U/mL penicillin and 100 µg/mL streptomycin solution (#15140-122 Gibco), maintained at 37 °C with 5% CO_2 atmosphere. Reverse transcription polymerase chain reaction (RT-PCR) was performed routinely in the laboratory to check the mycoplasma cell contamination. AnxA1 and FPR expression in melanoma cells were evaluated by flow cytometer as described below.

2.4. Collection of Plasma and Isolation of Blood Human Neutrophils

An aliquot of fresh and heparinized venous blood from patients and control donors was used to total leukocyte and smear blood count. The count of total leukocytes was performed using a Neubauer chamber, and smear blood was stained with Giemsa to circulating leukocyte differentiation. The NLR was calculated by the ratio between the number of circulating neutrophils and lymphocytes counted. Plasma was separated by centrifugation, recovered, and stored at −80 °C until AnxA1 serum levels measurement. Afterward, erythrocytes and leukocytes pellet were diluted in 0.9% NaCl, and neutrophil isolation was carried out by density gradient centrifugation, as described previously [49]. Isolated neutrophils were fixed and analyzed by flow cytometer as described in the following item.

2.5. Collection and Culture of Mice Neutrophils

Neutrophils were obtained from wild-type and AnxA1$^{-/-}$ mice, 4 h after intraperitoneal injection of 3 mL 1% oyster glycogen Type II solution (#G8751 Sigma-Aldrich, Saint Louis, MO, USA), previously prepared in phosphate-buffered saline (PBS) [50]. The animals were anesthetized, and the cells were collected by rinsing the abdominal cavity with 10 mL of PBS. To macrophage adherence, peritoneal cells were incubated for 2 h in DMEM supplemented with 10% FBS, 100 U/mL penicillin, and 100 µg/mL streptomycin. Afterward, non-adhered neutrophils were recovered and counted in the Neubauer chamber. Then, neutrophils (1×10^6) were seeded in a 96-well plate (Corning, New York, NY, USA) and cultured in DMEM supplemented with 10% FBS for 18 h. After culture, the cell-free supernatant was recovered as Neutrophil Conditioned Medium (NCM), filtered through a 45 µm filter (Corning), stored at −80 °C, and used according to assays. The purity of the peritoneal cell population and viability were analyzed by flow cytometry.

2.6. Induction of Melanoma Lung Metastasis in Mice

Cultured B16F10 cells were harvested, washed, and resuspended to give the appropriate concentration in serum-free DMEM. B16F10 cells suspension (5×10^5 cells/100 µL) was injected into the mice via the tail vein [51]. The animals were maintained under observation, and after 21 days of tumor cell injection, the mice were submitted to euthanasia by overexposure to nasal anesthesia (isoflurane; 2-chloro-2-(difluoromethoxy)-1,1,1-trifluoroethane; Cristália, Brazil). For neutrophil depletion, 150 µg anti-Gr1 (16-5931-95; clone RB6-8C5 Bioscience/Invitrogen, Waltham, MA, USA) or rat IgG2b kappa isotype (#14-4031-85 Bioscience/Invitrogen) were injected 24 h before melanoma cell inoculation. The antibodies were injected every 48 h for up to 21 days. The blood was recovered from aorta vein to obtain the plasma and circulating leukocytes for posterior analysis. The lung was recovered and perfused, and the number of B16F10 metastases was counted by visual inspection helped with stereo microscopy (CL 6000 LED, Zeiss, Oberkochen, Germany), followed by fixation.

2.7. Histology of Human Biopsies and Mice Lungs

Mice and human biopsies were fixed in 4% buffered paraformaldehyde, dehydrated and embedded in paraffin. Slides sections (4 µm) were dewaxed with xylene and rehydrated through gradient ethanol into water. Hydrated slides were stained with hematoxylin/eosin (H&E EasyPath, São Paulo, Brazil) for morphological analyses or used for immunofluorescence or immunohistochemistry assays.

2.8. Immunofluorescence

The immunofluorescence was performed according to Zaqout et al. (2020) [52]. Briefly, for antigen retrieval, sections were heated in citrate buffer (pH 6.0) for 40 min at 95 °C in a water bath. After cooling at room temperature, the sections were rinsed and permeabilized with 0.2% gelatin from cold water fish skin (#G7041 Sigma Aldrich) and 0.25% Triton-X-100 (#X100 Sigma-Aldrich) in PBS. Sections were blocked with 5% bovine serum albumin (BSA; #A7030 Sigma Aldrich), 0.2% gelatin, and 0.25% Triton-X-100 in PBS. Patients' samples were incubated with anti-AnxA1 mouse antibody (1:50; #610066 BD Biosciences, San Jose, CA, USA) overnight (4 °C), followed by incubation with anti-mouse Alexa Fluor 488 (1:250; #10680 Invitrogen). Lung sections were processed as mentioned previously and incubated with anti-rat Ly6G (1:25; clone 1A8—#16-9668-82 Bioscience/Invitrogen) and anti-AnxA1 rabbit antibody (1:50; #71-3400 Invitrogen). Afterwards, samples were incubated with anti-rat-Alexa-Fluor 488 (1:250; #A1106 Invitrogen) and anti-rabbit Alexa Fluor 568 (1:100; A11001 Invitrogen). The nuclei were stained with DAPI (1 µg/mL; #554907 BD Bioscience). Negative controls were obtained by omitting the primary antibody. Immunofluorescence was analyzed using an Axioskop 2 fluorescence microscope (Carl Zeiss, Jena, Germany), and images were captured using the software AxioVision 4.7 (Carl Zeiss). The $Ly6G^+$-positive cell count was performed using the cell counter tool from Fiji/ImageJ software (Version 2.9.0/1.53t National Institutes of Health, Bethesda, MD, USA). Five fields were analyzed from each lung section. The analysis of AnxA1 expression in Ly6G+positive cells was performed according to de Paula-Silva and collaborators [53]. Briefly, composite pictures (czi format) were imported to Fiji from ImageJ and split into blue and green or red channels. For densitometric analysis, the green or red channel was selected, further analyzed, and modified in the gray filter. Background pixel averages were then subtracted from the image pixels of interest to correct uneven illumination. Fluorescence measures were performed manually by the selection of positive regions; average values were expressed in arbitrary units.

2.9. Immunohistochemistry

After antigen retrieval and permeabilization with 0.1% Triton-X-100 in PBS, peroxidase was inactivated with 3% hydrogen peroxide (Synth, Diadema, Brazil), and nonspecific antibody binding was blocked by preincubating sections with 10% BSA in PBS at 37 °C for 60 min. Sections were incubated with diluted primary antibodies against melanoma marker Melan A (1:50; #PA5-99174 Invitrogen) or AnxA1 (1:500, #713400 Thermo Fisher) at 4 °C overnight. Then, slices were washed and incubated with HRP-conjugated anti-rabbit (#ab6721 Abcam, Cambridge, UK) at room temperature for 1 h. The sections were developed with 3,3-diaminobenzidine (DAB; #K3468 Dako, Carpinteria, CA, USA) and lightly counterstained with hematoxylin (Merck, Darmstadt, Germany), followed by dehydration and coverslip mounting. Negative controls were performed by omitting the primary antibody.

2.10. Serum and Cell Supernatant AnxA1 Measurement

The levels of AnxA1 in human and mouse blood and in the neutrophil-conditioned medium were quantified by ELISA using commercial kits (human: #MBS495574; mouse: #M704042, MyBioSource, San Diego, CA, USA) according to supplier instructions.

2.11. Flow Cytometry

Flow cytometry experiments were performed to characterize the expression of AnxA1, FPR1, FPR2, CD66b, Ly6G, and F4/80. To evaluate the expression of AnxA1 and CD66b

in human neutrophils, isolated cells were fixed with FACS lysing solution (#349202 BD Biosciences), washed with PBS containing 0.1M glycine (Synth), permeabilized with 0.01% Triton-X-100, washed with 1% BSA in PBS (BSA/PBS), and incubated with primary anti-rabbit antibody to AnxA1 (1:100) for 1 h at 37 °C. Next, cells were washed with BSA/PBS and incubated with secondary goat anti-rabbit antibody conjugated to Alexa Fluor 488 (1:250; Invitrogen) and anti-PerCP-Cy™5.5 anti-human CD66b-neutrophil marker (1:50; #562254 BD Pharmigen) for 40 min in the dark at room temperature. To verify the frequency of mice circulating neutrophils ($Ly6G^+$) and monocytes ($F4/80^+$), cells were fixed with FACS lysing solution for 30 min at room temperature, washed with PBS containing 0.1M glycine, and incubated with anti-Ly6G conjugated with FITC (1:50; #551460 BD Pharmigen) and anti-F4/80 conjugated with PerCP-Cy5.5 (1:200; # 15-4801-82 Biolegend, San Diego, CA, USA) for 40 min in the dark at room temperature. The cells were analyzed by a flow cytometer (BD Accuri C6), taking 10,000 events into consideration and using BD CSampler™ Analysis software (version: 1.0.2641-21 BD Biosciences, Franklin Lakes, NJ, USA).

2.12. Transwell Matrigel Invasion Assay

Transwell membranes (8 µm pore size; #353097 Falcon/Corning) were coated with 40 µL Matrigel (#356237 Corning diluted 1:6 in serum-free DMEM). B16F10 melanoma cells (2.0×10^4 cells/transwell) were resuspended in DMEM supplemented with 0.5% BSA and added to the inner compartment of the chamber [54]. One set of experiments was performed to investigate the role of the neutrophil-conditioned medium (NCM; supernatant from 18 h neutrophils cultured obtained from wild-type or $AnxA1^{-/-}$ mice) on melanoma cell invasion. Hence NCM:DMEM 5% FBS culture medium (300 µL; 1:1 dilution) or DMEM 5% FBS (Control) were added to the outer cup. Another set of experiments investigated the role of the contact of neutrophil–melanoma cells on invasion. In this case, neutrophils (obtained from wild-type or $AnxA1^{-/-}$ mice) and melanoma cells were co-cultured in a proportion of 5:1 for 24 h. The participation of FPRs on the effects was evaluated by treatment of melanoma cells with FPRs antagonists, cyclosporine H (1 µM; #AG CN2 0447-M005 Adipo Gen Life Sciences, San Diego, CA, USA), or WRW4 (1 µM; #2262 Tocris Bioscience, Bristol, UK) for 30 min and before adding to the inner compartment of the chamber. To confirm the involvement of AnxA1, NCM with low amounts of AnxA1 or $AnxA1^{-/-}$ NCM were supplemented with recombinant AnxA1 (1.5 and 3.5 ng/mL; donated by Professor Chris Reutelingsperger from Cardiovascular Research Institute Maastricht, Maastricht University, Maastricht, The Netherlands). After 24 h, cells that migrated through the Matrigel were fixed in 1.0% glutaraldehyde solution (#354400 Sigma Aldrich) and stained with 0.5% toluidine blue in 2% of Na_2CO_3 (Synth) for 20 min. The number of migrated cells was counted under a Leica DMi1 inverted microscope (Leica, Shinagawa, Tokyo, Japan). In each well, seven independent fields were considered for quantitation. The data are represented as change fold in relation to control or total number of invading cells.

2.13. Statistical Analysis

Statistical analyses were performed using Graph Pad Prism4 (Graph Pad Software Inc., San Diego, CA, USA). The data were expressed as mean ± standard error of the mean (SEM), and comparisons were made between the experimental groups using the *t*-test or one-way ANOVA followed by Tukey's post hoc test for multiple comparisons using GraphPad software version 5 (San Diego, CA, USA). The level of significance was set at $p < 0.05$.

3. Results

3.1. Expression and Serum AnxA1 Levels Were Increased in Melanoma Patients

The samples included were obtained from nevus or melanoma patients with different Breslow index and stages, or *in situ* melanoma (Table 1). The inflammatory infiltrate was classified as mild to severe, represented mainly by lymphocytes identified by morphological characteristics (Figure 1A–C—black arrows and inserts). AnxA1 expression was verified in four biopsy specimens (dysplastic nevus = 1; melanoma = 3). The selected melanoma

samples showed Breslow indexes around 0.8 mm (Figure 2F), 1.1 mm (Figure 2H), and 3.2 mm (Figure 2J). As observed by H&E staining, the samples showed pigmented cells (*) and melanoma cells (black arrow) characterized as large and rounded cells with large nuclei (Figure 1D,F,H,J). In the dysplastic nevus and first melanoma samples, cells scattered throughout the dermis, as seen by H&E staining (Figure 1D,F), were positive for AnxA1 in both samples (Figure 1E,G). In the second melanoma sample, an increased number of pigmented and melanoma cells (Figure 1H) and AnxA1-positive cells (Figure 1I) were detected. In the third sample, the majority of cell types found in the dermis were melanoma cells (Figure 1J), being that almost all of them expressed AnxA1 (Figure K). Peripheral blood was also analyzed. Patients with melanoma showed an increased circulating neutrophil compared to the nevus (Figure 1L). In melanoma patients, the NLR was around 2.5, while in nevus patients, the NLR was 1.69. Furthermore, a high expression of AnxA1 was found in circulating neutrophils (CD66b positive cells) from melanoma patients compared to nevus patients and the control (Figure 1M), and serum AnxA1 levels were increased in patients with melanoma (Figure 1N).

3.2. Neutrophils Were AnxA1$^+$ in The Lung Melanoma Metastasis Model

On the basis of the expression of AnxA1 in melanoma cells and neutrophils from melanoma patients, a model of lung melanoma metastasis was employed to investigate the pattern of AnxA1 expression and neutrophil infiltration in the metastatic site. As shown in Figure 2A, lung metastasis was observed 21 days after i.v. injection of B16F10. In the lungs of control animals, AnxA1 labeling was detected in the alveolar (arrowheads) but not in the bronchiolar epithelium (Br—Figure 2B,C). Conversely, the lung melanoma metastasis was composed of AnxA1$^+$ tumor cells (T—Figure 2D,E) and immune cells (arrows—Figure 2F,G). As verified by Ly6G-neutrophil marker labeling (Figure 2H,I), the number of neutrophils increased in the melanoma group (Figure 2J). Furthermore, Ly6G and AnxA1 double labeling (Figure 2K) or AnxA1 melanoma labeled cells (Figure 2L) showed that neutrophils expressed higher amounts of AnxA1 than melanoma cells (Figure 2M).

3.3. Peripheral Blood Neutrophils and AnxA1 Levels Were Enhanced in the Lung Melanoma Metastasis Model

The number of circulating neutrophils was elevated in melanoma metastasis mice in comparison to that found in the control group (Figure 3A). Moreover, levels of AnxA1 in the serum were augmented in lung melanoma metastasis mice (Figure 3B). To verify the ability of neutrophils to secrete AnxA1, peritoneal neutrophils were collected from naive mice, and greater amounts of AnxA1 release were found in the supernatant from these cells than B16F10 cells when cultured for 24 h (Figure 3C).

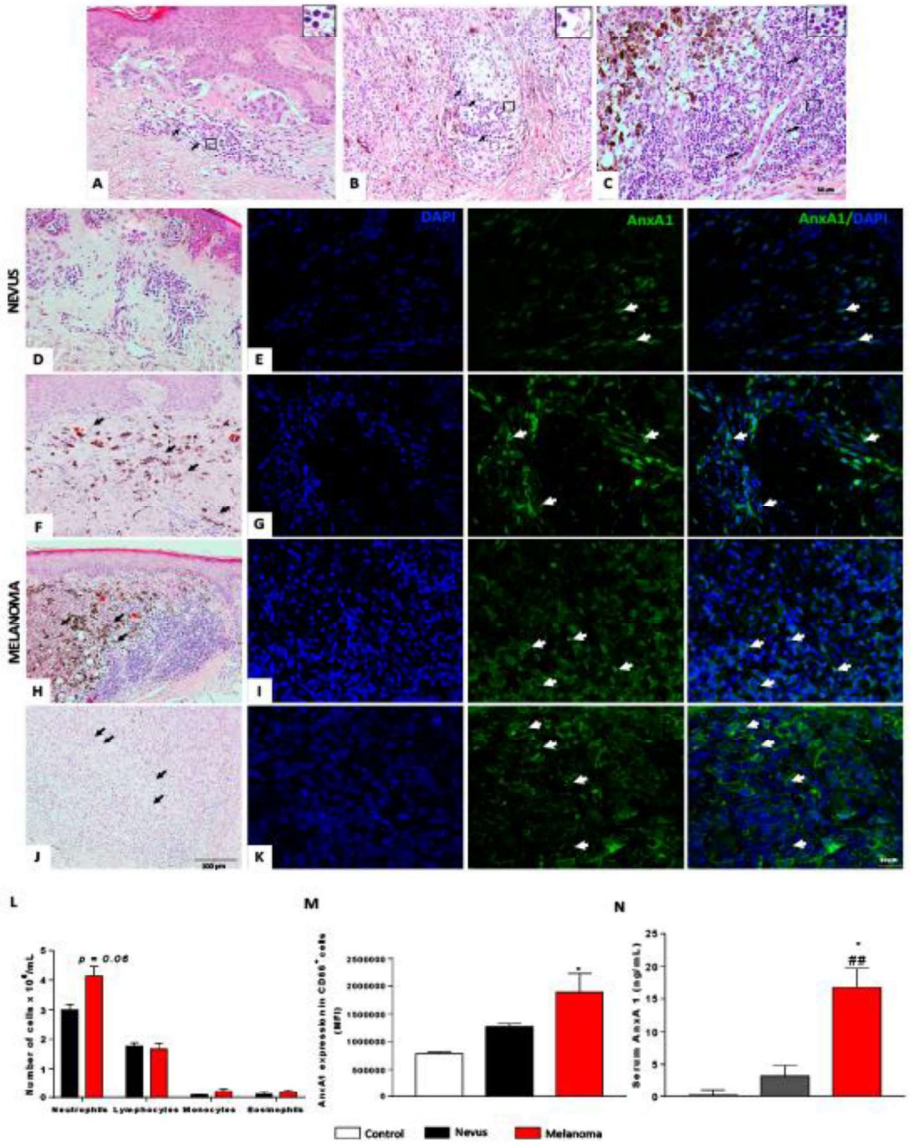

Figure 1. Expression and serum levels of AnxA1 were increased in melanoma patient samples. (**A–C**) Representative image of inflammatory infiltrate in biopsies obtained from melanoma patients—H&E staining (black arrows and inserts: lymphocytes). Scale bar: 100 µm. (**D**) H&E staining and (**E**) AnxA1 expression detected by immunofluorescence in nevus sample. (**F,H,J**) H&E staining and (**G,I,K**) AnxA1 expression detected by immunofluorescence in melanoma cells from melanoma biopsies. (*) pigmented cells. (Black arrows) melanoma cells. (White arrows) AnxA1-labeled cells. Scale bar: 50 µm. (**L**) Leukogram. (**M**) AnxA1 expression in circulating neutrophils ($CD66^+$) evaluated by flow cytometer. (**N**) AnxA1 serum levels. The data represent the average ± SEM. Control ($n = 4$); nevus ($n = 4$–5); melanoma ($n = 5$–9). * $p < 0.05$ vs. nevus; ## $p < 0.01$ vs. control.

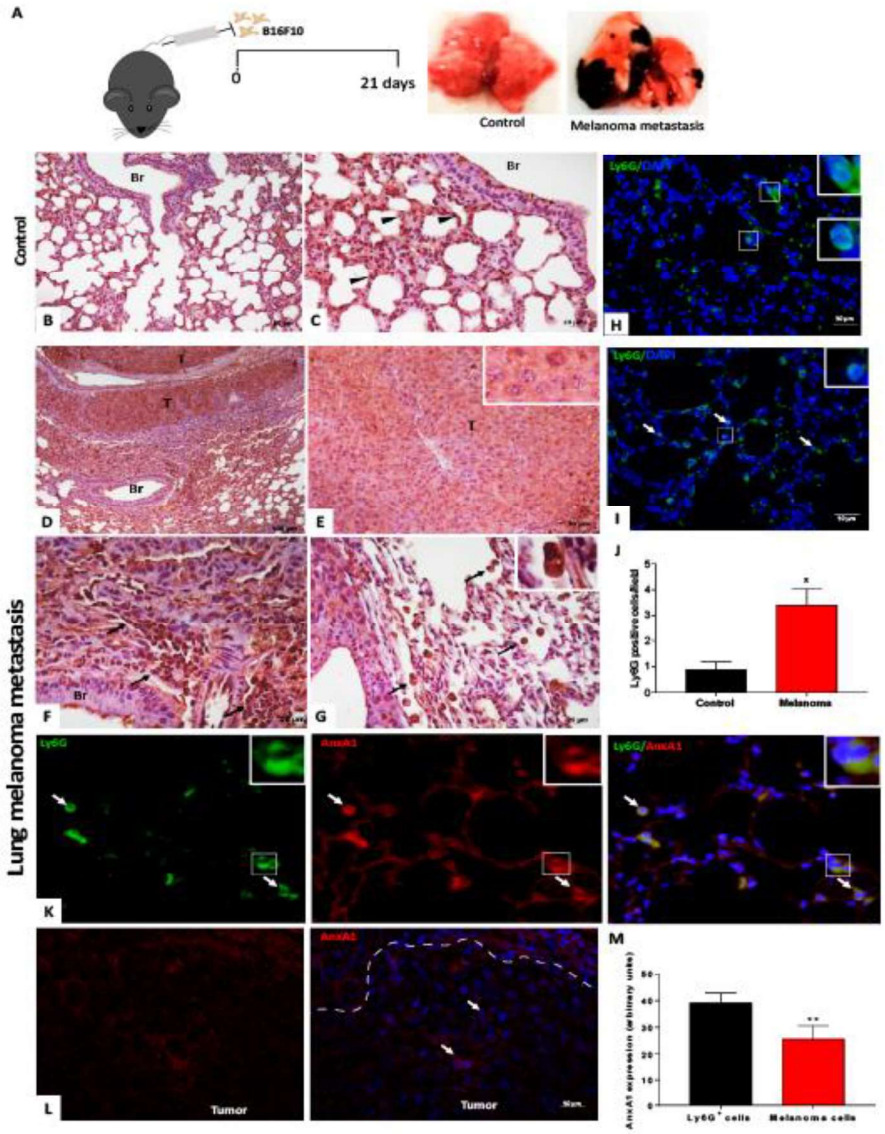

Figure 2. Increased expression and serum levels of AnxA1 in lung melanoma metastasis mice. (**A**) Experimental design. (**B**,**C**) Control group. Alveolar epithelium (arrowhead). Bronchiolar epithelium (Br). (**D**,**E**) Expression of AnxA1 in melanoma cells (T) from lung melanoma metastasis. (**F**,**G**) Immune cells labeled for AnxA1. Immune cells infiltrate (arrows). Inserts: Tumor and immune cells. Ly6G-positive cells in (**H**) control and (**I**) melanoma groups. (**J**) Increased number of neutrophils in lung melanoma metastasis mice. (**K**) AnxA1 expression in neutrophils ($Ly6G^+$) and (**L**) in melanoma cells from lung melanoma metastasis. (**M**) Amounts of AnxA1 expression in neutrophils and melanoma cells. The data represent the average ± SEM of at least 3–5 animals per group. p * < 0.05 vs. control; ** p < 0.01 vs. neutrophils.

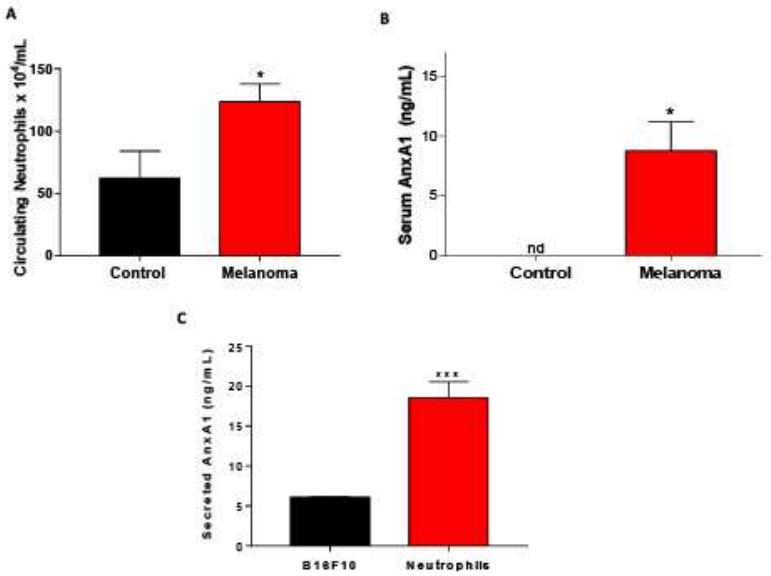

Figure 3. Increased blood neutrophils and AnxA1 levels in the lung melanoma metastasis model. (**A**) Amounts of neutrophils in the peripheral blood from lung melanoma metastasis mice. (**B**) Serum levels of AnxA1. (C) Secretion of AnxA1 by melanoma cells (B16F10) and neutrophils cultured for 24 h. The data represent the average ± SEM. * $p < 0.05$ vs. control; *** $p < 0.001$ vs. B16F10. Control group ($n = 5$); melanoma group ($n = 5$).

3.4. AnxA1 Secreted by Neutrophils Increased the Melanoma Cell Invasion via FPRs Pathways

On the basis of these previous data, we further investigated the involvement of AnxA1 secreted by neutrophils on melanoma cell invasion. Thus, neutrophils were recovered from the peritoneal cavity as depicted in Supplementary Figure S1A. Almost 80% of the total peritoneal cells were neutrophils, and 20% were macrophages as observed by Ly6G and F4/80 labeling, respectively (Supplementary Figure S1B). After macrophage removal by plated-adherence for 2 h, neutrophils were incubated for 18 h, and viability was reduced with an increase in Annexin V, an apoptosis marker (Supplementary Figure S1C), which was expected, since neutrophils' life span during *in vitro* incubation is around 7 to 10 h for both human and mice cells [55,56]. Furthermore, the levels of AnxA1 secreted by the neutrophil supernatant, named neutrophil-conditioned medium (NCM), was 2 up to 8 ng/mL (Supplementary Figure S1D). Considering that AnxA1 effects are attributed to its cleaved form, NCM was analyzed by Western blotting. As shown in Supplementary Figure S1E, the AnxA1 found in the NCM was cleaved. On the basis of the concentration of AnxA1, NCM was divided into high and low AnxA1 content and employed to investigate the invasion of melanoma cells. For this, murine melanoma B16F10 cells were applied, in which AnxA1 and its receptors (FPR1 and FPR2) were first characterized (Supplementary Figure S2A). B16F10 cells were incubated with NCM, at a proportion of 1:1, with a standard culture medium (DMEM supplemented with 5% FBS) or with standard medium (control) for 24 h (Figure 4A). In the assayed conditions, high AnxA1 content NCM increased the melanoma cell invasion in comparison to the control (Figure 4B), which was not associated with increased cell proliferation (Supplementary Figure S2B). To evaluate the involvement of AnxA1 in the effect promoted by NCM, melanoma cells were pre-treated with cyclosporine (CsH) or WRW4, antagonists for FPR1 and FPR2, respectively. As observed in Figure 4B, incubation with the antagonists reduced the melanoma cell invasion, which was not due to alterations in the cell viability (Supplementary Figure S2C). Further,

in NCM containing low levels of AnxA1 (lower than 2 ng/mL), the melanoma cell invasion was reduced in comparison to NCM with detectable AnxA1 levels. The addition of rAnxA1 to non-detectable AnxA1 NCM recovered the cell invasion previously observed (Figure 4C). The role of AnxA1 on cell invasion was corroborated using NCM from neutrophils collected from AnxA1 knockout mice ($AnxA1^{-/-}$). In this condition, the melanoma cell invasion was reduced, which was rescued by the addition of the rAnxA1 (Figure 4D).

The melanoma cell invasion was also evaluated in B16F10-neutrophil co-culture (Figure 4E). As observed in Figure 4F, neutrophil co-culture enhanced the melanoma cell invasion, which was inhibited if melanoma cells were pre-treated with FPR1 and FPR2 antagonists. The reduction of cell invasiveness was also observed if neutrophils were collected from $AnxA1^{-/-}$ mice (Figure 4G).

We also investigated whether melanoma-conditioned medium (MCM) could change the neutrophil's phenotype. Indeed, MCM reduced the expression of ICAM-1 at the neutrophil's surface (Supplementary Figure S3A) and increased the secretion of CXCCL1 KC, MCP-1, Arginase, VEGF, and IL-10 (Supplementary Figure S3C–E). As this neutrophil's profile is characteristic of the N2 phenotype, it may indicate that neutrophils at the site of metastasis display an anti-inflammatory phenotype.

3.5. Depletion of Circulating Neutrophils Reduced Lung Melanoma Metastasis and Serum Levels of AnxA1

Once AnxA1 secreted by neutrophils displayed a role in melanoma metastasis, we further investigated whether depletion of these cells during the disease progression was able to alter the disease outcomes. We depleted circulating neutrophils using anti-granulocyte antibody anti-Gr1 before B16F10 injection until the end of the lung melanoma metastasis model (Figure 5A). In our model, the antibody dosage and schedule reduced the number of peripheral neutrophils during the 48 h period after the antibody injection (Figure 5a). There was no detected modification in the number of circulating monocytes in the blood, while the number of blood neutrophils remained reduced up to day 21 (Supplementary Figure S4A). The remaining neutrophils showed morphology like an immature phenotype (Supplementary Figure S4A′), which may have been the result of bone marrow response to anti-rat antibody production (mitigation), due to limited depletion in peripheral tissue (low bioavailability), or due to the induction of neutrophil production in the spleen (extramedullary granulopoiesis), as discussed by recent literature [57,58].

Even the completed neutrophil depletion was not achieved; we observed a significant reduction of melanoma metastasis spots as observed by macroscopic analysis of the lungs from depleted neutrophils (anti-Gr1 treaded) in comparison to the isotype group (Figure 5B–D). Histologic analysis using H&E staining showed that the isotype group had metastasis in the external regions of lobes and near blood vessels (Figure 5E). The lungs of neutrophil-depleted mice showed tumor mass spots near vessels; however, the size was smaller than that found in the isotype group (Figure 5F). Further, we observed an increase in the circulating lymphocytes in the neutrophils depleted animals in comparison to isotype mice (Supplementary Figure S4B–D). Bronchoalveolar lavage (BAL) showed a reduced level of TGF-ß and VEFG-α (Supplementary Figure S4E,F), which may have been related to the reduced number of neutrophils in the lungs. To characterize lungs from neutrophil-depleted mice, we performed immunohistochemistry analysis using a melanoma marker (Melan A). Thus, it was verified that the Melan A-positive cells were restricted to the tumor (Figure 5G). On the other hand, in neutrophil-depleted mice, Melan A-positive cells were found to be mixed with other Melan A non-labeled cells also near vessels (Figure 5H). It was also observed that Melan A-positive cells were found spreading in the lung tissue of depleted-neutrophil mice (Figure 5H—insert). The AnxA1 expression was found in melanoma tumor cells (Figure 5I,J) and immune cells (Figure 5i,j) in the lung from both isotype and neutrophil-depleted mice. Furthermore, the depletion of neutrophils reduced the levels of serum AnxA1 (Figure 5E), reinforcing the potential of AnxA1 as a melanoma biomarker.

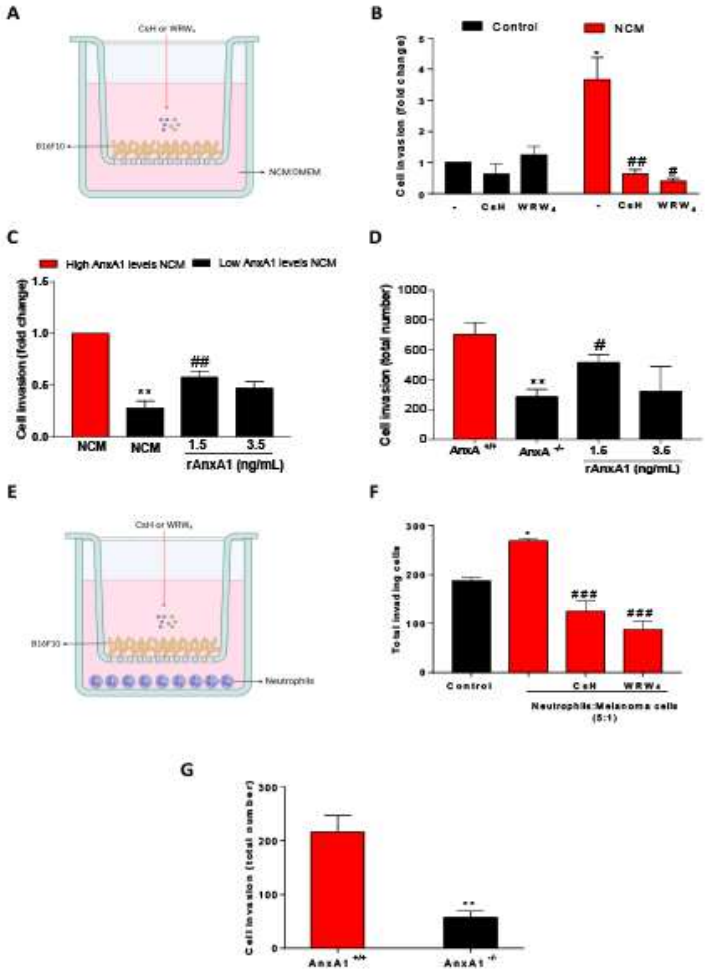

Figure 4. Neutrophil-conditioned medium or neutrophil cultured with melanoma cells increased the cell invasion by in a dependent manner of AnxA1. (**A**) Experimental design. (**B**) Invasion of melanoma cells in the absence and presence of FPR inhibitors incubated with standard culture medium (DMEM supplemented with 5% of FBS–control) or neutrophil-conditioned medium (NCM) for 24 h. Melanoma cells were pre-treated with 1 μM cyclosporine H (CsH; FPR1 inhibitor) or 1 μM WRW_4 (FPR2; inhibitor) for 15 min before seeding at the transwell bottom. * $p < 0.05$ vs. control; # $p < 0.05$; ## $p < 0.001$ vs. NCM. (**C**) Invasion of melanoma cells in the presence of NCM—detectable levels of AnxA1, NCM—undetectable levels of AnxA1, or NCM—undetectable levels of AnxA1 supplemented with recombinant AnxA1 (rAnxA1) at indicated concentrations. **/## $p < 0.01$ vs. NCM. (**D**) Invasion of melanoma cells in the presence of NCM from wild-type ($AnxA1^{+/+}$) or AnxA1 knockout ($AnxA1^{-/-}$) mice cultured for 24 h. (**E**) Experimental design. (**F**) Invasion of melanoma cells in the absence and presence of FPR inhibitors co-cultured for 24 h with neutrophils at proportion of 5 neutrophils to 1 melanoma cell. * $p < 0.05$ vs. control; ### $p < 0.001$ vs. untreated cells. (**G**) Invasion of melanoma cells in the presence of neutrophils from $AnxA1^{+/+}$ or $AnxA1^{-/-}$ mice cultured for 24 h. The data represent the average ± SEM of at least five to eight independent experiments. ** $p < 0.01$ vs. $AnxA1^{+/+}$.

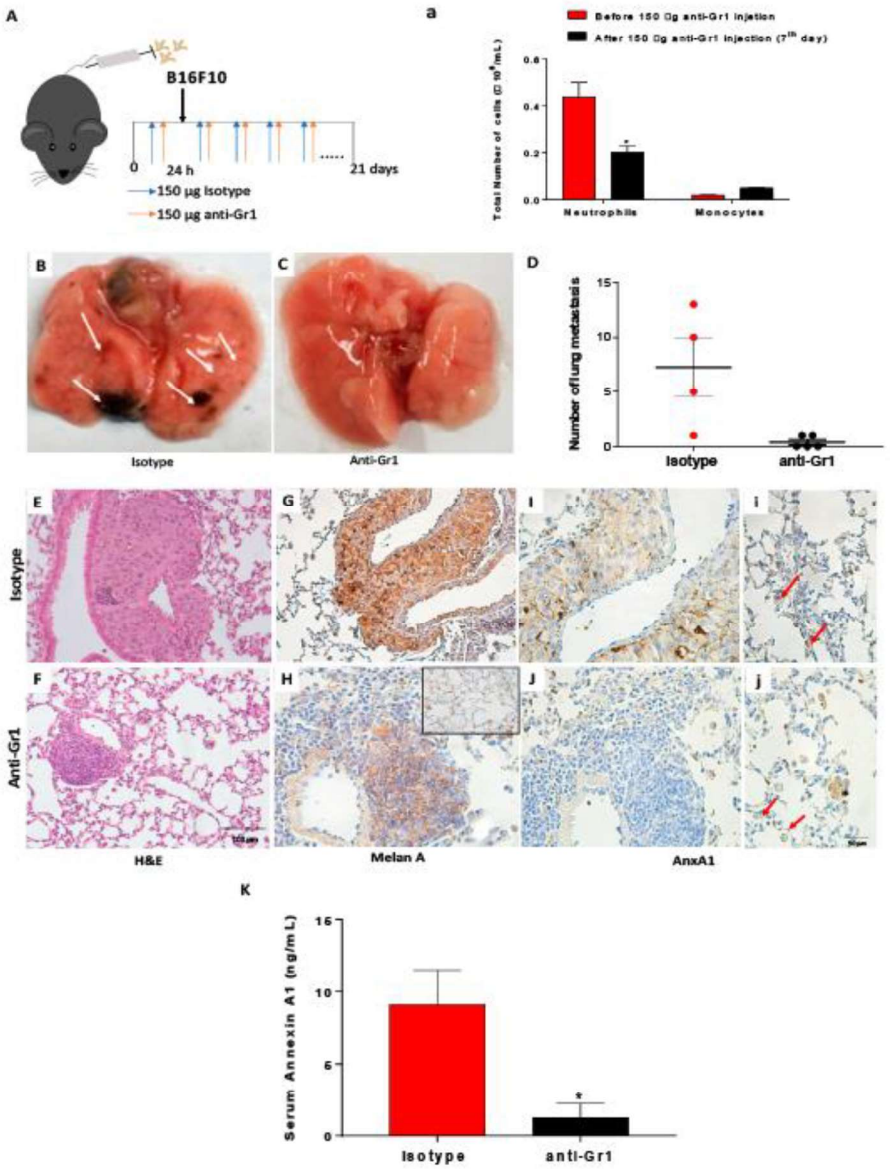

Figure 5. Neutrophil depletion reduced the number of melanoma lung metastasis and serum AnxA1 levels. (**A**) Experimental design. (a) Total number of neutrophils and monocytes in peripheral blood. (**B**,**C**) Images of the lungs from isotype or anti-Gr1-treated mice. (**D**) Number of melanoma metastasis spots. (**E**,**F**) Morphologic analysis by H&E staining. (**G**,**H**) Representative images of the Melan A expression (**I**,**i**) in isotype and (**J**,**j**) neutrophil-depleted mice. Insert: Melan A expressed in cells spread into the lungs. Red arrows: immune cells labeled for AnxA1. (**K**) Serum levels of AnxA1. The data represented the average ± SEM. * $p < 0.05$ vs. isotype. Melanoma group ($n = 4, 5$). Melanoma neutrophil-depleted group ($n = 5$).

4. Discussion

Neutrophils have been recognized as relevant players in cancer biology. Their actions are under robust investigation as they display anti- or pro-tumoral activities. The duality of neutrophil behavior is dependent on the phase of the disease, tumor environment contents, and the state of neutrophil activation in the blood or tumor sites. AnxA1^{+} neutrophils are fundamental to halting inflammation, and although AnxA1 secreted by cancer cells is involved in metastasis development, the role of AnxA1 derived from neutrophils in tumor invasiveness is underestimated. Hence, we addressed this issue, showing AnxA1 secreted by neutrophils contributes to the development of melanoma lung metastasis by promoting cancer invasiveness through FPR1/FPR2 pathways.

The up-expression of AnxA1 by tumor cells takes place in solid tumors of different origins and is associated with poor outcomes [59–62], implicating AnxA1 as a common mediator of cancer development. Indeed, aggressive human melanoma cell lines express high amounts of AnxA1 related to cell invasiveness, as verified by impairing melanoma cell invasion when endogenous AnxA1 protein levels were reduced [46]. Moreover, the treatment of the melanoma cells with the mimetic AnxA1 N-terminal peptide Ac2–26 stimulated the invasiveness by increasing MMP-2 expression, depending on FPR/MAPK/STAT3 activation pathways [46–48]. Furthermore, impaired melanoma lung metastasis in AnxA1$^{-/-}$ mice was associated with the inhibition of angiogenesis [63], pointing out that AnxA1 is a player protein such as on cancer as stromal cells. A previous retrospective clinical study showed that high AnxA1 expression in melanoma cells from primary tumors reduced metastasis-free survival, but AnxA1 expression levels were unchanged according to the Breslow index [46]. Here, data obtained in melanoma patients corroborate this evidence, as augmented AnxA1 expression in the cytoplasm of cells from a dysplastic nevus and melanoma patients was detected. However, the intensity of AnxA1 labeling did not change according to melanoma cells migrating deeper or spreading into the dermis, suggesting that maintenance of constitutive AnxA1 expression is an effector molecule mediating the tumor progression.

The NLR is a readily available metric with an emerging role in melanoma prognosis [15]. For localized melanoma, a high NLR is predictive of worse overall survival. However, the optimal cut-off for NLR is not established, varying between 2 and 5 [15]. Patients with NLR > 5 had significantly worse median overall survival in comparison with low NLR [64]. Similarly, NLR value has been considered in the prognostic of the patients receiving checkpoint inhibitors [24–26]. For instance, Bartlett et al. (2020) demonstrated that patients from the high-NLR group were more likely to have higher disease burden and poorer overall performance status. Furthermore, an NLR increase of ≥30% after initiation of therapy was also associated with shortened overall survival [65]. Although the number of patients included in our study was small, we observed a peripheral neutrophilia and the NLR was around 2.5, which is within the range considered for localized melanoma. Interestingly, we also observed that blood neutrophils from melanoma samples showed increased AnxA1 expression compared to nevus. The function of circulating AnxA1^{+} neutrophils in melanoma is not yet known and deserves further investigation. Nonetheless, AnxA1^{+} neutrophils in the blood are related to an immunosuppressive profile [39,41,66,67]. Furthermore, the potential of AnxA1 serum levels as a tumor biomarker has not been well explored. Its upregulation was only associated with pathological grade and clinical stage in patients with lung cancer [68]. Here, high serum AnxA1 levels and neutrophils expressing AnxA1 were consistent, such as that found in melanoma samples from patients as in the melanoma mice model. The fact that we found an increase in AnxA1 serum levels brings an alternative approach to help in the diagnosis of melanoma, and a large cohort is needed to support the potential of AnxA1 as a biomarker for melanoma detection or progression.

Further experimental data showed that neutrophils that infiltrated into the melanoma lung metastasis expressed elevated levels of AnxA1 in comparison to melanoma cells. A broad amount of data show that AnxA1 secreted by neutrophils into the inflammatory environment is phosphorylated and exerts autocrine and paracrine actions to halt the

inflammatory process and to induce efferocytosis [69]. To the best of our knowledge, we suggest, for the first time, that neutrophils secrete AnxA1 in melanoma metastasis and can influence tumor development. Hence, to confirm this hypothesis, an *in vitro* platform was carried out to detect the role of neutrophils or neutrophil-secreted products (NCM) on tumor cell invasiveness. Indeed, such melanoma cells co-cultured with neutrophils as incubated with NCM presented higher invasiveness, which was rescued if neutrophils were obtained from AnxA1$^{-/-}$ mice. The antagonisms of FPR1 or FPR2 also inhibited the augmented invasiveness of melanoma cells co-cultured with neutrophils or incubated with NCM. In the conditions where rAnxA1 was added to the medium, the melanoma cell invasion was lower than that found in NCM. Studies have shown that the active form of AnxA1 is associated with the N-terminal region, which can be exposed after a conformational change at the neutrophil plasma membrane or cleaved in a 33 kDa fragment by enzymes as elastase [70,71]. Here, we verified that AnxA1 secreted by neutrophils is cleaved. The lower effect promoted by rAnxA1 in comparison to NCM could be associated with the lack of the cleavage process. Hence, this body of data drives a pivotal role of AnxA1 secreted by neutrophils in melanoma invasion via the FPRs axis.

We here confirmed that B16F10 cells constitutively express FPR1 and FPR2, and data from the literature show that AnxA1 binds to both receptors and leads to cancer progression, such as breast cancer [67]. Interaction of AnxA1 with FPRs modulates signal transduction pathways, such as oncogenic signaling and extracellular-signal-related kinase (ERK) phosphorylation, resulting in cell invasion [72]. Indeed, the MAP kinase pathway is associated with melanoma development, as the inhibition of the members of the RAS–RAF–MEK–ERK axis has been a target of recent drugs to treat melanoma [73]. Moreover, previous studies showed that AnxA1 stimulated MMP-2 activity by interaction with FPRs, increasing cell invasiveness and promoting the proliferation and migration of melanoma cells *in vitro* [48,74].

Nonetheless, we may also suggest that AnxA1 secreted by N2 phenotype neutrophils influences stromal and immune cell behavior in the microenvironment, favoring the tumor progress. Indeed, AnxA1 via FPR1 potentiates the VEGF-A signaling in endothelial cells by promoting new vessel formation [75], and neutrophil-derived AnxA1 is related to angiogenesis during the development of the placenta [43]. Additionally, the reduction of lung melanoma metastasis in AnxA1$^{-/-}$ mice was associated with neovascularization impairment [63]. As mentioned before, N2 neutrophil-secreting AnxA1 displays immunoregulatory effects [39,41,66,67], which may effectively contribute to the immunosuppressive status of the metastasis sites. Robust evidences show a complex interplay of chemical mediators secreted by cancer cells and neutrophils on tumor progression when mediators secreted by cancer cells induce the switch of neutrophils to the N2 phenotype [75,76]. A recent report demonstrated that melanoma cell–neutrophil interaction supports cancer progression by priming neutrophils towards a pro-tumor N2 phenotype [77]. Indeed, the data here obtained show that melanoma-conditioned medium polarizes neutrophils into the N2 phenotype.

In addition, we observed a reduction of melanoma metastasis formation and serum levels of AnxA1 in neutrophil-depleted mice. Furthermore, an increase in lymphocytes was detected in lung metastasis, indicating that neutrophils at the tumor site may act as immunosuppressive cells. Indeed, neutrophil depletion has unveiled its role on cancer progression by suppressing antitumor T cells [78]. T-cell activation can be inhibited directly by TGF-β or IL-10 secreted by N2 phenotype [19] or indirectly by MMP-9 secretion that activates the TGF-β by proteolytic cleavage [79]. Moreover, neutrophils favor melanoma dissemination by releasing the neutrophil extracellular traps (NETs) induced by complement membrane attack complexes; NETs lead to the endothelial barrier opening that allows melanoma cells to enter the circulation and systemic spread [29]. Indeed, lung metastasis induced by melanoma cells expressing AnxA1 is impaired in AnxA1$^{-/-}$ mice [63], addressing the fact that constitutive AnxA1 secreted by other mice cells are involved in the metastasis.

Herein, the reduction of neutrophils implied in the serum AnxA1 secretion decrease, which may impair melanoma cell invasion and, consequently, its dissemination.

Our findings added AnxA1 secreted by neutrophils in the blood or at metastasis sites as a new player of the melanoma cell invasion, pointing to AnxA1 as a pivotal mediator secreted by neutrophils acting on cancer cells. These data open a venue for investigations about the mechanisms of AnxA1 secreted by neutrophils, such as in the blood as in tumor metastasis and to propose AnxA1 blood levels or $AnxA1^+$ neutrophils as a biomarker of early detection or melanoma progression.

Supplementary Materials: The following supporting information can be downloaded at https://www.mdpi.com/article/10.3390/cells12030425/s1. Figure S1: Obtention and characterization of mouse peritoneal cells; Figure S2: Characterization of melanoma cells. Figure S3: Neutrophil profile after 24 h of culture with melanoma-conditioned medium (MCM). Figure S4: Evaluation of the circulating neutrophils (Ly6G+) and monocytes (F4/80) on the 21st day after melanoma cells injection. Figure S5: Uncropped gel. Reference [80] is part of the Supplementary Materials document.

Author Contributions: Conceptualization: S.S., C.B.H. and S.H.P.F.; data curation: S.S., C.B.H., M.F.B., L.F.M., M.J.d.B.e.S., A.S.M., C.A.L.P. and J.P.D.N.; formal analysis: S.S., C.B.H., M.F.B., M.d.P.S., L.F.M., C.A.L.P. and C.D.G.; funding acquisition: S.H.P.F.; investigation: S.S., C.B.H. and S.H.P.F.; methodology: S.S., C.B.H., M.F.B., M.d.P.S., C.P.R. and C.D.G.; resources: S.H.P.F.; writing—review and editing: S.S., C.B.H., M.F.B., C.D.G. and S.H.P.F. All authors have read and agreed to the published version of the manuscript.

Funding: This work was supported by FAPESP (Fundação de Amparo á Pesquisa do Estado de São Paulo), grant number 2014/07328-4. S.H.P.F. is a fellow researcher of the CNPq (Conselho Nacional de Pesquisa); C.B.H. and S.S. were post-doctoral fellows of CAPES (Coordenação de Aperfeiçoamento de Pessoal de Nível Superior); M.F.B. is a PhD fellow of the FAPESP, grant number 2018/26383-7.

Institutional Review Board Statement: The study was conducted in accordance with the Declaration of Helsinki and approved by the Ethics in Research Committee of the School of Pharmaceutical Sciences/University of São Paulo (CAAE 27795120.0000.0067) and A.C. Camargo Cancer Center (CAAE 27795120.4.3001.5432). The animal use was approved by the Institutional Animal Care and Use Committee (IACUC) at the School of Pharmaceutical (CEUA FCF/USP 583).

Informed Consent Statement: Informed consent was obtained from all subjects involved in the study.

Data Availability Statement: Not applicable.

Acknowledgments: The authors thank Stephanie de Oliveira Duro for the technical support.

Conflicts of Interest: The authors declare no conflict of interest.

References

1. Hanahan, D.; Weinberg, R.A. Hallmarks of Cancer: The next Generation. *Cell* **2011**, *144*, 646–674. [CrossRef] [PubMed]
2. Angell, H.; Galon, J. From the Immune Contexture to the Immunoscore: The Role of Prognostic and Predictive Immune Markers in Cancer. *Curr. Opin. Immunol.* **2013**, *25*, 261–267. [CrossRef] [PubMed]
3. Ribas, A.; Wolchok, J.D. Cancer Immunotherapy Using Checkpoint Blockade. *Science* **2018**, *359*, 1350–1355. [CrossRef] [PubMed]
4. Waldman, A.D.; Fritz, J.M.; Lenardo, M.J. A Guide to Cancer Immunotherapy: From T Cell Basic Science to Clinical Practice. *Nat. Rev. Immunol.* **2020**, *20*, 651–668. [CrossRef] [PubMed]
5. Grivennikov, S.I.; Greten, F.R.; Karin, M. Immunity, Inflammation, and Cancer. *Cell* **2010**, *140*, 883–899. [CrossRef]
6. Gupta, A.K.; Hasler, P.; Holzgreve, W.; Gebhardt, S.; Hahn, S. Induction of Neutrophil Extracellular DNA Lattices by Placental Microparticles and IL-8 and Their Presence in Preeclampsia. *Hum. Immunol.* **2005**, *66*. [CrossRef]
7. Kumar, V.; Patel, S.; Tcyganov, E.; Gabrilovich, D.I. The Nature of Myeloid-Derived Suppressor Cells in the Tumor Microenvironment. *Trends Immunol.* **2016**, *37*, 208–220. [CrossRef]
8. Coffelt, S.B.; Wellenstein, M.D.; De Visser, K.E. Neutrophils in Cancer: Neutral No More. *Nat. Rev. Cancer* **2016**, *16*, 431–446. [CrossRef]
9. Rosales, C. Neutrophil: A Cell with Many Roles in Inflammation or Several Cell Types? *Front. Physiol.* **2018**, *9*, 113. [CrossRef]
10. Hellebrekers, P.; Vrisekoop, N.; Koenderman, L. Neutrophil Phenotypes in Health and Disease. *Eur. J. Clin. Investig.* **2018**, *48*, e12943. [CrossRef]

11. Schernberg, A.; Mezquita, L.; Boros, A.; Botticella, A.; Caramella, C.; Besse, B.; Escande, A.; Planchard, D.; Le Pechoux, C.; Deutsch, E. Neutrophilia as Prognostic Biomarker in Locally Advanced Stage III Lung Cancer. *PLoS ONE* **2018**, *13*, e0204490. [CrossRef]
12. Zou, P.; Yang, E.; Li, Z. Neutrophil-to-Lymphocyte Ratio Is an Independent Predictor for Survival Outcomes in Cervical Cancer: A Systematic Review and Meta-Analysis. *Sci. Rep.* **2020**, *10*, 21917. [CrossRef]
13. Kang, J.; Chang, Y.; Ahn, J.; Oh, S.; Koo, D.H.; Lee, Y.G.; Shin, H.; Ryu, S. Neutrophil-to-Lymphocyte Ratio and Risk of Lung Cancer Mortality in a Low-Risk Population: A Cohort Study. *Int. J. Cancer* **2019**, *145*, 3267–3275. [CrossRef]
14. Kim, J.Y.; Jung, E.J.; Kim, J.M.; Lee, H.S.; Kwag, S.J.; Park, J.H.; Park, T.; Jeong, S.H.; Jeong, C.Y.; Ju, Y.T. Dynamic Changes of Neutrophil-to-Lymphocyte Ratio and Platelet-to-Lymphocyte Ratio Predicts Breast Cancer Prognosis. *BMC Cancer* **2020**, *20*, 1206. [CrossRef]
15. Cohen, J.T.; Miner, T.J.; Vezeridis, M.P. Is the Neutrophil-to-Lymphocyte Ratio a Useful Prognostic Indicator in Melanoma Patients? *Melanoma Manag.* **2020**, *7*. [CrossRef]
16. Caruso, R.A.; Bellocco, R.; Pagano, M.; Bertoli, G.; Rigoli, L.; Inferrera, C. Prognostic Value of Intratumoral Neutrophils in Advanced Gastric Carcinoma in a High-Risk Area in Northern Italy. *Mod. Pathol.* **2002**, *15*, 831–837. [CrossRef]
17. Jensen, T.O.; Schmidt, H.; Møller, H.J.; Donskov, F.; Høyer, M.; Sjoegren, P.; Christensen, I.J.; Steiniche, T. Intratumoral Neutrophils and Plasmacytoid Dendritic Cells Indicate Poor Prognosis and Are Associated with PSTAT3 Expression in AJCC Stage I/II Melanoma. *Cancer* **2012**, *118*, 2476–2485. [CrossRef]
18. Jensen, H.K.; Donskov, F.; Marcussen, N.; Nordsmark, M.; Lundbeck, F.; Von Der Maase, H. Presence of Intratumoral Neutrophils Is an Independent Prognostic Factor in Localized Renal Cell Carcinoma. *J. Clin. Oncol.* **2009**, *27*, 4709–4717. [CrossRef]
19. Shaul, M.E.; Fridlender, Z.G. Tumour-Associated Neutrophils in Patients with Cancer. *Nat. Rev. Clin. Oncol.* **2019**, *16*, 601–620. [CrossRef]
20. Jaillon, S.; Ponzetta, A.; Di Mitri, D.; Santoni, A.; Bonecchi, R.; Mantovani, A. Neutrophil Diversity and Plasticity in Tumour Progression and Therapy. *Nat. Rev. Cancer* **2020**, *20*, 485–503. [CrossRef]
21. Cananzi, F.C.M.; Dalgleish, A.; Mudan, S. Surgical Management of Intraabdominal Metastases from Melanoma: Role of the Neutrophil to Lymphocyte Ratio as a Potential Prognostic Factor. *World J. Surg.* **2014**, *38*, 1542–1550. [CrossRef] [PubMed]
22. Blakely, A.M.; Cohen, J.T.; Comissiong, D.S.; Vezeridis, M.P.; Miner, T.J. Prognosis and Management of Thick and Ultrathick Melanoma. *Am. J. Clin. Oncol. Cancer Clin. Trials* **2019**, *42*, 824–829. [CrossRef] [PubMed]
23. Lino-Silva, L.S.; Salcedo-Hernández, R.A.; García-Pérez, L.; Meneses-García, A.; Zepeda-Najar, C. Basal Neutrophil-to-Lymphocyte Ratio Is Associated with Overall Survival in Melanoma. *Melanoma Res.* **2017**, *27*, 140–144. [CrossRef] [PubMed]
24. Robinson, A.V.; Keeble, C.; Lo, M.C.I.; Thornton, O.; Peach, H.; Moncrieff, M.D.S.; Dewar, D.J.; Wade, R.G. The Neutrophil–Lymphocyte Ratio and Locoregional Melanoma: A Multicentre Cohort Study. *Cancer Immunol. Immunother.* **2020**, *69*, 559–568. [CrossRef]
25. Ma, J.; Kuzman, J.; Ray, A.; Lawson, B.O.; Khong, B.; Xuan, S.; Hahn, A.W.; Khong, H.T. Neutrophil-to-Lymphocyte Ratio (NLR) as a Predictor for Recurrence in Patients with Stage III Melanoma. *Sci. Rep.* **2018**, *8*. [CrossRef]
26. Sandri, S.; Rodriguez, D.; Gomes, E.; Monteiro, H.P.; Russo, M.; Campa, A. Is Serum Amyloid A an Endogenous TLR4 Agonist? *J. Leukoc. Biol.* **2008**, *83*, 1174–1180. [CrossRef]
27. Bald, T.; Quast, T.; Landsberg, J.; Rogava, M.; Glodde, N.; Lopez-Ramos, D.; Kohlmeyer, J.; Riesenberg, S.; Van Den Boorn-Konijnenberg, D.; Hömig-Hölzel, C.; et al. Ultraviolet-Radiation-Induced Inflammation Promotes Angiotropism and Metastasis in Melanoma. *Nature* **2014**, *507*, 109–113. [CrossRef]
28. Wu, Y.; Zhao, Q.; Peng, C.; Sun, L.; Li, X.F.; Kuang, D.M. Neutrophils Promote Motility of Cancer Cells via a Hyaluronan-Mediated TLR4/PI3K Activation Loop. *J. Pathol.* **2011**, *225*. [CrossRef]
29. Liu, X.; Wang, Y.; Bauer, A.T.; Kirschfink, M.; Ding, P.; Gebhardt, C.; Borsig, L.; Tüting, T.; Renné, T.; Häffner, K.; et al. Neutrophils activated by membrane attack complexes increase the permeability of melanoma blood vessels. *Proc. Natl. Acad. Sci. USA* **2022**, *119*. [CrossRef]
30. Hyun, Y.M.; Seo, S.U.; Choi, W.S.; Kwon, H.J.; Kim, D.Y.; Jeong, S.; Kang, G.Y.; Yi, E.; Kim, M.; Ryu, H.J.; et al. Endogenous DEL-1 Restrains Melanoma Lung Metastasis by Limiting Myeloid Cell-Associated Lung Inflammation. *Sci. Adv.* **2020**, *6*. [CrossRef]
31. Jablonska, J.; Wu, C.F.; Andzinski, L.; Leschner, S.; Weiss, S. CXCR2-Mediated Tumor-Associated Neutrophil Recruitment Is Regulated by IFN-β. *Int. J. Cancer* **2014**, *134*. [CrossRef]
32. Soler-Cardona, A.; Forsthuber, A.; Lipp, K.; Ebersberger, S.; Heinz, M.; Schossleitner, K.; Buchberger, E.; Gröger, M.; Petzelbauer, P.; Hoeller, C.; et al. CXCL5 Facilitates Melanoma Cell–Neutrophil Interaction and Lymph Node Metastasis. *J. Investig. Dermatol.* **2018**, *138*, 1627–1635. [CrossRef]
33. Markman, J.L.; Porritt, R.A.; Wakita, D.; Lane, M.E.; Martinon, D.; Noval Rivas, M.; Luu, M.; Posadas, E.M.; Crother, T.R.; Arditi, M. Loss of Testosterone Impairs Anti-Tumor Neutrophil Function. *Nat. Commun.* **2020**, *11*. [CrossRef]
34. Schedel, F.; Mayer-Hain, S.; Pappelbaum, K.I.; Metze, D.; Stock, M.; Goerge, T.; Loser, K.; Sunderkötter, C.; Luger, T.A.; Weishaupt, C. Evidence and Impact of Neutrophil Extracellular Traps in Malignant Melanoma. *Pigment Cell Melanoma Res.* **2020**, *33*, 63–73. [CrossRef]
35. Uyanik, B.; Goloudina, A.R.; Akbarali, A.; Grigorash, B.B.; Petukhov, A.V.; Singhal, S.; Eruslanov, E.; Chaloyard, J.; Lagorgette, L.; Hadi, T.; et al. Inhibition of the DNA Damage Response Phosphatase PPM1D Reprograms Neutrophils to Enhance Anti-Tumor Immune Responses. *Nat. Commun.* **2021**, *12*. [CrossRef]

36. Qi, S.; Lu, L.; Zhou, F.; Chen, Y.; Xu, M.; Chen, L.; Yu, X.; Chen, W.R.; Zhang, Z. Neutrophil Infiltration and Whole-Cell Vaccine Elicited by N-Dihydrogalactochitosan Combined with NIR Phototherapy to Enhance Antitumor Immune Response and T Cell Immune Memory. *Theranostics* **2020**, *10*, 1814–1832. [CrossRef]
37. Headland, S.E.; Jones, H.R.; Norling, L.V.; Kim, A.; Souza, P.R.; Corsiero, E.; Gil, C.D.; Nerviani, A.; Dell'accio, F.; Pitzalis, C.; et al. Neutrophil-Derived Microvesicles Enter Cartilage and Protect the Joint in Inflammatory Arthritis. *Sci. Transl. Med.* **2015**, *7*, 315ra190. [CrossRef]
38. Jia, Y.; Morand, E.F.; Song, W.; Cheng, Q.; Stewart, A.; Yang, Y.H. Regulation of Lung Fibroblast Activation by Annexin A1. *J. Cell. Physiol.* **2013**, *228*, 476–484. [CrossRef]
39. Yang, Y.H.; Aeberli, D.; Dacumos, A.; Xue, J.R.; Morand, E.F. Annexin-1 Regulates Macrophage IL-6 and TNF via Glucocorticoid-Induced Leucine Zipper. *J. Immunol.* **2009**, *183*, 1435–1445. [CrossRef]
40. Sugimoto, M.A.; Vago, J.P.; Teixeira, M.M.; Sousa, L.P. Annexin A1 and the Resolution of Inflammation: Modulation of Neutrophil Recruitment, Apoptosis, and Clearance. *J. Immunol. Res.* **2016**, *2016*, 8239258. [CrossRef]
41. Walther, A.; Riehemann, K.; Gerke, V. A Novel Ligand of the Formyl Peptide Receptor: Annexin I Regulates Neutrophil Extravasation by Interacting with FPR. *Mol. Cell* **2000**, *5*, 831–840. [CrossRef] [PubMed]
42. Leoni, G.; Nusrat, A. Annexin A1: Shifting the Balance towards Resolution and Repair. *Biol. Chem.* **2016**, *397*, 971–979. [CrossRef] [PubMed]
43. Nadkarni, S.; Smith, J.; Sferruzzi-Perri, A.N.; Ledwozyw, A.; Kishore, M.; Haas, R.; Mauro, C.; Williams, D.J.; Farsky, S.H.P.; Marelli-Berg, F.M.; et al. Neutrophils Induce Proangiogenic T Cells with a Regulatory Phenotype in Pregnancy. *Proc. Natl. Acad. Sci. USA* **2016**, *113*, E8415–E8424. [CrossRef] [PubMed]
44. De Paula-Silva, M.; Barrios, B.E.; Macció-Maretto, L.; Sena, A.A.; Farsky, S.H.P.; Correa, S.G.; Oliani, S.M. Role of the Protein Annexin A1 on the Efficacy of Anti-TNF Treatment in a Murine Model of Acute Colitis. *Biochem. Pharmacol.* **2016**, *115*, 104–113. [CrossRef] [PubMed]
45. Foo, S.L.; Yap, G.; Cui, J.; Lim, L.H.K. Annexin-A1—A Blessing or a Curse in Cancer? *Trends Mol. Med.* **2019**, *25*, 315–327. [CrossRef]
46. Boudhraa, Z.; Rondepierre, F.; Ouchchane, L.; Kintossou, R.; Trzeciakiewicz, A.; Franck, F.; Kanitakis, J.; Labeille, B.; Joubert-Zakeyh, J.; Bouchon, B.; et al. Annexin A1 in Primary Tumors Promotes Melanoma Dissemination. *Clin. Exp. Metastasis* **2014**, *31*, 749–760. [CrossRef]
47. Rondepierre, F.; Bouchon, B.; Papon, J.; Bonnet-Duquennoy, M.; Kintossou, R.; Moins, N.; Maublant, J.; Madelmont, J.C.; D'Incan, M.; Degoul, F. Proteomic Studies of B16 Lines: Involvement of Annexin A1 in Melanoma Dissemination. *Biochim. Biophys. Acta Proteins Proteomics* **2009**, *1794*, 61–69. [CrossRef]
48. Boudhraa, Z.; Merle, C.; Mazzocut, D.; Chezal, J.M.; Chambon, C.; Miot-Noirault, E.; Theisen, M.; Bouchon, B.; Degoul, F. Characterization of Pro-Invasive Mechanisms and N-Terminal Cleavage of ANXA1 in Melanoma. *Arch. Dermatol. Res.* **2014**, *306*, 903–914. [CrossRef]
49. Oh, H.; Siano, B.; Diamond, S. Neutrophil Isolation Protocol. *J. Vis. Exp.* **2008**, *17*, 745. [CrossRef]
50. Santin, J.R.; Machado, I.D.; Drewes, C.C.; de Vinci Kanda Kupa, L.; Soares, R.M.; Cavalcanti, D.M.; da Rocha Pitta, I.; Farsky, S.H.P. Role of an Indole-Thiazolidiene PPAR Pan Ligand on Actions Elicited by G-Protein Coupled Receptor Activated Neutrophils. *Biomed. Pharmacother.* **2018**, *105*, 947–955. [CrossRef]
51. Overwijk, W.W.; Restifo, N.P. B16 as a Mouse Model for Human Melanoma. *Curr. Protoc. Immunol.* **2000**, *39*. [CrossRef]
52. Zaqout, S.; Becker, L.L.; Kaindl, A.M. Immunofluorescence Staining of Paraffin Sections Step by Step. *Front. Neuroanat.* **2020**, *14*, 582218. [CrossRef]
53. De Paula-Silva, M.; da Rocha, G.H.O.; Broering, M.F.; Queiroz, M.L.; Sandri, S.; Loiola, R.A.; Oliani, S.M.; Vieira, A.; Perretti, M.; Farsky, S.H.P. Formyl Peptide Receptors and Annexin A1: Complementary Mechanisms to Infliximab in Murine Experimental Colitis and Crohn's Disease. *Front. Immunol.* **2021**, *12*, 714138. [CrossRef]
54. Sandri, S.; Faião-Flores, F.; Tiago, M.; Pennacchi, P.C.; Massaro, R.R.; Alves-Fernandes, D.K.; Berardinelli, G.N.; Evangelista, A.F.; de Lima Vazquez, V.; Reis, R.M.; et al. Vemurafenib Resistance Increases Melanoma Invasiveness and Modulates the Tumor Microenvironment by MMP-2 Upregulation. *Pharmacol. Res.* **2016**, *111*, 523–533. [CrossRef]
55. Hu, Y. Isolation of Human and Mouse Neutrophils Ex Vivo and in Vitro. *Methods Mol. Biol.* **2012**, *844*, 101–113. [CrossRef]
56. Lahoz-Beneytez, J.; Elemans, M.; Zhang, Y.; Ahmed, R.; Salam, A.; Block, M.; Niederalt, C.; Asquith, B.; Macallan, D. Human Neutrophil Kinetics: Modeling of Stable Isotope Labeling Data Supports Short Blood Neutrophil Half-Lives. *Blood* **2016**, *127*, 3431–3438. [CrossRef]
57. Moses, K.; Klein, J.C.; Männ, L.; Klingberg, A.; Gunzer, M.; Brandau, S. Survival of Residual Neutrophils and Accelerated Myelopoiesis Limit the Efficacy of Antibody-Mediated Depletion of Ly-6G + Cells in Tumor-Bearing Mice. *J. Leukoc. Biol.* **2016**, *99*, 811–823. [CrossRef]
58. Stephens-Romero, S.D.; Mednick, A.J.; Feldmesser, M. The Pathogenesis of Fatal Outcome in Murine Pulmonary Aspergillosis Depends on the Neutrophil Depletion Strategy. *Infect. Immun.* **2005**, *73*, 114–125. [CrossRef]
59. Padden, J.; Ahrens, M.; Kälsch, J.; Bertram, S.; Megger, D.A.; Bracht, T.; Eisenacher, M.; Kocabayoglu, P.; Meyer, H.E.; Sipos, B.; et al. Immunohistochemical Markers Distinguishing Cholangiocellular Carcinoma (CCC) from Pancreatic Ductal Adenocarcinoma (PDAC) Discovered by Proteomic Analysis of Microdissected Cells. *Mol. Cell. Proteom.* **2016**, *15*, 1072–1082. [CrossRef]

60. Lin, Y.; Lin, G.; Fang, W.; Zhu, H.; Chu, K. Increased Expression of Annexin A1 Predicts Poor Prognosis in Human Hepatocellular Carcinoma and Enhances Cell Malignant Phenotype. *Med. Oncol.* **2014**, *31*, 327. [CrossRef]
61. Bai, X.F.; Ni, X.G.; Zhao, P.; Liu, S.M.; Wang, H.X.; Guo, B.; Zhou, L.P.; Liu, F.; Zhang, J.S.; Wang, K.; et al. Overexpression of Annexin 1 in Pancreatic Cancer and Its Clinical Significance. *World J. Gastroenterol.* **2004**, *10*, 1466–1470. [CrossRef] [PubMed]
62. Biaoxue, R.; Xiling, J.; Shuanying, Y.; Wei, Z.; Xiguang, C.; Jinsui, W.; Min, Z. Upregulation of Hsp90-Beta and Annexin A1 Correlates with Poor Survival and Lymphatic Metastasis in Lung Cancer Patients. *J. Exp. Clin. Cancer Res.* **2012**, *31*, 70. [CrossRef] [PubMed]
63. Yi, M.; Schnitzer, J.E. Impaired Tumor Growth, Metastasis, Angiogenesis and Wound Healing in Annexin A1-Null Mice. *Proc. Natl. Acad. Sci. USA* **2009**, *106*, 17886–17891. [CrossRef] [PubMed]
64. Kanatsios, S.; Melanoma Project, M.; Li Wai Suen, C.S.N.; Cebon, J.S.; Gyorki, D.E. Neutrophil to Lymphocyte Ratio Is an Independent Predictor of Outcome for Patients Undergoing Definitive Resection for Stage IV Melanoma. *J. Surg. Oncol.* **2018**, *118*. [CrossRef] [PubMed]
65. Bartlett, E.K.; Flynn, J.R.; Panageas, K.S.; Ferraro, R.A.; Jessica, J.M.; Postow, M.A.; Coit, D.G.; Ariyan, C.E. High Neutrophil-to-Lymphocyte Ratio (NLR) Is Associated with Treatment Failure and Death in Patients Who Have Melanoma Treated with PD-1 Inhibitor Monotherapy. *Cancer* **2020**, *126*, 76–85. [CrossRef]
66. Dalli, J.; Jones, C.P.; Cavalcanti, D.M.; Farsky, S.H.; Perretti, M.; Rankin, S.M. Annexin A1 Regulates Neutrophil Clearance by Macrophages in the Mouse Bone Marrow. *FASEB J.* **2012**, *26*, 387–396. [CrossRef]
67. Moraes, L.A.; Kar, S.; Foo, S.L.; Gu, T.; Toh, Y.Q.; Ampomah, P.B.; Sachaphibulkij, K.; Yap, G.; Zharkova, O.; Lukman, H.M.; et al. Annexin-A1 Enhances Breast Cancer Growth and Migration by Promoting Alternative Macrophage Polarization in the Tumour Microenvironment. *Sci. Rep.* **2017**, *7*, 17925. [CrossRef]
68. Rong, B.; Zhao, C.; Liu, H.; Ming, Z.; Cai, X.; Gao, W.; Yang, S. Elevated Serum Annexin A1 as Potential Diagnostic Marker for Lung Cancer: A Retrospective Case-Control Study. *Am. J. Transl. Res.* **2014**, *6*, 558–569.
69. Perretti, M.; D'Acquisto, F. Annexin A1 and Glucocorticoids as Effectors of the Resolution of Inflammation. *Nat. Rev. Immunol.* **2009**, *2016*, 8239258. [CrossRef]
70. Rosengarth, A.; Gerke, V.; Luecke, H. X-Ray Structure of Full-Length Annexin 1 and Implications for Membrane Aggregation. *J. Mol. Biol.* **2001**, *306*, 489–498. [CrossRef]
71. Rescher, U.; Goebeler, V.; Wilbers, A.; Gerke, V. Proteolytic Cleavage of Annexin 1 by Human Leukocyte Elastase. *Biochim. Biophys. Acta Mol. Cell Res.* **2006**, *1763*, 1320–1324. [CrossRef]
72. Kelly, L.; McGrath, S.; Rodgers, L.; McCall, K.; Tulunay Virlan, A.; Dempsey, F.; Crichton, S.; Goodyear, C.S. Annexin-A1: The Culprit or the Solution? *Immunology* **2022**, *166*, 2–16. [CrossRef]
73. Guo, W.; Wang, H.; Li, C. Signal Pathways of Melanoma and Targeted Therapy. *Signal Transduct. Target. Ther.* **2021**, *6*, 424. [CrossRef]
74. Delorme, S.; Privat, M.; Sonnier, N.; Rouanet, J.; Witkowski, T.; Kossai, M.; Mishellany, F.; Radosevic-Robin, N.; Juban, G.; Molnar, I.; et al. New insight into the role of ANXA1 in melanoma progression: Involvement of stromal expression in dissemination. *Am. J. Cancer Res.* **2021**, *11*, 1600–1615.
75. Shaul, M.E.; Fridlender, Z.G. Neutrophils as Active Regulators of the Immune System in the Tumor Microenvironment. *J. Leukoc. Biol.* **2017**, *102*, 343–349. [CrossRef]
76. Zou, J.M.; Qin, J.; Li, Y.C.; Wang, Y.; Li, D.; Shu, Y.; Luo, C.; Wang, S.S.; Chi, G.; Guo, F.; et al. IL-35 Induces N2 Phenotype of Neutrophils to Promote Tumor Growth. *Oncotarget* **2017**, *8*, 33501–33514. [CrossRef]
77. Anselmi, M.; Fontana, F.; Marzagalli, M.; Gagliano, N.; Sommariva, M.; Limonta, P. Melanoma Stem Cells Educate Neutrophils to Support Cancer Progression. *Cancers* **2022**, *14*, 3391. [CrossRef]
78. Giese, M.A.; Hind, L.E.; Huttenlocher, A. Neutrophil Plasticity in the Tumor Microenvironment. *Blood* **2019**, *133*, 2159–2167. [CrossRef]
79. Germann, M.; Zangger, N.; Sauvain, M.; Sempoux, C.; Bowler, A.D.; Wirapati, P.; Kandalaft, L.E.; Delorenzi, M.; Tejpar, S.; Coukos, G.; et al. Neutrophils Suppress Tumor-infiltrating T Cells in Colon Cancer via Matrix Metalloproteinase-mediated Activation of TGFβ. *EMBO Mol. Med.* **2020**, *12*, e10681. [CrossRef]
80. Rodrigues da Silva, M.; Schapochnik, A.; Peres Leal, M.; Esteves, J.; Bichels Hebeda, C.; Sandri, S.; Pavani, C.; Ratto Tempestini Horliana, A.C.; Farsky, S.H.P.; Lino-Dos-Santos-Franco, A. Beneficial effects of ascorbic acid to treat lung fibrosis induced by paraquat. *PLoS ONE* **2018**, *13*, e0205535. [CrossRef]

ORIGINAL RESEARCH

Development of Ac2-26 mesoporous microparticle system as a potential therapeutic agent for inflammatory bowel diseases

Milena Fronza Broering[1,2], Pedro Leonidas Oseliero Filho[3,4], Pâmela Pacassa Borges[1], Luis Carlos Cides da Silva[3], Marcos Camargo Knirsch[5], Luana Fillipi Xavier[1], Pablo Scharf[1], Silvana Sandri[1], Marco Antonio Stephano[5], Fernando Anselmo de Oliveira[6], Ibrahim M. Sayed[2], Lionel Fernel Gamarra[6], Soumita Das[2], Marcia C.A. Fantini[3], Sandra H.P. Farsky[1*]

[1]Department of Clinical and Toxicological Analyses, School of Pharmaceutical Sciences, University of Sao Paulo, São Paulo 05508-000, São Paulo, Brazil.

[2]Department of Biomedical and nutritional Sciences, University of Massachusetts-Lowell, 01854, Massachusetts, United States.

[3]Department of Applied Physics, Physics Institute, University of Sao Paulo, São Paulo, Brazil.

[4]Materials Innovation Factory, University of Liverpool, Liverpool, United Kingdom.

[5]Department of Biochemical and Pharmaceutical Technology, School of Pharmaceutical Sciences, University of São Paulo, São Paulo, Brazil

[6]Hospital Israelita Albert Einstein, São Paulo, Brazil.

Abstract

Inflammatory bowel diseases (IBDs) disrupt the intestinal epithelium, leading to severe chronic inflammation. Current therapies cause adverse effects and are expensive, invasive, and ineffective for most patients. Annexin A1 (AnxA1) is a pivotal endogenous anti-inflammatory and tissue repair protein in IBD. Nanostructured compounds loading AnxA1 or its active N-terminal mimetic peptides improve IBD symptomatology. To further explore their potential as a therapeutic candidate, the AnxA1 N-terminal mimetic peptide Ac2-26 was incorporated into SBA-15 ordered mesoporous silica and covered with Eudragit® L30-D55 to deliver it by oral treatment into the inflamed gut. The systems SBA-Ac2-26 developed Measurements revealed self-assembled rod-shaped particles, likely on the external surface of SBA-15, and 88% of peptide incorporation. SBA-15 carried the peptide Ac2-26 into cultured Raw 264.7 macrophages and Caco-2 epithelial cells. Moreover, oral administration of Eudragit-SBA-Ac2-26 (200 µg; once a day; for 4 days) to mice under dextran-sodium sulfate-induced colitis reduced colitis clinical symptoms, inflammation, and improved epithelium recovery. Our findings demonstrate a simple and cost-effective approach to delivering Ac2-26 orally into the inflamed gut, highlighting its potential as non-invasive IBD therapy.

Keywords: Annexin A1; SBA-15; oral route; tissue recovery; inflammation.

Introduction

The incidence of inflammatory bowel diseases (IBDs) has increased in the past years in developed and newly industrialized countries. Divided into two distinct types: ulcerative colitis (UC) and Crohn's disease (CD) are relapsing and chronic inflammatory diseases that mainly affect the large intestine.[1] Both UC and CD patients present debilitating symptoms like tenesmus, blood stool, diarrhea, and fatigue.[2] Notably, malignant colorectal cancer, small bowel cancer, intestinal lymphoma, and cholangiocarcinoma are enhanced in IBD patients; in addition, the high incidence of neoplasms is related to IBD-treated patients, implicating the adverse effects of available drugs.[3] Besides the considerable weakening situation that patients with IBD need to confront, around 50% of patients fail or present a loss of effectiveness of available drugs. Furthermore, the most recent biological treatments are expensive and require invasive administration. These features pose IBDs as a remarkable public health problem worldwide.[1,4] Hence, the look for novel biological targets and drugs and pharmaceutical approaches to deliver non-invasive drugs hallmarks IBDs as a subject in biological and drug development research.[5]

Annexin A1 (AnxA1) comprises a 37KDa endogenous protein of the calcium and phospholipid-binding Annexin superfamily.[6,7] Annexins present a C-terminal and an N-terminal domain; the last domain is specific for each superfamily component and confers specificity to biological activities.[7] AnxA1 was first characterized as a glucocorticoid-regulated anti-inflammatory protein;[6,8,9] nowadays, AnxA1 is recognized as a potent anti-inflammatory and resolvin molecule, being a mediator of cell proliferation, differentiation, and apoptosis of immune, epithelial, and cancer cells.[10–12] AnxA1 binds to intracellular structures, to membrane phospholipids, or to G-transmembrane coupled formyl peptide receptors to trigger the downstream activation of intracellular pathway. [8]

Robust evidence has associated the pivotal role of AnxA1 in the control of IBDs; as such, infiltrating leukocytes and epithelial intestinal cells express the protein during the course of the disease. Absence or low levels of the protein worsens and maintains the uncontrolled inflammation that perpetuates the disease.[13–17] AnxA1 interactions with formyl peptide receptor 1 (FPR1) mediate the IBD wound closure, and formyl peptide receptor 2 (FPR2) evokes mucosal healing by regulating the traffic and functions of leukocytes into the inflamed tissue.[18–22] Ac2-26 comprises the 25 amino acids of the N-terminal sequence

of AnxA1 that binds to FPR1 and 2 to display equivalent biological actions of the full-length protein,[8,23,24] including those evoked by AnxA1 on IBDs.[25–28]

Based on the data, the pharmacological administration of recombinant AnxA1 or its synthetic N-terminal-related peptides could address a mandatory role in IBD therapy. Indeed, this approach has been recently tested using lipid nanoparticles to load recombinant AnxA1 (rAnxA1) or Ac2-26. These strategies were more effective in treating colitis in mice than free rAnxA1 or Ac2-26 if locally administered, which demands non-feasible invasive routes of administration to treat chronic patients.[26–28] A nanoparticle-based on reactive oxygen species (ROS)-responsive material carrying Ac2-26 was effective in colitis treatment by oral route in mice, based on the release of the peptide by the action of ROS at the inflammatory site.[29] To strengthen the desirable oral delivery of novel drugs to treat IBDs, here we developed, characterized, and showed the effectiveness of a simple and cost-effective nanostructured silica mesoporous microparticle loading Ac2-26 to treat IBD by oral route. Data obtained point out the effectiveness of the treatment as a promising non-invasive approach to IBD therapy.

Material and Methods

Materials

SBA-15 was synthesized at the Physics Institute, University of São Paulo, Brazil, according to a previous work.[30] SBA-15 silanized with the amino-functional trimethoxysilanes (APTES); Eudragit® (L30-D55; Evonik Industries AG - Rellinghauser Straße – Essen Germany); peptide Ac2.26 (Proteinmax- São Paulo, Brazil); ethanol were of analytical grade (Sigma; St. Louis, USA); dextran sulfate sodium (DSS, MW 40,000, Dextran Products Limited, Ontario, Canada); anti-mouse MUC-2 (Invitrogen®, Waltham, Massachusetts, USA); anti-mouse F4/80 (eBioscience™, San Diego, California, USA); anti-mouse Claudin-1 and secondary antibody anti-rabbit conjugated with HRP (Abcam Plc, Cambridge, United Kingdom); anti-mouse Ly6G (BD, Becton Dickinson, New Jersey, US); DAB Substrate Chromogen System (Dako Omnis, Agilent, Santa Clara, California, USA); anti- proliferating cell nuclear antigen (PCNA)(Santa Cruz Biotechnology, Dallas, Texas, USA); anti-CD163 (Bioss Antibodies Inc, Massachusetts, USA); Collagenase II and Collagenase IV from *Clostridium histolyticum* and bovine serum albumin (BSA) (Gibco™, New York,

USA). ELISA kits anti-mouse TNF, IL-10, CXCL-1, IL-17 and IL-23 (BD OptEIA™ - BD, Becton Dickinson, New Jersey, US); isoflurane (Cristália Produto Químicos e Farmacêuticos Ltda, São Paulo, Brazil); paraformaldehyde, xilene, sodium citrate, peroxide and tris (hydroxymethyl) aminomethane (Synth® - Labsynth Produtos para Laboratórios LTDA, São Paulo, Brazil); cytochalasin D (Millipore Sigma, Darmstadt, Germany); pluronic P123 (BASF, German); tetraethyl orthosilicate; FITC; amino-functional trimethoxysilanes (APTES) (Sigma-Aldrich; St. Louis, USA). Cyanine-5.5 NHS ester (Cy5.5 - Lumiprobe Corporation, Hunt Valley, USA); Spectra/Por® 10 mm dialysis membrane tube (500 Da) (Spectrum® Laboratories; New Brunswick, USA); J774A.1 cells (ATCC®; Washington DC, USA); Raw 264.7 and Caco-2 cells (BCRJ®; Xerém, Brazil).

Synthesis of SBA-15

The synthesis of SBA-15 was made using 4 g of the Pluronic P123 ($PEO_{20}PPO_{70}PEO_{20}$). It was dissolved in 122 g of 2M HCl solution and kept under magnetic and mechanical stirring for 1 hour 8.6 g of tetraethyl orthosilicate was added, and the solution was kept under stirring for 24 hours. After this process, the mixture was submitted to a 48 hours hydrothermal treatment at 100ºC in an autoclave, washed with de-ionized water, and dried at room temperature. The polymer template was then removed through calcination at 540ºC under N_2 for 2 hours and in air for 4 hours.

Ac2-26 incorporation stemmed by dissolving the peptide in MilliQ water, then a 1:1 mixture of SBA-15:Ac2-26 was made, where 1 mg/mL of Ac2.26 was added at 1 mg of SBA-15. The mixture was dried in an oven at 35°C until complete drying. For coating with Eudragit® S100, a 1:2 ratio of SBA-15-Ac2-26 and Eudragit® was added. The material was dried in an oven at 35°C for 4 hours and then stored in a freezer at -20°C.

Characterization of SBA-15

Dynamic Light Scattering (DLS) measurement was performed at room temperature on a Brookhaven DM-5000 Particle Size Analyze (Brookhaven Instruments, NY, USA), using a wavelength of 635 nm. Data

120 analysis was conducted using the BIC software provided with the machine. The sample was diluted to 1
121 mg/mL to mitigate the influence of interparticle interaction on the diffusion coefficient of the particles and,
122 consequently, on the obtained data.

123 Small-angle X-ray Scattering (SAXS) was performed on a Nanostar (Bruker, Buffalo, USA)
124 instrument equipped with a microfocus Genix 3D system (Xenocs, Massachusetts, USA) and a Pilatus 300k
125 detector (Dectris, Baden Switzerland). The sample-to-detector distance was ~667 mm, which provided an
126 effective range of the modulus of the transfer moment vector, $q = 4\pi\sin(\theta)/\lambda$ (where 2θ is the scattering
127 angle and $\lambda = 1.5418$ Å is the X-ray wavelength), from 0.015 to 0.30 $Å^{-1}$. For the experiments, deionized
128 water (used in the sample preparation) and the same sample from DLS assays were measured, at room
129 temperature, in reusable quartz capillary with 1.5 mm in diameter mounted on stainless steel cases. Powder
130 samples of SBA-15 and SBA-15 plus peptide was placed in a sample holder between two mica sheets. The
131 set of mica sheets was also measured for background correction purposes. Data treatment, which includes
132 azimuthal integration, background subtraction and absolute scale normalization (for the liquid sample), was
133 performed using the XSACT software supplied by Xenocs.

134 The adsorption ®sotherms were obtained in the ASAP2020 equipment (Micromeritics®, Atlanta,
135 USA) using nitrogen gas.

136

137 ***SBA-15 uptake and cytotoxicity***

138 The analysis of SBA-15 uptake into cells was carried out by FITC labelling. For this, it was employed
139 SBA-15 silanized with APTES, according to protocol described by Appiah-Ntiamoah et al. (2015).[31] After
140 labeling, SBA-15 was analyzed by SAXS measurements. Mouse macrophage cell line J774A.1 were
141 cultured and seeded in 24 well plates as previously described.[32,33] Cytochalasin D (20 µM) was added 1
142 hour and removed before the treatment with FITC-SBA-15 (10 µg/mL). The cellular uptake was checked 4
143 and 24 hours after treatment using the cell imaging (CELENA ® Logos Biosystem, USA) and ten fields *per*
144 condition were analyzed. The percentage of phagocytic cells was quantified using the software ImageJ. In
145 addition, cytotoxicity for different concentrations of SBA-15 was performed using MTT assay.[34]

Murine 3D organoids and organoid-derived differentiated epithelial cells were isolated and cultured as previously described.[35,36] FITC-SBA (10 µg/mL) was added into organoids and on the apical part of the differentiated epithelial cells and analyzed 6 days or 24 hours later, respectively.

In vitro release of peptide by SBA-15

The peptide Ac2-26 was dissolved in phosphate buffes saline (PBS) (pH of 7.4) to reach a concentration of 1.0 mg/mL. Simultaneously, 1 mg of Cy5 dye was dissolved in 1 mL of 1 mM DMSO. The peptide and Cy5 dye were mixed in a 1:10 molar ratio, and any excess dye was removed through dialysis using a 10 mm membrane with a 500 Da cutoff. The Cy5-labeled peptide was purified with Sephadex G-25 and then lyophilized. Spectrophotometry at 215 nm (Shimadzu Scientific, Marlborough, USA) confirmed the success of the labeling process. The yield of the Cy5-labeled peptide was ten vials, each containing 450 µg.

Following, the labelled peptide was incorporated to SBA-15 (following item 2.2) and employed to test the release of the peptide into cells. The uptake of SBA-15-Ac2-26Cy.5.5 and FITC-SBA-15 was measure by flow cytometry (BD, Accuri C6, USA) in mouse macrophages Raw 264.7 and Caco-2 human intestinal epithelial cells. The presence of the peptide Ac2-26Cy.5.5 was analyzed after 30 minutes, 2, 6 and 24 hours after incubation with SBA-15-Ac2-26Cy.5.5. Caco-2 cell were used to measure the uptake of FITC-SBA-15 after 4 and 24 hours of incubation. After the incubation time, cells were collected and washed twice and resuspended in PBS. In order to quantify the percentage of cell positive, at least 10,000 events were collected. The events were collected with the delimitation of the principal population of healthy cells, and the percentage was set in relation to the untreated condition.

Animals

Male C57BL6 wild-type (WT) mice were obtained from Faculty of Pharmaceutical Sciences of the University of São Paulo, aged 8–10 weeks and weighting 20–25 g. They were maintained under pathogen-free conditions and in a 12-hours light/dark cycle, at temperatures between 20 to 25°C, with free access to

173 water and food. The protocol of study was approved by the Ethics Committee of Animal Use of the Faculty
174 of Pharmaceutical Sciences of the University of São Paulo (CEUA/FCF/ USP; protocol n°653), following
175 the Brazilian laws of animal ethics.
176

177 ***In vivo and ex vivo evaluation of SBA-15 and Ac2-26 in gastrointestinal tract***

178 The homing of the SBA-15 in the gastrointestinal tract (TGI) was evaluated by FITC-SBA-15 coated
179 with Eudragit. Eudragit-FITC-SBA-15 (400 µg/400 µL) was administered orally to health mice at day 6.
180 Animals were euthanatized 6 or 18 hours later to withdraw of the TGI. *Ex vivo* fluorescence images were
181 acquired using the IVIS ® Lumina LT Series III equipment (Xenogen Corp., Alameda, CA, USA) using the
182 following parameters: excitation/emission 465/520, automatic exposure time, F/stop 4 and binning of 4. For
183 Fluorescence intensity analysis we selected a region of interest and normalized by the corresponding areas.
184 The signals acquired were analyzed using Living Image Software version 4.7.2 in units of photons/s.
185

186 ***Experimental Colitis***

187 Experimental colitis was induced by gavage (v.o.) of dextran sodium sulfate (DSS) at 2%, conveyed
188 in the water of the animals from day 0-6, so that they receive constant doses of DSS. The animals were
189 divided into four groups: DSS, DSS + SBA-15-Eudragit (200 µg) and DSS + SBA-15-Ac2.26-Eudragit-SBA-
190 15-Ac2.26 (200 µg/200 µg), both in a final volume of 400 µL. Treatments were performed daily by oral route,
191 between days 6 ® Naive or DSS groups were manipulated as the other groups, but with the carrier solution
192 PBS only (Supplementary Figure 1). Clinical parameters (body weight, diarrhea, and rectal bleeding) were
193 evaluated daily (Day 0 to day 10), to assess the evolution of the colitis. The Disease Activity Index (DAI)
194 was calculated from the sum of the clinical parameters. On day 10, the animals were anesthetized by
195 isoflurane inhalation (2-chloro-2-(difluoromethoxy)-1,1,1-trifluoroethane) and euthanized. The intestinal
196 length and macroscopic analyses were evaluated. Colon samples were collected from the ileocecal junction
197 up to the proximity of the anus, and employed to histological (distal colon), enzymatic and flow cytometry
198 (mid/proximal colon) analyzes.
199

Histopathological analysis

Fragments collected from the distal part of the colon were fixed by 24 hours incubation in 4% paraformaldehyde for 24 hours. Histopathological analysis was performed in 4 µm sections. Samples were stained using hematoxylin and eosin solution and analyzed using an AxioCam coupled to a Zeiss microscope (Carl Zeiss, Jena, Germany). The histopathological score analysis was performed blindly by two analysts knowledgeable on characteristics of intestinal tissue. The score was adapted and considered: tissue edema, dysplasia/altered histoarchitecture, crypt edema, inflammatory infiltrates, and ulcerations. Ten photos were taken of each histological section using a 20x high power objective and scores were evaluated on a scale ranging from 0 to 4.

Immunohistochemistry analysis

Colon sections were deparaffinized, hydrated and incubated with sodium citrate buffer (pH 6.0) at 96°C for 30 minutes. Endogenous peroxidase activity was blocked with 3% hydrogen peroxide, three times washed after each in 10 minutes of incubation. Next, blocking of unspecific binding sites was carried out with 1% BSA diluted in Tris-buffer saline (TBS) for one hour. Sections obtained were incubated with antibodies for: Claudin-1 (1:50), MUC-2 (1:200), PCNA (1:10) and CD163 (1:100). Afterwards they were washed and incubated with a secondary antibody conjugated with HRP (1 hour, room temperature), and detected using 3,3′-diaminobenzidine. The sections were photographed using an AxioCam coupled to a Zeiss microscope (Carl Zeiss, Jena, Germany) with a 40x high power objective. The percentage of marked area of Claudin-1 was quantified using ImageJ software. Results were expressed as mean ± S.E.M. of percentage of marked area. The quantification of MUC-2, PCNA and CD163 were evaluated by using a 40x high power objective in ten fields of the mucosal layer from sections and the number of positive cells were quantified for each field assessed. Results were expressed as mean ± S.E.M. of cells per field.

Isolation of Leukocytes from Lamina Propria and Flow Cytometry

Leukocytes from proximal colonic lamina propria were isolated after washes with 2 mM EDTA followed by digestion with collagenase II and IV from *Clostridium histolyticum* (1 mg/mL). The cells were

washed through 40-µm strainers (Corning, Corning, NY, USA) and stained with Ly6G (PE) and F4/80 (PerCpCy5.5). Positive populations were determined by labeling with single antibodies. A minimum of 10,000 events per sample were acquired on a BD Accuri C6 Flow Cytometer (BD, Becton Dickinson, New Jersey, US). The results were expressed as percentages of positive cells normalized by controls from each experiment.

Statistical Analysis

The experimental colitis was subjected to analysis of clinical parameters using Two-way ANOVA with a subsequent Bonferroni post-test. In addition, for other analyses, One-way ANOVA was utilized, follow'd by Tukey's post-test. The significance level was set at $p < 0.05$, and the results were presented as mean ± SEM. GraphPad Prism Software 7.0 was employed to conduct the statistical analyses.

Results

Ac2-26 solution is composed of rod-like particles

Ac2-26 was successfully dispersed in deionized water at a concentration of 6 mg/mL, allowing future experiments that could require higher concentrations. It is interesting to observe that the sample is more viscous than pure water and slightly hazy, which points out the likely existence of large aggregates, being those features mitigated after dilution. To probe such aggregates, we proceeded with DLS assays. Figure 1A shows the obtained autocorrelation function (black filled circles), $C(\tau)$, fitted with the non-negatively constrained Least Squares (NNLS) method[37] (red continuous line). From the satisfactory fitting, the size distribution weighted by intensity, volume and number was evaluated (inset of Figure 1A). As observed, there are three populations of particles with sizes (23 ± 1) nm, (109 ± 28) nm and (58 ± 18) µm, being the first one the most numerous. Considering the results, none of these sets correspond to the peptide alone, with only 3089.46 Da of molecular weight, as informed by the manufacturer, but its self-assembled supramolecular structure and even aggregates. It is important to realize that such type of analysis assumes a spherical shape for the probed objects. To confirm this feature, we performed SAXS experiments on the same sample used for DLS.

254 The obtained SAXS data is shown in Figure 1B (black filled circles), and it was satisfactorily fitted
255 by the Indirect Fourier Transform (IFT),[38] implemented in the WIFT software [38]. From the fitting (blue
256 continuous line), the so-called pair distance distribution, p(r), is obtained (inset of Figure 1B, blue continuous
257 line), which provides the particle's longest length of ~23 nm (where p(r) ≈ 0), in agreement with the DLS
258 results concerning the population with the smallest objects. Furthermore, the pair distance distribution, p(r),
259 suggests the presence of elongated particles, for instance, with rod shape. In this context, a test was
260 performed in which the SAXS data was fitted with a simple cylinder model. A lognormal size distribution for
261 the radii values was also used, as in previous works.[39] The obtained satisfactory fit (Figure 1B, red
262 continuous line), corroborates the hypothesis of the cylindrical shape. In this case, the objects have average
263 radius of ~3 nm, according to the obtained size distribution (inset of Figure 1B, red continuous line) and
264 length of ~80 nm. The former value is out of the probed scale length, defined by the minimum value of the
265 q range, thus it cannot be precisely determined. Thus, the value ®icated by the p(r) function, ~23 nm, was
266 assumed as the cylinder length.
267 All in all, SAXS and DLS results suggest the peptide self-assembly into rod-shaped particles.
268

269 ***SBA-15 is a suitable mesoporous to anchorage Ac2-26***

270 The incorporation of peptide into SBA-15 was around 88,8% ± 1.2 (n=4) 88,8%, measured by the
271 Bradford dye-binding method. SAXS measurements were performed on powder samples of pure SBA-15
272 and SBA-15 containing the peptide (sample SBA-Ac-26). The obtained data is shown in Figure 1C (black-
273 filled circles) and the obtained results are comparable to already reported for ordered mesoporous silica
274 data.[40–42] It is interesting to note that both curves, with and without peptide, are very much alike.
275 To quantitively describe their nanostructure and eventual differences, we proceeded with the data
276 analysis using the model fully detailed by Losito *et al* 2021a.[41] The main fitting parameters, as well as their
277 values, are summarized in Table 1, while their meaning is explained in the following: R and T correspond
278 to the core radius and the shell thickness, respectively, of the core-shell cylinder modeling the mesopores,
279 being σ_{rel} the shared standard deviation of the log-normal size distribution of R and T. The parameter
280 $\frac{\Delta\rho_{core}}{\Delta\rho_{shell}}$ informs about the contrast electron density of the core relative to the shell. For ideally "empty"

281 mesopores, $\frac{\Delta\rho_{core}}{\Delta\rho_{shell}} = 0$. Otherwise, $\frac{\Delta\rho_{core}}{\Delta\rho_{shell}} \neq 0$ is an indication about the existence of some material inside
282 the mesopores. a is the lattice parameter and σ_a quantifies the distortion of the lattice relative to an ideal
283 2D-hexagonal one (for an ideal lattice, $\sigma_a = 0$). Finally, AP is the scale factor of the Porod term (proportional
284 to q^{-4} decaying law) and monitors, for instance, changes at the low q region of the SAXS curve related to
285 the presence of large aggregates, while $R_{G_{polymer}}$ is the radius of gyration related to the polymer-like
286 scattering at high q originated from the synthesis of the SBA-15.

287 As expected, both curves have structural parameters with close values, except for the AP
288 parameter. In comparison to pure SBA-15, its value increased ~3 times with the addition of peptide, which
289 suggests the presence of material on the SBA-15 macroporosity. Moreover, the parameter $\Delta\rho_{core}/\Delta\rho_{shell}$
290 slightly increased with the peptide incorporation, indicating that a fraction of material is inside the
291 mesopores. Considering the percentage of peptide anchorage was 87%, as previously discussed, possibly
292 most of the Ac-26, in its aggregated/self-assembled form, is in the SBA-15 macroporosity.

293 To have more information on the SBA-15 pore filling by the peptide, NAI experiments were
294 performed. The sorption results related to the SBA-15 samples, pristine and loaded with Ac2-26
295 (peptide:silica, 1:35 wt%), are shown in Figure 1D and are similar to those reported by Zhao et al 1998,[43]
296 for SBA-15 material. The isotherm of both samples shows hysteresis loops with sharp adsorption and
297 desorption branches, which indicates a narrow pore size distribution (PSD). From the quantitative analysis
298 using the Brunauer–Emmett–Teller (BET) and Barrett–Joyner–Halenda (BJH) models as well as the
299 calculations based on previous works,[44] the PSD was obtained (inset of Figure 1D) along other useful
300 parameters summarized in Table 1. Although the PSD of both samples are very similar, data presented in
301 Table 1 show a reduction of around ~55% in the surface area (internal mesopicroporosityxternal
302 macroporosity) after the incorporation of the peptide into SBA-15. Also considering the reduction of ~62%
303 in the available mesopore volume, that can either indicate their filling or blocking of the pore entrance, we
304 can conclude that the peptide is located inside the silica porosity (mesopores and/or macropores). In
305 combination with SAXS results, the hypothesis that likely most of the peptide is in the SBA-15 macroporosity
306 is reinforced. Furthermore, the possibility of increase the peptide concentration is evident, since there is
307 still “free space” in the SBA-15 porosity, with the care of preserving a homogenous distribution.
308

SBA-15 does not cause cytotoxicity and releases Ac2-26

Fluorophore labeling was employed to investigate the uptake of SBA-15 and the release of the Ac2-26 by SBA-15 into cells. SAXS measurement showed the incorporation of fluorophore to SBA-15 without robust changes in the SBA-15 scattering profile (Supplementary Figure 2). We here show the low uptake of SBA-15 by differentiated colonic epithelial cells (Figure 2A and D, Supplementary Figure 3) and 3D colonic organoids (Figure 2B, Supplementary Figure 3), which indicate SBA-15 may be low absorbed in the gut. Moreover, further flow cytometry analysis confirmed this data (Supplementary Figure 4). Nonetheless, enhanced epithelial permeability or even disruption of the epithelial barrier that occurs during gut inflammation may favor the microparticle influx into tissue.

Hence, SBA-15 may be taken up by phagocytes in the inflamed tissue. Data presented in Figure 2C showed that J774 murine macrophages engulfed the microparticle by phagocytosis, as the percentage of intake was blocked by cytochalasin D with a concentration of 20 µM. The uptake of microparticles increased with time (Figure 2E and F) and did not cause cytotoxicity until 48 hours of incubation (Figure 2G). Indeed, these data corroborate previous data depicting SBA-15 as a promising drug carrier into epithelial cells in the gut and inflammatory phagocytes.[45]

To evaluate the delivery of Ac2-26 by SBA-15, Caco-2 epithelial cells were incubated with SBA-15 loading Ac2-26-Cy5.5 labeled. Flow cytometry assay detected fluorescence emitted by Ac2-26-Cy5.5 in the epithelial cells after 30 minutes of incubation, which was increased 6 hours after incubation (Figure 2H). Furthermore, similar data was found in Raw 264.7 macrophages, which also evidences the capability of SBA-15 to deliver the peptide into phagocytes (Figure 2H).

Eudragit-SBA-15 biodistribution in gastrointestinal tract (GIT) and peptide release into gut

Notably, the in vitro dissolution analysis showed that the Ac2-26 peptide was released from Eudragit-SBA-15 in a pH solution close to that found in the duodenum (Supplementary Figure 5). Hence, to confirm if the peptide was delivered into the gut, Eudragit-SBA-15-Ac2-26Cy.5.5 was orally administered, and the

335 intensity of fluorescence was achieved in GIT after 3 hours of administration, which remained until 8 hours
336 of analysis (Figure 3A and B).
337 To evaluate the transit of Eudragit-FITC-SBA-15 in the GIT conditions and achieve the large intestine,
338 we track the treatment 6 and 18 hours after oral administration into mice. The measurement of signals
339 detected the Eudragit-FITC-SBA-15 in the small and large intestines at 6 hours and 18 hours after
340 administration, respectively (Figure 3C and D).
341 Associated data obtained showed Eudragit-SBA-15 remains in the GIT for at least 18 hours, which may
342 lead to sustained release of the peptide into the gut, addressing further analysis of the therapeutic efficacy
343 of the Eudragit-SBA-15-Ac2-26 by oral route on IBDs.
344

345 ***Eudragit-SBA-Ac2-26 reduces clinical symptoms and inflammation in the gut***

346 DSS-induced colitis is a standard model of experimental IBD.[46] DSS administration orally triggers the
347 peak of the disease on day 6, and the withdrawal of DSS promotes the initial recovery of tissue on day
348 10.[16,22,29,47] Hence, the Oral Eudragit-SBA-15-Ac2-26 treatment started at the peak of the disease (day 6)
349 and was maintained at the beginning of the recovery phase (day 10). Treatments were performed once a
350 day based on the TGI distribution of SBA-15 and peptide release. Data obtained showed that Eudragit-
351 SBA-15-Ac2-26 oral administration prevented weight loss and induced colon length recovery, leading to
352 lower DAI (Figure 4A-C). Moreover, the treatment inhibited the influx of neutrophils and macrophages into
353 the inflamed gut, reduced the secretion of inflammatory cytokines TNF-a and CXCL-1, and enhanced the
354 secretion of the anti-inflammatory cytokine IL-10 (Figure 4D-H). The beneficial effects of the treatment were
355 due to Ac2-26 loading, as treatment with Eudragit-SBA-15 did not prevent clinical symptoms and
356 inflammation parameters (Figure 4A-H).
357

358 ***Eudragit-SBA-Ac2-26 improves the gut histoarchitecture***

359 Histological analysis of the tissue showed that DSS administration induced ulcers, crypt abscesses,
360 vacuolar hydropic degeneration, submucosal edema, and mucosal/submucosal massive inflammatory cells

infiltrate. These alterations were reduced, and the colonic histological architecture was recovered by the Eudragit-SBA-15-Ac2-26 oral treatment (Figure 5A).

Immunohistochemical analysis was carried out to depict the mechanisms involved in the protection of gut architecture caused by Eudargit-SBA-15-Ac2-26 treatment. DSS administration led to lower expression of claudin-1, one major component of tight junctions, essential for the epithelial cells' barrier integrity; reduced mucin-2 marker, associated with goblet cells, leading to impaired mucus secretion; reduced epithelial cell proliferation and reduced the amount of anti-inflammatory M2 macrophage in the tissue. Eudragit-SBA-15-Ac2-26 oral treatment rescued all effects on tissue architecture (Figure 5B-E).

Discussion

The oral route is the most preferred for drug administration to treat IBD as it is not invasive, allows high patient compliance and flexibility on dose adjustment, and delivers the drug directly to the colonic region.[46] Nonetheless, small molecules and proteins present poor bioavailability by oral route administration and require suitable pharmaceutical technical approaches to resist the bacterial and enzyme-rich environment and different pHs in the gastrointestinal system.[46] Based on the robust beneficial actions of AnxA1 on IBD, we here inferred that AnxA1 mimetic peptide Ac2-26 could be incorporated into the SBA-15 ordered mesoporous silica microparticle, and the polymer coverage, using the well-known Eudragit® (L30 D55 polymer, Evonik), could protect the SBA-15-Ac2-26 from the unwanted harms of the TGI to deliver Ac2-26 into the inflamed colon area.

SBA-15 has a high thermic, hydrothermal, and mechanic-resistant material,[43] conferring its ability to resist pH and enzymatic actions [46]. The structural components of SBA-15 contain many essential sylanol groups (Si-OH)[43,48] to bond substances in its structure. SBA-15 also presents a high surface area, large pore volume, and narrow mesoporous pore size distribution, around 10 nm. Together, these properties allow the safe transport of small molecules through the TGI.[49–54] In fact, by means of the modeling of SAXS data, in combination with NAI results, it was possible to conclude that a fraction of the Ac2-26 peptide is loaded into the SBA-15 mesopores. In contrast, the remaining amount is somehow on the silica surface, a similar scenario observed in previous studies,[42,55] in which the authors loaded proteins instead of peptides.

As suggested by Rasmussen et al (2019),[56] the biological content of the SBA-15 macroporosity is still being protected against harsh environmental conditions such as the TGI.

Positively charged molecules can undergo electrostatic interactions with anionic components such as glycoproteins expressed on the epithelial cells. This results in charge neutralization and alteration of the tight junctions' permeability, allowing the transport of positively charged molecules.[57] For this reason, SBA-Ac2-26 was further covered with Eudragit®, a pH-responsive anionic copolymer produced from methyl methacrylate and methacrylic acid. It exhibits pH-dependent solubility characteristics, remaining stable under acidic conditions but dissolving in basic pH (pH >7.0)[58] to facilitate drug release, which in physiological conditions can start in the distal ileum. Eudragit is an efficient drug carrier in the lower pH of the inflamed gut, as it carries a significant negative charge,[59] enabling its preferential absorption to sites of inflammation. Image tomography analysis corroborated that Eudragit-SBA-15 administered by oral route remained in the GIT for an extended period, suitable for delivering drugs to the gut. Moreover, the Eudragit-SBA-15 uptake by in vitro gut epithelial cells in two or tri-dimensional cell models was deficient, reinforcing the hypothesis that SBA-15 is not absorbed in the gut and could be excreting by feces.[45] Further data addressed Eudragit-SBA-15 as a suitable platform to deliver the peptide into the gut, as Ac2-26 was detected in the epithelium after *in vitro* incubation with SBA-15-Ac2-26, and Eudragit-SBA-15 delivered Ac2-26 into the gut for an extended period after oral administration.

The inflammatory environment disrupts the intestinal barrier in IBD, resulting in increased permeability, allowing the leakage of nanoparticle-based therapies to the lamina propria and the subsequent engulfment by phagocytes.[60–62] It may be a suitable mechanism of SBA-15-Ac2-26 in IBD, as we here corroborated that macrophage efficiently phagocyte SBA-15.

The beneficial effects Ac2-26 on IBD symptomatology are related to its binding to FPR1 on the inflamed epithelium.[25,26] Moreover, AnxA1 is highly expressed by neutrophils and macrophages in the lamina propria and mediates the efferocytosis via FPR2 agonism.[16,22] Ac2-26 acts like AnxA1, binding to both receptors for downstream anti-inflammatory and tissue repair through intracellular pathways.[63] These concepts can be addressed to SBA-15 distribution and Ac2-26 biological response to oral treatment of colitis. The treatment promoted rapid beneficial effects, detected by the marked reduction of weight loss 24 hours after the first treatment, which was sustained for the following three administrations once a day during

the recovery phase of the disease. The effectiveness of the oral treatment of colitis could not be compared to the free Ac2-26 administration due to the poor bioavailability of peptides by oral intake.[64] On the 10th day of the disease, the treatment inhibited the influx of neutrophils and monocytes into inflamed tissue and reduced the levels of pro-inflammatory cytokines secreted in the tissue. The latter effect could reflect the lower number of inflammatory cells. Indeed, Ac2-26, similarly to AnxA1, detaches adhered cells to endothelial cells, thus limiting their trafficking to inflamed sites;[65–67] nonetheless, Ac2-26 inhibits the secretion of pro-inflammatory cytokines by transcriptional and post-transcriptional pathways.[28,68] Conversely, levels of the anti-inflammatory and pro-resolution IL-10 cytokine were enhanced by the treatment and agreed with the high amounts of anti-inflammatory CD163 M2 macrophages in the tissue of treated mice. Ac2-26 is a recognized resolvin peptide that polarizes M2 macrophages and induces neutrophil apoptosis to further phagocyted by M2 macrophages.[27,28,65–67]

Beyond reducing inflammation, Eudragit-SBA-15-Ac2-26 treatment favored tissue repair by rescuing the tight adhesion molecule and claudin-1 expression and promoting epithelial cell proliferation. Such AnxA1 as Ac2-26 induces epithelial repair in different models, and the underlying mechanisms involve the binding to FPR1/FPR2 receptors to downstream ERK1/2 phosphorylation pathway and inhibition of RhoA-ROCK signaling.[27,69–75]

Conclusion

We here designed a polymer-covered microparticle containing the antiinflammatory peptide Ac2-26 as a platform for targeted drug delivery to the inflamed colon by oral route administration. This conception was based on the high incorporation of small molecules into the microparticle mesoporous, which polymers could cover to protect it from the TGI adversities to drug delivery. Indeed, around 88% of the Ac2-26 peptide was incorporated, and the massive peptide release occurred in pH close to the gut microenvironment, suggesting that the peptide could be effectively protected from premature release until it reached the ileum and colon. Further data corroborated the platform's efficiency, as Eudragit-SBA-15 reached the large intestine in 18 hours, delivered the peptide in the gut, and clinical colitis recovery was detected in the first 24 hours of treatment. After four doses, once a day, the inflamed tissue was recovered, showing the peptide's anti-inflammation and tissue repair actions. Therefore, this platform holds promise, particularly in

444 safeguarding and delivering Ac2-26 at the inflamed colon to trigger the distinct intracellular pathways, which

445 are recognized as underlying mechanisms of AnxA1 protection in IBDs.

Disclosures

The authors declare no conflict of interest.

Acknowledgments

This work was supported by FAPESP (Fundação de Amparo à Pesquisa do Estado de São Paulo), grant numbers 2017/17844-8, 2019/07007-7, 2022/11602-0, 2019/12301-1. S.H.P.F., M.C.A. Fantini are researcher fellows of the CNPq (Conselho Nacional de Pesquisa, Brazil); M.F.B. is a PhD fellow of the FAPESP, grant number 2018/26383-7. CAPES (Coordenação de Aperfeiçoamento de Pessoal de Nível Superior) supported the Graduation Program on Pharmacy – Pathophysiology and Toxicology. A part of this work was supported by the intramural funds of University of Massachusetts- Lowell (to SD) and Leona M. and Harry B. Helmsley Charitable Trust (to SD and IMS).

References

1. Burisch J, Zhao M, Odes S, et al. The cost of inflammatory bowel disease in high-income settings: a Lancet Gastroenterology & Hepatology Commission. *Lancet Gastroenterol Hepatol*. 2023;8(5):458-492. doi:10.1016/S2468-1253(23)00003-1
2. Xavier RJ, Podolsky DK. Unravelling the pathogenesis of inflammatory bowel disease. *Nature*. 2007;448(7152):427-434. doi:10.1038/nature06005
3. Laredo V, García-Mateo S, Martínez-Domínguez SJ, López de la Cruz J, Gargallo-Puyuelo CJ, Gomollón F. Risk of Cancer in Patients with Inflammatory Bowel Diseases and Keys for Patient Management. *Cancers (Basel)*. 2023;15(3):871. doi:10.3390/cancers15030871
4. Spinelli A, Bonovas S, Burisch J, et al. ECCO Guidelines on Therapeutics in Ulcerative Colitis: Surgical Treatment. *J Crohn's Colitis*. 2022;16(2):179-189. doi:10.1093/ecco-jcc/jjab177
5. Kotla NG, Rochev Y. IBD disease-modifying therapies: insights from emerging therapeutics. *Trends Mol Med*. 2023;29(3):241-253. doi:10.1016/j.molmed.2023.01.001
6. Flower RJ, Rothwell NJ. Lipocortin-1: cellular mechanisms and clinical relevance. *Trends Pharmacol Sci*. 1994;15(3). doi:10.1016/0165-6147(94)90281-X
7. Moss SE, Morgan RO. The annexins. *Genome Biol*. 2004;5(4):219. doi:10.1186/gb-2004-5-4-219
8. Perretti M, D'Acquisto F. Annexin A1 and glucocorticoids as effectors of the resolution of inflammation. *Nat Rev Immunol*. Published online 2009. doi:10.1038/nri2470
9. Perretti M, Dalli J. Resolution Pharmacology: Focus on Pro-Resolving Annexin A1 and Lipid Mediators for Therapeutic Innovation in Inflammation. *Annu Rev Pharmacol Toxicol*. 2023;63(1):449-469. doi:10.1146/annurev-pharmtox-051821-042743
10. Machado ID, Spatti M, Hastreiter A, et al. Annexin A1 Is a Physiological Modulator of Neutrophil Maturation and Recirculation Acting on the CXCR4/CXCL12 Pathway. *J Cell Physiol*. 2016;231(11):2418-2427. doi:10.1002/jcp.25346
11. Sheikh M, Solito E. Annexin A1: Uncovering the Many Talents of an Old Protein. *Int J Mol Sci*. 2018;19(4):1045. doi:10.3390/ijms19041045
12. Foo SL, Yap G, Cui J, Lim LHK. Annexin-A1 – A Blessing or a Curse in Cancer? *Trends Mol Med*. 2019;25(4):315-327. doi:10.1016/j.molmed.2019.02.004

13. Vergnolle N, Comera C, Bueno L. Annexin 1 is Overexpressed and Specifically Secreted During Experimentally Induced Colitis in Rats. *Eur J Biochem*. 1995;232(2):603-610. doi:10.1111/j.1432-1033.1995.tb20850.x

14. Vergnolle N, Pagés P, Guimbaud R, et al. Annexin 1 is secreted in situ during ulcerative colitis in humans. *Inflamm Bowel Dis*. 2004;10(5):584-592. doi:10.1097/00054725-200409000-00013

15. Sena A, Grishina I, Thai A, et al. Dysregulation of Anti-Inflammatory Annexin A1 Expression in Progressive Crohns Disease. *PLoS One*. Published online 2013. doi:10.1371/journal.pone.0076969

16. de Paula-Silva M, Barrios BE, Macció-Maretto L, et al. Role of the protein annexin A1 on the efficacy of anti-TNF treatment in a murine model of acute colitis. *Biochem Pharmacol*. 2016;115:104-113. doi:10.1016/j.bcp.2016.06.012

17. Reischl S, Troger J, Jesinghaus M, et al. Annexin A1 Expression Capacity as a Determinant for Disease Severity in Crohn's Disease. *Dig Dis*. 2020;38(5):398-407. doi:10.1159/000505910

18. Babbin BA, Laukoetter MG, Nava P, et al. Annexin A1 Regulates Intestinal Mucosal Injury, Inflammation, and Repair. *J Immunol*. 2008;181(7):5035-5044. doi:10.4049/jimmunol.181.7.5035

19. Wentworth CC, Jones RM, Kwon YM, Nusrat A, Neish AS. Commensal-Epithelial Signaling Mediated via Formyl Peptide Receptors. *Am J Pathol*. 2010;177(6):2782-2790. doi:10.2353/ajpath.2010.100529

20. Vong L, Ferraz JGP, Dufton N, et al. Up-Regulation of Annexin-A1 and Lipoxin A4 in Individuals with Ulcerative Colitis May Promote Mucosal Homeostasis. *PLoS One*. 2012;7(6):e39244. doi:10.1371/journal.pone.0039244

21. Birkl D, O'Leary MN, Quiros M, et al. Formyl peptide receptor 2 regulates monocyte recruitment to promote intestinal mucosal wound repair. *FASEB J*. 2019;33(12):13632-13643. doi:10.1096/fj.201901163R

22. de Paula-Silva M, da Rocha GHO, Broering MF, et al. Formyl Peptide Receptors and Annexin A1: Complementary Mechanisms to Infliximab in Murine Experimental Colitis and Crohn's Disease. *Front Immunol*. 2021;12. doi:10.3389/fimmu.2021.714138

23. Galvão I, Vago JP, Barroso LC, et al. Annexin A1 promotes timely resolution of inflammation in murine gout. *Eur J Immunol*. 2017;47(3):585-596. doi:10.1002/eji.201646551

514 24. Alhasan H, Terkawi MA, Matsumae G, et al. Inhibitory role of Annexin A1 in pathological bone
515 resorption and therapeutic implications in periprosthetic osteolysis. *Nat Commun*. 2022;13(1):3919.
516 doi:10.1038/s41467-022-31646-0
517 25. Leoni G, Alam A, Neumann P-A, et al. Annexin A1, formyl peptide receptor, and NOX1 orchestrate
518 epithelial repair. *J Clin Invest*. 2013;123(1):443-454. doi:10.1172/JCI65831
519 26. Leoni G, Gripentrog J, Lord C, et al. Human neutrophil formyl peptide receptor phosphorylation and
520 the mucosal inflammatory response. *J Leukoc Biol*. 2015;97(1):87-101. doi:10.1189/jlb.4a0314-153r
521 27. Li C, Zhao Y, Cheng J, et al. A Proresolving Peptide Nanotherapy for Site-Specific Treatment of
522 Inflammatory Bowel Disease by Regulating Proinflammatory Microenvironment and Gut Microbiota.
523 *Adv Sci*. 2019;6(18). doi:10.1002/advs.201900610
524 28. Reischl S, Lee JH, Miltschitzky JRE, et al. Ac2-26-Nanoparticles Induce Resolution of Intestinal
525 Inflammation and Anastomotic Healing via Inhibition of NF-κB Signaling in a Model of Perioperative
526 Colitis. *Inflamm Bowel Dis*. Published online January 29, 2021. doi:10.1093/ibd/izab008
527 29. Broering MF, Leão M de C, da Rocha GHO, et al. Development of Annexin A1-surface-
528 functionalized metal-complex multi-wall lipid core nanocapsules and effectiveness on experimental
529 colitis. *Eur J Pharm Biopharm*. 2022;181(June):49-59. doi:10.1016/j.ejpb.2022.10.022
530 30. Matos JR, Mercuri LP, Kruk M, Jaroniec M. Toward the Synthesis of Extra-Large-Pore MCM-41
531 Analogues. *Chem Mater*. 2001;13(5):1726-1731. doi:10.1021/cm000964p
532 31. Appiah-Ntiamoah R, Chung WJ, Kim H. A highly selective SBA-15 supported fluorescent "turn-on"
533 sensor for the fluoride anion. *New J Chem*. 2015;39(7):5570-5579. doi:10.1039/c5nj00495k
534 32. Sayed IM, Ibeawuchi SR, Lie D, et al. The interaction of enteric bacterial effectors with the host
535 engulfment pathway control innate immune responses. *Gut Microbes*. 2021;13(1).
536 doi:10.1080/19490976.2021.1991776
537 33. Das S, Sarkar A, Choudhury SS, et al. Engulfment and Cell Motility Protein 1 (ELMO1) Has an
538 Essential Role in the Internalization of Salmonella Typhimurium Into Enteric Macrophages That
539 Impact Disease Outcome. *Cmgh*. 2015;1(3):311-324. doi:10.1016/j.jcmgh.2015.02.003
540 34. van Meerloo J, Kaspers GJL, Cloos J. Cell Sensitivity Assays: The MTT Assay. In: ; 2011:237-245.
541 doi:10.1007/978-1-61779-080-5_20

35. Sayed IM, Sahan AZ, Venkova T, et al. Helicobacter pylori infection downregulates the DNA glycosylase NEIL2, resulting in increased genome damage and inflammation in gastric epithelial cells. *J Biol Chem*. 2020;295(32):11082-11098. doi:10.1074/jbc.ra119.009981

36. Sharma A, Lee J, Fonseca AG, et al. E-cigarettes compromise the gut barrier and trigger inflammation. *iScience*. 2021;24(2):102035. doi:10.1016/j.isci.2021.102035

37. Morrison ID, Grabowski EF, Herb CA. Improved techniques for particle size determination by quasi-elastic light scattering. *Langmuir*. 1985;1(4):496-501. doi:10.1021/la00064a016

38. Glatter O. Data evaluation in small angle scattering: calculation of the radial electron density distribution by means of indirect Fourier transformation. *Acta Phys Austriaca*. 1977;47(1-2):83-102. Accessed June 2, 2023. https://inis.iaea.org/search/search.aspx?orig_q=RN:9355878

39. Pinto Oliveira CL. Investigating Macromolecular Complexes in Solution by Small Angle X-Ray Scattering. In: *Current Trends in X-Ray Crystallography*. InTech; 2011. doi:10.5772/30730

40. Martinez RM, Oseliero Filho PL, Gerbelli BB, et al. Influence of the Mixtures of Vegetable Oil and Vitamin E over the Microstructure and Rheology of Organogels. *Gels*. 2022;8(1):36. doi:10.3390/gels8010036

41. Losito DW, Lopes PS, Ueoka AR, et al. Biocomposites based on SBA-15 and papain: Characterization, enzymatic activity and cytotoxicity evaluation. *Microporous Mesoporous Mater*. 2021;325:111316. doi:10.1016/j.micromeso.2021.111316

42. Losito DW, de Araujo DR, Bezzon VDN, et al. Mesoporous Silica–Fe3O4 Nanoparticle Composites as Potential Drug Carriers. *ACS Appl Nano Mater*. 2021;4(12):13363-13378. doi:10.1021/acsanm.1c02861

43. Zhao D, Feng J, Huo Q, et al. Triblock Copolymer Syntheses of Mesoporous Silica with Periodic 50 to 300 Angstrom Pores. *Science (80-)*. 1998;279(5350):548-552. doi:10.1126/science.279.5350.548

44. Kruk M, Jaroniec M, Ko CH, Ryoo R. Characterization of the Porous Structure of SBA-15. *Chem Mater*. 2000;12(7):1961-1968. doi:10.1021/cm000164e

45. Li L, Liu T, Fu C, Tan L, Meng X, Liu H. Biodistribution, excretion, and toxicity of mesoporous silica nanoparticles after oral administration depend on their shape. *Nanomedicine Nanotechnology, Biol*

Med. 2015;11(8):1915-1924. doi:10.1016/j.nano.2015.07.004

46. Zhang F, Du Y, Zheng J, et al. Oral Administration of Multistage Albumin Nanomedicine Depots (MANDs) for Targeted Efficient Alleviation of Chronic Inflammatory Diseases. *Adv Funct Mater*. 2023;33(9):2211644. doi:10.1002/adfm.202211644

47. Mariano-Neto F, Matos JR, Cides da Silva LC, et al. Physical properties of ordered mesoporous SBA-15 silica as immunological adjuvant. *J Phys D Appl Phys*. 2014;47(42):425402. doi:10.1088/0022-3727/47/42/425402

48. Zhao D, Huo Q, Feng J, Chmelka BF, Stucky GD. Nonionic Triblock and Star Diblock Copolymer and Oligomeric Surfactant Syntheses of Highly Ordered, Hydrothermally Stable, Mesoporous Silica Structures. *J Am Chem Soc*. 1998;120(24):6024-6036. doi:10.1021/ja974025i

49. Scaramuzzi K, Oliveira DCA, Carvalho LV, et al. Nanostructured SBA-15 silica as an adjuvant in immunizations with hepatitis B vaccine. *Einstein (São Paulo)*. 2011;9(4):436-441. doi:10.1590/s1679-45082011ao2162

50. Xu C, Lei C, Yu C. Mesoporous Silica Nanoparticles for Protein Protection and Delivery. *Front Chem*. 2019;7. doi:10.3389/fchem.2019.00290

51. Mechler-Dreibi ML, Almeida HMS, Sonalio K, et al. Oral vaccination of piglets against Mycoplasma hyopneumoniae using silica SBA-15 as an adjuvant effectively reduced consolidation lung lesions at slaughter. *Sci Rep*. 2021;11(1):22377. doi:10.1038/s41598-021-01883-2

52. Rosenholm JM, Sahlgren C, Lindén M. Towards multifunctional, targeted drug delivery systems using mesoporous silica nanoparticles – opportunities & challenges. *Nanoscale*. 2010;2(10):1870. doi:10.1039/c0nr00156b

53. Lu J, Liong M, Li Z, Zink JI, Tamanoi F. Biocompatibility, Biodistribution, and Drug-Delivery Efficiency of Mesoporous Silica Nanoparticles for Cancer Therapy in Animals. *Small*. 2010;6(16):1794-1805. doi:10.1002/smll.201000538

54. Sarkar S, Ekbal Kabir M, Kalita J, Manna P. Mesoporous Silica Nanoparticles: Drug Delivery Vehicles for Antidiabetic Molecules. *ChemBioChem*. 2023;24(7). doi:10.1002/cbic.202200672

55. Trezena AG, Oseliero Filho PL, Cides da Silva LC, et al. Adjuvant effect of mesoporous silica SBA-15 on anti-diphtheria and anti-tetanus humoral immune response. *Biologicals*. 2022;80:18-26.

598 doi:10.1016/j.biologicals.2022.10.001

599 56. Rasmussen MK, Kardjilov N, Oliveira CLP, et al. 3D visualisation of hepatitis B vaccine in the oral
600 delivery vehicle SBA-15. *Sci Rep*. 2019;9(1):6106. doi:10.1038/s41598-019-42645-5

601 57. Bannunah AM, Vllasaliu D, Lord J, Stolnik S. Mechanisms of Nanoparticle Internalization and
602 Transport Across an Intestinal Epithelial Cell Model: Effect of Size and Surface Charge. *Mol Pharm*.
603 2014;11(12):4363-4373. doi:10.1021/mp500439c

604 58. Thakral S, Thakral NK, Majumdar DK. Eudragit®: a technology evaluation. *Expert Opin Drug Deliv*.
605 2013;10(1):131-149. doi:10.1517/17425247.2013.736962

606 59. Barbosa JAC, Abdelsadig MSE, Conway BR, Merchant HA. Using zeta potential to study the
607 ionisation behaviour of polymers employed in modified-release dosage forms and estimating their
608 pKa. *Int J Pharm X*. 2019;1:100024. doi:10.1016/j.ijpx.2019.100024

609 60. Beloqui A, Coco R, Alhouayek M, et al. Budesonide-loaded nanostructured lipid carriers reduce
610 inflammation in murine DSS-induced colitis. *Int J Pharm*. 2013;454(2).
611 doi:10.1016/j.ijpharm.2013.05.017

612 61. Hua S. Advances in Oral Drug Delivery for Regional Targeting in the Gastrointestinal Tract -
613 Influence of Physiological, Pathophysiological and Pharmaceutical Factors. *Front Pharmacol*.
614 2020;11(April):1-22. doi:10.3389/fphar.2020.00524

615 62. Mitchell MJ, Billingsley MM, Haley RM, Wechsler ME, Peppas NA, Langer R. Engineering precision
616 nanoparticles for drug delivery. *Nat Rev Drug Discov*. 2021;20(2):101-124. doi:10.1038/s41573-
617 020-0090-8

618 63. Cooray SN, Gobbetti T, Montero-Melendez T, et al. Ligand-specific conformational change of the
619 G-protein-coupled receptor ALX/FPR2 determines proresolving functional responses. *Proc Natl*
620 *Acad Sci*. 2013;110(45). doi:10.1073/pnas.1308253110

621 64. Langguth P, Bohner V, Heizmann J, et al. The challenge of proteolytic enzymes in intestinal peptide
622 delivery. *J Control Release*. 1997;46(1-2):39-57. doi:10.1016/S0168-3659(96)01586-6

623 65. Hayhoe RPG, Kamal AM, Solito E, Flower RJ, Cooper D, Perretti M. Annexin 1 and its bioactive
624 peptide inhibit neutrophil-endothelium interactions under flow: indication of distinct receptor
625 involvement. *Blood*. 2006;107(5):2123-2130. doi:10.1182/blood-2005-08-3099

626 66. Lim LHK, Pervaiz S. Annexin 1: the new face of an old molecule. *FASEB J*. 2007;21(4):968-975.
627 doi:10.1096/fj.06-7464rev
628 67. Girol AP, Mimura KKO, Drewes CC, et al. Anti-Inflammatory Mechanisms of the Annexin A1 Protein
629 and Its Mimetic Peptide Ac2-26 in Models of Ocular Inflammation In Vivo and In Vitro. *J Immunol*.
630 2013;190(11). doi:10.4049/jimmunol.1202030
631 68. Walther A, Riehemann K, Gerke V. A Novel Ligand of the Formyl Peptide Receptor. *Mol Cell*.
632 2000;5(5):831-840. doi:10.1016/S1097-2765(00)80323-8
633 69. Maderna P, Yona S, Perretti M, Godson C. Modulation of Phagocytosis of Apoptotic Neutrophils by
634 Supernatant from Dexamethasone-Treated Macrophages and Annexin-Derived Peptide Ac2–26. *J*
635 *Immunol*. 2005;174(6):3727-3733. doi:10.4049/jimmunol.174.6.3727
636 70. Sugimoto MA, Vago JP, Teixeira MM, Sousa LP. Annexin A1 and the Resolution of Inflammation:
637 Modulation of Neutrophil Recruitment, Apoptosis, and Clearance. *J Immunol Res*. 2016;2016.
638 doi:10.1155/2016/8239258
639 71. Cristante E, McArthur S, Mauro C, et al. Identification of an essential endogenous regulator of blood–
640 brain barrier integrity, and its pathological and therapeutic implications. *Proc Natl Acad Sci*.
641 2013;110(3):832-841. doi:10.1073/pnas.1209362110
642 72. Park J-C, Baik SH, Han S-H, et al. Annexin A1 restores $A\beta_{1-42}$ -induced blood-brain barrier
643 disruption through the inhibition of RhoA-ROCK signaling pathway. *Aging Cell*. 2017;16(1):149-161.
644 doi:10.1111/acel.12530
645 73. Lacerda JZ, Drewes CC, Mimura KKO, et al. Annexin A12–26 Treatment Improves Skin
646 Heterologous Transplantation by Modulating Inflammation and Angiogenesis Processes. *Front*
647 *Pharmacol*. 2018;9. doi:10.3389/fphar.2018.01015
648 74. Hebeda CB, Sandri S, Benis CM, et al. Annexin A1/Formyl Peptide Receptor Pathway Controls
649 Uterine Receptivity to the Blastocyst. *Cells*. 2020;9(5). doi:10.3390/cells9051188
650 75. Sheikh MH, Errede M, d'Amati A, et al. Impact of metabolic disorders on the structural, functional,
651 and immunological integrity of the blood-brain barrier: Therapeutic avenues. *FASEB J*. 2022;36(1).
652 doi:10.1096/fj.202101297R
653

654 **Legend for Figures**

655 **Figure 1 A** Autocorrelation function (filled black circles) fitted by the NNLS method (continuous line). Inset:
656 Hydrodynamic diameter distributions of the peptide weighted by number, volume, and intensity. **B** SAXS
657 data of the peptide in solution (filled circles) fitted by the IFT method (blue continuous line) and the cylinder
658 model (red continuous line). Inset: The obtained p(r) function, from IFT, and the size distribution function of
659 the cylinder radius, N(D), from the model fitting. **C** SAXS data (filled black circles) of the pure SBA-15 and
660 the SBA-15 incorporated with Ac2-26 (sample SBA-Ac2-26) fitted by the SBA-15 model (red continuous
661 line). The curves were vertically shifted for a clearer visualization. **D** NAI data of pristine SBA-15 and the
662 SBA-15 incorporated with Ac2-26 (sample SBA-Ac-26). Inset: Pore size distribution (PSD, adsorption and
663 desorption).

664

665 **Figure 2 A** Representatives pictures from differentiated EDMs treated FITC-SBA for 24 hours. **D** The
666 percentage of microparticles uptake was determined. **B** Representative pictures showed 3D murine
667 organoid challenged with microparticles and cultured for 6 days. **C** Representative pictures showed
668 macrophages J774 challenged or not with microparticles for 24 hours in presence or absent of phagocytosis
669 inhibitors (cytochalasin D). **E** and **F** represent the uptake quantification of FITC-SBA after 4 hours (4h) and
670 24 hours (24h) after treatment. **G** In All images, green inside the cells represent microparticles
671 internalization. Cytotoxicity by MTT assay using murine macrophages Raw 264.7. Ac2-26, SBA and
672 Ac2-26-SBA concentrations 1, 2, 3 and 4 corresponding to 0.5, 5, 10 and 50 µg/mL respectively. **H**
673 Representative graph showing the percentage of Caco-2 or Raw 264.7 cells positive for Ac2-26-Cy5 at
674 different time points: 30 minutes (30min), 2 hours, 6 hours and 24 hours. The lower left side represents the
675 Caco-2 and Raw 264.7 histogram median of fluorescence (upper line) and the percentage using forward
676 scatter height (FSC-H) vs fluorescence emission for Cy5. Data obtained from the flow cytometry Accuri C6
677 software after 30 min and 24 hours. **D** as determined by parametric Student's t-test. **E** and **F** as determined
678 by One-Way ANOVA and Tukey multiple comparisons. **H** as determined Two-Way ANOVA and Tukey
679 multiple comparisons. * <p 0.05, ** <p 0.01 and **** p< 0.0001. #### p< 0.0001.

680

681 **Figure 3** Biodistribution along the TGI of Eudragit-SBA-Ac2-26Cy5.5 Eudragit-FITC-SBA-15. Mice were
682 treated orally and the intensity of the distribution is represented by photons/s. **A** Eudragit-SBA-Ac2-26Cy5.5
683 distribution was analyzed after 3 hours and 8 hours *in vivo* (top) and the TGI analyzed separately *ex vivo*
684 (botton) at the same time points. The yellow color represents the higher intensity in the tissue. **B** Eudragit-
685 FITC-SBA-15 biodistribution *ex vivo* along the TGI after 6 hours and 18 hours. The red color represents the
686 higher intensity in the tissue.
687
688 **Figure 4** Clinical, cellular and secretory profile of DSS-induced colitis mice treated with Eudragit-SBA or
689 Eudragit-SBA-Ac2-16. **A** Percentage of body weight loss; **B** Anatomic evaluation of the colon and length
690 measure; **C** DAI; **D** Percentage of macrophages isolated from lamina propria ($CD45^+/F4/80^+$); **E** Percentage
691 of neutrophils isolated from lamina propria ($CD45^+/Ly6G^+$); **F** TNF-α; **G** CXCL-1; **H** IL-10. n = 10 mice/group.
692 * $p < 0.05$, ** $p < 0.01$, *** $p < 0.001$ vs DSS. & $p < 0.05$, && $p < 0.01$, &&& $p < 0.001$ vs Eudragit-SBA-15.
693 Abbreviations: DAI, disease activity index. DSS, dimethyl sulfoxide.
694
695 **Figure 5** Histopathological sections performed with HE dye. **A** Histopathological score represented by
696 arbitrary units. The sections were blindly evaluated and considered alterations were highlighted. Tissue
697 edema (square brackets), inflammatory infiltrates (black arrow head) and ulcerations (red arrow). Naïve
698 section presenting normal histoarchitecture. Mice colon sections submitted to IHC. **B** Representative
699 sections and percentage (%) of marked area for Claudin-1 marker. **C** Representative sections and, number
700 of positive cells per field for MUC-2 marker. **D** Representative sections and, number of positive cells per
701 slide for PCNA marker. **E** Representative sections and, number of positive cells per field for CD163 marker.
702 n = 10 mice/group. Scale bar: 50 µm. Sections: 4 µm. * $p < 0.05$, ** $p < 0.01$, *** $p < 0.001$, **** $p < 0.0001$
703 vs DSS. . & $p < 0.05$, &&&& $p < 0.0001$ vs DSS + Eudragit-SBA-15.
704
705 **Table 1** Structural and textural properties of the pristine SBA-15 sample and the SBA-15 incorporated with
706 Ac2-26 (sample SBA-Ac-26) obtained from SAXS and NAI techniques. All uncertainties in the last digit,
707 when exist, are presented between parentheses.
708

Anexo 5. Currículo lattes

Milena Fronza Broering

Endereço para acessar este CV: http://lattes.cnpq.br/5303105654305538
ID Lattes: **5303105654305538**
Última atualização do currículo em 30/11/2023

Possui graduação em Biomedicina pela Universidade do Vale do Itajai - UNIVALI (2016). Mestre em Ciências Farmacêuticas pela Universidade do Vale do Itajai (2019), área de concentração em Produtos Naturais e Substâncias Bioativas. Aluna de doutorado no programa de Pós-Graduação em Fisiopatologia e Toxicologia da Faculdade de Ciências Farmacêuticas da Universidade de São Paulo (FCF/USP) atuando na linha de pesquisa sobre processo inflamatório e nanotecnologia. **(Texto informado pelo autor)**

Identificação

Nome	Milena Fronza Broering
Nome em citações bibliográficas	BROERING, M. F.;BROERING, MILENA FRONZA;BROERING, M.F.
Lattes iD	http://lattes.cnpq.br/5303105654305538
Orcid iD	? https://orcid.org/0000-0001-6748-882X

Endereço

Formação acadêmica/titulação

2017 - 2019
Mestrado em Programa de Mestrado em Ciências Farmacêuticas.
Universidade do Vale do Itajaí, UNIVALI, Brasil.
Título: Efeitos do estrato de Tithonia diversifolia (Asteraceae) sobre a inflamação inata.
Ano de Obtenção: 2019.
Orientador: José Roberto Santin.
Coorientador: Nara Lins Meira Quintão.
Bolsista do(a): Conselho Nacional de Desenvolvimento Científico e Tecnológico, CNPq, Brasil.
Palavras-chave: Inflamação; Migração; Neutrófilos; Tithonia.
Grande área: Ciências Biológicas
Grande Área: Ciências Biológicas / Área: Farmacologia / Subárea: Imunologia Celular.

2013 - 2016
Graduação em Biomedicina.
Universidade do Vale do Itajaí, UNIVALI, Brasil.
Título: Avaliação toxicológica in vivo, in vitro e in silico do extrato metanólico e compostos isolados das partes aéreas de Rubus rosaefolius.
Orientador: José Roberto Santin.
Bolsista do(a): Programa Universidade para Todos, PROUNI, Brasil.

2010 - 2012
Ensino Médio (2º grau).
Escola de Educação Básica Luiz Bertoli, EEBLB, Brasil.

Formação Complementar

2019 - 2019
Cultivo Celular em 3D. (Carga horária: 32h).
Banco de Células do Rio de Janeiro, BCRJ, Brasil.

Atuação Profissional

Universidade de São Paulo, USP, Brasil.

Vínculo institucional

2019 - Atual	Vínculo: Bolsista, Enquadramento Funcional: Doutorado, Carga horária: 40, Regime: Dedicação exclusiva.

Idiomas

Português	Compreende Bem, Fala Bem, Lê Bem, Escreve Bem.
Inglês	Compreende Bem, Fala Bem, Lê Bem, Escreve Bem.

Produções

Produção bibliográfica

Artigos completos publicados em periódicos

Ordenar por

Ordem Cronológica

1. DE CASTRO LEÃO, MATHEUS ; DI PIAZZA, ISABELLA ; CARIA, SARAH JORGE ; **BROERING, MILENA FRONZA** ; FARSKY, SANDRA HELENA POLISELLI ; UCHIYAMA, MAYARA KLIMUK ; ARAKI, KOITI ; BONJOUR, KENNEDY ; COGLIATI, BRUNO ; POHLMANN, ADRIANA RAFFIN ; GUTERRES, SILVIA STANISÇUASKI ; CASTRO, INAR ALVES . Effect of nanocapsules containing docosahexaenoic acid in mice with chronic inflammation. BIOMEDICINE & PHARMACOTHERAPY JCR , v. 167, p. 115474, 2023.

2. SANDRI, SILVANA ; HEBEDA, CRISTINA BICHELS ; **BROERING, MILENA FRONZA** ; DE PAULA SILVA, MARINA ; MOREDO, LUCIANA FACURE ; DE BARROS E SILVA, MILTON JOSÉ ; SAPATA MOLINA, ANDRÉ ; LOPES PINTO, CLÓVIS ANTÔNIO ; DUPRAT NETO, JOÃO PEDREIRA ; REUTELINGSPERGER, CHRIS P. ; GIL, CRISTIANE DAMAS ; FARSKY, SANDRA HELENA POLISELLI . Role of Annexin A1 Secreted by Neutrophils in Melanoma Metastasis. Cells JCR, v. 12, p. 425, 2023.

   Citações: WEB OF SCIENCE℠ 1 | 1

3. SANTIN, JOSÉ ROBERTO ; BENVENUTTI, LARISSA ; **BROERING, MILENA FRONZA** ; NUNES, ROBERTA ; GOLDONI, FERNANDA CAPITANIO ; PATEL, YASMIN BEATRISSE KLEIN ; DE SOUZA, JADE ANDRÉ ; KOPP, MAINARA ADRIANE TESSER ; DE SOUZA, PRISCILA ; DA SILVA, RITA DE CÁSSIA VILHENA ; PASTOR, MARIA VERÔNICA DÁVILA ; DE SOUZA, ANGELITA BOLDIERI ; TESTONI, LETÍCIA DEBATIN ; COUTO, ANGÉLICA GARCIA ; BRESOLIN, TANIA MARI BELLE ; QUINTÃO, NARA LINS MEIRA . Sambucus nigra: A traditional medicine effective in reducing inflammation in mice. JOURNAL OF ETHNOPHARMACOLOGY JCR, v. 283, p. 114736, 2022.

   Citações: WEB OF SCIENCE℠ 7 | 7

4. **BROERING, MILENA FRONZA**; LEÃO, MATHEUS DE CASTRO ; DA ROCHA, GUSTAVO HENRIQUE OLIVEIRA ; SCHARF, PABLO ; XAVIER, LUANA FILLIPI ; ALVES, ALINE DE CRISTO SOARES ; CASTRO, INAR ; REUTELINGSPERGER, CHRIS ; UCHIYAMA, MAYARA KLIMUK ; ARAKI, KOITI ; GUTERRES, SÍLVIA STANISÇUASKI ; POHLMANN, ADRIANA RAFFIN ; FARSKY, SANDRA HELENA POLISELLI . Development of Annexin A1-surface-functionalized metal-complex multi-wall lipid core nanocapsules and effectiveness on experimental colitis. EUROPEAN JOURNAL OF PHARMACEUTICS AND BIOPHARMACEUTICS JCR, v. 181, p. 49-59, 2022.

5. DE PAULA-SILVA, MARINA ; DA ROCHA, GUSTAVO HENRIQUE OLIVEIRA ; **BROERING, MILENA FRONZA** ; QUEIROZ, MARIA LUÍZA ; SANDRI, SILVANA ; LOIOLA, RODRIGO AZEVEDO ; OLIANI, SONIA MARIA ; VIEIRA, ANDREA ; PERRETTI, MAURO ; FARSKY, SANDRA HELENA POLISELLI . Formyl Peptide Receptors and Annexin A1: Complementary Mechanisms to Infliximab in Murine Experimental Colitis and Crohn?s Disease. Frontiers in Immunology JCR, v. 12, p. 714138, 2021.

   Citações: WEB OF SCIENCE℠ 3 | 3

6. BENVENUTTI, LARISSA ; NUNES, ROBERTA ; VENTURI, IVONILCE ; RAMOS, SILVIA APARECIDA ; **BROERING, MILENA FRONZA** ; GOLDONI, FERNANDA CAPITANIO ; PAVAN, SARAH ESKELSEN ; PASTOR, MARIA VERÔNICA DÁVILA ; MALHEIROS, ANGELA ; QUINTÃO, NARA LINS MEIRA ; FERNANDES, ELIZABETH SOARES ; SANTIN, JOSÉ ROBERTO . Anti-Inflammatory and Healing Activity of the Hydroalcoholic Fruit Extract of Solanum diploconos (Mart.) Bohs. JOURNAL OF IMMUNOLOGY RESEARCH JCR, v. 2021, p. 1-13, 2021.

   Citações: WEB OF SCIENCE℠ 4 | 5

7. DE PAULA-SILVA, MARINA ; **BROERING, MILENA FRONZA** ; SCHARF, PABLO ; DA ROCHA, GUSTAVO HENRIQUE OLIVEIRA ; FARSKY, SANDRA ; LINO-DOS-SANTOS-FRANCO, ADRIANA . Red light-emitting diode treatment improves tissue recovery in DSS-induced colitis in mice. JOURNAL OF PHOTOCHEMISTRY AND PHOTOBIOLOGY B-BIOLOGY JCR, v. 212, p. 112018, 2020.

   Citações: WEB OF SCIENCE℠ 2 | 2

8. SCHARF, PABLO ; **BROERING, MILENA FRONZA** ; OLIVEIRA DA ROCHA, GUSTAVO HENRIQUE ; FARSKY, SANDRA HELENA POLISELLI . Cellular and Molecular Mechanisms of Environmental Pollutants on Hematopoiesis. INTERNATIONAL JOURNAL OF MOLECULAR SCIENCES JCR, v. 21, p. 6996, 2020.

   Citações: WEB OF SCIENCE℠ 12 | 17

9.

DE FAVERI, ALINE ; DE FAVERI, RENATA ; **BROERING, MILENA FRONZA** ; BOUSFIELD, IZABEL TERRANOVA ; GOSS, MARINA JAGIELSKI ; MULLER, SAMUEL PAULO ; PEREIRA, RAQUEL OLIVEIRA ; DE OLIVEIRA E SILVA, ANA MARA ; MACHADO, ISABEL DAUFENBACK ; QUINTÃO, NARA LINS MEIRA ; SANTIN, JOSÉ ROBERTO . Effects of passion fruit peel flour (Passiflora edulis f. flavicarpa O. Deg.) in cafeteria diet-induced metabolic disorders. JOURNAL OF ETHNOPHARMACOLOGY JCR, v. 250, p. 112482, 2020.

Citações: WEB OF SCIENCE ℠ 17 | 16

10. DA ROCHA, GUSTAVO HENRIQUE OLIVEIRA ; DE PAULA-SILVA, MARINA ; **BROERING, MILENA FRONZA** ; SCHARF, PABLO RHASAN DOS SANTOS ; MATSUYAMA, LARISSA SATIKO ALCÂNTARA SEKIMOTO ; MARIA-ENGLER, SILVYA STUCHI ; FARSKY, SANDRA HELENA POLISELLI . Pioglitazone-Mediated Attenuation of Experimental Colitis Relies on Cleaving of Annexin A1 Released by Macrophages. Frontiers in Pharmacology JCR, v. 11, p. 1-19, 2020.

Citações: WEB OF SCIENCE ℠ 9 | 8

11. SANTIN, J. R. ; SILVA, G. ; PASTOR, M. V. ; **BROERING, M. F.** ; NUNES, R. ; BRAGA, R. ; SOUSA, I. ; STIZ, D. ; SILVA, K. ; STOEBERL, L. C. ; CORREA, R. ; CECHINEL FILHO, V. ; SANTOS, C. E. ; QUINTÃO, N. L. M. . Biological and toxicological evaluation of N-(4methyl-phenyl)-4-methylphthalimide on bone cancer in mice.. Anti-Cancer Agents in Medicinal Chemistry JCR, v. 19, p. 667-676, 2019.

12. ★ **BROERING, MILENA FRONZA**; NUNES, ROBERTA ; DE FAVERI, RENATA ; DE FAVERI, ALINE ; MELATO, JÉSSICA ; VIEIRA, MARIA EDUARDA ; MALHEIROS, ANGELA ; MEIRA QUINTÃO, NARA LINS ; SANTIN, JOSÉ ROBERTO . Effects of Tithonia diversifolia (asteraceae) extract on innate inflammatory responses. JOURNAL OF ETHNOPHARMACOLOGY JCR, v. 1, p. 112041, 2019.

Citações: WEB OF SCIENCE ℠ 9 | 10

13. GOLDONI, FERNANDA CAPITANIO ; BARRETTA, CLAIZA ; NUNES, ROBERTA ; **BROERING, MILENA FRONZA** ; DE FAVERI, RENATA ; MOLLERI, HELOISA TACHINI ; CORRÊA, THIAGO PATRÍCIO ; FARIAS, INGRID VICENTE ; AMORIN, CLARISSA KRIEGER ; PASTOR, MARIA VERONICA DAVILA ; DA SILVA, CHRISTIANE MEYRE ; BRESOLIN, TANIA MARI BELLE ; DE FREITAS, RILTON ALVES ; QUINTÃO, NARA LINS MEIRA ; SANTIN, JOSÉ ROBERTO . Effects of Eugenia umbelliflora O. Berg (Myrtaceae)-leaf extract on inflammation and hypersensitivity. JOURNAL OF ETHNOPHARMACOLOGY JCR, v. 244, p. 112133, 2019.

Citações: WEB OF SCIENCE ℠ 4 | 8

14. NUNES, ROBERTA ; **BROERING, MILENA FRONZA** ; DE FAVERI, RENATA ; GOLDONI, FERNANDA CAPITANIO ; MARIANO, LUISA NATHÁLIA BOLDA ; MAFESSOLI, PAMELA CECÍLIA MÜLLER ; DELLE MONACHE, FRANCO ; CECHINEL FILHO, VALDIR ; NIERO, RIVALDO ; SANTIN, JOSÉ ROBERTO ; QUINTÃO, NARA LINS MEIRA . Effect of the metanolic extract from the leaves of Garcinia humilis Vahl (Clusiaceae) on acute inflammation. INFLAMMOPHARMACOLOGY JCR, v. 1, p. 1-16, 2019.

Citações: WEB OF SCIENCE ℠ 11 | 13

15. SHANMUGAM, SARAVANAN ; THANGARAJ, PARIMELAZHAGAN ; DOS SANTOS LIMA, BRUNO ; TRINDADE, GABRIELA G.G. ; NARAIN, NARENDRA ; MARA DE OLIVEIRA E SILVA, ANA ; SANTIN, JOSÉ ROBERTO ; **BROERING, MILENA FRONZA** ; SERAFINI, MAIRIM RUSSO ; QUINTANS-JÚNIOR, LUCINDO JOSÉ ; ANTUNES DE SOUZA ARAÚJO, ADRIANO . Protective effects of flavonoid composition rich P. subpeltata Ortega. on indomethacin induced experimental ulcerative colitis in rat models of inflammatory bowel diseases. JOURNAL OF ETHNOPHARMACOLOGY JCR, v. 248, p. 112350, 2019.

Citações: WEB OF SCIENCE ℠ 13 | 13

16. ROCHA, LILIAN W. ; SONZA, DANIELE R. ; **BROERING, MILENA FRONZA** ; NUNES, ROBERTA ; DE CAMPOS-BUZZI, FÁTIMA ; CORRÊA, ROGÉRIO ; SILVA, RANGEL L. ; CUNHA, THIAGO M. ; SANTIN, JOSÉ ROBERTO ; QUINTÃO, NARA L.M. . Synthetic chalcones as potential tool for acute- and chronic-pain control. BIOMEDICINE & PHARMACOTHERAPY JCR, v. 104, p. 437-450, 2018.

Citações: WEB OF SCIENCE ℠ 4 | 4

17. WOLFF, FELLIPPE RAMOS ; **BROERING, MILENA FRONZA** ; JURCEVIC, JOCILENE DEMÉTRIO ; ZERMIANI, TAYLIN ; BRAMORSKI, ADRIANA ; DE CARVALHO VITORINO, JOSIANE ; MALHEIROS, ANGELA ; SANTIN, JOSÉ ROBERTO . Safety assessment of Piper cernuum Vell. (Piperaceae) leaves extract: Acute, sub-acute toxicity and genotoxicity studies. JOURNAL OF ETHNOPHARMACOLOGY JCR, v. 5, p. 109-116, 2018.

Citações: WEB OF SCIENCE ℠ 8 | 10

18. TONIN, TALITA DACROCE ; THIESEN, LILIANI CAROLINI ; DE OLIVEIRA NUNES, MARIA LUISA ; **BROERING, MILENA FRONZA** ; DONATO, MARCOS PAULO ; GOSS, MARINA JAGIELSKI ; PETREANU, MARCEL ; NIERO, RIVALDO ; MACHADO, ISABEL DAUFENBACK ; SANTIN, JOSÉ ROBERTO . Rubus imperialis (Rosaceae) extract and pure compound niga-ichigoside F1: wound healing and anti-inflammatory effects. NAUNYN-SCHMIEDEBERG'S ARCHIVES OF PHARMACOLOGY JCR, v. 389, p. 1235-1244, 2016.

Citações: WEB OF SCIENCE ℠ 12 | 12

19. PETREANU, MARCEL ; GUIMARÃES, ÁGATHA AMANDA ALVES ; **BROERING, MILENA FRONZA** ; FERREIRA, EMILI KAMILA ; MACHADO, ISABEL DAUFENBACK ; GOIS, ANA LÚCIA TASCA ; DE CARVALHO, JOÃO ERNESTO ; MONACHE, FRANCO DELLE ; NIERO, RIVALDO ; SANTIN, JOSÉ ROBERTO . Antiproliferative and toxicological properties of methanolic extract obtained from Solanum capsicoides All. seeds and carpesterol. Naunyn-Schmiedeberg´s Archives of Pharmacology JCR, v. 389, p. 1123-1131, 2016.

Citações: WEB OF SCIENCE ℠ 7 | 9

Resumos publicados em anais de congressos

1. **BROERING, M. F.**; NUNES, ROBERTA ; DE FAVERI, A ; DE FAVERI, R. ; GOLDONI, F. C. ; QUINTÃO, N. L. M. ; SANTIN, J. R. . ETHANOLIC EXTRACT OF Tithonia diversifolia (ASTERACEAE) LEAVES INHIBITHIS NEUTROFIL INFLUX AND CYTOKINE SECRETION. In: IV Congress of the Brazilian Association of Pharmaceutical Sciences - Biological Drugs: From Technology to Pharmaceutical Care, 2018, São Paulo. Brazilian Journal of Pharmaceutical Sciences, 2018. v. 35.

2. NUNES, ROBERTA ; **BROERING, M. F.** ; DE FAVERI, R. ; QUINTÃO, N. L. M. ; SANTIN, J. R. . METHANOLIC EXTRACT OF GARCINIA ACHACHAIRU RUSBY (CLUSIACEAE) LEAVES INHIBITHIS NEUTROFIL INFLUX AND CYTOKINE SECRETION. In: IV Congress of the Brazilian Association of Pharmaceutical Sciences - Biological Drugs: From Technology to Pharmaceutical Care, 2018, São Paulo. Brazilian Journal of Pharmaceutical Sciences, 2018. v. 35.

Apresentações de Trabalho

1. **BROERING, M. F.**. Nanotecnologia: aplicação a ciência da vida. 2019. (Apresentação de Trabalho/Outra).
2. DE FAVERI, A ; **BROERING, M. F.** ; ROSA, R. G. ; NASCIMENTO, M. M. V. S. ; DALMARCO, E. M. ; QUINTÃO, N. L. M. ; SANTIN, J. R. . Avaliação da atividade anti-inflamatória das cascas de Aleurites moluccana in vivo. 2017. (Apresentação de Trabalho/Congresso).
3. **BROERING, M. F.**; TONIN, T. D. ; MACHADO, I. D. ; PETREANU, M. ; NIERO, R. ; SANTIN, J. R. . Avaliação toxicológica in vivo, in vitro e in silico do extrato e compostos isolados obtidos das partes aéreas de Rubus rosaefolis. 2015. (Apresentação de Trabalho/Congresso).
4. **BROERING, M. F.**; SANTIN, JOSÉ ROBERTO . Avaliação toxicológica in vivo, in vitro e in silico do extrato metanólico e compostos isolados das partes aéreas de Rubus rosaefolius. 2015. (Apresentação de Trabalho/Seminário).
5. **BROERING, M. F.**. Avaliação toxicológica in vivo, in vitro e in silico do extrato metanólico e compostos isolados das partes aéreas de Rubus rosaefolius. 2015. (Apresentação de Trabalho/Outra).
6. **BROERING, M. F.**; TONIN, T. D. ; PETREANU, M. ; NIERO, R. ; SANTIN, J. R. . Avaliação toxicológica do extrato obtido das partes aéreas de Rubus rosaefolius. 2014. (Apresentação de Trabalho/Outra).

Eventos

Participação em eventos, congressos, exposições e feiras

1. V Congresso da Associação Brasileira de Ciências Farmacêuticas. Efeitos da nanocápsula de núcleo lipídico contendo anexina a1 em modelo de colite ulcerativa induzida em camundongos. 2020. (Congresso).
2. I Simpósio Internacional em Investigação Químico Farmacêutico.Avaliação da Atividade Anti-inflamatória do Extrato de Tithonia diversifolia (Asteracea). 2018. (Simpósio).
3. IV Congress of the Brazilian association of Pharmaceutical sciences - Biological Drugs: From Technologies to Pharmaceutical Care. ETHANOLIC EXTRACT OF Tithonia diversifolia (ASTERACEAE) LEAVES INHIBITHIS NEUTROFIL INFLUX AND CYTOKINE SECRETION. 2018. (Congresso).
4. IV Semana Integrada: Ensino, Pesquisa e Extensão do Centro de Ciências da Saúde - CCSias. 2016. (Outra).
5. VI Simpósio Biomédico e VIII Semana de Iniciação Científica de Biomedicina. 2016. (Simpósio).
6. Grupo de Pesquisa em Análises Clínicas. 2015. (Outra).
7. Grupo de Pesquisa em Farmacologia.Avaliação toxicológica in vivo, in vitro e in silico do extrato metanólico e compostos isolados das partes aéreas de Rubus rosaefolius. 2015. (Outra).
8. Grupo de Pesquisa em Farmacologia. 2015. (Outra).
9. III Congresso de Biomedicina de Santa Catarina. Avaliação toxicológica in vivo e in silico do extrato e compostos isolados das partes aéreas de Rubus rosaefolius. 2015. (Congresso).
10. III Congresso de Biomedicina de Santa Catarina. 2015. (Congresso).
11. V Semana de Iniciação Científica do Curso de Biomedicina. 2015. (Outra).
12. V Simpósio Biomédico e VI Semana de iniciação Científica do Curso de Biomedicina.Avaliação toxicológica in vivo, in vitro e in silico do extrato e compostos isolados das partes aéreas de Rubus rosaefolius. 2015. (Simpósio).
13. V Simpósio Biomédico e VI Semana de iniciação Científica do Curso de Biomedicina. 2015. (Simpósio).
14. XIV Seminário de Iniciação Científica.Avaliação toxicológica in vivo, in vitro e in silico do extrato metanólico e compostos isolados das partes aéreas de Rubus rosaefolius. 2015. (Seminário).
15. III Semana de Iniciação Científica do Curso de Biomedicina. 2014. (Outra).
16. IV Simpósio Biomédico e IV Semana de Iniciação Científica da Biomedicina. 2014. (Simpósio).
17. VIII Fórum Internacional CISDEM: Desafios e Avanços em Tecnologia Farmacêutica. 2014. (Congresso).
18. VIII Fórum Internacional CISDEM: Desafios e Avanços em Tecnologia Farmacêutica. Avaliação Toxixológica do Extrato Obtido das Partes Aéreas de Rubus rosaefolius (Rosaceae). 2014. (Congresso).
19. XIII Seminário de Iniciação Científica. 2014. (Seminário).
20. III Simpósio Biomédico da Univali e II Semana de Iniciação Científica do Curso de BIomedicina. 2013. (Simpósio).
21. III Simpósio Biomedico e II Semana de Iniciação Científica. 2013. (Outra).
22. II Semana Acadêmica e I Semana de Iniciação Científica da Biomedicina. 2013. (Outra).

Organização de eventos, congressos, exposições e feiras

1. SANTIN, J. R. ; DE FAVERI, R. ; VALADARES, M. C. ; **BROERING, M. F.** . I Workshop ABCF-UNIVALI: Atualização em Toxicologia Clínica e Experimental. 2018. (Outro).

Educação e Popularização de C & T

Anexo 6. Ficha do aluno

Universidade de São Paulo

FICHA DO ALUNO

Janus

9142 - 11144151 / 1 - Milena Fronza Broering

Email:	milenafbroering@usp.br
Data de Nascimento:	30/10/1995
Cédula de	RG - 5844437 - SC
Local de	Estado de Santa Catarina
Nacionalidade:	Brasileira
Graduação:	Biomédica - Universidade do Vale do Itajaí - Santa Catarina - Brasil - 2016
Mestrado:	Mestra em Ciências Farmacêuticas (1) - Universidade do Vale do Itajaí - Santa Catarina - Brasil - 2019

Curso:	Doutorado
Programa:	Farmácia (Fisiopatologia e Toxicologia)
Modalidade:	Acadêmica
Área:	Fisiopatologia
Data de Matrícula:	11/02/2019
Início da Contagem de Prazo:	11/02/2019
Data Limite para o Depósito:	06/02/2024
Orientador:	Prof(a). Dr(a). Sandra Helena Poliselli Farsky - 11/02/2019 até o presente Email: sfarsky@usp.br

Proficiência em Línguas:

Inglês, Aprovado em 11/02/2019

Data de Aprovação no Exame de Qualificação:	Aprovado em 11/08/2021
Estágio no Exterior:	University of Massachusetts, Estados Unidos da América - Período de 15/11/2022 até 14/11/2023

USP Universidade de São Paulo

FICHA DO ALUNO

Janus

Data do Depósito do Trabalho:

Título do Trabalho:

Data Máxima para Aprovação da Banca:

Data de Aprovação da Banca:

Data Máxima para Defesa:

Data da Defesa:

Resultado da Defesa:

Histórico de Ocorrências: Primeira Matrícula em 11/02/2019
Aluno matriculado no Regimento da Pós-Graduação USP (Resolução nº 6542 em vigor de 20/04/2013 até 28/03/2018).

Última ocorrência: Matrícula de Acompanhamento em 07/07/2023

Sigla	Nome da Disciplina	Início	Término	Carga Horária	Cred.	Freq.	Conc.	Exc.	Situação	Pres.
BMI5881-6/2	Regulação da Resposta Imune (Instituto de Ciências Biomédicas - Universidade de São Paulo)	11/03/2019	05/05/2019	120	8	100	B	N	Concluída	S
FBC5792-5/2	Tópicos em Fisiopatologia e Toxicologia III	12/03/2019	24/06/2019	15	1	88	B	N	Concluída	S
FBC5958-1/1	Sinalização por GPCRs e descoberta de novos fármacos	18/03/2019	24/03/2019	30	2	100	A	N	Concluída	S
FBC5766-6/3	Tópicos em Fisiopatologia e Toxicologia IV	06/08/2019	18/11/2019	15	1	87	A	N	Concluída	S
FBF5805-2/7	Delineamento de Experimentos e Ferramentas Estatísticas Aplicadas às Ciências Farmacêuticas	20/08/2019	28/10/2019	90	6	100	A	N	Concluída	S
PGF5357-1/1	Técnicas de Caracterização de Sistemas de Relevância Biológica (Instituto de Física - Universidade de	11/10/2019	17/10/2019	15	0	-	-	N	Matrícula cancelada	S

USP Universidade de São Paulo

FICHA DO ALUNO

Janus

Sigla	Nome da Disciplina	Início	Término	Carga Horária	Cred.	Freq.	Conc.	Exc.	Situação	Pres.
	São Paulo)									
Atividade do Programa	Publicação de Trabalho Original completo ou Artigo de Revisão, intitulado Red light-emitting diode treatment improves tissue recovery in DSSinduced colitis in mice (2)	04/12/2019	04/12/2019	-	2	-	-	-	-	-
QBQ5903-1/1	Técnicas Aplicadas ao Desenvolvimento de Processos Biotecnológicos (Instituto de Química - Universidade de São Paulo)	17/02/2020	31/05/2020	105	0	-	-	N	Matrícula cancelada	S
FBA5728-4/9	Aprimoramento Pedagógico	17/03/2020	13/04/2020	60	0	-	-	N	Turma cancelada	S
Atividade do Programa	Publicação de Trabalho Original completo ou Artigo de Revisão, intitulado Cellular and Molecular Mechanisms of Environmental Pollutants on Hematopoiesis" (2)	26/08/2020	26/08/2020	-	2	-	-	-	-	-
Atividade do Programa	Publicação de Trabalho Original completo ou Artigo de Revisão, intitulado Pioglitazone-Mediated Attenuation of Experimental Colitis Relies on Cleaving of Annexin A1 Released by Macrophages (2)	21/12/2020	21/12/2020	-	2	-	-	-	-	-
BTC5743-5/2	Seminários Gerais (Curso Interunidades: Biotecnologia - Universidade de São Paulo)	24/03/2021	06/07/2021	30	2	90	B	N	Concluída	N

Universidade de São Paulo

FICHA DO ALUNO

Janus

	Créditos mínimos exigidos		Créditos obtidos
	Para exame de qualificação	Para depósito de tese (Totais/Presenciais)	Totais/Presenciais
Disciplinas:	0	20 / 12	26 / 26*
Estágios:			
Total:	0	20 / 12	26 / 26*

Créditos Atribuídos à Tese: 167

*Créditos obtidos anteriormente a 01/01/2024 serão computados como presenciais de acordo com a Resolução CoPGr 8546, de

Observações:

1) Curso com validade nacional, de acordo com o disposto na Portaria nº 656, de 22.05.2017

Observações:

2) Créditos atribuídos de acordo com o Artigo 64 do Regimento de Pós-Graduação e aprovados pela Comissão de Pós-Graduação, em Sessão de 14/04/2021

Conceito a partir de 02/01/1997:

A - Excelente, com direito a crédito; B - Bom, com direito a crédito; C - Regular, com direito a crédito; R - Reprovado; T - Transferência.

Um(1) crédito equivale a 15 horas de atividade programada.